Non-perturbative renormalization in Quantum Chromodynamics and Heavy Quark Effective Theory

als Habilitationsschrift
dem
Fachbereich Physik
der
Westfälischen Wilhelms-Universität zu Münster

vorgelegt von

Jochen Heitger

2005

Für meine Frau Margret
mit Tizian, Thalia und Tristan

Contents

Introduction

1 From continuum to lattice QCD

Already about thirty years ago, the three fundamental forces between elementary particles, the electromagnetic, the weak and the strong nuclear interactions have found their unified description in the *Standard Model* of particle physics. This unification — and even more the great success of the Standard Model on its own, reflecting in a so far impressively precise agreement between theory and experiment — would not have been possible without the theoretical insight that these three kinds of interactions can be formulated in a way consistent with both quantum theory and the special theory of relativity on the one hand, while on the other hand they have to obey a local gauge principle which demands invariance under certain local symmetry transformations. The theory of elementary particles and their interactions is therefore founded on so-called *gauge field theories*.[1]

The gauge field theory of the strong nuclear interactions, which bind the constituents of atomic nuclei together, is *Quantum Chromodynamics, QCD*. As such it is a key component of the Standard Model, describing the constituents of all nuclear matter, the *quarks*, and their mutual interactions by the exchange of massless vector bosons that are referred to as *gluons*. They carry SU(3) quantum numbers associated with internal, *colour* degrees of freedom and couple to all flavours of quarks with equal strength proportional to the *gauge coupling constant, g*. QCD shares some common structural and qualitative features with Quantum Electrodynamics (QED), the quantized theory of electrons and photons, which historically was the first of the three aforementioned gauge theories of particle physics. The general form of the basic field equations looks rather similar, and in both cases the interactions are mediated by massless field quanta: in QED these are the photons that are responsible for the electromagnetic interactions of charged particles, whereas in QCD the gluons mediate the strong force among the quarks.

However, there are also essential differences between both theories. The gauge group of QED is U(1), an abelian group, which implies that there is no self-interaction of photons and the electromagnetic force decreases as the distance between the charges grows. Moreover, physical quantities of interest can be expanded in powers of the electromagnetic coupling, the finestructure constant α, that is numerically small ($\alpha \approx 1/137$). The *smallness* of this number is just the deeper reason for the very accurate predictions made in QED, which in turn led to experimental tests of the theory with highest precision. In contrast, the coupling strength of the strong interactions is *not small* at all, and it is actually the non-abelian character of the gauge group of QCD, SU(3), that has crucial consequences for the properties of this theory.

To illuminate this more closely, let us write down the Lagrange density of QCD, which may be regarded as the defining equation of the theory and usually serves as the starting

[1] The gravitational force does not play an important rôle in the physics of elementary particles.

point of any of its calculational schemes:

$$\mathcal{L}_{\mathrm{QCD}} \;=\; -\frac{1}{2g^2}\,\mathrm{Tr}\,\{F_{\mu\nu}F_{\mu\nu}\} \;+\; \sum_{f=\mathrm{u,d,s,...}} \overline{\psi}_f\,\{\gamma_\mu\,(\partial_\mu + gA_\mu) + m_f\}\,\psi_f\,, \tag{1.1}$$

where in this form a rotation from Minkowski to Euclidean space is already implied. Without going into all details, we only mention that the first term is the square of the non-abelian gauge field tensor

$$F_{\mu\nu} = \partial_\mu A_\nu - \partial_\nu A_\mu + [\,A_\mu, A_\nu\,] \tag{1.2}$$

with $A_\mu(x) = A^a_\mu(x)T^a$ being the gauge (or gluon) fields and T^a, $a = 1,\ldots,8$ the generators of the colour group SU(3), while the second term in eq. (1.1) sums the contributions of the quark flavours up, down, charm, strange, top and bottom, represented by the Dirac spinor fields $\psi_f(x)$ with associated quark masses m_f (and internal colour indices suppressed here).

In fact, from the $g\overline{\psi}_f\gamma_\mu A_\mu\psi_f$ piece in the QCD Lagrangian (1.1) one now concludes that the quarks are interacting with each other by exchanging massless quanta of the gauge field, the gluons, where the interaction strength is parameterized by the gauge coupling g. At first sight, this suggests a fall off like $1/r^2$ of the force at large distances r, similar to the situation with photons in QED, which then would also mean that the amount of energy necessary to break up a quark-antiquark bound state is finite. Such an interpretation stands, however, in clear contradiction to a famous phenomenon of the strong interactions known as *confinement*: Quarks have never been detected in isolation, always several of them appear as constituents to build up bound-state hadrons. From the theoretical point of view, this corresponds to the fact that all physical states are singlets w.r.t. the colour group.

In addition to the quark-gluon interaction, however, the gluons do also *interact with each other* by virtue of the squared field strength term in (1.2) — a term that is absent in QED. As a consequence, it turns out (and can be explicitly shown in a perturbative expansion of the theory defined by eq. (1.1) with the coupling as expansion parameter) that, once exchanges of virtual quarks and vector bosons are included, the interaction strength mediated by the gluons depends on the magnitude μ of the energy-momentum transfer between the quarks. More precisely, if one introduces a suitable quantity, say $\bar{g}$, that is designed to be a measure for the strength of the interaction accounting for all possible higher-order corrections from virtual quark and gluon excitations[2], the corresponding *strong coupling constant* α_s behaves for large momenta μ as

$$\alpha_\mathrm{s}(\mu) \equiv \frac{\bar{g}^2(\mu)}{4\pi} = \frac{c}{\ln(\mu/\Lambda)} \;+\; \ldots\,, \tag{1.3}$$

[2]In a more theoretical language, such a quantity would be called an *effective* or *renormalized*, physical coupling.

with a calculable constant c and an intrinsic, low-energy QCD scale of mass dimension one, the Λ*–parameter*, which governs the dynamics and particularly the large-energy asymptotics of the theory and which in a sense can be looked at as a fundamental QCD parameter equivalent to the coupling itself. The logarithmic decay of the coupling α_s encoded in eq. (1.3) is the other prominent property of QCD and called *asymptotic freedom*. As illustrated in the left diagram of Figure 1.1, it is indeed confirmed in high-energy scattering experiments; from such measurements it was possible to estimate the value of Λ to be $210\,^{+34}_{-30}$ MeV [1,2], where this number refers to the five-flavour theory and the '$\overline{\text{MS}}$ scheme of dimensional regularization' as a particular definition of the effective coupling used in (1.3).

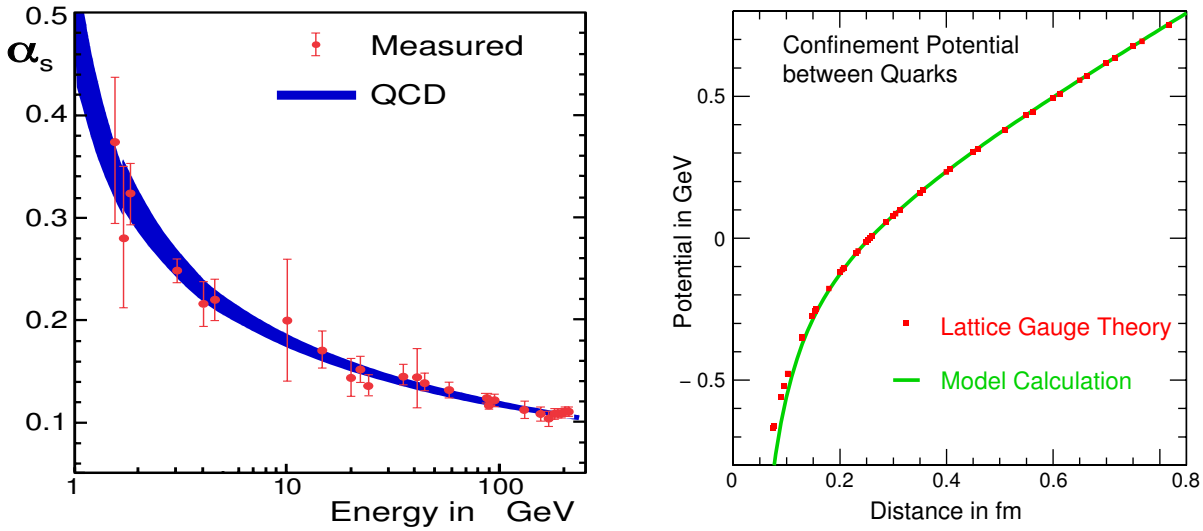

Figure 1.1: *Left*: The strength of the strong interaction (α_s) decreases as the energy increases. Known as *asymptotic freedom*, this property is one of the crucial predictions of the underlying quantum field theory, QCD. *Right*: The QCD potential between quarks and antiquarks computed non-perturbatively with the methods of lattice gauge theory. The potential increases with the separation distance between the quarks, with the result that quarks are never encountered free. This phenomenon is known as *confinement*. (The compilation of the data in both figures is taken from Ref. [3].)

The physical picture emerging from the foregoing discussion, namely the 'running' of the QCD coupling with the energy scale as e.g. expressed by eq. (1.3), makes evident that the supposed conflict between theory and the non-observation of free quarks is avoided. As one moves towards *higher energies*, the coupling becomes increasingly weak. Hence, for energies beyond a few GeV, perturbation theory as a systematic expansion in powers of the coupling, which multiply contributions pictorially representable by Feynman diagrams, will generally be applicable to yield reliable results for the observables of interest in this regime. Opposed to that, if we approach the confinement regime at *low energies* of some hundred MeV, i.e. of the order of the QCD scale Λ, the QCD force begins to become strong and constant at large distances of $\mathrm{O}(1\,\mathrm{GeV}^{-1})$ (see the right graph of Figure 1.1), and the associated growth of the coupling consequently renders the perturbative expansion

invalid. It is also worth to note here that the breakdown of this expansion immediately implies that the characteristic low-energy scale of QCD itself, Λ, can *not* be directly computed with perturbative methods.

The scope of most theoretical investigations of QCD may be grouped into two branches. On the one hand, one would like to demonstrate that QCD indeed yields the correct explanation for the observed diversity of the strong interaction phenomena in both the high- and low-energy regimes and thereby to confirm it as the undoubtedly accepted framework to describe this sector of the Standard Model. On the other hand, QCD computations are needed to determine the basic properties of the quark bound states such as pions, kaons or, for instance, mesons involving heavy quarks, since results from the hadronic sector of the theory constitute valuable information for experimentalists in order to interpret the outcome of their current and future experiments at particle accelerators. In practice, though, it turns out to be difficult to perform such precision tests of QCD by comparing theory with experiment or to arrive at concrete numerical predictions, and the reason for that has already been touched above: Contrary to the situation in QED as a weakly coupled theory where perturbation theory always works well and gives applicable series expansions, the coupling strength of the strong interactions is by no means small and thus cannot serve as a feasible expansion parameter of perturbative series in QCD, unless one allows for ad hoc assumptions or approximations such as e.g. restricting the investigations to the domain of very high energies. Therefore, a different computational scheme is required to address questions that are of generically non-perturbative nature or take (direct or indirect) reference to the whole energy range of the theory.

To be able to deal with such problems in a reliable way, one first of all needs a formulation of the theory that is mathematically well-defined at the *non-perturbative* level. A viable framework to achieve this is provided by the *lattice formulation of QCD*, which was initiated by K. Wilson in 1974 [4] and opened already from the very beginning the interesting perspective to solve the theory by applying numerical simulation methods. The lattice approach to quantum field theory has nowadays established itself as an integral part of theoretical elementary particle physics[3] and provides a non-perturbative framework to compute relations between Standard Model parameters and experimental quantities from first principles. As the lattice formulation of QCD also represents the basis for the work presented in the following, we will continue with a brief summary of its key elements. For a more general and comprehensive indroduction to the whole field see, for instance, the textbooks [5, 6].

[3]The current status of this field of theoretical physics as well as an representative overview of its concrete results and new developments can be drawn from the periodically published Proceedings of the annual *International Symposium on Lattice Field Theory*.

1.1 A survey of the lattice formulation of QCD

In order to formulate QCD on a discrete grid of points, the four-dimensional space-time continuum is replaced by a Euclidean, hypercubic lattice with lattice spacing a and volume $L^3 \times T$ of (in practice finite) space- and timelike extents, L and T. Next, one needs a sensible prescription for the discretization of the action belonging to the Lagrange density (1.1) of QCD. To this end the quark and antiquark fields ψ and $\overline{\psi}$ are restricted to the lattice points, while the gauge field is associated with matrix-valued link variables $U(x,\mu) \in \mathrm{SU}(3)$, $\mu = 1,\ldots,4$, which live on the lattice bonds pointing from site x into the positive μ–direction with unit vector $\hat{\mu}$ and which act as parallel transporters between the fields defined on different sites of the lattice. In this way it is possible to find discretizations of the terms in eq. (1.1) that fully preserve the gauge symmetry of the theory and coincide in the classical continuum limit, $a \to 0$, with their continuum counterparts. In case of the purely gluonic part, the commonly used discretization is the Wilson action [4],

$$S_{\mathrm{gluon}}[U] = \frac{1}{g_0^2} \sum_p \mathrm{Tr}\left\{1 - U(p)\right\} , \tag{1.4}$$

which is defined in terms of (oriented) plaquette variables $U(p)$, where a plaquette denotes the product of link variables along a closed curve of extent 1×1 (in units of the lattice spacing) as the smallest possible of all closed curves of arbitrary size and shape on the lattice. This expression is gauge invariant and reproduces as its leading term for small a the Euclidean Yang-Mills action in the continuum, $-\frac{1}{2g_0^2}\int \mathrm{d}^4x\, \mathrm{Tr}\left\{F_{\mu\nu}F_{\mu\nu}\right\}$, with g_0 being the (bare) gauge coupling. The construction introduced so far is schematically drawn in Figure 1.2. It is also important note here that the inverse lattice spacing naturally imposes a cutoff $\propto 1/a$ on all entering momenta; thereby the lattice serves at the same time as a (non-perturbative) regulator of the ultraviolet divergences that are usually encountered in quantum field theory.

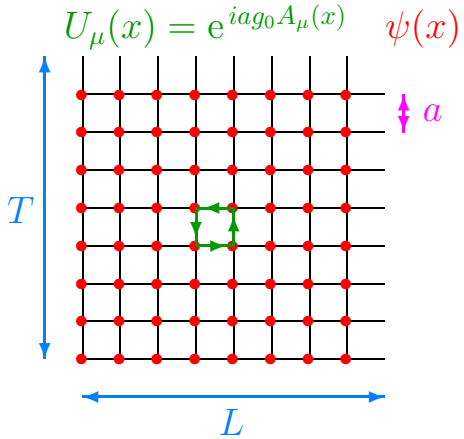

Figure 1.2: Sketch of lattice-discretized two-dimensional space-time of extent $L \times T$ and the lattice versions of the field variables that build up the Lagrange density of QCD. Links $U(x,\mu)$, representing the lattice gauge field, connect neighbouring sites, whereas the quark field $\psi(x)$ resides on the lattice sites x.

The discretization of the part in $\mathcal{S}_{\rm QCD} = \int \mathrm{d}^4x\, \mathcal{L}_{\rm QCD}$ involving the quark fields simply reads

$$S_{\rm quark}[U,\overline{\psi},\psi] = a^4 \sum_x \overline{\psi}(x) D[U] \psi(x)\,, \tag{1.5}$$

where x runs over all points of the lattice and $D[U] = \frac{1}{2}\gamma_\mu(\nabla^*_\mu + \nabla_\mu) + m_0$ stands for the lattice Dirac operator in which the naive lattice forward and backward (i.e. the corresponding nearest neighbour finite-difference) operators ∇_μ and ∇^*_μ acting on the quark fields are understood to be substituted by their gauge covariant forms, i.e.

$$\nabla_\mu \psi(x) = \frac{1}{a}\left[\, U(x,\mu)\psi(x+a\hat{\mu}) - \psi(x)\,\right] \tag{1.6}$$

for the forward difference operator and analogously for the backward case, in order to ensure gauge invariance. The lattice action (1.5) is, however, afflicted with the so-called 'doubler' problem reflecting in the occurrence of additional unphysical degrees of freedom that would persist in the continuum limit and thus deteriorate the physical spectrum of the theory. One of the proposals to cure this deficiency is again due to Wilson and amounts to include a term $-\frac{1}{2}a\nabla^*_\mu\nabla_\mu$ in eq. (1.5), which causes the unwanted fermion modes to acquire masses proportional to $1/a$. The corrections assigned to the low-momentum physical modes then vanish proportionally to a so that for $a \to 0$ the former become infinitely heavy and disappear from the physical spectrum while only the latter survive. Thanks to its simplicity (and, as will become clear below, despite the difficulties it introduces for its own) it is widely used in many lattice QCD applications. The complete lattice action of QCD is now written as

$$\begin{aligned} S_{\rm QCD} &= S_{\rm gluon} + S_{\rm quark} \\ &= \beta \sum_p \left\{1 - \tfrac{1}{3}\,\mathrm{Re}\,U(p)\right\} + a^4 \sum_x \overline{\psi}(x) \left\{\tfrac{1}{2}\left[\gamma_\mu\left(\nabla^*_\mu + \nabla_\mu\right) - a\nabla^*_\mu\nabla_\mu\right] + m_0\right\}\psi(x)\,, \end{aligned} \tag{1.7}$$

where the convenient parameter β is related to the bare gauge coupling through $\beta \equiv 6/g_0^2$ and m_0 is the bare quark mass[4].

The quantization of the lattice field theory is founded on the Feynman path integral formalism and bears a nice as well as very useful analogy between Euclidean quantum field theory and statistical mechanics, which finally allows the application of many, particularly numerical methods borrowed from the statistical mechanics of lattice systems and to develop new tools from them. Therefore, given an observable $\mathcal{O}$ (which generally will be a local gauge invariant function $\mathcal{O}[U,\overline{\psi},\psi]$ of the link variables and quark fields), the starting point of any calculation in lattice QCD is to specify the functional integral that defines the expectation value of O via the representation,

$$\langle\mathcal{O}\rangle = \frac{1}{\mathcal{Z}}\int \mathcal{D}[U]\mathcal{D}[\overline{\psi},\psi]\,\mathcal{O}\,\mathrm{e}^{-S_{\rm QCD}[U,\overline{\psi},\psi]}\,, \quad \mathcal{Z} = \int \mathcal{D}[U]\mathcal{D}[\overline{\psi},\psi]\,\mathrm{e}^{-S_{\rm QCD}[U,\overline{\psi},\psi]}\,, \tag{1.8}$$

[4]For simplicity it is assumed here that the quark mass is the same for all flavours, making obsolete the subscript f on the quark fields in (1.1).

where S_{QCD} is the discretized action from eq. (1.8) and $\mathcal{Z}$ is called the partition function. The discretization procedure has hence given a meaning to the functional integral measure $\mathcal{D}[U]\mathcal{D}[\overline{\psi},\psi]$ as a simple *product measure* $\prod_{x,\mu} \mathrm{d}U(x,\mu) \prod_x \mathrm{d}\overline{\psi}(x)\mathrm{d}\psi(x)$ comprising a discrete (and in practice even *finite*) set of integration variables so that the lattice in fact leads to a regularization of the theory with finite, mathematically well-defined expressions for the quantities of interest. On top of these more theoretical advantages, expressions such as (1.8) are also optimally suited for a *numerical evaluation* by Monte Carlo methods.

Before coming to introduce the main ideas underlying the numerical studies of lattice QCD, we want to give one example for an observable $\mathcal{O}$ that typically enters in spectroscopy calculations to obtain the mass of a hadron from the asymptotic behaviour of Euclidean-time correlation functions. Let $\Phi(x)$ be a suitable combination of quark fields at a point x, which has the quantum numbers of some hadron H. A prominent quantity is then the *two-point correlation function* defined as the expectation value $\left\langle \Phi(x)\Phi^\dagger(y)\right\rangle$, because it is proportional to the quantum-mechanical amplitude for the propagation of the hadron from y to x, from which the mass m_{H} of the hadronic bound state may be extracted. More precisely, if one takes $\Phi(x) = \overline{\psi}(x)\Gamma\psi(x)$ with a Dirac matrix Γ (say $\gamma_0\gamma_5$ in case of pseudoscalar mesons like pions or kaons) and sums over the spatial coordinates to Fourier-project onto zero spatial momentum, the correlation function is saturated by those hadron states among an inserted complete set of intermediate states, which $\Phi(x)$ can create from the vacuum, and its time dependence becomes a sum of damped exponentials,

$$C(t) = \sum_{\mathbf{x}} \left\langle \Phi(x_0,\mathbf{x})\Phi^\dagger(0,\mathbf{0})\right\rangle = \frac{|\langle 0|\Phi|\mathrm{H}\rangle|^2}{2m_{\mathrm{H}}} \times \mathrm{e}^{-m_{\mathrm{H}}x_0} + \cdots , \tag{1.9}$$

where the lowest-lying (i.e. lightest) state $|\mathrm{H}\rangle$ of mass m_{H} dominates and the omitted higher excitations are exponentially suppressed. Employing the rules to contract creation and annihilation operators into quark propagators $G(x_0,\mathbf{x};0,\mathbf{0}) \equiv \langle 0|\psi(x_0,\mathbf{x})\overline{\psi}(0,\mathbf{0})|0\rangle$, the correlator can be shown to be representable as a product of these propagators:

$$C(t) = \sum_{\mathbf{x}} \mathrm{Tr}\left\{G(x_0,\mathbf{x};0,\mathbf{0})\Gamma G(0,\mathbf{0};x_0,\mathbf{x})\Gamma\right\} , \tag{1.10}$$

with the trace running over spin and colour indices. In an actual calculation on the lattice, the quark propagators are obtained by a numerically cumbersome inversion of the (huge but sparse) matrix associated with the lattice Dirac operator $D[U]$, while the hadron mass is eventually estimated through a fit to the exponential decay form of the resulting correlation function.

1.2 Numerical simulations

As anticipated before, the central objects of interest in a lattice QCD calculation are the expectation values of eq. (1.8), whose formal path integral representation on a *finite* lattice

translates into a finite product of finite-dimensional integrals. This immediately suggests to apply numerical methods on a computer for their evaluation; but owing to the even now very large number of variables involved any straightforward numerical integration method would be highly inefficient or just impossible. The goal of numerical simulations of field theories on a lattice is therefore to compute physical observables through a *stochastic evaluation* of these integrals by *Monte Carlo* integration, and not least by the growing performance of the available computer platforms they have developed to one the most powerful tools for obtaining predictions from QCD and other models of elementary particle physics.

Opposed to more traditional theoretical approaches, a simulation by means of Monte Carlo techniques may better be understood as numerical 'experiment', which is performed on a computer; as such it has an a priori unknown outcome and is naturally affected by statistical and systematic errors. The key for an efficient estimation of the multi-dimensional integrals (1.8) is to generate field configurations with a probability distribution which follows the Boltzmann factor, e^{-S}. In this way the dominant part of the integrand is incorporated into the sampling of the phase space and thereby yields configurations that have the most substantial weight in the path integral; the method is thus known as *importance sampling*. Restricting to the pure gauge sector of QCD for a moment, an ensemble of configurations is then defined as an infinite number of gauge field configurations with a probability density $p[U]$ and, in the language of statistical mechanics, the density associated to the canonical ensemble is proportional to the Boltzmann factor: $p[U] \propto \mathrm{e}^{-S_{\mathrm{gluon}}[U]}$. Of course, in an actual simulation only samples consisting of a large but finite number N of field configurations can be created, where for the generation of this sequence of gauge configurations one makes use of suitable updating algorithms, which have to satisfy certain conditions defining a stochastic process called Markov chain and are constructed such that the distribution within a sample reproduces the desired equilibrium distribution in the canonical ensemble.

Assuming now to have generated in such a Monte Carlo procedure a representative sample of full QCD configurations (i.e. where both the dynamics of the gauge-link *and* fermion field variables has participated in), the *sample average* of some observable $\mathcal{O} = \mathcal{O}[U, \overline{\psi}, \psi]$ is given by

$$\overline{\mathcal{O}} = \frac{1}{N} \sum_{n=1}^{N} \mathcal{O}_n[U, \overline{\psi}, \psi] \tag{1.11}$$

with $\mathcal{O}_n$ being the value of the observable computed on the n-th configuration, sometimes also dubbed the n-th 'measurement' of $\mathcal{O}$. As we work with a finite number of configurations, it is an estimator of the ensemble average corresponding to the expectation value of $\mathcal{O}$ up to some finite precision, viz.

$$\langle \mathcal{O} \rangle = \overline{\mathcal{O}} \pm \Delta_{\mathcal{O}} \,, \tag{1.12}$$

where generically the statistical error $\Delta_{\mathcal{O}}$ is proportional to $1/\sqrt{N}$.[5] Hence, a correct and controlled evaluation of the statistical errors to be assigned to the observables, particularly accounting for the (in principle unavoidable) intrinsic autocorrelations among the configurations of a Monte Carlo sequence, is always a crucial (but more technical) ingredient of any serious analysis of numerical simulation data.

In summary, the numerical evaluation of the QCD path integral by Monte Carlo simulations then appears a two-step process, where in the first stage sets of gluon fields, the configurations, are created which are the representative 'snapshots' of the QCD vacuum. In the second stage, the quarks are allowed to propagate on these background gluon fields and the physical quantities are extracted from sample averages of ('measurements' of) products of gauge invariant local fields like, for instance, a hadron correlation function as discussed around eq. (1.9), which during the simulation has been composed out of the quark propagators calculated on each gauge background. Finally, it should be emphasized once more that — in contrast to other fields in physics where numerical simulations are often to be looked at as an approximate tool to primarily gain qualitative information on the behaviour of complex systems — lattice QCD simulations rather provide an 'ab initio' approach relying on the basic Lagrangian as the defining element of the theory, which produce results that are (on the given lattice) exact up to statistical errors.

1.3 Problems and uncertainties

Despite its attractivity as a genuine non-perturbative approach to perform computations in QCD, realistic simulations of lattice QCD are difficult and various theoretical as well as practical issues have to be addressed.

Regarding the latter, one first has to realize that the usual approach of applying numerical simulations to problems in high-energy physics consists in performing them in boxes large enough for the relevant correlation lengths, or the Compton wave lengths $1/(am_i)$ of the lightest particles with masses m_i, to live comfortably inside. Obviously this would be an 'ideal' world, resembling the infinite-volume situation extremely well.[6] In order to eventually reach the point where the corresponding continuum field theory is defined, the lattice spacing a has to be sent to zero such that particle masses in lattice units vanish, $am_i \to 0$, while renormalized physical quantities have to remain finite in this limit. Equivalently, the associated correlation lengths $\xi_i \sim 1/(am_i)$ will diverge and the theory in the continuum is recovered at the critical point of a second-order phase transition that

[5] Accordingly, statistical errors roughly scale with computing time, t_{CPU}, as $1/\sqrt{t_{\mathrm{CPU}}}$.

[6] In current calculations the lattice spacing is typically around $a \approx 0.1\,\mathrm{fm}$ (or even $a \approx 0.05\,\mathrm{fm}$ in the case of the quenched approximation introduced below), while the length of a side of the box is about $L \approx 3.0\,\mathrm{fm}$. Thus, lattice QCD simulations are covering energy scales in an approximate range from 2 GeV down to 100 MeV.

the lattice theory would undergo if it were considered as a statistical mechanical system. In the simulations, this scenario of increasing correlation lengths towards the continuum limit must be accounted for by decreasing the resolution of the lattice accompanied by an extension of the box size to keep the volume in physical units fixed. For lattice QCD and models in high-energy physics in general, the number of lattice points needed in the simulations scales with the fourth power along this limit, where additional factors originating from the scaling behaviour of the employed algorithms are not even included. Therefore, simulations of lattice QCD are numerically very hard and time-consuming, and one actually may forced be to deviate from this ideal world to some extent. The possible effects induced, for instance, by the finiteness of the lattice resolution or volume then have to be assessed carefully.

Apart from these more practical limitations, which are mainly due to the fact that the accessible lattice volumes and resolutions are restricted by the available (finite) computer performance and memory, one also faces various problems and sources of uncertainties on the theoretical side. Some of the characteristic ones are listed here, where I give most room to those that will play a major rôle for the material covered later.

Continuum limit and lattice artifacts

Once one has computed a certain observable according to eq. (1.11) from the data obtained in a numerical simulation, it still depends on the non-zero, finite values of the lattice spacing a one has worked at and needs to be related to the continuum physical world. An essential prerequisite for uncovering this relation and obtaining physically meaningful results from it is the existence of a well-defined and unique *continuum limit*. The approach to this limit is governed by so-called *renormalization group equations* that describe how the parameters of the theory behave under a change of its scale, here the lattice spacing. If the latter is sufficiently small, one expects dimensionless ratios of physical quantities to become nearly independent on a; in this case one speaks of scaling, whereas the corrections are the scaling violations.

To see how the problem of uncertainties due to the non-zero lattice spacing is addressed in practice, let $\mathcal{O}$ denote the dimensionless quantity one wishes to compute on the lattice. Then its expectation value on the lattice and in the continuum differ by corrections of the order of some power of the lattice spacing,

$$\langle \mathcal{O} \rangle^{\mathrm{latt}} = \langle \mathcal{O} \rangle^{\mathrm{cont}} + \mathrm{O}\left(a^n\right) , \tag{1.13}$$

where the term $\mathrm{O}(a^n)$ stands for the lattice artifacts (cutoff effects) and the power n depends on the chosen discretization of the QCD action. The size of the correction term can in some cases be as large as 20%, again depending on the discretization but also on the quantity under study. It appears quite clear now that usually it will be required to

calculate the quantities of interest at different values of the lattice spacing and to obtain the desired continuum results by an *extrapolation* (of the corresponding results at finite lattice spacing as on the l.h.s. in eq. (1.13)) to the continuum limit at $a = 0$. Since it is computationally very expensive or impossible to perform numerical simulations at arbitrarily small lattice spacings, these extrapolations can be brought much better under control, if the chosen discretization avoids small values of n (i.e. particularly $n = 1$) which in turn would correspond to a higher rate of convergence to the continuum limit. The systematic construction of lattice actions and observables by which their leading-order lattice artifacts are reduced or even completely eliminated goes under the name *improvement*.

The basic idea of improvement is easily explained. To begin with, recall that discretization errors, which manifest themselves as a dependence of the physical result on the (unphysical) lattice spacing, always arise whenever equations are discretized and solved numerically. Hence, it will generally be possible to correct these errors by the adoption of a higher-order discretization scheme. In the context of lattice field theories a very similar picture reflects in the important observation that a given lattice action is not unique: one can add any number of operators which formally vanish in the continuum limit $a \to 0$, provided that that they comply with the correct symmetry and locality requirements. This relative freedom may now be exploited to define an higher-order (or *improved*) discretization scheme via supplementing the lattice action by appropriate combinations of irrelevant operators (i.e. operators of dimension larger than four), where their coefficients have to be tuned such that the lattice artifacts are reduced. The concept of *universality* then tells us that the details of the discretization become irrelevant in the continuum limit, i.e. any reasonable lattice formulation will give the same physical continuum theory up to finite renormalizations of, as e.g. in QCD, the gauge coupling and the quark masses.

The theoretical understanding that at finite lattice spacing a the irrelevant operators govern the discretization errors of renormalized dimensionless quantities and as such are the deeper origin of lattice artifacts has led to a systematic and successful approach for their removal order by order in a. It is often referred to as the Symanzik improvement programme [7,8], and its implementation to design improved lattice QCD Lagrangians (as well as improved bilinear quark operators for the extraction of hadron masses and matrix elements) is one of the greatest advances in the field over the past years. As a particular aspect it deserves to be mentioned here that in a quantum field theory like QCD the improvement coefficients entering the higher-order discretization of the continuum action receive radiative corrections, which must be determined. This can be done, for instance, in lattice perturbation theory. To achieve a *complete* removal of the lattice artifacts at a given order, however, calls for a *non-perturbative* determination of these coefficients [9].

For the rest of this paragraph we come back to the lattice QCD action in eq. (1.8). Here one finds that the leading-order cutoff effects implied by S_{gluon} in observables composed

of only gauge degrees of freedom are of order a^2, whereas the O(a) term $-\frac{1}{2}a\nabla_\mu^*\nabla_\mu$ in the Wilson-Dirac operator $D[U]$ of S_{quark} introduces lattice artifacts that already start at order a. As a consequence, one usually encounters large cutoff effects in physical observables involving also fermionic degrees of freedom. In this case the implementation of Symanzik improvement to lowest order amounts to add one dimension–5 counterterm by replacing [10]

$$S_{\mathrm{QCD}}[U,\overline{\psi},\psi] \;\rightarrow\; S_{\mathrm{QCD}}^{\mathrm{I}}[U,\overline{\psi},\psi] = S_{\mathrm{QCD}}[U,\overline{\psi},\psi] + c_{\mathrm{sw}}\frac{ia}{4}\sum_{x,\mu,\nu}\overline{\psi}(x)\sigma_{\mu\nu}F_{\mu\nu}(x)\psi(x)\,. \quad (1.14)$$

Here, c_{sw} is an improvement coefficient (depending on the bare gauge coupling) and $F_{\mu\nu}$ is a lattice transcription of the field strength tensor. In order to remove all O(a) lattice artifacts in hadron masses, c_{sw} has to be fixed by imposing a suitable improvement condition. A sensible condition is offered by requiring that the restoration of the axial Ward identity — which in the first place is violated at O(a) by the Wilson term (see below) — holds up to terms of O(a^2) and has been applied to determine c_{sw} non-perturbatively in the range of bare couplings relevant for the simulation of QCD.

Further improvement coefficients appear in the definitions of the improved versions of local composite operators such as vector and axial vector currents and have to be considered, if their matrix elements need to be computed. For instance, upon O(a) improvement the axial current $A_\mu(x) = \overline{\psi}(x)\gamma_0\gamma_5\psi(x)$, which was already mentioned as one of the possible operators entering the correlation function (1.9) and whose matrix element $\langle\, 0\,|A_0|\,\mathrm{PS}\,\rangle$ defines the pseudoscalar decay constant F_{PS}, takes the form

$$A_\mu(x) \;\rightarrow\; A_\mu^{\mathrm{I}}(x) = (1 + b_{\mathrm{A}}am_{\mathrm{q}})\left\{A_\mu(x) + c_{\mathrm{A}}a\partial_\mu P(x)\right\}, \quad (1.15)$$

where again b_{A} and c_{A} are improvement coefficients (the former compensating for quark mass dependent cutoff effects) and $P(x) = \overline{\psi}(x)\gamma_5\psi(x)$ is the pseudoscalar density. Provided that all these improvement coefficients, and similar ones necessary for other operators, are chosen properly, one can show that lattice artifacts of O(a) are cancelled completely in masses and matrix elements. As has been demonstrated in various lattice QCD investigations of the hadron spectrum and hadronic matrix elements, calculations with O(a) improved Wilson fermions are feasible and have the main advantage that more accurate results in the continuum limit are obtained.

Effects of dynamical light quarks

One of the biggest challenges in lattice QCD simulations is the inclusion of dynamical sea quark pairs that appear as a result of energy fluctuations in the vacuum. Moreover, it will be necessary to push the mass values of light dynamical quark flavours u, d and s towards their physical values, as they (in contrast to the heavier b-, c- and t-quarks) can

have significant effects on many phenomenologically interesting quantities and e.g. also on the running on the coupling constant.

The problem originates from the fact that the quark fields cannot be handled straightforwardly on a computer, because the quarks are fermions and as such to be represented in the functional integral by anti-commuting variables. Instead, to still prepare for a numerical evaluation of the expectation values (1.8), the quark degrees of freedom are integrated out of the functional integral analytically. The expression for $\langle O \rangle$ then becomes:

$$\langle O \rangle = \frac{1}{\mathcal{Z}} \int \mathcal{D}[U]\, \mathcal{O}_{\text{eff}} \left\{ \det D[U] \right\}^{N_{\text{f}}} \mathrm{e}^{-S_{\text{gluon}}[U]} \,. \tag{1.16}$$

With $\mathcal{O}_{\text{eff}}$ we denote the representation of the observable $\mathcal{O}$ in the effective theory, where only gluon fields remain in the path integral measure: $\mathcal{D}[U] = \prod_{x,\mu} \mathrm{d}U(x,\mu)$. N_{f} is the number of quark flavours, whose masses are assumed to be equal in eq. (1.16). This leaves us with the exponentiated pure gauge part of the QCD action alone but at the expense of factors $\{\det D[U]\}$, where the Wilson-Dirac operator D is an enormous (typically $10^7 \times 10^7$) sparse matrix, so that the exact treatment of the highly non-local determinant in numerical simulations is exceedingly costly in terms of computer time — even on today's massively parallel computers —, because the available simulation techniques become very inefficient once the quark polarization effects inherent in this matrix are taken into account. In many applications one therefore has set the determinant of the fermion matrix to unity or, equivalently, $N_{\text{f}} = 0$. This defines the *quenched approximation*. Physically it means that the quantum fluctuations of quarks (i.e. all the fermion loops) are neglected in the determination of $\langle O \rangle$ and only those due to the gluons are included exactly. Although this seems to be a rather drastic assumption about the influence of quantum effects induced by the quarks, the quenched approximation works surprisingly well and is still a sensible, widely employed approximation, not least also as a laboratory to test new ideas and to study more complicated physical problems.

From comparisons of quenched lattice results with experimentally accessible quantities such as the hadron spectrum one finds that in most cases this approximation introduces a systematic error at the level of 10%, but sometimes also up to 20%. Nevertheless, the proper treatment of $N_{\text{f}} > 0$ to overcome these obstacles is certainly one of the major issues in current simulations.

A more indirect consequence of this approximation to ignore the fermion dynamics is an intrinsic quenched scale ambiguity that leads to an internal inconsistency reflecting in some non-negligible dependence of the results on how the parameters of QCD were fixed. Namely, the so-called *calibration* of the lattice spacing in physical units depends on the quantity which is commonly used to set the scale:

$$a^{-1}\,[\text{MeV}] = \frac{\mathcal{Q}\,[\text{MeV}]}{(a\mathcal{Q})}\,, \quad \mathcal{Q} = F_\pi, F_{\text{K}}, m_{\text{N}}, m_\rho, \ldots \,. \tag{1.17}$$

The origin of this ambiguity lies in the different ways in which one expects quark loops to affect different quantities.

The huge computational overhead caused by the evaluation of the quark determinant in eq. (1.16) does even grow considerably, when the quark masses, to which the lattice parameters one simulates at correspond, are diminished towards the small values which we know the physical u- and d-quarks have. The reason is twofold. First, exceptionally small eigenvalues of the Wilson-Dirac operator may drastically deteriorate the performance of the algorithms used to evaluate expressions like (1.16). Second, the inequality $\xi \ll L$ that must hold between the correlation length of a typical hadronic state (serving as a measure of the quark mass) and the spatial extent of the lattice volume places restrictions on the light quark masses that can be simulated: if those are too light, ξ becomes large, and one will suffer from finite-size effects, unless L is enlarged accordingly. The typically tractable spatial extensions of $L \lesssim 3\,\mathrm{fm}$ imply that the pion mass cannot be reached yet.[7] In many applications one therefore has to rely on *chiral extrapolations* in the (light) quark mass variables in order to connect to the physical u- and d-quarks.

Renormalization

In many cases, the task of relating quantities calculated in the lattice-regularized theory to their continuum counterparts does not merely demand to take the continuum limit but also involves renormalization constants that match the lattice to a convenient continuum renormalization scheme.

Frequent examples are QCD matrix elements of vector and axial vector flavour currents, because the electroweak vector bosons mediating semileptonic weak decay of hadrons couple to quarks through linear combinations of these currents so that, treating the electroweak interactions at lowest order, the decay rates are given in terms of those matrix elements. A priori, the bare currents need renormalization; but thanks to the invariance of the formal continuum QCD Lagrangian under $\mathrm{SU}(2)_\mathrm{V}\times\mathrm{SU}(2)_\mathrm{A}$ flavour symmetry transformations in the limit of vanishing quark masses (if only two flavours are considered), there exist non-linear relations between the currents known as *current algebra* which protect them against renormalization. In the lattice-regularized theory, however, $\mathrm{SU}(2)_\mathrm{V}\times\mathrm{SU}(2)_\mathrm{A}$ is not an exact symmetry any more but explicitly broken by terms of order a induced by the Wilson term $-\frac{1}{2}a\nabla^*_\mu\nabla_\mu$ in the lattice fermion action. Consequently, lattice versions of the local vector and axial currents are are not conserved. Instead of this, they are related to the currents in the continuum by *finite (re-)normalizations* Z_V and Z_A, respectively, where finite here means that they do not contain any logarithmic or power-law divergences (in a) and also do not depend on any physical scale. These normalizations may either be

[7] There is also a restriction on the masses of heavy quarks on the lattice, which follows from meeting the inequality $a \ll \xi$. We will turn to this question in Section 3.

approximated in perturbation theory as $Z_{\rm X} = 1 + Z_{\rm X}^{(1)} g_0^2 + \cdots$, X = A, V, or can be fixed on the non-perturbative level by imposing current algebra relations [11–13].

Picking out again the axial current for illustration, its correctly normalized form in the O(a) improved lattice theory (cf. eq. (1.15)) reads

$$\begin{aligned} \left(A_{\rm R}\right)_\mu^a(x) &= Z_{\rm A} \times \left(A_\mu^{\rm I}\right)_\mu^a(x)\,, \\ \left(A^{\rm I}\right)_\mu^a(x) &= (1 + b_{\rm A} a m_{\rm q}) \left\{ A_\mu^a(x) + c_{\rm A}\, \tfrac{1}{2}\, a\, (\partial_\mu + \partial_\mu^*)\, P^a(x) \right\}, \end{aligned} \tag{1.18}$$

where for the axial vector current and the pseudoscalar density,

$$A_\mu^a(x) = \overline{\psi}(x)\gamma_\mu\gamma_5 \tfrac{1}{2}\,\tau^a\psi(x)\,, \quad P^a(x) = \overline{\psi}(x)\gamma_5 \tfrac{1}{2}\,\tau^a\psi(x)\,, \tag{1.19}$$

we write down here their more general expressions for the case of two flavours of quarks with the Pauli matrices τ^a acting on the isospin indices of the quark fields in flavour space. In the quenched approximation, for instance, non-perturbatively determined values for the renormalization constant $Z_{\rm A} = Z_{\rm A}(g_0)$ are available in the relevant range of simulation parameters.

Another, perhaps even more demanding class of renormalization problems are *scale dependent renormalizations*. Most prominently, the fundamental parameters of QCD — the renormalized running coupling and quark masses — belong to this class and will be the subject of the next section.

Chiral symmetry breaking

Finally, we briefly mention a further source of systematic uncertainties, which is caused by the violation of chiral symmetry at finite values of the lattice spacing through the Wilson discretization of the fermion action. From the expression $D^{(0)} = \frac{1}{2}\gamma_\mu(\nabla_\mu^* + \nabla_\mu) - \frac{1}{2} a \nabla_\mu^* \nabla_\mu$ for the massless free Wilson-Dirac operator one easily proves that it enjoys a set of sensible properties to ensure a smooth contact to the continuum theory: locality, a leading-order behaviour in momentum space as in the continuum and (per construction via the second term) no additional poles at non-zero momentum that would correspond to spurious fermion states in the spectrum. A last, particularly important property, however, is obviously not satisfied: the invariance of the lattice action $a^4 \sum_{x,y} \overline{\psi}(x) D(x-y) \psi(y)$ under chiral symmetry transformations, which is equivalent to a vanishing anti-commutator $\gamma_5 D + D\gamma_5 = 0$.

The issue of chiral symmetry breaking has already been formalized a long time ago in the Nielsen-Ninomiya 'no-go' theorem [14]. It implies that (under fairly mild assumptions) exact chiral symmetry can not be realized at non-zero lattice spacing and hence, chiral and continuum limits cannot be separated. Contrary to the situation for the electroweak sector, where this is a really fundamental problem for any lattice formulation, chiral

symmetry breaking in a vector-like theory such as QCD may be regarded more as an 'inconvenience', since its chiral invariance is still recovered when the continuum limit is performed. Although not being of influence on the work summarized here, I want to remark that a lot of progress has been made recently in the formulation of chiral fermions on the lattice and of lattice chiral gauge theories preserving locality and gauge invariance (see e.g. Ref. [15] for a review).

One implication of the violation of chiral invariance with Wilson fermions are severe complications in the renormalization pattern of local composite operators with definite chirality, such as the four-quark operators whose weak hadronic matrix elements describe the famous mixings in the neutral kaon or B-meson systems, because on the lattice they are then allowed to mix with operators of opposite chirality under renormalization. The general relation between the desired physical matrix element in the continuum and the matrix element of the leading bare operator $\mathcal{O}_{\rm bare}$ on the lattice, supplemented by additional matrix elements of operators $\mathcal{O}_k^{\rm mix}$ of different chirality contributing via this mixing, thus looks in the unimproved theory like:

$$\langle\,\mathrm{f}\,|\mathcal{O}_{\rm R}|\,\mathrm{i}\,\rangle^{\rm cont}(\mu) = Z_{\mathcal{O}}(a\mu)\Big\{\langle\,\mathrm{f}\,|\mathcal{O}_{\rm bare}|\,\mathrm{i}\,\rangle^{\rm latt} + \sum_k Z_k\langle\,\mathrm{f}\,|\mathcal{O}_k^{\rm mix}|\,\mathrm{i}\,\rangle^{\rm latt} + \mathrm{O}(a)\Big\}\,. \qquad (1.20)$$

The Z_k are the appropriate normalization factors multiplying the operators allowed by the mixing, which together with their matrix elements and $\langle\,\mathrm{f}\,|\mathcal{O}_{\rm bare}|\,\mathrm{i}\,\rangle$ have to be determined on the lattice to match to the continuum matrix element at the end.[8] Afterwards, an overall scale dependent renormalization $Z_{\mathcal{O}}(a\mu)$ might be necessary as well, then usually obtained in a subsequent computation.

2 Determination of fundamental parameters of QCD

As it was outlined at the beginning of Section 1, QCD is a theory with only a few parameters, namely the gauge coupling and the masses of the quarks, and therefore — at least in principle — also extremely predictive. One of the fundamental questions in this context is how precisely the low-energy world with its rich spectrum of bound states of quarks and gluons, which derives from the strongly coupled sector of QCD, is related to the properties of the theory at high energies, where owing to asymptotic freedom these constituents more and more behave as if they were free particles and the running coupling becomes small enough so that perturbative methods can be expected to furnish reliable predictions for physical observables. Establishing such a link between these two complementary energy regimes of QCD demands in the first place to investigate the *running* of the coupling and the quark masses over the relevant range in the scale at a quantitative level. After having gained detailed knowledge of the scale dependence of

[8] The $\mathrm{O}(a)$ lattice artifacts arise through mixing with higher-dimensional operators.

these basic parameters, it is then of course also of great importance to arrive at *accurate estimates* for the QCD coupling and quark masses at particular values of the energy (or renormalization) scale using experimentally well-determined observables from our low-energy world as physical input, either to confront them with values deduced from high-energy scattering experiments combined with standard perturbation theory or, in the case of quark masses, as contributions to a variety of phenomenological quantities such as decay rates, hadronic matrix elements and lifetimes that often parametrically depend on the masses of the quarks.

At first sight it seems quite unlikely that the two distinct energy regimes of QCD or characteristic observable quantities associated with them such as, for instance, the mass of the pion and the hadronic decay width of the Z-boson can be connected at all. On the other hand, however, at least some relations of this kind have to exist, because all strong interaction physics is described by the same underlying field theory. To uncover these relations on a quantitative level thus provides a stringent test that will only be passed if QCD is the correct theory at *all* energies. Recalling that in QCD any physical quantity is a function of the parameters in the Lagrangian (1.1), we can formulate the problem even more explicitly in terms of dimensionless universal functions G and H, which must exist to relate the masses of the pseudoscalar mesons, e.g. expressed in units of their decay constants, to the basic parameters of QCD, viz.

$$\frac{F_{\rm PS}}{\Lambda} = G\left(\frac{m_{\rm u}}{\Lambda}, \frac{m_{\rm d}}{\Lambda}, \ldots\right), \quad \frac{m_{\rm PS}^2}{F_{\rm PS}^2} = H\left(\frac{m_{\rm u}}{\Lambda}, \frac{m_{\rm d}}{\Lambda}, \ldots\right), \quad {\rm PS} \in \{\pi, {\rm K}, \ldots\}, \tag{2.1}$$

where in this parametrization it is more natural to consider the low-energy scale Λ as a basic parameter of the theory equivalent to the gauge coupling g (see eq. (1.3)). But rather than being an academic exercise, these equations are of physical importance now: taking, say, m_π^2/F_π^2 as experimental input, the second equation can be solved for the quark masses in units of Λ, and via the first one the ratio F_π/Λ then becomes a calculable quantity, which constitutes the desired link between the low-energy world (typically characterized by the physics of pions and kaons) and the Λ–parameter governing the high-energy asymptotics of the running QCD coupling constant and which, moreover, may also be confronted with experiment. Once relations as those in eq. (2.1) will be known, the theory is in fact 'solved' in the aforementioned sense that any physical quantity in QCD can finally be predicted given the values of its fundamental parameters at the scales where this quantity (or the process from which it is inferred) is considered. This in turn amounts to a *renormalization of QCD at all scales*, and it is then clear that the only possible way to achieve this ultimate goal starting from first principles is to employ the non-perturbative tools of lattice QCD.[9]

Unfortunately, the practical realization of a lattice computation of quantities acquiring a scale dependence upon the renormalization process (such as the gauge coupling and

[9]For a more general introduction to the subject and an extended discussion of non-perturbative renormalization in QCD see e.g. Ref. [16].

quark masses we are concerned with here but, for instance, also matrix elements of certain four-quark operators as mentioned in the last paragraph of the previous section) by means of numerical simulations is not straightforward. The new difficulty arising here is a consequence of the *large range of scales* that refer to properties of the theory at energies lying orders of magnitude apart but ideally would have be covered simultaneously in the simulations. To understand which scales typically contribute to the task of reliably matching the low- and high-energy regimes of QCD, we first note that on the one side it is necessary to reach high energy scales $\mu \sim 10\,\mathrm{GeV}$ — and thereby the applicability domain of perturbation theory — in order to be able to connect to other calculational (or renormalization) schemes with controlled perturbative errors. At the same time this high energy scale must be kept remote from the lattice cutoff a^{-1} to avoid large discretization effects and to allow for safe continuum limit extrapolations. On the other side, the linear extent of the system size, L, has to be kept much larger than the confinement scale $\Lambda^{-1} \sim (0.2\,\mathrm{GeV})^{-1}$ to avoid substantial finite-size effects. These conditions are summarized in the hierarchy of scales

$$L \gg 1/(0.2\,\mathrm{GeV}) \gg 1/\mu \sim 1/(10\,\mathrm{GeV}) \gg a\,, \tag{2.2}$$

which in one Monte Carlo simulation would have to be well separated from each other. Given the practical limitations imposed by the available present-day computer resources, however, the number of manageable lattice points per direction, L/a, in current simulations of typically $L/a \leq 32$ with a physical box size of at least $L \approx 2\,\mathrm{fm}$, to sufficiently suppress finite-size effects, implies that the accessible lattice resolutions are roughly bounded from below as $a \gtrsim 0.05\,\mathrm{fm}$ and that one hence can deal reasonably only with energies $\mu \ll a^{-1} \lesssim 4\,\mathrm{GeV}$. From these consideration we conclude that lattice QCD is well suited for the computation of low-energy properties of hadrons, while a clean extraction of short-distance parameters (i.e. those as Λ characterizing the high-energy regime) are problematic because high energies seem to be too demanding for a Monte Carlo calculation and therefore impossible to reach.

An elegant solution to overcome the problem of disparate scales is inspired by the even more general and fascinating discovery that many physical models of interest can be considered in unphysical situations, in which its relevant properties do not change while it is still possible to extract correct physical information from them. In the present context the idea is to study a system that is formulated in a box of finite size in such a way that the size variable becomes the only scale in the system, on which a physical observables can depend upon. The main advantage is that under these conditions numerical simulations are much easier than in the case of a large physical volume.[10]

The crucial step to translate the idea of a finite system size into a viable approach for

[10]Similar studies of systems as a function of the finite size of the box and finite-size scaling arguments have also proved to be fruitful in other fields like, for instance, in investigations of turbulence and critical phenomena.

addressing various scale dependent renormalization problems in QCD non-perturbatively is to *identify* two of the scales in eq. (2.2):

$$\mu = \frac{1}{L}\,. \tag{2.3}$$

Assuming for the moment that a formulation of the theory exists where such an identification is possible in a natural way, one next has to introduce an effective gauge coupling measuring the interaction strength at momenta proportional to $1/L$ so that the finite lattice size becomes a device to probe the interactions rather than being a source of systematic errors. In other words, the finite-size effect itself is taken as the physical observable. As it was already devised in the first implementation of this general idea within an investigation of the σ–model [17], the remaining large scale difference can then be very efficiently bridged via applying a *recursive finite-size scaling technique*. This will be explained in the following two subsections.

2.1 Strategy for scale dependent renormalizations

The general strategy for a non-perturbative computation of scale dependent quantities and associated short-distance parameters is schematically drawn in the diagram below, restricting to the running QCD coupling $\alpha \equiv \alpha_{\rm s}$ as the representative example. By a proper adaption of this strategy it then becomes quite straightforward to also solve scale dependent renormalization problems occurring in other places in lattice QCD. Further examples that will be discussed later are the running quark masses (cf. Section 2.4), as well as the non-perturbative renormalization of the heavy-light axial current in the static approximation, entering the computation of the B-meson decay constant (cf. Section 3.2).

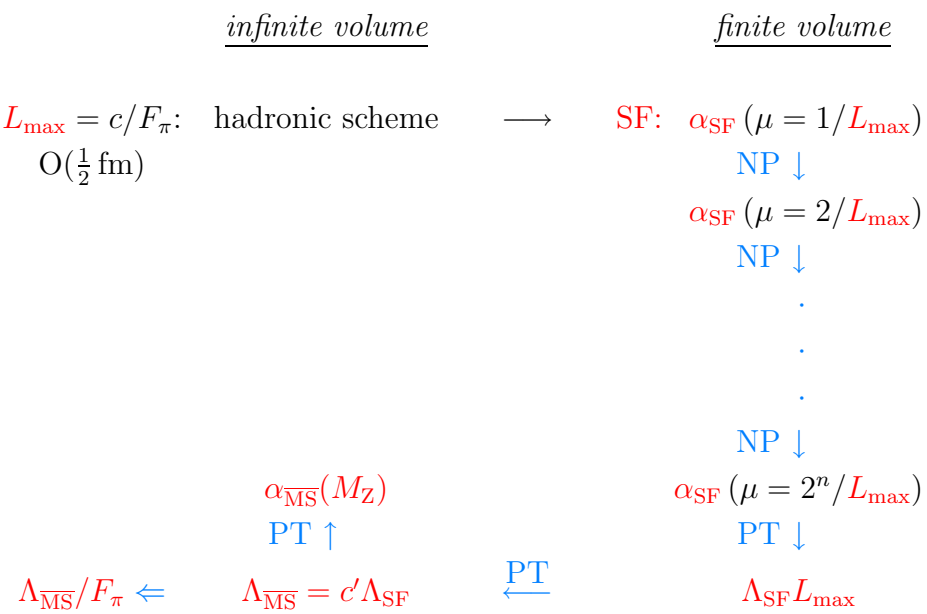

The computation follows the arrows in the diagram, starting at the upper-left corner. The energy is increasing from top to bottom, while the entries in the left and right columns refer to quantities in the infinite- and finite-volume situation, respectively. In the first step, low-energy data are taken as input in order to renormalize QCD via replacing the bare parameters by hadronic observables. A convenient candidate for such a physical observable would be the pion decay constant, F_π, since it is known experimentally as well as calculable on the lattice. This defines a *hadronic scheme*. Next, the chosen hadronic scheme is matched at low energies with a suitable *finite-volume renormalization scheme*, which will be specified soon but for the moment is still arbitrary and just abbreviated with 'SF'. In practice, this amounts to determine the quantity defining the hadronic scheme, here F_π, in physically large (ideally infinite) volume in units of a low-energy scale $\mu = 1/L_{\max}$, where $L_{\max} \sim 0.5\,\mathrm{fm}$ is the external scale fixing the maximal linear extent of the box in which the finite-volume scheme is prepared. The running coupling in this scheme ($\alpha_{\mathrm{SF}} \equiv \bar{g}^2_{\mathrm{SF}}/(4\pi)$) is then evolved non-perturbatively (NP) to higher and higher energies employing a *recursive* procedure through constructing a sequence of matching lattices whose linear extents are shortened by powers of two in each step. Once the computation of the scale evolution of α_{SF} within this scheme has reached the desired high scale $\mu = 2^n/L_{\max}$ where the coupling is small enough and hence perturbation theory (PT) expected to apply, the Λ–parameter $\Lambda_{\mathrm{SF}} L_{\max}$ can be extracted with negligible systematic uncertainty by perturbatively continuing the evolution to infinite energy while obeying the behaviour dictated by the renormalization group,

$$\Lambda = \mu \left(b_0 \bar{g}^2\right)^{-b_1/(2b_0^2)} \mathrm{e}^{-1/(2b_0\bar{g}^2)} \exp\left\{ -\int_0^{\bar{g}} \mathrm{d}g \left[\frac{1}{\beta(g)} + \frac{1}{b_0 g^3} - \frac{b_1}{b_0^2 g} \right] \right\} . \qquad (2.4)$$

Here, $\beta(\bar{g})$ is a *renormalization group function*, defined in eq. (2.5) below, describing the change of the renormalized coupling under a change of the scale. At this point the conversion to a continuum renormalization scheme such as $\overline{\mathrm{MS}}$ and a subsequent evaluation at a common reference scale (say the Z–boson mass $M_{\mathrm{Z}} \sim 90\,\mathrm{GeV}$) are trivial, and upon inserting $\Lambda_{\overline{\mathrm{MS}}}$ or $\alpha_{\overline{\mathrm{MS}}}$ into perturbative expressions, predictions for jet cross sections and other high-energy observables may be obtained.

Given the link between the SF-specific low-energy scale $L_{\max}$ to the hadronic world represented by F_π we started from, together with the contact that now has recursively been made to the high-energy regime in form of the value for $\Lambda_{\overline{\mathrm{MS}}} L_{\max}$, any reference to (and details on) the intermediate, finite-volume renormalization scheme SF has entirely disappeared and the desired connection between the (supposedly unrelated) low- and high-energy domains of QCD is finally established in a controlled manner, reflecting in a numerical result for $\Lambda_{\overline{\mathrm{MS}}}/F_\pi$ at the end. Moreover, a particularly important aspect of the whole strategy to be emphasized is that it is designed in such a way that the lattice calculations of all the steps involved can be readily extrapolated to the *continuum limit*; all arrows in the foregoing diagram thus correspond to universal relations in the

continuum limit.

For the practical success of this general approach, the intermediate scheme and the finite-volume coupling $\bar{g} \equiv \bar{g}_{\mathrm{SF}}$ (and analogously any other quantities whose scale dependence is studied) have to meet a number of criteria:

(i) The finite-volume scheme must be relatable to the infinite-volume theory at low and high energies.

(ii) Perturbation theory in the finite-volume scheme should be manageable and the coupling should have an easy perturbative expansion so that through a perturbative determination of the β–function

$$\beta(\bar{g}) \equiv -L\,\frac{\partial \bar{g}}{\partial L} \overset{\bar{g}\to 0}{\sim} -\bar{g}^3\left\{b_0 + b_1\bar{g}^2 + b_2\bar{g}^4 + \ldots\right\}, \tag{2.5}$$

at least to the indicated order[11], the scale dependence of the finite-volume coupling for large energies becomes known analytically.

(iii) A non-perturbative definition of the renormalized finite-volume coupling has to exist, and in Monte Carlo simulations it should be computable efficiently and with good statistical accuracy (i.e. with small variance).

(iv) The discretization errors of the coupling (and possibly other relevant quantities) must be small to allow for safe extrapolations to the continuum limit. This means to ensure that the lattice calculations are feasible in the regime respecting $1/L = \mu \ll a^{-1}$ while requiring only moderate resolutions of $a/L = \mathrm{O}(0.1)$, i.e. $O(10)$ lattice points per coordinate, to be sufficient.

2.2 The finite-volume renormalization scheme

A specific finite-volume scheme, which fulfils all the just mentioned criteria and allows to find — amongst several other observables that will turn out to be useful later — a coupling with the appropriate properties, is the *QCD Schrödinger Functional (SF)* [18]. It therefore proves to be particularly suited to serve as the intermediate renormalization scheme we are looking for. To introduce the Schrödinger functional, one imposes periodic boundary conditions for the quark and gluon fields as functions of the three space directions, whereas at time 0 and T these fields are required to satisfy Dirichlet boundary conditions. In the practical applications to follow, the latter are chosen to be homogeneous except for the spatial components of the gluon gauge potentials, A_k. With this choice of boundary conditions the space-time manifold assumes the topology of a four-dimensional cylinder as shown in the left part of Figure 2.1.

[11] The first two leading coefficients in this expansion are independent of the chosen renormalization

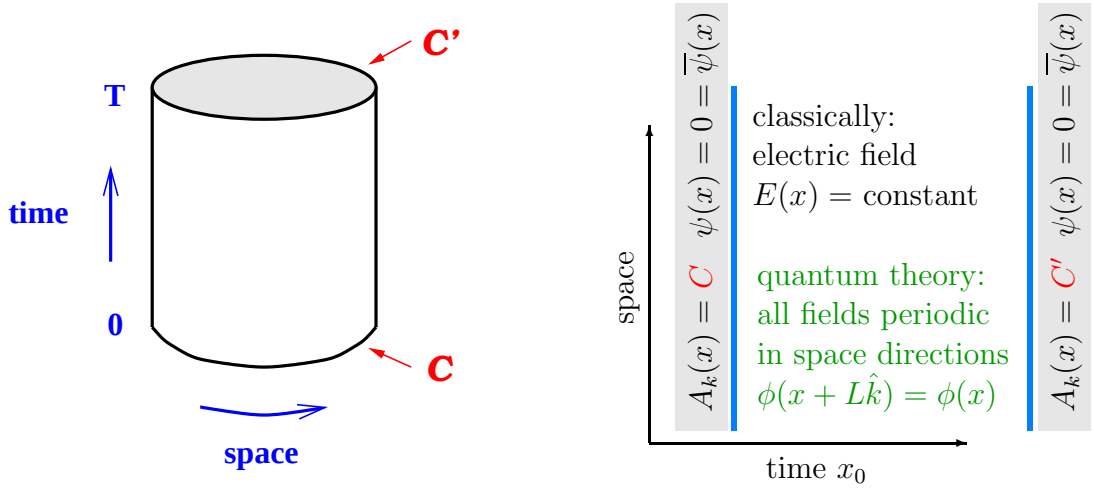

Figure 2.1: *Left*: Illustration of the Schrödinger functional. The specific choice of boundary conditions gives the space-time world the shape of a cylinder. *Right*: Sketch of the SF setup used for the definition of the finite-size coupling $\bar{g}(L)$ in QCD. The Dirichlet boundary conditions can be imagined as to correspond to walls at times $x_0 = 0, T$ that act similarly to the plates of an electric condensor. This means that classically they lead to a homogeneous (i.e. $\mathbf{x}$ and x_0 independent) colour-electric field inside the cylinder. The QCD interaction strength can then be defined in terms of the field at the condensor plates as $\bar{g}^2(L) = E_{\text{classical}}/\langle E\rangle$, where E is a special colour component of the electric field.

More specifically, the spatial components of the gauge field at the boundaries are set to some prescribed values for the classical (chromoelectric) gauge potentials C and C',

$$U(x,k)\,|_{x_0=0} = \mathrm{e}^{\,aC_k(\boldsymbol{x})}\,, \quad U(x,k)\,|_{x_0=T} = \mathrm{e}^{\,aC'_k(\boldsymbol{x})}\,, \tag{2.6}$$

where the matrices C and C' are taken to be constant diagonal, while the dynamical degrees of freedom of the gauge field are the link variables $U(x,\mu)$ residing in the interior of the lattice. Similarly, the quark and antiquark fields are fixed on the boundary surfaces according to

$$\begin{aligned} \tfrac{1}{2}\,(1+\gamma_0)\,\psi(x)\,\big|_{x_0=0} &= \rho(\mathbf{x})\,, & \tfrac{1}{2}\,(1-\gamma_0)\,\psi(x)\,\big|_{x_0=T} &= \rho'(\mathbf{x})\,, \\ \overline{\psi}(x)\,\tfrac{1}{2}\,(1-\gamma_0)\,\big|_{x_0=0} &= \bar{\rho}(\mathbf{x})\,, & \overline{\psi}(x)\,\tfrac{1}{2}\,(1+\gamma_0)\,\big|_{x_0=T} &= \bar{\rho}'(\mathbf{x}) \end{aligned} \tag{2.7}$$

with ρ and ρ' (and also $\bar{\rho}, \bar{\rho}'$) being some externally given anti-commuting fields. The field components $\psi(x)$ and $\overline{\psi}(x)$ at times $0 < x_0 < T$ remain unconstrained and represent the dynamical part of the quark and antiquark fields.

The SF is now defined as the Euclidean QCD partition function with these boundary conditions:

$$\mathcal{Z}[C', \bar{\rho}', \rho'; C, \bar{\rho}, \rho] = \int_{T\times L^3} \mathcal{D}[U, \overline{\psi}, \psi]\, \mathrm{e}^{\,-S[U,\overline{\psi},\psi]}\,. \tag{2.8}$$

scheme anyway. Its universal values for QCD with N_f quark flavours are: $b_0 = \left(11 - \frac{2}{3}N_\mathrm{f}\right)/(4\pi)^2$ and $b_1 = \left(102 - \frac{38}{3}N_\mathrm{f}\right)/(4\pi)^4$.

It is a gauge invariant functional of the boundary fields and, pertaining to its quantum mechanical interpretation in the transfer matrix formalism, equals the transition amplitude for going from the field configuration $\{C, \bar{\rho}, \rho\}$ at time $x_0 = 0$ to the configuration $\{C', \bar{\rho}', \rho'\}$ at time $x_0 = T$. The lattice action S in finite volume is essentially given by the expressions that were written down for $S_{\rm QCD}$ in eq. (1.8) of Section 1.1 for the infinite-volume theory. E.g. in the case of O(a) improvement, the only modification is that in the counterterm proportional to $c_{\rm sw}$ of eq. (1.14) the sum is restricted to all points x in the interior of the lattice.[12] Expectation values of products of local fields in this framework are obtained in the usual way through the functional integral, whereby the integration is performed at fixed boundary values; thus, the only dependence on these values arises from the action.

To prepare the ground for the definition of a renormalized coupling within the SF in the next paragraph, I consider the theory without quark fields for a moment. Then it can be shown that at small couplings g_0 the functional integral is dominated by gauge fields close to some (up to gauge transformations unique) minimal action configuration $U(x, \mu) = \mathrm{e}^{aB_\mu(x)}$ with the specified boundary values [18]. As a consequence, the SF admits a regular perturbative expansion by expanding about this minimum B at weak coupling (which is sometimes called the background field). The associated perturbative series is conveniently expressed in terms of the effective action (or free energy) Γ as

$$\Gamma[B] \equiv -\ln \mathcal{Z}[C', C] = \frac{1}{g_0^2}\,\Gamma_0[B] + \Gamma_1[B] + g_0^2\,\Gamma_2[B] \,+\, \cdots\,, \quad \Gamma_0[B] \equiv g_0^2\,S[B]\,, \qquad (2.9)$$

and is also the starting point of any perturbative study such as, for instance, that of the renormalization properties of the functional $\mathcal{Z}$. Concerning the renormalizability of the SF, explicit perturbative calculations as well as numerical, non-perturbative Monte Carlo simulations have yielded strong support for the validity of Symanzik's conjecture [19] that including the usual counterterms plus a few additional boundary counterterms in the action is sufficient to renormalize the QCD Schrödinger functional in four dimensions.

Definition of the effective coupling

As was already noticed before, in the Schrödinger functional formulation of QCD the effect of the finite volume itself can serve as a measure of the interaction strength of the theory and may hence be exploited to arrive at a suitable definition of an effective coupling. A more illustrative introduction of this coupling, which should help to motivate its exact definition below, is reproduced in the right part of Figure 2.1. (The subscript 'SF' on the SF coupling is dropped from now on.)

[12] In addition to this well-known clover counterterm in the lattice bulk, there are two further, SF-specific boundary improvement coefficients $c_{\rm t}$ and $\widetilde{c}_{\rm t}$, which multiply certain O(a) time-boundary counterterms in the pure gauge action and analogous time-boundary O(a) improvement terms involving quark fields, respectively.

To define a renormalized coupling in the SF scheme, one first distinguishes a certain choice of boundary conditions by assigning two particular sets of angles, which themselves are parameterized in dependence of some parameter η, to the diagonals of the matrices representing the boundary gauge potentials C and C' in eq. (2.6). It is then obvious that the response of the system to an infinitesimal variation of this specific one-parameter family of prescribed constant abelian boundary fields measures the interaction strength through $1/\bar{g}^2 \propto \delta(\text{free energy})/\delta(\text{boundary conditions})$, and if we take into account the perturbative expansion of the effective action, eq. (2.9), proper normalization leads us to the definition of the renormalized coupling [18]

$$\bar{g}^2(L) \equiv \left\{ \frac{\partial \Gamma_0}{\partial \eta} \Big/ \frac{\partial \Gamma}{\partial \eta} \right\} \Bigg|_{\eta=0\,,\,T=L} . \tag{2.10}$$

By the very construction of the SF, the linear extent L of the cylinder is now the only external scale in this formula as it should be in a finite-volume renormalization scheme.[13]

Moreover, since $\partial\Gamma/\partial\eta = \langle \partial S/\partial\eta \rangle$ is an expectation value of some combination of the gauge field variables close to the boundaries, the numerical calculation of $\bar{g}^2$ in a Monte Carlo simulation of the path integral is straightforward, and it thereby also complies with the demand raised under (iii) at the end of Section 2.1. For small L (i.e. at weak coupling), where the path integral is dominated by field configurations corresponding to small fluctuations about the configuration that minimizes the classical action, the commonly used simulation algorithms remain effective thanks to the boundary conditions excluding possible gluon zero modes for very small L in physical units. By contrast, for $L \lesssim 1\,\text{fm}$ the field configurations may deviate significantly from the classical solution. A smooth connection between these two regimes — perturbative for small L and increasingly non-perturbative for growing L — is achieved by adopting a recursive simulation strategy.

Returning finally to the functional $\mathcal{Z}$ containing the quarks again, eq. (2.8), we remark that in this case no additional renormalization of the SF is necessary for vanishing boundary values of the fermionic boundary fields $\rho, \ldots, \bar{\rho}'$, apart from the renormalization of the coupling and the quark mass [20, 21]. So, after imposing homogeneous boundary conditions for the fermion fields, the foregoing definition of the renormalized SF coupling carries over to this situation without changes. A further important aspect of the SF setup, which offers practical as well as theoretical advantages and therefore deserves to be pointed out in this context, is the following. Since the boundary conditions (2.7) induce a gap into the spectrum of the (lattice) Dirac operator, the lattice SF may be simulated for vanishing physical quark masses, m. It is then convenient to supplement the definition of the renormalized coupling (2.10) by the requirement $m = 0$. This entails that our chosen intermediate scheme SF also becomes a *mass independent renormalization scheme* with

[13] One has to note here that the precise choice of the boundary values is largely arbitrary and mainly based on practical considerations. The final physical results will not depend on any of these details.

simplified renormalization group equations. Particularly the β–function, introduced in eq. (2.5) above, stays independent of the quark mass in such a scheme.

Step scaling functions

The SF coupling $\bar{g}^2(L)$ genuinely depends only on one renormalization scale, $L = 1/\mu$. Therefore, a determination of its energy dependence amounts to quantify the behaviour of the coupling under changes of the size of the finite-volume system. The quantity devised for this purpose is the *step scaling function (SSF)* $\sigma(u)$ defined through

$$\sigma(u) \equiv \bar{g}^2(2L)\,\big|_{\bar{g}^2(L)=u}\ . \tag{2.11}$$

It describes the change in the coupling when the physical box size is doubled. From the renormalization group equation (2.5) of the continuum theory, which governs the scale evolution of the coupling by determining it at any scale if it is known at some point, we infer that such a well-defined function σ must exist and is implicitly given as the solution of the recursion equation

$$\bar{g}^2(2L) = \sigma\left(\bar{g}^2(L)\right) \tag{2.12}$$

equivalent to (2.11). The SSF may thus be regarded as an integrated form of the β–function for finite length scale transformations with rescaling factor 2, and its computation will enable us to map out the scale evolution of $\bar{g}^2$.

The central observation is now that $\sigma(u)$ can be calculated on the lattice by numerical simulations. On a lattice with finite spacing a, however, the SSF will in the first place still be a quantity with an additional dependence on the resolution a/L, denoted as $\Sigma(u, a/L)$. The continuum limit $\sigma(u) = \Sigma(u, 0)$ is then obtained by performing the calculations for one rescaling step at several different resolutions and extrapolation $a/L \to 0$. By iterating this stepwise procedure, in which the physical size L is increased successively by factors of s (where mostly $s = 2$ in practice), one eventually gains full control over the exact SSF $\sigma(u)$ and can trace the non-perturbative evolution of the coupling in discrete steps $\bar{g}^2(L) \to \bar{g}^2(sL) \to \bar{g}^2(s^2L) \to \cdots$ over a wide range of momenta. What one actually constructs in this way is a *non-perturbative renormalization group.*

The sequential computation of the lattice SSF $\Sigma(u, a/L)$, which upon extrapolating away its inherent discretization errors implements the recursion (2.12) to be obeyed by the continuum SSF $\sigma(u)$, is sketched in Figure 2.3. In fact, because the relevant energy scale for the running, $\mu = 1/L$, is cleanly separated from the lattice spacing a, it can be calculated recursively over a wide range of momenta μ, whilst keeping the number of lattice points at a manageable level (i.e. $L/a = \mathrm{O}(10)$). Sample numerical results for one horizontal step of Figure 2.3, repeated several times with different resolutions, are displayed in Figure 2.2 for the case of the quenched approximation to QCD (i.e. in the theory without fermions). As a consequence of the careful choice of the coupling itself

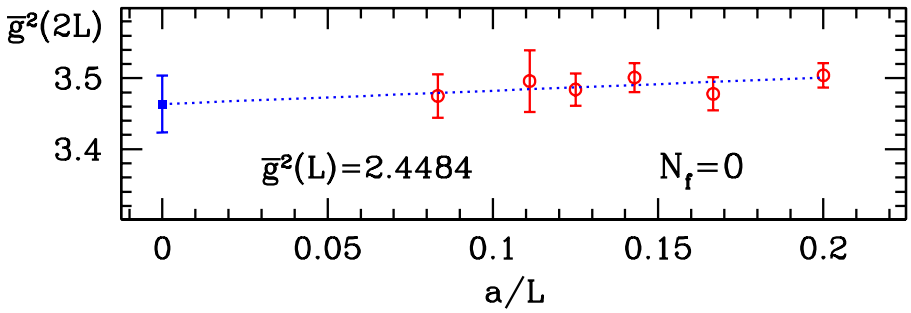

Figure 2.2: The extrapolation of the SSF $\bar{g}^2(2L) = \sigma\left(\bar{g}^2(L)\right)$ from the data at finite lattice spacing (red circles) to the continuum limit (blue square) at some representative value of the renormalized SF coupling, which corresponds to a physical box size in the low-energy domain. This example is taken from a computation in quenched QCD (i.e. $N_\mathrm{f} = 0$ or pure SU(3) gauge theory), where a high numerical precision as well as very fine lattice resolution could be achieved [22, 23].

as well as of other details of the discretization, the dependence of the SSF on the lattice resolution turns out to be extremely weak so that the extrapolations $a/L \to 0$ to arrive at the desired continuum limits are very safe.

As the outcome of the numerical simulation procedure outlined so far, the continuum SSF $\sigma(u)$ becomes non-perturbatively known (up to statistical errors) for a sequence of discrete coupling values $u \in \{u_0 < u_1 < u_2 < \cdots\}$, corresponding to physical box sizes of the intermediate SF scheme of

$$L_0 = L = 2^0 L \to L_1 = 2^1 L \to L_2 = 2^2 L \to \cdots \to L_n = 2^n L \quad (\text{typically } n \sim 8) \tag{2.13}$$

that span several orders of magnitude in $\mu = 1/L$. Guided by the observation that the SSF has a well-behaved perturbative expansion at weak coupling (small L), it is now easily possible to parameterize the numerical, non-perturbative results on σ by a continuous function in form of some low-order polynomial with only the leading coefficient(s) constrained to perturbation theory. This eventually solves the recursion we originally started from in eq. (2.12).

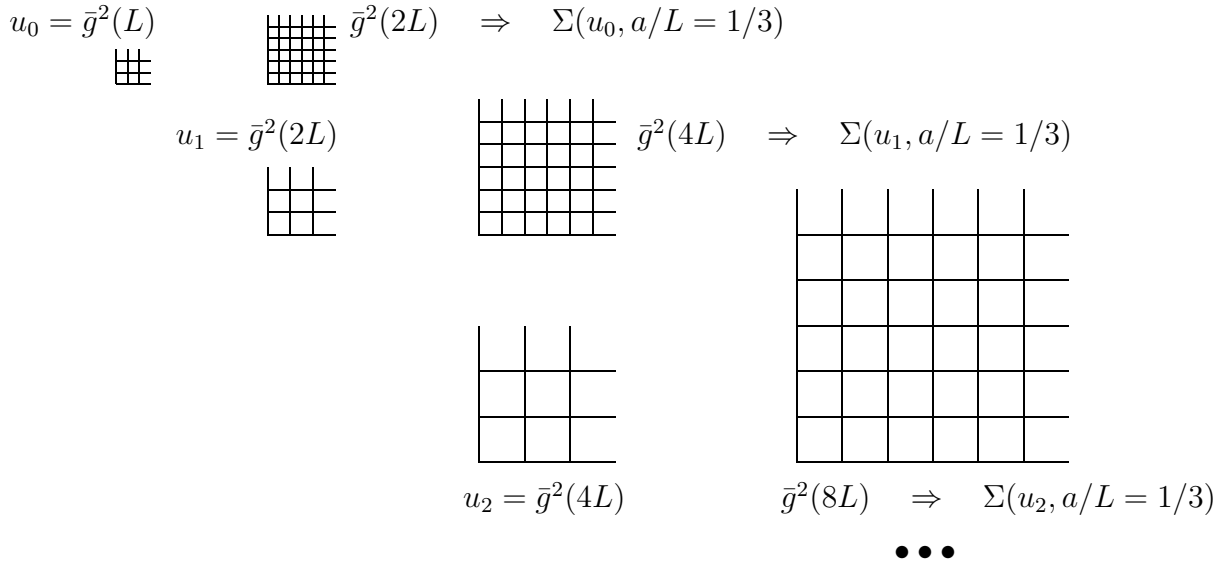

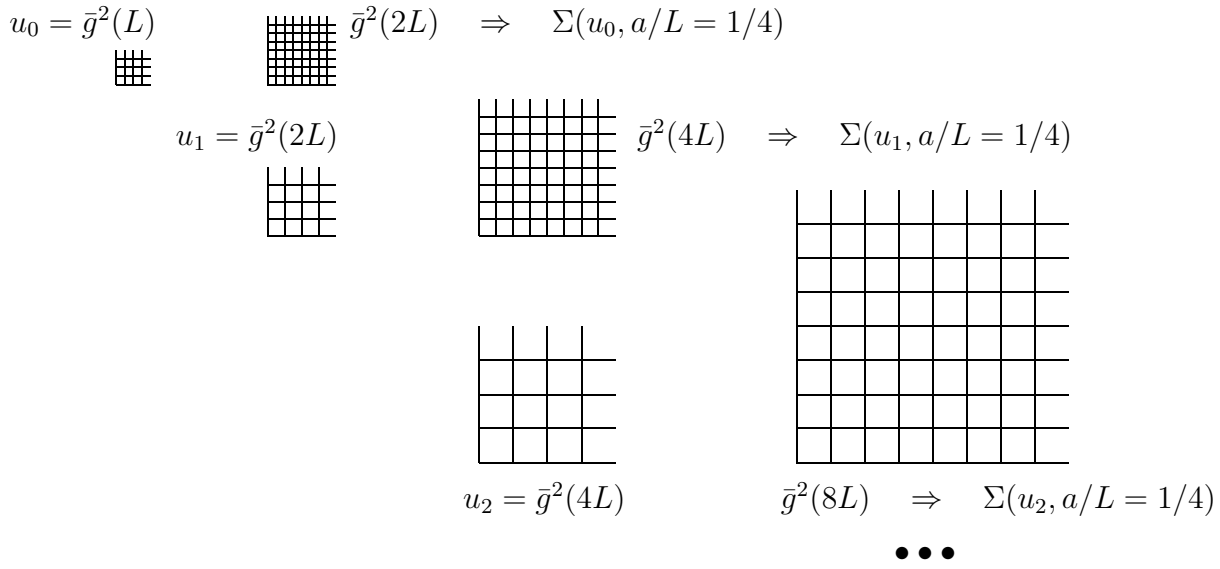

Figure 2.3: Illustration of the recursive finite-size scaling method, by which the evolution of the SF coupling $\bar{g}$ with the energy scale $\mu = 1/L$ can be computed in several steps, changing μ by factors of two in each of them. To implement the recursion (2.12) by a series of lattice simulations, one always alternates between keeping a fixed and increasing $L \to 2L$ (horizontal direction in the figure) and keeping L fixed and decreasing a (vertical direction in the figure). In this way, no large scale ratios appear and discretization errors are small for $L/a \gg 1$. More explicitly, the individual steps are the following: 1. Choose a lattice with L/a points in each direction. (The artificial choice $L/a = 3$ above is just to avoid the figure getting oversized. A convenient lattice size to start with in practice is $L/a = 4 - 6$ at least.) 2. Tune the bare gauge coupling g_0 of the lattice action so that $\bar{g}^2(L) = u_0$. (This takes care of renormalization.) 3. At the same value of g_0, simulate a lattice with twice the linear extent and calculate $u_1 = \bar{g}^2(2L)$ on it to obtain the lattice SSF $\Sigma(u_0, a/L)$, which equals $\sigma(u_0)$ up to cutoff effects. (This determines the evolution of the renormalized coupling.) 4. Repeat steps 1.-3. for several, successively larger values of L/a (i.e. finer resolutions) and extrapolate $a/L \to 0$ to get rid of the lattice effects. To continue the recursion, the steps 1.-4. have to be iterated n times, where the respective bare couplings have to be adjusted such that $\bar{g}^2(2^n L) = u_n$ with u_n being known from the previous iteration step.

Renormalized trajectories in lattice parameter space. A crucial byproduct of the finite-size scaling analysis of the running coupling in the intermediate SF scheme is that it provides a one-to-one correspondence between the bare parameters of the theory, which occur in the lattice action and as such are the input parameters of the Monte Carlo simulations, and a series of values of the renormalized couplings $\bar{g}^2$. In the course of the calculation, these bare parameters are moreover adjusted to enforce (the renormalization condition of) fixed SF coupling at any of the physical box sizes in (2.13) for various lattice resolutions in order to take the SSF's continuum limit.

The resulting sets of lattice parameters (e.g., in case of pure SU(3) gauge theory, the pairs $(L/a, \beta)$ with $g_0^2 = 6/\beta$ being the bare coupling) thereupon define lines of constant physics in the bare parameter space, along which the approach to the continuum limit of other arbitrary quantities depending on the renormalization scale may now be followed as well. Because the construction of Figure 2.3 then automatically ensures that they pick up the correct, built-in dependence on the renormalized coupling $u = \bar{g}^2(L)$ in the finite-volume renormalization scheme, the evolution of those quantities in the direction of varying L in physical units can be explored in parallel to that of the coupling itself.

Generic scale dependent renormalization problems. To make this somewhat more explicit, let us focus on scale dependent renormalizations in QCD that are multiplicative, similar to the overall renormalization in eq. (1.20) at the end of Section 1.3. Furthermore we suppose that the renormalized operator in question, whose definition is assumed to be readily transferable to our intermediate, finite-volume renormalization scheme, decomposes into

$$\mathcal{O}_{\rm inter}(\mu) = Z_{\rm inter}(g_0, a\mu) \times \mathcal{O}_{\rm bare}(g_0) \tag{2.14}$$

with $\mathcal{O}_{\rm bare}$ the bare operator and a renormalization factor $Z_{\rm inter}$ depending on the bare gauge coupling and the scale in lattice units, $a\mu$. This factor is typically fixed by posing a suitable normalization condition in the intermediate scheme. In the case of the Schrödinger functional scheme one may e.g. require

$$\langle\, \beta \,|\mathcal{O}_{\rm inter}(\mu)|\, \alpha \,\rangle = \langle\, \beta \,|\mathcal{O}_{\rm bare}|\, \alpha \,\rangle^{\rm tree-level} \tag{2.15}$$

to hold, where $|\alpha\rangle, |\beta\rangle$ are convenient states that are given in terms of some boundary states propagated in Euclidean time. As $\mathcal{O}_{\rm bare}$ one might imagine local composite operators such as quark bilinears $\overline{\psi}(x)\Gamma\psi(x)$ with some Dirac structure Γ, hadronic matrix elements of which are of phenomenological relevance in infinite-volume QCD; an explicit example will be touched in the context of the determination of $F_{\rm B_s}$ (Section 3.2 and Publication H). If a massless renormalization scheme such as the SF in employed as the intermediate scheme, the renormalization constant $Z_{\rm inter}$ can be evaluated at zero quark mass.

To non-perturbatively compute the change of $\mathcal{O}_{\rm inter}$ under finite changes of the renormalization scale, we again identify $\mu = 1/L$ and define associated (continuum and lattice) step scaling functions according to

$$\sigma_{\mathcal{O}}(u) = \lim_{a/L\to 0} \Sigma_{\mathcal{O}}(u, a/L)\,, \quad \Sigma_{\mathcal{O}}(u, a/L) = \left.\frac{Z_{\mathcal{O}}(g_0, 2L/a)}{Z_{\mathcal{O}}(g_0, L/a)}\right|_{\bar{g}^2(L)=u}\,, \tag{2.16}$$

using here the subscript '$\mathcal{O}$' as shorthand notation to indicate the very origin (2.14) of the scale dependence carried by the suitably defined renormalization factor $Z_{\mathcal{O}} \equiv Z_{\rm inter}$ in the intermediate scheme. The argument $u \equiv \bar{g}^2(L)$ of $\sigma_{\mathcal{O}}$ is taken to be exactly the renormalized SF coupling studied above. Eq. (2.16) gives rise to a recursion

$$Z_{\mathcal{O}}(2L) = \sigma_{\mathcal{O}}(u) Z_{\mathcal{O}}(L)\,, \quad u = \bar{g}^2(L)\,, \tag{2.17}$$

that now has to accompany the corresponding recursion (2.12) determining the evolution of the renormalized coupling $\bar{g}^2$. Then, by evaluating the finite-size renormalization constant $Z_{\mathcal{O}}(L)$ in numerical simulations at the same bare lattice parameters as done for the running of the SF coupling, one automatically moves along a renormalized trajectory and — having solved the recursion (2.17) analogously as for the coupling — is finally able to also trace the scale evolution of the operator renormalized in the intermediate scheme, $\mathcal{O}_{\rm inter}$, from low to high energies.

Extraction of the renormalization group invariants

In view of the strategy explained in Section 2.1 we now turn the logics around and consider the largest value u_n of the renormalized coupling $\bar{g}^2$, i.e. the one at the largest $L_n = 2^n L \equiv L_{\rm max}$ among the physical sizes (2.13) of the finite-volume system that were covered in the non-perturbative calculation, as initial datum in the recursion (2.12) and scale $u = \bar{g}^2$ by iterated application of the inverse of the previously obtained step scaling function,

$$u_n \equiv u_{\rm max}\,, \quad u_{k-1} = \sigma^{-1}(u_k)\,, \quad k = n, n-1, \ldots, 1\,, \tag{2.18}$$

to higher and higher energies (increasingly small physical box sizes). Once the smallest value of L in the covered range of data, L_0 in our notation and which is assumed to be selected such that the accompanying coupling u_0 is accurately known as well as sufficiently small (typically $\bar{g}^2 \sim 1$ or $\alpha = \bar{g}^2/(4\pi) \sim 0.08$), is met, perturbation theory is expected to safely apply in the corresponding domain of very high energies. Particularly the perturbative expansion for the β–function, eq. (2.5), may thus be trusted so that the Λ–parameter, which in a given renormalization scheme is just the integration constant in the solution of the renormalization group equation $\mu(\partial\bar{g}/\partial\mu) = \beta(\bar{g})$, can be computed through the exact formula (2.4) via integrating the renormalization group function β up to infinite energies. In our intermediate SF renormalization scheme we only have to set

$\mu = 1/L$ and to evaluate the expression starting the integration at $\bar{g}^2(L)$

$$\Lambda = \frac{1}{L}\left[b_0\bar{g}^2(L)\right]^{-b_1/(2b_0^2)} \mathrm{e}^{-1/(2b_0\bar{g}^2(L))} \exp\left\{-\int_0^{\bar{g}(L)} \mathrm{d}g \left[\frac{1}{\beta(g)} + \frac{1}{b_0 g^3} - \frac{b_1}{b_0^2 g}\right]\right\} \quad (2.19)$$

with $L = L_0 = 2^{-n}L_{\max}$ lying deep enough in the perturbative regime as anticipated above. Owing to the perturbative series for $\beta(\bar{g})$ in the SF renormalization scheme being worked out to three loops and the scale evolution of the coupling being accurately reproduced by perturbation theory at high energies (cf. Figure 2.4), the uncertainty stemming from the perturbative approximation used in this integration turns out to be negligible compared to the statistical and other systematic errors.

At last, our strategy demands to convert the Λ–parameter in the SF scheme to a convenient continuum renormalization scheme, preferably the $\overline{\mathrm{MS}}$ scheme. Utilizing the known relation between the finite-volume and the $\overline{\mathrm{MS}}$ coupling to one-loop order of perturbation theory, the (exact) conversion factor $\Lambda_{\overline{\mathrm{MS}}}/\Lambda$ is now easily calculated and leads to a numerical value for $\Lambda_{\overline{\mathrm{MS}}}L_{\max}$. To end up with a final, solid result for the QCD Λ–parameter, one still needs to relate the SF scale $L_{\max}$ to some low-energy reference scale with an unambiguous physical meaning. Only then the reference to the intermediate finite-volume scheme has disappeared, and the expression for the Λ–parameter in the $\overline{\mathrm{MS}}$ scheme in terms of the this low-energy scale provides the solution of the non-perturbative renormalization problem for the running coupling.

Also the extraction of the renormalization group invariant Λ belonging to the running QCD coupling generalizes to arbitrary renormalized operators carrying a multiplicative renormalization scale dependence. Returning to the operator $\mathcal{O}_{\mathrm{inter}}$ in the intermediate SF scheme, which was introduced through eq. (2.14) at the end of the foregoing paragraph, the continuum limit $a \to 0$ of the matrix element

$$\Omega_{\mathrm{inter}}(\mu) \equiv \langle\, \mathrm{f}\,|\mathcal{O}_{\mathrm{inter}}(\mu)|\,\mathrm{i}\,\rangle = Z_{\mathrm{inter}}(g_0, a\mu)\,\langle\, \mathrm{f}\,|\mathcal{O}_{\mathrm{bare}}(g_0)|\,\mathrm{i}\,\rangle \quad (2.20)$$

is independent of the regularization. In a massless renormalization scheme as the SF, the entering renormalization constant $Z_{\mathcal{O}} = Z_{\mathrm{inter}}$ is evaluated (via eq. (2.15)) at zero quark masses. Associated with any such renormalized matrix element is a renormalization group function $\gamma^{\mathcal{O}}(\bar{g})$, the so-called *anomalous dimension*; in the case of the intermediate scheme at hand its definition reads

$$\begin{aligned} \mu\frac{\partial\,\Omega_{\mathrm{inter}}(\mu)}{\partial\mu} &= \gamma^{\mathcal{O}}\left(\bar{g}(\mu)\right)\,\Omega_{\mathrm{inter}}(\mu)\,, \\ \gamma^{\mathcal{O}}(\bar{g}) &\overset{\bar{g}\to 0}{\sim} -\bar{g}^2\left\{\gamma_0^{\mathcal{O}} + \gamma_1^{\mathcal{O}}\bar{g}^2 + \gamma_2^{\mathcal{O}}\bar{g}^4 + \ldots\right\}\,, \end{aligned} \quad (2.21)$$

where the perturbative expansion comprises a scheme independent (universal) leading-order coefficient $\gamma_0^{\mathcal{O}}$ and further ones $\gamma_1^{\mathcal{O}}, \gamma_2^{\mathcal{O}}, \ldots$ depending on the chosen renormalization scheme. In principle, these can be computed using dimensional or a lattice regularization.

For phenomenological applications, however, we are interested in the matrix elements at some convenient energy scale in a common renormalization scheme, which we may take again to be the $\overline{\rm MS}$ scheme: $\Omega_{\overline{\rm MS}}(\mu_{\rm ref})$ where usually $\mu_{\rm ref} = 2\,{\rm GeV}$ or beyond.

To reliably connect to such a scheme, it is most attractive to perform this step by a *matching at infinite energies through the renormalization group invariant operator.* In close analogy to eq. (2.19), the *renormalization group invariant (RGI)* matrix element, associated with $\mathcal{O}_{\rm inter}$ and its anomalous dimension $\gamma^{\mathcal{O}}$, is given by:

$$\Omega_{\rm RGI} \;=\; \Omega_{\rm inter}(\mu)\left[2b_0\bar{g}^2(\mu)\right]^{-\gamma_0^{\mathcal{O}}/(2b_0)}\exp\left\{-\int_0^{\bar{g}(\mu)}{\rm d}g\left[\frac{\gamma^{\mathcal{O}}(g)}{\beta(g)}-\frac{\gamma_0^{\mathcal{O}}}{b_0 g}\right]\right\}. \tag{2.22}$$

These RGI matrix elements are scheme and scale independent by definition and hence should be — from the theoretical point of view — looked upon as the fundamental quantities of QCD whose precise determination from the lattice theory similarly as surveyed for the Λ–parameter is of primary importance. In order to connect $\Omega_{\rm RGI}$ to $\Omega_{\overline{\rm MS}}(\mu_{\rm ref})$, one has to adopt the analogues of eqs. (2.21) and (2.22) for the $\overline{\rm MS}$ scheme[14] so that all the individual steps, which turn a bare lattice matrix element $\Omega_{\rm bare}$ of $\mathcal{O}_{\rm bare}$ into a renormalized one in the $\overline{\rm MS}$ scheme and thereby solve the underlying generic multiplicative renormalization problem as discussed here, consist in the decomposition

$$\Omega_{\overline{\rm MS}}(\mu_{\rm ref}) = \frac{\Omega_{\overline{\rm MS}}(\mu_{\rm ref})}{\Omega_{\rm RGI}}\times\frac{\Omega_{\rm RGI}}{\Omega_{\rm inter}(\mu)}\times Z_{\rm inter}(g_0,a\mu)\times\Omega_{\rm bare}(g_0)\,. \tag{2.23}$$

While the first two factors are universal in the sense of being independent of the lattice regularization (e.g. the choice of action), the renormalization constant $Z_{\rm inter}(g_0,a\mu)$ refers to a specific low-energy scale in the intermediate scheme (i.e. $\mu\sim{\rm O}(1/L_{\rm max})$ in case of the SF) and thus would have to be recomputed once the discretization of the theory or the scheme itself is altered.

2.3 The running strong coupling constant

So far, computations of the running coupling $\alpha(\mu)$ along the lines of the preceding subsections have been performed in the quenched approximation to QCD (pure gauge theory) [22–24] and in QCD with two flavours of quarks. In the case of two dynamical quarks the numerical calculations involved become much more expensive in terms of computer time compared to the former, owing to the quark polarization effects rendering the available simulation techniques increasingly inefficient. First promising results of a study in this already more realistic approximation to the full theory (by which one would ideally understand QCD with all flavours of quarks properly included) are reported in Ref. [25].

[14] Since this conversion to the matrix element in the $\overline{\rm MS}$ scheme at some finite renormalization scale is mostly done by perturbation theory, its reliability needs generally to be investigated.

In the meantime, the simulations have been completed and the analysis of all available data is finished. Its final results have been published recently in Publication A.

The status of the results is summarized in Figure 2.4, both for the case of quenched QCD (left) and including two flavours of dynamical quarks (right). With the step scaling function at hand, the recursive application of eq. (2.12) yields the series of couplings that is shown as the points in the figure and likewise represents the range covered in the non-perturbative calculation of the SSF; thus, no approximation is involved. For comparison, the diagrams also contain the perturbative evolution starting at the smallest value of $\alpha = \bar{g}^2/(4\pi)$ that was reached. Three-loop accuracy here means that the renormalization group function β is truncated at three-loop order and the resulting differential equation (2.5) is integrated exactly. An important observation is now that this truncation of the renormalization group equation (which governs the running of the coupling) is verified in the region of low enough α. It may hence also be used to compute the Λ–parameter, through continuation of the non-perturbative scale evolution with the perturbative one to infinite energies as indicated in eq. (2.19), with negligible errors due to higher-order terms that are not included in the perturbative approximation of the β–function.

At first sight, the attentive reader will find it quite surprising that the perturbative evolution in the SF renormalization scheme is so precise down to very low energy scales. Of course, this property may *not* be generalized to other renormalization schemes, in particular not to the $\overline{\rm MS}$ scheme, where the β–function is only defined in perturbation theory anyhow.[15]

Results in the quenched approximation

After converting to the $\overline{\rm MS}$ scheme, a step that utilizes the one-loop perturbative relation between the finite-volume and the $\overline{\rm MS}$ coupling leading to an exact conversion factor $\Lambda_{\overline{\rm MS}}/\Lambda$, Ref. [22] arrives at the result

$$\Lambda_{\overline{\rm MS}} = 0.602(48)/r_0 \qquad (N_{\rm f} = 0)\,, \tag{2.24}$$

which upon assigning physical units to the appropriate overall physical scale — in this case the hadronic radius parameter $r_0 = 0.5\,\mathrm{fm}$ — translates into

$$\Lambda_{\overline{\rm MS}} = 238(19)\,\mathrm{MeV} \qquad (N_{\rm f} = 0) \tag{2.25}$$

for the Λ–parameter in QCD with zero quark flavours, i.e. the pure Yang-Mills theory. Recall that all reference to the intermediate finite-volume scheme has disappeared at this point. Eq. (2.24) simply expresses the Λ–parameter in the $\overline{\rm MS}$ scheme in terms of the low-energy scale r_0 and thus provides the solution of the non-perturbative renormalization

[15] Furthermore, our non-perturbative coupling was designed to have a good perturbative expansion, since one relies on the 3–loop β–function in the (high-energy part of the) computation of the Λ–parameter.

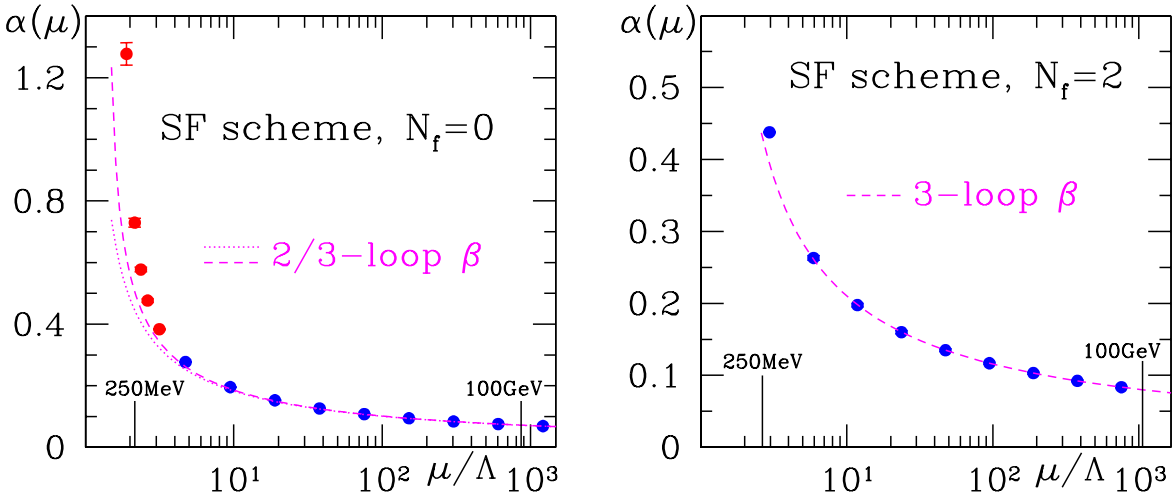

Figure 2.4: Energy dependence of the effective gauge coupling in our particular finite-volume scheme, translated to $\alpha(\mu) = \bar{g}^2(\mu)/(4\pi)$, in the pure SU(3) gauge theory (left) [22, 23] and in QCD with two flavours of massless quarks (right) as published in the preliminary report [25] and finally in Publication A. The results from the computation in lattice QCD are also compared with the evolution predicted by perturbation theory, where here 3–loop means that eq. (2.5) is evaluated including the b_2–term. The observation that both for zero and two flavours the momentum dependence of the SF coupling α that has been studied is accurately matched by perturbation theory already at fairly low momenta will be discussed further in the text.

problem for the running coupling. Rather than eq. (2.25), it is this first equation that is the solid result, because the conversion to physical units was already stressed to be ambiguous in the pure gauge theory.

If the result (2.24) is combined with the computation of pseudoscalar decay constants reported in the context of Publication F and a careful analysis of the systematic errors is made, we obtain

$$\frac{F_\pi}{\Lambda_{\overline{\rm MS}}} = 0.56(5) \qquad (N_{\rm f} = 0) \tag{2.26}$$

and thereby finally achieve our initial aim of relating the parameter characterizing the high-energy asymptotics of the running QCD coupling ($\Lambda_{\overline{\rm MS}}$) to a low-energy hadronic, observable physical quantity (F_π). That actually the figure (2.26) even agrees with the experimental number $F_\pi/\Lambda_{\overline{\rm MS}} = 0.62(10)$ within the quoted errors is somewhat unexpected since the quark polarization effects have been neglected. Although one may speculate that the ratio is not strongly affected by them, there is currently no good theoretical argument for this and the coincidence can thus not be taken as a solid confirmation of QCD at this point.

Despite the fact that the result on $F_\pi/\Lambda_{\overline{\rm MS}}$ still refers to the unphysical situation of disregarding the dynamics of the quarks, it can already be foreseen that a similar ab initio computation in the case of full QCD will provide one of the most stringent tests of the theory one can think of. Also note that the error in eq. (2.26) already sums up all

uncertainties except the quenched approximation, including those from the extrapolations to the continuum limit that were done in the various intermediate steps.

The running of the coupling in the $\overline{\mathrm{MS}}$ scheme, $\alpha_{\overline{\mathrm{MS}}}(\mu)$, at normalization masses μ given in units of r_0 (or equivalently F_π) may finally be calculated by solving the perturbative renormalization group equation in the $\overline{\mathrm{MS}}$ scheme, taking eq. (2.24) (or $\Lambda_{\overline{\mathrm{MS}}}/F_\pi$ of eq. (2.26)) as input. The numbers that one obtains tend to be significantly lower than the experimentally measured values of the strong coupling constant, but since we have not included the quark polarization effects so far, there is no reason to be worried. Sea quarks affect the evolution of the coupling (it becomes flatter) and they also influence the low-energy reference scale in some way which is difficult to guess at this stage.

$\alpha(\mu)$ for two flavours of massless quarks

Encouraged by the quenched computations, which yielded important insights into how precisely the low- and the high-energy regimes of the theory are connected to each other and which demonstrated the potential of the lattice approach to pursue very stringent tests of QCD, the calculations explained so far were extended to the numerically very demanding case of $N_\mathrm{f} = 2$ in Ref. [25] and Publication A. In these works, QCD is considered with two massless quark flavours. Since the SF invokes a massless renormalization scheme by its very construction, the definition (2.11) of the step scaling function has now to be supplemented by the additional condition of vanishing quark mass,

$$\sigma(u) \equiv \bar{g}^2(2L)\,\big|_{\bar{g}^2(L)=u\,,\,m=0}\ , \tag{2.27}$$

where m denotes the common mass of the two degenerate quark flavours that is understood to be properly computable (and then also tunable) on the lattice.

Apart from this more technical detail, the whole computation principally proceeds in the same way as in the zero-flavour case. Again, one of the key ingredients for a successful end of this calculation may be attributed to the fact that before mapping out the μ–dependence non-perturbatively and joining it with the perturbative evolution, the a–effects can be well controlled in each step of the recursion which has to be solved to obtain the SSF σ.

Algorithmic issues. On the algorithmic side, however, a new challenge of the situation with $N_\mathrm{f} > 0$ consists in the incorporation of the quark dynamics, which slows down the numerical calculations by a large factor. Therefore, in order to ensure efficiency and correctness of the required dynamical fermion simulations, the development and testing of suitable Monte Carlo algorithms was from the very beginning also an essential goal of the project to compute the running QCD coupling for $N_\mathrm{f} = 2$. The outcome of a study, which had these issues as its primary objective while particularly concentrating on

the observables of relevance in our finite-volume, Schrödinger functional scheme, can be found in Publication B. Since, as emphasized before, in the dynamical fermion case the generation of the lattice field configurations, on basis of which the physical quantities of interest are evaluated, is very expensive (in terms of CPU time), this investigation has been done in the course of the data production runs that had to be carried out for the determination of the coupling anyway.

A particular calculational step, both in dynamical fermion simulations employing the widely used Hybrid Monte Carlo (HMC) algorithm or its variants and in the computation of quark propagators as they enter the construction of fermionic correlation functions (see, for instance, Section 2.4), is the inversion of the Dirac operator. In actual lattice simulations, this amounts to invert the huge but sparse quark matrix or, equivalently, to determine the numerical solution of an associated system of linear equations. To accelerate the convergence of the iterative solvers that are commonly used here, it has by now become quite standard to *precondition* the quark matrix by transformations designed such that the new linear system can be numerically solved more efficiently than the original one. One of those preconditioners goes under the name 'SSOR preconditioning' [26]. Its implementation for QCD with SF boundary conditions on a massively parallel computer platform is worked out and tested in Publication C. In conjunction with the HMC algorithm, this preconditioner also entered the $N_{\rm f} = 2$ simulations to compute the running of the QCD coupling reported in Ref. [25] and Publication A.

Results. The $N_{\rm f} = 2$ results on the scale evolution of the QCD coupling in the SF scheme, displayed on the r.h.s. of Figure 2.4, represent the final status of the complete set of data collected in Publication A. At the time when the preliminary study [25] was published, these points were still awaiting a final check for the absence of discretization errors. The analysis of Publication A finally confirmed this, indeed.

As shown in the figure, the data obtained for the coupling cover a large range of energies from approximately 600 MeV to 100 GeV, similarly to the quenched case. The perturbative scaling of the coupling sets in rather early, and once $\alpha \approx 0.2$ and smaller, the data lie on top of the three-loop curve so that perturbation theory can be used with a negligible error. This feature of an absence of large corrections to the perturbative evolution, however, refers to a property of the particular observable under study and is definitely not to be interpreted as a reflection of some universal property of QCD couplings. In other schemes the coupling behaves differently in general, and there is usually no way to tell in advance at which energy the non-perturbative contributions become small. Let me illustrate this more explicitly here: If, instead of evolving non-perturbatively, one were only using perturbation theory to evolve the coupling over the range considered here, then the Λ–parameter would be overestimated by up to 14% (depending on the value of the coupling $u_{\rm max}$ that defines the low-energy scale $L_{\rm max}$). This in turn corresponds to an extra

error of 3% for the coupling in the range where its value is close to 0.12, i.e. the physical value of $\alpha_{\overline{\rm MS}}$ at the Z-boson mass. Needless to add that, of course, this uncertainty could even hardly be quantified *without* non-perturbative information, as perturbation theory appears rather well-behaved when looked at in isolation.

In Figure 2.4 we see the momentum dependence of the SF coupling $\alpha = \bar{g}^2/(4\pi)$ studied in the two-flavour case to be accurately matched by perturbation theory even at already fairly low momenta, similar to the quenched theory. Contact with the asymptotic behaviour (2.19) of the coupling can hence be made, and since also the low-energy regime is safely reached, these calculations eventually provide the desired link between that regime and the Λ–parameter. One should not forget, though, that only at the point, when the SF-specific reference energy scale $1/L_{\rm max}$ (implicitly still contained in the r.h.s. of Figure 2.4) is related to a physical low-energy observable, the scale dependent renormalization problem of the running coupling will have been successfully solved. This is an important piece within the calculation, which will serve, for instance, to transfer the scale dependence of the QCD coupling α initially determined as a function of the dimensionless ratio μ/Λ into a function of the energy μ in physical units.

To expose this last step a little further, we recall from Section 2.1 that the computational strategy described there yields $\Lambda L_{\rm max}$ with $L_{\rm max}$ defined by the value of the coupling itself. This is the central numerical result obtained in Publication A:

$$-\ln(\Lambda L_{\rm max}) = 1.09(7) \quad \text{at} \quad u_{\rm max} = 5.5 \qquad (N_{\rm f} = 2)\,. \tag{2.28}$$

Since this SF-specific scale is not experimentally measurable, it remains to connect it to a hadronic one. Ideally, the connection of the low-energy scale $L_{\rm max}$ to a low-energy, experimentally accessible property of a hadron should be again performed by adopting the decay rate of the K- or the π-meson for the latter, because chiral perturbation theory offers an analytic understanding of the pion dynamics, which is expected to help to control the extrapolations to the physical quark mass as well as to infinite volume. A computation of $F_\pi L_{\rm max}$ requires the knowledge of the decay constant in lattice units, aF_π, at a quark mass where m_π/F_π takes its experimental value, and of $L_{\rm max}/a$ with $\bar{g}^2(L_{\rm max}) = u_{\rm max}$, both as functions of the bare coupling in a range belonging to lattice spacings accessible in large-volume simulations. Unfortunately, as discussed in more detail in Publication A, the $N_{\rm f} = 2$ results for aF_π so far available in the literature still suffer from substantial systematic uncertainties and theoretical shortcomings, the most severe being (i) an only perturbative knowledge of the renormalization of the axial current as well as (ii) of its O(a) improvement and (iii) reasonable doubts whether these calculations have reached quark masses where chiral perturbation theory is applicable at all. At present, it hence appears preferable to relate $L_{\rm max}$ to the frequently used hadronic radius r_0, which has an unambiguous definition in terms of the force $F(r)$ between static quarks via $r_0^2 F(r_0) = 1.65$ and, according to phenomenological considerations, has a value of around 0.5 fm [27]. The

radius r_0 has also been the reference scale in the zero-flavour theory, i.e. the quenched approximation (cf. [22] and the preceding subsection).

Thus, in order to be able to end up with an evaluation of $\Lambda_{\overline{\rm MS}}\, r_0$, the low-energy scale of the intermediate scheme in units of this radius parameter, $L_{\rm max}/r_0$, was estimated in Publication A employing existing raw $N_{\rm f} = 2$ data on r_0/a at finite bare quark masses from the literature. One then gets in place of eqs. (2.24) and (2.25) as *results in QCD with two dynamical flavours*

$$\Lambda_{\overline{\rm MS}} = 0.62(8)/r_0 \qquad (N_{\rm f} = 2)\,, \tag{2.29}$$

where the quoted error covers the 7% error on $\Lambda L_{\rm max}$ in eq. (2.28) and statistical plus systematic uncertainties deriving from the determination of $L_{\rm max}/a$ and the extrapolation of the entering external, finite-mass data on r_0/a to zero quark mass, and

$$\Lambda_{\overline{\rm MS}} = 245(32)\,{\rm MeV} \qquad (N_{\rm f} = 2)\,. \tag{2.30}$$

Notwithstanding the fact that the analogue of the relation (2.26) is still missing here and that also the four-flavour theory has not yet been reached, it is a very non-trivial test of QCD that the non-perturbative results, which use experimental input at low energies of order $1/r_0 \approx 400\,{\rm MeV}$, agree roughly with high-energy, perturbative extractions of Λ. Some further work will still be required, of course, to unravel the details in this comparison.

Conclusion and open questions

The fact that the relation between the parameters in the Lagrangian and the basic properties of the mesons and nucleons can be established on the lattice, along with the ability to compute the non-perturbative evolution of the effective coupling from very low to high energies, is the key to show that quark confinement and asymptotic freedom are just two complementary aspects of QCD. In this respect, Ref. [25] and Publications A have its share with the many other lattice calculations and investigations, which are devoted to different phenomenological as well as fundamental issues, in making QCD the unique candidate of the theory of the strong interactions.

In these publications, the hadronic radius $r_0 \approx 0.5\,{\rm fm}$ was chosen for technical reasons to calibrate the overall energy scale and to therefrom relate the high-energy experiments to the theoretical predictions also in the case of QCD with dynamical quarks. Although one expects it to be quite unlikely that r_0 differs by 10% from this value, a *true* error on the results (2.29) and (2.30) in physical units is thus difficult to estimate until a reliable non-perturbative determination of e.g. $r_0 F_\pi$ has been performed. Such a computation (or more directly the computation of $L_{\rm max} F_\pi$ for $N_{\rm f} = 2$) is therefore still an urgent computational task that is left to connect $\Lambda L_{\rm max}$ in eq. (2.28) to an experimentally observable quantity, in order to complete the programme of solving QCD non-perturbatively on the same footing as already achieved in the quenched approximation.

The main reason that until recently comparisons of the lattice results with experimental numbers could not be regarded as hard tests of QCD lies in the quark polarization effects (i.e. those from dynamical sea quarks), which often were and at some places still are neglected in the numerical simulations, because their inclusion causes an enormous amount of computer time required to simulate them. Moreover, by the same token, neither was the number of relevant flavours used so far the physical one in most cases, nor could their simulated masses be adequately lowered — or let alone exactly set — to the actual values met in nature. However, once these limitations which are presently being overcome by many current projects within the lattice community, are finally gone, clean precision tests of QCD will become a reality.

2.4 Quark masses

Before I am going to discuss the determination of quark masses by virtue of probing low-energy physics within the scope of lattice regularized QCD, it is worth to remind that the masses of quarks are of a very different nature from the mass of other elementary particles such as, for instance, the electron. The basic difference lies in the property of confinement mentioned at the beginning of Section 1, which means that a quark cannot be prepared in isolation in order to perform an experimental measurement of its mass. Instead of this, quark masses have to be regarded — equally to the strong coupling constant — as fundamental parameters of the theory, and consequently their proper definition very much resembles that of an effective coupling, especially in that they have an energy dependence similar to the one of α.

Based on the past (and partly still ongoing) progress in lattice QCD concerning the non-perturbative renormalization of local composite operators and the removal of leading discretization errors which entailed a natural interest and much activity to evaluate hadron masses and matrix elements in the continuum limit, lattice calculations have become particularly capable to address the problem of a determination of the light quark masses with confidence. This is all the more so, because their complete renormalization (or, differently speaking, their overall energy dependence) is known non-perturbatively, at least in the quenched approximation [22], so that lattice determinations of quark masses have entered a mature stage where the dominant systematic error is quenching.

As an alternative to more standard methods, I here review the work presented in Publications E and F, where, as a necessary prerequisite for the Schrödinger functional (SF) framework to allow for a reliable computation of spectral quantities with high accuracy in lattice QCD, it is demonstrated explicitly that SF correlation functions are dominated by hadron intermediate states at Euclidean time separations of around 3 fm. This technique is then applied to physical observables in the meson sector of QCD, and in particular to the strange quark mass as the representative example out of the set of light quark masses.

The quenched data underlying the investigations of Publications E and F stem from four lattices with physically large volumes of $T \times L^3 \sim (3\,\mathrm{fm}) \times (1.5\,\mathrm{fm})^3$ and SF boundary conditions; lattice spacings, a, range from 0.1 fm to 0.05 fm, with four values of the quark mass each so that all results can first be properly extrapolated in the pseudoscalar mass and finally to the continuum limit. Among the more technical issues of the work (such as full $\mathrm{O}(a)$ improvement of the theory and a confirmation of the negligibility of finite-size effects as predicted by chiral perturbation theory), which due to its rather introductory character are ignored in this overview and can be found in the original references, it deserves to be noted that in the course of the generation of the raw numerical data the aforementioned, very efficient and parallelized implementation of an SSOR preconditioner for QCD with SF boundary conditions developed in Publication C was adopted as well. The underlying decomposition of the Dirac matrix speeds up the inversion algorithm solving the system of linear equations belonging to the boundary value problem of the Dirac operator to 'measure' the quark propagators within the evaluation of the correlation functions and thereby leads to a substantial gain in the overall computational cost. In the remaining paragraphs, I only emphasize the general concepts and our strategy for the computation of quark masses.

Correlation functions with SF boundary conditions

To begin with, we come back to the expectation values of products of local fields $\mathcal{O}$, introduced in Section 2.2, and will convey a rough idea of how SF correlation functions are constructed.

Namely, it is an interesting option at this point to include derivatives w.r.t. the quark and antiquark boundary values in the field product $\mathcal{O}$. An example for such a product is the operator

$$\mathcal{O}^a = -a^6 \sum_{\mathbf{y},\mathbf{z}} \frac{\delta}{\delta\rho(\mathbf{y})}\,\gamma_5 \tfrac{1}{2}\,\tau^a\,\frac{\delta}{\delta\bar{\rho}(\mathbf{z})}\,. \tag{2.31}$$

In the functional integral the derivatives act on the weight factor e^{-S} and induce an insertion of certain combinations of the dynamical fields localized near the boundaries of the lattice, and thereupon one finds the derivatives $-\delta/\delta\rho(\mathbf{x})$ and $\delta/\delta\bar{\rho}(\mathbf{x})$ to effectively behave like an antiquark and a quark field at time $x_0 = 0$, respectively. The generated field product associated with this example is an isovector pseudoscalar field at the boundary of the SF cylinder. Hence, we can define the correlation function

$$\left\langle A_\mu^a(x)\mathcal{O}^a \right\rangle = \left\{ \frac{1}{\mathcal{Z}} \int_{\text{fields}} A_\mu^a(x)\mathcal{O}^a\,\mathrm{e}^{-S} \right\} \Bigg|_{\rho=\bar{\rho}=\rho'=\bar{\rho}'=0}\,, \tag{2.32}$$

in which the summation over the positions $\mathbf{y}$ and $\mathbf{z}$ from eq. (2.31) causes the operator $\mathcal{O}^a$ to create a quark and an antiquark at time zero with vanishing spatial momentum. This

correlation function is then proportional to the probability amplitude that the quark-antiquark pair propagates to the interior of the space-time volume and annihilates at the point x, as illustrated in Figure 2.5.[16]

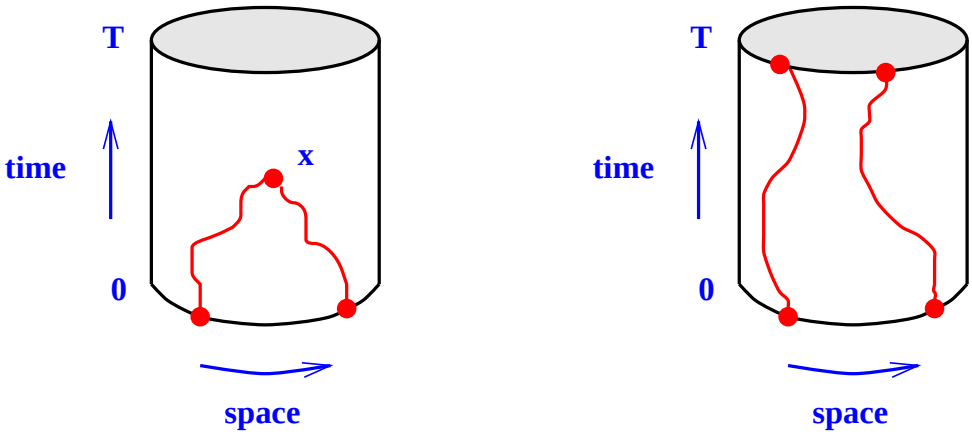

Figure 2.5: *Left*: Sketch of a fermionic boundary-to-bulk correlation function $f_{\rm X}(x_0)$ defined in the Schrödinger functional. The irregular lines represent the space-time trajectories of a quark and an antiquark, which have been created at time 0 (through the operator $\mathcal{O}^a$ in (2.31)) and annihilate each other at the point x. *Right*: The boundary-to-boundary correlation function f_1. Correlation functions of this type have been used before, for instance, to study current conservation and quark mass renormalization on the lattice [9, 13, 22].

According to this formal recipe, a variety of multiplicatively renormalizable, gauge-invariant correlation functions in the SF can be formed from suitable pairings of local composite fields in the interior of the manifold and boundary quark fields. Two prominent candidates involve the axial vector current and the pseudoscalar density in the bulk; the corresponding correlators read

$$f_X(x_0) \propto \left\langle \sum_{\mathbf{y},\mathbf{z}} X(x)\, \bar{\zeta}(\mathbf{y})\gamma_5 \tfrac{1}{2}\tau^a\, \zeta(\mathbf{z}) \right\rangle , \quad X = A^a_\mu \text{ or } P^a , \tag{2.33}$$

where the boundary fields, located at the $x_0 = 0$ surface, are now denoted by $-\delta/\delta\rho(\mathbf{x}) \to \overline{\zeta}(\mathbf{x})$ and $\delta/\delta\bar{\rho}(\mathbf{x}) \to \zeta(\mathbf{x})$ and create fermions and antifermions in the sense outlined above. Their partners at $x_0 = T$ are $-\delta/\delta\rho'(\mathbf{x}) \to \overline{\zeta}'(\mathbf{x})$ and $\delta/\delta\bar{\rho}'(\mathbf{x}) \to \zeta'(\mathbf{x})$ and give rise to primed analogues of eq. (2.31), viz.

$$\mathcal{O}'^a = a^6 \sum_{\mathbf{y},\mathbf{z}} \bar{\zeta}'(\mathbf{y})\, \gamma_5 \tfrac{1}{2}\tau^a\, \zeta'(\mathbf{z})\,.$$

A correlation function between two pseudoscalar boundary sources at $x_0 = 0$ and $x_0 = T$, as sketched on the r.h.s. of Figure 2.5, is

$$f_1 \propto \langle \mathcal{O}'^a\, \mathcal{O}^a \rangle \propto \left\langle \sum_{\mathbf{u},\mathbf{v},\mathbf{y},\mathbf{z}} \bar{\zeta}'_i(\mathbf{u})\gamma_5\zeta'_j(\mathbf{v})\, \bar{\zeta}_j(\mathbf{y})\gamma_5\zeta_i(\mathbf{z}) \right\rangle \quad (i,j\text{: flavour indices}) \tag{2.34}$$

[16] Such pictures receive an exact meaning if the quark lines are thought of to represent quark propagators at the current gauge field.

and will later serve to cancel the multiplicative renormalization of the boundary quark fields $\zeta, \ldots, \bar{\zeta}'$ in order to compose these fermionic SF correlation functions to renormalized quantities with a well-defined continuum limit.

Verification of O(a) improvement in intermediate volume

As a preparation for the following calculation of hadron masses, matrix elements and light quark masses in large volume, renormalized SF correlation functions and a few observables constructed such that they turn into meson masses and decay constants have been thoroughly examined in an intermediate physical volume ($T \times L^3 \sim (1.5\,\mathrm{fm}) \times (0.75\,\mathrm{fm})^3$) within O($a$) improved quenched lattice QCD in Publication D.

Upon extrapolating to the continuum limit results on these observables from numerical simulations of renormalized and improved correlation functions at decreasing lattice spacings a, the quality of scaling as well as the size of its violation were studied, and the impact of O(a) improvement was quantified therefrom. The outcome of this investigation is that all quantities under consideration show an overall behaviour completely compatible with being linear in a^2 at $a \lesssim 0.1\,\mathrm{fm}$ and that changing a by a factor of about two gives very stable continuum extrapolations — though there are also still quantities (e.g. in the vector meson channel), for which even in the O(a) improved theory the remaining O(a^2) effects have to be assessed by *varying* the lattice spacing.

Low-energy physics from SF correlation functions

Whereas in other applications, e.g. those described in Sections 2.3 and 3 that rather address scale dependent renormalization problems, correlation functions in the SF are mainly considered in the perturbative regime (i.e. small extensions of the space-time volume), the focus in the present context is on the properties of SF correlators in intermediate to large volumes with extensions significantly larger than the typical QCD scales of order 1 fm, where now their behaviour at *large* time separations will carry the physical information.

Starting from the quantum mechanical interpretation of the SF, one can derive explicit expressions for the representation of its correlation functions in terms of intermediate physical states (Publication E). Let us discuss an example, which is directly relevant later. We consider the correlation functions introduced in eqs. (2.33) and (2.34),

$$f_X(x_0) = -\frac{L^3}{2}\,\langle X(x)\,\mathcal{O}\rangle\ , \quad f_1 = -\frac{1}{2}\,\langle \mathcal{O}'\,\mathcal{O}\rangle\ , \tag{2.35}$$

where $\mathcal{O}$ is a pseudoscalar field, constructed from a $\mathbf{p} = 0$ quark field and a $\mathbf{p} = 0$ antiquark field at $x_0 = 0$:

$$\mathcal{O} = \frac{a^6}{L^3}\sum_{\mathbf{y},\mathbf{z}} \overline{\zeta}_i(\mathbf{y})\gamma_5\zeta_j(\mathbf{z})\,, \tag{2.36}$$

i and j being flavour indices. Analogously, $\mathcal{O}'$ is located at the boundary $x_0 = T$. One may think of the fields $\zeta, \ldots, \overline{\zeta}'$ as quark fields at the boundary; their precise definition is given in [9] and was motivated before. Here, we shall be interested in f_{A} and f_{P}, defined by choosing

$$X(x) \equiv A_0(x) = \overline{\psi}_j(x)\gamma_0\gamma_5\psi_i(x) \quad \text{and} \quad X(x) \equiv P(x) = \overline{\psi}_j(x)\gamma_5\psi_i(x)\,, \tag{2.37}$$

respectively.

For large separations x_0 and $T - x_0$, the correlation functions are dominated by the lowest lying intermediate states with the appropriate quantum numbers. These are the pseudoscalar ground state and the vacuum, the latter contributing between x_0 and T in both f_{A} as well as f_{P}. Following the arguments in Publication E, one may then arrive at the asymptotic behaviour including the first non-leading corrections in the transfer matrix formalism, viz.

$$\begin{aligned} f_X(x_0) &\propto \rho\,\langle\, 0,0 \,|\, \mathbb{X} \,|\, 0,\mathrm{PS}\,\rangle\, \mathrm{e}^{-x_0 m_{\mathrm{PS}}} \left\{1 + \mathrm{O}\left(\mathrm{e}^{-x_0\Delta}, \mathrm{e}^{-(T-x_0)m_{\mathrm{G}}}\right)\right\}\,, \\ f_1 &\propto \rho^2\,\mathrm{e}^{-T m_{\mathrm{PS}}}\,. \end{aligned} \tag{2.38}$$

In leading order, an unknown matrix element (ρ) and the desired matrix elements of the Schrödinger picture operators $\mathbb{X}$, associated with the fields X, arise. Moreover, the mass of the 0^{++} glueball, m_{G}, and the energy gap to the first excited state in the pseudoscalar channel, Δ, enter the corrections with coefficients, which can be expressed through certain matrix elements but whose exact form does not need not be repeated here. Apart from the pseudoscalar mass, m_{PS}, the formulae (2.38) thus enable us to calculate the decay constant, F_{PS}, and the so-called pseudoscalar coupling, G_{PS}, via their definitions through the matrix elements just occurring in eq. (2.38):

$$\langle\, 0,0 \,|\, \mathbb{A}_0 \,|\, 0,\mathrm{PS}\,\rangle = N_{\mathrm{PS}} \times m_{\mathrm{PS}} F_{\mathrm{PS}}\,, \tag{2.39}$$

$$\langle\, 0,0 \,|\, \mathbb{P} \,|\, 0,\mathrm{PS}\,\rangle = N_{\mathrm{PS}} \times G_{\mathrm{PS}}\,, \quad N_{\mathrm{PS}} = \frac{1}{\sqrt{2 m_{\mathrm{PS}} L^3}}\,. \tag{2.40}$$

Also note the particular rôle of the boundary-to-boundary correlator f_1 that consists in its use to eliminate the unknown factor ρ, the only place where the (divergent) renormalizations of the boundary quark fields are hidden, by taking suitable ratios with f_{A} or f_{P} (e.g. $f_{\mathrm{A}}/\sqrt{f_1}$). A generalization to other channels such as that of the vector meson is straightforward.

Turning to the numerical tests of the practicability of the method, I pick out as a representative example the ratio of correlation functions

$$\frac{f_{\mathrm{A}}}{f_{\mathrm{P}}} = \frac{m_{\mathrm{PS}} F_{\mathrm{PS}}}{G_{\mathrm{PS}}} \left\{1 + \mathrm{O}\left(\mathrm{e}^{-x_0\Delta}, \mathrm{e}^{-(T-x_0)m_{\mathrm{G}}}\right)\right\}\,, \tag{2.41}$$

which will become the key observable in the approach to follow of computing quark masses. This ratio shows approximate plateaux between $x_0 \approx 1\,\mathrm{fm}$ and $T - x_0 \approx 1\,\mathrm{fm}$,

compare Figure 2.6. Their height determines $m_{\rm PS}F_{\rm PS}/G_{\rm PS}$. Before simply reading these off, however, the magnitude of the 'contaminations' by excited state contributions should be carefully assessed. Given the fact that estimates for Δ and $m_{\rm G}$ are available in the literature, this may be achieved by analyzing the data on $f_{\rm A}/f_{\rm P}$ as functions of the leading corrections. The corresponding slopes, estimated from plotting this ratio against these correction terms, then allow to deduce the (nearly central) timeslice range, where the excited state contributions are below a certain systematic error margin that in turn is chosen to be negligible compared to the envisaged statistical errors, and within which the quantity $f_{\rm A}/f_{\rm P}$ is subsequently averaged to obtain the final results. This procedure is also easily extended to the calculation of $m_{\rm PS}$, $F_{\rm PS}$ and $G_{\rm PS}$ separately.

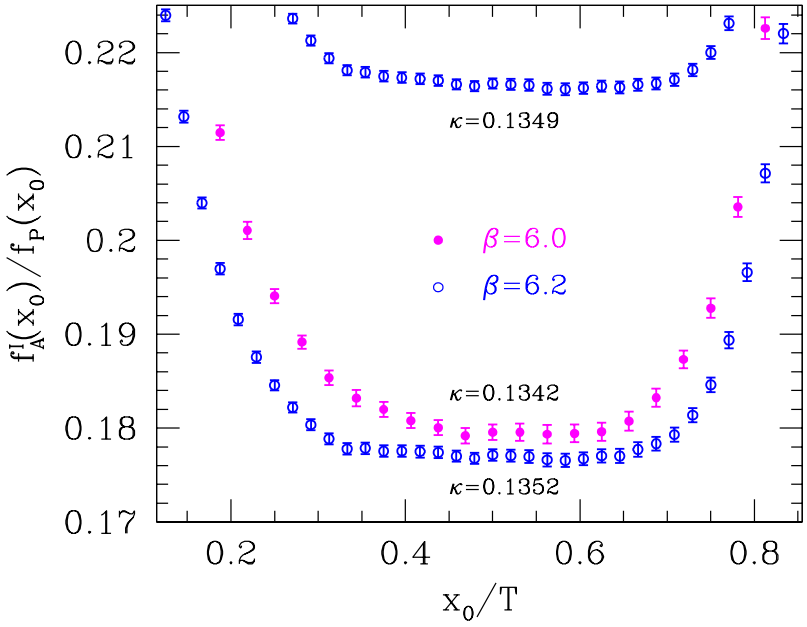

Figure 2.6: The ratio $f_{\rm A}/f_{\rm P}$ of SF correlation functions for $a \approx 0.07\,$fm (open circles) and $a \approx 0.09\,$fm (filled circles). The label 'I' at $f_{\rm A}$ on the horizontal axis indicates that the O(a) improved correlator is employed.

Though the SF applied for extracting hadron physics appears similar in spirit to the method of wall sources, one should note that gauge invariance is kept at all stages of the present formulation and furthermore, as a consequence of the dimensionless non-local fields used to create the boundary states, dimensional analysis implies that the pre-asymptotic decay of SF correlation functions is slow, hence leaving large and precise signals at hadronic length scales of $1-2\,$fm. Since the correlators are renormalizable by simple factors (see also Publication D), this property is indeed independent of the lattice spacing once one is sufficiently close to the continuum limit.

Light quark masses: The strategy

Before we come to exploit the aforementioned nice features of large-volume SF correlation functions in the low-energy regime, I want to explain in more detail the strategy for the computation of light quark masses advocated here. Their ratios can be calculated from chiral perturbation theory [28], where the currently best results read

$$\frac{M_{\rm u}}{M_{\rm d}} = 0.55 \pm 0.04\,, \quad \frac{M_{\rm s}}{M_{\rm l}} = 24.4 \pm 1.5 \tag{2.42}$$

with the average light quark mass $M_{\rm l} = \frac{1}{2}\,(M_{\rm u} + M_{\rm d})$ [29].

Despite this success of chiral perturbation theory, there are still substantial questions that can be answered decisively only in the framework of lattice QCD.

(i) The applicability of chiral perturbation theory needs to be checked. This concerns the practical question, in how far the lowest orders dominate the full result.

(ii) The parameters in the chiral Lagrangian (at a given order in the expansion) cannot be inferred with great precision from experimental data alone. Their determination can be improved significantly by help of lattice QCD results. (This aspect is discussed in Section 2.5 and Publication G.)

(iii) In particular, there is one parameter in the chiral Lagrangian that is impossible to determine from experimental data. This is the overall scale of the quark masses, which is only defined once the connection with the fundamental theory, QCD, is made.

An important point to realize is that all of the above problems can be dealt with by working with *unphysical quark masses* (where, obviously, they should not be too large). For the first two problems, it is in fact essential to explore a range of quark masses, and also for the last problem, which is addressed here, this is of significant advantage.

The above considerations lead one to determine a reference quark mass, $M_{\rm ref}$, implicitly defined through the condition

$$m_{\rm PS}^2\,(M_{\rm ref})\,r_0^2 = 1.5736 = (m_{\rm K} r_0)^2\,, \tag{2.43}$$

where $m_{\rm PS}^2(M)$ is the pseudoscalar meson mass as a function of the quark mass (for mass-degenerate quarks), and r_0 again denotes the dimensionful hadronic radius defined through the force between static quarks [27] to set the physical scale ($r_0 = 0.5\,\mathrm{fm}$), entering as well as the experimental value $\frac{1}{2}(m_{\rm K^+}^2 + m_{\rm K^0}^2)|_{\rm pure\ QCD} = (495\,\mathrm{MeV})^2$ on the r.h.s. of this equation. Chiral perturbation theory *in full QCD* relates $M_{\rm ref}$ to the other light quark masses, that is to say

$$2M_{\rm ref} \approx M_{\rm s} + M_{\rm l}\,. \tag{2.44}$$

Publication F provides further evidence for this relation, employing the results of quenched QCD. Hence, the remaining task is to calculate $M_{\rm ref}$ from lattice QCD.

What was said so far is valid literally in mass independent renormalization schemes, in which quark masses are renormalized with a flavour independent factor. The resulting running quark masses, $\overline{m}(\mu)$, are however scheme and scale dependent quantities. Therefore, as already explained in Section 2.2, it is advantageous to calculate directly the renormalization group invariant (RGI) quark masses, which are pure numbers and do *not* depend on the scheme. In terms of $\overline{m}(\mu)$, they are given as

$$M = \overline{m}(\mu)\left[2b_0\bar{g}^2(\mu)\right]^{-d_0/(2b_0)}\exp\left\{-\int_0^{\bar{g}(\mu)}\mathrm{d}g\left[\frac{\tau(g)}{\beta(g)}-\frac{d_0}{b_0 g}\right]\right\}, \qquad (2.45)$$

with the leading β–function coefficient $b_0 = 11/(4\pi)^2$ and $d_0 = 8/(4\pi)^2$ the leading coefficient of the function $\tau(\bar{g})$ that describes the RG evolution of the quark masses with the renormalization scale (i.e. d_0 characterizes the asymptotic behaviour of $\overline{m}(\mu)$ for large energy). For O(a) improved quenched QCD, the quark mass renormalization has been performed non-perturbatively in Ref. [22]. As a result, the flavour independent total renormalization factor $Z_{\rm M}$, relating the bare current quark masses m — defined by the partially conserved axial current (PCAC) relation

$$\langle\partial_0 A_0(x)\mathcal{O}\rangle \;=\; 2m\,\langle P(x)\mathcal{O}\rangle \;+\; \mathrm{O}\left(a^2\right) \qquad (2.46)$$

that is to be read as a renormalized operator identity with $\mathcal{O}$ being some O(a) improved field localized in a region not containing x — to the RGI masses according to

$$\begin{aligned} M &= \frac{M}{\overline{m}(\mu)}\,\frac{Z_{\rm A}(g_0)}{Z_{\rm P}(g_0,L)}\times m(g_0) \;+\; \mathrm{O}\left(a^2\right) \\ &\equiv Z_{\rm M}(g_0)\times m(g_0) \;+\; \mathrm{O}\left(a^2\right)\,, \quad \mu = 1/L \equiv 1/(2L_{\rm max}) \approx 275\,\mathrm{MeV}\,, \end{aligned} \qquad (2.47)$$

is non-perturbatively known for the range of bare couplings g_0 commonly used in simulations in physically large volumes.

Then, combining the PCAC relation (2.46), applied to the vacuum-to-pseudoscalar matrix elements in eqs. (2.39) and (2.40), with eq. (2.43) leads to the central formula

$$2r_0 M_{\rm ref} = Z_{\rm M}\times\frac{R\,|_{\,m_{\rm PS}^2 r_0^2 = 1.5736}}{r_0}\times 1.5736\,, \quad R \equiv \frac{F_{\rm PS}}{G_{\rm PS}}\,. \qquad (2.48)$$

Of course, as anticipated in this equation by the K-meson scale $1.5736 = (m_{\rm K}r_0)^2$ where the ratio R is to be evaluated at, as well as by the omission of any lattice spacing dependence, it is understood that the r.h.s. is chirally extrapolated in the pseudoscalar mass to the mass scale of the light quark in question (the strange quark in the case at hand), prior to a continuum limit extrapolation, $a \to 0$.

An application: Computation of the strange quark's mass

With the aid of the numerical methods outlined two paragraphs before, the ratio R and the meson mass m_{PS} in lattice units can be computed accurately as a function of the bare quark mass and the bare gauge coupling. As discussed and explicitly demonstrated in Publication F, a mild extrapolation then yields R/a at the point $m_{\mathrm{PS}}^2 r_0^2 = 1.5736$.[17] Next, the sum of the RGI strange quark mass and the average light quark mass, implicit in eqs. (2.43) and (2.44) through the combination $r_0 M_{\mathrm{ref}}$, is extrapolated to the continuum limit. Since this latter extrapolation, which is displayed in the upper diagram of Figure 2.7, involves a significant slope, the point furthest away from the continuum has been discarded. This is a safeguard against higher-order lattice spacing effects. Nevertheless, we clearly see the data points to approach the continuum limit with a rate consistent with leading discretization errors proportional to a^2.

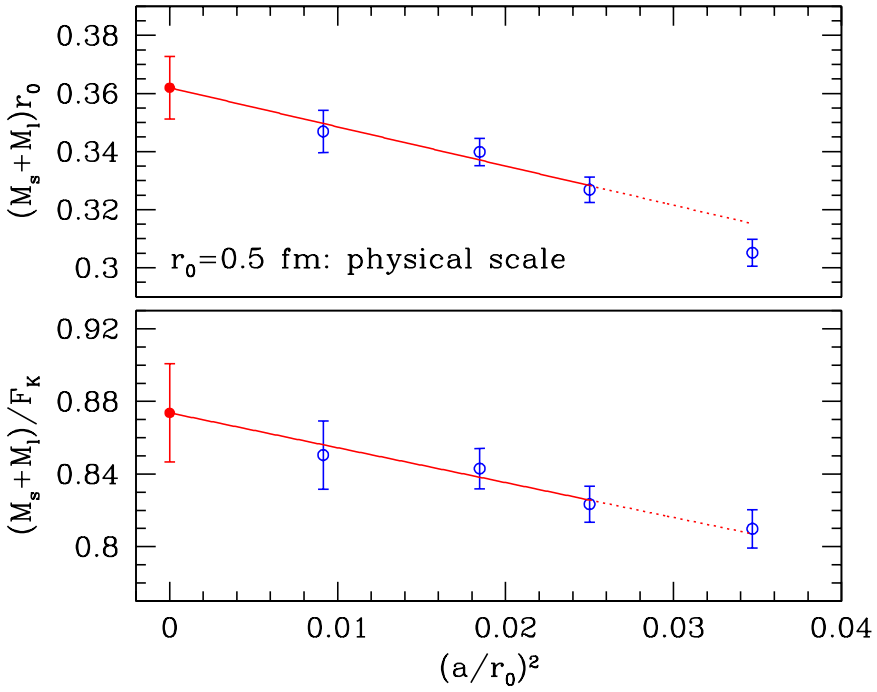

Figure 2.7: Continuum limit extrapolations of the sum of the RGI strange and average light quark masses, in units of a particular physical scale given by the hadronic radius $r_0 = 0.5\,\mathrm{fm}$ (top), as well as in units of the K-meson decay constant (bottom).

Moreover, the entire analysis was repeated for M_{ref} in units of the kaon decay constant. This amounts to substitute eq. (2.48), here exposed again but in the more familiar form

[17] The reason for not computing directly at or below the quark mass corresponding to $m_{\mathrm{PS}}^2 r_0^2 = 1.5736$ was that this is the region where unphysical zero modes of the O(a) improved Dirac operator become relevant ('exceptional configurations'). However, even without entering this region, the quark mass points imposed in the Monte Carlo simulations are close enough to perform a safe extrapolation.

directly referring to the strange quark mass scale,

$$r_0\,(M_{\rm s}+M_{\rm l}) = Z_{\rm M}\times\frac{\langle\,0\,|\,A_0\,|\,{\rm K}\,\rangle}{(m_{\rm K}r_0)\langle\,0\,|\,P\,|\,{\rm K}\,\rangle}\times(m_{\rm K}r_0)^2\,\big|_{\rm exp}\,+\,{\rm O}\left(a^2\right)\,, \tag{2.49}$$

by the expression

$$\frac{M_{\rm s}+M_{\rm l}}{F_{\rm K}} = \frac{M}{\overline{m}(\mu)}\,\frac{1}{Z_{\rm P}(g_0,L)\,r_0^2\,G_{\rm K}}\times(m_{\rm K}r_0)^2\,\big|_{\rm exp}\,+\,{\rm O}\left(a^2\right)\,, \tag{2.50}$$

owing to the PCAC relation now written as $m_{\rm K}^2F_{\rm K}=(\overline{m}_{\rm u}+\overline{m}_{\rm s})\langle 0|\overline{u}\gamma_5 s|{\rm K}\rangle\equiv(\overline{m}_{\rm u}+\overline{m}_{\rm s})G_{\rm K}$. Note that, in the same way as via $Z_{\rm M}$ in eq. (2.49), all reference to the intermediate scheme used to trace the renormalization scale dependence of the quark masses is cancelled in the product $M/(\overline{m}Z_{\rm P})$, eq. (2.47). In the case of $(M_{\rm s}+M_{\rm l})/F_{\rm K}$ we observe a weaker lattice spacing dependence, as illustrated in the lower diagram of Figure 2.7. The final results of these two analyses are completely consistent with each other; as shown in Publication F, the numerical agreement between them is even better than one would expect it to be in the quenched approximation.

Using the experimental value $F_{\rm K}=160(2)\,{\rm MeV}$, one now obtains for the sum of the RGI strange and average light quark masses in the continuum limit of the quenched approximation

$$M_{\rm s}+M_{\rm l}=140(5)\,{\rm MeV}\quad\Leftrightarrow\quad\overline{m}_{\rm s}^{\,\overline{\rm MS}}(2\,{\rm GeV})=97(4)\,{\rm MeV}\,, \tag{2.51}$$

where the number on the r.h.s. follows from combining the result for $M_{\rm s}+M_{\rm l}$ with the prediction of chiral perturbation theory, $M_{\rm s}/M_{\rm l}=24.4(1.5)$ (cf. eq. (2.42)), and a subsequent conversion to the $\overline{\rm MS}$ scheme at the convenient, finite renormalization scale $\mu=2\,{\rm GeV}$ via integration of the four-loop perturbative renormalization group functions (which also accounts for the uncertainty in $\Lambda^{(N_{\rm f}=0)}=238(19)\,{\rm MeV}$ [22]). The uncertainty of $\pm4\,{\rm MeV}$ quoted in eq. (2.51) comprises all errors but those due to quenching. But, as already pointed out earlier, an intrinsic ambiguity is encountered when assigning physical units to lattice results in the quenched approximation. For $\overline{m}_{\rm s}^{\,\overline{\rm MS}}(2\,{\rm GeV})$, eq. (2.51), the associated uncertainty was estimated to be $\sim 10\%$.

Concluding remarks

In Publications E and F, other interesting results both at finite lattice spacing and after extrapolation to the continuum limit were gained along similar lines for the pseudoscalar decay constant and the vector meson mass, $r_0F_{\rm K}$ and $r_0m_{\rm K^*}$. Summing up, it may be said that, also through the explicit comparisons with numbers from the literature not reproduced here, the SF has been shown to be not only useful for the extraction of low-energy matrix elements from suitable SF correlators but to also lead to numerically efficient and beyond that, for the particular cases of vacuum-to-pseudoscalar matrix elements (e.g. as

crucial elements of a reliable calculation of the light quark masses), to significantly more precise results than those from standard methods — in addition to the SF's other important area of applications that addresses to solve various renormalization problems in QCD.

In the meantime, the just summarized strategy and practical procedure devised in these publications to determine quark masses through low-energy physics from the QCD Schrödinger functional has also successfully been adapted to a precision computation of the mass of the charm quark in the quenched approximation [30].

2.5 Chiral Lagrangian parameters from lattice QCD

A notorious problem particularly for numerical simulations of QCD with dynamical quarks is to reach the region of realistic, small quark masses. Among the different attempts being pursued to deal with this problem, a sound method on the theoretical side is *chiral perturbation theory (ChPT)*. It describes the dynamics of the Goldstone boson fields as they appear as a consequence of a spontaneously broken continuous symmetry, the chiral symmetry in the case of QCD with massless quarks. The associated effective Lagrangian originates from a systematic higher-order expansion of the underlying, more fundamental theory — QCD — in the four-momentum and the quark masses m_{u}, m_{d} and m_{s} about the massless limit [31]. While with increasing order of the expansion more complicated terms together with corresponding additional, so-called low-energy constants (LECs) multiplying them arise in this Lagrangian, it is designed such that it obeys the same global symmetries as QCD to yield a trustworthy description of the fundamental theory. These LECs are free parameters of the Lagrangian; they can only be determined by the comparison with sources beyond ChPT, and in principle, their values have to follow from QCD itself.

The fact that in the low-energy regime the information content of ChPT is equivalent to that of QCD has been exploited in many ways. It supplies us, for instance, with formulae, which model the quark mass dependence of pseudoscalar masses, decay constants and other observables and thereby provides valuable input and information for lattice simulations: ChPT predictions can serve as a guide to extrapolate the numerical results from medium to small quark masses and are widely used for this purpose by the lattice community. However, this line of reasoning may also be turned around by viewing at numerical simulations as a powerful tool to *determine the low-energy parameters of ChPT* from first principles, because simulations of lattice QCD employ the fundamental Lagrangian of the theory.

Tuning the quark masses such that the regime of validity of ChPT is reached, a comparison of numerically generated QCD data and the predictions of ChPT can be performed. In practice, the LECs are extracted by a fit of the numerical data to the

analytical formulae of ChPT (which contain the LECs as free parameters), and the values of the LECs obtained in this way from QCD can then be related to experimental data, which eventually leads to direct tests of QCD. Furthermore, an estimation of the LECs is an important ingredient to supplement the numerical simulations themselves, since simulations at small values of the quark mass, i.e. corresponding to their physical values, are very expensive. (For a recent review on this topic, see e.g. Ref. [32]). But if we would know, at what values of the quark mass ChPT is valid, its use to extrapolate many observables to physical values of the quark mass could be put on solid grounds. Obviously, for this procedure a sufficiently precise knowledge of the LECs is an inevitable prerequisite.

A general method that allows for the determination of LECs with good statistical accuracy through combining ChPT with numerical simulations of lattice QCD has been introduced in Publication G. Here I will only highlight one particularly interesting aspect of the applications discussed in this reference, which explores the question of the masslessness of the up quark by testing whether such a scenario would be compatible with the real world.

Interplay between lattice simulations and chiral perturbation theory

Chiral perturbation theory is an effective (non-renormalizable) theory parameterized in terms of a set of empirical couplings, which are usually referred to as Gasser-Leutwyler coefficients or, as already done above, 'low-energy constants'. At lowest order, the effective chiral Lagrangian reads

$$\mathcal{L}_{\text{eff}}^{(2)} = \frac{F_0^2}{2}\left\{\frac{1}{2}\,\text{Tr}\left(\partial_\mu U^\dagger \partial^\mu U\right) \,+\, B_0\,\text{Tr}\left(\mathcal{M}(U+U^\dagger)\right)\right\}\,, \tag{2.52}$$

where

$$U = \exp\left\{i\,\frac{\varphi^a T^a}{\sqrt{2}\,F_0}\right\} \qquad \text{and} \qquad \mathcal{M} = \text{diag}\,(m_\text{u}, m_\text{d}, m_\text{s}) \tag{2.53}$$

are the field of Goldstone bosons and the quark mass matrix, respectively. Among the leading-order LECs contained in eq. (2.52), B_0 and F_0, the latter corresponds to the pion decay constant in the chiral limit, while the former is related to the order parameter of chiral symmetry breaking, the so-called scalar condensate. At next-to-leading order there are twelve more interaction terms and hence new LECs $L_1, \ldots, L_{12}$.

The values of the LECs can be fixed by using experimental data and comparing with the relevant expressions obtained in ChPT. It turns out, however, that the complete set of LECs cannot be extracted in this way, because the values of some of them cannot be fixed without resorting to additional theoretical assumptions. One example is B_0, appearing in the leading-order chiral expansion of the pion mass, $m_\pi^2 = 2B_0 m_\text{l}$ with $m_\text{l} = \frac{1}{2}(m_\text{u} + m_\text{d})$, which shows that B_0 can only be determined from m_π if the physical value of the average

light quark mass m_l is known already. Vice versa, m_l can only be inferred if an estimate for B_0 is available in advance. Therefore, while ChPT enables us to compute quark mass ratios (cf. eq. (2.42)) since B_0 drops out in suitably chosen pseudoscalar mass ratios, it fails to predict an absolute normalization of their masses.

Another reason why the complete set of LECs cannot be determined from chiral symmetry considerations alone is the fact that the low-energy effective Lagrangian beyond leading order is invariant under a symmetry transformation involving the LECs and the mass matrix $\mathcal{M}$ in (2.52). This is the famous 'Kaplan-Manohar ambiguity' raised in Ref. [33]. The potential of lattice QCD in this respect is quite obvious now. By studying the quark mass dependence of Goldstone bosons in a simulation, one can estimate the value of B_0 or, equivalently, calculate the absolute normalization of quark masses. Since the Kaplan-Manohar ambiguity is not a symmetry of QCD, it is thus possible to resolve it by determining the values of LECs from an ab initio based approach. It must still be kept in mind, though, that a successful combination of lattice QCD and ChPT requires sufficient overlap between the range of quark masses used in simulations and the region of validity of the chiral expansion. This demand is crucial, if ChPT is used to extrapolate results from simulations performed for relatively heavy quarks to the regime of the physical up and down quark masses.

Is the up quark massless?

As announced above, the hypothesis of a massless up quark emphasizes a particularly interesting application of a lattice determination of LECs, and we hence return to the Kaplan-Monohar ambiguity and those couplings in the chiral Lagrangian that are required to test this hypothesis.

The aforementioned invariance of the effective chiral Lagrangian beyond leading order under simultaneous transformations of the mass matrix and a subset of LECs implies an uncertainty in the size of the next-to-leading order correction to the mass ratio $m_\mathrm{u}/m_\mathrm{d}$. This correction, Δ_M, is given by

$$\Delta_\mathrm{M} = \frac{(m_\mathrm{K}^2 - m_\pi^2)}{(4\pi F_\pi)^2}\,(2\alpha_8 - \alpha_5) \;+\; \{\text{chiral logarithms}\}\;. \tag{2.54}$$

Since α_5 can be estimated from the ratio of decay constants F_K/F_π but at the same time there exists no experimental information which would allow an unambiguous determination of α_8 or rather the linear combination $2\alpha_8 - \alpha_5$ itself [34], the value of α_8 and thus Δ_M must be fixed by invoking plausible assumptions beyond chiral symmetry arguments. Although in this way [29] the possibility that $m_\mathrm{u}/m_\mathrm{d} = 0$ (which necessitates a large negative value for Δ_M) was excluded and a massless up quark, which would present a simple and elegant mechanism to solve the strong CP-problem, appears already as an unlikely scenario, an estimate on Δ_M based on first principles is still lacking. Therefore, not least

owing to the importance of the strong CP-problem, it is desirable to tackle this question by means of lattice determinations of $2\alpha_8 - \alpha_5$.[18]

To briefly sketch the investigation of Publication G directed to the issue of a massless up quark, we first note that the expressions of ChPT are valid for arbitrary quark mass. Now one specifies a certain reference quark mass value $m_{\rm ref}$ and defines the ratios

$$R_{\rm F}(x) = \frac{F_{\rm PS}(m)}{F_{\rm PS}(m_{\rm ref})}\,, \tag{2.55}$$

$$R_{\rm M}(x) = \left[\frac{2m}{m^2_{\rm PS}(m)}\right] \Big/ \left[\frac{2m_{\rm ref}}{m^2_{\rm PS}(m_{\rm ref})}\right], \quad x \equiv \frac{m}{m_{\rm ref}}\,, \tag{2.56}$$

which become universal functions of the dimensionless mass parameter x and, due to the correlations between numerator and denominator, are expected to yield good statistical precision in their numerical evaluations. As all renormalization factors drop out in the ratios, these quantities can also be extrapolated to the continuum limit straightforwardly. The LECs at next-to-leading order are then extracted by confronting numerical data for $R_{\rm F}$ and $R_{\rm M}$ with the corresponding expressions in quenched (or partially quenched) ChPT.

In Publication G this 'ratio method' is implemented and numerically tested in the quenched approximation for $m_{\rm ref} \approx m_{\rm s}$ and x in the range $0.75 \lesssim x \lesssim 1.4$. (This range corresponds to the quark mass interval covered in the generation of the raw data for the computation of the strange quark mass in Publication F, which are also employed here, and it is limited from below by the constraint of evading exceptional configurations). The numerically evaluated functions in eqs. (2.55) and (2.56) are compiled together with the associated combinations of LECs in Figure 2.8. There it is found that the ratio $R_{\rm F}$, which is predicted by quenched ChPT to rise linearly with the quark mass, is modelled very well by the data and results in stable estimates for α_5, whereas the numerical data for $R_{\rm M}$ exhibit an almost constant behaviour, in contrast to quenched ChPT predicting the presence of linear terms as well as chiral logarithms. Hence, if the accessible range of simulated masses lies indeed within the regime where ChPT at next-to-leading order is valid, we can interpret this constant behaviour of the data as the result of a strong cancellation between the various contributions at next-to-leading order.

A comparison with the 'standard' values for the LECs estimated in the continuum, as well as with those values that would be necessary to support the notion of a massless up quark, shows that the latter scenario is strongly disfavoured already by the quenched

[18] In this context it is worth to mention the relevance of partially quenched simulations, where the Monte Carlo updates are performed with large enough sea quark masses to allow for a tolerable simulation speed, while quark propagators and the quantities derived from them are evaluated with smaller valence quark masses. As for unequal sea and valence quark masses the chiral Lagrangian is parameterized in terms of the same LECs as the physical theory, simulations with unphysical quark mass combinations do provide phenomenological information as long as the correct number of dynamical quark flavours (i.e. $N_{\rm f} = 3$) is used and, of course, the regime of validity of ChPT and the range of simulated masses overlap.

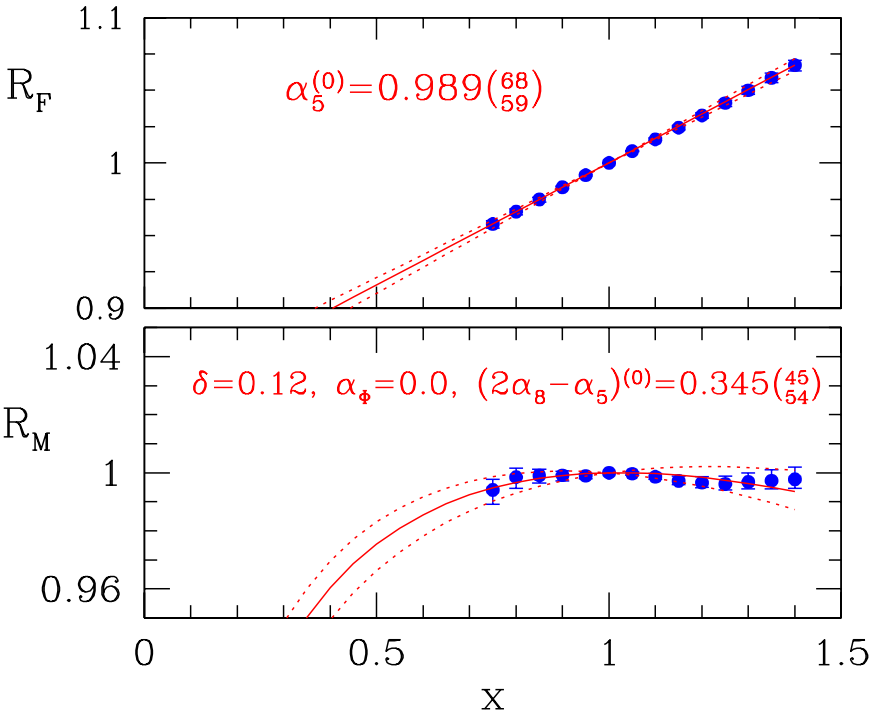

Figure 2.8: Numerical results for the ratios $R_{\rm F}$ and $R_{\rm M}$, eqs. (2.55) and (2.56), in the quenched approximation, taken from Publication G. (The additional LECs α_Φ and δ are induced by quenching artifacts in the chiral expansion: Incorporating flavour-singlet fields, which do not decouple in the quenched version of the effective low-energy theory, explicitly into the chiral Lagrangian introduces a parameter α_Φ multiplying the kinetic term in the flavour-singlet part of the effective Lagrangian as well as a new type of chiral logarithm, δ, proportional to the mass scale squared of the flavour-singlet.)

lattice calculation reported here: the (valence) quark mass behaviour of $R_{\rm M}$ would have to be radically different to accommodate a large negative value for α_8 as a massless up quark does demand it.

Meanwhile, the ratio method, which appears to be most stable against systematic errors from renormalization effects and lattice artifacts, has also been applied by other groups, for instance in Ref. [35] to the case of $N_{\rm f} = 2$ partially quenched QCD and in Ref. [36] where $N_{\rm f} = 3$ flavours of dynamical staggered quarks were simulated. Taking them together with our quenched study, one observes a quite weak $N_{\rm f}$ dependence of the LECs and even a broad consistency of the results on α_5 and $2\alpha_8 - \alpha_5$ within errors (particularly, if the $N_{\rm f} = 3$ expressions of ChPT are used, though the data were actually generated for $N_{\rm f} = 0, 2$). In short, under the assumption that the quarks entering the simulations are light enough to justify the comparison with ChPT[19], these first principles calculations in quest of a massless up quark provide clear indications to *exclude* this possibility, because it is not reflected at all in the valence quark mass behaviour of the relevant

[19]In fact, there is evidence that the dependence of $m_{\rm PS}^2$ and $F_{\rm PS}$ on the *sea* quark mass is not in agreement with ChPT if the sea quark mass corresponds to $m_{\rm PS} = 550 - 1000\,{\rm MeV}$, which would affect attempts to perform extrapolations in $m_{\rm sea}$ to the physical point defined by $m_{\rm PS}/m_{\rm V} \approx 0.17$ (see e.g. [37]).

pseudoscalar observables, and they thereby support the earlier, more phenomenologically oriented analysis of [29] based on suppositions beyond ChPT.

Of course, further simulations with smaller dynamical sea quark masses should be performed to corroborate these findings and primarily to settle the issue of the mass range, in which ChPT at next-to-leading order can be expected to hold true, in order to exploit its predictions to finally make contact with the region of very light quarks that is difficult to access directly in numerical simulations. This subject is recently growing into a major activity among current investigations of lattice QCD [38–40].

3 Physics of heavy-light quark systems

Not least by the influence of the challenging experimental programme of B-factories that aim at exploring such phenomenologically very interesting questions as the CP-violation in the B-system [41], the physical understanding of heavy quark physics and the study of the physics of B-mesons in particular have become a vivid area of research. In order to interpret the experimental observations within (or beyond) the Standard Model, matrix elements between low-energy hadron states must be known. Current investigations, in the context of which heavy-light hadronic matrix elements typically appear, focus on the extraction of elements of the CKM matrix that mixes quark flavours under the weak interactions of the Standard Model as well as on its internal self-consistency. But since these QCD matrix elements live in the strongly coupled sector of the theory, they call once more for a genuinely non-perturbative, 'ab initio' approach for their determination: the lattice formulation of QCD, which enables a numerical computation of its low-energy properties through Monte Carlo evaluation of the underlying Euclidean path integral.

For these reasons, B-physics has now developed to one of the fields, where lattice QCD can make most impact and will be a key factor in the precision with which the associated decay rates might be determined. In fact, lattice QCD calculations with b-quarks are already valuably contributing to precision CKM-physics by (over-)constraining the unitarity triangle and help to obtain other phenomenologically relevant predictions. Two examples for experimentally inaccessible quantities that are of great importance for this purpose are the mass of the b-quark, m_{b}, and the B leptonic decay rate parameterized by the B-meson decay constant, F_{B}. Before we will concentrate on the determination of these quantities in more detail, however, we have to discuss a technical obstacle that one faces when studying B-physics on the lattice.

As the inverse lattice spacing acts as an ultraviolet cutoff, its value in physical units places constraints on the scales one is able afford. In simulations on present-day computers typical values lie in the range $a^{-1} = 2 - 4\,\mathrm{GeV}$. These relatively low values of the cutoff imply that one expects already large cutoff effects for the charm quark (whose mass in

GeV is not too far below a^{-1}), while — more importantly for the following — the b-quark cannot be studied directly at all because its mass lies above the cutoff, i.e. huge discretization errors would render a realistic treatment of B-systems with a *propagating* b-quark on the lattice impossible.

This motivates to recourse to a theoretically very attractive framework, within which hadronic systems involving one heavy quark, such as the B-meson system we will be interested in from now on, can be investigated reliably also in the lattice formulation: the *heavy quark effective theory (HQET)*. It basically allows the lattice to predominantly handle scales appropriate to those degrees of freedom governing the non-perturbative dynamics of QCD in the low-energy ($\sim \Lambda_{\mathrm{QCD}}$) regime, while explicitly eliminating the high scale originating from the b-quark mass. In the sequel, we first outline the idea of the effective theory approach to heavy-light systems in the continuum and then turn our attention to recent work that solves two peculiar problems encountered in studying HQET non-perturbatively on the lattice.

3.1 Heavy quark effective theory

The properties of hadronic bound states containing heavy quarks are characterized by a large separation of energy scales. Effects associated with the heavy quark mass, m_{Q}, are perturbative and can be controlled once they have been separated from the other, long-distance effects. This separation is most conveniently done using an effective low-energy theory. For external states of hadrons containing a single heavy quark, the relevant effective quantum field theory to describe their transition amplitudes is the heavy quark effective theory (HQET).

The effective Lagrangian of the continuum HQET is

$$\mathcal{L}_{\mathrm{HQET}} = \overline{h}_v \, (iv \cdot D) \, h_v + \frac{C_{\mathrm{kin}}}{2m_{\mathrm{Q}}} \, \overline{h}_v \, (iD)^2 \, h_v + \frac{C_{\mathrm{spin}}(m_{\mathrm{Q}})}{4m_{\mathrm{Q}}} \, \overline{h}_v \sigma_{\mu\nu} G^{\mu\nu} h_v \, + \, \ldots \, , \qquad (3.1)$$

where $h_v(x)$ denotes the (velocity dependent) field describing a heavy quark inside a hadron moving with velocity v, D the covariant derivative orthogonal to v and $G^{\mu\nu}$ is the gluon field strength tensor. The field h_v is subject to the constraint $\not{v} h_v = h_v$. HQET then provides a systematic expansion of the QCD amplitudes around the *static limit* $m_{\mathrm{Q}} \to \infty$, in which new symmetries of the strong interactions arise, relating the long-distance properties of many observables to a small number of hadronic hadronic matrix elements. The leading term in the effective Lagrangian, which gives rise to the Feynman rules of HQET, is invariant under a global SU($2N_{\mathrm{h}}$) spin-flavour symmetry group, where N_{h} is the number of heavy quark flavours. This symmetry is broken by the higher-dimensional operators arising at order $1/m_{\mathrm{Q}}$. The first operator corresponds to the kinetic energy of the heavy quark inside the hadron, and the second one describes the chromomagnetic interaction of the heavy quark spin with the gluon field. Hadronic matrix

elements of these operators appear in many applications of HQET, while the coefficients $C_{\rm kin}$ and $C_{\rm spin}$ result from short-distance effects and, in general, depend on the energy scale at which the operators are renormalized. Following power counting arguments, it can be shown that this effective theory is renormalizable at any finite order in $1/m_{\rm Q}$.

A schematic view on the construction of the effective theory for heavy quarks is given in Figure 3.1; for an extensive presentation of the theoretical aspects of HQET and its computational methods and applications, as well as for a guide to the original literature, the reader may consult, for instance, the reviews [42, 43].

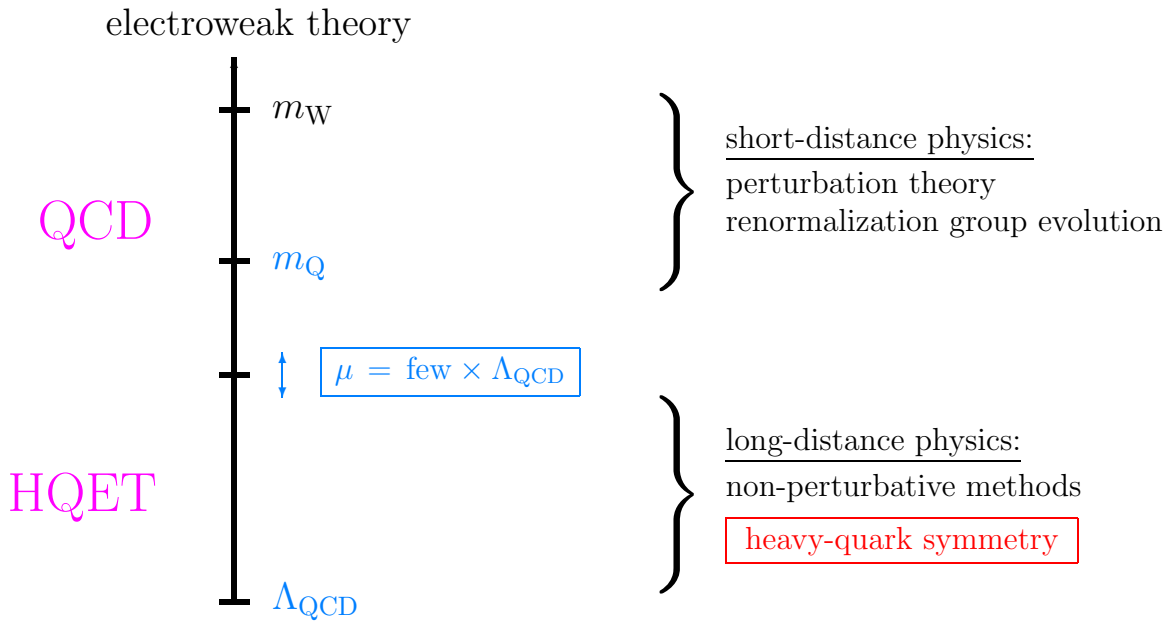

Figure 3.1: Sketch of the construction of HQET.

Problems of the lattice formulation

Being a convenient and successful tool to describe the physics of hadrons containing a heavy quark — while at the same time having in mind the aforementioned difficulty to treat a heavy flavour such as the b-quark directly in numerical simulations —, it appears natural to transfer the effective theory approach to the lattice.

The Lagrangian of HQET in lattice formulation is, to first order in the inverse heavy quark mass $1/m$, formally identical to the continuum one:[20]

$$\mathcal{L}_{\rm HQET}(x) \;=\; \overline{\psi}_{\rm h}(x)\left\{ D_0 + m - \frac{\omega_{\rm kin}}{2m}\,\mathbf{D}^2 - \frac{\omega_{\rm spin}}{2m}\,\sigma\cdot\mathbf{B} \right\}\psi_{\rm h}(x) \;+\; \ldots\ . \qquad (3.2)$$

Here, $\psi_{\rm h}(x)$ is the heavy quark field discretized on the lattice, and only the velocity-zero part is written, since non-vanishing velocities will not be relevant to our discussion;

[20] For short, m is now used as a generic symbol for the heavy quark mass when its precise definition is irrelevant and the renormalized mass needs not to be distinguished from the bare one.

the ellipsis stands for higher-dimensional operators with coefficients of $O(1/m^2)$. As an expansion similar to (3.2) holds for the hadronic matrix elements in question, lattice HQET constitutes a systematic expansion in terms of $1/m_b$ for B-mesons at rest [44] that also has a continuum limit order by order in the $1/m$–expansion.

Despite its favourable theoretical properties, however, lattice HQET has not received so much attention in past non-perturbative investigations of heavy-light physics using numerical simulations. There were mainly two reasons for that:

(i) The rapid growth of statistical errors as the time separation of correlation function is made large. This unwanted feature is already encountered in the lowest-order effective theory (static approximation) and limits a reliable extraction of masses and matrix elements in practice.

(ii) The number of parameters in the effective theory (such as $m, \omega_{\mathrm{spin}}, \ldots$ in eq. (3.2)) does not only increase with the order of the expansion, but they have also to be determined non-perturbatively, since otherwise — as a consequence of the mixings among operators of different dimensions allowed in the cutoff theory (e.g. of $\frac{1}{2m}\,\overline{\psi}_{\mathrm{h}}\mathbf{D}^2\psi_{\mathrm{h}}$ with $\overline{\psi}_{\mathrm{h}}D_0\psi_{\mathrm{h}}$) — one is always left with a perturbative remainder that diverges as $a \to 0$. Hence, these power-law divergences cause the continuum limit not to exist unless the theory is renormalized *non-perturbatively*.

In the subsequent sections I summarize recent work on two concrete applications in the combined static and quenched approximation that reflect significant progress in both directions. These are a determination of the B_s-meson decay constant (Publication H and Publication I), where a correction due to the finite mass of the b-quark is estimated by interpolating between the leading-order HQET result and the D-meson decay constant F_{D_s}, and a fully non-perturbative computation of the mass of the b-quark, which is based on the idea of a *non-perturbative matching of HQET and QCD in finite volume* proposed in Publication J. In both cases, the involved renormalization problems are solved non-perturbatively, and the continuum limit is taken. Apart from being of mere conceptual relevance for the theoretical and practical feasibility of lattice HQET, the results reported there already offer an interesting numerical precision, which can (and will) be further improved in the future.

3.2 Towards a computation of the B-meson decay constant

The issue of enhancing the numerical precision of static-light correlation functions is addressed on our way towards a precision computation of F_{B_s} in quenched QCD as detailed in Publication I and Ref. [45]. To this end, a two-step strategy is employed. First, the decay constant is calculated in lowest order of HQET, and then it is combined with

available results for the pseudoscalar decay constant $F_{\rm PS}(m_{\rm PS})$ in QCD around the charm quark mass region by interpolation in $1/m_{\rm PS}$.

The pseudoscalar decay constant at finite mass is related to the *renormalization group invariant (RGI)* matrix element of the static axial current,

$$\Phi_{\rm RGI} \equiv Z_{\rm RGI} \, \langle \, {\rm PS} \, | \, A_0^{\rm stat} \, | \, 0 \, \rangle \tag{3.3}$$

where in case of the pseudoscalar ${\rm PS} = {\rm B_s}$ the static-light axial vector current reads

$$A_0^{\rm stat}(x) = \overline{\psi}_{\rm s}(x) \gamma_0 \gamma_5 \psi_{\rm b}^{\rm stat}(x) \, , \tag{3.4}$$

through:

$$F_{\rm PS} \sqrt{m_{\rm PS}} = C_{\rm PS} \, (M/\Lambda_{\overline{\rm MS}}) \times \Phi_{\rm RGI} \, + \, {\rm O} \, (1/M) \, . \tag{3.5}$$

Here, M denotes the RGI mass of the heavy quark and $\Lambda_{\overline{\rm MS}}$ the QCD Λ–parameter in the $\overline{\rm MS}$ scheme. The renormalization factor $Z_{\rm RGI}$, turning any bare matrix element of $A_0^{\rm stat}$ into the RGI one, has been non-perturbatively determined in Publication H.

In contrast to the relativistic current, there is no axial Ward identity which protects the renormalized static-light axial current

$$(A_{\rm R}^{\rm stat})_0(x) = Z_{\rm A}^{\rm stat} \, \overline{\psi}_{\rm s}(x) \gamma_0 \gamma_5 \psi_{\rm b}^{\rm stat}(x) \tag{3.6}$$

from a scale dependence: $Z_{\rm A}^{\rm stat} = Z_{\rm A}^{\rm stat}(\mu)$, respectively, $\Phi = \Phi(\mu)$ with Φ being some matrix element of the renormalized static current. The renormalization of the static-light axial current (3.4) thus constitutes a further example for a scale dependent renormalization problem, whose non-perturbative solution was found in Publication H by applying the same finite-size scaling ideas as described in Section 2.2 in conjunction with the calculation of the running QCD coupling and its generalization to arbitrary renormalized matrix elements with an intrinsic multiplicative energy scale dependence.

The function $C_{\rm PS}$ in eq. (3.5) accounts for the fact that in order to extract predictions for QCD from results computed in the effective theory, its matrix elements are to be related to those in QCD at finite quark mass values. In this sense $C_{\rm PS}$ translates to a so-called *'matching scheme'*, which is defined by the condition that matrix elements in the (static) effective theory, renormalized in this scheme and at scale $\mu = m$, equal those in QCD up to $1/m$–corrections. In leading order it is given via the large-mass asymptotics

$$\Phi_{\rm RGI} = \lim_{M \to \infty} \, [\, \ln(M/\Lambda_{\overline{\rm MS}}) \,]^{\gamma_0/(2b_0)} \, F_{\rm PS} \sqrt{m_{\rm PS}} \tag{3.7}$$

with γ_0 and β_0 being the leading-order coefficients in the perturbative expansions of the renormalized static current's anomalous dimension and of the β–function, respectively. Thanks to the recent 3–loop computation of the anomalous dimension of the static axial current [46], the function $C_{\rm PS}(M/\Lambda_{\overline{\rm MS}}) = F_{\rm PS} \sqrt{m_{\rm PS}}/\Phi_{\rm RGI}$ translating a RGI matrix element of $A_0^{\rm stat}$ at infinite mass to the one at finite mass is now known perturbatively up to

and including $\bar{g}^4(\overline{m})$–corrections. From the numerical evaluation as explained and shown in Publication H one can infer that the remaining perturbative uncertainty induced by the conversion factor $C_{\rm PS}$ has become very small.

RGI matrix element in the static theory

As mentioned before, heavy-light correlation functions on the lattice, from which B-physics matrix elements such as the B-meson decay constant in question are obtained at large Euclidean time, are affected by large statistical errors in the static approximation. Their noise-to-signal ratio grows exponentially with the time separation, and in particular for the Eichten-Hill action [44],

$$S_{\rm h} = a^4 \sum_x \overline{\psi}_{\rm h}(x) D_0 \psi_{\rm h}(x)\,, \tag{3.8}$$

this ratio roughly behaves as $\exp\{x_0(E_{\rm stat} - m_\pi)\}$ with $E_{\rm stat}$ the bare ground state energy of a B-meson in the static theory, diverging linearly in the continuum limit.

To overcome this difficulty, a few alternative discretizations of the static theory that retain the O(a) improvement properties of the action (3.8) but lead to a substantial reduction of the statistical fluctuations have been introduced in Publication I. These new static quark actions rely on changes of the form $U(x,0) \to W(x,0)$ of the parallel transporters $U(x,\mu)$ in the covariant derivative

$$D_0\psi_{\rm h}(x) = \frac{1}{a}\left[\,\psi_{\rm h}(x) - U^\dagger(x - a\hat{0},0)\psi_{\rm h}(x - a\hat{0})\,\right]\,, \tag{3.9}$$

where now $W(x,0)$ is a function of the gauge fields in the immediate neighbourhood of x and $x + a\hat{0}$. Its best version employs 'HYP-smearing' that takes for $W(x,0)$ the so-called HYP-link, which is a function of the gauge links located within a hypercube [47]. Comparing the noise-to-signal ratios of a B-meson correlation function in static approximation for the various actions, one then finds that around $x_0 \approx 1.5\,\mathrm{fm}$ more than an order of magnitude can be gained in the case of the alternative discretization with HYP-links w.r.t. to the original Eichten-Hill action and that, in addition, the statistical errors grow only slowly as x_0 is increased. Even more importantly, in Publication I quite the same, small lattice artifacts are observed with the new discretizations.

In the computational setup to determine the bare matrix element $\langle \mathrm{B_s}|A_0^{\rm stat}|0\rangle$ entering eq. (3.3) we use the Schrödinger functional (SF) formulation of QCD with non-perturbatively O(a) improved Wilson actions in the gauge and light (i.e. relativistic) quark sectors. For technical details and the exact definitions of the correlation functions, which are composed out of the light and static quark fields in formal analogy to the relativistic theory surveyed earlier, the reader is again referred to Publications H and I. Here I only record that (in the same way as in the course of the light quark mass determination

outlined in Section 2.4 and derived in detail in Publication E) the matrix element in question can be extracted from a proper ratio of correlators, viz.

$$\langle\, \mathrm{B_s} \,|\, A_0^{\mathrm{stat}} \,|\, 0 \,\rangle \;\propto\; \frac{f_{\mathrm{A}}^{\mathrm{stat}}(x_0)}{\sqrt{f_1^{\mathrm{stat}}}}\, \mathrm{e}^{\,(x_0-T/2)E_{\mathrm{stat}}(x_0)} \tag{3.10}$$

modulo volume factors, where $f_{\mathrm{A}}^{\mathrm{stat}}$ is a proper SF correlation function of the (O(a) improved) static axial current with the quantum numbers of a B-meson and f_1^{stat} is a corresponding boundary-to-boundary correlator, which serves to cancel the renormalization factors of the boundary quark fields. Moreover, wave functions at the boundaries of the SF-cylinder are implemented to construct an interpolating B-meson field that suppresses unwanted contaminations from excited B-meson states to the correlators.

So far, the bare matrix element (3.10) has been calculated for three lattice spacings ($a \approx 0.1\,\mathrm{fm}$, $0.08\,\mathrm{fm}$ and $0.07\,\mathrm{fm}$), and the regularization dependent part of the factor Z_{RGI}, which according to (3.3) must be attached to get the RGI matrix element, has been computed for the new actions as it was done for the Eichten-Hill action in Publication H. The continuum extrapolation quadratic in the lattice spacing of our results stemming from the static action with HYP-links is displayed in the right part of Figure 3.2. To illustrate the gain in precision and control of the systematic errors, I confront our O(a) improved results with an analysis based on older unimproved Wilson data for the same bare matrix element, reproduced from the aforementioned publications in the left part of the figure.

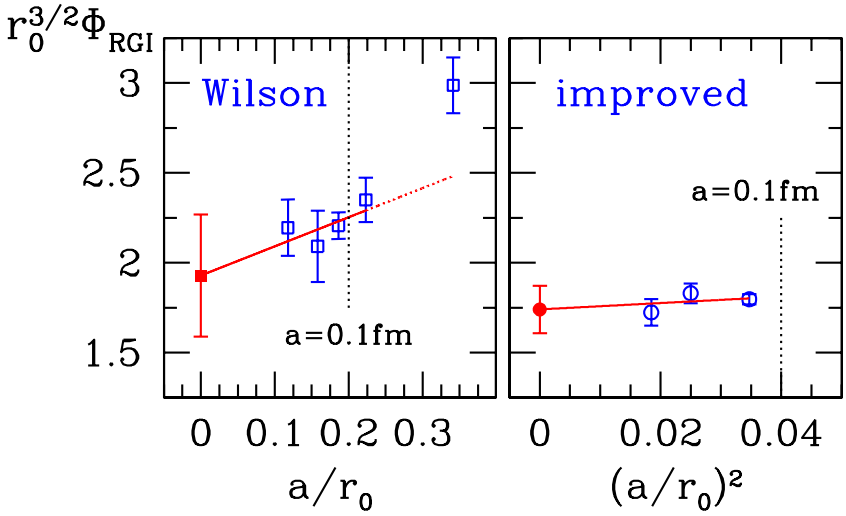

Figure 3.2: RGI matrix element of A_0^{stat}, based on unimproved bare data from the literature (left) and on simulations of the O(a) improved theory with the new discretization of Publication I (right). A continuum extrapolation of the latter yields: $r_0^{3/2}\Phi_{\mathrm{RGI}} = 1.74(13)$.

Extrapolation in the heavy quark mass

To finally arrive at a value for $F_{\mathrm{B_s}}$, we combine Φ_{RGI}, referring to the static limit and thus being independent of the heavy quark mass, with numbers of F_{PS} in the continuum limit at finite values of the quark mass, which have been collected in the context of the (quenched) computation of $F_{\mathrm{D_s}}$ in Refs. [48,49]. In incorporating the mass dependence (3.5) predicted by HQET, we are then led to extrapolate $r_0^{3/2} F_{\mathrm{PS}} \sqrt{m_{\mathrm{PS}}}/C_{\mathrm{PS}}(M/\Lambda_{\overline{\mathrm{MS}}})$ from the charm region to the static estimate $r_0^{3/2}\Phi_{\mathrm{RGI}}$ by a linear fit in $1/(r_0 m_{\mathrm{PS}})$. This interpolation is shown in Figure 3.3, where the zigzag error bands around the relativistic data indicate a small systematic effect that is due to the mass dependence of the discretization errors in the decay constant near the charm quark mass as discussed in [45, 49]. While an extrapolation in $1/(r_0 m_{\mathrm{PS}})$ from the charm region without the constraint through the static approximation would look similar, it is obvious that the *interpolation* is much safer, since extrapolating to the (quite distant) $\mathrm{B_s}$-meson scale depends significantly on the functional form assumed.

Using $m_{\mathrm{B_s}} = 5.4\,\mathrm{GeV}$, $r_0 = 0.5\,\mathrm{fm}$ and the numerical perturbative value of the matching factor $C_{\mathrm{PS}}(M_{\mathrm{b}}/\Lambda_{\overline{\mathrm{MS}}})$ in eq. (3.5) translating to finite b-quark mass, one finds from the interpolation to $1/(r_0 m_{\mathrm{B_s}})$ in Figure 3.3 as a present result [45]

$$r_0 F_{\mathrm{B_s}} = 0.52(3) \quad \rightarrow \quad F_{\mathrm{B_s}} = 206(10)\,\mathrm{MeV}\,. \tag{3.11}$$

This number includes all errors except for the quenched approximation; the (unavoidable) scale ambiguity introduced by this approximation can be estimated to be about 12%.

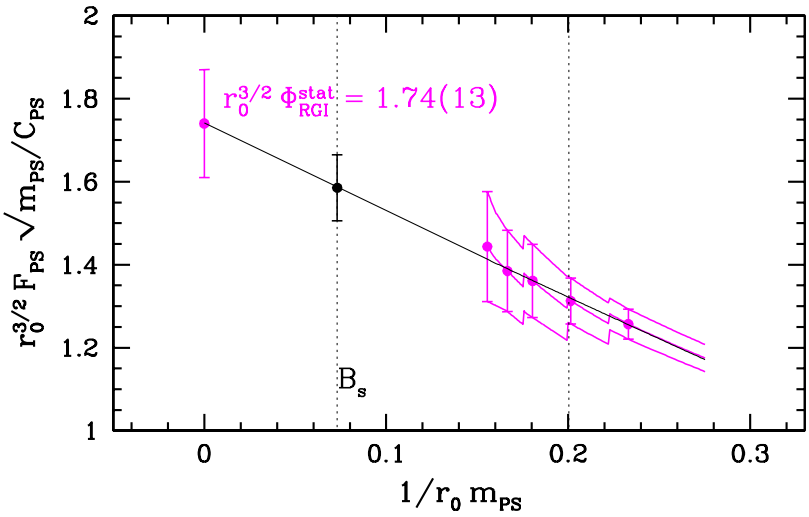

Figure 3.3: Interpolation in the inverse heavy-strange meson mass, m_{PS}, between the RGI matrix element of the static axial current and relativistic data around the charm quark mass. (The latter are taken from Refs. [48, 49]).

3.3 Non-perturbative renormalization of HQET

The second of the problems exposed at the end of Section 3.1, which so far hampered the use of HQET on the lattice, is the occurrence of power-law divergences in the lattice spacing upon renormalization of the parameters in the effective Lagrangian (3.2). It already shows up in the static approximation and thereby affects, for instance, the computation of the mass of the b-quark in leading order of HQET. In this case the kinetic and the mass terms in the static action mix under renormalization and give rise to a local mass counterterm $\delta m \propto 1/a$, the self-energy of the static quark, which implies a linearly divergent truncation error if one relies on an only perturbative subtraction of this divergence. Therefore, past lattice computations in the framework of HQET could not reach the continuum limit [50, 51].

The idea: Matching in small volume

A strategy for a solution to this longstanding problem, which offers the opportunity to perform clean, non-perturbative calculations in HQET, was developed and first presented in Ref. [52]. This strategy is worked out and implemented in Publications J and K and basically consists of three parts that I want to briefly describe in the following by sketching the computation of the b-quark's mass as an example:

1.) Renormalization of the effective theory amounts to relate the parameters of the HQET Lagrangian to those of QCD, a step usually called *matching*. In order to realize the matching in a *non-perturbative* way, one imposes matching conditions of the form

$$\Phi^{\mathrm{HQET}}(L_0, M) = \Phi^{\mathrm{QCD}}(L_0, M) \,+\, \mathrm{O}\,(1/M)\;, \tag{3.12}$$

in a *physically small volume* of linear extent $L_0 = \mathrm{O}(0.2\,\mathrm{fm})$, for suitably chosen observables Φ^{HQET} and Φ^{QCD} in HQET and QCD to be calculated with the aid of numerical simulations. The finiteness of the matching volume ensures that lattice resolutions satisfying $am_{\mathrm{b}} \ll 1$ are possible and the b-quark can be treated as standard relativistic fermion, whereby at the same time the energy scale $1/L_0 = \mathrm{O}(1\,\mathrm{GeV})$ is still significantly below m_{b} and HQET applies quantitatively. Figure 3.4 illustrates this idea. Of course, owing to the very construction of the effective theory, it is clear that the matching conditions (3.12) must also carry a dependence on the heavy quark mass. (For convenience, we now identify the heavy quark mass parameter with the scheme and scale independent renormalization group invariant mass, M, see eq. (2.45) in Section 2.4.) Thus, in determining the parameters of the effective theory from those of QCD via such a non-perturbative matching in finite volume — while maintaining the physical quark mass dependence in QCD since its Lagrangian is blind to the finiteness of the volume —, the predictive power of QCD is transferred to HQET.

To sacrifice as little predictability of the theory as can be, the quantities Φ should not be experimental observables but certain renormalized quantities calculable in the continuum limit of lattice QCD. In the concrete case of the b-quark mass computation, definite choices for Φ have to be made to formulate a sensible matching condition between the quark mass in the full, relativistic theory (QCD) and HQET. Those are $\Gamma(L, M_\mathrm{b})$, denoting the energy of a state with the quantum numbers of a B-meson but defined in a *small volume* of extent L, and $\Gamma_\mathrm{stat}(L)$ as its counterpart in (leading order of) the effective theory. As detailed in Publications J and K, both can be expressed as logarithmic derivatives of appropriate finite-volume, heavy- and static-light correlation functions, respectively, and numerically evaluated with high precision.

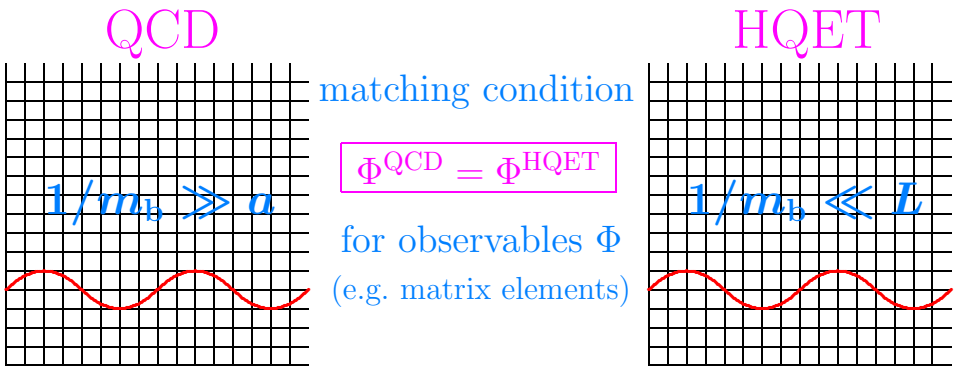

Figure 3.4: Non-perturbative matching of HQET and QCD in a finite volume: The lattice setup is arranged such that the Compton wavelength of the b-quark (red solid line) still just fits into a box, which is small enough for this wavelength to be reasonably resolved without exceeding the number of lattice points manageable in a numerical simulation. In this way, via certain matching conditions, the parameters of the effective theory are fixed through its relation to QCD observables in small volume.

2.) Next we need to establish a connection to a physical situation, where observables of the infinite-volume theory such as masses or matrix elements are accessible at the end. The accompanying gap between the small volume with its fine lattice resolution, where the matching of HQET and QCD is done, on the one side and larger lattice spacings (and also larger volumes) on the other is bridged by a few recursive finite-size scaling steps, which are inspired by the procedure reviewed in Section 2.3 to probe the running of the QCD coupling: The volume to compute the quantity $\Gamma_\mathrm{stat}(L)$ in HQET is iteratively enlarged until one reaches a volume of linear extent $L = \mathrm{O}(1\,\mathrm{fm})$ so that, at the same resolutions a/L (i.e. at the same bare parameters) met there, *large volumes* with $L \approx 2\,\mathrm{fm}$ to accommodate physical observables of the infinite-volume theory eventually become affordable. Also note that, apart from terms of $\mathrm{O}(1/(L_0 M_\mathrm{b})^{n+1})$ if considering HQET up to order n, any dependence on the unphysical small-volume physics is gone.

3.) Finally, a physical, dimensionful input is still missing. In the case at hand this means to link the energy Γ_stat, which turns into the B-meson's static binding energy,

$E_{\rm stat}$, as the volume grows, to the mass of the B-meson as the physical observable in large volume whose numerical value is taken from experiment.

An application: The mass of the b-quark

To join the foregoing three steps, we have to recall that energies in the effective theory differ from the corresponding ones in QCD by a linearly divergent mass shift $m_{\rm bare}$, which has its origin in the mixing of $\overline{\psi}_{\rm h} D_0 \psi_{\rm h}$ with the lower-dimensional operator $\overline{\psi}_{\rm h}\psi_{\rm h}$ under renormalization — the central problem we started from. As a consequence of its universality (i.e. its independence of the state), however, $m_{\rm bare}$ obeys at any fixed lattice spacing

$$m_{\rm B} = E_{\rm stat} + m_{\rm bare}\,, \tag{3.13}$$

$$\Gamma(L, M_{\rm b}) = \Gamma_{\rm stat}(L) + m_{\rm bare}\,. \tag{3.14}$$

Imposing eq. (3.14) for $L = L_0$ as the non-perturbative matching condition in small volume implicitly determines the parameter $m_{\rm bare}$ and may hence be exploited to replace it in eq. (3.13). Then, after adding and subtracting a term $\Gamma_{\rm stat}(L_2)$ (where $L_2 = 2^2 L_0 \approx 1\,\mathrm{fm}$ with lattice spacings commonly used in large-volume simulations), the resulting equation may be cast into the basic formula

$$m_{\rm B} = \underbrace{E_{\rm stat} - \Gamma_{\rm stat}(L_2)}_{a \to 0 \text{ in HQET}} + \underbrace{\Gamma_{\rm stat}(L_2) - \Gamma_{\rm stat}(L_0)}_{a \to 0 \text{ in HQET}} + \underbrace{\Gamma(L_0, M_{\rm b})}_{a \to 0 \text{ in QCD}} + \mathrm{O}\left(\Lambda^2/M_{\rm b}\right) \tag{3.15}$$

(with Λ the typical low-energy QCD scale), where the terms are just arranged such that the unknown $m_{\rm bare}$ cancels in the energy differences,

$$\Delta E \equiv E_{\rm stat} - \Gamma_{\rm stat}(L_2) \qquad \text{and} \qquad \Gamma_{\rm stat}(L_2) - \Gamma_{\rm stat}(L_0)\,, \tag{3.16}$$

and the continuum limit exists separately for each of the pieces entering eq. (3.15). The physical picture underlying the 'master equation' (3.15) is illustrated in Figure 3.5.

The entire heavy quark mass dependence is contained in $\Gamma(L_0, M)$, defined in QCD with a relativistic b-quark. This mass dependence has been non-perturbatively mapped out in Publication K, where as a particular ingredient of the numerical calculation, which demands to keep fixed the dimensionless RGI heavy quark mass while approaching the continuum limit, the knowledge of several renormalization factors and improvement coefficients relating the bare to the RGI quark mass is required. Although they were already available in some (but quite distant) region of parameter space, it was desirable to improve their precision and to estimate them directly in the bare coupling range relevant for the present application. These necessary renormalization factors and improvement coefficients were determined in Publication K and, as exemplified in Figure 3.6 taken from

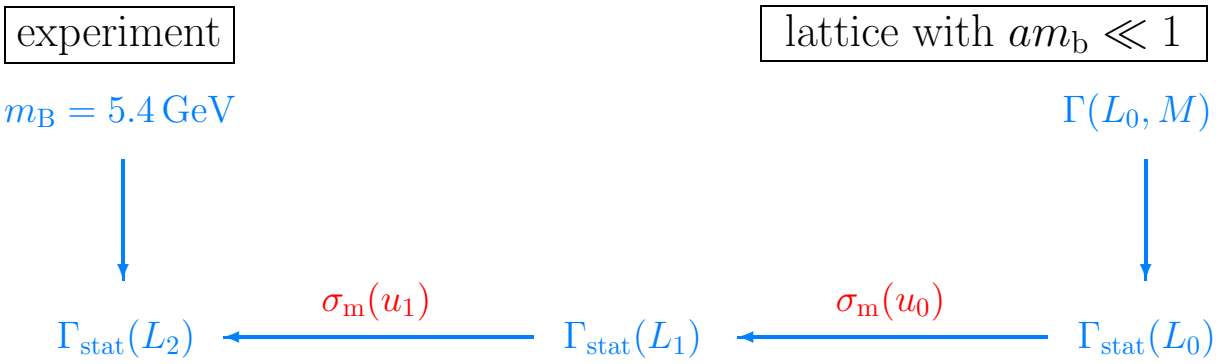

Figure 3.5: Connecting the matching condition in small volume to physical observables in large volumes by a recursive finite-size technique. The quantity σ_m represents the associated step scaling function, defined as $\sigma_\mathrm{m}(u) \equiv 2L \times [\,\Gamma_\mathrm{stat}(2L) - \Gamma_\mathrm{stat}(L)\,]$.

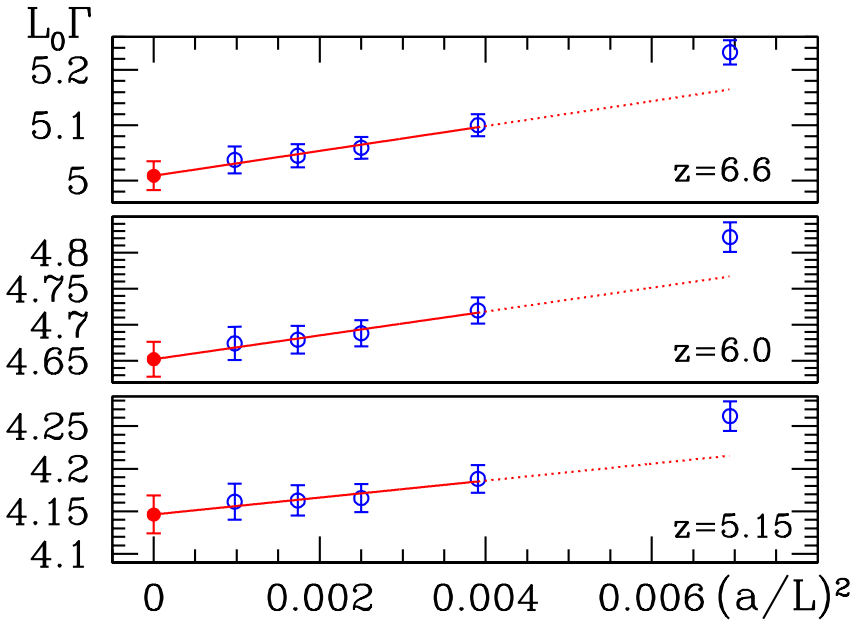

Figure 3.6: Continuum limit extrapolations of $L_0\Gamma(L_0, M)$ in relativistic QCD and in a small volume (of linear extent $L_0 \approx 0.2\,\mathrm{fm}$) for representative values of $z \equiv L_0 M$.

there, performing controlled continuum extrapolations provides $\omega \equiv \lim_{a/L\to 0} L_0\Gamma(L_0, M)$ as function of $z \equiv L_0 M$.

In view of eq. (3.15), the b-quark mass may now be extracted from the interception point of $\omega(z)$ with the combination

$$\begin{aligned} \omega_\mathrm{stat} &\equiv L_0 m_\mathrm{B} - L_0\,\{\Gamma_\mathrm{stat}(L_2) - \Gamma_\mathrm{stat}(L_0)\} - L_0\Delta E \\ &= L_0 m_\mathrm{B} - \left\{\tfrac{1}{2}\sigma_\mathrm{m}(u_0) + \tfrac{1}{4}\sigma_\mathrm{m}(u_1)\right\} - L_0\Delta E\,, \end{aligned} \tag{3.17}$$

σ_m denoting the step scaling function introduced in Figure 3.5. The associated graph

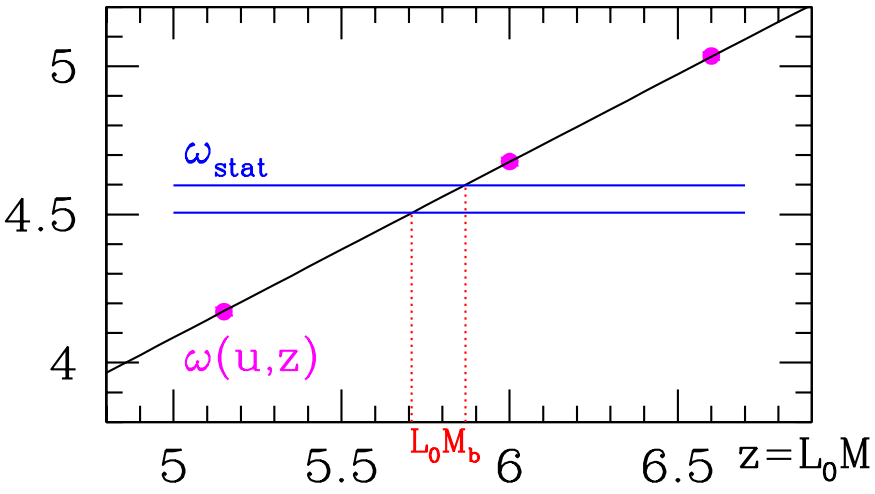

Figure 3.7: Solution of eq. (3.15) for the dimensionless RGI b-quark mass, $L_0 M_\mathrm{b}$. (As explained in Publications J and K, the argument u of ω simply indicates that during the computation one had to work at a certain fixed value of the renormalized SF coupling.)

is reproduced from Publication J in Figure 3.7, where for the time being the analysis was restricted to unimproved Wilson fermion data for the subtracted, dimensionless $\mathrm{B_s}$–meson energy aE_stat from the literature; this results in $L_0\Delta E = 0.46(5)$. Then we obtain in combined static and quenched approximations:

$$r_0 M_\mathrm{b} = 16.12(29) \quad \rightarrow \quad \overline{m}_\mathrm{b}^{\overline{\mathrm{MS}}}\left(\overline{m}_\mathrm{b}^{\overline{\mathrm{MS}}}\right) = 4.12(8)\,\mathrm{GeV}\,, \tag{3.18}$$

up to corrections of $\mathrm{O}(\Lambda^2/M_\mathrm{b}) = \mathrm{O}(\Lambda/(L_0 M_\mathrm{b}))$. However, from a — not yet finally completed — evaluation of aE_stat with the alternative static action discussed in Section 3.2 (which also has linear $\mathrm{O}(a)$ lattice artifacts removed), one can already anticipate that a continuum limit of $L_0\Delta E$ with by a factor about 3 smaller error is within reach and, therefore, will still substantially enhance the accuracy of the result (3.18).

3.4 Non-perturbative tests of the effective theory

Although it is generally accepted (and also supported, though in a more indirect way, by the satisfactory leading-order calculations just described) that HQET represents an effective theory for QCD, quantitative tests of this equivalence are rare and mostly based on phenomenological analyses of experimental results. A direct, pure theory test can only be performed, however, if QCD including a sufficiently heavy quark can be simulated on the lattice at lattice resolutions which are fine enough to be able to take the continuum limit. This has been achieved in Publication L, and I conclude my review of non-perturbative computations in HQET with a brief summary of this work.

On the QCD side of these tests we adopt the same setup as in Section 3.3 and exploit the fact that lattice spacings such that $am_\mathrm{b} \ll 1$ can be reached if one puts the theory

in a finite volume, $L^3 \times T$, with L and T not too large. Here, $T = L$ and once more, for various practical reasons, Schrödinger functional boundary conditions are chosen. As has been shown in [53], equivalent boundary conditions are easily imposed in the effective theory, and SF correlation functions are constructed as already sketched around eq. (2.33) in Section 2.4 before, but now in a situation where one quark flavour is light ('l') and the other one is either heavy ('b') or treated in the effective theory ('h'). After these preparations it becomes possible to quantitatively investigate the heavy quark mass dependence of current matrix elements and energies, which are derived from heavy-light meson correlation functions and calculated over a wide range of quark masses in the continuum limit. Then, by a precise comparison of these observables as functions of the heavy quark mass with the predictions of HQET, one is able to verify that their large quark mass behaviour is described by the effective theory and, in addition, first non-perturbative estimates on the size of the $1/m$–corrections to the static theory may be obtained.

Illustration

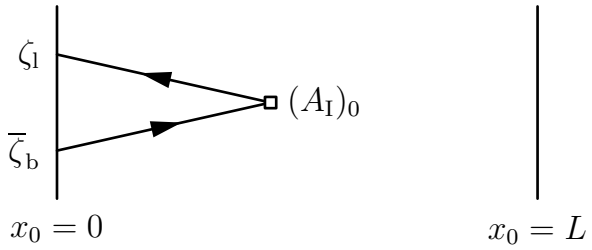

Figure 3.8: The correlation function $f_{\rm A}$. In case of $f_{\rm A}^{\rm stat}$, the operator in the bulk is $(A_{\rm I}^{\rm stat})_0$ connected to $\overline{\zeta}_{\rm h}$ (instead of $\overline{\zeta}_{\rm b}$) by a static quark propagator.

As an example let us consider correlation functions built from boundary quark fields ζ (located at $x_0 = 0$) and the time component of the axial current as composite field in the bulk ($0 < x_0 < T$), both in the relativistic and in the static effective theory:

$$f_{\rm A}(x_0) = -\frac{a^6}{2}\sum_{\mathbf{y},\mathbf{z}} \left\langle (A_{\rm I})_0(x)\, \overline{\zeta}_{\rm b}(\mathbf{y})\gamma_5\zeta_{\rm l}(\mathbf{z})\right\rangle , \tag{3.19}$$

$$f_{\rm A}^{\rm stat}(x_0) = -\frac{a^6}{2}\sum_{\mathbf{y},\mathbf{z}} \left\langle (A_{\rm I}^{\rm stat})_0(x)\, \overline{\zeta}_{\rm h}(\mathbf{y})\gamma_5\zeta_{\rm l}(\mathbf{z})\right\rangle . \tag{3.20}$$

The SF correlator $f_{\rm A}$ is schematically drawn in Figure 3.8. The quark bilinears $A_{\rm I}$ and $A_{\rm I}^{\rm stat}$ are the O(a) improved versions of the axial current in QCD and in the effective theory, respectively, for which lattice artifacts linear in the lattice spacing are absent. In order to form suitable ratios such as

$$Y_{\rm PS}(L,M) \equiv Z_{\rm A}\,\frac{f_{\rm A}(L/2)}{\sqrt{f_1}}\bigg|_{T=L} , \tag{3.21}$$

in which the renormalization factors of the boundary fields cancel, we again need another correlation function, f_1, that traces the propagation of a quark-antiquark pair from the $x_0 = 0$ to the $x_0 = T$ boundary. As worked out in Publication L, eq. (3.21) gives rise to a representation of $Y_{\rm PS}$ as a matrix element of the axial current between a normalized state $|B(L)\rangle$ with the quantum numbers of a B-meson and $|\Omega(L)\rangle$ having vacuum quantum numbers, while their time evolution $\propto \mathrm{e}^{-LH/2}$ ensures that both of these states are dominated by energy eigenstates with energies around $2/L$ and less. From this we infer that HQET is applicable if $1/L \ll M$ (and, of course, $\Lambda \ll M$ too).[21]

For fixed $L\Lambda_{\overline{\rm MS}}$ we hence expect

$$Y_{\rm PS}(L,M)/C_{\rm PS}\,(M/\Lambda_{\overline{\rm MS}}) = X_{\rm RGI}(L) \,+\, \mathrm{O}\,(1/z)\;, \quad z = LM\,, \tag{3.22}$$

where the $1/M$–corrections are written in the dimensionless variable $1/z$ and $X_{\rm RGI}$ is defined as $Y_{\rm PS}$ but at lowest order in the effective theory and renormalized according to eq. (3.3) in Section 3.2. Relations such as (3.22), however, are only expected to hold *after* the continuum limits of both sides have been taken separately. For the case of $Y_{\rm PS}(L,M)$ at hand, this is done by (i) fixing a value u_0 for the renormalized SF coupling $\bar{g}^2(L_0 \approx 0.2\,\mathrm{fm})$ at vanishing light quark mass, (ii) a determination of the bare coupling from the condition $\bar{g}^2(L_0) = u_0$ for a given L/a, (iii) fixing the (O(a) improved) subtracted bare quark mass $\widetilde{m}_{\rm q}$ of the heavy quark such that $LM = z$ using the known renormalization factor $Z_{\rm m}$ in $M = Z_{\rm m}\widetilde{m}_{\rm q}$ (see Ref. [22] and Publication K), (iv) an evaluation of $Y_{\rm PS}$ by Monte Carlo and subsequently repeating (i)–(iii) for better resolutions a/L, and followed by (v) an extrapolation to the continuum limit.

The continuum extrapolation of $Y_{\rm PS}(L,M)$ is shown in the left panel of Figure 3.9. As can be seen in the figure, the continuum extrapolation becomes more difficult as the mass of the heavy quark is increased and O($(aM)^2$) discretization errors become more and more important. By contrast, the continuum extrapolation in the static effective theory (not reproduced here) turns out to be much easier, particularly owing to the renormalization factor relating the bare to the RGI current, which was non-perturbatively determined in Publication H. After the continuum limit has been taken, the finite-mass QCD observable $Y_{\rm PS}(L,M)/C_{\rm PS}(M/\Lambda_{\overline{\rm MS}})$ is compatible with smoothly approaching, as $1/z \to 0$, the leading-order prediction from the effective theory. The right panel of Figure 3.9 clearly illustrates this. It also makes evident that the perturbative $C_{\rm PS}$ reduces the mass dependence of $Y_{\rm PS}$ significantly; the coefficients of the $1/z^n$–terms in the polynomial fits to the finite-mass results are roughly of order unity, and thus the corrections are reasonably small.

In Publication L, several successful tests in a very similar spirit were actually performed: one of them — due to a property called reparameterization invariance [54] — even

[21] Recall that M denotes the renormalization group invariant (heavy) quark mass and Λ the QCD Λ–parameter in some generic scheme.

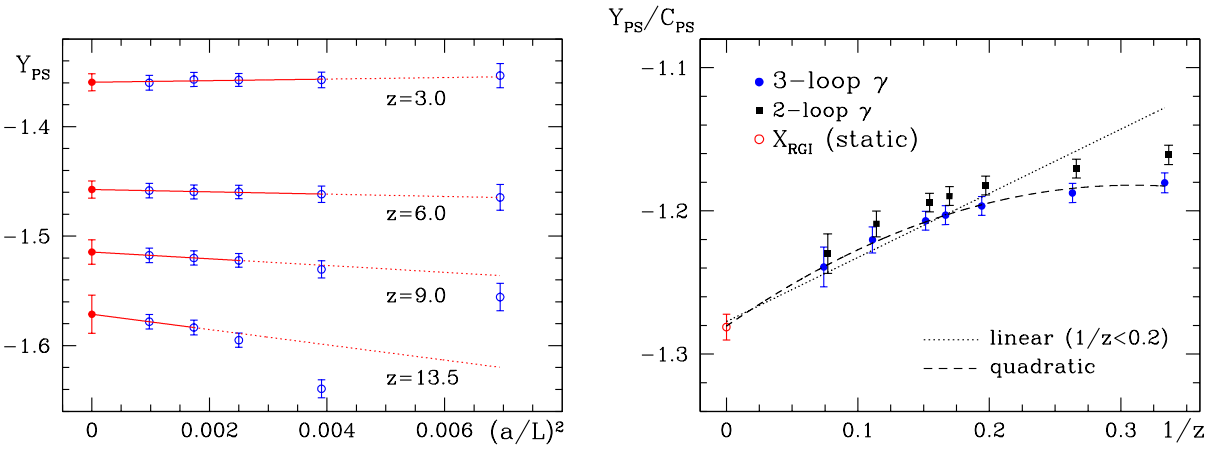

Figure 3.9: Testing eq. (3.22) through numerical simulations in the quenched approximation and for $L \approx 0.2\,\mathrm{fm}$ (Publication L). *Left*: Continuum extrapolations of $Y_{\mathrm{PS}}(L, M)$ for z–values spanning the entire range of z. *Right*: Polynomial fits in $1/z$ of $Y_{\mathrm{PS}}(L, M)/C_{\mathrm{PS}}(M/\Lambda_{\overline{\mathrm{MS}}})$ to quantify deviations from the static limit. C_{PS} uses the two- and the three-loop anomalous dimension of the static axial current.

free of any remaining perturbative uncertainty that a conversion function such as C_{PS} in eq. (3.22) still might introduce, and two others with the associated static (i.e. $M \to \infty$) limits known from the heavy quark spin symmetry of HQET. Despite finite-mass lattice QCD results have been confronted with the static limit over the years, the new features of the tests discussed in this work are that the composite fields were renormalized non-perturbatively throughout and that, by studying the theory in a small volume, the continuum limit could be taken at *large* quark masses.

3.5 Outlook

By virtue of recent theoretical as well as technical advances, non-perturbative calculations using the lattice regularized heavy quark effective theory have reached a new quality. As demonstrated by both applications discussed in the previous subsections, the determination of the $\mathrm{B_s}$-meson decay constant and of the b-quark mass, the status of non-perturbative HQET at lowest order in $1/m$ has become satisfactory in the quenched approximation. And still, there is some room for reducing the quoted uncertainties of the numerical results further.

Since it is one of the benefits of the theoretical concepts addressed here that describing the b-quark by an *effective theory* circumvents the need for prohibitively large lattices — because it completely eliminates the mass scale of the b-quark — it is worth to also emphasize at this point the interesting potential of these methods for systematic and (at least partly) straightforward extensions. First, applying them to the theory incorporating dynamical fermions is possible without major obstacles, apart from the 'usual' problems with the light quarks that have to be solved. Moreover, one has to note that lowest-order results as those reported above are by themselves not expected to have an interesting

precision for phenomenological applications, though for sure they can not only constrain the large-mass behaviour computed with other methods but do also help, through *inter*polation between data obtained in QCD and in the static limit, to render results (such as the one for $F_{\mathrm{B_s}}$ presented in Section 3.2) almost independent of any effective theory. Therefore, a second direction appears even more important: going beyond the static approximation by inclusion of $1/m$–corrections.

In principle, $1/m$–corrections can be calculated in the effective theory. The general matching strategy between HQET and QCD (cf. Section 3.3) to solve renormalization problems in HQET entirely non-perturbatively, while taking the continuum limit in all steps involved, as well as the use of modified static actions that in the static approximation have already proven to enable the computation of B-meson lattice correlation functions with good statistical precision for $x_0 > 1\,\mathrm{fm}$, are designed to also cope with the sub-leading order in the HQET expansion. These ingredients make us believe in promising perspectives for an inclusion of $1/m_{\mathrm{b}}$–corrections that will hopefully lead to further considerable improvements in applying non-perturbative HQET and thereby would have a great impact on the achievable precision in B-physics computations employing HQET.

References

[1] S. Bethke, *Determination of the QCD coupling α_s*, J. Phys. **G26** (2000) R27, [hep-ex/0004021].

[2] S. Bethke, *α_s at Zinnowitz 2004*, Nucl. Phys. Proc. Suppl. **135** (2004) 345, [hep-ex/0407021].

[3] Komitee für Elementarteilchenphysik KET, *Teilchenphysik in Deutschland — Status und Perspektiven*, 2002. http://www.dpg-fachgremien.de/t/ket/ket.html.

[4] K. G. Wilson, *Confinement of quarks*, Phys. Rev. **D10** (1974) 2445.

[5] I. Montvay and G. Münster, *Quantum Fields on a Lattice*. Cambridge University Press, Cambridge, 1st ed., 1994.

[6] J. Smit, *Introduction to quantum fields on a lattice: A robust mate*, Cambridge Lect. Notes Phys. **15** (2002) 1–271.

[7] K. Symanzik, *Continuum limit and improved action in lattice theories: 1. Principles and ϕ^4 theory*, Nucl. Phys. **B226** (1983) 187.

[8] K. Symanzik, *Continuum limit and improved action in lattice theories: 2. O(N) non-linear sigma model in perturbation theory*, Nucl. Phys. **B226** (1983) 205.

[9] M. Lüscher, S. Sint, R. Sommer, and P. Weisz, *Chiral symmetry and O(a) improvement in lattice QCD*, Nucl. Phys. **B478** (1996) 365, [hep-lat/9605038].

[10] B. Sheikholeslami and R. Wohlert, *Improved continuum limit lattice action for QCD with Wilson fermions*, Nucl. Phys. **B259** (1985) 572.

[11] M. Bochicchio, L. Maiani, G. Martinelli, G. C. Rossi, and M. Testa, *Chiral symmetry on the lattice with Wilson fermions*, Nucl. Phys. **B262** (1985) 331.

[12] L. Maiani and G. Martinelli, *Current algebra and quark masses from a Monte Carlo simulation with Wilson fermions*, Phys. Lett. **B178** (1986) 265.

[13] **ALPHA** Collaboration, M. Lüscher, S. Sint, R. Sommer, and H. Wittig, *Non-perturbative determination of the axial current normalization constant in O(a) improved lattice QCD*, Nucl. Phys. **B491** (1997) 344, [hep-lat/9611015].

[14] H. B. Nielsen and M. Ninomiya, *No-go theorem for regularizing chiral fermions*, Phys. Lett. **B105** (1981) 219.

[15] M. Lüscher, *Chiral gauge theories revisited*, Lectures given at *International School of Subnuclear Physics, 38th Course: Theory and Experiment Heading for New Physics, Erice*, Italy, 27 August – 5 September 2000 [hep-th/0102028].

[16] M. Lüscher, *Advanced lattice QCD*, Lectures given at *Les Houches Summer School in Theoretical Physics, Probing the Standard Model of Particle Interactions*, Les Houches, France, 28 July – 5 September 1997 [hep-ph/9802029].

[17] M. Lüscher, P. Weisz, and U. Wolff, *A numerical method to compute the running coupling in asymptotically free theories*, Nucl. Phys. **B359** (1991) 221.

[18] M. Lüscher, R. Narayanan, P. Weisz, and U. Wolff, *The Schrödinger functional: A renormalizable probe for non-abelian gauge theories*, Nucl. Phys. **B384** (1992) 168, [hep-lat/9207009].

[19] K. Symanzik, *Schrödinger representation and Casimir effect in renormalizable quantum field theory*, Nucl. Phys. **B190** (1981) 1.

[20] S. Sint, *On the Schrödinger functional in QCD*, Nucl. Phys. **B421** (1994) 135, [hep-lat/9312079].

[21] S. Sint, *One-loop renormalization of the QCD Schrödinger functional*, Nucl. Phys. **B451** (1995) 416, [hep-lat/9504005].

[22] **ALPHA** Collaboration, S. Capitani, M. Lüscher, R. Sommer, and H. Wittig, *Non-perturbative quark mass renormalization in quenched lattice QCD*, Nucl. Phys **B544** (1999) 669, [hep-lat/9810063].

[23] **ALPHA** Collaboration, J. Heitger, H. Simma, R. Sommer, and U. Wolff, *The Schrödinger functional coupling in quenched QCD at low energies*, Nucl. Phys. Proc. Suppl. **106** (2002) 859–861, [hep-lat/0110201].

[24] M. Lüscher, R. Sommer, P. Weisz, and U. Wolff, *A precise determination of the running coupling in the SU(3) Yang-Mills theory*, Nucl. Phys. **B413** (1994) 481, [hep-lat/9309005].

[25] **ALPHA** Collaboration, A. Bode, R. Frezzotti, B. Gehrmann, M. Hasenbusch, J. Heitger, K. Jansen, S. Kurth, J. Rolf, H. Simma, S. Sint, R. Sommer, P. Weisz, H. Wittig, and U. Wolff, *First results on the running coupling in QCD with two massless flavours*, Phys. Lett. **B515** (2001) 49, [hep-lat/0105003].

[26] U. Block, A. Frommer, and G. Mayer, *Block coloring schemes for the SOR method on local memory parallel computers*, Parallel Computing **14** (1990) 61.

[27] R. Sommer, *A new way to set the energy scale in lattice gauge theories and its applications to the static force and $\alpha_{\rm s}$ in SU(2) Yang-Mills theory*, Nucl. Phys. **B411** (1994) 839, [hep-lat/9310022].

[28] J. Gasser and H. Leutwyler, *Quark masses*, Phys. Rept. **87** (1982) 77.

[29] H. Leutwyler, *The ratios of the light quark masses*, Phys. Lett. **B378** (1996) 313, [hep-ph/9602366].

[30] **ALPHA** Collaboration, J. Rolf and S. Sint, *A precise determination of the charm quark's mass in quenched QCD*, J. High Energy Phys. **12** (2002) 007, [hep-ph/0209255].

[31] J. Gasser and H. Leutwyler, *Chiral perturbation theory to one loop*, Ann. Phys. **158** (1984) 142.

[32] K. Jansen, *Actions for dynamical fermion simulations: Are we ready to go?*, Nucl. Phys. Proc. Suppl. **129** (2004) 3, [hep-lat/0311039].

[33] D. B. Kaplan and A. V. Manohar, *Current mass ratios of the light quarks*, Phys. Rev. Lett. **56** (1986) 2004.

[34] A. G. Cohen, D. B. Kaplan, and A. E. Nelson, *Testing $m_{\rm u} = 0$ on the lattice*, J. High Energy Phys. **11** (1999) 027, [hep-lat/9909091].

[35] **UKQCD** Collaboration, A. C. Irving, C. McNeile, C. Michael, K. J. Sharkey, and H. Wittig, *Is the up quark massless?*, Phys. Lett. **B518** (2001) 243, [hep-lat/0107023].

[36] D. R. Nelson, G. T. Fleming, and G. W. Kilcup, *Is strong CP due to a massless up quark?*, Phys. Rev. Lett. **90** (2003) 021601, [hep-lat/0112029].

[37] C. Bernard *et. al.*, *Panel discussion on chiral extrapolation of physical observables*, Nucl. Phys. Proc. Suppl. **119** (2003) 170, [hep-lat/0209086].

[38] **qq+q** Collaboration, F. Farchioni, I. Montvay, and E. Scholz, *Quark mass dependence of pseudoscalar masses and decay constants on a lattice*, Eur. Phys. J. **C37** (2004) 197, [hep-lat/0403014].

[39] K.-I. Ishikawa, *Hadron spectrum from dynamical lattice QCD simulations*, Nucl. Phys. Proc. Suppl. **140** (2005) 20, [hep-lat/0410050].

[40] O. Bär, *Chiral perturbation theory at non-zero lattice spacing*, Nucl. Phys. Proc. Suppl. **140** (2005) 106, [hep-lat/0409123].

[41] S. Stone, *Experimental results in heavy flavor physics*, Plenary talk at International Europhysics Conference on High-Energy Physics (HEP 2003), Aachen, Germany, 17 – 23 July 2003, Eur. Phys. J. **C33** (2004) S129, [hep-ph/0310153].

[42] M. Neubert, *Heavy quark symmetry*, Phys. Rept. **245** (1994) 259, [hep-ph/9306320].

[43] T. Mannel, *Effective theory for heavy quarks*, Lectures given at *35th Internationale Universitätswochen für Kern- und Teilchenphysik*, Schladming, Austria, 2 – 9 March 1996 [hep-ph/9606299].

[44] E. Eichten and B. Hill, *An effective field theory for the calculation of matrix elements involving heavy quarks*, Phys. Lett. **B234** (1990) 511.

[45] **ALPHA** Collaboration, J. Rolf, M. Della Morte, S. Dürr, J. Heitger, A. Jüttner, H. Molke, A. Shindler, and R. Sommer, *Towards a precision computation of $F_{\mathrm{B_s}}$ in quenched QCD*, Nucl. Phys. Proc. Suppl. **129** (2004) 322, [hep-lat/0309072].

[46] K. G. Chetyrkin and A. G. Grozin, *Three-loop anomalous dimension of the heavy-light quark current in HQET*, Nucl. Phys. **B666** (2003) 289, [hep-ph/0303113].

[47] A. Hasenfratz and F. Knechtli, *Flavor symmetry and the static potential with hypercubic blocking*, Phys. Rev. **D64** (2001) 034504, [hep-lat/0103029].

[48] **ALPHA** Collaboration, A. Jüttner and J. Rolf, *A precise determination of the decay constant of the D_{s} meson in quenched QCD*, Phys. Lett. **B560** (2003) 59, [hep-lat/0302016].

[49] A. Jüttner and J. Rolf, *A precise determination of the decay constant of the D_{s} in quenched QCD*, Nucl. Phys. Proc. Suppl. **129** (2004) 319, [hep-lat/0309069].

[50] S. M. Ryan, *Heavy quark physics from lattice QCD*, Nucl. Phys. Proc. Suppl. **106** (2002) 86, [hep-lat/0111010].

[51] L. Lellouch, *Phenomenology from lattice QCD*, Nucl. Phys. Proc. Suppl. **117** (2003) 127, [hep-ph/0211359].

[52] **ALPHA** Collaboration, J. Heitger and R. Sommer, *A strategy to compute the b-quark mass with non-perturbative accuracy*, Nucl. Phys. Proc. Suppl. **106** (2002) 358, [hep-lat/0110016].

[53] **ALPHA** Collaboration, M. Kurth and R. Sommer, *Renormalization and O(a) improvement of the static axial current*, Nucl. Phys. **B597** (2001) 488, [hep-lat/0007002].

[54] M. E. Luke and A. V. Manohar, *Reparametrization invariance constraints on heavy particle effective field theories*, Phys. Lett. **B286** (1992) 348, [hep-ph/9205228].

Publications

A

Computation of the strong coupling in QCD with two dynamical flavours

Nucl. Phys. B713 (2005) 378-406

Available online at www.sciencedirect.com
SCIENCE DIRECT®
ELSEVIER
Nuclear Physics B 713 (2005) 378–406
NUCLEAR PHYSICS B

Computation of the strong coupling in QCD with two dynamical flavors

ALPHA Collaboration

M. Della Morte [a], R. Frezzotti [b], J. Heitger [c], J. Rolf [a], R. Sommer [d], U. Wolff [a]

[a] *Institut für Physik, Humboldt Universität, Berlin, Germany*
[b] *INFN, Milano and Università di Milano "Bicocca", Milano, Italy*
[c] *Institut für Theoretische Physik, Universität Münster, Münster, Germany*
[d] *DESY, Zeuthen, Germany*

Received 22 November 2004; accepted 11 February 2005

Available online 8 March 2005

Abstract

We present a non-perturbative computation of the running of the coupling α_s in QCD with two flavors of dynamical fermions in the Schrödinger functional scheme. We improve our previous results by a reliable continuum extrapolation. The Λ-parameter characterizing the high-energy running is related to the value of the coupling at low energy in the continuum limit. An estimate of Λr_0 is given using large-volume data with lattice spacings a from 0.07 fm to 0.1 fm. It translates into $\Lambda^{(2)}_{\overline{\rm MS}} = 245(16)(16)$ MeV [assuming $r_0 = 0.5$ fm]. The last step still has to be improved to reduce the uncertainty.

PACS: 11.10.Hi; 11.15.Ha; 12.38.Gc; 02.70.Lq

Keywords: Lattice QCD; Strong coupling constant

E-mail address: uwolff@physik.hu-berlin.de (U. Wolff).

0550-3213/$ – see front matter
doi:10.1016/j.nuclphysb.2005.02.013

1. Introduction

The QCD sector of the Standard Model of elementary particles constitutes a renormalizable quantum field theory. After determining one mass parameter for each quark species and the strong coupling constant (at some reference energy) which fixes the interaction strength, QCD is believed—and so far found—to predict all phenomena where only strong interactions are relevant. Due to asymptotic freedom, this programme could be successfully implemented for processes with energies $E \gg 1$ GeV by using perturbation theory to evaluate QCD. A recent report on such determinations of the coupling implied by a multitude of experiments is found in [1].

At smaller energy the lattice formulation together with the tool of numerical simulation is used to systematically extract predictions of the theory. Here the free parameters are typically determined by a sufficient number of particle masses or matrix elements associated with low energies, and then for instance the remaining hadron spectrum becomes a prediction. See [2] for a recent reference on such large scale simulations.

While this almost looks like two theories having disjoint domains of applicability, we really view QCD as one theory for all scales. Then the adjustable parameters mentioned above are not independent but half of them should in fact be redundant or, in other words, predictable. The ALPHA Collaboration is pursuing the long-term programme of computing the perturbative parameters in the theory matched with Nature at hadronic energies. Here a non-perturbative multi-scale problem has to be mastered: hadronic and perturbative energies have to be covered and kept remote from inevitable infrared and ultraviolet cutoffs. To nevertheless gain good control over systematic errors in such a calculation, a special strategy had to be developed; it will be reviewed in the next section.

As done for many other applications of lattice QCD, also our collaboration has recently set out to overcome the quenched approximation and include vacuum fluctuations due to the two most important light quark flavors. In this article we publish detailed results on the energy dependence of a non-perturbative coupling from hadronic to perturbative energies and thereby connect the two regimes of QCD. This connection has been broken into two parts. It is first established with reference to a scale $L_{\max}$ in the hadronic sector that is not yet directly physical but rather technically convenient within our non-perturbative renormalization scheme. This part is, however, a universal continuum result and represents what is mainly reported here. In a second step, which does not anymore involve large physical scale ratios, one number relating our intermediate result to physics, like for instance $L_{\max} F_\pi$, has to be computed. Here we can cite in this publication only a first estimate and not yet a systematic continuum extrapolation, which is left as a future task.

Earlier milestones of our programme consisted of the formulation of the finite-size scaling technique [3], its adaptation to QCD [4,5], check of universality [6] and the complete numerical execution of all steps in the quenched approximation [7–9]. A shorter account of the present study with a subset of the data was published in [10].

We would like to mention that beside our finite-volume technique there are also efforts to compute the coupling and quark masses in a more direct “one-lattice” approach. Some recent references with unquenched results include [11–13]. Since it is not possible to accommodate all scales involved on one lattice in a satisfactory fashion, in these works a perturbative connection is established between the bare coupling associated with the lat-

tice cutoff scale a and a renormalized coupling at high energy in a continuum scheme such as $\overline{\mathrm{MS}}$. In our view, this step represents the main weakness of the method.[1] Series in the non-universal bare coupling are usually worse behaved than renormalized perturbation theory. There are techniques to improve this (tadpole improvement, boosted perturbation theory) which, in cases where a non-perturbative check is possible, sometimes help more and sometimes help less. Thus it is not easy to verify that one uses this perturbation theory in a regime where it is accurate and to quote realistic errors on this step. On the other hand, this approach is much easier to carry through and typically yields approximate results before an application of our strategy is available.

2. Strategy

A non-perturbative renormalization of QCD addresses the question how the high-energy regime, where perturbation theory has been successfully applied in many cases, is related to the observed hadrons and their interactions at small energies. This relation involves large scale separations and thus is difficult to study by numerical simulation. Naively, it would require simulations with a cutoff a^{-1} much larger than the largest-energy scale, combined with a large system size L, much larger than the Compton wavelength of the pion. In summary this would mean

$$a^{-1} \gg \mu_{\mathrm{perturbative}} \gg \mu_{\mathrm{hadronic}} \gg L^{-1}, \tag{2.1}$$

to avoid discretization and finite-size errors. This clearly corresponds to—with the current computing power—inaccessibly large lattices.

Our method to overcome these problems has been developed in [3–5,10,15–17]; pedagogical introductions can be found in [18,19]. The key concept is an intermediate finite-volume renormalization scheme, in which the scale evolution of the coupling (and the quark masses) can be computed recursively from low to very high energies. At sufficiently high energies, the scale evolution is verified to match with perturbation theory and there the Λ-parameter is determined.

2.1. Renormalization

Any physical quantity P should be independent of the renormalization scale μ. This is expressed by the Callan–Symanzik equation [20,21]

$$\left\{\mu\frac{\partial}{\partial\mu} + \beta(\bar{g})\frac{\partial}{\partial\bar{g}} + \tau(\bar{g})\bar{m}\frac{\partial}{\partial\bar{m}}\right\}P = 0. \tag{2.2}$$

Here, the β-function is given by

$$\beta(\bar{g}) = \mu\frac{\partial\bar{g}(\mu)}{\partial\mu}. \tag{2.3}$$

[1] As for Ref. [13], an additional relevant question concerns the correctness of the formulation of fermions on the lattice. We refer to [14] and references therein for an introduction to the problem.

Hence, once the coupling has been defined non-perturbatively for all scales (see Section 2.2), also the β-function is defined beyond perturbation theory.[2] For weak couplings or high energies only, the β-function can be asymptotically expanded as

$$\beta(\bar{g}) = -\bar{g}^3\big(b_0 + b_1\bar{g}^2 + b_2\bar{g}^4 + \cdots\big). \tag{2.4}$$

In the following we only consider mass independent renormalization schemes [22], in which the renormalization conditions are imposed at zero quark mass. Particular examples are the Schrödinger functional scheme described below, and the $\overline{\mathrm{MS}}$ scheme. If in two such schemes the couplings can[3] be mutually expanded as Taylor series of each other (once they are small enough),

$$\bar{g}'^2 = \bar{g}^2\big(1 + C_g^{(1)}\bar{g}^2 + \cdots\big), \tag{2.5}$$

then the 1- and 2-loop coefficients b_0 and b_1 in (2.4) are universal,

$$b_0 = \frac{1}{(4\pi)^2}\left(11 - \frac{2}{3}N_{\mathrm{f}}\right), \tag{2.6}$$

$$b_1 = \frac{1}{(4\pi)^4}\left(102 - \frac{38}{3}N_{\mathrm{f}}\right), \tag{2.7}$$

while the higher-order coefficients depend on the choice of the coupling. Starting from the 3-loop coefficient in the $\overline{\mathrm{MS}}$ scheme [24] and its conversion to the minimal subtraction scheme of lattice regularization [25–28], the 3-loop coefficient in the Schrödinger functional scheme (with all the parameters as specified below)

$$b_2 = \big(0.483(7) - 0.275(5)N_{\mathrm{f}} + 0.0361(5)N_{\mathrm{f}}^2 - 0.00175(1)N_{\mathrm{f}}^3\big)/(4\pi)^3 \tag{2.8}$$

could be obtained in [29].

Now, a special exact solution of the Callan–Symanzik equation (2.2) is the renormalization group invariant Λ-parameter,

$$\Lambda = \mu\big(b_0\bar{g}^2(\mu)\big)^{-b_1/(2b_0^2)}e^{-1/(2b_0\bar{g}^2(\mu))}\exp\left\{-\int_0^{\bar{g}(\mu)}dx\left[\frac{1}{\beta(x)} + \frac{1}{b_0x^3} - \frac{b_1}{b_0^2x}\right]\right\}. \tag{2.9}$$

Λ is scale independent but renormalization scheme dependent. The transition to other mass independent schemes is accomplished exactly by a 1-loop calculation. If in another scheme the coupling is given through (2.5) with both $\bar{g}'$ and $\bar{g}$ taken at the same μ, the Λ-parameters are related by

$$\Lambda' = \Lambda e^{C_g^{(1)}/(2b_0)}. \tag{2.10}$$

[2] For the τ-function similar statements and expressions are valid, once the running quark mass $\bar{m}$ has been defined non-perturbatively.

[3] See [23] for an example that this restriction can be non-trivial for non-perturbative couplings.

In particular, the transition from the Schrödinger functional scheme with two dynamical flavors to the $\overline{\rm MS}$ scheme of dimensional regularization is provided through [30]

$$\Lambda^{(2)}_{\overline{\rm MS}} = 2.382035(3)\Lambda^{(2)}. \tag{2.11}$$

2.2. Schrödinger functional

Since we want to connect the perturbative regime of QCD with the non-perturbative hadronic regime, we have to employ a non-perturbative definition of the coupling. Furthermore, the definition of the coupling should be practical. This means that one has to be able to evaluate it on the lattice with a small error, that cutoff effects are reasonably small and that its perturbative expansion to 2-loop order is computable with a reasonable effort. In principle there is a large freedom for the choice of the coupling, however, it turns out that the conditions above are hard to fulfill simultaneously.

To this end we consider the Schrödinger functional, which is the propagation amplitude for going from some field configuration at the time $x_0 = 0$ to another field configuration at the time $x_0 = T$. Here the space–time is a hyper-cubic Euclidean lattice with discretization length a and volume $T \times L^3$. We choose $T = L$ so that L is the only remaining external scale in the continuum limit $a \to 0$ of the massless theory.

The SU(3) gauge fields U are defined on the links of the lattice, while the fermion fields are defined on the lattice sites. The partition function of this system is given by

$$Z = e^{-\Gamma} = \int_{T\times L^3} \mathrm{D}[U,\psi,\bar\psi] e^{-S[U,\psi,\bar\psi]}. \tag{2.12}$$

Here, the action is the sum $S[U,\psi,\bar\psi] = S_{\rm g}[U] + S_{\rm f}[U,\psi,\bar\psi]$ of the O(a) improved plaquette action

$$S_{\rm g}[U] = \frac{1}{g_0^2}\sum_p w(p)\,\mathrm{tr}\big(1 - U(p)\big) \tag{2.13}$$

and the fermionic action

$$S_{\rm f}[U,\psi,\bar\psi] = \sum_x \bar\psi(x)(D + m_0)\psi(x) \tag{2.14}$$

for two degenerate flavors implicit in ψ. For the special boundary conditions considered below, the weight factor $w(p)$ is the boundary improvement term $c_{\rm t}$ [4] for time-like plaquettes at the boundary and one in all other cases. The value of $c_{\rm t}$ has become available to 2-loop order in perturbation theory [29] in the course of this work. Thus some of our data sets use the 1-loop value of $c_{\rm t}$, hence our simulations adopt two different actions. Because of universality we expect them to yield the same continuum limits for our observables.

The O(a) improved Wilson Dirac operator D includes the Sheikholeslami–Wohlert term [31] multiplied with the improvement coefficient $c_{\rm sw}$ that has been determined with non-perturbative precision in [32], and a boundary improvement term that is multiplied by the coefficient $\tilde c_{\rm t}$, which is known to 1-loop order. For details and notation we refer to [33,34].

The boundary conditions in the space directions are periodic for the gauge fields and periodic up to a global phase θ for the fermion fields. The value of θ was optimized at 1-loop order of perturbation theory [30]. It turns out that a value close to $\theta = \pi/5$ leads to a significantly smaller condition number of the fermion matrix than other values of θ and thus to a smaller computational cost. Benchmarks in the relevant parameter range for our project have shown this too, and therefore we adopt the choice $\theta = \pi/5$ in this work.

In the time direction, Dirichlet boundary conditions are imposed at $x_0 = 0$ and $x_0 = T$. The quark fields at the boundaries are given by the Grassmann valued fields $\rho, \bar{\rho}$ at $x_0 = 0$ and $\rho', \bar{\rho}'$ at $x_0 = T$, respectively. They are used as sources that are set to zero after differentiation. The gauge fields at the boundaries are chosen such that a constant color-electric background field, which is the unique (up to gauge transformations) configuration of least action, is generated in our space–time [4]. This is achieved by the diagonal color matrices specified in Ref. [16], parametrized by two dimensionless real parameters η and ν.

A renormalized coupling $\bar{g}^2$ may then be defined by differentiating the effective action Γ at the boundary point "A" of [16] that corresponds to the choice $\eta = \nu = 0$,

$$\left.\frac{\partial \Gamma}{\partial \eta}\right|_{\eta=\nu=0} = \frac{k}{\bar{g}^2}. \tag{2.15}$$

The normalization k is chosen such that the tree-level value of $\bar{g}^2$ equals g_0^2 for all values of the lattice spacing. The boundary point "A" and especially the value $\nu = 0$ are used, since the statistical error of the coupling turns out to be small for this choice. For general values of ν we find another renormalized quantity $\bar{v}$,

$$\left.\frac{\partial \Gamma}{\partial \eta}\right|_{\eta=0} = k\left\{\frac{1}{\bar{g}^2} - \nu\bar{v}\right\}, \tag{2.16}$$

that we have investigated as well to study the effects of dynamical fermions.

The renormalized coupling depends on the system size, the lattice spacing a and on the quark mass. The bare quark mass m_0 is additively renormalized on the lattice because chiral symmetry is broken for Wilson fermions [35]. Thus we define the bare mass by the PCAC relation that relates the axial current $A_\mu^a(x) = \bar{\psi}(x)\frac{\tau^a}{2}\gamma_\mu\gamma_5\psi(x)$ to the pseudoscalar density $P^a(x) = \bar{\psi}(x)\frac{\tau^a}{2}\gamma_5\psi(x)$. Using the matrix elements f_A and f_P of A_μ^a and P^a, respectively (cf. [33]), the $\mathrm{O}(a)$ improved PCAC mass is defined as

$$m(x_0) = \frac{\frac{1}{2}(\partial_0 + \partial_0^\star) f_\mathrm{A}(x_0) + c_\mathrm{A} a \partial_0^\star \partial_0 f_\mathrm{P}(x_0)}{2 f_\mathrm{P}(x_0)}. \tag{2.17}$$

We have used 1-loop perturbation theory for c_A [34].

To fix all the details of our scheme, we define the bare current mass through

$$m = \begin{cases} m(T/2), & \text{if } T/a \text{ is even,} \\ \big[m\big((T-a)/2\big) + m\big((T+a)/2\big)\big]/2, & \text{if } T/a \text{ is odd.} \end{cases} \tag{2.18}$$

This mass is tuned to zero,

$$m(g_0, m_0, L/a) = 0, \tag{2.19}$$

so that we have a massless renormalization scheme, in which the only remaining external scale in the continuum limit is the system size L.

2.3. Computational strategy

In the last section we have defined the Schrödinger functional coupling $\bar{g}^2$. This finite-volume coupling runs with $\mu = 1/L$ and—assuming monotonicity—there is a one-to-one relation between the value of the coupling and the system size L or energy scale μ. In an abuse of notation we will from now on write $\bar{g}^2(L)$ instead of $\bar{g}^2(1/L)$.

Our goal is to calculate the scale evolution of the strong coupling and the Λ-parameter of QCD in terms of a low-energy scale. We start the computation by choosing a value u for the renormalized coupling (which implicitly determines L) and by choosing a lattice resolution L/a. The theory can then be renormalized by tuning the bare parameters $\beta = 6/g_0^2$ and $\kappa = 1/(8 + 2am_0)$ such that

$$\bar{g}^2(L) = u \quad \text{and} \quad m = 0. \tag{2.20}$$

Now we simulate a lattice with twice the linear size at the same bare parameters, that means at the same value of the lattice spacing, and thus with the physical extent $2L$, corresponding to a new renormalized coupling $u' = \bar{g}^2(2L)$.[4] This determines the scale evolution of the renormalized coupling. It can be expressed through the lattice step scaling function

$$\Sigma(u, a/L) = \bar{g}^2(2L)|_{\bar{g}^2(L)=u, m=0}, \tag{2.21}$$

which is the key observable we compute. Finally, we obtain the step scaling function

$$\sigma(u) = \lim_{a/L \to 0} \Sigma(u, a/L) \tag{2.22}$$

in the continuum limit by repeating these three steps with finer and finer lattice resolutions. This algorithm is iterated for a sequence of values for u to get the functional form of $\sigma(u)$.

For small values of u the step scaling function $\sigma(u)$ can be expanded in renormalized perturbation theory,

$$\sigma(u) = u + s_0 u^2 + s_1 u^3 + \cdots, \tag{2.23}$$

with the coefficients

$$s_0 = 2b_0 \ln 2, \tag{2.24}$$

$$s_1 = (2b_0 \ln 2)^2 + 2b_1 \ln 2, \tag{2.25}$$

$$s_2 = (2b_0 \ln 2)^3 + 10 b_0 b_1 (\ln 2)^2 + 2b_2 \ln 2. \tag{2.26}$$

The step scaling function $\sigma(u)$ can be interpreted as an integrated discrete β-function. Indeed, by using Eq. (2.3) we get

$$\beta\big(\sqrt{\sigma(u)}\big) = \beta\big(\sqrt{u}\big)\sqrt{\frac{u}{\sigma(u)}}\sigma'(u) \tag{2.27}$$

for the β-function, which allows to calculate it recursively once the step scaling function $\sigma(u)$ is known.

[4] The mass m on this larger lattice is different from zero by a lattice artifact which is expected to vanish in the continuum limit proportionally to a^2. This has been verified in Ref. [10].

To arrive at our main result, that is the Λ-parameter in terms of a low-energy scale, we solve the equation

$$\sigma\big(\bar{g}^2(L/2)\big) = \bar{g}^2(L) \tag{2.28}$$

recursively for $\bar{g}^2(L/2)$. We start this recursion at a maximal value $u_{\max} = \bar{g}^2(L_{\max})$ of the coupling. The value of $u_{\max}$ is chosen such that the associated scale $L_{\max}$ is a scale in the hadronic regime of QCD. Following the recursion (2.28) to larger and larger energies, we obtain the values for

$$u_i = \bar{g}^2\big(2^{-i} L_{\max}\big), \quad i = 0, \ldots, n, \qquad u_0 = u_{\max}. \tag{2.29}$$

We perform $n = 7$ or $n = 8$ steps of this recursion and can in this way cover a scale separation of a factor 100 to 250. Eventually, for sufficiently large energies, perturbation theory can safely be applied. Then we use (2.9) with $\mu = 2^n/L_{\max}$ and with the β-function truncated at 3-loop order, (2.6)–(2.8). The final result for $\Lambda L_{\max}$ in the Schrödinger functional scheme can be converted to the $\overline{\mathrm{MS}}$ scheme with (2.11). We also check the admissibility of employing perturbation theory by studying the variation of our final result with respect to the number of non-perturbative steps n in the scale evolution of the strong coupling.

2.4. Discretization effects

The influence of the underlying space–time lattice on the evolution of the coupling can be estimated perturbatively [29], by generalizing Symanzik's discussion [36–38] to the present case. Close to the continuum limit we expect that the relative deviation

$$\delta(u, a/L) = \frac{\Sigma(u, a/L) - \sigma(u)}{\sigma(u)} = \delta_1(a/L)u + \delta_2(a/L)u^2 + \cdots \tag{2.30}$$

of the lattice step scaling function from its continuum limit converges to zero with a rate roughly proportional to a/L. More precisely, since the action is $\mathrm{O}(a)$ improved, we expect

$$\delta_1(a/L) \sim \left(d_{0,1} + d_{1,1} \ln \frac{a}{L}\right)\left(\frac{a}{L}\right)^2 + \cdots, \tag{2.31}$$

$$\delta_2(a/L) \sim e_{0,2}\frac{a}{L} + \left(d_{0,2} + d_{1,2} \ln \frac{a}{L} + d_{2,2}\left(\ln \frac{a}{L}\right)^2\right)\left(\frac{a}{L}\right)^2 + \cdots \tag{2.32}$$

for the 1-loop value of c_{t} and the same form with $e_{0,2} = 0$ for the 2-loop value of c_{t}. Note that the tree-level discretization effects vanish exactly, since we normalize the coupling such that its perturbative expansion starts with g_0^2 for all values of the lattice spacing.

The coefficients δ_1 and δ_2 are collected in Table 1 for the resolutions needed in this work. An expanded version of this table can be found in [39]. The entries in the last column are very small. For larger values of L/a than shown in the table, $\delta_2^{c_{\mathrm{t}}=2\text{-loop}}$ decreases as expected. Since $\delta_2^{c_{\mathrm{t}}=1\text{-loop}}$ is of the order a/L, it is no surprise that it is much larger than $\delta_2^{c_{\mathrm{t}}=2\text{-loop}}$. In fact, it is of the same size as δ_1, for which the linear term in a/L is absent.

The largest coupling at which the step scaling function has been computed with the 1-loop value of c_{t} is $u = 1.7319$. With the 2-loop value of c_{t}, this is $u = 3.334$. Table 1

Table 1
Discretization error of the step scaling function

L/a	δ_1	$\delta_2^{\text{ct=1-loop}}$	$\delta_2^{\text{ct=2-loop}}$
4	−0.0103	0.0063	−0.00007
5	−0.0065	0.0049	−0.00019
6	−0.0042	0.0038	−0.00041
8	−0.0021	0.0029	−0.00030

suggests that the step scaling function is only mildly affected by discretization effects. This will be demonstrated by our numerical results in Section 4.

We cancel the known perturbative cutoff effects for the respective actions by using

$$\Sigma^{(2)}(u, a/L) = \frac{\Sigma(u, a/L)}{1 + \delta_1(a/L)u + \delta_2(a/L)u^2} \tag{2.33}$$

in the analysis of our Monte Carlo data. The perturbative estimate of the relative cutoff effects behaves as $(a/L) \times u^3$ close to the continuum limit.

2.5. Matching to a hadronic scheme

As described so far, our computational strategy yields $\Lambda L_{\max}$, with $L_{\max}$ defined by the value of the coupling itself. Since the latter is not experimentally measurable, it remains to relate $L_{\max}$ to a hadronic scale. Here, the natural choice is the pion decay constant F_π, since chiral perturbation theory provides an analytic understanding of the pion dynamics [40,41], which is expected to help to control the extrapolations to the physical quark mass [41] as well as to infinite volume [42].

A computation of $L_{\max} F_\pi$ requires the knowledge of $f(\tilde{g}_0^2) = aF_\pi$ (at a quark mass where m_π/F_π takes its experimental value) and $l(g_0^2) = L_{\max}/a$, where $\bar{g}^2(L_{\max}) = u_{\max}$. We remind the reader that $\bar{g}^2$ is defined at vanishing quark mass. The difference between the improved bare coupling $\tilde{g}_0$ [33] and g_0 is proportional to the light quark mass and can safely be neglected for physical values of the light quark mass. We therefore replace $\tilde{g}_0 \approx g_0$ in the following. The value of $u_{\max}$ is restricted to be in the range covered by the computation of the scale dependence of the coupling and, for lattice spacings accessible in large-volume simulations, $l(g_0^2)$ should be sufficiently large. With both functions, l and f, defined for the same discretization, one finally wants to evaluate

$$L_{\max} F_\pi|_{\text{continuum}} = \lim_{f \to 0} l\big(g_0^2\big) f\big(g_0^2\big). \tag{2.34}$$

Unfortunately, the results available in the literature [43,44] for $f(g_0^2)$ with our action [32] suffer from an uncertainty in the renormalization of the axial current, which has not yet been performed non-perturbatively. Also the $\mathrm{O}(a)$ improvement of the current is known only perturbatively and it is not obvious that quark masses have been reached where chiral perturbation theory is applicable.

At present, we thus prefer to relate $L_{\max}$ to the frequently used hadronic radius r_0, which, according to phenomenological considerations, has a value of around 0.5 fm [45] and which has also been the reference scale in the zero-flavor theory, i.e., the quenched

approximation [7]. Note that in a calculation in this approximation agreement was found (within its 3% precision) between $F_K r_0$ and the product of the experimental number for F_K times 0.5 fm [8]. Below, we thus evaluate $L_{\max}/r_0 = l(g_0^2)/\rho(g_0^2)$ where $\rho(g_0^2) = r_0/a$ and translate to physical units via $r_0 = 0.5$ fm.

3. Details of the numerical simulation and analysis

In addition to the piece present in the pure gauge theory [16], the central observable, $\partial\Gamma/\partial\eta$, receives a contribution due to the quark determinant. We describe its numerical evaluation by a stochastic estimator in Appendix A. Also detailed tables with simulation results are deferred to an Appendix B.

3.1. Tuning

With a number of tuning runs we determine the bare parameters β and κ such that Eq. (2.20) is valid. Fulfilling the condition $m(L) = 0$ precisely would require a fine tuning of the hopping parameter κ. However, the uncertainty in Σ owing to a small mismatch of m can be estimated perturbatively. To this end we compute the derivative of Σ with respect to $z = mL$,

$$\frac{\partial}{\partial z}\bar{g}^2(2L)\bigg|_{\bar{g}^2(L)=u,\, m(L)=z/L} = \Phi(a/L)u^2 + \cdots. \tag{3.1}$$

It turns out that Φ is a slowly varying function of a/L. Thus, for our purpose it suffices to approximate it by its universal part,

$$\Phi(0) = -\frac{N_f}{4\pi}\frac{\partial}{\partial z}c_{1,1}(z)\bigg|_{z=0} = 0.00957N_f, \tag{3.2}$$

where $c_{1,1}(z)$ has been taken from [30]. The typical precision in Monte Carlo simulations is $\Delta(\bar{g}^{-2}) = \bar{g}^{-4}\Delta(\bar{g}^2) = 0.003$, as can be seen from Tables 10 and 11 in Appendix B. This means that an additional error of $0.001 \times u^2$ due to a slight mismatch of the mass $m(L)$ is tolerable. Then it suffices to require

$$am < 0.1\frac{a}{L}\frac{1}{N_f}. \tag{3.3}$$

Tables 10 and 11 in Appendix B show that we have reached this precision in our simulations.

Analogously, we stop the fine tuning of β if $\bar{g}^2(L) = u$ well within the errors. Then we can correct for a small mismatch owing to $\bar{g}^2(L) = \tilde{u} \neq u$ by using

$$\Sigma(u, a/L) = \Sigma(\tilde{u}, a/L) + \Sigma'(u, a/L) \times (u - \tilde{u}), \tag{3.4}$$

with the perturbative estimate

$$\Sigma'(u, a/L) \equiv \frac{\partial\Sigma(u, a/L)}{\partial u} \approx \frac{\partial\sigma(u)}{\partial u} \approx 1 + 2s_0u + 3s_1u^2 + 4s_2u^3 \tag{3.5}$$

Table 2
Step scaling functions Σ and $\Sigma^{(2)}$

u	L/a	$\Sigma(u,a/L)$	$\Sigma^{(2)}(u,a/L)$	u	L/a	$\Sigma(u,a/L)$	$\Sigma^{(2)}(u,a/L)$
0.9793	4	1.0643(35)	1.0686(35)	1.5031	4	1.7204(56)	1.7477(57)
	5	1.0720(40)	1.0738(41)		5	1.737(11)	1.755(11)
	6	1.0802(46)	1.0807(46)		6	1.730(13)	1.743(13)
	8	1.0736(59)	1.0729(59)		8	1.723(16)	1.730(16)
1.1814	4	1.3154(55)	1.3199(56)	2.0142	4	2.481(18)	2.535(18)
	5	1.3296(61)	1.3307(61)		5	2.438(20)	2.473(20)
	6	1.3253(70)	1.3249(70)		6	2.507(27)	2.533(28)
	8	1.3342(71)	1.3323(71)		8	2.475(35)	2.489(35)
1.5031	4	1.7310(61)	1.7332(61)	2.4792	4	3.251(28)	3.338(29)
	5	1.756(12)	1.754(12)		5	3.336(52)	3.394(53)
	6	1.745(12)	1.741(12)		6	3.156(57)	3.198(58)
					8	3.326(52)	3.351(53)
1.7319	4	2.0583(76)	2.0562(76)	3.334	4	5.588(54)	5.791(56)
	5	2.083(21)	2.076(21)		5	5.43(11)	5.56(11)
	6	2.058(20)	2.049(20)		6	5.641(99)	5.75(10)
					8	5.48(13)	5.53(13)

The left-hand side of the table contains the data with the 1-loop value of c_t, while the data with $c_t = 2$-loop are shown on the right.

for the derivative of the step scaling function Σ. This correction is always smaller than the statistical error of the step scaling function.

Similarly, we convert the statistical error on u into an additional error of Σ,

$$\Delta\big(\Sigma(u)\big) \approx \Sigma'(u,a/L) \times \Delta(u) \approx (1 + 2s_0 u + \cdots) \times \Delta(u). \tag{3.6}$$

This additional error is always much smaller than the error of $\bar{g}^2(2L)$, to which it is added in quadrature.

In some cases we have stopped the fine tuning of β and κ after a number of runs and interpolated the results such that exactly the target coupling and mass zero with the errors as shown in Tables 10 and 11 were obtained.

The step scaling function $\Sigma(u,a/L)$ and its partner with the perturbative cutoff effects being divided out, $\Sigma^{(2)}(u,a/L)$ (cf. (2.33)), are listed in Table 2.

3.2. Parameters

Our choice of parameters is displayed in Tables 10 and 11 in Appendix B. The parameters shown are the results of a careful application of the tuning procedure explained in the last section. The tables reveal that the condition $\bar{g}^2(L) = u$ is fulfilled to a good precision. The remaining deviations and the errors are then propagated into an additional error for $\Sigma(u)$, as described above.

Table 3
Cost estimates for two $L/a = 16$ runs; $t_{\text{update}}/[s]$ is the time in seconds needed for one trajectory of length 1

Algorithm	Step size	τ_{int}	$t_{\text{update}}/[s]$	$\bar{g}^2$	N_{traj}	M_{cost}
HMC	0.0625	3.6(3)	380	2.46(5)	4800	6.9(6)
HMC 2 pf	0.111	4.6(4)	262	2.55(5)	5900	5.6(5)

The reference machine is an APEmille board.

3.3. Simulation costs and proper sampling of the configuration space

Most of our results have been produced with the hybrid Monte Carlo algorithm (HMC) [46], the polynomial hybrid Monte Carlo (PHMC) in the version proposed in [47,48] and for some of the $L/a = 16$ runs the hybrid Monte Carlo algorithm generalized to two pseudofermion fields (HMC 2 pf) [49,50].

We measure the cost of our simulations with the quantity

$$M_{\text{cost}} = (\text{update time in seconds on machine M}) \times \left(\text{error of } 1/\bar{g}^2\right)^2 \times (4a/T)(4a/L)^3. \tag{3.7}$$

In [51] the cost of a subset of the simulations discussed here (essentially up to $L/a = 12$ and $\bar{g}^2 \approx 2.5$) has been analyzed. A typical value for HMC at $L/a = 10$ and $\bar{g}^2 \approx 2.5$ is $M_{\text{cost}} \approx 3.5$, with respect to one board of APEmille [52]. To give an idea about the increase of the cost for the $L/a = 16$ simulations, we collect results from two different runs at the coupling $\bar{g}^2 \approx 2.5$ in Table 3. We compute the autocorrelation time τ_{int} in units of trajectories in the way suggested in [53].

Related to the issue of estimating the autocorrelation time is always the question whether the algorithm samples the entire relevant configuration space efficiently. If this is not the case, autocorrelation times may be largely underestimated and even systematically wrong results may be obtained. We now discuss two at least rough checks that our simulations do not suffer from such problems.

(1) To investigate the contributions to the coupling from sectors of configuration space with non-trivial topology, we have performed a set of simulations at the coupling $\bar{g}^2 \approx 2.5$ with $L/a = 8, 12$. The topological charge $Q(U)$ is determined through a cooling procedure. Since sampling different topological sectors might be algorithmically very difficult, we have employed the PHMC algorithm, whose flexibility can be exploited to enhance the transition rate among different sectors (at the price of increasing the fluctuations of the reweighting factor), and checked the results to be independent of the polynomial approximation used.

Starting from a hot, random configuration, several of the independent replica were in a non-trivial topological sector. For these replica the smallest eigenvalue of D^2 (even–odd preconditioned) turns out to be one order of magnitude smaller than typical values in the topologically trivial sectors. After O(100) trajectories for $L/a = 8$, respectively O(1000) trajectories for $L/a = 12$, all the replica have zero topological charge and transitions to sectors with $Q(U) \neq 0$ have not been observed in additional O(10^4) trajectories.

From this we conclude that the PHMC algorithm can tunnel between different topological sectors, but for large L/a the transition rate is very small. In addition, the weight of

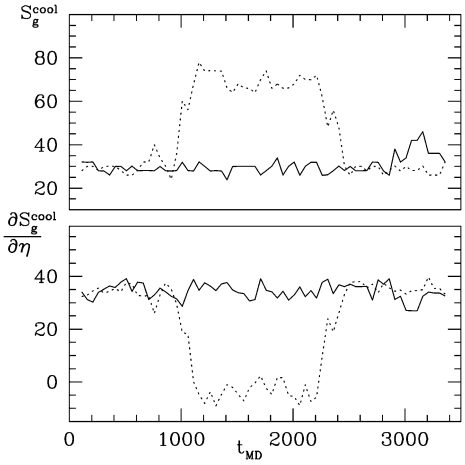

Fig. 1. Monte Carlo histories of $S_{\mathrm{g}}^{\mathrm{cool}}$ and $\partial S_{\mathrm{g}}^{\mathrm{cool}}/\partial\eta$ from two independent replica (solid and dotted lines) in a simulation of a 16^4 lattice at $\bar{g}^2 \approx 3.3$.

the non-trivial sectors is too small for them to occur in a practical simulation at all (all tunnelings went to $Q(U) = 0$ and none in the reverse direction). Their weight in the path integral is negligible. These statements have been checked for $L/a = 8, 12$, and it appears safe to assume their validity also for larger L/a. Therefore, we decided to always start from a cold configuration, especially for the $L/a = 16$ simulations, to avoid thermalization problems.

(2) For the two largest couplings discussed here the distribution of $\partial S/\partial\eta$ shows long tails toward negative values. The same effect was also observed in the computation of the Schrödinger functional coupling in pure SU(3) gauge theory [16]. We have related this tail to secondary local minima of the action [54] by measuring on cooled configurations the pure gauge contribution to the action $S_{\mathrm{g}}^{\mathrm{cool}}$ and to the coupling $\partial S_{\mathrm{g}}^{\mathrm{cool}}/\partial\eta$. This leads to metastabilities as shown for an $L/a = 16$ simulation with $\bar{g}^2 \approx 3.3$ in Fig. 1. The upper panel is the Monte Carlo history (t_{MD} is the Monte Carlo time in units of molecular dynamics trajectories) of the gauge part of the action after cooling for two independent replica. The lower panel shows the history of $\partial S_{\mathrm{g}}^{\mathrm{cool}}/\partial\eta$ for the same two replica. The correlation between metastable states and small (even negative) values of $\partial S_{\mathrm{g}}^{\mathrm{cool}}/\partial\eta$ appears evident in this case. The action $S_{\mathrm{g}}^{\mathrm{cool}}$ for the metastability in the figure is consistent with the value for a secondary solution of the field equations [16], given our choice for the boundary fields. Numerical evidence suggests that this solution is a local minimum.

In order to estimate the weight of these contributions in our expectation values properly, we have enhanced their occurrence through a modified sampling similar to [16], adding to the HMC effective action a term

$$\gamma \left.\frac{\partial S_{\mathrm{g}}}{\partial\eta}\right|_{\eta=0} + \frac{1}{w_\gamma}(\gamma - \gamma_0)^2, \tag{3.8}$$

where γ_0 and w_γ are fixed to suitable (positive) values, while γ is a dynamical variable. The expectation values in the original ensemble are then obtained by reweighting. By some

deterministic cooling procedure with a fixed number of cooling steps we now define a quantity q whose value is 1 for metastable configurations, and 0 otherwise, such that $\delta_{q1} + \delta_{q0} \equiv 1$. For an arbitrary observable O we have an exact identity

$$\langle O \rangle = \langle \delta_{q1} O \rangle + \langle \delta_{q0} O \rangle = \langle \delta_{q1} O \rangle + \langle O \rangle_{\bar{1}} \big(1 - \langle \delta_{q1} \rangle\big), \tag{3.9}$$

with $\langle O \rangle_{\bar{1}} = \langle \delta_{q0} O \rangle / \langle \delta_{q0} \rangle$. If the main contribution to $\langle O \rangle$ comes from the configurations with $q = 0$, a precise estimate of $\langle O \rangle$ just requires a precise estimate of $\langle O \rangle_{\bar{1}}$, which can be obtained by an algorithm that samples only the $q = 0$ sector, together with rough estimates of $\langle \delta_{q1} \rangle$ and $\langle \delta_{q1} O \rangle$ that can be obtained by the modified sampling.

At $\bar{g}^2 \approx 3.3$ we get $\langle \delta_{q1} \rangle = 0.3(2)\%$, independent of $L/a = 8, 12$ within the error. The effect of metastable states on the coupling is 0.10(2)%. At the coupling $\bar{g}^2 \approx 5.5$ the occurrence of metastable states is much more frequent, as expected, and we get $\langle \delta_{q1} \rangle = 5(1)\%$. At the same time their sampling is much easier already in the original ensemble, using either the PHMC or the HMC algorithm. In fact, we have repeated the $L/a = 12$ simulation for $\bar{g}^2 \approx 5.5$ using PHMC for the ordinary ensemble (without (3.8)) as in [10], but measuring in addition the occurrence of metastable states. This turned out to be around 6%, and for $\bar{g}^2$ we have obtained a result fully consistent with the number in [10].

In summary, we can be confident that topologically non-trivial sectors are irrelevant for our observables with our choice of parameters and at the present level of precision. In contrast, there are secondary minima in the action, which are visible as metastable states in the Monte Carlo sequence. They are relevant starting at $\bar{g}^2 \approx 3$ and have been taken into account efficiently by deviating from naive importance sampling and combining two different properly chosen ensembles.

4. Results

4.1. The strong coupling

In Fig. 2 we show the approach of the step scaling function $\Sigma^{(2)}(u, a/L)$ to the continuum limit. The cutoff effects are small. Actually, all the data are compatible with constants. If we use simple fits to constants, the combined χ^2 per degree of freedom for all the eight continuum extrapolations is about 1.4 regardless of the number of lattices included in the fit. Even the points at $L/a = 4$ are compatible with a constant continuum extrapolation. One possible strategy for the continuum extrapolation is thus a fit to a constant that uses the lattices with $L/a = 6, 8$.

In this fit to constants we exclude the two coarsest lattices since there is always the danger of including systematic cutoff effects into the results coming from the lattices with large a/L. Therefore, we have also investigated two alternative fit procedures. The first and most conservative one (denoted as "global fit" in the tables) is a combined continuum extrapolation of all the data sets, but excluding $L/a = 4$. Here we use the two-parameter ansatz

$$\Sigma^{(2)}(u, a/L) = \sigma(u) + \rho^X u^4 (a/L)^2, \quad X \in \{\text{1-loop}, \text{2-loop}\}, \tag{4.1}$$

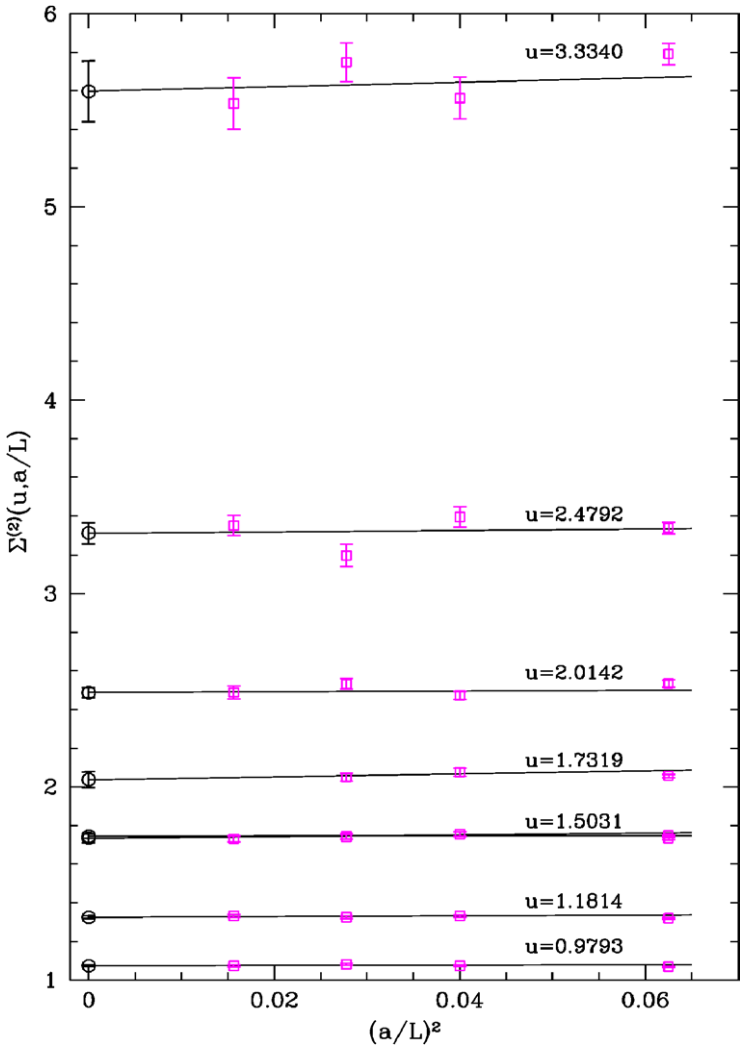

Fig. 2. Continuum extrapolation of the step scaling function.

for the lattice artifacts, where the coefficients ρ^X are understood to be associated to the data with the 1-loop and the 2-loop value of c_t, respectively.[5] This fit results in $\rho^{1\text{-loop}} = 0.08(13)$ and $\rho^{2\text{-loop}} = 0.01(4)$, quantifying that lattice artifacts are not detectable in our data. Moreover we have studied a mixed fit procedure, using a fit to constants for the lattices with $L/a = 6, 8$ for the 2-loop improved data sets and the global fit ansatz (4.1), which includes a slope for the cutoff effects, for the 1-loop improved data sets.

[5] We have also considered fits that use a common ansatz for the step scaling function for all the data sets. These lead to slightly smaller error bars of the final results.

Table 4
Continuum limit of the step scaling function

u	$\sigma(u)$		
	Global fit	Fit to constants	Mixed fit
0.9793	1.0736(44)	1.0778(36)	1.0736(44)
1.1814	1.3246(81)	1.3285(50)	1.3246(81)
1.5031	1.733(23)	1.741(12)	1.733(23)
1.7319	2.037(41)	2.049(20)	2.037(41)
1.5031	1.7440(97)	1.738(10)	1.738(10)
2.0142	2.488(26)	2.516(22)	2.516(22)
2.4792	3.311(52)	3.281(39)	3.281(39)
3.3340	5.60(16)	5.670(80)	5.670(80)

These different fits are performed to investigate the uncertainties in the continuum results. All our plots refer to the most conservative of these three fit procedures, which leaves both $\rho^{\text{1-loop}}$ and $\rho^{\text{2-loop}}$ unconstrained.

The results of the continuum limit extrapolation of the step scaling function $\Sigma^{(2)}(u, a/L)$ are recorded in Table 4. At $u = 1.5031$ we have two sets of data, one of which was produced with the 1-loop value and the other with the 2-loop value of c_{t}. Both continuum results agree well within their errors, which is an independent check of our extrapolation procedures.

We interpolate the values of Table 4 by a polynomial of degree 6 in u, the first coefficients up to u^3 being fixed by 2-loop perturbation theory, cf. (2.23). This interpolation is depicted in Fig. 3. For small values of $u < 2$, the step scaling function is well described by perturbation theory. Actually, the perturbative lines shown in this plot are the solution of

$$-2\ln 2 = \int_{u}^{\sigma(u)} \frac{dx}{\sqrt{x}\beta(\sqrt{x})} \tag{4.2}$$

for $\sigma(u)$ using the 2-loop and the 3-loop β-function. Looking at the comparison of successive perturbative approximations to the non-perturbative results, it appears likely that higher orders would not improve the agreement at the largest coupling. Rather we appear to have reached a value for the coupling, where the perturbative expansion has broken down. In fact, already in Section 3.3 we have discussed the indications that fluctuations around a secondary minimum of the action are important at this value of the coupling. Such a mechanism may represent one *possible* source of non-perturbative effects.[6]

We adopt the parametrized form of the step scaling function to compute the Λ-parameter. To this end we start a recursion with a maximal coupling $u_{\max} = \bar{g}^2(L_{\max})$. For $u_{\max} = 5.5$, the recursive step (2.28) is solved numerically to get the couplings u_i, corresponding to the energy scales $\mu = 2^i/L_{\max}$, that are quoted in Table 5. We then insert

[6] In this context we note further that for the pure gauge theory it has been demonstrated that the Schrödinger functional coupling grows exponentially with L at even larger values of L [9]. We do not expect that any semi-classical picture is applicable in that regime but rather see this as a disorder phenomenon.

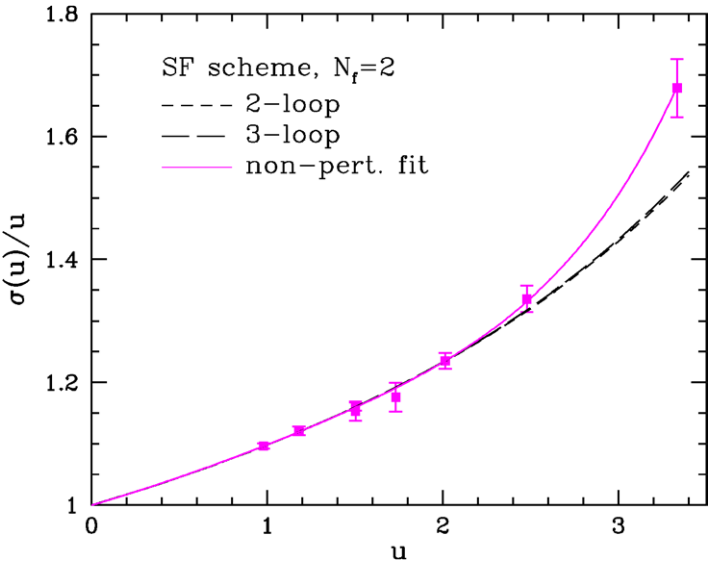

Fig. 3. Step scaling function $\sigma(u)$. The dashed lines show the perturbative results from the integration of the 2-loop and 3-loop β-function, respectively.

Table 5
Recursive computation of the Λ-parameter starting at $u_0 = u_{\max} = 5.5$

i	Global fit		Constant fit, $L/a = 6, 8$		Mixed cont. extrap.	
	u_i	$-\ln(\Lambda L_{\max})$	u_i	$-\ln(\Lambda L_{\max})$	u_i	$-\ln(\Lambda L_{\max})$
0	5.5	0.957	5.5	0.957	5.5	0.957
1	3.306(40)	1.071(25)	3.291(18)	1.081(12)	3.291(19)	1.081(12)
2	2.482(31)	1.093(37)	2.479(20)	1.096(23)	2.471(20)	1.106(24)
3	2.010(27)	1.093(48)	2.009(19)	1.096(35)	2.003(19)	1.106(35)
4	1.695(22)	1.089(57)	1.691(16)	1.099(43)	1.690(17)	1.103(44)
5	1.468(18)	1.087(65)	1.462(14)	1.109(49)	1.464(15)	1.100(52)
6	1.296(16)	1.086(73)	1.288(12)	1.122(55)	1.292(14)	1.100(63)
7	1.160(14)	1.086(82)	1.151(11)	1.138(62)	1.157(13)	1.101(74)
8	1.050(13)	1.088(93)	1.041(10)	1.155(70)	1.048(13)	1.103(87)

these couplings into Eq. (2.9) for the Λ-parameter, using there the 3-loop β-function. This gives the results in the third column of Table 5. Employing the 2-loop β-function leads to results that are larger by roughly 0.02. The table shows that for $u < 2$ the Λ-parameter barely moves within its error bars. To be conservative, we use the global fit result and quote

$$-\ln(\Lambda L_{\max}) = 1.09(7) \quad \text{at } u_{\max} = 5.5 \tag{4.3}$$

as our final result, if the hadronic scale $L_{\max}$ is defined through $u_{\max} = 5.5$.

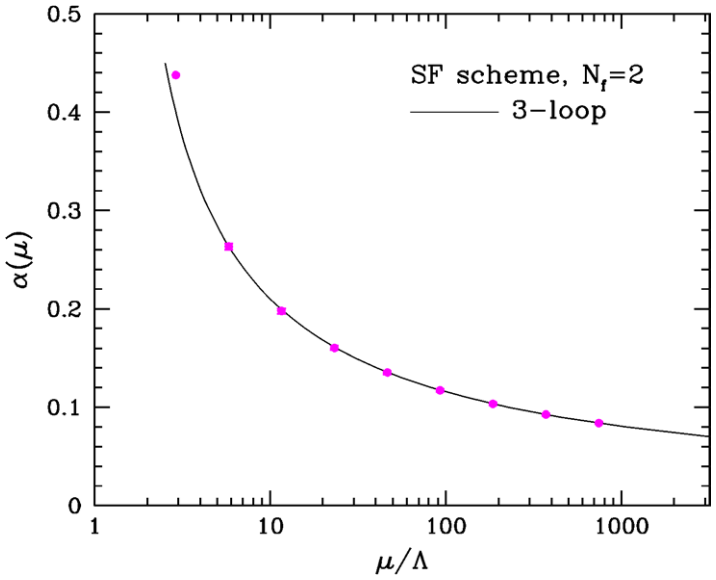

Fig. 4. Running of the strong coupling in the Schrödinger functional scheme.

We have in addition computed the Λ-parameter as a function of $u_{\max}$ in the interval $u_{\max} = 3.0 \ldots 5.5$. The results can be parametrized as

$$-\ln(\Lambda L_{\max}) = \frac{1}{2b_0 u_{\max}} + \frac{b_1}{2b_0^2}\ln(b_0 u_{\max}) - 0.1612 + 0.0379 u_{\max}. \tag{4.4}$$

This parametrization is motivated by (2.9) and represents the central values of our data with a precision better than one permille. The absolute error of $-\ln(\Lambda L_{\max})$ that we quote for all the values of $u_{\max}$ is 0.07. This means that we have calculated the Λ-parameter in units of $L_{\max}$ with a precision of seven percent.

The running of the Schrödinger functional coupling $\alpha(\mu) = \bar{g}^2(1/\mu)/(4\pi)$ as a function of μ/Λ is displayed in Fig. 4. The points refer to the entries of the second column of Table 5. The symbol size is larger than their error. The difference between the perturbative and the non-perturbative running of the coupling looks small in this plot. However, if we had used perturbation theory only to evolve the coupling over the range considered here, the Λ-parameter would have been overestimated by up to 14%, depending on $u_{\max}$. This corresponds to an extra error of 3% for the coupling in the range where its value is close to 0.12, corresponding to the physical value of $\alpha_{\overline{\rm MS}}$ at M_Z. Needless to add, this error could of course not even be quantified without non-perturbative information.

Furthermore, our non-perturbative coupling was designed to have a good perturbative expansion, since we rely on the 3-loop β-function in the (high-energy part of the) computation of the Λ-parameter. With our computation we have *shown* that for the Schrödinger functional coupling there is an overlapping region where both, perturbative and non-perturbative methods apply. In no way is this to be interpreted as a general statement about QCD observables or couplings at certain energies.

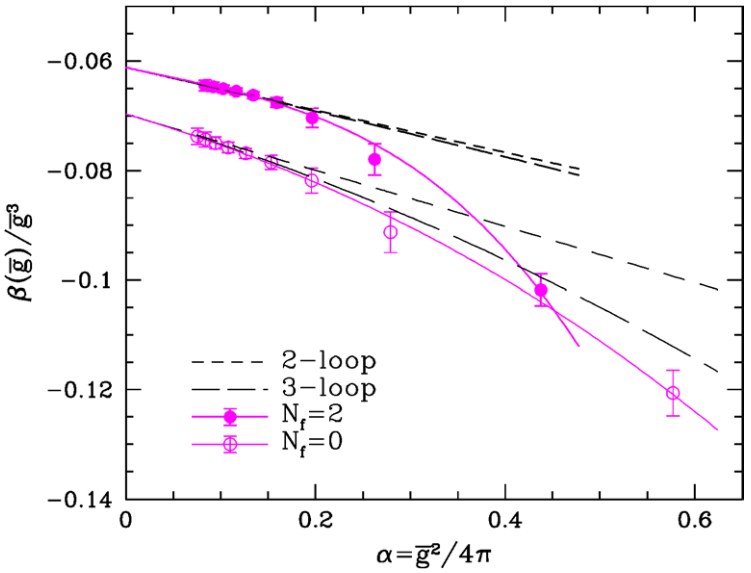

Fig. 5. Non-perturbative β-function in the Schrödinger functional scheme.

In Fig. 5 we show the non-perturbative β-function in the Schrödinger functional scheme, together with the 2-loop and the 3-loop perturbation theory. It has been obtained recursively from (2.27). The derivative of the step scaling function needed there has been calculated from the polynomial interpolating $\sigma(u)$ (see continuous line in Fig. 3). The non-perturbative data are fitted with two parameters beyond the 2-loop β-function. The plot again shows an overlapping region in $\bar{g}$, where the perturbative and the non-perturbative β-functions agree well with each other. For $\alpha > 0.2$, however, perturbation theory is no longer valid. Furthermore, the plot shows the difference between $N_f = 0$ and $N_f = 2$. Already the leading coefficient b_0 of the β-function depends on the number of flavors, and this is nicely reflected in the figure.

4.2. Computation of $\bar{v}$ as a function of the strong coupling

The difference between the quenched approximation and the two-flavor theory is also apparent in the renormalized quantity $\bar{v}$ defined in (2.16). As a function of the coupling u we write (at zero quark mass)

$$\bar{v} = \omega(u) = \lim_{a/L \to 0} \Omega(u, a/L). \tag{4.5}$$

In perturbation theory, Ω is known to 2-loop order,

$$\Omega(u, a/L) = (v_1 + v_2 u)\big(1 + \epsilon_1(a/L) + \epsilon_2(a/L)u\big) + \mathrm{O}\big(u^2\big). \tag{4.6}$$

Here [16,30,55],

$$v_1 = 0.0694603(1) + 0.0245370(1)N_f, \tag{4.7}$$

Table 6
Cutoff effects of $\bar{v}$ in perturbation theory

L/a	$N_f = 0$		$N_f = 2$	
	$\epsilon_1(a/L)$	$\epsilon_2(a/L)$	$\epsilon_1(a/L)$	$\epsilon_2(a/L)$
4	0.1880609(17)	−0.02020(24)	0.3044344(25)	0.03725(43)
5	0.1085045(16)	−0.01347(22)	0.1822083(22)	0.01255(39)
6	0.0677292(15)	−0.00910(22)	0.1114033(21)	0.00325(36)
7	0.0460993(15)	−0.00660(21)	0.0727865(20)	−0.00047(35)
8	0.0335967(15)	−0.00513(21)	0.0502340(20)	−0.00130(34)
10	0.0203927(15)	−0.00357(21)	0.0280832(19)	−0.00118(34)
12	0.0138002(15)	−0.00273(20)	0.0181305(19)	−0.00091(33)
14	0.0099904(15)	−0.00219(20)	0.0127946(19)	−0.00074(33)
16	0.0075781(15)	−0.00181(20)	0.0095635(19)	−0.00064(33)
20	0.0047983(14)	−0.00133(20)	0.0059634(19)	−0.00050(33)
24	0.0033132(14)	−0.00103(20)	0.0040873(19)	−0.00040(33)

$$v_2 = -0.001364(14) - 0.000101(17)N_f - 0.0003362(30)N_f^2, \tag{4.8}$$

and the perturbative cutoff effects are listed in Table 6. Note that the tree-level coefficient of $\bar{v}$ vanishes exactly because of the definition of the couplings. The perturbative results indicate a large effect for going from the zero- to the two-flavor theory.

The first step in the analysis is to project $\bar{v}$ on zero mass. To this end we have obtained the crude estimate $\partial\bar{v}/\partial(am) \approx -0.15(4)$ at constant u from the matching runs at the smallest coupling and with $L/a = 4$. We use it also at the other couplings. After this projection, the perturbative cutoff effects are eliminated (similarly to (2.33)) by replacing Ω by

$$\Omega^{(2)}(u, a/L) = \frac{\Omega(u, a/L)}{1 + \epsilon_1(a/L) + \epsilon_2(a/L)u} \tag{4.9}$$

in the analysis. In contrast to the coupling, this correction is substantial and the resulting continuum extrapolation is much smoother [10].

Then we project $\Omega^{(2)}(u, a/L)$ on some reference couplings in the range $u = 0.9793\ldots 5.5$, using a numerical estimate for the slope. In principle, we would have to propagate the error of $u = \bar{g}^2$ into an extra error of $\Omega^{(2)}(u, a/L)$. However, it turns out, both from perturbation theory and from the non-perturbative fits later, that the variation of $\bar{v}$ with u is so small that this extra error can safely be neglected.

We make an ansatz linear in $(a/L)^2$ for the continuum extrapolation. The data for the two different actions are extrapolated separately and the continuum results are then averaged according to their weight. The data at $L/a = 4, 5$ are left out.

The results are displayed in Fig. 6 together with $\bar{v}$ at $N_f = 0$ from Ref. [16]. The comparison shows that $\bar{v}$ increases by almost a factor two when going from the quenched approximation to $N_f = 2$.

4.3. *Evaluation of Λr_0*

For the O(a) improved action [32] used in our computations, the low-energy scale r_0 has been calculated at $\beta \equiv 6/g_0^2 = 5.2$ (or $a \approx 0.1$ fm) by two groups [44,56]. Recently,

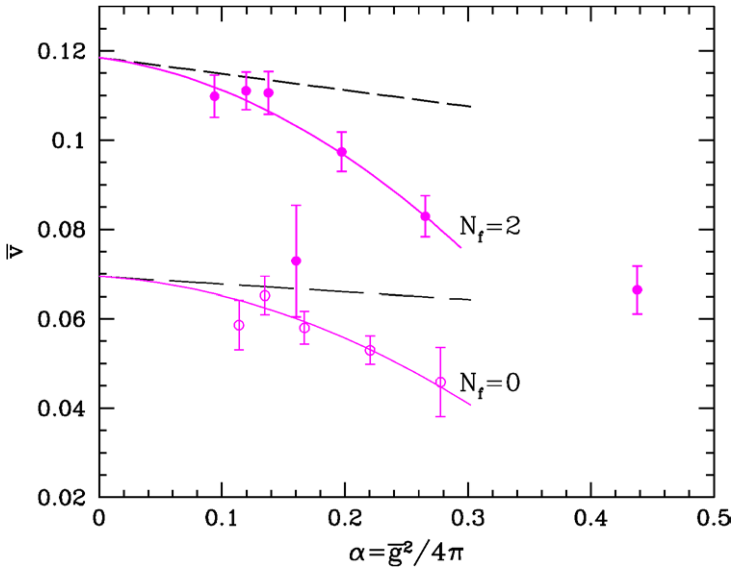

Fig. 6. $\bar{v}$ as a function of the strong coupling α. The dashed lines show the 2-loop perturbation theory while the solid lines are non-perturbative fits for $\alpha < 0.3$ including an additional α^2-term.

Table 7
Simulation results for $\bar{g}^2(L)$ at low β

β	κ	L/a	$\bar{g}^2(L)$	
			$c_t = 1$-loop	$c_t = 2$-loop
5.20	0.13600	4	3.32(2)	3.65(3)
5.20	0.13600	6	4.31(4)	4.61(4)
5.29	0.13641	4	3.184(16)	3.394(17)
5.29	0.13641	6	4.059(32)	4.279(37)
5.29	0.13641	8	5.34(8)	5.65(9)
5.40	0.13669	4	3.016(20)	3.188(24)
5.40	0.13669	6	3.708(31)	3.861(34)
5.40	0.13669	8	4.704(59)	4.747(63)

The hopping parameters κ are set to the critical ones (κ_c) of [57].

these large-volume $N_f = 2$ simulations of QCD have been extended to smaller values of the lattice spacing, namely $5.2 \leqslant \beta \leqslant 5.4$ [57]. In order to obtain Λr_0 and to study its dependence on the lattice spacing, we here use results for r_0/a of [57] at $\beta = 5.2, 5.29, 5.4$ and compare also to the numbers resulting from r_0/a of [44].

First, we obtain the renormalized coupling on lattices with extent $L/a = 4, 6, 8$ at the three chosen values of β. It is listed in Table 7. The hopping parameters κ are taken from [57]. They correspond to roughly massless pions and thus massless quarks. We checked that reasonable changes of κ, e.g., requiring Eq. (2.19), affect our analysis only to a negligible amount. We then set the improvement coefficient c_t to its 2-loop value and obtain

Table 8
Low-energy scale r_0 in the chiral limit and the combination $\Lambda_{\overline{\rm MS}} r_0$ as obtained for two values of $u_{\rm max} = \bar{g}^2(L_{\rm max})$

β	r_0/a	$L_{\rm max}/a$	$\Lambda_{\overline{\rm MS}} r_0$	$L_{\rm max}/a$	$\Lambda_{\overline{\rm MS}} r_0$
		$u_{\rm max} = 3.65$		$u_{\rm max} = 4.61$	
5.20	5.45(5)(20)	4.00(6)	0.655(27)	6.00(8)	0.610(25)
5.29	6.01(4)(22)	4.67(6)	0.619(25)	6.57(6)	0.614(24)
5.40	7.01(5)(15)	5.43(9)	0.621(17)	7.73(10)	0.609(16)

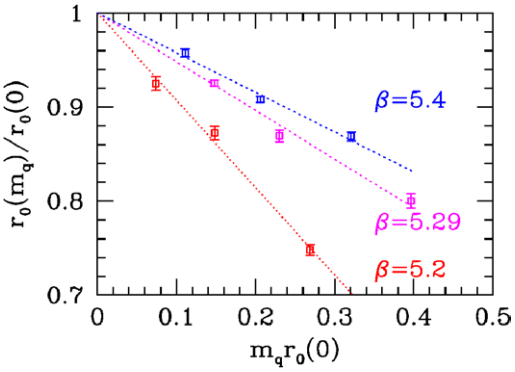

Fig. 7. Dependence of r_0 on the bare quark mass $m_{\rm q} = (1/\kappa - 1/\kappa_{\rm c})/2$. Both quantities are rescaled (made dimensionless) by the extrapolated value of r_0, denoted by $r_0(0)$. The uncertainty of this rescaling is not propagated into the errors. For $\kappa_{\rm c}$, we take the values of [57], listed in Table 7.

$L_{\rm max}/a$ for the three values of β combined with two fixed values $u_{\rm max} \equiv \bar{g}^2(L_{\rm max}) = 3.65$ and $u_{\rm max} = 4.61$ by an interpolation of the data in Table 7. These values of $L_{\rm max}/a$, which are recorded in Table 8, are insensitive to the interpolation formula used.

Second, we analyze the raw data for r_0/a at finite bare quark masses, $m_{\rm q}$, in order to obtain the value corresponding to massless quarks (the up- and down-quark masses may safely be neglected in this context). At each bare coupling, three different quark masses, corresponding to pion masses between about 500 MeV and 1 GeV, have been simulated in [57]. As seen in Fig. 7, the radius r_0 depends approximately linearly on the bare quark mass in this range. The figure also demonstrates that the slope is strongly cutoff dependent; its magnitude decreases quite rapidly as β increases (the lattice spacing decreases).[7] This has been noted earlier [58] and reminds us that the study of lattice artifacts is important. On the other hand, we are here not interested in the slope but in r_0 at zero quark mass. We estimate it by a simple linear extrapolation in $m_{\rm q}$. Since the linear behavior is not guaranteed to extend all the way to zero quark mass, we include a systematic error of the extrapolation in addition to the statistical one: an uncertainty of half the difference of the

[7] The slope visible in Fig. 7 is not directly a physical observable, since (up to a-effects) the renormalized quark mass is given by $m_{\rm R} = Z_{\rm m} m_{\rm q}$ rather than by $m_{\rm q}$. However, it appears unlikely that the strong dependence of the slope on g_0 is canceled by $Z_{\rm m}$, since the latter is expected to be a weak function of the bare coupling. More details can be found in [58], where also a properly renormalized slope has been analyzed.

last data point and the extrapolated value is added as the second error in Table 8. Within the total error, dominated by the systematic one due to the extrapolation, our values of r_0/a do agree with those quoted in [44,56,57], where somewhat different ansätze—and in [44] also different data—have been used.

Third, combining Eqs. (4.4) and (2.11) with r_0/a and $L_{\max}/a$ of Table 8, one arrives at the columns $\Lambda_{\overline{\rm MS}} r_0$ in that table. Here we have added errors in quadrature, except for the one attributed to Eq. (4.4), which is independent of the bare coupling. The resulting $\Lambda_{\overline{\rm MS}} r_0$ are remarkably stable with respect to the change of the lattice spacing and also the choice of $u_{\max}$. In particular, for $L_{\max}/a > 4.5$ all numbers including their errors are covered by the interval $0.58 \leqslant \Lambda_{\overline{\rm MS}} r_0 \leqslant 0.66$ and also the central value obtained with the worst discretization $L_{\max}/a = 4$ is inside. We thus quote

$$\Lambda^{(2)}_{\overline{\rm MS}} r_0 = 0.62(4)(4) \tag{4.10}$$

as our result, the second error deriving from the 7% error on $\Lambda L_{\max}$.

We finally mention that we repeated the above analysis also for $c_{\rm t}$ to 1-loop precision and the values $u_{\max} = 3.32$ and 4.31 suggested by Table 7. The central values for $\Lambda_{\overline{\rm MS}} r_0$ are then up to 15% lower than for $c_{\rm t}$ at 2-loop precision, but this difference shrinks as $L_{\max}/a$ grows. At the largest value of $L_{\max}/a$, the number for $\Lambda_{\overline{\rm MS}} r_0$ is again fully contained in the range $\Lambda_{\overline{\rm MS}} r_0 = 0.62(4)$.

5. Conclusions

This non-perturbative QCD computation has required extensive simulations of $N_{\rm f} = 2$ QCD with O(a) improved massless Wilson fermions in finite volume. In our situation, discretization errors turned out to be very small, as seen for example in Fig. 2 and also in [10]. Although we could achieve the necessary precision only on lattices up to a size 16^4, the smallness of discretization errors allowed to obtain the running of the QCD coupling in the continuum limit and to good accuracy. As in the $N_{\rm f} = 0$ (pure gauge) theory, the energy dependence of the coupling in the Schrödinger functional scheme is now known over more than two orders of magnitude in the energy scale. This is the main result of our investigation.

The $N_{\rm f}$-dependence is best illustrated in Fig. 5, where we also observe excellent agreement with 3-loop perturbation theory for $\alpha \leqslant 0.2$, while for larger α, the non-perturbative β-function breaks away rapidly from the perturbative approximation. At $\alpha \approx 0.3 \ldots 0.4$, a couple of additional higher-order perturbative terms with *coefficients of a reasonable size* would not be able to come close to the non-perturbative β-function.

To calibrate the overall energy scale, one fixes a large enough value of the coupling to be in the low-energy region and relates the associated distance, $L_{\max}$, to a non-perturbative, large-volume observable. For technical reasons, explained in Section 2.5, we have chosen the hadronic radius r_0, which has an unambiguous definition in terms of the force $F(r)$ between static quarks, via $r_0^2 F(r_0) = 1.65$ [45]. This quantity has also been chosen in the computation of the Λ-parameter for $N_{\rm f} = 0$ [7]. We compare Λr_0 for various numbers of flavors in Table 9.

Table 9
The QCD Λ-parameter in units of r_0

N_f	$\Lambda_{\overline{MS}}^{(N_f)} r_0$	Reference	Remarks
0	0.60(5)	[7]	
2	0.62(4)(4)	This work	
4	0.57(8)	[59–61]	DIS @ NNLO & $r_0 = 0.5$ fm
4	0.74(10)	[1]	World average & $r_0 = 0.5$ fm
5	0.54(8)	[1]	World average & $r_0 = 0.5$ fm

Non-perturbative, purely theoretical determinations for $N_f = 0, 2$ are compared to extractions of Λ from high-energy scattering experiments, using high-order perturbation theory combined with the phenomenological estimate $r_0 \approx 0.5$ fm [45].

The last two entries in the table represent one and the same world average by S. Bethke of α-measurements. They are related by the *perturbative* matching of the effective theories with $N_f = 4$ and $N_f = 5$ massless quarks [62]. While little can be said on the N_f-dependence of $\Lambda_{\overline{MS}}^{(N_f)} r_0$ on general grounds, the prediction that there should be a significant drop from $N_f = 4$ to $N_f = 5$ depends only on perturbation theory at the scale of the b-quark mass and should thus be reliable. A similar statement for the change from $N_f = 3$ to $N_f = 4$ is less certain as it involves physics at and below the mass of the charm quark.

Another relevant issue in the above comparison is that we used $r_0 \approx 0.5$ fm to relate the high-energy experiments to our theoretical predictions. Although it appears unlikely that r_0 differs by 10% from this value, a true error is difficult to estimate until a reliable non-perturbative computation of, e.g., $r_0 F_\pi$ has been performed. Indeed, such a computation, or more directly the computation of $L_{max} \times F_\pi$ for $N_f = 2$, is the most urgent next step to be taken in our programme. After that, the effect of the remaining (massive) quarks needs to be estimated.

Keeping the above caveats in mind, we still may convert the Λ-parameter to physical units and obtain

$$\Lambda_{\overline{MS}}^{(2)} = 245(16)(16)\ \text{MeV} \quad [\text{with } r_0 = 0.5\ \text{fm}]. \tag{5.1}$$

Although in this case the four-flavor theory has not yet been reached, it is a very non-trivial test of QCD that the non-perturbative results, which use experimental input at low energies of order $1/r_0 \approx 400$ MeV, agree roughly with the high energy, perturbative extractions of Λ. Unraveling the details in this comparison will still require some work; some of it was just mentioned.

Now, that $\alpha(\mu)$ is known, the tables presented in this work also provide the bare parameters of our lattice action needed in the computation of the energy dependence of the renormalized quark mass and composite operators. These are then readily related to the appropriate renormalization group invariants.

Acknowledgements

We are indebted to Martin Lüscher who founded the ALPHA Collaboration and who led ground-breaking work for this project—as demonstrated by the references we quote. We

further thank Achim Bode, Bernd Gehrmann, Martin Hasenbusch, Karl Jansen, Francesco Knechtli, Stefan Kurth, Hubert Simma, Stefan Sint, Peter Weisz and Hartmut Wittig for many useful discussions and collaboration in early parts of this project [10]. We are grateful to Gerrit Schierholz for communicating the results of [57]. We further thank DESY for computing resources and the APE Collaboration and the staff of the computer center at DESY Zeuthen for their support.

The computation of α_s is one project of SFB Transregio 9 "Computational Particle Physics" and has been strongly supported there as well as in Graduiertenkolleg GK 271 by the Deutsche Forschungsgemeinschaft (DFG). We thank our colleagues in the SFB for discussions, in particular Johannes Blümlein, Kostia Chetyrkin and Fred Jegerlehner. This work has also been supported by the European Community's Human Potential Programme under contract HPRN-CT-2000-00145.

Appendix A. Evaluation of $\partial\Gamma/\partial\eta$

Our central observable, Eq. (2.15), translates into the expectation value

$$\left.\frac{\partial\Gamma}{\partial\eta}\right|_{\eta=0} = \left\langle\frac{dS}{d\eta}\right\rangle = \left\langle\frac{dS_g}{d\eta}\right\rangle + \left\langle\frac{dS_f^{\text{eff}}}{d\eta}\right\rangle, \tag{A.1}$$

where the pure gauge part $dS_g/d\eta$ has been discussed in [16] and

$$\frac{dS_f^{\text{eff}}}{d\eta} = -N_f \operatorname{Tr} Q^{-1}\frac{dQ}{d\eta} = -N_f\left\langle\varphi^\dagger Q^{-1}\frac{dQ}{d\eta}\varphi\right\rangle_\varphi. \tag{A.2}$$

Here we have used $S_f^{\text{eff}} = -N_f \operatorname{Tr}\ln Q$ with $Q = \gamma_5(D+m_0) = Q^\dagger$ and D the (one-flavor) Dirac operator including improvement terms. As usual, S_f^{eff} is obtained after integrating out the fermion fields and the trace extends over color and Dirac indices as well as over the space–time points. The last expression in Eq. (A.2) represents an average over a complex random field $\varphi(x)$ with the property

$$\left\langle\varphi^*_{c\alpha}(x)\varphi_{d\beta}(y)\right\rangle_\varphi = \delta_{cd}\delta_{\alpha\beta}\delta_{xy}, \tag{A.3}$$

where c, d denote color indices and α, β are Dirac indices. We may finally rewrite $dS_f^{\text{eff}}/d\eta$ in the form

$$\begin{aligned}\frac{dS_f^{\text{eff}}}{d\eta} &= -N_f\left\langle\sum_{x|x_0\in\{a,T-a\}}\frac{1}{2}\operatorname{tr}\frac{dQ(x,x)}{d\eta}\left[\varphi(x)X^\dagger(x) + X(x)\varphi^\dagger(x)\right]\right\rangle_\varphi,\\ QX &= \varphi,\end{aligned} \tag{A.4}$$

where we have used the fact that $dQ/d\eta$ vanishes except for the clover terms, which are diagonal in the coordinate x and contribute only on the time slices $x_0 = a$ and $x_0 = T - a$. Now "tr" is over spin and color only. Eq. (A.4) is in the form used in [63] for the contribution of the clover terms to the pseudofermionic force in the HMC algorithm and is evaluated analogously. Only one solution of the Dirac equation is needed.

Of course, the average over the gauge fields can be interchanged with the one over the field φ and one may replace (A.2) by an average over a finite number of fields φ drawn from a distribution satisfying (A.3). We found that the fluctuations of such a noisy (unbiased) estimator for $dS_{\mathrm{f}}^{\mathrm{eff}}/d\eta$ are small compared to the ones of $dS_{\mathrm{g}}/d\eta$, already when only one field φ (from a Gaussian distribution) is used per gauge configuration. This has hence been our method of choice in all simulations.

Appendix B. Detailed numerical results

Tables 10 and 11 list detailed parameters and results of our simulations.

Table 10
Simulation parameters and results using the 1-loop value for c_{t}

L/a	β	κ	$\bar{g}^2$	$\Delta(\bar{g}^2)$	$\bar{v}$	$\Delta(\bar{v})$	m	$\Delta(m)$
$u = 0.9793$								
4	9.2364	0.1317486	0.9793	0.0007	0.1557	0.0019	−0.00600	0.00011
5	9.3884	0.1315391	0.9794	0.0009	0.1322	0.0023	0.00197	0.00005
6	9.5000	0.1315322	0.9793	0.0011	0.1266	0.0016	−0.00014	0.00003
8	9.7341	0.131305	0.9807	0.0017	0.1177	0.0042	0.00074	0.00006
8	9.2364	0.1317486	1.0643	0.0034	0.1244	0.0061	0.00010	0.00004
10	9.3884	0.1315391	1.0721	0.0039	0.1151	0.0077	0.00210	0.00003
12	9.5000	0.1315322	1.0802	0.0044	0.1227	0.0072	−0.00091	0.00002
16	9.7341	0.131305	1.0753	0.0055	0.1047	0.0080	−0.00008	0.00003
$u = 1.1814$								
4	8.2373	0.1327957	1.1814	0.0005	0.1483	0.0016	0.00100	0.00011
5	8.3900	0.1325800	1.1807	0.0012	0.1353	0.0018	−0.00018	0.00009
6	8.5000	0.1325094	1.1814	0.0015	0.1269	0.0014	−0.00036	0.00003
8	8.7223	0.1322907	1.1818	0.0029	0.1141	0.0048	−0.00115	0.00004
8	8.2373	0.1327957	1.3154	0.0055	0.1209	0.0061	0.00020	0.00005
10	8.3900	0.1325800	1.3287	0.0059	0.1128	0.0070	0.00097	0.00007
12	8.5000	0.1325094	1.3253	0.0067	0.1304	0.0068	−0.00102	0.00002
16	8.7223	0.1322907	1.3347	0.0061	0.1065	0.0049	−0.00194	0.00002
$u = 1.5031$								
4	7.2103	0.1339411	1.5031	0.0010	0.1437	0.0010	−0.00074	0.00010
5	7.3619	0.1339100	1.5044	0.0027	0.1250	0.0031	0.00052	0.00010
6	7.5000	0.1338150	1.5031	0.0025	0.1201	0.0024	−0.00078	0.00004
8	7.2103	0.1339411	1.7310	0.0059	0.1151	0.0037	0.00959	0.00004
10	7.3619	0.1339100	1.7581	0.0113	0.1062	0.0084	0.00257	0.00005
12	7.5000	0.1338150	1.7449	0.0119	0.1223	0.0073	−0.00138	0.00004
$u = 1.7319$								
4	6.7251	0.1347424	1.7319	0.0020	0.1378	0.0009	−0.00181	0.00013
5	6.8770	0.1346900	1.7333	0.0032	0.1272	0.0025	−0.00005	0.00011
6	7.0000	0.1345794	1.7319	0.0034	0.1161	0.0023	−0.00002	0.00005
8	6.7251	0.1347424	2.0583	0.0070	0.1008	0.0032	0.01051	0.00005
10	6.8770	0.1346900	2.0855	0.0208	0.0934	0.0080	0.00335	0.00006
12	7.0000	0.1345794	2.0575	0.0196	0.0833	0.0082	−0.00049	0.00006

Table 11
Simulation parameters and results using the 2-loop value for c_t

L/a	β	κ	$\bar{g}^2$	$\Delta(\bar{g}^2)$	$\bar{v}$	$\Delta(\bar{v})$	m	$\Delta(m)$
$u = 1.5031$								
4	7.2811	0.1338383	1.5031	0.0012	0.1434	0.0013	0.00043	0.00015
5	7.4137	0.1338750	1.5033	0.0026	0.1310	0.0027	−0.00083	0.00009
6	7.5457	0.1337050	1.5031	0.0030	0.1247	0.0031	0.00072	0.00008
8	7.7270	0.133488	1.5031	0.0035	0.1219	0.0032	−0.00084	0.00003
8	7.2811	0.1338383	1.7204	0.0054	0.1091	0.0037	0.00928	0.00004
10	7.4137	0.1338750	1.7372	0.0104	0.1110	0.0063	0.00109	0.00004
12	7.5457	0.1337050	1.7305	0.0122	0.0893	0.0079	−0.00006	0.00008
16	7.7270	0.133488	1.7231	0.0151	0.1017	0.0092	−0.00154	0.00019
$u = 2.0142$								
4	6.3650	0.1353200	2.0142	0.0024	0.1349	0.0017	0.00000	0.00023
5	6.5000	0.1353570	2.0142	0.0044	0.1236	0.0024	0.00002	0.00011
6	6.6085	0.1352600	2.0146	0.0056	0.1205	0.0029	0.00030	0.00009
8	6.8217	0.134891	2.0142	0.0102	0.0991	0.0045	0.00049	0.00007
8	6.3650	0.1353200	2.4814	0.0172	0.1016	0.0049	0.01318	0.00008
10	6.5000	0.1353570	2.4383	0.0188	0.0900	0.0050	0.00367	0.00005
12	6.6085	0.1352600	2.5077	0.0259	0.1074	0.0069	0.00013	0.00004
16	6.8217	0.134891	2.475	0.031	0.0916	0.0076	−0.00053	0.00006
$u = 2.4792$								
4	5.8724	0.1360000	2.4792	0.0034	0.1206	0.0016	0.00000	0.00026
5	6.0000	0.1361820	2.4792	0.0073	0.1085	0.0023	−0.00009	0.00014
6	6.1355	0.1361050	2.4792	0.0082	0.1025	0.0032	0.00000	0.00013
8	6.3229	0.1357673	2.4792	0.0128	0.1015	0.0053	0.00000	0.00016
8	5.8724	0.1360000	3.2511	0.0277	0.0859	0.0043	0.01819	0.00011
10	6.0000	0.1361820	3.3356	0.0502	0.0796	0.0064	0.00579	0.00009
12	6.1355	0.1361050	3.1558	0.0552	0.0801	0.0079	0.00078	0.00007
16	6.3229	0.1357673	3.3263	0.0472	0.0806	0.0074	0.00039	0.00017
$u = 3.3340$								
4	5.3574	0.1356400	3.3340	0.0109	0.1087	0.0013	0.00000	0.00040
5	5.5000	0.1364220	3.3340	0.0182	0.0965	0.0018	−0.00004	0.00017
6	5.6215	0.1366650	3.3263	0.0196	0.0894	0.0031	0.00051	0.00018
8	5.8097	0.1366077	3.334	0.019	0.0887	0.0042	0.00000	0.00004
8	5.3574	0.1356400	5.588	0.049	0.0576	0.0036	0.03163	0.00019
10	5.5000	0.1364220	5.430	0.098	0.0585	0.0048	0.01126	0.00012
12	5.6215	0.1366650	5.624	0.089	0.0607	0.0043	0.00334	0.00015
16	5.8097	0.1366077	5.4763	0.1236	0.0689	0.0052	0.00048	0.00004

References

[1] S. Bethke, Nucl. Phys. B (Proc. Suppl.) 135 (2004) 345, hep-ex/0407021.
[2] K.I. Ishikawa, Plenary talk at LATTICE '04, Fermilab, Batavia IL, USA, Nucl. Phys. B (Proc. Suppl.) 140 (2005) 20, hep-lat/0410050.
[3] M. Lüscher, P. Weisz, U. Wolff, Nucl. Phys. B 359 (1991) 221.
[4] M. Lüscher, et al., Nucl. Phys. B 384 (1992) 168, hep-lat/9207009.
[5] S. Sint, Nucl. Phys. B 451 (1995) 416, hep-lat/9504005.
[6] ALPHA Collaboration, G. de Divitiis, et al., Nucl. Phys. B 437 (1995) 447, hep-lat/9411017.
[7] ALPHA Collaboration, S. Capitani, et al., Nucl. Phys. B 544 (1999) 669, hep-lat/9810063.

[8] ALPHA Collaboration, J. Garden, et al., Nucl. Phys. B 571 (2000) 237, hep-lat/9906013.
[9] ALPHA Collaboration, J. Heitger, et al., Nucl. Phys. B (Proc. Suppl.) 106 (2002) 859, hep-lat/0110201.
[10] ALPHA Collaboration, A. Bode, et al., Phys. Lett. B 515 (2001) 49, hep-lat/0105003.
[11] TXL Collaboration, A. Spitz, et al., Phys. Rev. D 60 (1999) 074502, hep-lat/9906009.
[12] QCDSF Collaboration, M. Göckeler, et al., Nucl. Phys. B (Proc. Suppl.) 140 (2005) 228, hep-lat/0409166.
[13] C. Davies, et al., Nucl. Phys. B (Proc. Suppl.) 119 (2003) 595, hep-lat/0209122.
[14] B. Bunk, et al., Nucl. Phys. B 697 (2004) 343, hep-lat/0403022.
[15] M. Lüscher, et al., Nucl. Phys. B 389 (1993) 247, hep-lat/9207010.
[16] M. Lüscher, et al., Nucl. Phys. B 413 (1994) 481, hep-lat/9309005.
[17] S. Sint, Nucl. Phys. B (Proc. Suppl.) 42 (1995) 835, hep-lat/9411063.
[18] R. Sommer, Non-perturbative renormalization of QCD, Lectures given at 36th Internationale Universitätswochen für Kernphysik und Teilchenphysik, Schladming, Austria, hep-ph/9711243.
[19] M. Lüscher, Advanced lattice QCD, Lectures given at Les Houches Summer School in Theoretical Physics, Les Houches, France, hep-lat/9802029.
[20] C.G. Callan Jr., Phys. Rev. D 2 (1970) 1541.
[21] K. Symanzik, Commun. Math. Phys. 18 (1970) 227.
[22] S. Weinberg, Phys. Rev. D 8 (1973) 3497.
[23] Y. Frishman, R. Horsley, U. Wolff, Nucl. Phys. B 183 (1981) 509.
[24] O.V. Tarasov, A.A. Vladimirov, A.Y. Zharkov, Phys. Lett. B 93 (1980) 429.
[25] M. Lüscher, P. Weisz, Nucl. Phys. B 452 (1995) 213, hep-lat/9504006.
[26] M. Lüscher, P. Weisz, Nucl. Phys. B 452 (1995) 234, hep-lat/9505011.
[27] B. Allés, A. Feo, H. Panagopoulos, Nucl. Phys. B 491 (1997) 498, hep-lat/9609025.
[28] A. Bode, H. Panagopoulos, Nucl. Phys. B 625 (2002) 198, hep-lat/0110211.
[29] ALPHA Collaboration, A. Bode, P. Weisz, U. Wolff, Nucl. Phys. B 576 (2000) 517, hep-lat/9911018;
ALPHA Collaboration, A. Bode, P. Weisz, U. Wolff, Nucl. Phys. B 600 (2001) 453, Erratum;
ALPHA Collaboration, A. Bode, P. Weisz, U. Wolff, Nucl. Phys. B 608 (2001) 481, Erratum.
[30] S. Sint, R. Sommer, Nucl. Phys. B 465 (1996) 71, hep-lat/9508012.
[31] B. Sheikholeslami, R. Wohlert, Nucl. Phys. B 259 (1985) 572.
[32] ALPHA Collaboration, K. Jansen, R. Sommer, Nucl. Phys. B 530 (1998) 185, hep-lat/9803017.
[33] M. Lüscher, et al., Nucl. Phys. B 478 (1996) 365, hep-lat/9605038.
[34] M. Lüscher, P. Weisz, Nucl. Phys. B 479 (1996) 429, hep-lat/9606016.
[35] K.G. Wilson, Phys. Rev. D 10 (1974) 2445.
[36] K. Symanzik, Some topics in quantum field theory, in: R. Schrader, et al. (Eds.), Mathematical Problems in Theoretical Physics, in: Lecture Notes in Physics, vol. 153, Springer-Verlag, New York, 1982.
[37] K. Symanzik, Nucl. Phys. B 226 (1983) 187.
[38] K. Symanzik, Nucl. Phys. B 226 (1983) 205.
[39] B. Gehrmann, et al., Nucl. Phys. B 612 (2001) 3, hep-lat/0106025.
[40] S. Weinberg, Physica A 96 (1979) 327.
[41] J. Gasser, H. Leutwyler, Ann. Phys. 158 (1984) 142.
[42] G. Colangelo, Plenary talk at LATTICE '04, Fermilab, Batavia IL, USA, Nucl. Phys. B (Proc. Suppl.) 140 (2005) 120, hep-lat/0409111.
[43] UKQCD Collaboration, A.C. Irving, et al., Phys. Lett. B 518 (2001) 243, hep-lat/0107023.
[44] JLQCD Collaboration, S. Aoki, et al., Phys. Rev. D 68 (2003) 054502, hep-lat/0212039.
[45] R. Sommer, Nucl. Phys. B 411 (1994) 839, hep-lat/9310022.
[46] S. Duane, et al., Phys. Lett. B 195 (1987) 216.
[47] R. Frezzotti, K. Jansen, Nucl. Phys. B 555 (1999) 395, hep-lat/9808011.
[48] R. Frezzotti, K. Jansen, Nucl. Phys. B 555 (1999) 432, hep-lat/9808038.
[49] M. Hasenbusch, Phys. Lett. B 519 (2001) 177, hep-lat/0107019.
[50] M. Hasenbusch, K. Jansen, Nucl. Phys. B 659 (2003) 299, hep-lat/0211042.
[51] ALPHA Collaboration, R. Frezzotti, et al., Comput. Phys. Commun. 136 (2001) 1, hep-lat/0009027.
[52] A. Bartoloni, et al., Nucl. Phys. B (Proc. Suppl.) 106 (2002) 1043, hep-lat/0110153.
[53] ALPHA Collaboration, U. Wolff, Comput. Phys. Commun. 156 (2004) 143, hep-lat/0306017.
[54] ALPHA Collaboration, M. Della Morte, et al., Nucl. Phys. B (Proc. Suppl.) 119 (2003) 439, hep-lat/0209023.

[55] A. Bode, $\bar{v}$ to two loop including cutoff effects, unpublished notes, 2001.
[56] UKQCD Collaboration, C.R. Allton, et al., Phys. Rev. D 65 (2002) 054502, hep-lat/0107021.
[57] QCDSF Collaboration, M. Göckeler, et al., hep-ph/0409312.
[58] ALPHA Collaboration, R. Sommer, et al., Nucl. Phys. B (Proc. Suppl.) 129 (2004) 405, hep-lat/0309171.
[59] J. Blümlein, H. Böttcher, A. Guffanti, Nucl. Phys. B (Proc. Suppl.) 135 (2004) 152, hep-ph/0407089.
[60] S. Moch, J.A.M. Vermaseren, A. Vogt, Nucl. Phys. B 688 (2004) 101, hep-ph/0403192.
[61] W.L. van Neerven, E.B. Zijlstra, Phys. Lett. B 272 (1991) 127.
[62] W. Bernreuther, W. Wetzel, Nucl. Phys. B 197 (1982) 228.
[63] K. Jansen, C. Liu, Comput. Phys. Commun. 99 (1997) 221, hep-lat/9603008.

B

Comparative benchmarks of full QCD algorithms

Comput. Phys. Commun. 136 (2001) 1-13

Computer Physics Communications 136 (2001) 1–13

Computer Physics Communications

www.elsevier.nl/locate/cpc

Comparative benchmarks of full QCD algorithms

Roberto Frezzotti [a], Martin Hasenbusch [b], Ulli Wolff [b,*], Jochen Heitger [c], Karl Jansen [d]

[a] *Dipt. di Fisica, Univ. di Milano Bicocca, Via Celoria 16, I-20133 Milano, Italy*
[b] *Institut für Physik, Humboldt Universität, Invalidenstr. 110, D-10099 Berlin, Germany*
[c] *DESY, Platanenallee 6, D-15738 Zeuthen, Germany*
[d] *CERN, Theory Division, CH-1211 Geneve 23, Switzerland*

Received 20 September 2000; received in revised form 10 November 2000

Abstract

We report performance benchmarks for several algorithms that we have used to simulate the Schrödinger functional with two flavors of dynamical quarks. They include hybrid and polynomial hybrid Monte Carlo with preconditioning. An appendix describes a method to deal with autocorrelations for nonlinear functions of primary observables as they are met here due to reweighting.

1. Introduction

In the past years the ALPHA Collaboration has pursued the goal to reliably compute the QCD gauge coupling at high energy in terms of non-perturbative low energy parameters. The concomitant necessity to deal with a large energy ratio in the continuum limit was solved by a breakup into recursive steps. Here one employs finite size rescaling by repeated factors of two and extrapolates to the continuum each step by itself. By a combination of theoretical reasoning and numerical tests the Schrödinger functional was determined as a particularly convenient framework for this purpose. The programme has been completed for the quenched approximation, see Refs. [1,2] for reviews of the approach and Ref. [3] for a summary of data. First tests with a non vanishing flavor number have been reported [4]. As is well known, by the inclusion of dynamical quarks the numerical cost is boosted by a large factor. The importance of algorithmic optimization can hence hardly be overestimated. The finite size technique with the Schrödinger functional — beside its uses for QCD physics — offers the possibility of an investigation of the lattice spacing dependence of the performance of fermion algorithms with all physical scales held fixed. Here we report on such results for several algorithms.

The Schrödinger functional can be regarded as the free energy Γ of QCD in a finite volume $L^3 \times T$,

$$\exp(-\Gamma) = \int D[U]D[\overline{\psi}]D[\psi] \times \exp\bigl(-S[U,\overline{\psi},\psi]\bigr). \tag{1.1}$$

The action S consists of the usual plaquette action for SU(3) gauge fields U and two degenerate flavors of clover-improved Wilson fermions. The box is periodic in space, and fixed gluon potentials and vanishing quark fields [1] are prescribed on the temporal bound-

* Corresponding author.
E-mail address: uwolff@physik.hu-berlin.de (U. Wolff).

[1] Non-vanishing quark sources are also possible but will not be needed here.

0010-4655/01/$ – see front matter
PII: S0010-4655(00)00242-3

aries. The boundary potentials C and C' at $x_0 = 0$ and $x_0 = T$ are specified in terms of the scale L and dimensionless parameters, one of which is called η and is kept variable. A convenient practical choice with $T = L$, introduced as point "A" in [5], is used throughout. Quark fields are periodic in space up to a phase $\theta = \pi/5$. An Abelian background field is induced which can be varied by changing η. The response to such an infinitesimal variation is used to define the renormalized coupling

$$g^2_{\rm SF}(L) = \left.\frac{\partial \Gamma_0/\partial\eta}{\partial \Gamma/\partial\eta}\right|_{\eta=0}, \tag{1.2}$$

where Γ_0/g_0^2 is the tree level value of Γ for bare coupling g_0. For a lattice realization we now have to choose values for L/a, g_0 and bare quark mass m_0 as well as coefficients for the improvement terms in the action. We take the latter as smooth functions of g_0 either by a perturbative expression or by a non-perturbative fit [6]. The mass m_0 is fixed by demanding zero PCAC-mass [7]. Hence we may approach the continuum limit by a sequence of lattices with growing L/a and g_0 adjusted to maintain a fixed value $g_{\rm SF}$. Conceptually this is exactly the same situation as in our quenched computations. The regularizing lattice spacing a varies while renormalized physics is held fixed. It is on such 'trajectories', that we study algorithm performance.

Our most extensive simulations of the O(a) improved Schrödinger functional have been conducted with the well-known hybrid Monte Carlo method (HMC) [8]. In our implementation we took advantage of preconditioning and the refinement proposed in [9]. It amounts to the introduction of two different step sizes for fermion-gluon and gluonic self-couplings in an approximately optimal proportion depending on their relative computational cost. In other long runs we applied the polynomial hybrid Monte Carlo (PHMC) [10,11]. Here, as for the multiboson technique [12], an approximately inverting polynomial of the Dirac operator is used to bosonize the theory. In the multiboson proposal the resulting action is represented by many boson fields with nearest neighbor couplings. For unimproved Wilson fermions finite step-size updates are employed, which however become impractical when the clover term is included — the case on that we concentrate here. A further disadvantage is the additional slowing down due to collective effects of the many bosons [13]. With PHMC the operator polynomial is employed to construct a non-local Gaussian action for only one boson field which is simulated by HMC. The imperfection of the polynomial can be corrected by an acceptance or reweighting step. Some results are reported which have been obtained by a recently proposed multi-level Metropolis procedure (MLM) [14]. Further details of the various algorithms will be given below.

2. Algorithms in this study

In this section we briefly describe our implementations of fermion Monte Carlo algorithms as they are benchmarked in this study. With each of them the goal is the inclusion of effects of the weight factor $\det(Q)^2$ which arises from integrating two degenerate flavors of quarks out of (1.1),

$$\exp(-\Gamma) = \int D[U]\exp\bigl(-S_{\rm gauge}[U]\bigr)\det(Q)^2. \tag{2.1}$$

Here the Hermitian operator Q for Sheikholeslami–Wohlert improved Wilson quarks has the structure

$$Q = c_0\gamma_5 M; \quad M = 1 - T - H. \tag{2.2}$$

The constant c_0 is chosen to contain the eigenvalues of Q in the interior of the interval $(-1, 1)$. The matrix M contains nearest neighbor hopping terms in H and the clover term in T, which is diagonal with respect to the lattice index. The detailed form of these components, including boundary improvement, can for instance be found in Ref. [15].

2.1. Hybrid Monte Carlo

The HMC method [8] has so far been the most popular fermion algorithm for QCD. In choosing a trajectory length of unity we followed the general experience that this is close to optimal. In [16] this was confirmed for the quenched Schrödinger functional, and a test with dynamical fermions at $L/a = 8$ showed an almost doubling of computational costs for $g^2_{\rm SF}$ as we lowered the trajectory length to one half. We reduced discretization errors by the multiple time scale method proposed in Ref. [9] taking the version given there in Eq. (6.7) with $n = 4$. A test of the performance gain of the above integration scheme in

practical simulations was performed in [17], where it was demonstrated that a substantial gain is achieved as compared to a standard leap-frog integrator. The value of n was not varied any further in this study.

As an essential sophistication we made use of two different forms of preconditioning. Both rely on our ability to factor out of Q matrix factors which on the one hand are easy to invert and on the other hand capture a part of its spectral variation to leave us with a better conditioned remaining factor. For even–odd preconditioning we exhibit the block structure of M with respect to even (e) and odd (o) lattice sites and factorize

$$M = \begin{pmatrix} M_{\mathrm{ee}} & M_{\mathrm{eo}} \\ M_{\mathrm{oe}} & M_{\mathrm{oo}} \end{pmatrix} = \begin{pmatrix} M_{\mathrm{ee}} & 0 \\ M_{\mathrm{oe}} & 1 \end{pmatrix} \begin{pmatrix} 1 & M_{\mathrm{ee}}^{-1} M_{\mathrm{eo}} \\ 0 & M_{\mathrm{oo}} - M_{\mathrm{oe}} M_{\mathrm{ee}}^{-1} M_{\mathrm{eo}} \end{pmatrix}, \tag{2.3}$$

where the left (lower) block-triangular factor and the block-diagonal M_{ee} are easy to invert. This factorization can now be used in a two-fold way. If the original Q under the determinant in (2.1) is plugged into the HMC algorithm we have to continuously solve linear systems with coefficient matrices given by Q. With (2.3) these can be transformed into better conditioned systems with accelerated iterative inversion of

$$\widehat{Q} = \tilde{c}_0 \gamma_5 \big(M_{\mathrm{oo}} - M_{\mathrm{oe}} M_{\mathrm{ee}}^{-1} M_{\mathrm{eo}}\big). \tag{2.4}$$

The constant $\tilde{c}_0$ is again used to normalize the spectrum of $\widehat{Q}$. On the other hand we may also conclude from (2.3) that up to irrelevant constant factors the relation

$$\det(Q) \propto \det(M_{\mathrm{ee}}) \det(\widehat{Q}) \tag{2.5}$$

holds. Now $\widehat{Q}$ enters into the HMC and leads to a different Monte Carlo dynamics, which also takes $\det(M_{\mathrm{ee}})$ into account. When we refer to even–odd preconditioning in this paper, this second variant will always be meant. Further details on our implementation of HMC may be found in [18]. As we only have to invert the squared operator $\widehat{Q}^2$ we use the conjugate gradient method (CG), which was found to be close to optimal in this case.

For SSOR preconditioning a different factorization of M based on factors triangular with respect to a lexicographic ordering of lattice sites is used [19–21]. Due to its complexity, in particular if the clover term is included, this has to our knowledge only been used to accelerate linear systems and was for that purpose reported to be superior over even–odd preconditioning if combined with the BiCGstab [22] inversion algorithm for the preconditioned M and $M^\dagger$. In the following SSOR will refer to such an implementation. For the unimproved case, a simplified form of SSOR preconditioning (ILU) was implemented under the determinant with very positive results [10].

We compared the performance of our two HMC program versions on our largest lattice, i.e. 12^4 at $\beta = 9.5$. In solving the linear systems with the respective preconditioned operators we confirmed that in terms of operations associated with applying these operators to fields, the BiCGstab algorithm with SSOR preconditioning outperforms the CG algorithm with even–odd preconditioning by a factor of about 1.6. Part of this advantage is however lost in terms of CPU time, because on our Alenia Quadrics (APE) machines inner products are relatively expensive. Since in the BiCGstab algorithm inner products and linear combinations are much more frequent than in the CG algorithm, this is a non-negligible overhead. The overall advantage that we find for the even–odd version derives however from the different operators under the determinant. A clear sign of this is the behaviour of the acceptance rate in both cases. While for the even–odd preconditioned determinant we could obtain an acceptance rate of 91% with a step size of $\Delta\tau = 0.08$, for $\det(Q^2)$ it went down to 75% already at a step size of $\Delta\tau = 0.07$.

In principle, one could also conceive of the following combination yet untested by us. One uses the even–odd preconditioned determinant and, when linear systems with $\widehat{Q}$ have to be solved, one transforms them to the SSOR preconditioned form, solves, and translates back. It is unclear at present, whether the overhead still leaves this variant profitable.

2.2. Polynomial hybrid Monte Carlo

We recall here some basics of the PHMC algorithm. For technical details the reader is referred to Refs. [23, 24]. In the PHMC algorithm the inverse of $\widehat{Q}^2$ is approximately computed by a suitable [12] Chebyshev polynomial of degree n,

$$\widehat{Q}^{-2} \approx P_{n,\epsilon}(\widehat{Q}^2). \tag{2.6}$$

Defining the relative deviation

$$R_{n,\epsilon}(\lambda) = \lambda P_{n,\epsilon}(\lambda) - 1, \tag{2.7}$$

the inversion error for eigenvalues $\lambda \in [\epsilon, 1]$ of $\widehat{Q}^2$ is bounded by

$$\delta = \sup_{\lambda} \left| R_{n,\epsilon}(\lambda) \right| = 2\left(\frac{1-\sqrt{\epsilon}}{1+\sqrt{\epsilon}}\right)^{n+1}. \tag{2.8}$$

For a given degree n the free parameter ϵ in $P_{n,\epsilon}$ allows to trade between approximation range and accuracy. For eigenvalues $\lambda < \epsilon$ the error monotonically moves from $R_{n,\epsilon}(\epsilon) = -\delta$ to $R_{n,\epsilon}(0) = -1$. With the help of $P_{n,\epsilon}$ we represent the determinant by a bosonic spinor field (pseudofermion) ϕ

$$\det(\widehat{Q}^2) = \int D[\phi] D[\phi^\dagger] \exp(-S_P) W \tag{2.9}$$

with the Gaussian action

$$S_P = \phi^\dagger P_{n,\epsilon}\big(\widehat{Q}^2[U]\big)\phi \tag{2.10}$$

and the remainder

$$W = \det\big(\widehat{Q}^2 P_{n,\epsilon}(\widehat{Q}^2)\big) \tag{2.11}$$

rendering (2.9) exact. As long as the spectrum of $\widehat{Q}^2$ is in the approximation range $[\epsilon, 1]$, W is a small correction close to one. Expectation values in the full QCD ensemble are now given by reweighting with W as

$$\langle \mathcal{O} \rangle = \frac{\langle \mathcal{O} W \rangle_P}{\langle W \rangle_P}, \tag{2.12}$$

where $\mathcal{O}$ is some observable and the average $\langle \ldots \rangle_P$ is taken with the action $S_{\text{gauge}} + S_P$. Since W is still given by a determinant, a straightforward evaluation is hard. As it is a small correction, however, stochastic (unbiased) estimates should be adequate. For each measurement we construct an estimator $\overline{W}$ given by

$$\overline{W} = \frac{1}{N_{\text{corr}}} \sum_{i=1}^{N_{\text{corr}}} \exp\big\{\eta_i^\dagger \big(1 - [\widehat{Q}^2 P_{n,\epsilon}(\widehat{Q}^2)]^{-1}\big)\eta_i\big\} \tag{2.13}$$

with independent Gaussian random fields η_i. Averaging over N_{corr} such estimates allows us to reduce and control the extra noise inflicted here. The true QCD average is then estimated by Eq. (2.12) with W replaced by $\overline{W}$.

The update of the gauge field and the pseudofermionic field ϕ follows the standard HMC pattern with global heatbath for ϕ and molecular dynamics for U including the speedup from [9] discussed before. This is chosen, because, in contrast to the multiboson algorithm [12], finite step size updates for U are impractical here due to the complicated non-local effective action.

At this point the parameters n, ϵ and, less importantly, N_{corr} are at our disposal for optimization. For small eigenvalues the growth of the 'inverter' $P_{n,\epsilon}(\lambda) \sim 1/\lambda$ is cut off at $\lambda \sim \epsilon$. For the HMC dynamics ϵ hence, in some sense, takes over the role of the smallest eigenvalue. It was found advantageous [23,24] to choose ϵ a few times larger than the typical smallest eigenvalue of $\widehat{Q}^2$. This allows us to keep the degree of the polynomial lower for the same approximation accuracy. Configurations with small eigenvalues of $\widehat{Q}^2$ are produced more frequently than they would be with the exact determinantal weight. As the algorithm is still exact, this is precisely compensated by W or respectively $\overline{W}$ giving smaller weight to the observables evaluated on these configurations. It should be borne in mind that the unquenched lattice path integral is always well-defined. The potential problem with nearly 'exceptional' configurations is a statistical one with rarely sampled large contributions, which is alleviated by our sampling and reweighting technique. This is the reason for us to prefer the reweighting correction over an acceptance step.

There is a special round-off problem for PHMC that we briefly summarize now with more details available in [23,25]. To generate ϕ with action (2.10) it is necessary to factorize

$$P_{n,\epsilon}(\widehat{Q}^2) = F_n(\widehat{Q})^\dagger F_n(\widehat{Q}) \tag{2.14}$$

with an nth degree polynomial F_n. For gauge field updating U-derivatives of S_P have to be taken at fixed ϕ. To this end we factorize further

$$\begin{aligned} F_n(\widehat{Q})\phi = {} & \big[\sqrt{c_n}(\widehat{Q} - r_n)\big]\big[\sqrt{c_{n-1}}(\widehat{Q} - r_{n-1})\big]\cdots \\ & \big[\sqrt{c_1}(\widehat{Q} - r_1)\big]\phi \end{aligned} \tag{2.15}$$

and store the occurring subproducts to facilitate the force computation. While the complex roots r_k are determined by $P_{n,\epsilon}$, the real factors $\sqrt{c_k}$ only serve to prevent the partial products from growing too large or too small. It is known [25] that the evaluation of a high order matrix polynomial in factorized form is in principle rather susceptible to round-off error. In

particular, the ordering of factors in (2.15) is of crucial importance in this context. In [23,25] orderings were found which make this source of errors negligible for the runs with n up to 46 reported in this paper, even on the 32-bit APE 100 machines. Further details on tuning the polynomial parameters are deferred to Appendix B.

Another variant of PHMC could be devised by applying an inverting polynomial to the complex spectrum of $\gamma_5\widehat{Q}$ instead of the real positive $\widehat{Q}^2$. A corresponding multiboson algorithm was investigated in Ref. [26]. We shall investigate this method in the near future.

2.3. Multi-level metropolis algorithm

As for the previous algorithms it is our aim to represent $\det(Q^2) \propto \det(M^\dagger M)$ in a way suitable for simulation. Here this will be done in part by the explicit use of a few terms of the hopping parameter expansion in powers of $T + H$ (see Eq. (2.2)) and by integrals over a collection of pseudofermion fields to represent the remainder.

The series for the logarithm of the determinant is given by

$$\log\det(M) = \operatorname{tr}\ln(M) = -\operatorname{tr}(T+H) - \tfrac{1}{2}\operatorname{tr}(T+H)^2 - \tfrac{1}{3}\operatorname{tr}(T+H)^3 + \cdots. \tag{2.16}$$

In our algorithm, we separate off the series up to some order k. In the present work we found it convenient to use $k = 3$, since $\operatorname{tr}(T+H)^i = \operatorname{tr} T^i$ can easily be computed for $i = 1, 2, 3$. At higher orders also mixed terms would contribute. In order to deal with the remaining terms, we define

$$\widetilde{M} = M\exp\left(\sum_{j=1}^{k}\frac{1}{j}(T+H)^j\right). \tag{2.17}$$

For the inverse of $\widetilde{M}$ we introduce a hierarchical approximation by polynomials P_i of order n_i in $T + H$,

$$\widetilde{M}^{-1} = \prod_{i=1}^{j} P_i^{r_i} + \mathrm{O}\big((T+H)^{n_j+1}\big). \tag{2.18}$$

The full required inversion accuracy is reached for the maximal value $j = l$. This is used with $r_1 + r_2 + \cdots + r_l$ pseudofermion fields to derive the representation

$$\det(\widetilde{M}^\dagger\widetilde{M}) \propto \int\prod_{i=1}^{l}\prod_{a=1}^{r_i} D[\phi_{ia}^\dagger]D[\phi_{ia}] \times \exp\left(-\sum_{i,a}|P_i\,\phi_{ia}|^2\right). \tag{2.19}$$

The powers $r_i > 1$ are advantageous as they lead to a smaller force on the gauge field which allows larger update steps [14].

Let us summarize the action that is simulated,

$$S = S_{\text{gauge}}[U] + S_{\text{hop}}[U] + S_{\text{PF}}[U,\phi] \tag{2.20}$$

with [2]

$$S_{\text{hop}}[U] = \operatorname{tr} T + \tfrac{1}{2}\operatorname{tr} T^2 + \tfrac{1}{3}\operatorname{tr} T^3 \tag{2.21}$$

and

$$S_{\text{PF}}[U,\phi] = \sum_{i,a}|P_i\phi_{ia}|^2. \tag{2.22}$$

We now consider $S_{\text{gauge}}[U]$ as a zeroth approximation which is taken into account in generating finite stepsize primary update *proposals*. All further terms will eventually be implemented by accept–reject filters. In the first level action

$$S^{(1)} = S_{\text{gauge}} + S_{\text{hop}} + \sum_{a=1}^{r_1}|P_1\phi_{1a}|^2 \tag{2.23}$$

the hopping term is included as it would otherwise lead to a single link action too complex for level zero. All further levels $j > 1$ are straightforwardly given by

$$S^{(j)} = S^{(j-1)} + \sum_{a=1}^{r_j}|P_j\phi_{ja}|^2 \tag{2.24}$$

up to $j = l$.

We now describe the steps of the multi-level Metropolis update scheme. A proposal at level 0 is given by multiple local updates with the Cabibbo–Marinari heatbath or the overrelaxation algorithm. One possibility is to randomly select v links to be updated. In Ref. [14] we found it advantageous to actually update several times a sublattice chosen at random from a set that covers the lattice. The size of the sublattices is chosen such that a reasonable acceptance at level one of the algorithm is achieved. The whole proposal obeys detailed balance with respect to the level zero

[2] $\operatorname{tr} T$ is small but nonzero, as we also included boundary improvement terms in it.

action as we reverse the order of link updates with probability $1/2$. The remaining levels now proceed recursively as follows. Generate a proposal $\widetilde{U}$ by performing t_j update steps at level $j-1$. Accept $\widetilde{U}$ as new configuration at level j with the probability

$$A^{(j)} = \min\bigl[1, \exp\bigl(-\Delta S^{(j)}[\widetilde{U}] + \Delta S^{(j)}[U]\bigr)\bigr], \tag{2.25}$$

where $\Delta S^{(j)} = S^{(j)} - S^{(j-1)}$.

In our implementation, the auxiliary fields ϕ_{ia} are kept fixed during the update cycle of the gauge field after they have been generated by a global heatbath by solving

$$\phi_{i,a} = P_i^{-1}\eta, \tag{2.26}$$

where η is a Gaussian random field.

In its present form the MLM algorithm will not be the method of choice for large lattices. The reason is that its cost will ultimately grow proportional to the square of the number of lattice sites. This is because the size of the updated blocks cannot grow while maintaining the acceptance rate and thus their number is proportional to the volume. Each evaluation of $\Delta S^{(j)}$ is however also of order volume in complexity. On the other hand, as we shall see shortly, MLM can produce precise results at $L/a = 5$ where we have tested it here. As it contains interesting elements, for instance being a finite step-size method for improved dynamical fermions, we still found the idea and the practical test worth reporting and comparing with other methods here, for instance as a basis for further modification.

3. Benchmarks of algorithmic performance

3.1. Our measure of efficiency

We now define two quantities, $M_{\rm cost}$ and $D_{\rm cost}$, which allow to compare simulation costs for a certain physics output between different algorithms and parameters. The first measure is machine dependent and refers to actual CPU time on the APE100 line of parallel computers currently in use by the ALPHA Collaboration. The second one is machine independent with the number of Dirac operator applications to a spinor field being our currency. As a target quantity, whose statistical accuracy is used for weighing costs in either units, we take our coupling $g^2_{\rm SF}$. The precise definitions are

$$\begin{aligned} M_{\rm cost} = {} & (\text{update time in seconds on machine } M) \\ & \times (\text{error of } 1/g^2_{\rm SF})^2 \times (4a/T)(4a/L)^3 \end{aligned} \tag{3.1}$$

and

$$\begin{aligned} D_{\rm cost} = {} & (\text{number of applications } Q\phi) \\ & \times (\text{error of } 1/g^2_{\rm SF})^2. \end{aligned} \tag{3.2}$$

Since the squared error in both formulas goes down inversely proportional to the run length, both quantities, extracted from given Monte Carlo simulations, do not depend on their lengths. The reason for focusing on absolute errors of $1/g^2_{\rm SF}$ is as follows. We assume for the *purpose of error analysis only* that the running of $g_{\rm SF}$ with L has the structure of 1-loop perturbation theory, $1/g^2_{\rm SF} \approx -2b_0 \log L + \text{const}$. Then

$$\frac{\delta L}{L} = \frac{1}{2b_0}\delta(1/g^2_{\rm SF}) \approx 8\,\delta(1/g^2_{\rm SF}) \tag{3.3}$$

holds, and we approximately aim at a certain relative scale uncertainty, independently of the size of $g_{\rm SF}$. In (3.1) the trivial growth proportional to the number of lattice sites is cancelled such that both quantities scale in the same way. The reference machine M in this publication will always be the smallest 8-node machine of type Q1. Most of our data actually come from bigger machines with up to 512 nodes. The costs on these machines are converted by multiplying naively by the ratio of nodes, e.g., $512/8$. This means, we neglect communication overheads, which is a small effect on our hardware and implementation. Note that with our definitions costs can be meaningfully compared also under trivial (replica) parallelization, of which we make extensive use.

While most of the CPU time with dynamical fermions is spent on applications of the Dirac operator there is also quite some overhead from other operations, in particular on small lattices. This was neglected in $D_{\rm cost}$ except for the contribution to the gauge field force in the PHMC algorithm which is proportional to the polynomial degree n. As a consequence, the ratio $D_{\rm cost}/M_{\rm cost}$ varies between 50 and 80% of the theoretical value referring to $Q\phi$ operations only. Applications of Q and $\widehat{Q}$ are so close to each other both in theoretical complexity and actual CPU time, that

Table 1
Summary of the simulated parameter sets, which enter our performance studies of dynamical fermion algorithms. Quark masses are close to their critical values

Set	L/a	β	Algorithm	$\Delta\tau$	P_{acc}
12a	12	9.5	HMC (e/o)	0.080	0.91
12b	12	9.5	HMC (SSOR)	0.060	0.86
12c	12	9.5	HMC (SSOR)	0.070	0.75
12d	12	9.5	PHMC (e/o)	0.091	0.83
12e	12	9.5	PHMC (e/o)	0.100	0.76
12f	12	8.5	HMC (e/o)	0.070	0.93
12g	12	8.5	PHMC (e/o)	0.091	0.80
12h	12	8.5	PHMC (e/o)	0.114	0.75
12i	12	7.5	HMC (e/o)	0.075	0.89
12j	12	7.5	PHMC (e/o)	0.098	0.77
12k	12	7.5	PHMC (e/o)	0.098	0.78
10a	10	9.3884	HMC (SSOR)	0.080	0.78
10b	10	8.39	HMC (SSOR)	0.080	0.75
10c	10	7.3619	HMC (SSOR)	0.070	0.79
10d	10	6.877	HMC (SSOR)	0.070	0.72
10e	10	6.5	HMC (SSOR)	0.060	0.80
10f	10	6.0	HMC (SSOR)	0.050	0.83
10g	10	5.5	HMC (SSOR)	0.040	0.82
8a	8	9.2364	HMC (e/o)	0.080	0.96
8b	8	8.2373	HMC (e/o)	0.120	0.91
8c	8	7.2103	HMC (SSOR)	0.100	0.71
6a	6	9.5	HMC (e/o)	0.110	0.97
6b	6	9.0	HMC (e/o)	0.110	0.97
6c	6	8.5	HMC (e/o)	0.100	0.97
6d	6	7.5	HMC (e/o)	0.070	0.98
5a	5	9.3884	HMC (SSOR)	0.120	0.92
5b	5	7.3619	HMC (SSOR)	0.120	0.90
4a	4	9.2364	HMC (e/o)	0.130	0.98
4b	4	8.24	HMC (e/o)	0.120	0.98
4c	4	7.21	HMC (e/o)	0.200	0.93

we neglect their difference. The SSOR preconditioned operator, on the other hand, is counted as $4/3$ Q operations due to extra multiplications of the diagonal (clover) part.

A typical run that entered our benchmarks is entry 12k in Table 1. With $M_{\rm cost} \approx 12$ and $D_{\rm cost} \approx 3000$ we ran a total of 13 000 trajectories on an $L/a = T/a = 12$ lattice and achieved 6% scale accuracy in about 6 days on 256 nodes of APE100.

3.2. Numerical results

In Table 1 we list the most important parameters for a subset of our HMC and PHMC runs performed to investigate the QCD running gauge coupling with two massless flavors.[3] The fourth column indicates which of the algorithms discussed before was used. This table has to be read in conjunction with Table 2, where the measured values for $M_{\rm cost}$ and $D_{\rm cost}$ are given. Results for $D_{\rm cost}$ of MLM follow in Table 4 below. Error estimates for the costs stem from the error of $\tau_{\rm int}$ of $g_{\rm SF}^{-2}$ which is determined by the method of Appendix A. Its value here refers to a unit given by complete update cycles (trajectories). The update time in seconds for one such cycle is normalized to the APE100-Q1 as discussed with the definition of $M_{\rm cost}$. In Fig. 1 we plot $M_{\rm cost}$ against L/a for all our runs at a fixed scale L in physical units that is implicitly determined by the condition $g_{\rm SF}^2 \approx 1.1$. The line corresponding to a growth proportional to a^{-3} is shown as a reference and roughly represents the rise of the data. This combines effects of a growing variance of our observable in the Schrödinger functional for $g_{\rm SF}^2$ and of critical slowing down. The latter accounts for about two powers of $1/a$. In Fig. 2 the number of conjugate gradient iterations is shown for our even–odd preconditioned HMC runs. At least for smaller $g_{\rm SF}^2$ there is an approximately linear growth with L/a which contributes one power to critical slowing down. This is the expected behaviour since $1/L$ is the infrared cutoff here analogous to the quark mass in other applications. At larger coupling $N_{\rm CG}$ moderately rises in the range that has been explored here.

The actual cost to determine the running coupling at fixed error for $g_{\rm SF}^{-2}$ as discussed before hence seems

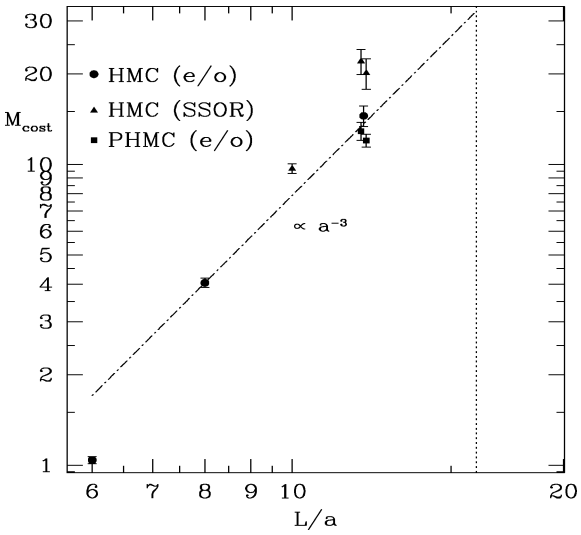

Fig. 1. Measured values of $M_{\rm cost}$ for runs with constant physics fixed by $g_{\rm SF}^2 \approx 1.1$ and vanishing quark mass.

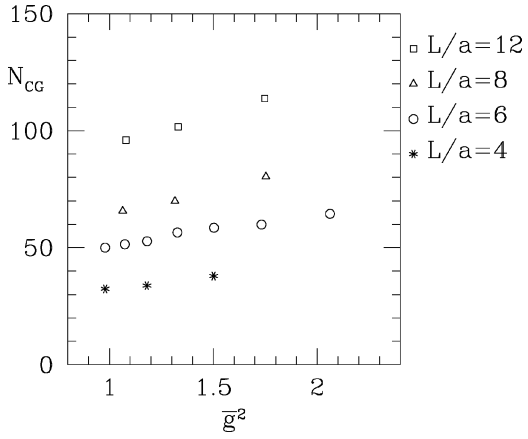

Fig. 2. Average number of iterations of the conjugate gradient algorithm in even–odd preconditioned HMC runs.

to roughly grow like $1/a^7$ in the continuum limit, at least at the relatively weak coupling considered here. This seems to be more optimistic than the quark mass dependence in some previous estimates, for instance[4] in [27]. One reason may be that our growth may be slightly underestimated due to overhead on the small lattices. Closer inspection reveals as another source of difference that in our molecular dynamics steps we are

[3] The physical implications of these data will be analyzed in a separate paper [29] while here we focus on algorithmic aspects.

[4] See also the discussion in [28].

Table 2
Cost estimates for the simulations in the parameter sets specified in Table 1. Precise results and analysis on the running of $g^2_{\rm SF}$ will appear in [29]

Set	$g^2_{\rm SF}$	$\tau_{\rm int}$	$t_{\rm update}/[s]$	$M_{\rm cost}$	$D_{\rm cost}/10^2$
12a	1.1	2.00(16)	1582	15(1)	36(3)
12b	1.1	1.98(23)	2392	20(2)	30(4)
12c	1.1	2.82(27)	1773	22(2)	37(4)
12d	1.1	1.41(10)	1636	12.9(9)	30(2)
12e	1.1	1.35(7)	1335	12.0(6)	28(2)
12f	1.3	2.19(12)	1768	15.0(8)	38(2)
12g	1.3	1.16(7)	1518	18.3(1.1)	44(3)
12h	1.3	2.47(15)	1103	11.6(7)	27(2)
12i	1.7	2.35(14)	1895	14.7(9)	39(2)
12j	1.7	2.05(14)	1554	12.6(9)	32(2)
12k	1.7	1.81(13)	1371	11.6(9)	28(2)
l0a	1.1	1.95(7)	707	9.7(4)	16.2(6)
10b	1.3	2.35(10)	719	10.7(5)	17.5(8)
10c	1.7	2.63(13)	804	11.5(6)	18.7(9)
10d	2.1	3.42(20)	806	14.4(8)	25(1)
10e	2.4	3.46(21)	991	16(1)	28(2)
10f	3.3	3.42(21)	1274	19(1)	33(2)
10g	5.4	3.94(22)	1932	30(2)	49(3)
8a	1.1	1.14(4)	260	4.0(1)	8.2(3)
8b	1.3	1.40(6)	183	3.0(1)	6.2(3)
8c	1.7	2.40(9)	239	5.8(2)	8.4(3)
6a	1.0	0.70(2)	49	1.00(3)	1.98(6)
6b	1.1	0.75(2)	49	1.04(3)	2.09(6)
6c	1.2	0.80(2)	55	1.15(3)	2.34(6)
6d	1.5	1.08(2)	74	2.08(4)	4.50(8)
5a	1.1	0.67(1)	22	0.70(1)	1.03(2)
5b	1.5	1.02(3)	22	0.83(2)	1.26(4)
4a	1.0	0.53(1)	6	0.268(5)	0.428(8)
4b	1.2	0.57(1)	7	0.271(5)	0.445(8)
4c	1.5	0.74(1)	5	0.222(3)	0.397(5)

Table 3
Parameters of the MLM update cycle, where $l = 4$, $r_2 = r_3 = r_4 = 1$ and a_j denotes the acceptance rate at the level j

β	r_1	n_1	n_2	n_3	n_4	t_1	t_2	t_3	t_4	a_1	a_2	a_3	a_4
8.39	4	15	31	63	255	1	6	6	10	0.313	0.828	0.966	0.998
8.854	4	15	31	63	255	1	6	6	10	0.347	0.835	0.969	0.999
9.40	3	11	23	63	255	1	8	10	10	0.355	0.742	0.923	0.996

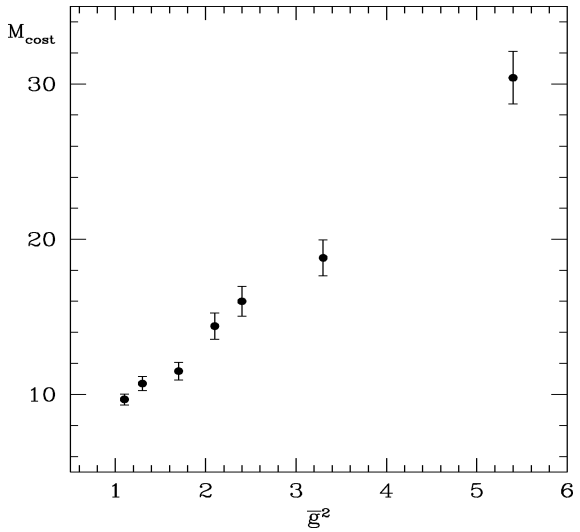

Fig. 3. Measured values of M_{cost} for runs with HMC-SSOR on $L/a = 10$ lattices versus renormalized coupling.

not forced to lower the step size $\Delta\tau$ at the rate usually estimated for constant acceptance while lowering the quark mass. Keeping L however fixed in physical units means that β rises when a/L becomes smaller which makes the gauge field smoother at the same time. This could lead to smaller discretization errors and partly be responsible for the observed behaviour. The integration method [9] may in addition interfere with standard scaling on intermediate size lattices.

The vertical dotted line in Fig. 1 is located at $L/a = 16$ and points to $M_{\text{cost}} \approx 30$. This implies about 100 days on 512 nodes for 3% scale accuracy. Thus at least with the next generation of APE1000 machines a serious continuum calculation should be within reach. For $L/a = 12$, our most expensive lattices so far, we found a slight preference for PHMC. This conclusion holds also among the larger couplings simulated, with the costs being approximately independent of g^2_{SF} in the present range between 1.1 and 1.8. All runs with $L/a = 10$ have been performed employing HMC with SSOR [5] and reach up to much larger couplings. Here the growth of M_{cost} and D_{cost} with g^2_{SF} becomes clearly visible but not dramatic, see Fig. 3.

Table 4
D_{cost} for simulations with the multi-level algorithm of 5^4 lattices at various β-values

β	8.39	8.854	9.40
g^2_{SF}	1.1807(12)	1.0778(10)	0.9767(16)
D_{cost}	290(6)	287(6)	372(15)

With the MLM algorithm for improved fermions we only have results for $L/a = 5$ whose parameters are collected in Table 3. As updates on level zero (gauge action only) we used heatbath sweeps and overrelaxation sweeps over certain sets of links. With probability $1/2$ we update either set A or set B. Set A consists of all spatial links of one randomly selected timeslice together with the temporal links at this timeslice in either positive or negative time direction. Set B are all links with a randomly selected spatial direction plus the temporal boundary links. In the case of set A we perform a heatbath sweep over all links followed by five overrelaxation sweeps. In the case of set B we perform a heatbath sweep over the temporal boundary links followed by five overrelaxation sweeps over the spatial links of one direction. In both cases the order of the updating is exactly reversed with probability $1/2$ to fulfill detailed balance. Given the large set of free parameters, some of them had to be chosen rather ad hoc. As we implemented and ran MLM on PCs but not on APE100, to which our M_{cost}-values refer, we only quote the machine independent D_{cost} here. Together with results for the coupling, which were found consistent with HMC results, they are given in Table 4.

[5] Our even–odd preconditioned (P)HMC code is unsuitable for this lattice size due to machine topology.

4. Conclusions

We have studied several simulation algorithms for the Schrödinger functional of full QCD with two flavors of massless quarks. Due to relatively high statistics on lattices up to 12^4 we obtained precise information on integrated autocorrelation times. Although our results are relatively close for the algorithms compared, there is a slight advantage for the polynomial hybrid Monte Carlo for our parameter range and observable. For this numerical reason and for the expected advantages from its modified sampling at larger coupling, we plan to focus on PHMC for our coming runs with $L/a = 16$. In simulations with ordinary HMC we found even–odd preconditioning of the *determinant* more efficient than SSOR preconditioning the *solver* alone.

Acknowledgement

We would like to thank Rainer Sommer for numerous discussions and for a critical reading of the manuscript. We are grateful to DESY for allocating computer time on the APE machines at DESY Zeuthen.

Appendix A. Integrated autocorrelation time for functions of observables

In this appendix we discuss a method to assess the effect of autocorrelations on the statistical error of nonlinear functions of simple expectation values. We consider a number of observables in a statistical system, and by $A_\alpha,\ \alpha = 1, 2, \ldots,$ we denote their *exact* mean values. For each observable we have a chain of N unbiased but (auto-)correlated Monte Carlo estimates $a_\alpha^i,\ i = 1, \ldots, N$. Assume that we want to estimate $F = f(A_\alpha)$, where f is an in principle arbitrary function. A simple case arising in the context of reweighting is the quotient $F = A_1/A_2$, while fit parameters extracted from a correlation function at a sequence of separations would be a more complicated case.

The obvious estimator for F is given by $f(\bar{a}_\alpha)$, where

$$\bar{a}_\alpha = \frac{1}{N}\sum_{i=1}^{N} a_\alpha^i \tag{A.1}$$

are the ensemble-means for our simulation. In a correct and equilibrated Monte Carlo we expect

$$\langle A_\alpha - \bar{a}_\alpha \rangle = 0, \tag{A.2}$$

$$\left\langle (A_\alpha - \bar{a}_\alpha)^2 \right\rangle = \mathrm{O}(1/N) \tag{A.3}$$

to hold, where the expectation values in this appendix mean the *average over* an infinite number of identical *Monte Carlo simulations* of length N. Loosely speaking, A_α and $\bar{a}_\alpha$ differ by $\mathrm{O}(1/\sqrt{N})$ in an individual Monte Carlo run.

By Taylor expanding f around the argument A_α we find

$$\left\langle F - f(\bar{a}_\alpha) \right\rangle = \mathrm{O}(1/N), \tag{A.4}$$

$$\sigma^2 = \left\langle (F - f(\bar{a}_\alpha))^2 \right\rangle = \mathrm{O}(1/N). \tag{A.5}$$

The first line reveals the (in general unavoidable) bias of our estimator which has to be suppressed [6] by large enough N. The statistical error σ of order $1/\sqrt{N}$ will be discussed in the following. With the gradient vectors

$$H_\beta = f_{|\beta}(A_\alpha), \quad \bar{h}_\beta = f_{|\beta}(\bar{a}_\alpha) \tag{A.6}$$

we define projected observables

$$A_H = \sum_\alpha A_\alpha H_\alpha \tag{A.7}$$

and analogously with $\bar{h}_\alpha$ and for $\bar{a}_\alpha$. Now we conclude that up to higher orders in $1/N$ we just need to know the variance of the projected observable,

$$\sigma^2 \approx \left\langle (A_H - \bar{a}_H)^2 \right\rangle \approx \left\langle (A_{\bar{h}} - \bar{a}_{\bar{h}})^2 \right\rangle. \tag{A.8}$$

In practice, the projection can only be performed with $\bar{h}$, taken from the data, of course.

From here on one may proceed just like in the case of simple expectation values. We may estimate the relevant autocorrelation function at separation t for instance [7] as

$$\Gamma(t) = \frac{1}{N-t}\sum_{i=1}^{N-t}\left(a_{\bar{h}}^i - \frac{1}{N-t}\sum_{j=1}^{N-t} a_{\bar{h}}^j\right) \times \left(a_{\bar{h}}^{(i+t)} - \frac{1}{N-t}\sum_{k=t+1}^{N} a_{\bar{h}}^k\right). \tag{A.9}$$

[6] In principle it is also possible to cancel the leading bias-term, for instance by the jackknife method.

[7] Less symmetrically, one might also subtract $\bar{a}_{\bar{h}}$ in each bracket.

From it the error follows as

$$\sigma^2 = \frac{\Gamma(0)}{N} 2\tau_{\mathrm{int}} \tag{A.10}$$

with

$$\tau_{\mathrm{int}} = \frac{1}{2} + \sum_{t=1}^{W} \frac{\Gamma(t)}{\Gamma(0)}. \tag{A.11}$$

The summation window W is usually chosen large enough that τ_{int} saturates to a constant within statistical errors. Often this can be achieved by self-consistently summing until W/τ_{int} reaches numbers like $5\ldots10$. Below the role of W will be discussed further. In summary, the deviation of $2\tau_{\mathrm{int}}$ from one for the projected observable describes the complete effect of (auto)correlations on the estimation of F. Obviously, σ, Γ and τ_{int} all depend on the function $f(A_\alpha)$ which has remained implicit in our notation.

We would like to conclude this appendix by indicating the advantage of explicitly summing Γ compared to the jackknife binning procedure which is often applied for the estimation of errors of secondary quantities like best-fit parameters. There one divides N estimates into N/B bins of length B. The individual bins are treated as uncorrelated. The fact that this is not exactly true leads to a systematic error in the error estimate which is of order τ/B from the correlation of neighboring bins. Here τ is a general scale of autocorrelation times involved. This is usually controlled by demanding a plateau of the errors as the bin length is varied. The statistical uncertainty of the error estimate is of order $\sqrt{B/N}$. These two errors have to be balanced at an optimal bin length, which incidentally scales as $B \propto (N\tau^2)^{1/3}$.

If we sum Γ up to separation W (summation window), systematic errors due to the neglected remainder are of order $\exp(-W/\tau)$. The statistical error of the error estimate is expected to be of order $\sqrt{W/N}$ from the number of independent windows. In fact, Madras and Sokal quote the formula [30]

$$\frac{\delta\tau_{\mathrm{int}}}{\tau_{\mathrm{int}}} = \sqrt{\frac{2(2W+1)}{N}}, \tag{A.12}$$

which follows if one approximates the required summed 4-point autocorrelation function by its disconnected part which falls back to the sum over Γ entering into τ_{int} itself. In practice, these errors usually look very reasonable under repeated runs. The conclusion is that the systematic errors for the "summation method" are much smaller, which, in balancing systematic with statistical errors, leads to more accurate error estimates. Taking the idea of balancing totally seriously, one would conclude that the "error of the error" decays like $[1/N]^{1/3}$ with binning and with $[\ln(N)/N]^{1/2}$ with the Γ-summation method.

Appendix B. Tuning of the PHMC algorithm

Here we summarize our strategy for tuning the free parameters of the PHMC algorithm, in particular for the Schrödinger functional at small volume or weak coupling. We are interested in the error $\sigma_{N_{\mathrm{corr}}}$ of the estimate

$$\langle\mathcal{O}\rangle = \frac{\langle\mathcal{O}\overline{W}\rangle_P}{\langle\overline{W}\rangle_P}, \tag{B.1}$$

for some observable $\mathcal{O}$ (mainly g_{SF}^{-2} at present) and $\overline{W}$ given in Eq. (2.13). All errors are assessed by the method of the previous appendix. Here the error can be decomposed as

$$\sigma^2_{N_{\mathrm{corr}}} = \sigma^2_P + \left[\sigma^2_\infty - \sigma^2_P\right] + \left[\sigma^2_{N_{\mathrm{corr}}} - \sigma^2_\infty\right]. \tag{B.2}$$

Here σ^2_∞ corresponds to $N_{\mathrm{corr}} = \infty$, or equivalently to the use of the exact reweighting with W as in Eq. (2.12), while σ^2_P refers to the simple mean $\langle\mathcal{O}\rangle_P$. The second term in (B.2) reflects a contribution from "ideal" reweighting and hence from the imperfection of the polynomial approximation, while the third one is due to our non-ideal stochastic estimation of the correction. Both would vanish for a perfect polynomial and are naively proportional to δ^2, the scale of polynomial errors. The third term has a factor $1/N_{\mathrm{corr}}$ in addition. We can roughly disentangle them by measuring $\langle\mathcal{O}\rangle_P$ and $\langle\mathcal{O}\rangle$ and their errors for at least two values of N_{corr}. The goal now is to take $N_{\mathrm{corr}} = 1\ldots4$ and find δ, ϵ such that the reweighting part of the error remains acceptable, less than 20%, say. This is to be achieved at the smallest possible value of the polynomial degree n.

In [24] we found for β between 5.4 and 6.8 on $8^3 \times 16$ the rule $\delta \approx 0.01$ and $\epsilon \approx 2\lambda_{\mathrm{min}}$ to be very efficient, where λ_{min} is the average smallest eigenvalue of $\widehat{Q}^2$. At the larger β-values of the present study we expect the intrinsic fluctuations caused by the

Table 5
Parameters controlling the polynomial approximation to $\widehat{Q}^{-2}$ for PHMC runs on 12^4

Set	β	$N_{\rm corr}$	ϵ	n	δ
12d	9.5	4	0.0050	44	0.0034
12e	9.5	2	0.0050	44	0.0034
12g	8.5	4	0.0044	44	0.0050
12h	8.5	2	0.0069	42	0.0016
12j	7.5	4	0.0050	46	0.0026
12k	7.5	2	0.0050	46	0.0026

Table 6
Average smallest and largest eigenvalue of $\widehat{Q}^2$ (see Eq. (2.4) for $\tilde{c}_0$) and ratio of errors in Eq. (B.2)

Set	$\langle\lambda_{\rm min}\rangle$	$\langle\lambda_{\rm max}\rangle$	$\tilde{c}_0$	$\sigma^2_{N_{\rm corr}}/\sigma^2_P$
12d	0.002477(15)	0.8582(1)	0.6738653	1.05
12e	0.002474(12)	0.8582(1)	0.6738653	1.10
12g	0.002284(14)	0.8765(1)	0.6686256	1.35
12h	0.002270(13)	0.8765(1)	0.6686256	1.14
12j	0.001869(14)	0.8664(1)	0.6477127	1.06
12k	0.001860(15)	0.8667(1)	0.6477127	1.03

gauge field to be smaller and correspondingly found a too large relative contribution from the third term in (B.2) when the above tuning is employed. Instead we found it much more efficient to attenuate this term with a smaller δ. This turned out to be possible essentially without enlarging n, i.e. we could allow ϵ to grow even larger than $2\lambda_{\rm min}$. This is probably due to smaller fluctuations of the small eigenvalues as well. In Tables 5 and 6 we report simulation parameters of the PHMC runs on 12^4. As to the choice of $\tilde{c}_0$ it is noted that one has to ensure $\lambda_{\rm max} < 1$ for all configurations for a numerically stable evaluation of (2.15). On the other hand, the efficiency is not very sensitive to the precise value of $\langle\lambda_{\rm max}\rangle$ which we hence kept safely below one.

References

[1] M. Lüscher, Lectures given at Les Houches Summer School, 1997, hep-lat/9802029.
[2] R. Sommer, ALPHA Collaboration, Lectures given at 36, Internationale Universitätswochen für Kern- und Teilchenphysik, Schladming, 1997, hep-ph/9712218.
[3] S. Capitani, M. Lüscher, R. Sommer, H. Wittig, ALPHA Collaboration, Nucl. Phys. B 544 (1999) 669, hep-lat/9810063.
[4] J. Rolf, U. Wolff, Nucl. Phys. Proc. Suppl. 83–84 (2000) 899, hep-lat/9907007.
[5] M. Lüscher, R. Sommer, P. Weisz, U. Wolff, Nucl. Phys. B 413 (1994) 481, hep-lat/9309005.
[6] K. Jansen, R. Sommer, ALPHA Collaboration, Nucl. Phys. B 530 (1998) 185, hep-lat/9803017.
[7] M. Lüscher, S. Sint, R. Sommer, P. Weisz, Nucl. Phys. B 478 (1996) 365, hep-lat/9605038.
[8] S. Duane, A.D. Kennedy, B.J. Pendleton, D. Roweth, Phys. Lett. B 195 (1987) 216.
[9] J.C. Sexton, D.H. Weingarten, Nucl. Phys. B 380 (1992) 665.
[10] P. de Forcrand, T. Takaishi, Nucl. Phys. Proc. Suppl. 53 (1997) 968, hep-lat/9608093.
[11] R. Frezzotti, K. Jansen, Phys. Lett. B 402 (1997) 328, hep-lat/9702016.
[12] M. Lüscher, Nucl. Phys. B 418 (1994) 637, hep-lat/9311007.
[13] B. Jegerlehner, Nucl. Phys. B 465 (1996) 487, hep-lat/9512001.
[14] M. Hasenbusch, Phys. Rev. D 59 (1999) 054505, hep-lat/9807031.
[15] M. Lüscher, P. Weisz, Nucl. Phys. B 479 (1996) 429, hep-lat/9606016.
[16] B. Gehrmann, U. Wolff, Nucl. Phys. Proc. Suppl. 83–84 (2000) 801, hep-lat/9908003.
[17] K. Jansen, C. Liu, Nucl. Phys. B 453 (1995) 375, hep-lat/9506020.
[18] K. Jansen, C. Liu, Comput. Phys. Commun. 99 (1997) 221, hep-lat/9603008.
[19] S. Fischer, A. Frommer, U. Glassner, T. Lippert, G. Ritzenhofer, K. Schilling, Comput. Phys. Commun. 98 (1996) 20, hep-lat/9602019.
[20] N. Eicker, W. Bietenholz, A. Frommer, H. Hoeber, T. Lippert, K. Schilling, Nucl. Phys. Proc. Suppl. 63 (1998) 955, hep-lat/9709143.
[21] M. Guagnelli, J. Heitger, ALPHA Collaboration, Comput. Phys. Commun. 130 (2000) 12, hep-lat/9910024.
[22] A. Frommer, V. Hannemann, B. Nockel, T. Lippert, K. Schilling, Int. J. Mod. Phys. C 5 (1994) 1073, hep-lat/9404013.
[23] R. Frezzotti, K. Jansen, Nucl. Phys. B 555 (1999) 395, hep-lat/9808011.
[24] R. Frezzotti, K. Jansen, Nucl. Phys. B 555 (1999) 432, hep-lat/9808038.
[25] B. Bunk, S. Elser, R. Frezzotti, K. Jansen, Comput. Phys. Commun. 118 (1999) 95, hep-lat/9805026.
[26] A. Borrelli, P. de Forcrand, A. Galli, Nucl. Phys. B 477 (1996) 809, hep-lat/9602016.
[27] R. Gupta, A. Patel, C.F. Baillie, G. Guralnik, G.W. Kilcup, S.R. Sharpe, Phys. Rev. D 40 (1989) 2072.
[28] K. Jansen, Nucl. Phys. Proc. Suppl. 53 (1997) 127, hep-lat/9607051.
[29] ALPHA Collaboration, in preparation.
[30] N. Madras, A.D. Sokal, J. Stat. Phys. 21 (1988) 109.

C

SSOR preconditioning in simulations of the QCD Schrödinger functional

Comput. Phys. Commun. 130 (2000) 12-21

Computer Physics Communications 130 (2000) 12–21

Computer Physics Communications

www.elsevier.nl/locate/cpc

SSOR preconditioning in simulations of the QCD Schrödinger functional

Marco Guagnelli [a], Jochen Heitger [b,*]

[a] *Dipartimento di Fisica, Università di Roma "Tor Vergata", and INFN, Sezione di Roma II, Via della Ricerca Scientifica 1, I-00133 Rome, Italy*

[b] *Deutsches Elektronen-Synchrotron, DESY Zeuthen, Platanenallee 6, D-15738 Zeuthen, Germany*

Received 2 November 1999; received in revised form 21 December 1999

Abstract

We report on a parallelized implementation of locally-lexicographic SSOR preconditioning for O(a) improved lattice QCD with Schrödinger functional boundary conditions. Numerical simulations in the quenched approximation at parameters in the light quark mass region demonstrate that a performance gain of a factor ∼1.5 over even–odd preconditioning can be achieved.

PACS: 11.15.Ha; 12.38.Gc; 2.60.Cb; 2.60.Dc

Keywords: Lattice QCD; O(a) improvement; Schrödinger functional; SSOR preconditioning; Parallelization; Quenched simulations

1. Introduction

One of the severe problems in lattice QCD from the practical point of view is the numerical inversion of sparse matrices. It nearly enters every Monte Carlo simulation, either in the quenched approximation of the theory in applying the inverse of the discretized Dirac operator on source vectors for the computation of quark propagators, or in full QCD with Hybrid Monte Carlo like algorithms, where a similar operation is necessary when calculating the fermionic force in order to include the quark field dynamics in the updating process of the gauge fields.

In recent years substantial progress has been made by the use of Krylov subspace iterative solvers in conjunction with preconditioning techniques. (See, e.g., [1] for a textbook reference and the reviews [2–4], which contain an extensive bibliography.) Popular choices for the inverter to be mentioned in the context of lattice simulations are the Conjugate Gradient (CG) algorithm [5,6], the Minimal Residual (MR) algorithm [7,8] and above all the stabilized Bi-Conjugate Gradient (BiCGStab) algorithm [9,10]. The latter now seems commonly established as the most efficient solver in a vast majority of QCD applications [11,12], particularly in the parameter region of small quark masses.

In the area of preconditioning, any new (and potentially competitive) idea should be confronted with an even–odd (e/o) decomposition of the Dirac matrix [13,14], which both for ordinary Wilson fermions and together with

* Corresponding author. E-mail: heitger@ifh.de.

0010-4655/00/$ – see front matter
PII: S0010-4655(00)00012-6

an O(a) improvement term [15] has become the state-of-the-art method. An earlier step towards an alternative approach was the incomplete LU factorization [16] utilizing a *globally*-lexicographic ordering of the lattice points and thereby already related to SSOR. However, it turns out to be unsatisfactory when an implementation on grid-oriented parallel computers is envisaged [17]. Finally, the Wuppertal group invented a parallelization of symmetric successive overrelaxed (SSOR) preconditioning, a variant of the classical Gauss–Seidel iteration [1], resting upon a *locally*-lexicographic ordering of the points within a given (sub-)grid of the total space-time lattice [18–22]. They showed that at least for Wilson fermions an SSOR preconditioner can perform much better that the standard e/o one.

Since many comparative studies of the properties of the various inversion algorithms and preconditioning methods are already available in the literature [4,12,17], we restrict ourselves in the sequel exclusively to the case of the O(a) improved Wilson–Dirac operator involving the Sheikholeslami–Wohlert clover term [23] within the Schrödinger functional of QCD [24,25].

The *Schrödinger functional* (*SF*) is defined as the partition function of QCD in a space-time cylinder of extension $L^3 \times T$ with periodic boundary conditions in the space directions and (inhomogeneous) Dirichlet boundary conditions at times 0 and T. As detailed, e.g., in Refs. [25,26], the SF has proven to be a valuable tool for computing the running coupling constant in a finite-size scaling analysis as well as for extracting phenomenological quantities from simulations in physically large volumes [27,28]. On the other hand, the O(a) *improved Wilson–Dirac operator* is now a good candidate to probe continuum QCD by means of numerical simulations on the lattice: most coefficients multiplying the counterterms required for a complete removal of the leading O(a) lattice artifacts of action and quark currents are known non-perturbatively in the quenched approximation [25,29,30], and also for the action in the case of two flavors of dynamical quarks [31]. Therefore, a quantitative investigation of the performance of a (parallelized locally-lexicographic) SSOR preconditioner for the SF setup incorporating O(a) improvement appears to be of natural interest. This is what we intend with the present communication.

One might ask what should be different from periodic boundary conditions in space *and* time. At first, the lattice Dirac operator within the SF scheme is by definition distinct from its counterpart with periodic boundary conditions in all directions and may behave differently in a numerical inversion algorithm. Thus it is in principle, e.g., not excluded that with Dirichlet boundary conditions a (specifically preconditioned) solver has generally lower iteration numbers. Another point concerns a definite advantage in the actual implementation, since the SF allows to circumvent inefficient conditional statements as will be explained later.

2. SSOR preconditioning

Let us start with shortly repeating the fundamental formulae to prepare the ground for the following discussion. (Please notice that the material covered in the first, more introductory part of this section is not original and quite similar to the presentation in Refs. [19,21].)

The basic problem posed is to solve a system of linear equations of the type

$$\mathcal{A}X = Y \Leftrightarrow R \equiv \mathcal{A}X - Y = 0. \tag{1}$$

To fix some notation, small Greek letters denote scalars, capital Latin ones vectors with components in small letters, and matrices have calligraphic symbols; $(X, Y) = \sum_i x_i^* y_i$ is the usual scalar product. In lattice QCD, $\mathcal{A}$ represents the discretized Dirac operator, a huge sparse matrix of rank $\Omega \times 4 \times 3$ emerging from the nearest neighbor couplings of the quark and gluon field variables in position space after discretization of the interacting continuum theory. More precisely, Ω is the volume of the four-dimensional space-time lattice, and the latter factors are connected to Dirac and SU(3) colour spaces. Physically, the solution of Eq. (1) can be regarded as a fermionic Green function (i.e. a quark propagator).

SSOR preconditioning consists of solving the system

$$\mathcal{V}_1^{-1}\mathcal{A}\mathcal{V}_2^{-1}\widetilde{X} = \widetilde{Y}, \quad \widetilde{X} = \mathcal{V}_2 X, \quad \widetilde{Y} = \mathcal{V}_1^{-1} Y \tag{2}$$

instead of $\mathcal{A}X = Y$, where in the present context $\mathcal{A}$ stands for $\widehat{\mathcal{Q}}$, the lattice Dirac operator of Wilson fermions supplemented with a local O(a) improvement term $a\sigma_{\mu\nu}F_{\mu\nu}(x)$, which is composed of the SU(3)-valued gauge link variables $U(x,\mu)$ to form a clover leaf [23]:

$$\begin{aligned}\widehat{\mathcal{Q}} = {} & \mathbf{1}\delta_{x,y} \\ & - \kappa \sum_{\mu} \big\{(\mathbf{1}-\gamma_\mu)U(x,\mu)\delta_{x,y-a\hat{\mu}} + (\mathbf{1}+\gamma_\mu)U(x-a\hat{\mu},\mu)^+\delta_{x,y+a\hat{\mu}}\big\} \\ & + c_{\rm sw}\frac{i}{2}a\kappa\sum_{\mu,\nu}\sigma_{\mu\nu}F_{\mu\nu}(x)\delta_{x,y}\end{aligned} \tag{3}$$

with $F_{\mu\nu}(x)$ equal to

$$\begin{aligned}\tfrac{1}{8}\big\{\big[& U(x,\mu)U(x+a\hat{\mu},\nu)U(x+a\hat{\nu},\mu)^+U(x,\nu)^+ \\ & + U(x,\nu)U(x+a\hat{\nu}-a\hat{\mu},\mu)^+U(x-a\hat{\mu},\nu)^+U(x-a\hat{\mu},\mu) \\ & + U(x-a\hat{\mu},\mu)^+U(x-a\hat{\nu}-a\hat{\mu},\nu)^+U(x-a\hat{\nu}-a\hat{\mu},\mu)U(x-a\hat{\nu},\nu) \\ & + U(x-a\hat{\nu},\nu)^+U(x-a\hat{\nu},\mu)U(x-a\hat{\nu}+a\hat{\mu},\nu)U(x,\mu)^+\big] \\ & - \big[\cdots\big]^+\big\}.\end{aligned} \tag{4}$$

$c_{\rm sw}$ is an improvement coefficient non-perturbatively determined in quenched and two-flavor QCD [29,31]. (The slight modification to (3) induced by the Dirichlet boundary conditions in time direction are not written out here.) If one introduces the decomposition [1]

$$\widehat{\mathcal{Q}} = \mathcal{D} - \mathcal{L} - \mathcal{U} \tag{5}$$

into block diagonal, block lower-triangular and block upper-triangular parts with respect to position space, the SSOR preconditioner is defined in terms of these matrices and a non-zero relaxation parameter $\omega_{\rm SSOR}$ (which serves to reduce the iteration number) through the choice

$$\mathcal{V}_1 = \left(\frac{1}{\omega_{\rm SSOR}}\mathcal{D}-\mathcal{L}\right)\left(\frac{1}{\omega_{\rm SSOR}}\mathcal{D}\right)^{-1}, \qquad \mathcal{V}_2 = \frac{1}{\omega_{\rm SSOR}}\mathcal{D}-\mathcal{U}. \tag{6}$$

Now it is advantageous to exploit in (2) the so-called 'Eisenstat trick' [32], embodied in the identity

$$\begin{aligned}& \frac{1}{\omega_{\rm SSOR}}\mathcal{D}\left(\frac{1}{\omega_{\rm SSOR}}\mathcal{D}-\mathcal{L}\right)^{-1}(\mathcal{D}-\mathcal{L}-\mathcal{U})\left(\frac{1}{\omega_{\rm SSOR}}\mathcal{D}-\mathcal{U}\right)^{-1} \\ & \quad = \big(\mathbf{1}-\omega_{\rm SSOR}\mathcal{L}\mathcal{D}^{-1}\big)^{-1}\big\{\mathbf{1}+(\omega_{\rm SSOR}-2)\big(\mathbf{1}-\omega_{\rm SSOR}\mathcal{U}\mathcal{D}^{-1}\big)^{-1}\big\} \\ & \qquad + \big(\mathbf{1}-\omega_{\rm SSOR}\mathcal{U}\mathcal{D}^{-1}\big)^{-1},\end{aligned} \tag{7}$$

to save on computational costs: namely, it implies that any matrix–vector product with the preconditioned matrix $\mathcal{V}_1^{-1}\widehat{\mathcal{Q}}\mathcal{V}_2^{-1}$ essentially gives rise to a backward substitution and a subsequent forward substitution process, corresponding to the application of the (non-block) upper and lower triangular matrices $\mathbf{1}-\omega_{\rm SSOR}\mathcal{U}\mathcal{D}^{-1}$ and $\mathbf{1}-\omega_{\rm SSOR}\mathcal{L}\mathcal{D}^{-1}$, respectively. These relations reflect that SSOR splits any application of $\widehat{\mathcal{Q}}$, which usually enters the inversion procedure associated with (1), into an equivalent but much simpler sequence of arithmetic operations with the set of matrices $\{\mathcal{D},\mathcal{L},\mathcal{U}\}$.

[1] The case of Wilson–Dirac fermions is recovered by setting $\mathcal{D}$ to the unit matrix.

Then, combining the BiCGStab algorithm with SSOR preconditioning, an iterative numerical solution of the system in Eq. (1) up to a given precision ε is obtained by the prescription [2] (preconditioned quantities carry a tilde and the backward/forward solves according to Eq. (7) are indented):

{initialization}

$$
\begin{aligned}
R_0 &= Y - \widehat{\mathcal{Q}} X_0 \\
&\quad (\mathbf{1} - \omega_{\mathrm{SSOR}} \mathcal{L}\mathcal{D}^{-1}) \widetilde{R}_0 = R_0 \\
\widetilde{\mathrm{R}} &\equiv \widetilde{R}_0 \\
\widetilde{V}_0 &= \widetilde{P}_0 \equiv 0 \\
\rho_0 &\equiv 1 \\
\alpha_0 &= \omega_0 \equiv 1
\end{aligned}
$$

{iteration:} for $k = 1, 2, \ldots$

$$
\begin{aligned}
\rho_k &= (\widetilde{\mathrm{R}}, \widetilde{R}_{k-1}) \\
\beta &= \frac{\rho_k \alpha_{k-1}}{\rho_{k-1} \omega_{k-1}} \\
\widetilde{P}_k &= \widetilde{R}_{k-1} + \beta \widetilde{P}_{k-1} - \beta \omega_{k-1} \widetilde{V}_{k-1} \\
&\quad (\mathbf{1} - \omega_{\mathrm{SSOR}} \mathcal{U}\mathcal{D}^{-1}) W = \widetilde{P}_k \\
&\quad Z' = \widetilde{P}_k + (\omega_{\mathrm{SSOR}} - 2) W \\
&\quad (\mathbf{1} - \omega_{\mathrm{SSOR}} \mathcal{L}\mathcal{D}^{-1}) Z = Z' \\
\widetilde{V}_k &= W + Z \\
\alpha_k &= \frac{\rho_k}{(\widetilde{\mathrm{R}}, \widetilde{V}_k)} \\
\widetilde{S} &= \widetilde{R}_{k-1} - \alpha_k \widetilde{V}_k \\
&\quad (\mathbf{1} - \omega_{\mathrm{SSOR}} \mathcal{U}\mathcal{D}^{-1}) U = \widetilde{S} \\
&\quad Z' = \widetilde{S} + (\omega_{\mathrm{SSOR}} - 2) U \\
&\quad (\mathbf{1} - \omega_{\mathrm{SSOR}} \mathcal{L}\mathcal{D}^{-1}) Z = Z' \\
\widetilde{T} &= U + Z \\
\omega_k &= \frac{(\widetilde{T}, \widetilde{S})}{(\widetilde{T}, \widetilde{T})} \\
\widetilde{X}_k &= \widetilde{X}_{k-1} + \omega_k U + \alpha_k W \\
\widetilde{R}_k &= \widetilde{S} - \omega_k \widetilde{T}
\end{aligned}
$$

{stopping criterion}

$$
\varepsilon^2 \geqslant \frac{(\widetilde{R}_k, \widetilde{R}_k)}{(\widetilde{X}_k, \widetilde{X}_k)}
$$

[2] The algorithm can straightforwardly formulated for other solvers, like MR for instance. Note, however, that in the chiral quark mass regime MR is generally of worse performance.

Some comments are in order.

- Taking the forward substitution as example, one calculates recursively in terms of the (block) components Z_i, Z'_i, $\mathcal{D}_{ij}$ and $\mathcal{L}_{ij}$ of Z, Z', $\mathcal{D}$ and $\mathcal{L}$:

$$\forall i: \quad Z_i = Z'_i + \sum_{j=1}^{i-1} \mathcal{L}_{ij} H_j, \qquad H_j = \omega_{\mathrm{SSOR}} (\mathcal{D}^{-1})_{jj} Z_j|_{j \leqslant i-1}. \tag{8}$$

  I.e. thanks to the triangularity of $\mathcal{L}$ (and $\mathcal{U}$) it can be done economically without involving a plain matrix multiplication, and owing to the sparsity of $\widehat{\mathcal{Q}}$ only a few j actually contribute to the sum. Provided that the inverses $(\mathcal{D}^{-1})_{ii}$ are pre-computed, the backward and forward solves together are exactly as expensive as one application of the whole matrix $\widehat{\mathcal{Q}}$ plus one additional $\mathcal{D}$ multiplication.
- In contrast to the unimproved case (where $X_k = \widetilde{X}_k$ follows immediately), the solution of the original system $\widehat{\mathcal{Q}} X = Y$ is now $X_k = \omega_{\mathrm{SSOR}}^{-1} \mathcal{D}^{-1} \widetilde{X}_k$.
- Choose $X_0 = 0 = \widetilde{X}_0$ as initial guess for the solution to avoid an application of $\mathcal{D}$, as part of $\widehat{\mathcal{Q}}$, at the beginning, which yields $R_0 = Y - \widehat{\mathcal{Q}} X_0 = Y$. If $\mathcal{D}$ is not needed elsewhere, this might be favorable in view of possible memory limitations of the hardware (e.g., setting an upper bound on the accessible lattice volumes), because we made the experience that savings in iteration number when using an available solution of a foregoing inversion as initial guess are generically negligible.
- Since in order to save on computational cost the stopping criterion (in our runs $\varepsilon^2 = 10^{-12}, 10^{-13}$) is conveniently based on the preconditioned residual $\widetilde{R}_k$, one might want to re-compute R_k at the end to test for convergence again and eventually – if the solution is not yet accurate enough – to continue the iteration with a stronger stopping criterion imposed on $\widetilde{R}_k$.
- In the SSOR-preconditioned BiCGStab scheme the minimal number of vectors to be stored at each iteration k is 9, if $\widetilde{R}_{k-1}$ and $\widetilde{S}$ share the same memory location, and if the source vector Y is overwritten by the iterative solutions $\widetilde{X}_k$.
- Due to the overall Dirac and colour structure of the fermion field variables at every lattice point, $\widehat{\mathcal{Q}}$ is genuinely partitioned into blocks of dimension 12×12. The dependence of the speed of the SSOR preconditioner on the diagonal (sub-)block size of $\mathcal{D}_{ij}$ was not studied.

2.1. Implementation for the Schrödinger functional

For the implementation of SSOR preconditioning on a parallel computer, the ordering of the lattice points plays a key rôle. [3] It determines the shape of $\widehat{\mathcal{Q}}$ via the pattern of its non-zero entries and thereby the degree of parallelism and the efficiency of the preconditioner. Via adapting a locally-lexicographic scheme we closely follow Refs. [19, 21], where different orderings and their consequences on the parallelization have been discussed. Hence we only describe the salient issues characteristic for the SF approach.

Assume that a given space-time lattice is matched on the, say, three-dimensional grid of processing nodes of a parallel computer. Then each node occupies a local lattice, where three of its extensions are ratios of the total lattice sizes in the respective directions and the corresponding numbers of processors. The locally-lexicographic ordering ('coloring') is ensured by an alphabetic ordering of the lattice sites belonging to these local lattices. Associating a colour with each fixed position within the local lattices, the original lattice is divided into groups, whose members couple to sublattice points of different colours only. In this way it becomes obvious that the forward and backward substitutions, e.g., to get Z_i as in Eq. (8), can be handled in parallel within the colored groups, since for all positions of a given colour only their predecessors – in the lexicographic sense – enter the necessary computations. [4] Because

[3] We remark that traditional e/o preconditioning can be interpreted as SSOR preconditioning of the even–odd ordered system [19].

[4] So the general strategy would be to maximize the number of colored groups, while maintaining its strengths in accordance with the desired parallelization.

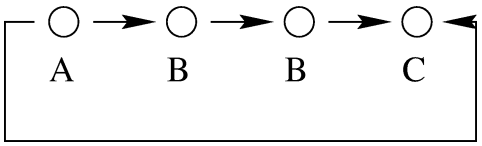

Fig. 1. A one-dimensional example. The direction of the arrows shows the data flow: sites of kind **B** need information from site **A**, and so forth.

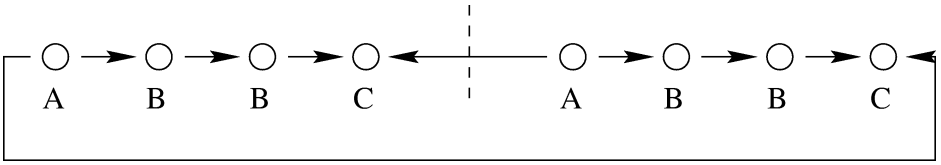

Fig. 2. A one-dimensional parallel example. As in the non-parallel case, Fig. 1, the arrows represent the data flow involved.

among these lexicographically preceding sites, lattice points living on the neighboring processors contribute too, the quantities H_i of (8) will have to be communicated from those processing nodes to the site in question.

At this point we have to note that there is a crucial difference between a situation with ordinary (anti-)periodic boundary conditions in all four space-time directions and our SF setup with Dirichlet boundary conditions in time. To see this difference in more detail, let us resort to an example in one dimension. The four points in Fig. 1 define a one-dimensional lattice with periodic boundary conditions, and one can think of a 'coupling matrix' between the sites of mutual dependence. Since only nearest neighbor sites are coupled, we immediately see that in applying Eq. (8) one has to distinguish between three cases. (We restrict to the forward solve, because it is straightforward to work out the necessary changes for the backward solve.)

A The point is on the 'left', i.e. it has coordinate $x = 1$: (8) simply becomes

$$Z_1 = Z'_1. \tag{9}$$

B The point lies within the 'bulk', i.e. it has coordinate $x = 2, 3$: (8) becomes

$$Z_x = Z'_x + \mathcal{L}_{x,x-1} H_{x-1}, \quad x = 2, 3. \tag{10}$$

C The point is on the 'right', i.e. it has coordinate $x = 4$: then (8) becomes

$$Z_4 = Z'_4 + \mathcal{L}_{4,3} H_3 + \mathcal{L}_{4,1} H_1. \tag{11}$$

It is clear that we have those three cases for each dimension, in which either periodic or antiperiodic boundary conditions are prescribed. For a four-dimensional lattice this leads to $3^4 = 81$ different cases to be handled, and it is natural to implement the algorithm with a `do`-loop over all the lattice points and some `if`-statements to discriminate between the 81 cases. The *parallel* version of the algorithm just described needs minor modifications: looking at Fig. 2, only the case **C** has to be replaced with

$$Z_4 = Z'_4 + \mathcal{L}_{4,3} H_3 + \mathcal{L}_{4,1} H_1^{(\text{next processor})}, \tag{12}$$

where now the coordinate index has a local meaning, labeling the sites inside the sublattice residing on a given processor, and also the processor's mesh is assumed to have periodic boundary conditions in the sense that the processor 'next' to the last one in each direction (rightmost in Fig. 2) is to be identified with the first one in the same direction (leftmost in Fig. 2).

Our numerical simulations were done on the 8–512 nodes APE-100 massively parallel computers with cubic topology and nearest neighbor communication, built up of an array of elementary processing boards with $2 \times 2 \times 2$

nodes [33,34]. They possess a SIMD (single-instruction multiple-data) architecture and are either suited to distribute a single, typically large, lattice over the whole machine or to simulate in parallel several independent copies of a lattice on subsets of the machine in the case of smaller volumes.

With such a cubic topology it suggests itself to keep the whole time extent of the lattice within the processors, and to only split the spacelike volume into sublattice fractions with respect to the three-dimensional processor grid. If *SF boundary conditions* are adopted, one can make sure that, as far as the time direction with its first and last timeslices fixed to the boundary values is concerned, a site belongs always to the 'bulk'. This lowers the number of cases to be distinguished in order to implement the forward and backward solves to $3^3 = 27$. So it becomes rather near at hand to encode these cases explicitly in a sensible arrangement of nested `do`-loops alone, i.e. via an outer loop over the full time coordinate and inner ones over the coordinates of the local space directions on every processor to exhaust the total lattice volume; thereby the usage of any `if`-statements is completely avoided. Here arises the significant advantage of our implementation: the latter type of statements cause – especially so on the APE-100 machines – a drastic deterioration of the performance by breaking the so-called 'optimization blocks' recognized by the compiler. In practice, the contents of the registers is lost each time a branching statement like `if`, `do`, `call subroutine`, ... is encountered, because this amounts to a break in the memory pipeline preloaded before. Writing out the 27 distinct cases explicitly, however, reduces the impact of the largest part of such statements, so that finally we are able to arrive at a substantial speed-up of the code. [5]

2.2. Performance tests

After realizing the implementation outlined above, we first have investigated the influence of the relaxation parameter ω_{SSOR} on the numerical solution procedure for the linear system in Eq. (1). It is quantified through the ratio of the numbers of iterations to solve the system with the e/o preconditioned matrix, $N_{\mathrm{e/o}}$, and with the locally-lexicographic SSOR-preconditioned one, N_{SSOR}, under otherwise identical conditions. We show these ratios in dependence on ω_{SSOR}, averaged over a set of O(10) propagator computations occurring in quenched simulations, for two lattice sizes with SF boundary conditions in Fig. 3. Upon distributing these lattices over the meshes of nodes of the APEs, the lattice extensions per node were $4^3 \times 8$ and $2^3 \times 32$. The course of $N_{\mathrm{e/o}}/N_{\mathrm{SSOR}}$ confirms a conclusion of the Wuppertal group [21] that between $\omega_{\mathrm{SSOR}} \simeq 1.3$ and $\omega_{\mathrm{SSOR}} \simeq 1.6$ the gain in the number of iterations needed for the fermion matrix inversions reaches its maximum: the corresponding improvement factor is around or even above 2, while the tendency for a further increase of $N_{\mathrm{e/o}}/N_{\mathrm{SSOR}}$ towards the chiral limit (i.e. larger κ and smaller quark mass) is also seen. Above $\omega_{\mathrm{SSOR}} \simeq 1.6$–$1.8$ this ratio drops rapidly and the gain gets lost; therefore, we take over $\omega_{\mathrm{SSOR}} = 1.4$ to be considered as an 'optimal' compromise irrespective of the definite values for lattice sizes and/or parameters.

Now we pass to the central question, whether the gain in the number of iterations also translates into a visible CPU time gain. Of course, as already pointed out previously, this will depend on the hardware architecture of the machine in use as well as on the individual implementation. At the peak in the upper diagram of Fig. 3, for instance, a total saving of 1.5 in the spent simulation time can be attained. In Table 1 we collect the approximate performance gain factors in units of iteration number and net CPU time, which were found in the situation of a realistic (quenched) QCD simulation in physically large volumes. Here we applied locally-lexicographic SSOR and e/o preconditioning for a set of 300 fermion matrix inversions on thermalized $16^3 \times 32$ configurations at $\beta = 6.0$ and $\kappa = 0.1335, 0.1342$, where the relaxation parameter was set to $\omega_{\mathrm{SSOR}} = 1.4$ throughout and the pseudoscalar mass at those couplings is $am_{\mathrm{PS}} = 0.388, 0.300$ [27,28]. Moreover, we examined the dependence of the SSOR preconditioner on the fractional grid size per node treated by a single processor. As illustrated by the numbers in Table 1 and in Fig. 4, the iteration number ratio and thus the preconditioning efficiency slightly increases with growing volumes of the different local subgrids, $2^3 \times 32$, $2^2 \times 4 \times 32$ and $2 \times 4^2 \times 32$, if the $16^3 \times 32$ lattice

[5] Of course one can imagine to write down analogously the 81 different cases for the familiar periodic situation [19], but then the size of the executable file might easily exceed the integer and/or program memory limits of the machine.

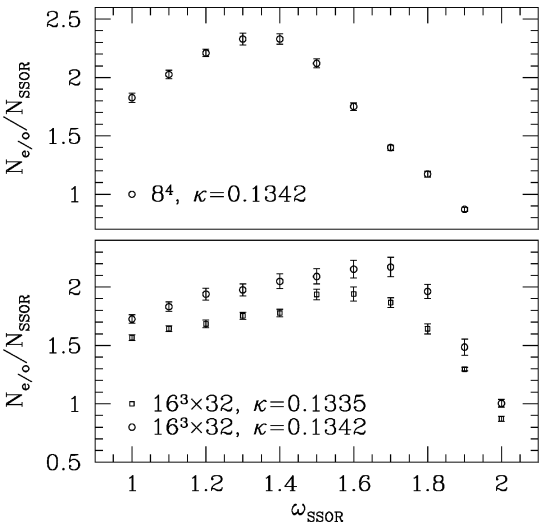

Fig. 3.

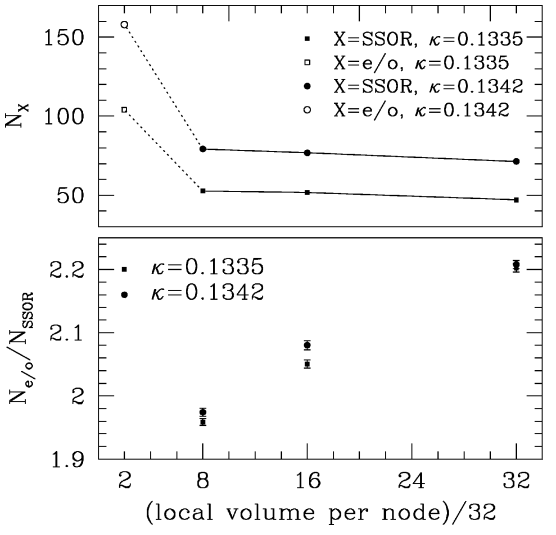

Fig. 4.

Fig. 3. Improvement factor in the number of BiCGStab iterations, when simulating with (locally-lexicographic) SSOR and different choices for ω_{SSOR} instead of e/o preconditioning. The lattice sizes are 8^4 and $16^3 \times 32$, with parameters $\beta = 6.0$ and $\kappa = 0.1335, 0.1342$.

Fig. 4. Upper part: BiCGStab iteration number in dependence of the local lattice volume per node after distributing a $16^3 \times 32$ lattice on different three-dimensional meshes of processing nodes. Note that the common time extent of the local lattices, $T = 32$, has been divided out. The e/o iteration numbers are included for comparison, and the lines are only meant to guide the eye. Lower part: Associated improvement factors in the number of iterations.

Table 1
Approximate gain factors of SSOR over e/o in iteration number and net CPU time

sublattice/node	subvolume/node	iteration gain	performance gain
$2^3 \times 32$	$8 \cdot 32$	2.0	1.4
$2^2 \times 4 \times 32$	$16 \cdot 32$	2.1	1.4
$2 \times 4^2 \times 32$	$32 \cdot 32$	2.2	1.5

is spread over the 512, 256 and 128 processors of the available machines, respectively. This complies with the heuristic expectation that an enlarged number of colored groups, i.e. sets of points at the same fixed position within the local sublattices (according to their locally-lexicographic ordering), entails a measurable iteration gain in the inverter, whereas the performance stays nearly unchanged owing to less parallelism and hence a small accompanying inter-processor communication overhead. Because of the equivalence of e/o preconditioning to a coloring into two groups assigned to the even and odd sublattice, one can accommodate the e/o iteration number in the upper part of Fig. 4 too. Additionally, the points in both diagrams indicate once more the even better behaviour of locally-lexicographic BiCGStab-SSOR in the range of lighter quark masses.

The foregoing observations are supported by the large scale simulations in the strange quark mass region underlying the extraction of hadron masses and matrix elements in quenched QCD with the SF reported in Refs. [27,28]. There, at $\beta = 6.1, 6.2$ on $24^3 \times T$ lattices (with $3^3 \times T$ sublattices per node and $T = 40, 48$) and at $\beta = 6.45$ on a $32^3 \times 64$ lattice (with $4^2 \times 8 \times 64$ sublattice per node), locally-lexicographic SSOR enabled to save against e/o always CPU time factors of around 1.5–1.6.

Altogether these results clearly reveal that the replacement of e/o by locally-lexicographic SSOR preconditioning to solve the O(a) improved Wilson–Dirac equation in the SF scheme pays off in real simulation costs. In contrast to what the authors in [21] obtain, for the same local diagonal block size of $\widehat{Q}$ and computer class, from QCD simulations including the clover term with ordinary boundary conditions, the SF type of boundary conditions allow for an efficient implementation of SSOR preconditioning also on massively parallel machines with an architecture equal or similar to that of the APE-Quadrics systems.

3. Conclusion

We have demonstrated in numerical simulations of quenched lattice QCD with the Sheikholeslami–Wohlert quark action that the increase of performance between even–odd and locally-lexicographic SSOR preconditioning in a parallel implementation can be a factor $\sim$1.5, when Schrödinger functional boundary conditions are employed.

Opposed to the more standard situation with periodic boundary conditions in all directions studied in Ref. [21], the gain factors in real time consumption come out to be significantly better here. The main reason for this originates in the lower number of cases (27 versus 81) to be distinguished explicitly, when the contributions to a given site among the locally-lexicographically ordered points of the local sublattices residing on the processors have to be collected: the avoidance of any conditional statements in the solver routines evades unwanted breaks in the data flow within the registers of the computer, which then directly translates into a considerable gain in units of CPU time. We have to emphasize that this inherent sensitivity to pipeline optimization might be – at least partly – a special feature of the APE-100 environment. Nevertheless, since some conclusions drawn from the investigations in [20–22] refer to the identical particular machines, our findings should be of interest in the same context and can be compared with the results stated there.

As the Schrödinger functional formulation of QCD is physically already well accepted to be a viable framework to address many problems in the non-perturbative low energy regime of the theory [25,28], the observed evidence for a performance gain of SSOR (together with BiCGStab as the inverter) for the O(a) improved Wilson–Dirac operator in actual run time – also on a parallel computer – constitutes a further benefit of this scheme. Therefore, the feasibility of an efficient implementation of this preconditioner does not only provide an important algorithmic information by itself, but even more is also promising for any kind of future applications of the Schrödinger functional in lattice QCD.

Acknowledgements

This work is part of the ALPHA collaboration research programme. We thank DESY for allocating computer time on the APE-Quadrics computers at DESY Zeuthen to this project and the staff of the computer centre at Zeuthen for their support. We are grateful to Rainer Sommer for discussions, useful suggestions and a critical reading of the manuscript. J.H. also thanks Burkhard Bunk and Andreas Hoferichter for discussions.

References

[1] G.H. Golub, C.F.V. Loan, Matrix Computations, 3rd edn. (The Johns Hopkins University Press, Baltimore, 1996).
[2] R. Freund, G.H. Golub, N. Nachtigal, Acta Numerica (1992) 57.
[3] R. Barrett et al., Templates for the Solution of Linear Systems: Building Blocks for Iterative Methods (SIAM, Philadelphia, PA, 1994).
[4] A. Frommer, Nucl. Phys. Proc. Suppl. B 53 (1997) 120, hep-lat/9608066.
[5] M.R. Hestenes, E. Stiefel, J. Res. Nat. Bur. Stand. 49 (1952) 409.
[6] V. Faber, T. Manteuffel, SIAM J. Numer. Anal. 21 (1984) 352.
[7] S.C. Eisenstat, H.C. Elman, M.H. Schultz, SIAM J. Numer. Anal. 20 (1983) 345.
[8] P. Rossi, C.T.H. Davies, G.P. Lepage, Nucl. Phys. B 297 (1988) 287.

[9] H. van der Vorst, SIAM J. Sci. Stat. Comput. 13 (1992) 631.
[10] M.H. Gutknecht, SIAM J. Sci. Stat. Comput. 14 (1993) 1020.
[11] A. Frommer, V. Hannemann, B. Nöckel, T. Lippert, K. Schilling, Int. J. Mod. Phys. C 5 (1994) 1073, hep-lat/9404013.
[12] G. Cella, A. Hoferichter, V.K. Mitrjushkin, M. Müller-Preussker, A. Vicere, Int. J. Mod. Phys. C 7 (1996) 787, hep-lat/9606003.
[13] T.A. DeGrand, Comput. Phys. Commun. 52 (1988) 161.
[14] T.A. DeGrand, P. Rossi, Comput. Phys. Commun. 60 (1990) 211.
[15] K. Jansen, C. Liu, Comput. Phys. Commun. 99 (1997) 221, hep-lat/9603008.
[16] Y. Oyanagi, Comput. Phys. Commun. 42 (1986) 333.
[17] G. Hockney, Nucl. Phys. Proc. Suppl. B 17 (1990) 301.
[18] U. Block, A. Frommer, G. Mayer, Parallel Comput. 14 (1990) 61.
[19] S. Fischer et al., Comput. Phys. Commun. 98 (1996) 20, hep-lat/9602019.
[20] N. Eicker et al., Nucl. Phys. Proc. Suppl. B 63 (1998) 955, hep-lat/9709143.
[21] W. Bietenholz et al., Comput. Phys. Commun. 119 (1999) 1, hep-lat/9807013.
[22] N. Eicker et al., Nucl. Phys. Proc. Suppl. B 73 (1999) 850, hep-lat/9809038.
[23] B. Sheikholeslami, R. Wohlert, Nucl. Phys. B 259 (1985) 572.
[24] M. Lüscher, R. Narayanan, P. Weisz, U. Wolff, Nucl. Phys. B 384 (1992) 168, hep-lat/9207009.
[25] R. Sommer, Non-perturbative renormalization of QCD, Lectures given at 36th Internationale Universitätswochen für Kernphysik und Teilchenphysik, Schladming, Austria, 1–8 March 1997, hep-ph/9711243.
[26] M. Lüscher, R. Sommer, P. Weisz, U. Wolff, Nucl. Phys. B 413 (1994) 481, hep-lat/9309005.
[27] ALPHA, M. Guagnelli, J. Heitger, R. Sommer, H. Wittig, Nucl. Phys. B 560 (1999) 465, hep-lat/9903040.
[28] ALPHA & UKQCD, J. Garden, J. Heitger, R. Sommer, H. Wittig, hep-lat/9906013.
[29] ALPHA, M. Lüscher, S. Sint, R. Sommer, P. Weisz, U. Wolff, Nucl. Phys. B 491 (1997) 323, hep-lat/9609035.
[30] R. Sommer, Nucl. Phys. Proc. Suppl. 60 A (1998) 279, hep-lat/9705026.
[31] ALPHA, K. Jansen, R. Sommer, Nucl. Phys. B 530 (1998) 185, hep-lat/9803017.
[32] S.C. Eisenstat, SIAM J. Sci. Stat. Comput. 2 (1981) 1.
[33] M. Albanese et al., Comput. Phys. Commun. 45 (1987) 345.
[34] C. Battista et al., The APE-100 computer: 1. The architecture, in: Field Theory, Disorder and Simulations, G. Parisi (Ed.) (World Scientific, Singapore, 1993).

D

Scaling investigation of renormalized correlation functions in O(a) improved quenched lattice QCD

Nucl. Phys. B557 (1999) 309-326

ELSEVIER

Nuclear Physics B 557 (1999) 309–326

NUCLEAR PHYSICS B

www.elsevier.nl/locate/npe

Scaling investigation of renormalized correlation functions in O(a) improved quenched lattice QCD

ALPHA Collaboration

Jochen Heitger

Deutsches Elektronen-Synchrotron, DESY Zeuthen, Platanenallee 6, D-15738 Zeuthen, Germany

Received 11 March 1999; accepted 7 June 1999

Abstract

We present a scaling investigation of some correlation functions in O(a) improved quenched lattice QCD. In particular, as one observable the renormalized PCAC quark mass is considered. Others are constructed such that they become the vector meson mass and the pseudoscalar meson decay constant when the volume is large. For the present discussion we remain in intermediate volume, $(0.75^3 \times 1.5)$ fm^4 with Schrödinger functional boundary conditions. By fixing the 'pion mass' and the spatial lattice size in units of the hadronic scale r_0, we simulated four lattices with resolutions ranging from 0.1 fm to 0.05 fm and performed the extrapolation to the continuum limit. The maximal scaling violation found in the improved theory is a $\sim 6\%$ effect at $a \simeq 0.1$ fm.

PACS: 11.15.Ha; 12.38.Gc
Keywords: Lattice QCD; Non-perturbative improvement; Quenched approximation; Schrödinger functional; Numerical simulations; Scaling tests

1. Introduction

One of the major drawbacks in the standard formulation of lattice QCD, induced by the Wilson–Dirac operator violating chiral symmetry at the scale of the cutoff [1,2], reflects among others in the fact that the quark masses are not protected from additive renormalizations and that the leading lattice effects in physical matrix elements and amplitudes are proportional to the lattice spacing a rather than being of O(a^2).

Nowadays, a systematic approach based on the Symanzik improvement programme [3,4] is well established to permit a removal of these discretization errors of O(a) in lattice QCD with confidence. It has been elaborated for on-shell quantities in Refs. [5,6]

0550-3213/99/$ - see frontmatter
PII S0550-3213(99)00354-5

and adds appropriate higher-dimensional operators to the action and fields in order to compensate for any correction terms at $O(a)$.

Within this framework a mostly non-perturbative $O(a)$ improvement of the action and the quark currents as well as their renormalization has been achieved in the quenched case, where quark loops are ignored. The basic idea for the practical implementation of on-shell improvement to enable a numerical computation of these improvement coefficients – pioneered by the ALPHA Collaboration – is to exploit chiral symmetry restoration and certain chiral Ward identities from Euclidean current algebra relations on the lattice at $O(a)$ [7,8]. Most prominently, demanding the PCAC relation $\partial_\mu A^a_\mu = 2mP^a$ between the isovector axial current A^a_μ and pseudoscalar density P^a to hold as a renormalized operator identity, imposes a sensible improvement condition in this respect. As a result, the values of the improvement coefficients $c_{\rm sw}$, $c_{\rm A}$ and $c_{\rm V}$, which are required to completely eliminate the corresponding $O(a)$ effects, are known for $\beta = 6/g_0^2 \geqslant 6.0$, g_0 being the bare gauge coupling [9–11].

Therefore, one is now interested in the quality of scaling behaviour and the size of its possible violation. During the last two years it was reported in this context [12–14] that at $a \simeq 0.1$ fm the residual $O(a^2)$ lattice artifacts may be still fairly large e.g. for the kaon decay constant $f_K r_0$ ($\sim 10\%$), while they are very small already for other quantities like the rho meson mass $m_\rho/\sqrt{\sigma}$ ($\sim 2\ \%$) [14,15]. Thus, restricting to an intermediate physical volume, the present scaling tests are intended to examine the impact of full $O(a)$ improvement in quenched lattice QCD thoroughly and with high accuracy for different observables. Some of these are designed to coincide with phenomenologically relevant observables in the limit of large physical volumes. A preliminary status of this work has been briefly surveyed recently in Ref. [16].

We wish to point out that the present investigation must be distinguished from similar studies like [13,17,18] for an important reason. Namely, since we address directly the scaling behaviour of correlation functions in finite volume, we do not have to rely on the asymptotic behaviour of (ratios of) usual timeslice correlation functions to extract, for instance, hadron masses or decay constants; these more conventional techniques often reveal to be genuinely affected by systematic errors difficult to control. Actually, an avoidance of such intrinsic uncertainties is supplied in part by the Schrödinger functional: its finite-volume fermionic correlation functions are scaling quantities at any fixed distance in time, if the renormalization factors of the quark fields at the boundaries are properly divided out. Beyond that, they decay very slowly for small time separations, allow to gain a good numerical precision and hence offer the appealing possibility to probe the theory for $O(a)$ improvement without unwanted additional sources of errors. Finally, for sufficiently large volumes the correlators can be shown to embody standard hadronic masses and matrix elements [19]. These aspects provide the real advantages of our method. The price to pay for it is, however, that within the Schrödinger functional formulation there exist two further improvement coefficients multiplying the boundary counterterms. These are perturbatively known only and as a consequence, one can in principle not exclude that the theory is to some extent still contaminated with uncancelled $O(a)$ contributions. That this fear can be dismissed in

practice has recently been demonstrated for the renormalization group invariant running quark mass [20], but we will make sure of it in the present context as well.

The paper is organized as follows. In Section 2 we introduce the fermionic correlation functions under study and sketch how spectral observables can be constructed from them in the Schrödinger functional scheme. After a short account on the numerical simulations, Section 3 contains a detailed description of the scaling test and the careful evaluation of the data. Section 4 gives the results. Here, also the question will be answered whether an improvement condition, chosen to fix a certain improvement coefficient non-perturbatively, is unambiguous in the sense that it automatically implies appreciably small scaling violations of $O(a^2)$ in other quantities not related to this specific condition. We conclude with a discussion in Section 5.

2. Correlation functions and hadronic observables

The basic framework for our lattice setup is the QCD Schrödinger functional (SF), whose concepts and characteristic features have been published in much detail in Refs. [21–23]; consult also Refs. [24,25] for comprehensive overviews on the subject.

It is defined as the partition function of QCD in a cylindrically shaped space-time manifold of extension $L^3 \times T$ with periodic boundary conditions in the space directions and (in general inhomogeneous) Dirichlet boundary conditions at times $x_0 = 0$ and $x_0 = T$. This means in the case of the gluons to require the spatial gauge field components at the boundaries to satisfy $A_k(x)|_{x_0=0} = C_k(\boldsymbol{x})$ and $A_k(x)|_{x_0=T} = C'_k(\boldsymbol{x})$, where C_k and C'_k are some prescribed smooth classical (chromo-electric) gauge potentials, and a similar assignment is imposed on the quark fields as well. One of the bold advantages of such a choice is that it ensures frequency gaps for the gluon and quark fields, and thereby numerical simulations at vanishing quark masses become tractable. As in most of the other applications of the QCD SF, we assume the special choice of homogeneous boundary conditions from now on: $C_k = C'_k = 0$ for the spatial components of the gauge potentials and vanishing fermion boundary fields.

2.1. Correlation functions in the Schrödinger functional

Although the definitions of fermionic correlation functions within the SF already appeared in the literature [7,9–11], let us recall them here and collect the essential properties and formulae in order to make the paper self-contained.

If ζ and $\bar{\zeta}$ denote 'boundary quark and antiquark fields' at Euclidean time $x_0 = 0$ and primed symbols the corresponding objects at $x_0 = T$ [7], one builds up the boundary field products

$$\mathcal{O}^a = a^6 \sum_{y,z} \bar{\zeta}(y)\gamma_5 \tfrac{1}{2}\tau^a \zeta(z)\,, \qquad \mathcal{O}'^a = a^6 \sum_{u,v} \bar{\zeta}'(u)\gamma_5 \tfrac{1}{2}\tau^a \zeta'(v) \tag{2.1}$$

and analogously,

$$\mathcal{Q}_k^a = a^6 \sum_{y,z} \bar{\zeta}(y)\gamma_k \tfrac{1}{2}\tau^a \zeta(z)\,, \qquad \mathcal{Q}_k'^a = a^6 \sum_{u,v} \bar{\zeta}'(u)\gamma_k \tfrac{1}{2}\tau^a \zeta'(v)\,, \tag{2.2}$$

where τ^a, $a = 1,2,3$, are the Pauli matrices acting on the first two flavour components of the quark fields ψ. In the operator language of quantum field theory they create initial and final quark–antiquark states with zero momenta, respectively, and transform according to the vector representation of the exact isospin symmetry. For the axial-vector current A_μ^a and the pseudoscalar density P^a we use the local expressions

$$A_\mu^a(x) = \overline{\psi}(x)\gamma_\mu\gamma_5 \tfrac{1}{2}\tau^a \psi(x)\,, \qquad P^a(x) = \overline{\psi}(x)\gamma_5 \tfrac{1}{2}\tau^a \psi(x)\,, \tag{2.3}$$

while the vector current V_μ^a and the anti-symmetric tensor field $T_{\mu\nu}^a$ read

$$V_\mu^a(x) = \overline{\psi}(x)\gamma_\mu \tfrac{1}{2}\tau^a \psi(x)\,, \qquad T_{\mu\nu}^a(x) = i\overline{\psi}(x)\sigma_{\mu\nu} \tfrac{1}{2}\tau^a \psi(x)\,. \tag{2.4}$$

Now we consider correlation functions on the lattice in the SF. By inserting the preceding densities at some inner point x of the SF cylinder (with support on the hypersurface at x_0) between the appropriate external quark–antiquark states, one introduces the expectation values

$$f_{\mathrm{A}}(x_0) = -a^6 \sum_{y,z} \tfrac{1}{3} \left\langle A_0^a(x)\, \bar{\zeta}(y)\gamma_5 \tfrac{1}{2}\tau^a \zeta(z) \right\rangle = -\tfrac{1}{3} \left\langle A_0^a(x)\, \mathcal{O}'^a \right\rangle, \tag{2.5}$$

$$f_{\mathrm{P}}(x_0) = -a^6 \sum_{y,z} \tfrac{1}{3} \left\langle P^a(x)\, \bar{\zeta}(y)\gamma_5 \tfrac{1}{2}\tau^a \zeta(z) \right\rangle = -\tfrac{1}{3} \left\langle P^a(x)\, \mathcal{O}'^a \right\rangle, \tag{2.6}$$

analogously,

$$k_{\mathrm{V}}(x_0) = -\tfrac{1}{9} \left\langle V_k^a(x)\, \mathcal{Q}_k'^a \right\rangle, \tag{2.7}$$

$$k_{\mathrm{T}}(x_0) = -\tfrac{1}{9} \left\langle T_{k0}^a(x)\, \mathcal{Q}_k'^a \right\rangle, \tag{2.8}$$

and the boundary–boundary correlation function

$$f_1 = -\frac{1}{3L^6} \left\langle \mathcal{O}'^a \mathcal{O}'^a \right\rangle. \tag{2.9}$$

Gauge invariant correlators of this type have already been used to study the conservation of currents on the lattice and to deduce suitable improvement and normalization conditions in lattice QCD in order to calculate the corresponding coefficients and constants non-perturbatively by numerical simulations [9–11]. One of them, f_1, will be utilized later to cancel the multiplicative renormalization of the boundary quark fields $\zeta, \ldots, \bar{\zeta}'$. Besides on the SF characteristic kinematical variables [7], the correlation functions depend on the bare parameters g_0, m_0 and the improvement coefficient $c_{\mathrm{sw}} = c_{\mathrm{sw}}(g_0)$ in the fermionic part of the lattice action, but not on the spatial coordinates of x owing to translation invariance. There is also a dependence on the improvement coefficients c_{t} and $\tilde{c}_{\mathrm{t}}$, which account for specific boundary $\mathrm{O}(a)$ counterterms arising in the SF approach [7].

After contracting the quark fields, all the bare and unimproved correlation functions have the general structure $h_{\rm X}(x_0) \propto \langle {\rm Tr}\{H^+(x)\Gamma_{\rm X}H(x)\}\rangle$, $h = f, k$, where the respective insertions are $\Gamma_{\rm X} \in \{-\gamma_0, 1, \gamma_k, -\sigma_{k0}\}$, X = A, P, V, T; the trace extends over colour, Dirac and (in principle as well) flavour indices, and the matrix H is the quark propagator from the boundary at $x_0 = 0$ to the point x in the interior of the space-time volume [9]. In the quenched approximation the expectation values are understood to be taken as path integral averages in the pure gauge theory.

We should mention that also the primed correlation functions $h'_{\rm X}$, which are connected to $h_{\rm X}$ through a time reflection and vice versa, become relevant. Those are in the case of Eqs. (2.5) and (2.6)

$$f'_{\rm A}(T-x_0) = +\tfrac{1}{3}\,\langle A_0^a(x)\,\mathcal{O}'^a\rangle\,, \qquad f'_{\rm P}(T-x_0) = -\tfrac{1}{3}\,\langle P^a(x)\,\mathcal{O}'^a\rangle\,, \tag{2.10}$$

and similar relations apply to $k_{\rm V}, k'_{\rm V}$ and $k_{\rm T}, k'_{\rm T}$. Obviously, in $h'_{\rm X}$ the currents and densities are probed by the boundary quark fields at $x_0 = T$ instead, and the argument $T - x_0$ indicates that they fall off with this distance. For vanishing gauge fields C and C' at the boundaries, our correlation functions possess the useful time reflection invariance $h_{\rm X}(x_0) = h'_{\rm X}(x_0)$. This allows to sum them up accordingly, and averaging over the spatial components helps to reduce the statistical noise in the Monte Carlo simulation further.

On-shell improvement at $\mathrm{O}(a)$ for the axial and vector currents is achieved by adding the derivatives of the pseudoscalar density and the tensor current as the suitable $\mathrm{O}(a)$ counterterms,

$$(A_{\rm I})^a_\mu(x) \equiv A^a_\mu(x) + ac_{\rm A}\tilde\partial_\mu P^a(x), \tag{2.11}$$

$$(V_{\rm I})^a_\mu(x) \equiv V^a_\mu(x) + ac_{\rm V}\tilde\partial_\nu T^a_{\mu\nu}(x)\,, \tag{2.12}$$

where the improvement coefficients $c_{\rm A}$ and $c_{\rm V}$ are determined by the demand to cancel the $\mathrm{O}(a)$ errors in lattice Ward identities, emerging from a mixing with higher-dimensional operators with the same quantum numbers [10,11]. Then the corresponding improved fermionic correlation functions are given by

$$f^{\rm I}_{\rm A}(x_0) = f_{\rm A}(x_0) + ac_{\rm A}\tilde\partial_0 f_{\rm P}(x_0), \tag{2.13}$$

$$k^{\rm I}_{\rm V}(x_0) = k_{\rm V}(x_0) + ac_{\rm V}\tilde\partial_0 k_{\rm T}(x_0)\,. \tag{2.14}$$

The lattice derivative $\tilde\partial_\mu \equiv \frac{1}{2}(\partial_\mu + \partial^*_\mu)$ is the symmetrized combination of the usual forward and backward difference operators ∂_μ and ∂^*_μ, acting as

$$\partial_\mu f(x) = \frac{f(x+a\hat\mu) - f(x)}{a}\,, \qquad \partial^*_\mu f(x) = \frac{f(x) - f(x-a\hat\mu)}{a}\,.$$

Herewith we are already in the position to write down the unrenormalized PCAC quark mass as a function of the timeslice location $a \leqslant x_0 \leqslant T - a$:

$$m(x_0) = \frac{\tilde\partial_0 f_{\rm A}(x_0) + ac_{\rm A}\partial^*_0\partial_0 f_{\rm P}(x_0)}{2f_{\rm P}(x_0)}\,. \tag{2.15}$$

For the properly chosen value of $c_A = c_A(g_0)$ at given gauge coupling g_0 and any hopping parameter κ it is defined by obeying the PCAC relation (for two degenerate quark flavours) up to cutoff effects of $O(a^2)$,

$$\tilde{\partial}_\mu [\, (A_I)^a_\mu(x) \,] = 2mP^a(x) + O(a^2)\,, \tag{2.16}$$

which more rigorously must be looked at as a renormalized operator identity

$$\tilde{\partial}_\mu \langle (A_R)^a_\mu(x)\mathcal{O}\rangle = 2m_R \langle P^a_R(x)\mathcal{O}\rangle + O(a^2)$$

in terms of some arbitrary renormalized on-shell $O(a)$ improved field $\mathcal{O}$ localized in a region not containing x.

2.2. *Construction of renormalized observables*

Now we want to introduce the renormalized correlation functions and design the scaling combinations of them, which will be studied numerically in the next section.

The QCD SF serves as a particular intermediate finite-volume renormalization scheme which is, however, not necessarily related to a special regularization [7,24,25]. Here, the SF is employed as a mass-independent renormalization scheme, while the ratio T/L is assumed to be kept fixed to a certain value. The freedom in choosing the boundary fields C and C' (as well as the boundary conditions on the quark fields specified by angles θ_μ, cf. Subsection 3.1) different from zero are left for other applications, see e.g. Refs. [9,20,26]. Moreover, the SF respects $O(a)$ improvement after adding the $O(a)$ counterterms $\propto c_t, \tilde{c}_t$ so that by attaching additive and multiplicative renormalization constants, the quantities

$$(A_R)^a_\mu(x) = Z_A(1 + b_A am_q)(A_I)^a_\mu(x), \tag{2.17}$$

$$(V_R)^a_\mu(x) = Z_V(1 + b_V am_q)(V_I)^a_\mu(x), \tag{2.18}$$

$$P^a_R(x) = Z_P(1 + b_P am_q)P^a(x) \tag{2.19}$$

induce the renormalized and improved correlation functions

$$f^R_A(x_0) = Z_A(1 + b_A am_q)Z^2_\zeta(1 + b_\zeta am_q)^2 f^I_A(x_0), \tag{2.20}$$

$$k^R_V(x_0) = Z_V(1 + b_V am_q)Z^2_\zeta(1 + b_\zeta am_q)^2 k^I_V(x_0), \tag{2.21}$$

$$f^R_P(x_0) = Z_P(1 + b_P am_q)Z^2_\zeta(1 + b_\zeta am_q)^2 f_P(x_0), \tag{2.22}$$

$$f^R_1 = Z^4_\zeta(1 + b_\zeta am_q)^4 f_1\,. \tag{2.23}$$

The constants Z_ζ and b_ζ (the former being scale dependent [7]) have to be attributed to the boundary values of the quark and antiquark fields appearing in the products (2.1) and (2.2) in the renormalized theory. In a mass-independent renormalization scheme the underlying $O(a)$ counterterm enters as

$$\zeta_R(x) = Z_\zeta(1 + b_\zeta am_q)\zeta(x)$$

and similarly for the antiquark field $\bar{\zeta}$, giving $\mathcal{O}^a_R = Z^2_\zeta(1 + b_\zeta am_q)^2\mathcal{O}^a$ for instance.

Because the renormalization does not distinguish between different flavours in a mass-independent scheme, the knowledge of the Z-factors suffices to link the lattice theory at finite cutoff to the renormalized continuum theory. Here, all normalization conditions to fix and determine the renormalization constants Z_X and b_X, X = A, V, P, were imposed on appropriate matrix elements at *zero quark mass*, which is safe within the SF scheme as the finite lattice extent L provides the before-mentioned natural infrared cutoff for the theory [9,10]. Because of the zero quark mass condition they are functions of g_0 only and *not* of the subtracted bare quark mass, which equals

$$am_q = am_0 - am_c(g_0) = \frac{1}{2}\left(\frac{1}{\kappa} - \frac{1}{\kappa_c}\right) \tag{2.24}$$

and vanishes along a critical line $m_0 = m_c(g_0)$ in the plane of bare parameters, implicitly defining the critical hopping parameter κ_c. Any remaining corrections of $O(am_q)$ are supposed to be cancelled by adjusting the b_X alone.

Now we can pass to the set of observables we have constructed for the present study. We start with the renormalized PCAC (current) quark mass in the SF scheme, which in view of Eqs. (2.15), (2.17) and (2.19) may be defined as

$$\overline{m} = \frac{Z_A}{Z_P(L)}\, m\,(T/2) \tag{2.25}$$

by multiplying the proper renormalization constants Z_A and $Z_P(L)$, the latter assumed to be taken at some renormalization scale $\mu = 1/L$ [20,27]. Strictly speaking, the ratio of the additive renormalization factors $1 + b_A am_q$ and $1 + b_P am_q$ would have been to be accounted for as well, but it turns out perturbatively [28] and non-perturbatively [29] that $(b_A - b_P)am_q$ is numerically quite small at the interesting values of the bare gauge coupling and the hopping parameter. Hence we neglect it here.

Beyond that, we compose the following (time dependent) combinations of renormalized and improved fermionic correlation functions. Firstly, the logarithmic time derivatives

$$\mu_{PS}(x_0) = \frac{\tilde{\partial}_0 f_P^R(x_0)}{f_P^R(x_0)} = \frac{\tilde{\partial}_0 f_P(x_0)}{f_P(x_0)}, \tag{2.26}$$

$$\mu_V(x_0) = \frac{\tilde{\partial}_0 k_V^R(x_0)}{k_V^R(x_0)} = \frac{\tilde{\partial}_0 k_V^I(x_0)}{k_V^I(x_0)} \tag{2.27}$$

of the respective SF correlation functions in the pseudoscalar and vector meson channel; they deviate from the ordinary definition of effective masses ($\sim \partial_0 \ln h_X$) by terms of $O(a^2)$. Secondly, we will consider the ratios

$$\eta_{PS}(x_0) = C_{PS}\frac{f_A^R(x_0)}{\sqrt{f_1^R}} = C_{PS}\frac{Z_A(1 + b_A am_q) f_A^I(x_0)}{\sqrt{f_1}},$$
$$C_{PS} = \frac{2}{\sqrt{L^3 \mu_{PS}(\frac{T}{2})}}, \tag{2.28}$$

$$\eta_{\mathrm{V}}(x_0) = C_{\mathrm{V}} \frac{k_{\mathrm{V}}^{\mathrm{R}}(x_0)}{\sqrt{f_1^{\mathrm{R}}}} = C_{\mathrm{V}} \frac{Z_{\mathrm{V}}(1 + b_{\mathrm{V}} a m_{\mathrm{q}}) k_{\mathrm{V}}^{\mathrm{I}}(x_0)}{\sqrt{f_1}},$$
$$C_{\mathrm{V}} = \frac{2}{\sqrt{L^3 \left[\mu_{\mathrm{V}}(\tfrac{T}{2}) \right]^3}}. \tag{2.29}$$

Since through the division by $\sqrt{f_1^{\mathrm{R}}}$ the renormalization factors of the boundary quark fields, $Z_\zeta(1 + b_\zeta a m_{\mathrm{q}})$, drop out, it is ensured that η_{PS} and η_{V} (at fixed argument x_0) exhibit scaling and have a well-defined continuum limit. We note in passing that alternatively the correlation function $f_{\mathrm{A}}^{\mathrm{I}}$ also could have been used instead of f_{P} to define a 'local mass' in the pseudoscalar channel. But as $f_{\mathrm{A}}^{\mathrm{I}}$ amounts to somewhat larger statistical errors in the time derivatives, we here preferred f_{P} for the purpose of $\mu_{\mathrm{PS}}(x_0)$.

In the present scaling test we fix a definite temporal separation from the boundaries, $x_0 = T/2$. Thus one arrives at the objects

$$\text{pseudoscalar channel}: \quad \mu_{\mathrm{PS}}(T/2) \quad \eta_{\mathrm{PS}}(T/2) \tag{2.30}$$
$$\text{vector channel}: \quad \mu_{\mathrm{V}}(T/2) \quad \eta_{\mathrm{V}}(T/2)\ . \tag{2.31}$$

Their continuum limits are expected to be approached like $\mu_{\mathrm{X}}(T/2) + \mathrm{O}(a^2)$ and $\eta_{\mathrm{X}}(T/2) + \mathrm{O}(a^2)$, X = PS, V, in the $\mathrm{O}(a)$ improved theory. The choice $x_0 = T/2$ is motivated by the fact that in the SF scheme cutoff effects are generically larger when sitting closer to the boundaries. It is possible to construct other quantities in a similar way, but we consider the foregoing ones as reasonably representative.

Let us emphasize, however, a final point. Adopting the quantum mechanical representation of the field operators associated to (2.3) and (2.4), it can be shown in the transfer matrix formalism that asymptotically for large Euclidean times the quantities in Eqs. (2.30) and (2.31) become the pseudoscalar and vector meson masses ($\mu_{\mathrm{PS}}, \mu_{\mathrm{V}}$) as well as the pseudoscalar decay constant (η_{PS}). For instance, the proportionality constant C_{PS} in (2.28) is such that this ratio turns, as the temporal lattice extent goes to infinity ($x_0, T - x_0 \to \infty$), into a familiar matrix element, which complies with the standard definition of the pion decay constants in continuum QCD:

$$Z_{\mathrm{A}} \langle 0 | \overline{\psi}(x) \gamma_0 \gamma_5 \tfrac{1}{2} \tau^a \psi(x) | \pi^a(\mathbf{0}) \rangle = m_\pi f_\pi .$$

More formally, the observables $\mathcal{O}$ just introduced should be regarded as functions $\mathcal{O}(T/L, x_0/L, L/r_0, a/r_0)$, and in the spirit of the above a physically meaningful situation is realized if, as the spatial volume $(L/a)^3$ tends to infinity, $x_0 \gg r_0$ and $T - x_0 \gg r_0$ are valid for some typical hadronic radius of $r_0 \simeq 0.5$ fm. Masses and matrix elements of interest in hadron phenomenology can then be extracted [19].

3. Scaling tests

Before going into the details of the investigation, one has to keep in mind that the chosen lattice volumes in physical units are only of intermediate magnitude. Therefore, any of the following results are prevented from resembling the large volume limit, where our observables were argued to receive a really physical meaning. Instead of this, most emphasis is on the scaling properties of the theory, which should not depend on the specific choice of the lattice size and the SF characteristic boundary conditions. Nevertheless, we refer from now on to the (first three of the) quantities in Eqs. (2.30) and (2.31) as the 'pion mass', its decay constant and the 'rho meson mass' and assign the common symbols m_π, f_π and m_ρ to them in the obvious manner. We also denote $\overline{\eta}_{\rm V} \equiv \eta_{\rm V}(T/2)$ in the vector meson channel.

The advantage of working at finite quark mass in a direct test of improvement should be stressed explicitly. Namely, this avoids any extrapolations and evades the potential problems with so-called exceptional configurations one runs into, when the parameter region of zero quark mass is attempted to be reached [9,30].

3.1. Monte Carlo simulation

The cost of a quenched QCD simulation is always governed by the computation of fermion propagators required for the correlation functions to be covered. This involves the action of the Wilson–Dirac operator on quark fields $\psi(x)$, which for the O(a) improved theory in the framework of the SF is conveniently decomposed as $D+\delta D+m_0$ with

$$(D+m_0)\psi(x) \equiv \frac{1}{2\kappa} M\psi(x)\,, \qquad \kappa = \frac{1}{8+2m_0}, \tag{3.1}$$

$$\begin{aligned} M\psi(x) = \psi(x) - \kappa \sum_{\mu=0}^{3} \Big\{ & \lambda_\mu U(x,\mu)(1-\gamma_\mu)\psi(x+a\hat{\mu}) \\ & + \lambda_\mu^* U(x-a\hat{\mu},\mu)^+(1+\gamma_\mu)\psi(x-a\hat{\mu}) \Big\}, \end{aligned} \tag{3.2}$$

where, as usual, the fermionic degrees of freedom $\psi(x)$ live on the sites x of the lattice, and $U(x,\mu)$ denotes the SU(3)-valued gauge links in lattice direction $x+a\hat{\mu}$, $\mu = 0,\ldots,3$. The factors $\lambda_\mu = \mathrm{e}^{ia\theta_\mu/L}$, $\theta_0 \equiv 0$, give rise to a modified covariant derivative equivalent to demanding spatial periodicity of the quark field up to a phase $\mathrm{e}^{i\theta_k}$; for our purposes θ_k, $k=1,2,3$, was set to zero throughout.[1] The local O(a) counterterm $\delta D = \delta D_{\rm v} + \delta D_{\rm b}$ now consists of two contributions, namely the Sheikholeslami–Wohlert clover term [31]

$$\delta D_{\rm v}\psi(x) = c_{\rm sw}\frac{i}{4} a\sigma_{\mu\nu}F_{\mu\nu}(x)\psi(x) \tag{3.3}$$

[1] In general, θ_k can serve as an additional kinematical variable to formulate proper improvement and normalization conditions, see for instance [9,20].

and a term

$$\delta D_{\mathrm{b}}\psi(x) = (\tilde{c}_{\mathrm{t}} - 1)\Big\{\delta_{x_0/a,1}\big[\psi(x) - U(x - a\hat{0}, 0)^{+}P_{+}\psi(x - a\hat{0})\big] + \delta_{x_0/a,T-1}\big[\psi(x) - U(x,0)P_{-}\psi(x + a\hat{0})\big]\Big\} \tag{3.4}$$

with

$$P_{+}\psi(x)|_{x_0=0} = 0\,, \qquad P_{-}\psi(x)|_{x_0=T} = 0\,, \qquad P_{\pm} \equiv \tfrac{1}{2}(1 \pm \gamma_0)\,,$$

which is specific for the SF type of boundary conditions in our setup. The improvement coefficient $\tilde{c}_{\mathrm{t}}$ and a further one, c_{t} which enters the calculation as well but is independent of the local composite operators containing quark fields and thus not written down here, are set to their one-loop perturbative values.[2]

Since the technicalities of the Monte Carlo simulations are identical to those already detailed in Ref. [9], it is not necessary to repeat them here in full length. Our data were taken on the APE-100 massively parallel computers with 128–512 nodes at DESY Zeuthen, whose topology also allows to simulate independent replica of the system at the same time in the case of smaller lattice volumes (sets A–C below). The gauge field ensembles were generated by a standard hybrid overrelaxation algorithm, where each iteration consists of one heatbath step followed by several microcanonical reflection steps (typically $N_{\mathrm{OR}} = L/2a + 1$), and the correlation functions have been evaluated by averaging over sequential gauge field configurations separated by 50 iterations. To solve the system of linear equations belonging to the boundary value problem of the Dirac operator within the measurements of the correlators, the BiCGStab algorithm with even–odd preconditioning was used as inverter. Finally, a single-elimination jackknife procedure was applied to estimate the statistical errors of all the secondary quantities, because the data stemming from the same configurations must be considered as strongly correlated. By dividing the full ensemble of measurements into bins we also checked for the statistical independence of our data samples.

3.2. *Method and numerical analysis*

For the analysis we use c_{sw}, c_{X}, Z_{X}, X = A, V, P, and b_{V} non-perturbatively determined in [9–11,20] for $\beta \geqslant 6.0$, while b_{A} and b_{P} are taken from one-loop perturbation theory [7,8,28]. If available, we always adopted the rational formulas for the former with overall, i.e. statistical and systematic, uncertainties stated in the references. As opposed to Z_{A} and Z_{V} (and as already anticipated below Eq. (2.25) in Subsection 2.2), the normalization constant of the pseudoscalar density, $Z_{\mathrm{P}} = Z_{\mathrm{P}}(L)$, acquires a scale dependence through its renormalization. The scale evolution of Z_{P}, which due to its definition at the point of vanishing PCAC quark mass (but in the absence of exact chiral symmetry at finite a) is unique only up to $\mathrm{O}(a^2)$ errors, has been recently

[2] Recently, the coefficient c_{t} has also been computed up to two-loop order of perturbation theory in the quenched case [32].

Table 1
Simulation points and its statistics N_{meas} denoting the number of gauge field configurations, on which the fermionic correlation functions were computed. L/r_0 and $m_\pi L$ are the quantities chosen to fix renormalization conditions for the LCP studied

Set	L/a	β	κ	N_{meas}	L/r_0	am_π	$m_\pi L$
A	8	6.0	0.13458	12800	1.490(6)	0.2505(11)	2.004(9)
B	10	6.14	0.13538	3840	1.486(7)	0.1945(14)	1.946(14)
C	12	6.26	0.13546	2560	1.495(7)	0.1709(13)	2.050(16)
D	16	6.48	0.13541	3000	1.468(8)	0.1244(9)	1.991(15)

computed non-perturbatively in [20]. In the SF the appropriate renormalization scale is $\mu = 1/L \equiv 1/2L_{\max}$, with $L_{\max}/r_0 = 0.718$ [33], and we take over the needed numbers for Z_{P} from the last but one reference. In the case of c_{V} and the critical hopping parameter κ_c in Eq. (2.24), where no closed expressions are recommended yet, we adapted the numbers at discrete values of the gauge coupling from Refs. [9,11] to our simulated β-values by linear interpolation.

The strategy was then to keep a finite physical volume and the quark mass fixed by prescribing the geometry $T/L = 2$ and two further renormalization conditions, which we decided to chose as

$$m_\pi L = 2.0 \quad \text{and} \quad \frac{L}{r_0} = 1.49 \tag{3.5}$$

for the 'pseudoscalar meson (pion) mass' and the spatial lattice size, respectively. The first condition on m_π can be, at least approximately,[3] satisfied by a careful tuning of the hopping parameter ($a^2 m_\pi^2 \sim \kappa$). Here the reference scale is expressed by the hadronic radius r_0 defined in [34] through the force between static quarks to yield the phenomenologically motivated value of $r_0 \simeq 0.5$ fm. Using the latest results on the hadronic scale r_0/a in Ref. [33], quoted there as

$$\ln\left(\frac{a}{r_0}\right) = -1.6805 - 1.7139(\beta - 6) + 0.8155(\beta - 6)^2 - 0.6667(\beta - 6)^3, \tag{3.6}$$

one can solve numerically for β after inserting $a/r_0 = 1.49a/L$ to find the desired pairs $(L/a, \beta)$ in order to fulfill the second condition in Eq. (3.5) within errors. In practice, the particular value $L/r_0 = 1.49$ was determined by the initial simulations at $\beta = 6.0$ on lattices with spatial size $L/a = 8$, and the larger lattices were adjusted thereafter. The simulation parameters and some results are compiled in Table 1. These settings give an intermediate volume of $(0.75^3 \times 1.5)$ fm^4, and one moves on a line of constant physics (LCP) in bare lattice parameter space with lattice resolutions ranging from 0.1 fm to 0.05 fm.

[3] In our actual simulations we have some mismatch in $m_\pi L$ between the individual points in parameter space, which will be discussed later.

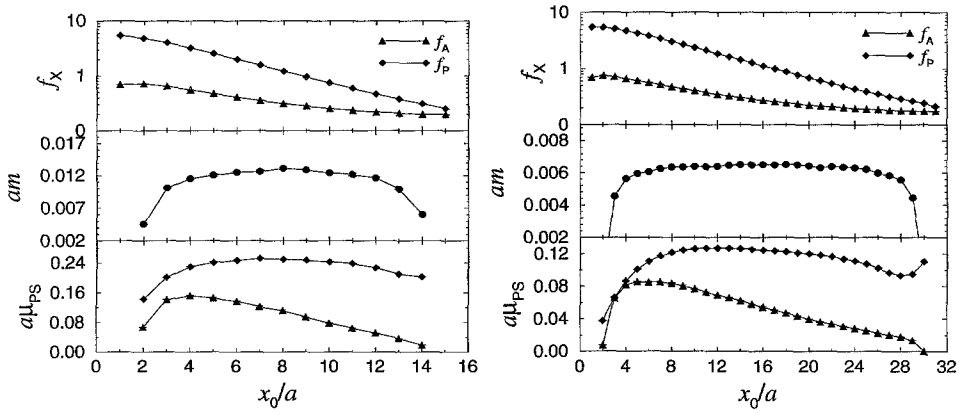

Fig. 1. Correlation functions f_A and f_P (upper parts) and O(a) improved local masses extracted from them: PCAC current quark mass via Eq. (2.15) (middle part) and 'pseudoscalar meson masses' via Eq. (2.26) and the same with f_P substituted by f_A^I (lower parts). The left figure depicts simulation point A ($L/a = 8$) and the right one point D ($L/a = 16$), with $T/L = 2$ in both cases. The solid lines are only meant to guide the eye, and the statistical errors are smaller than the symbols.

As an important prerequisite for the reliability of the scaling test we had, of course, to estimate the dependence of our results on the SF specific (and solely perturbatively known) improvement coefficients of the boundary counterterms c_t and $\tilde{c}_t$, which with respect to full non-perturbative O(a) improvement represent the only imperfectly known input parameters for the simulation. Otherwise a complete suppression of errors linear in a would not be guaranteed, and continuum limit extrapolations with an O(a^2) term as the dominant scaling violation is a priori not justified. To this end we verified by an artificial variation of the one-loop coefficients in the expansions [26,35]

$$c_t^{1\text{-loop}} = 1 - 0.089 g_0^2 + \mathrm{O}(g_0^4), \tag{3.7}$$

$$\tilde{c}_t^{1\text{-loop}} = 1 - 0.018 g_0^2 + \mathrm{O}(g_0^4) \tag{3.8}$$

by a factor 2 for $c_t^{1\text{-loop}}$ and by a factor 10 for $\tilde{c}_t^{1\text{-loop}}$ that at unchanged renormalization conditions (3.5) their influence on the level of numerical precision in our data is small enough to be neglected: it typically came out to be below 1% for af_π, below 2% for $\overline{\eta}_V$, and nearly not visible for am and am_ρ, at parameters corresponding to simulation point A ($T/a = 16$). It was sufficient to do these replacements for the lattice with the largest a, since the relative contribution of the boundaries to the field variables residing on the bulk of lattice points among a given gauge field configuration decreases with decreasing lattice spacing. Therefore, the leading scaling violations can be regarded as being purely O(a^2) within our precision.

In Fig. 1 we first illustrate for simulation points A and D the correlation functions f_A, f_P and some of the quantities deduced from them in the previous section in dependence of the time coordinate. The correlators reflect that a good signal remains also at larger distances in time. The PCAC quark mass (2.15) already exposes a plateau for the rather moderate temporal extensions of the lattice, whereas the 'local pion mass' (2.26),

Table 2
Analysis results for the observables under consideration in lattice units. The first error is only the statistical one, the second one (where given) includes in addition the uncertainties from the renormalization constants

Set	$am(\frac{T}{2})$	am_ρ	af_π	$\overline{\eta}_V$
A	0.0132(2)	0.3438(10)	0.1248(5)(13)	0.3283(19)(25)
B	0.0083(1)	0.2688(15)	0.1013(7)(12)	0.3387(36)(40)
C	0.0096(1)	0.2337(14)	0.0851(7)(11)	0.3289(40)(43)
D	0.00651(6)	0.1689(10)	0.0650(5)(8)	0.3561(41)(44)

and even more the logarithmic derivative of the improved correlation of the axial current (2.13), show significant contributions from higher intermediate states in small volumes. On physically large volumes, however, this pattern disappears: plateaux develop around $x_0 = T/2$, i.e. the lightest excitations, which coincide with the pseudoscalar meson mass when defined either by f_A^I or by f_P, govern the exponential decay of these functions. This will be explicitly demonstrated elsewhere [19]. An analogous statement holds for the vector meson mass via the correlation functions k_V^I and k_T.

The expectation values in the simulation points of Table 1 for the observables Eqs. (2.15), (2.30) and (2.31) are now summarized in Table 2. Within all potential sources of errors to be incorporated in the analysis, i.e. the statistical one and those coming from Z_A/Z_P, Z_A, Z_V, L/r_0 and $m_\pi L$, the contributions caused by the uncertainties of the renormalization factors Z_X ever dominate the combined errors quoted in the second parentheses in the table. Furthermore, any inherent small mismatch of the central values with the renormalization conditions (3.5) on $m_\pi L$ and L/r_0 in sets B, C and D was corrected by a conservative estimation of the slopes $\partial\mathcal{O}/\partial(am_\pi)$ and $\partial\mathcal{O}/\partial\beta$ with $\mathcal{O} = \mathcal{O}(m_\pi L, L/r_0, L/a) \in \{am, am_\rho, af_\pi, \overline{\eta}_V\}$, which enter the identities for the required partial derivatives

$$\frac{\partial\mathcal{O}}{\partial(m_\pi L)} \simeq \frac{a}{L}\frac{\partial\mathcal{O}}{\partial(am_\pi)}, \tag{3.9}$$

$$\frac{\partial\mathcal{O}}{\partial(L/r_0)} \simeq \frac{a}{L}\frac{\partial\beta}{\partial(a/r_0)}\frac{\partial\mathcal{O}}{\partial\beta} \simeq \frac{r_0}{a}\frac{\partial\mathcal{O}}{\partial(L/a)}. \tag{3.10}$$

They were numerically extracted in linear approximation from several simulations in set A at neighbouring values of κ and β, where in the latter case they had to be combined with the derivative $\partial\beta/\partial(a/r_0)$ to be read off from the parametrization (3.6). The slopes obtained in this way were carried over to the finer lattices as well, since for increasing lattice resolution ($\beta > 6.0$) their corrections are of $O(a)$ and, with respect to the other sources of errors, can safely be ignored.

4. Results

We pass to the final results. After the procedure of matching the conditions characterizing the LCP under study, one finds the numbers collected in Table 3; note that

Table 3
Dimensionless results for the quantities of Table 2 with total errors after they have been corrected to fulfill exactly the simultaneous renormalization conditions (3.5) as described in the text (Subsection 3.2). The errors on r_0/a quoted in [33] have been taken into account as well

Set	$\overline{m}r_0$	$m_\rho r_0$	$f_\pi r_0$	$\overline{\eta}_V$
A	0.1069(50)	1.846(13)	0.6701(82)	0.3283(46)
B	0.1029(35)	1.839(15)	0.684(11)	0.3296(72)
C	0.1045(36)	1.848(18)	0.681(13)	0.3360(95)
D	0.1103(35)	1.860(18)	0.699(12)	0.3457(75)

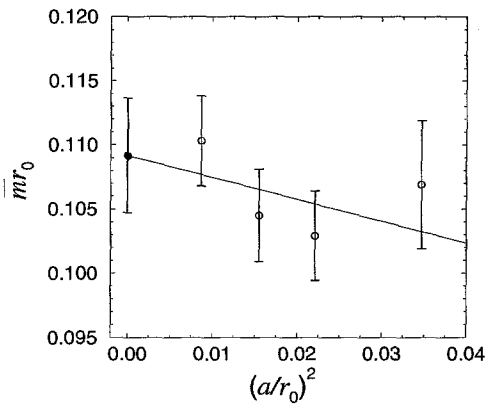

Fig. 2. Scaling behaviour of the renormalized PCAC current quark mass in units of r_0. An intermediate volume with SF boundary conditions is considered. The renormalization constant Z_P refers to a scale of $L = 1.436\, r_0$. Non-perturbative O(a) improvement allows to extrapolate linearly with $(a/r_0)^2 \to 0$ to the continuum limit.

according to (2.25) the bare PCAC quark mass $m(T/2)$ translates through multiplication with Z_A/Z_P into the renormalized quantity $\overline{m}$. Now we are prepared to perform extrapolations of these data to the continuum limit, assuming convergence with a rate proportional to a^2.

The fits are displayed in Figs. 2–5 and exemplify the scaling behaviour on the course from simulation points A to D. One evidently observes the leading corrections to the continuum to be compatible with O(a^2). Moreover, it can be inferred from Table 4 that the differences of the continuum limits from the values at $\beta = 6.0$ ($a \simeq 0.1$ fm) are around or even below 5% in the improved theory. These appear to be partly smaller than it was to be expected on basis of the experiences reported previously in Refs. [13,14].

At this point we have to add the remark that the results in the vector channel had to be revised compared to those listed in [16]. Due to some incorrect normalization of the correlation functions k_V and k_T during an earlier data analysis, we erroneously observed a quite steep slope when carrying out the $(a/r_0)^2 \to 0$ fit for the ratio $\overline{\eta}_V$ defined in Eq. (2.31). Looking at the final numbers now, it does no longer stand in contradiction to the findings in the pseudoscalar channel. By contrast, since the scaling violations of $\overline{\eta}_V$ are only slightly larger than for $f_\pi r_0$, we interpret this as a further compelling and

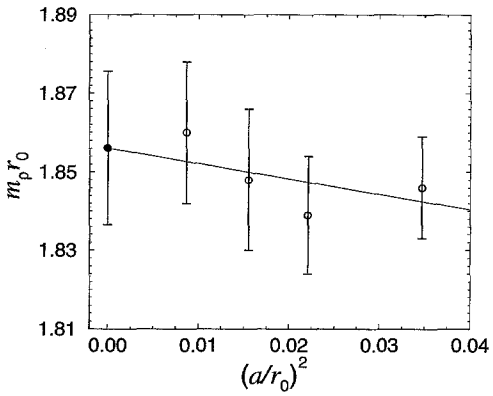

Fig. 3. Continuum limit extrapolation as in Fig. 2 but for the 'rho meson mass' in intermediate volume.

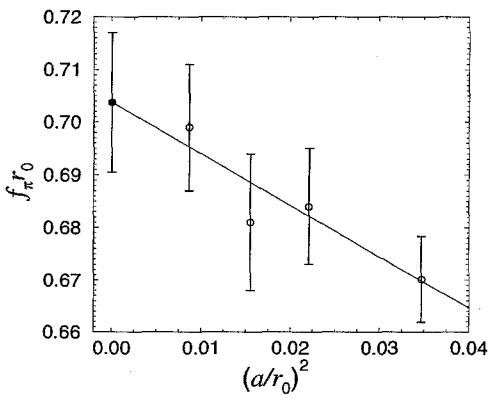

Fig. 4. The same as in Fig. 3 but for the 'pion decay constant'.

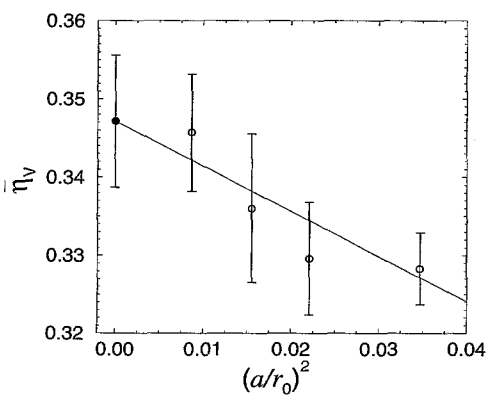

Fig. 5. Again as in Fig. 3 but now for the observable $\overline{\eta}_V$, which is composed of a (renormalized and improved) correlation function involving the vector current.

Table 4
Continuum limits and their percentage deviations from $\beta = 6.0$ ($a \simeq 0.1$ fm). The lower numbers belong to a data evaluation, where the improvement coefficients c_A and c_V have been artificially taken to vanish

Case	$\overline{m}r_0$	$m_\rho r_0$	$f_\pi r_0$	$\overline{\eta}_V$
Fully improved	0.1092(45)	1.856(20)	0.704(13)	0.3472(84)
	2%	< 1%	5%	6%
$c_A = 0$ and $c_V = 0$	0.1069(46)	1.856(20)	0.698(13)	0.3439(85)
	17%	< 1%	1%	2%

satisfactory indication for the effectiveness of non-perturbative $O(a)$ improvement.

In Ref. [14] the suspicion was raised that scaling looks even slightly better, if the perturbative estimates for the improvement coefficients c_A and c_V are used. This issue deserves some comments here. In order to address the sensitivity of the analysis to the improvement terms in the pseudoscalar and vector channel proportional to c_A and c_V, we just evaluated our data with setting these coefficients arbitrarily to zero. Then, of course, the theory is only partially $O(a)$ improved, and a residual contamination with uncancelled $O(a)$ contributions has still to be expected. The surprising outcome is that upon omitting those terms, two quantities ($f_\pi r_0, \overline{\eta}_V$) have somewhat smaller a-effects in total magnitude. At the same time, however, the renormalized PCAC quark mass $\overline{m}r_0$ gets much larger ones. Nevertheless, as seen from Table 4, the continuum limits of both data sets agree within errors. Such a result might suggest that the *qualitative* scaling behaviour of our quantities (apart from $\overline{m}r_0$) is only marginally influenced by the definite choice of c_X, X = A, V, still meeting the condition of a dominant a^2-behaviour. On the other hand, we observed a tendency in the $c_A = c_V = 0$ data points to disperse around the straight line fits to the continuum, which hints at some remnant of admixture of $O(a)$ discretization errors; hence a scaling violating term $\propto a^2$ in leading order rather seems to be ruled out in that case. This is particularly pronounced for $\overline{m}r_0$, where the correction to the continuum limit grows distinctly (from 2% to 17% in Table 4) if the improvement of the axial quark current is switched off. Opposed to that, in the fully improved case including the $O(a)$ correction terms, the required continuum limit extrapolations are generically not critical. In conclusion – and as a further convincing argument for the use of its non-perturbative values – this finally supports the physical insight that c_A and c_V are essentially relevant for chiral symmetry restoration at finite cutoff.

5. Discussion and outlook

In confirmation of similar investigations [12–15], $O(a)$ improvement implies a substantial reduction of scaling violations. Our numerical simulations of renormalized correlation functions in intermediate physical volume within the Schrödinger functional give clear evidence for an overall behaviour completely consistent with being linear in a^2 at $a \leqslant 0.1$ fm, for all quantities under consideration. Changing a by a factor two yields very stable fits and honest continuum limit extrapolations. Actually, the residual $O(a^2)$

cutoff effects at $a \simeq 0.1$ fm stay around ($f_\pi r_0$ and $\overline{\eta}_V$) or significantly below 5% ($\overline{m} r_0$ and $m_\rho r_0$).

To quantify directly the influence of the improvement coefficients c_A and c_V on the scaling behaviour, we examined also the partially improved case $c_A = c_V = 0$. In this case $f_\pi r_0$ and $\overline{\eta}_V$ show an even weaker dependence on the lattice spacing, *but now one finds* $\sim$ *17% lattice spacing effects* at $a \simeq 0.1$ fm in the renormalized current quark mass $\overline{m} r_0$. Additionally, as outlined in Section 4, the functional form of the leading a-effects then appears no longer compatible with a^2 alone; furthermore, chiral Ward identities are badly violated for $c_A = c_V = 0$ at $O(a)$ level [9,11]. Thus there is in general no choice for the improvement coefficients c_A and c_V, which diminishes the size of $O(a^2)$ lattice artifacts simultaneously for *all* relations and observables below a level of 5%. However, one should not feel tempted to judge this fact as a kind of principal conflict with the improvement programme itself, since the criterion of small $O(a^2)$ corrections has only been touched when selecting a definite set of kinematical variables to formulate the respective improvement conditions within the Schrödinger functional.

To summarize, the scaling tests in hand illustrate that also in the $O(a)$ improved theory the remaining $O(a^2)$ discretization errors have to be assessed – and consequently can be extrapolated away reliably – by varying the lattice spacing.

An extension of the present study to physically large volumes, where hadronic masses and matrix elements can be computed, is in progress [19].

Acknowledgements

This work is part of the ALPHA Collaboration research programme. We thank DESY for allocating computer time on the APE-Quadrics computers at DESY Zeuthen to this project and the staff of the computer centre at Zeuthen for their support. I am grateful to Rainer Sommer for numerous discussions, useful suggestions and a critical reading of the manuscript. I also thank Hartmut Wittig and Andreas Hoferichter for discussions.

References

[1] M. Bochicchio, L. Maiani, G. Martinelli, G.C. Rossi and M. Testa, Nucl. Phys. B 262 (1985) 331.
[2] L. Maiani and G. Martinelli, Phys. Lett. B 178 (1986) 265.
[3] K. Symanzik, Nucl. Phys. B 226 (1983) 187.
[4] K. Symanzik, Nucl. Phys. B 226 (1983) 205.
[5] M. Lüscher and P. Weisz, Phys. Lett. B 158 (1985) 250.
[6] M. Lüscher and P. Weisz, Commun. Math. Phys. 97 (1985) 59.
[7] ALPHA, M. Lüscher, S. Sint, R. Sommer and P. Weisz, Nucl. Phys. B 478 (1996) 365, hep-lat/9605038.
[8] R. Sommer, Nucl. Phys. B (Proc. Suppl.) 60A (1998) 279, hep-lat/9705026.
[9] ALPHA, M. Lüscher, S. Sint, R. Sommer, P. Weisz and U. Wolff, Nucl. Phys. B 491 (1997) 323, hep-lat/9609035.
[10] ALPHA, M. Lüscher, S. Sint, R. Sommer and H. Wittig, Nucl. Phys. B 491 (1997) 344, hep-lat/9611015.
[11] M. Guagnelli and R. Sommer, Nucl. Phys. B (Proc. Suppl.) 63 (1998) 886, hep-lat/9709088.
[12] QCDSF, M. Göckeler et al., Phys. Lett. B 391 (1997) 388, hep-lat/9609008.

[13] QCDSF, M. Göckeler et al., Phys. Rev. D 57 (1998) 5562, hep-lat/9707021.
[14] H. Wittig, Nucl. Phys. B (Proc. Suppl.) 63 (1998) 47, hep-lat/9710013.
[15] R.G. Edwards, U.M. Heller and T.R. Klassen, Phys. Rev. Lett. 80 (1998) 3448, hep-lat/9711052.
[16] ALPHA, J. Heitger, Nucl. Phys. B (Proc. Suppl.) 73 (1999) 921, hep-lat/9809002.
[17] A. Cucchieri, M. Masetti, T. Mendes and R. Petronzio, Phys. Lett. B 422 (1998) 212, hep-lat/9711040.
[18] D. Becirevic et al., hep-lat/9809129.
[19] ALPHA, M. Guagnelli, J. Heitger, R. Sommer and H. Wittig, hep-lat/9903040.
[20] ALPHA, S. Capitani, M. Lüscher, R. Sommer and H. Wittig, Nucl. Phys. B 544 (1999) 669, hep-lat/9810063.
[21] M. Lüscher, R. Narayanan, P. Weisz and U. Wolff, Nucl. Phys. B 384 (1992) 168, hep-lat/9207009.
[22] S. Sint, Nucl. Phys. B 421 (1994) 135, hep-lat/9312079.
[23] S. Sint, Nucl. Phys. B 451 (1995) 416, hep-lat/9504005.
[24] R. Sommer, Non-perturbative Renormalization of QCD, Lectures given at 36th Internationale Universitätswochen für Kernphysik und Teilchenphysik, Schladming, Austria, 1–8 March 1997, hep-ph/9711243.
[25] M. Lüscher, Advanced Lattice QCD, Lectures given at Les Houches Summer School in Theoretical Physics, Probing the Standard Model of Particle Interactions, Les Houches, France, 28 July–5 Sept. 1997, hep-ph/9802029.
[26] M. Lüscher, R. Sommer, P. Weisz and U. Wolff, Nucl. Phys. B 413 (1994) 481, hep-lat/9309005.
[27] ALPHA, S. Capitani et al., Nucl. Phys. B (Proc. Suppl.) 63 (1998) 153, hep-lat/9709125.
[28] S. Sint and P. Weisz, Nucl. Phys. B 502 (1997) 251, hep-lat/9704001.
[29] G.M. de Divitiis and R. Petronzio, Phys. Lett. B 419 (1998) 311, hep-lat/9710071.
[30] W. Bardeen, A. Duncan, E. Eichten, G. Hockney and H. Thacker, Phys. Rev. D 57 (1998) 1633, hep-lat/9705008.
[31] B. Sheikholeslami and R. Wohlert, Nucl. Phys. B 259 (1985) 572.
[32] A. Bode and U. Wolff, Nucl. Phys. B 540 (1999) 491, hep-lat/9809175.
[33] ALPHA, M. Guagnelli, R. Sommer and H. Wittig, Nucl. Phys. B 535 (1998) 389, hep-lat/9806005.
[34] R. Sommer, Nucl. Phys. B 411 (1994) 839, hep-lat/9310022.
[35] M. Lüscher and P. Weisz, Nucl. Phys. B 479 (1996) 429, hep-lat/9606016.

E

Hadron masses and matrix elements from the QCD Schrödinger functional

Nucl. Phys. B560 (1999) 465-481

ELSEVIER

Nuclear Physics B 560 (1999) 465–481

NUCLEAR PHYSICS B

www.elsevier.nl/locate/npe

Hadron masses and matrix elements from the QCD Schrödinger functional

ALPHA Collaboration

Marco Guagnelli [a], Jochen Heitger [b], Rainer Sommer [b], Hartmut Wittig [c,1]

[a] *Dipartimento di Fisica, Università di Roma Tor Vergata and INFN, Sezione di Roma II, Rome, Italy*

[b] *DESY-Zeuthen, Platanenallee 6, D-15738 Zeuthen, Germany*

[c] *Theoretical Physics, University of Oxford, 1 Keble Road, Oxford OX1 3NP, UK*

Received 1 April 1999; accepted 5 August 1999

Abstract

We explain how masses and matrix elements can be computed in lattice QCD using Schrödinger functional boundary conditions. Numerical results in the quenched approximation demonstrate that good precision can be achieved. For a statistical sample of the same size, our hadron masses have a precision similar to what is achieved with standard methods, but for the computation of matrix elements such as the pseudoscalar decay constant the Schrödinger functional technique turns out to be much more efficient than the known alternatives.

PACS: 11.15.Ha; 12.38.Gc

Keywords: Hadron masses; Matrix elements; Lattice gauge theory; Quantum chromodynamics; Monte Carlo

1. Introduction

In recent years, lattice QCD calculations in the quenched approximation have reached a new quality [1–3]. The renormalization of many local composite operators can be treated non-perturbatively, and the leading discretization errors have been removed. Consequently one would now like to perform continuum extrapolations for various

[1] PPARC Advanced Fellow.

0550-3213/99/$ - see frontmatter
PII S0550-3213(99)00466-6

hadron masses and matrix elements in the improved theory [4–9] and compare to recent results obtained with more standard techniques [3]. In particular, the problem of a determination of the light quark masses can be addressed with confidence, since the complete renormalization is known non-perturbatively [10].

However, continuum extrapolations require masses and matrix elements for finite values of the lattice spacing which are sufficiently accurate [3]. Efficient methods are needed to obtain such precise results. Standard methods use correlation functions in a sufficiently large box with periodic boundary conditions [11]. Usually one seeks to enhance the dominance of the low lying hadrons by using tuned hadron wave functions [12–21], possibly combined with variational techniques [22,23,17].

In this paper we investigate an alternative to these standard methods. Again we choose a sufficiently large box but impose Dirichlet boundary conditions in time, as they are used to formulate the QCD Schrödinger functional . We shall demonstrate that correlation functions in the Schrödinger functional are dominated by hadron intermediate states at large Euclidean time. Moreover, it is shown that a time extent of 3 fm for the box is sufficient to extract masses and matrix elements. An advantage compared to the standard methods is that the pre-asymptotic decay of Schrödinger functional correlation functions is very slow, which means that a large signal remains at large separations.

In the following, we briefly discuss the foundation of the method (Section 2) and test its applicability in practice in the quenched approximation (Section 3). We also attempt to quantify the efficiency compared to more standard calculations (Section 4). Finally we discuss open questions as well as possible further improvements.

2. Correlation functions at large time separations

We now derive explicit expressions for the representation of Schrödinger functional correlation functions in terms of intermediate physical states. Throughout this section we assume that the lattice Schrödinger functional is defined using the standard Wilson action as in Ref. [24]. In this situation the relations presented here hold exactly. If one considers the $O(a)$ improved theory, as we will do later, we cannot derive the equations given in this section directly from the transfer matrix. However, universality implies that the renormalized correlation functions of the improved theory and the unimproved theory agree in the continuum limit. Since the correlation functions considered below are renormalized multiplicatively, their time dependence (bare or renormalized) is given by the expressions derived for the Wilson theory up to lattice spacing effects. For the $O(a)$ improved theory this means that all relations derived in this section are valid for physical distances large compared to the lattice spacing (up to corrections of order a^2).

The correlation functions considered here have been introduced before [25–27]. In those references the emphasis was largely on the perturbative regime, which means choosing small extensions of the space-time volume. By contrast, in this work we are interested in the correlation functions for intermediate to large volumes, i.e. extensions which are significantly larger than typical QCD scales. Provided that the pion mass is

not too small, such typical QCD scales are of order 1 fm.

The QCD Schrödinger functional is defined as the QCD partition function in a cylindrical geometry, i.e. periodic boundary conditions with periodicity length L in three of the four Euclidean dimensions, and Dirichlet boundary conditions in time at the hypersurfaces $x_0 = 0$ and $x_0 = T$. Its quantum mechanical interpretation has first been discussed for the pure gauge theory [28] and subsequently for the theory with quarks [24]. In these references it was shown that the Schrödinger functional partition function can be written as

$$\mathcal{Z} = \langle \mathrm{f}|\mathrm{e}^{-T\mathbb{H}}\mathbb{P}|\mathrm{i}\rangle\,, \tag{2.1}$$

with states $|\mathrm{i}\rangle$ and $|\mathrm{f}\rangle$ which are given in terms of the boundary values specified at $x_0 = 0$ and $x_0 = T$, respectively. In the above equation $\mathbb{H}$ denotes the Hamilton operator of QCD formulated on a torus of volume L^3. More precisely, in the lattice theory it is proportional to the (negative) logarithm of the transfer matrix.[2]

Of course, the same operator describes the correlation functions when the Dirichlet boundary conditions are replaced by periodic boundary conditions in time. The projector $\mathbb{P}$ projects onto the gauge invariant subspace of the Hilbert space [28,24]; only gauge invariant intermediate states are physical and can contribute.

For our present investigation, we have considered only the case of homogeneous boundary conditions, where the spatial components of the gauge potentials are set to zero at the boundaries and also the fermion boundary fields are taken to vanish. In this case we have $|\mathrm{i}\rangle = |\mathrm{f}\rangle = |\mathrm{i}_0\rangle$ and this state carries the quantum numbers of the vacuum. Other choices for the boundary conditions may be of interest as well and can be treated similarly.

As an example we will discuss two specific correlations, which allow for a calculation of the pion mass and decay constant. The generalization to other channels and other matrix elements is straightforward.

We start from the dimensionless fields

$$\mathcal{O} = \frac{a^6}{L^3}\sum_{y,z}\bar{\zeta}_{\mathrm{u}}(y)\gamma_5\zeta_{\mathrm{d}}(z)\,, \qquad \mathcal{O}' = \frac{a^6}{L^3}\sum_{y,z}\bar{\zeta}'_{\mathrm{d}}(y)\gamma_5\zeta'_{\mathrm{u}}(z) \tag{2.2}$$

and a local composite (gauge invariant) field $X(x)$ (which will have mass dimension three in our applications) to define the gauge invariant correlation functions

$$f_X(x_0) = -\frac{L^3}{2}\langle X(x)\,\mathcal{O}\rangle\,, \tag{2.3}$$

$$f_1 = -\frac{1}{2}\langle \mathcal{O}'\,\mathcal{O}\rangle\,, \tag{2.4}$$

where the average denotes the usual path integral average and u, d are flavour indices. The "boundary quark fields", $\zeta, \ldots, \bar{\zeta}'$, have been discussed in [26]. In the lattice theory, ζ is given explicitly in terms of the gauge fields connecting hypersurfaces $x_0 = 0$

[2] For the unimproved Wilson action, $\mathbb{H}$ is known to be hermitian [29].

and $x_0 = a$ and the quark fields on the hypersurface $x_0 = a$. Analogous properties hold for the other boundary quark fields. Our choices for X are $X = A_0$ (defining, through Eq. (2.3), the correlation function f_A) and $X = P$ (which gives f_P), where

$$A_0(x) = \overline{\psi}_d(x)\gamma_0\gamma_5\psi_u(x)\,, \tag{2.5}$$

$$P(x) = \overline{\psi}_d(x)\gamma_5\psi_u(x)\,. \tag{2.6}$$

The correlation functions f_X have the quantum mechanical representation

$$f_X(x_0) = \mathcal{Z}^{-1}\,\frac{L^3}{2}\,\langle \mathrm{i}_0|\mathrm{e}^{-(T-x_0)\mathbb{H}}\mathbb{P}\mathbb{X}\mathrm{e}^{-x_0\mathbb{H}}\mathbb{P}|\mathrm{i}_\pi\rangle\,, \quad a \leqslant x_0 \leqslant T-a\,, \tag{2.7}$$

where $\mathbb{X}$ is the corresponding operator in the Schrödinger picture, and the state $|\mathrm{i}_\pi\rangle$ has the quantum numbers of the π^+ with momentum zero. To conclude that Eq. (2.7) holds, one only requires that the combination of fields $\mathcal{O}$, Eq. (2.2), has support for $x_0 \leqslant a$ and that it carries the quantum numbers of a π^+. The former is guaranteed by the very construction of the boundary fields $\zeta, \bar{\zeta}$ [26]. Furthermore we have

$$f_1 = \mathcal{Z}^{-1}\,\frac{1}{2}\,\langle \mathrm{i}_\pi|\mathrm{e}^{-T\mathbb{H}}\mathbb{P}|\mathrm{i}_\pi\rangle\,. \tag{2.8}$$

It is now apparent that (for large separations x_0 and $T - x_0$) the mass of the pion and its decay constant can be extracted. To see this explicitly we insert a complete set of eigenstates of the Hamiltonian,

$$|n,q\rangle\,, \quad n = 0,1,\ldots\,, \tag{2.9}$$

$$\mathbb{H}\,|n,q\rangle = E_n^{(q)}|n,q\rangle\,, \tag{2.10}$$

with normalization $\langle n',q'|n,q\rangle = \delta_{n,n'}\,\delta_{q,q'}$. Here the energy levels in the sector of the Hilbert space with internal quantum numbers q are enumerated by n. Only quantum numbers $q = \pi$, a shorthand for $(J,P,C,I,I_3) = (0,-,+,1,1)$, and $q = 0$, which denotes vacuum quantum numbers are considered in the following. We do not indicate the momentum of the states $|n,q\rangle$, since both $|\mathrm{i}_0\rangle$ and $|\mathrm{i}_\pi\rangle$ are invariant under spatial translations and only states $|n,q\rangle$ with vanishing (spatial) momentum contribute.

The representations given so far hold for arbitrary L, T and x_0. In this paper, we shall be interested in the special case of the asymptotic behaviour of $f_A(x_0)$, f_1 for large values of both x_0 and $T - x_0$, while L remains unspecified at this stage. We include the first non-leading corrections but neglect any contributions which are suppressed by terms of order

$$\exp(-TE_1^{(0)})\,, \qquad \exp(-x_0E_1^{(\pi)} - (T-x_0)E_1^{(0)})\,,$$
$$\exp(-(T-x_0)E_2^{(0)}) \quad \text{and} \quad \exp(-x_0E_2^{(\pi)})\,,$$

compared to the leading terms in the correlation functions. In this approximation we obtain

$$f_X(x_0) \approx \frac{L^3}{2}\,\rho\,\langle 0,0|\mathbb{X}|0,\pi\rangle\,\mathrm{e}^{-x_0 m_\pi}\left\{1+\eta_X^\pi \mathrm{e}^{-x_0\Delta}+\eta_X^0\mathrm{e}^{-(T-x_0)m_G}\right\}, \tag{2.11}$$

$$f_1 \approx \frac{1}{2}\,\rho^2\,\mathrm{e}^{-Tm_\pi}, \tag{2.12}$$

where we have introduced the ratios

$$\rho = \frac{\langle 0,\pi|\mathrm{i}_\pi\rangle}{\langle 0,0|\mathrm{i}_0\rangle}, \tag{2.13}$$

$$\eta_X^\pi = \frac{\langle 0,0|\mathbb{X}|1,\pi\rangle\langle 1,\pi|\mathrm{i}_\pi\rangle}{\langle 0,0|\mathbb{X}|0,\pi\rangle\langle 0,\pi|\mathrm{i}_\pi\rangle}, \tag{2.14}$$

$$\eta_X^0 = \frac{\langle \mathrm{i}_0|1,0\rangle\langle 1,0|\mathbb{X}|0,\pi\rangle}{\langle \mathrm{i}_0|0,0\rangle\langle 0,0|\mathbb{X}|0,\pi\rangle}. \tag{2.15}$$

The energy difference $m_G = E_1^{(0)} - E_0^{(0)}$ is the mass of the 0^{++} glueball and $\Delta = E_1^{(\pi)} - E_0^{(\pi)}$ is an abbreviation for the gap in the pion channel. As indicated above, we have dropped contributions of higher excited states which decay even faster as x_0 and $T - x_0$ become large.

Considering the special case of f_A, we find that it is proportional to the matrix element $\langle 0,0|\mathbb{A}_0|0,\pi\rangle$, which is related to the pion decay constant F_π through

$$Z_A\langle 0,0|\mathbb{A}_0|0,\pi\rangle = F_\pi m_\pi (2m_\pi L^3)^{-1/2}. \tag{2.16}$$

Here, Z_A is the renormalization constant of the isovector axial current, and the factor $(2m_\pi L^3)^{-1/2}$ takes account of the conventional normalization of one-particle states (in our convention the experimental value of the pion decay constant is 132 MeV).

Eq. (2.11) is used to determine m_π, while the pion decay constant, F_π, may be conveniently extracted from the ratio

$$Z_A\, f_A(x_0)/\sqrt{f_1} \approx \frac{1}{2}F_\pi\,(m_\pi L^3)^{1/2}\mathrm{e}^{-(x_0-T/2)m_\pi} \times\left\{1+\eta_A^\pi \mathrm{e}^{-x_0\Delta}+\eta_A^0\mathrm{e}^{-(T-x_0)m_G}\right\}. \tag{2.17}$$

The above formulas show explicitly how masses and matrix elements can be obtained from Schrödinger functional correlation functions. Before we describe the numerical tests of the practicability, we wish to point out some properties of the present method and list the differences to conventional approaches.

- Eqs. (2.11) and (2.12) can be expected to be rather accurate when all time separations are larger than typical hadronic length scales (say, 1 fm, provided m_π is not too small). Schrödinger functional correlation functions decay slowly for small x_0, leaving a large and precise signal at separations of 1–2 fm. This is easily seen by applying asymptotic freedom and a simple-dimensional analysis. As a comparison, consider correlation functions of standard local composite fields such as $\sum_x\langle\Phi^\dagger(x)\Phi(0)\rangle$, with $\Phi(x) = \overline{\psi}_u(x)\Gamma\psi_d(x)$, $\Phi^\dagger(x) = \overline{\psi}_d(x)\gamma_0\Gamma\gamma_0\psi_u(x)$. At distances $x_0 \approx 1$ fm, such correlation functions are typically very small which usually means low statistical precision. The reason why they are small is because

they decay like $(x_0)^{-3}$ for short time separations, as may be inferred by the same arguments used above. This qualitative difference arises from the fact that in the Schrödinger functional a dimensionless (non-local) field, $\int \mathrm{d}\boldsymbol{y}\, \bar{\zeta}_{\mathrm{u}}(\boldsymbol{y})\gamma_5\zeta_{\mathrm{d}}(\boldsymbol{0})$, is used to create hadronic states at the boundary.

- The ratio ρ, Eq. (2.13) is divergent, since the state $|\mathrm{i}_\pi\rangle$ involves the bare boundary quark fields. However, in the final quantities of interest ρ is cancelled explicitly (see Eq. (2.17)).
- In particular, the combination $Z_{\mathrm{A}}\, f_{\mathrm{A}}(x_0)/\sqrt{f_1}$ has a continuum limit for all values of x_0. One may therefore choose some (not too large) value of the lattice spacing to determine the time separations x_0 and $T - x_0$ where the contamination due to excited states is small. The same separations (in physical units) can then be used for other values of the lattice spacing. This holds also for the "local masses" which are commonly used to extract hadron masses. When one applies smearing or fuzzing the validity of such a statement is not immediately evident.
- Spatial translation invariance is used fully and reduces statistical errors.
- The present approach is similar to using "wall sources" to create hadronic states [13], but here we keep gauge invariance in all stages of the formulation!

3. Extraction of masses and decay constants

In this section we demonstrate the practicability of the method in the case of quenched lattice QCD.

3.1. Computational details

We work in $\mathrm{O}(a)$ improved QCD as detailed in [26], using the non-perturbative estimates of the improvement coefficients c_{sw} and c_{A} reported in Ref. [30].

The full $\mathrm{O}(a)$ improvement of the Schrödinger functional correlation functions requires also $\mathrm{O}(a)$ counterterms (with coefficients $c_{\mathrm{t}}, \widetilde{c}_{\mathrm{t}}$) at the boundary [26]. These do not affect the lattice spacing dependence of hadron masses and matrix elements, and therefore their coefficients are not very important in the present context. The only place where they do play a role is the size of the correction terms in Eq. (2.11), since the lattice spacing errors in the amplitude ratios η_X^π, η_X^0 are $\mathrm{O}(a^2)$ when $c_{\mathrm{t}}, \widetilde{c}_{\mathrm{t}}$ are chosen appropriately. Otherwise cutoff effects of order a remain in these excited state contributions. We used one-loop estimates for $c_{\mathrm{t}}, \widetilde{c}_{\mathrm{t}}$ [31,32]. For these values the $\mathrm{O}(a)$ effects are expected to be quite small [10,33].

In the pseudoscalar channel we consider the correlation functions $f_{\mathrm{P}}(x_0)$ and $f_{\mathrm{A}}^{\mathrm{I}}(x_0)$, where the latter is obtained from Eq. (2.3) by inserting the time component of the improved axial current [25,26], viz.

$$(A_{\mathrm{I}})_\mu(x) = A_\mu(x) + ac_{\mathrm{A}}\frac{1}{2}\left(\partial_\mu^* + \partial_\mu\right) P(x). \tag{3.1}$$

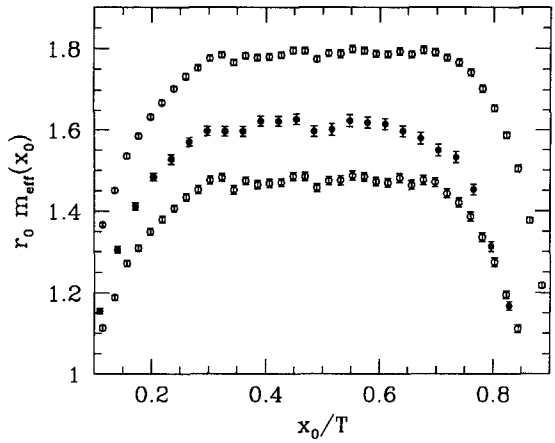

Fig. 1. The effective mass of the correlation function f_A^I, as defined in Eq. (3.4). The three sets of data points correspond to $(\beta, \kappa) = (6.2, 0.1349), (6.0, 0.1342), (6.2, 0.1352)$ from top to bottom. In all cases the time extent is $T \approx 3$ fm.

The correlation function in the vector channel is defined by

$$k_V^I(x_0) = -a^6 \sum_{y,z} \frac{1}{6} \sum_k \langle (V_I)_k(x)\ \bar{\zeta}_u(y)\gamma_k\zeta_d(z)\rangle\,, \tag{3.2}$$

where

$$(V_I)_\mu(x) = \overline{\psi}_d(x)\gamma_\mu\psi_u(x) + ac_V\frac{i}{2}(\partial_\nu + \partial_\nu^*)[\overline{\psi}_d(x)\sigma_{\mu\nu}\psi_u(x)] \tag{3.3}$$

is the $O(a)$ improved vector current. For the improvement coefficient c_V we have used the values from its non-perturbative determination reported in [34].

We have chosen the parameters of our simulations such that $L \approx 1.5$ fm and $T \approx 3$ fm. Our calculations have been performed for four different values of the lattice spacing, but for the purpose of demonstrating the practicability of the method we restrict ourselves to results obtained at $\beta = 6.0$ and $\beta = 6.2$. These couplings correspond to lattice spacings $a = 0.093$ fm and $a = 0.068$ fm, when $r_0 = 0.5$ fm is used to set the scale [35,36]. For these parameters a direct comparison with results obtained using conventional methods [4,5,8,9] can be made.

The numerical computations of Schrödinger functional correlation functions have been explained earlier [30], and further details can be found in that reference. Here we only mention that in addition to the previously used even/odd preconditioned version of the BiCGStab solver, we have also implemented SSOR-preconditioning [37,38]. The latter reduced the number of BiCGStab iterations needed to solve the Dirac equation by more than a factor 2. This turned into a gain in CPU-time of a factor of around 1.5 in our implementation on the APE-100 machines.

Our statistical samples consist of 1000 "measurements" of Schrödinger functional correlation functions at $\beta = 6.0$ and 800 measurements at $\beta = 6.2$. All statistical errors were computed using the jackknife method.

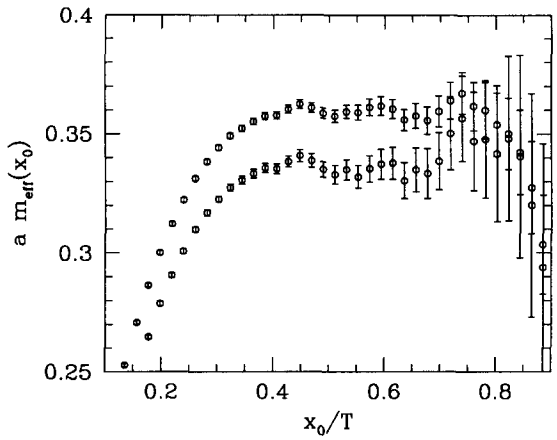

Fig. 2. The effective mass of the correlation function k_V^I for $a \approx 0.07$ fm.

3.2. Plateaux

Let us first get a rough impression of the range of x_0, where the leading term in Eq. (2.11) dominates. To this end we follow the tradition of looking for a plateau in the effective mass,

$$m_{\mathrm{eff}}(x_0 + a/2) = \frac{1}{a} \ln\big(f(x_0)/f(x_0 + a)\big) \ . \tag{3.4}$$

Here, f denotes any of the two-point correlation functions defined above. In the pseudoscalar channel we use $f = f_A^I$, and the resulting effective masses are shown in Fig. 1. There is good evidence for plateaux starting at $x_0 \approx 1$ fm and extending to approximately $T - x_0 \approx 1$ fm. As expected, the location of the plateaux is approximately independent of the lattice spacing.

Turning to the vector channel, we use Eq. (3.4) with $f = k_V^I$. In this channel the effective mass, shown in Fig. 2, turns into a plateau only at $x_0 \approx 1.5$ fm. Furthermore, statistical errors grow more rapidly as x_0 becomes large. By comparing Fig. 1 and Fig. 2 one may anticipate that it is more difficult to obtain a reliable determination of the vector meson mass than it is to compute m_π. However, this is not much different when standard methods are employed.

3.3. Excited state corrections – averaging intervals

Let us now discuss the extraction of masses and matrix elements in some detail. A standard method is to perform fits to the leading term in Eq. (2.11). Alternatively one can average the effective mass over the plateau region. Both of these procedures reduce the error in the mass compared to just taking one point of the effective mass in the plateau. One must then ensure that the final statistical error is not accompanied by a noticeable systematic error due to a small contamination by excited states. In other

words, one needs a rough estimate of the size of the contribution of excited states in the region of x_0 considered.

In order to arrive at such an estimate, one requires some information about the values of m_G and the gap Δ in Eq. (2.11) and the analogous equation for the vector channel. Glueball masses from the literature [39], combined with r_0/a [36], give

$$m_G r_0 \approx 4.3\,. \tag{3.5}$$

For our two values of the bare coupling, the results of Ref. [36] read $\frac{r_0}{a}(\beta = 6.0) = 5.37(2)$, $\frac{r_0}{a}(\beta = 6.2) = 7.36(4)$. We have also obtained a rough estimate for Δ in the pseudoscalar channel by analyzing correlation functions with periodic boundary conditions in time, which were made available to us by the *Tor Vergata* group [5]. Since this analysis is not of immediate interest for our discussion of Schrödinger functional correlation functions we relegate the details to Appendix A.

The typical uncertainties associated with the gaps and the scalar glueball mass are of order 10% for the range of quark masses considered here. The gaps and m_G can now be used to take a closer look at the effective masses and obtain estimates for the excited state contributions and the range of x_0 where these are small compared to the statistical errors. We discuss this separately for the two channels.

3.4. The pseudoscalar channel

The analysis described in Appendix A yields

$$r_0\Delta \approx 3.2\,, \tag{3.6}$$

which agrees with an estimate of the same quantity using data by UKQCD [9]. Using Eq. (2.11), the time dependence of the effective mass is given by

$$\begin{aligned} m_{\mathrm{eff}}(x_0) &\approx m_\pi \left\{ 1 + \frac{2\sinh(a\Delta/2)}{am_\pi}\eta_A^\pi \mathrm{e}^{-x_0\Delta} - \frac{2\sinh(am_G/2)}{am_\pi}\eta_A^0 \mathrm{e}^{-(T-x_0)m_G} \right\} \\ &\approx m_\pi \left\{ 1 + \frac{\Delta}{m_\pi}\eta_A^\pi \mathrm{e}^{-x_0\Delta} - \frac{m_G}{m_\pi}\eta_A^0 \mathrm{e}^{-(T-x_0)m_G} \right\}, \end{aligned} \tag{3.7}$$

where the second line is valid close to the continuum limit ($a\Delta \ll 1$, $am_G \ll 1$). In order to check whether this time dependence is reproduced by the data, we plot the effective masses directly against the expected form of the asymptotic correction terms, $\mathrm{e}^{-x_0\Delta}$ and $\mathrm{e}^{-(T-x_0)m_G}$ in Fig. 3.

One observes that the data fall approximately onto straight lines. It is important to bear in mind that m_G, Δ on the one hand and $m_{\mathrm{eff}}(x_0)$ on the other, have been obtained independently from correlation functions computed for different boundary conditions where excited state corrections have different amplitudes. The apparent compatibility of the data with the expected form of the correction terms is therefore non-trivial, and we conclude that we have a semi-quantitative understanding of the excited state corrections.

It is now easy to deduce values for t_{min} and $T - t_{\mathrm{max}}$ such that for $t_{\mathrm{min}} \leqslant x_0 \leqslant t_{\mathrm{max}}$ these corrections are below a certain margin, ϵ, which is allowed as a systematic

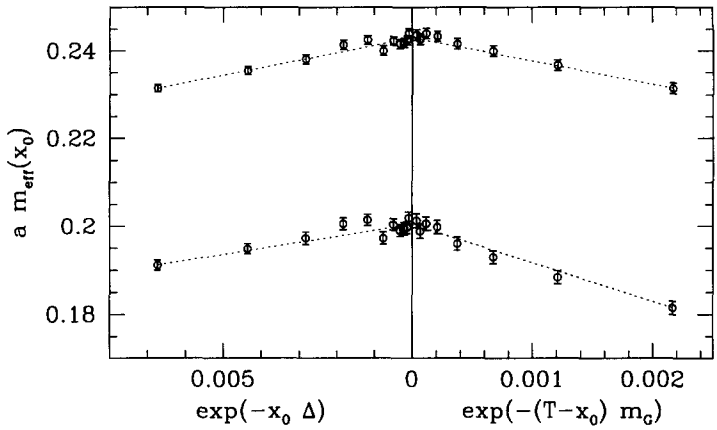

Fig. 3. The effective mass of the correlation function f_A^I against the two leading corrections. Small values of x_0 are omitted in the right half of the graph and large values of x_0 in the left half. Data are for a lattice spacing of $a \approx 0.07$ fm; the dashed lines indicate the agreement with linear behaviour.

Table 1
Ranges of x_0, where (relative) excited state contribution are smaller than ϵ

Channel	ϵ	t_{min}/r_0	$(T - t_{max})/r_0$
f_A^I	0.2%	2.6	2.3
f_A^I/f_P, f_P	0.1%	2.8	2.5
k_V^I	0.2%	3.0	2.2

uncertainty. We list t_{min} and $T - t_{max}$ together with the chosen values for ϵ in Table 1. Reliable estimates for m_π are then obtained by averaging m_{eff} for $t_{min} \leqslant x_0 \leqslant t_{max}$, and representative results are collected in Table 2.

A widely used method to extract hadron masses is to fit the correlation functions, using the expected asymptotic behaviour as an ansatz. In order to check the consistency of results obtained by averaging m_{eff} for $t_{min} \leqslant x_0 \leqslant t_{max}$, we have also performed single exponential fits to $f_A^I(x_0)$ over the same interval. A comparison of the two methods shows that the estimates for m_π are entirely consistent. Furthermore, the quality of the fits is very good, with typical values of the correlated χ^2/n_{df} in the range 0.6–0.9. Moreover, the stability of the fits under variations of the fitting interval has been used as an additional check that our values of t_{min}, t_{max} were chosen appropriately. In Table 2 we compare our results for am_π to those obtained using conventional techniques and find good agreement.

Next, we discuss the bare pion decay constant, F_π^{bare}, which is obtained from an average of

$$F_\pi^{bare} = 2(m_\pi L^3)^{-1/2} e^{(x_0 - T/2)m_\pi} \frac{f_A^I(x_0)}{\sqrt{f_1}}, \tag{3.8}$$

Table 2
Results in the pseudoscalar channel compared to values from the literature

β	κ	am_π	Ref. [4]	Ref. [5]	Ref. [8]
6.0	0.1338	0.3529(11)			
	0.1342	0.3001(12)	0.2988(17)		
6.2	0.1349	0.2430(6)	0.2444(9)		0.2440(21)
	0.1352	0.2004(6)	0.2016(11)	0.2007(40)	0.2007(26)
β	κ	$m_\pi F_\pi^{\rm bare}/G_\pi^{\rm bare}$	$aF_\pi^{\rm bare}$	Ref. [4]	Ref. [8]
6.0	0.1338	0.2125(7)	0.0943(4)		
	0.1342	0.1794(8)	0.0905(4)	0.0907(8)	
6.2	0.1349	0.2165(5)	0.0721(3)	0.0727(9)	0.0740(35)
	0.1352	0.1769(5)	0.0687(3)	0.0690(30)	0.0706(46)

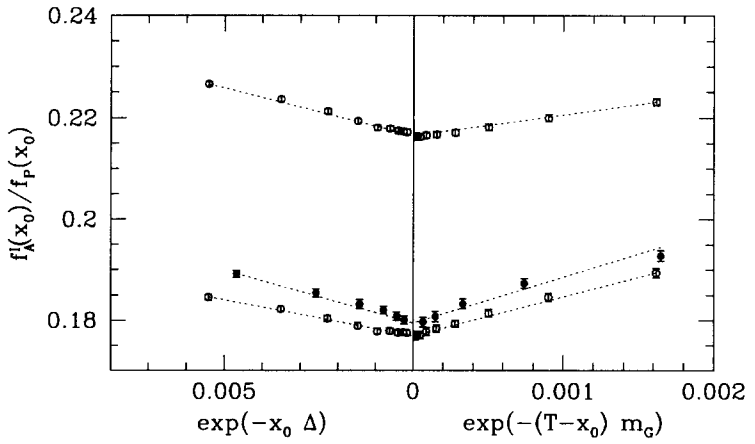

Fig. 4. Influence of excited states on the ratio $f_{\rm A}^{\rm I}(x_0)/f_{\rm P}(x_0)$ for $a \approx 0.07$ fm (open circles) and $a \approx 0.09$ fm (filled circles).

over the same interval of x_0, with m_π taken from the previous analysis.[3] Values for $F_\pi^{\rm bare}$ are also included in Table 2. Note that in the improved theory which we consider, the renormalized decay constant is given by $F_\pi = Z_{\rm A}(1 + b_{\rm A}\, am_{\rm q})F_\pi^{\rm bare}$ [26].

A further example for the determination of matrix elements is the combination $m_\pi F_\pi^{\rm bare}/G_\pi^{\rm bare}$ which is related to the ratio $f_{\rm A}^{\rm I}/f_{\rm P}$ via

$$\frac{f_{\rm A}^{\rm I}(x_0)}{f_{\rm P}(x_0)} \approx \frac{m_\pi F_\pi^{\rm bare}}{G_\pi^{\rm bare}} \frac{\left\{1 + \eta_{\rm A}^\pi e^{-x_0\Delta} + \eta_{\rm A}^0 e^{-(T-x_0)m_{\rm G}}\right\}}{\left\{1 + \eta_{\rm P}^\pi e^{-x_0\Delta} + \eta_{\rm P}^0 e^{-(T-x_0)m_{\rm G}}\right\}}\,. \tag{3.9}$$

Again one may average the l.h.s. over a range of x_0 where excited state corrections are negligible. To find the proper range for the ratio $f_{\rm A}^{\rm I}(x_0)/f_{\rm P}(x_0)$, we literally repeat the

[3] The leading correction terms to Eq. (3.8) are suppressed by factors m_π/Δ and $m_\pi/m_{\rm G}$ compared to Eq. (3.7). However, we did not enlarge the interval in this case, since m_π is not very small in comparison to the other masses.

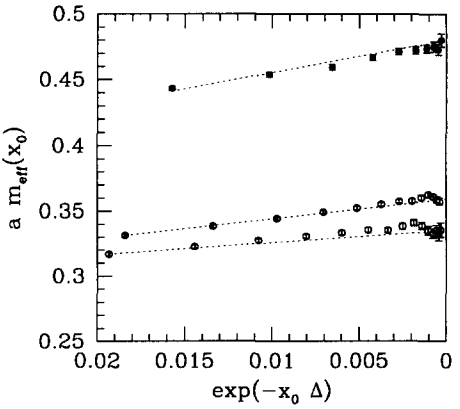

Fig. 5. The effective mass of the correlation function $k_{\mathrm{V}}^{\mathrm{I}}$ against the leading correction. The meaning of the symbols is as in Fig. 4.

analysis performed before for m_{eff}. As shown in Fig. 4 the corrections of order $\mathrm{e}^{-x_0\Delta}$ are of the same order as before. They originate predominantly from the denominator, since the PCAC relation predicts

$$\eta_{\mathrm{P}}^{\pi} = \frac{\Delta + m_{\pi}}{m_{\pi}} \eta_{\mathrm{A}}^{\pi} . \tag{3.10}$$

This enhancement factor compensates for the missing factor Δ/m_{π} compared to (3.7), and a similar value of t_{min} has to be chosen (see Table 1). Results for $m_{\pi} F_{\pi}^{\mathrm{bare}}/G_{\pi}^{\mathrm{bare}}$ are included in Table 2.

3.5. The vector channel

In analogy to the pseudoscalar case, the analysis of the correlation function $k_{\mathrm{V}}^{\mathrm{I}}$ requires information about the gap in the vector channel. The effective masses are plotted in Fig. 5. Here, the estimate for Δ has been obtained by tuning its value until a roughly linear behaviour was observed. Thus, unlike the case of the pseudoscalar, the gap is not known independently through a separately determined correlation function. However, from additional runs performed on a larger volume, we know that the contribution from excited states has approximately the same magnitude for $L = 2.2$ fm, which adds further credibility to the analysis of the gaps presented here.

Our statistical errors are too large to observe a significant signal for the glueball contribution at large x_0. The value of t_{max} was therefore determined by requiring that the maximally allowed glueball amplitude be contained within the statistical errors in the range of x_0 corresponding to $\exp(-(T - x_0)m_{\mathrm{G}}) \leqslant 0.002$. As before, our results for m_{ρ} obtained using the averaging procedure were consistent with single exponential fits to $k_{\mathrm{V}}^{\mathrm{I}}$. All parameters and numerical results are listed in the tables.

The comparison of our estimates for m_{ρ} to results employing standard methods in Table 3 shows that our numbers are slightly lower, although the difference is mostly not statistically significant. In view of the many checks of our analysis, we are confident

Table 3
Vector meson masses

β	κ	am_ρ	Ref. [4]	Ref. [5]	Ref. [8]
6.0	0.1338	0.508(3)			
	0.1342	0.480(4)	0.487(3)		
6.2	0.1349	0.359(3)	0.363(4)		0.363(8)
	0.1352	0.335(4)	0.343(5)	0.353(15)	0.335(12)

that the vector mass has been extracted correctly. It is well known that in general the determination of the mass in the vector channel is not easy, so that differences at the level of around 1.5 standard deviations are not too surprising.

4. Numerical efficiency

We can now assess the numerical efficiency of our method in relation to results obtained using conventional techniques. Comparing the errors in Tables 2 and 3, one has to take into account that the statistics for the simulation in [4] is approximately the same as ours, whereas in Refs. [5] and [8] the number of "measurements" is smaller by roughly a factor 8. If one compensates for trivial statistical factors, the tables demonstrate that correlation functions computed in the Schrödinger functional allow for the determination of hadron masses with similar precision compared to conventional methods. This is also the case for ratios of correlation functions like $f_{\mathrm{A}}^{\mathrm{I}}(x_0)/f_{\mathrm{P}}(x_0)$, which serves to extract the combination $m_\pi F_\pi^{\mathrm{bare}}/G_\pi^{\mathrm{bare}}$ [40,9].

Another relevant issue for the overall precision is the tolerated maximum contamination by excited states, ϵ. In order to avoid the total error to be noticeably affected by systematic effects, the averaging or fitting intervals must be chosen such that the statistical error is still significantly larger than ϵ. It then turns out that in our approach one can use very small values for ϵ without compromising the statistical accuracy. This is illustrated by a direct comparison to the results of Ref. [8] in the pseudoscalar channel. From the formulas in Appendix A we have

$$\epsilon = \chi_{\mathrm{P}}^2 \, \mathrm{e}^{\Delta t_{\mathrm{min}}}, \tag{4.1}$$

for the analysis of [8]. Inserting our estimates for Δ and χ_{P} obtained from fits described in Appendix A and the value of t_{min} used in [8], one obtains $\epsilon \approx 0.6\%$ in the pseudoscalar channel for Ref. [8]. Thus, in our simulation *both* the statistical error and the residual contamination by excited states is smaller by about a factor three.

The overall errors of the observables discussed above are similar to the ones achievable with standard methods, but perhaps – as we just argued – the Schrödinger functional correlation functions give somewhat more precise results. In addition the Schrödinger functional enables one to compute the pseudoscalar decay constant with much better precision compared to what is usually achieved with conventional correlation functions. The

reason for this is not entirely clear, but it may be because F_π^{bare} defined in Eq. (3.8) is obtained from a straight ratio of correlation functions times a function involving m_π only.

5. Discussion

In this paper we have shown how correlation functions with Schrödinger functional boundary conditions can be used to compute hadronic quantities like meson masses and matrix elements with high precision. An integral part of our analysis was the detailed investigation of the influence of excited states: in the pseudoscalar channel we have used independent information about the gap Δ and the lightest glueball mass to select the appropriate averaging intervals.

As explained in Section 2, correlation functions with Schrödinger functional boundary conditions decay slowly, resulting in accurate results for masses and matrix elements. In particular, we have seen that our method produces *very precise* results for the pion decay constant. One may expect that a similarly good efficiency applies to pseudoscalar-to-pseudoscalar matrix elements such as B_{K}. Such applications should be investigated in the future.

A separate issue is the generalization of our method to incorporate different channels. In particular one might be interested which hadrons are accessible from the quark Greens functions already computed in our present work. For all quantum numbers which can be reached by combining upper component $\mathbf{p} = 0$ quark fields and lower component $\mathbf{p} = 0$ anti-quark fields, hadron correlation functions can be constructed from the known quark Greens functions without additional "matrix inversions". An interesting example is a nucleon correlation function. We had not considered it in our present work: our spatial sizes are probably not big enough to accommodate nucleon states without significant finite size effects. On the other hand, an efficient treatment of states like the scalar meson would require boundary quark-antiquark fields in a relative P-wave. This represents a new numerical problem, which merits a separate investigation.

All our detailed investigations have been done for $L \approx 1.5\,\mathrm{fm}$. How does the size of excited state corrections depend on L? For smaller L, we expect the dominance by the ground state to be similar or even better. For significantly larger L, however, our correlation functions might receive bigger contributions from excited states and the efficiency might deteriorate. We have investigated also $L \approx 2.2\,\mathrm{fm}$ (keeping T fixed) for two different pairs of (β, κ). The magnitude of excited state corrections is hardly different from our results on the smaller system. So the location of the window of x_0, which allows for an extraction of physical masses and matrix elements, is independent of L between $1.5\,\mathrm{fm} \leqslant L \leqslant 2.2\,\mathrm{fm}$. Even larger values of L can not be reached with our computing resources but are also not necessary for the quantities studied here.

Further improvements of the method are possible. So far we have used only the simplest implementation of composite boundary fields in the calculation of f_1, $f_{\mathrm{A}}^{\mathrm{I}}$ and $k_{\mathrm{V}}^{\mathrm{I}}$. More refined choices of sources involving the boundary fields, such as tuned hadron

wavefunctions, can surely be made, whilst preserving gauge invariance at all stages of the calculation. This might further enhance the efficiency of the method.

Acknowledgements

This work is part of the ALPHA collaboration research programme. We thank DESY for allocating computer time on the APE/Quadrics computers at DESY-Zeuthen and the staff of the computer centre at Zeuthen for their support. We are grateful to the Tor Vergata group and to the UKQCD collaboration for access to their data. We also thank R. Horsley and D. Pleiter for a discussion of their results [4] and U. Wolff for a critical reading of the manuscript.

Appendix A. Determination of Δ

Here we describe the determination of the gap Δ in the pseudoscalar channel using correlation functions with periodic boundary conditions in all four space-time directions. The quark propagators were made available by the *Tor Vergata* group, and more details about the simulation can be found in [5]. Here we only state that Δ has been determined at $\beta = 6.2$ on a lattice of size $24^3 \times 48$, with the $O(a)$ improved action. In order to distinguish the correlation function computed using periodic boundary conditions from those defined within the Schrödinger functional , we use the letter 'C', defining

$$C_{\mathrm{PP}}(x_0) = a^3 \sum_{\mathbf{x}} \langle P(x) P^\dagger(0) \rangle, \tag{A.1}$$

$$C_{\mathrm{AP}}(x_0) = a^3 \sum_{\mathbf{x}} \langle (A_\mathrm{I})_0(x) P^\dagger(0) \rangle, \tag{A.2}$$

$$C_{\mathrm{AA}}(x_0) = a^3 \sum_{\mathbf{x}} \langle (A_\mathrm{I})_0(x) (A_\mathrm{I}^\dagger)_0(0) \rangle, \tag{A.3}$$

with $P(x)$ and $(A_\mathrm{I})_0(x)$ as given in Eqs. (2.6) and (3.1). Furthermore, we here use $P^\dagger(x) = -\overline{\psi}_\mathrm{u}(x)\gamma_5\psi_\mathrm{d}(x)$, and similarly for $A_\mathrm{I}^\dagger$. The spectral decomposition of the correlation functions in terms of the two lowest intermediate states is

$$C_{XX}(x_0) \approx \xi_X^2 \, \mathrm{e}^{-x_0 m_\pi} \times \left\{ 1 + \chi_X^2 \, \mathrm{e}^{-x_0 \Delta} \right\}, \quad X = \mathrm{A}, \mathrm{P}, \tag{A.4}$$

$$C_{\mathrm{AP}}(x_0) \approx \xi_\mathrm{A} \xi_\mathrm{P} \, \mathrm{e}^{-x_0 m_\pi} \times \left\{ 1 + \chi_\mathrm{A} \chi_\mathrm{P} \, \mathrm{e}^{-x_0 \Delta} \right\}, \tag{A.5}$$

when terms proportional to $\exp(-m_\pi(T-x_0))$ and $\exp(-m_G(T-x_0))$ can be neglected. We now consider the ratio

$$R_{\mathrm{AP}}(x_0) = \frac{C_{\mathrm{PP}}(x_0) C_{\mathrm{AA}}(x_0)}{[C_{\mathrm{AP}}(x_0)]^2}, \tag{A.6}$$

which – in the same approximation – is given by

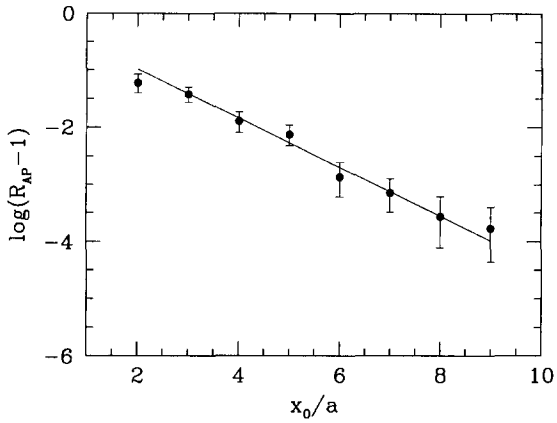

Fig. A.1. $R_{\mathrm{AP}} - 1$ for $\kappa = 0.1345$, $\beta = 6.2$. The line represents a fit in the window $3a \leqslant x_0 \leqslant 8a$.

$$R_{\mathrm{AP}}(x_0) - 1 \approx (\chi_{\mathrm{P}} - \chi_{\mathrm{A}})^2 \mathrm{e}^{-\Delta x_0}. \tag{A.7}$$

As in Eq. (3.10), χ_{P} and χ_{A} are related by the PCAC relation,

$$\chi_{\mathrm{P}} = \frac{\Delta + m_\pi}{m_\pi} \chi_{\mathrm{A}}, \tag{A.8}$$

and hence

$$R_{\mathrm{AP}}(x_0) - 1 \approx \chi_{\mathrm{P}}^2 \left(\frac{\Delta}{m_\pi} \right)^2 \mathrm{e}^{-\Delta x_0}. \tag{A.9}$$

By fitting $(R_{\mathrm{AP}}(x_0) - 1)$ to the above functional form in the appropriate range of x_0, one can extract the gap Δ. A typical fit is shown in Fig. A.1 from which we obtain the result quoted in the text,

$$r_0 \Delta \approx 3.2. \tag{A.10}$$

It turns out that Δ depends very little on the bare quark mass, so that this result is used in the analysis of correlation functions in Section 3 at all values of the quark mass.

References

[1] M. Lüscher, (1997), hep-ph/9711205.
[2] R.D. Kenway, (1998), hep-lat/9810054.
[3] CP-PACS Collaboration, R. Burkhalter et al., (1998), hep-lat/9810043.
[4] M. Göckeler et al., Phys. Rev. D 57 (1998) 5562, hep-lat/9707021.
[5] A. Cucchieri, M. Masetti, T. Mendes and R. Petronzio, Phys. Lett. B 422 (1998) 212, hep-lat/9711040.
[6] A. Cucchieri, T. Mendes and R. Petronzio, J. High Energy Phys. 05 (1998) 006, hep-lat/9804007.
[7] R.G. Edwards, U.M. Heller and T.R. Klassen, Phys. Rev. Lett. 80 (1998) 3448, hep-lat/9711052.
[8] D. Becirevic et al., (1998), hep-lat/9809129.
[9] UKQCD Collaboration, K.C. Bowler et al., in preparation (1999).
[10] ALPHA Collaboration, S. Capitani, M. Lüscher, R. Sommer and H. Wittig, (1998), hep-lat/9810063.
[11] R. Gupta, (1997), hep-lat/9807028.

[12] P. Bacilieri et al., Phys. Lett. B 214 (1988) 115;
APE Collaboration, P. Bacilieri et al., Nucl. Phys. B 317 (1989) 509.
[13] G. Kilcup, Nucl. Phys. B (Proc. Suppl.) 9 (1988) 201;
R. Gupta, G. Guralnik, G.W. Kilcup and S.R. Sharpe, Phys. Rev. D 43 (1991) 2003.
[14] T.A. DeGrand and R.D. Loft, Comput. Phys. Commun. 65 (1991) 84.
[15] F. Butler, H. Chen, J. Sexton, A. Vaccarino and D. Weingarten, Nucl. Phys. B (Proc. Suppl.) 26 (1992) 287.
[16] T. DeGrand and M. Hecht, Phys. Lett. B 275 (1992) 435.
[17] A. Duncan et al., Phys. Rev. D 51 (1995) 5101, hep-lat/9407025.
[18] S. Güsken, Nucl. Phys. B (Proc. Suppl.) 17 (1990) 361;
S. Güsken et al., Phys. Lett. B 227 (1989) 266.
[19] C. Alexandrou, S. Güsken, F. Jegerlehner, K. Schilling and R. Sommer, Nucl. Phys. B 414 (1994) 815, hep-lat/9211042.
[20] UKQCD Collaboration, C.R. Allton et al., Phys. Rev. D 47 (1993) 5128, hep-lat/9303009.
[21] UKQCD Collaboration, P. Lacock, A. McKerrell, C. Michael, I.M. Stopher and P.W. Stephenson, Phys. Rev. D 51 (1995) 6403, hep-lat/9412079.
[22] C. Michael, Nucl. Phys. B 259 (1985) 58.
[23] M. Lüscher and U. Wolff, Nucl. Phys. B 339 (1990) 222.
[24] S. Sint, Nucl. Phys. B 421 (1994) 135, hep-lat/9312079.
[25] K. Jansen et al., Phys. Lett. B 372 (1996) 275, hep-lat/9512009.
[26] M. Lüscher, S. Sint, R. Sommer and P. Weisz, Nucl. Phys. B 478 (1996) 365, hep-lat/9605038.
[27] S. Sint and P. Weisz, Nucl. Phys. B 502 (1997) 251, hep-lat/9704001.
[28] M. Lüscher, R. Narayanan, P. Weisz and U. Wolff, Nucl. Phys. B 384 (1992) 168, hep-lat/9207009.
[29] M. Lüscher, Commun. Math. Phys. 54 (1977) 283.
[30] M. Lüscher, S. Sint, R. Sommer, P. Weisz and U. Wolff, Nucl. Phys. B 491 (1997) 323, hep-lat/9609035.
[31] M. Lüscher, R. Sommer, P. Weisz and U. Wolff, Nucl. Phys. B 413 (1994) 481, hep-lat/9309005.
[32] M. Lüscher and P. Weisz, Nucl. Phys. B 479 (1996) 429, hep-lat/9606016.
[33] J. Heitger, (1999), hep-lat/9903016.
[34] M. Guagnelli, R. Sommer, (1997), hep-lat/9709088.
[35] R. Sommer, Nucl. Phys. B 411 (1994) 839, hep-lat/9310022.
[36] ALPHA Collaboration, M. Guagnelli, R. Sommer and H. Wittig, Nucl. Phys. B 535 (1998) 389, hep-lat/9806005.
[37] S. Fischer et al., Comp. Phys. Commun. 98 (1996) 20, hep-lat/9602019.
[38] W. Bietenholz et al., hep-lat/9807013.
[39] M.J. Teper, hep-th/9812187.
[40] UKQCD Collaboration, C.R. Allton et al., Phys. Rev. D 49 (1994) 474, hep-lat/9309002.

F

Precision computation of the strange quark's mass in quenched QCD

Nucl. Phys. B571 (2000) 237-256

ELSEVIER

Nuclear Physics B 571 (2000) 237–256

NUCLEAR PHYSICS B

www.elsevier.nl/locate/npe

Precision computation of the strange quark's mass in quenched QCD

ALPHA and UKQCD Collaborations

Joyce Garden [a], Jochen Heitger [b], Rainer Sommer [b], Hartmut Wittig [c,d,1]

[a] *Department of Physics & Astronomy, University of Edinburgh, Edinburgh EH9 3JZ, Scotland, UK*
[b] *DESY-Zeuthen, Platanenallee 6, D-15738 Zeuthen, Germany*
[c] *Theoretical Physics, University of Oxford, 1 Keble Road, Oxford OX1 3NP, UK*
[d] *Center for Computational Physics, University of Tsukuba, Tsukuba, Ibaraki 305-8571, Japan*

Received 16 July 1999; received in revised form 29 October 1999; accepted 9 November 1999

Abstract

We determine the renormalization group invariant quark mass corresponding to the sum of the strange and the average light quark mass in the quenched approximation of QCD, using as essential input the mass of the K-mesons. In the continuum limit we find $(M_s + \hat{M})/F_K = 0.874(29)$, which includes systematic errors. Translating this non-perturbative result into the running quark masses in the $\overline{\rm MS}$ scheme at $\mu = 2$ GeV and using the quark mass ratios from chiral perturbation theory, we obtain $\overline{m}_s(2\,{\rm GeV}) = 97(4)\,{\rm MeV}$. With the help of recent results by the CP-PACS Collaboration, we estimate that a 10% higher value would be obtained if one replaced F_K by the nucleon mass to set the scale. This is a typical ambiguity in the quenched approximation.

PACS: 11.15.Ha; 12.38.Gc; 12.39.Fe
Keywords: Quark masses; Lattice gauge theory; Chiral perturbation theory; Non-perturbative renormalization; Quantum chromodynamics; Monte Carlo

1. Introduction

Quark masses are fundamental parameters of the standard model, which have to be determined from experimental observations confronted with theoretical predictions [1].

[1] PPARC Advanced Fellow.

0550-3213/00/$ - see front matter
PII: S0550-3213(99)00714-2

At present the most precise theoretical predictions which allow for the determination of ratios of the three light quark masses are based on chiral perturbation theory [2]. A detailed analysis yielded [3]

$$M_{\mathrm{u}}/M_{\mathrm{d}} = 0.55 \pm 0.04\,, \qquad M_{\mathrm{s}}/\hat{M} = 24.4 \pm 1.5 \tag{1.1}$$

with

$$\hat{M} = \tfrac{1}{2}(M_{\mathrm{u}} + M_{\mathrm{d}})\,. \tag{1.2}$$

Unlike these ratios, the overall magnitude of the quark masses is not accessible to chiral perturbation theory combined with experimental data alone. One should therefore determine a particular linear combination of quark masses by comparing lattice QCD predictions [4–19] or QCD sum rules [20–31] to experiments.

In this work we use the masses of the K-mesons and a computation in the quenched approximation to QCD to determine $M_{\mathrm{s}} + \hat{M}$. Our analysis employs the O(a) improved lattice theory, the quark mass is renormalized completely non-perturbatively [32] and the continuum limit is taken (with a rate proportional to a^2). Hence, with respect to the last two points, it improves on many previous calculations.

In general quark masses are scale- and scheme dependent quantities. It is therefore desirable to compute the *renormalization group invariant quark masses*, which – being both scale- and scheme-independent – are naturally taken as fundamental parameters of QCD. We recall that they are defined in terms of the high energy behaviour of the running masses $\overline{m}(\mu)$:

$$M_i \equiv \lim_{\mu\to\infty} \left\{ \left(2b_0\bar{g}^2(\mu)\right)^{-d_0/2b_0}\, \overline{m}_i(\mu) \right\}, \tag{1.3}$$

$$b_0 = 11/(4\pi)^2,\; d_0 = 8/(4\pi)^2\,. \tag{1.4}$$

On the other hand, the renormalization group invariant masses M_i are related to the bare current quark masses m_i by

$$M_i = Z_{\mathrm{M}}\, m_i \tag{1.5}$$

with a (flavour independent) renormalization factor Z_{M} which was recently computed by the ALPHA Collaboration [32,33]. This non-perturbative result is the basis of our present calculation.[2] The renormalization problem and its solution were discussed in detail in Refs. [32,33]. The current quark masses themselves, are defined through the PCAC relation

$$\partial_\mu A_\mu(x) = (m_i + m_j)\, P(x), \tag{1.6}$$

[2] Since the bare mass is involved, Z_{M} depends on the regularization. The complete calculation of [32] was done in O(a) improved quenched lattice QCD, which we use here as well.

in terms of the axial current

$$A_\mu(x) = \bar{\psi}_i(x)\gamma_\mu\gamma_5\psi_j(x), \tag{1.7}$$

and the pseudoscalar density

$$P(x) = \bar{\psi}_i(x)\gamma_5\psi_j(x). \tag{1.8}$$

Applied to the vacuum-to-K matrix elements it reads

$$M_s + \hat{M} = Z_M(m_s + \hat{m}) = Z_M\frac{F_K}{G_K}m_K^2, \tag{1.9}$$

where F_K is the K-meson decay constant, and G_K denotes the vacuum-to-K matrix element of the pseudoscalar density.[3] Eq. (1.9) is the fundamental relation which we shall exploit in this work. It is used in the following way: we compute $Z_M\frac{F_K}{G_K}$ and multiply with the experimental squared mass,

$$m_K^2 = \tfrac{1}{2}\left(m_{K^+}^2 + m_{K^0}^2\right)_{QCD} = (495\,\mathrm{MeV})^2, \tag{1.10}$$

to obtain $M_s + \hat{M}$. By the subscript ''QCD'' we indicate that we have used the masses in pure QCD with electromagnetic interactions switched off, since obviously the lattice QCD result is valid for a world where $\alpha_{em} = 0$. In practice this is achieved by subtracting an estimate of the electromagnetic effects from the experimental numbers. The numerical estimate in Eq. (1.10) was obtained from Dashen's theorem [34] being well aware that the accuracy of this estimate may be only around 0.5% in m_K^2 [35–39].

The combination $\frac{F_K}{G_K}$ carries the dimension of an inverse mass. Therefore it is necessary to choose another dimensionful observable to form a dimensionless ratio which has a continuum limit (this is often called ''setting the scale''). Choosing r_0 [40] or F_K for this second observable and extrapolating to the continuum limit yields the results quoted in the abstract.

In the following we shall first explain our strategy to deal with some technical difficulties in the computation of F_K/G_K. Since our strategy involves replacing F_K/G_K by the ratio F_{PS}/G_{PS} for mass-degenerate mesons, we discuss in Section 3 the dependence of various observables on the difference of quark masses $m_i - m_j$. In Section 4 we show that finite size effects are negligibly small in our calculation. The main result for the quark mass is presented in Section 5, where, among other issues, the extrapolations to the continuum are discussed. We then proceed to estimate the *ambiguity* which originates from the fact that the *quenched approximation* can not be expected to describe the real world properly. As a byproduct, we present the calculation of the kaon decay constant and masses in the vector channel in the continuum limit. We finish with a discussion of our results and some comments on how the method may be extended to determine coefficients of the chiral Lagrangian.

[3] Our convention is that F_K, G_K denote the matrix elements of the bare operators. Renormalization factors are written explicitly. For the O(a) improved lattice theory they can be found in Appendix A.

2. Strategy

2.1. Chiral perturbation theory

Let us first recall what chiral perturbation theory can predict concerning the quark masses [2,3,41,42]. Chiral perturbation theory is based on nothing but the very general assumption that chiral symmetry is broken spontaneously in the limit $\hat{M} = M_s \to 0$. This allows for a quantitative description of the pseudoscalar sector in terms of a low-energy effective Lagrangian, where quark masses appear as ''kinematical variables'' just like the energy in scattering processes. The parameters in the chiral Lagrangian are independent of the quark masses. At order p^4, most of the parameters have been determined by comparison to experimental data (see e.g. Ref. [43] for numerical values). However, the coefficient of the chiral symmetry breaking quark mass term in the Lagrangian (denoted by B in [42]), cannot be determined from experimental data alone. It can only be fixed when one particular quark mass is known. Since all parameters are independent of the quark masses, this may be done at a convenient reference point. It is important to realize that this reference point does not have to correspond to a physical quark mass. The procedure can then be extended to determine other parameters in the chiral Lagrangian more precisely, once additional observables are known for suitable quark masses and with sufficient accuracy. All of this can potentially be achieved by lattice QCD calculations and can improve predictions such as Eq. (1.1). Also the justification for the truncation of chiral perturbation theory can and should, of course, be checked.

A particularly convenient way of applying this idea in practice is as follows. We introduce the ratio

$$R(m_i, m_j) = \frac{F_{\mathrm{PS}}}{G_{\mathrm{PS}}}\,, \tag{2.1}$$

such that

$$m_i + m_j = R(m_i, m_j)\, m_{\mathrm{PS}}^2(m_i, m_j)\,. \tag{2.2}$$

Defining a reference quark mass

$$m_{\mathrm{PS}}(m_{\mathrm{ref}}, m_{\mathrm{ref}}) = m_{\mathrm{K}}\,, \tag{2.3}$$

with the kaon mass already discussed in the introduction, the ratio R for the physical quark masses may be written as

$$R(m_i, m_j) = T(x_i, x_j)\, R(m_{\mathrm{ref}}, m_{\mathrm{ref}})\,, \quad x_i = m_i/m_{\mathrm{ref}} \tag{2.4}$$

with a function $T(x_i, x_j)$ which can be computed in chiral perturbation theory. In particular, using [41,43] one finds

$$T(m_s/m_{\mathrm{ref}}, \hat{m}/m_{\mathrm{ref}}) \approx 1 \quad \text{and thus } 2\, m_{\mathrm{ref}} \approx m_s + \hat{m}\,. \tag{2.5}$$

The corrections to the above equation are small, but the overall uncertainties associated with this statement require a detailed investigation of the phenomenology. The reason is that the errors of the parameters in the chiral Lagrangian are correlated, which makes it non-trivial to estimate uncertainties. Nevertheless we expect Eq. (2.5) to be correct to within about 10%.

In Section 3 we shall follow a complementary approach, by investigating pseudoscalar meson observables as a function of the average quark mass and the difference of the quark masses. We find that the dependence on the latter variable is rather small. It then follows trivially from our definition of T that Eq. (2.5) is valid rather precisely.

Before turning to that investigation let us briefly explain why our strategy is advantageous. The reasons for quenched QCD and full QCD are somewhat different but related, having both to do with the difficulties of extrapolations to the region of small quark masses which is at present inaccessible to direct Monte Carlo calculations.

2.2. Quenched approximation and full QCD

The lattice calculations presented in this paper have been performed in the O(a) improved theory [44] with non-perturbative improvement coefficients [45] and mass-renormalization factor, Z_{M} [32]. Details pertaining to, for instance, O(a) correction terms in the currents can be found in the appendix.

To motivate our strategy let us first review the straightforward approach for computing light quark masses. First one assumes isospin symmetry of the ratios R, i.e. effects of $\mathrm{O}(m_{\mathrm{u}} - m_{\mathrm{d}})$ are neglected, which is well justified given the smallness of this mass difference. Then one chooses an overall scale, say the hadronic radius r_0, and determines the bare light quark mass and strange quark mass such that $r_0 m_\pi$ and $r_0 m_{\mathrm{K}}$ agree with the experimental numbers. Except for the bare coupling, all parameters in the QCD Lagrangian are then fixed and the current quark masses are given by Eqs. (2.1), (2.2), with

$$\langle 0|A_\mu(0)|\mathrm{K}(p)\rangle = ip_\mu F_{\mathrm{K}}\,, \quad \langle 0|P(0)|\mathrm{K}(p)\rangle = G_{\mathrm{K}}\,. \tag{2.6}$$

Here $|\mathrm{K}(p)\rangle$ denotes a pseudoscalar state with momentum p, standard infinite volume normalization and the proper flavour quantum numbers. After renormalization the quark masses can be extrapolated to the continuum.

While this approach will ultimately be a clean and straightforward way to determine the quark masses, it poses two problems in the quenched approximation.

- The quenched approximation is expected to be misleading for very light quark masses such as $\hat{m}$. A particular indication of the failure of the quenched approximation in this regime is the presence of logarithmic terms in chiral perturbation theory which have no counterpart in the full theory [46–50].
- With our fermion action and lattice spacings, we cannot perform calculations for quark masses which are below approximately half of the strange quark mass. For smaller masses, the Dirac operator has unphysical zero-modes on a certain fraction of configurations contributing to the path integral (''exceptional configuration'') [45,51].

The second problem is of a more technical nature. It can in principle be circumvented by choosing a suitable action, but then also Z_{M} has to be recomputed. However, the first point must be taken seriously, since we want to obtain results which are not misleading with respect to the real theory of interest, full QCD.

It is furthermore advantageous to use the same strategy in full QCD. The reason is that it is very likely that for some time to come, lattice simulations will only reach down

to quark masses somewhere around $m = m_{\rm ref} (\approx m_{\rm s}/2)$. The most precise way to extrapolate further is then given by chiral perturbation theory as discussed above.

3. Non-degenerate quarks

In this section we investigate quantitatively how the pseudoscalar mass and decay constant depend on the difference of the two quark masses in quenched QCD. Apart from some consistency checks which were performed with the data of the ALPHA Collaboration, the numerical results presented here were obtained during the course of the UKQCD simulations [52] using the O(a) improved action.

We consider the observables of interest as a function of the average current quark mass $m = \frac{m_i + m_j}{2}$ and the parameter y defined by

$$y = (x_i - x_j)^2 = (m_i - m_j)^2 / m_{\rm ref}^2 , \tag{3.1}$$

with $m_{\rm ref}$ as determined later in Section 5. In particular, we want to show that the functions

$$H_{\rm M}(m,y) = m_{\rm PS}^2 \text{ and } H_{\rm F}(m,y) = F_{\rm PS}\left[1 + b_{\rm A} a m_{\rm q}\right] \tag{3.2}$$

have little dependence on y. In other words, the ratios

$$Q_{\rm M}(m,y) = H_{\rm M}(m,y)/H_{\rm M}(m,0) , \tag{3.3}$$

$$Q_{\rm F}(m,y) = H_{\rm F}(m,y)/H_{\rm F}(m,0) \tag{3.4}$$

are close to unity. Note that the two functions $Q_{\rm M}$ and T are equivalent at the special point $m = m_{\rm ref}$, since $Q_{\rm M}(m_{\rm ref},y) = 1/T(1 + \frac{1}{2}\sqrt{y}, 1 - \frac{1}{2}\sqrt{y})$. In order to investigate the y-dependence numerically, we start from the results for $am_{\rm PS}$ and $aF_{\rm PS}$ of UKQCD

Table 1
Results for masses and unrenormalized (ratios of) matrix elements in all simulation points

β	κ	am	$am_{\rm PS}$	$am_{\rm V}$	$aF_{\rm PS}$	$F_{\rm PS}/aG_{\rm PS}$
6.0	0.1335	0.0466(1)	0.3884(10)	0.5289(26)	0.0969(4)	0.5997(31)
	0.1338	0.03856(6)	0.3529(11)	0.5077(31)	0.0943(4)	0.6022(34)
	0.1340	0.03311(7)	0.3275(11)	0.4938(36)	0.0924(4)	0.6015(39)
	0.1342	0.02759(8)	0.3001(12)	0.4804(44)	0.0905(4)	0.5978(45)
6.1	0.1342	0.04161(3)	0.3306(5)	0.4542(17)	0.0870(3)	0.7454(22)
	0.1345	0.03305(3)	0.2947(5)	0.4328(23)	0.0841(3)	0.7476(26)
	0.1347	0.02734(3)	0.2687(6)	0.4188(28)	0.0820(3)	0.7458(30)
	0.1349	0.02160(4)	0.2399(7)	0.4056(39)	0.0799(3)	0.7405(37)
6.2	0.1347	0.03241(3)	0.2683(5)	0.3748(21)	0.0743(3)	0.8887(33)
	0.1349	0.02661(3)	0.2430(6)	0.3588(26)	0.0721(3)	0.8908(38)
	0.13515	0.01934(3)	0.2080(6)	0.3388(39)	0.0693(3)	0.8857(48)
	0.1352	0.01788(3)	0.2004(6)	0.3348(43)	0.0687(3)	0.8830(51)
6.45	0.13485	0.02477(2)	0.1975(8)	0.2749(25)	0.0533(5)	1.261(10)
	0.1351	0.01734(2)	0.1650(9)	0.2558(37)	0.0503(4)	1.265(14)
	0.1352	0.01439(2)	0.1505(9)	0.2480(46)	0.0490(4)	1.261(16)
	0.1353	0.01142(2)	0.1347(10)	0.2398(59)	0.0477(4)	1.250(19)

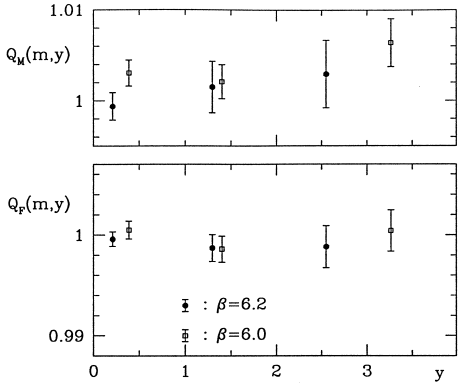

Fig. 1. The functions $Q(m,y)$. Q_{M} denotes the case of pseudoscalar masses and Q_{F} their decay constants. The average of m_i and m_j is between $\approx 1.4\, m_{\mathrm{ref}}$ and $\approx 2.4\, m_{\mathrm{ref}}$.

[52] for three values of the quark masses at each of the two bare couplings $\beta = 6.0, 6.2$. Three combinations with $m_j \neq m_i$ are then available for each of the two corresponding lattice spacings, 0.09 fm and 0.07 fm. The only numerical difficulty in examining the ratios Q_X is that the denominators $H_X(m,0)$ are in general not available directly. They may, however, be replaced by an interpolation

$$H_{\mathrm{M}}(m,0) = h_1^{\mathrm{M}} m + h_2^{\mathrm{M}} m^2 + h_3^{\mathrm{M}} m^3\,, \tag{3.5}$$

$$H_{\mathrm{F}}(m,0) = h_0^{\mathrm{F}} + h_1^{\mathrm{F}} m + h_2^{\mathrm{F}} m^2\,, \tag{3.6}$$

with h_k^X determined from the observables computed for the three available degenerate mesons ($m_i = m_j$). One has to check that these interpolations are stable. This was tested by taking different subsets of three mass points of the data in Table 1, extracting h_k^X and comparing the resulting functions $H_X(m,0)$. Deviations between these different interpolations were found to be negligible compared to the statistical precision of the ratios Q themselves.

Before discussing the results, let us mention one technical point in the numerical analysis. For convenience, the above procedure was carried out using the subtracted, improved bare quark masses, $\tilde{m}_{\mathrm{q}} = m_{\mathrm{q}}(1 + b_{\mathrm{m}} a m_{\mathrm{q}})$, $m_{\mathrm{q}} = m_0 - m_{\mathrm{c}}$, instead of the current quark masses themselves.[4] For the question addressed in this section, this makes no difference because $m = Z_{\mathrm{m}} \tilde{m}_{\mathrm{q}}$ holds up to the usual $\mathrm{O}(a^2)$ errors, with some mass-independent renormalization factor Z_{m}.

In Fig. 1 we show our numerical results.[5] They show that Q_{M} has a dependence on y which is below the level of a percent, and Q_{F} is seen to be independent of y to within our statistical precision of around 0.3%. It should be kept in mind that Fig. 1 tests the y-dependence for $m/m_{\mathrm{ref}} = 1.4$–2.4, while later we shall be interested in kaon physics, where $m/m_{\mathrm{ref}} \approx 1$. It remains a (plausible!) hypothesis that Q_X are close to unity also for this lower value of m. Nevertheless, our investigation quantifies the smallness of y-effects for the first time and suggests that the correction terms in Eq. (2.5) are

[4] Flavour indices are suppressed, here, and we use [53] $b_{\mathrm{m}} = -1/2 - 0.0962\, g_0^2$.
[5] The numerical values for $(\tilde{m}_{\mathrm{q}})_{\mathrm{ref}}$ were taken from the analysis described in Section 5.

negligible.[6] Based on this analysis we shall not distinguish between $2m_{\rm ref}$ and $m_{\rm s}+\hat{m}$ from now on.

4. Finite size effects

Our numerical results, which are listed in Table 1, have been obtained for approximately constant physical volume, $T\times L^3$, where $T=2L$ and $L\approx 3r_0=1.5$fm. We used exactly the numerical methods described in [55], and in particular systematic errors due to excited state contributions were checked to be small compared to the statistical errors. Further details about the simulation are described in the appendix. Since the precision of the results is quite good one has to investigate whether they may be affected by the finite size of the system at the level of their statistical accuracy. The most relevant observable for the determination of the quark masses is the ratio $R=(m_i+m_j)/m_{\rm PS}^2$. Since m_i is defined through the PCAC relation, it is independent of the volume [44] (apart from small lattice artefacts of order a^2). We are therefore predominantly interested in the volume dependence of the pseudoscalar masses but will also consider the decay constant $F_{\rm PS}$.

In the pseudoscalar sector the leading finite size effects can be reliably calculated in chiral perturbation theory. The reason is that for vanishing quark masses the pseudoscalar mesons are Goldstone bosons. Their interactions become weak for small energies and these are responsible for the leading finite size effects for large but finite volumes.

Gasser and Leutwyler have reported results for the two-point function of the axial current at space-like separations in Eqs. (25) and (26) of Ref. [56]. These expressions hold at finite temperature and in finite volume. They are easily adapted to the situation which is of interest here, namely the pseudoscalar mass on an L^3-torus (temperature zero) $m_{\rm PS}(L)$, and the corresponding decay constant $F_{\rm PS}(L)$. The resulting formulae are

$$\frac{m_{\rm PS}(L)}{m_{\rm PS}(\infty)}-1=\frac{1}{N_{\rm f}}\,\frac{m_{\rm PS}^2}{F_{\rm PS}^2}\,g(z)+{\rm O}\big({\rm e}^{-\sqrt{2}z}\big),\quad z=m_{\rm PS}\,L \tag{4.1}$$

$$\frac{F_{\rm PS}(L)}{F_{\rm PS}(\infty)}-1=-N_{\rm f}\,\frac{m_{\rm PS}^2}{F_{\rm PS}^2}\,g(z)+{\rm O}\big({\rm e}^{-\sqrt{2}z}\big), \tag{4.2}$$

$$g(z)=\frac{3}{8\pi^2 z^2}\int_0^\infty \frac{{\rm d}x}{x^2}\,{\rm e}^{-z^2x-1/(4x)}=\frac{3}{2\pi^2 z}\,K_1(z), \tag{4.3}$$

where $K_1(z)$ denotes a modified Bessel function. Here a comment is in order. This is a result of the first non-trivial order in chiral perturbation theory in full QCD. A priori one cannot expect it to be accurate if the pseudoscalar meson masses are too large. On the other hand, one knows that the finite size effects discussed here are of order ${\rm e}^{-z}$, as long as the pseudoscalar is the lightest particle in the theory [57,58]. It is plausible that the

[6] From earlier results of Ref. [54] it was already possible to infer that – for light quark masses – $Q_{\rm F}$ does not depend on y beyond a level of 5%. Our investigation now excludes y-effects which are 10 times smaller.

prefactor of the exponential is not dramatically different for heavier pseudoscalar mesons. We may therefore take the above equations as a reasonable estimate of finite size effects. Being interested in the order of magnitude of these effects, we also do not worry about the difference of the quenched approximation and full QCD.

In our numerical calculations (see Tables 1 and 4), we are in the range $z = m_{\rm PS} L \geqslant 4.3$ and consequently Eqs. (4.1)–(4.2) predict corrections which are below the level of 0.5% for $F_{\rm PS}$ and 0.1% for $m_{\rm PS}$. In order to check this estimate, we have done some calculations on lattices which are larger than our standard $L \approx 1.5$ fm. Entirely consistent with the above formulae, we found no significant changes in $F_{\rm PS}, m_{\rm PS}$, for instance

$$\beta = 6.2\,,\ am_{\rm PS} = 0.208: \quad \frac{m_{\rm PS}(24a)}{m_{\rm PS}(32a)} - 1 = 0.003(4) \quad (\approx 0.0009)\,, \tag{4.4}$$

$$\frac{F_{\rm PS}(24a)}{F_{\rm PS}(32a)} - 1 = -0.003(8) \quad (\approx -0.003)\,, \tag{4.5}$$

where the numbers in parentheses are the estimates from the above equations with $N_{\rm f} = 2$.

We conclude that even with the numerical precision of Table 1, finite size effects are negligible for the quark masses considered. Of course, as described by the above formulae, finite size effects grow rapidly when the pseudoscalar mass becomes smaller and larger volumes would be necessary for quark masses which are significantly smaller than the ones we used.

5. Degenerate quarks, continuum limit

We can now proceed to compute the desired quantity $r_0(M_{\rm s} + \hat{M})$. The first step is to evaluate R for degenerate quarks as a function of $r_0^2 m_{\rm PS}^2$. Relegating all details of the exact numerical procedure, such as the definition of $m_{\rm q}$ and the different improvement coefficients, to the appendix we directly show the mass dependence of R in Fig. 2a. It is apparent that R is almost constant as a function of the quark mass (or $r_0^2 m_{\rm PS}^2$). It is therefore easy to extrapolate to the desired point $r_0^2 m_{\rm PS}^2 = r_0^2 m_{\rm K}^2 = 1.5736$, slightly outside of the range where we have numerical results. The extrapolation is performed linearly in $r_0^2 m_{\rm PS}^2$, using the three closest data points. Simply taking for instance the closest data point or an average of all of them would change the final result for the quark mass by a negligible amount.

The second step is now to form the combination

$$r_0\big(M_{\rm s} + \hat{M}\big) = Z_{\rm M} \frac{R|_{r_0^2 m_{\rm PS}^2 = 1.5736}}{r_0} \times 1.5736 \tag{5.1}$$

collecting all errors, including the ones on r_0 [59] and the β-dependent one of $Z_{\rm M}$ [32]. We then extrapolate to the continuum limit linearly in a^2. As seen in Fig. 3a, the dependence on the lattice spacing is significant – in contrast to the quark mass on smaller volume [60]. As a safeguard against higher order terms in the lattice spacing, we

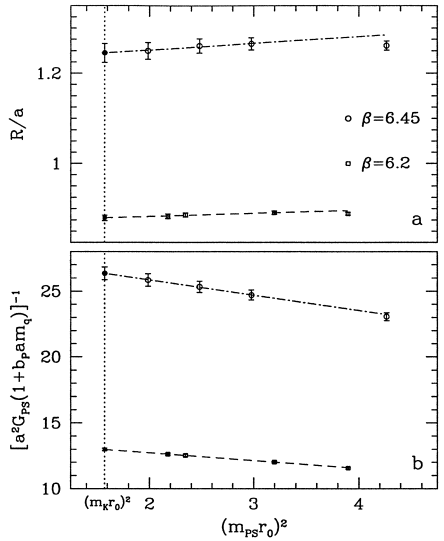

Fig. 2. Mass dependence and extrapolations for the two smallest values of the lattice spacing. The ratio R is defined in Eq. (A.6).

therefore include only the three points with smallest lattice spacing in the extrapolation and obtain our main result

$$r_0\left(M_s + \hat{M}\right) = 0.362(12)\,. \tag{5.2}$$

This result contains the β-independent part of the uncertainty in Z_M of 1.3% [32]. At this point one may be concerned about the validity of an a^2-extrapolation, since $b_A - b_P$

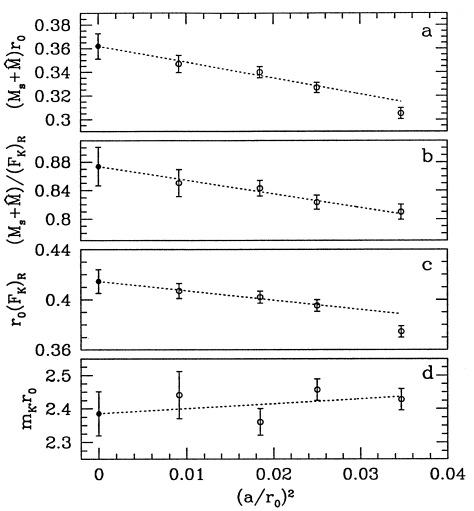

Fig. 3. Continuum limit extrapolations of several observables. Full symbols show the extrapolated values. Dashed lines represent the extrapolation function, which are continued outside the fit range towards larger lattice spacings.

is mostly known only in perturbation theory. However, this combination is found to be tiny at the one-loop level [53] and turns out to be rather small also non-perturbatively [62,63]. We have checked explicitly that such small values of $b_A - b_P$ do not affect our continuum extrapolation.

In the whole procedure one may replace R, defined in Eq. (2.2), by the ratio of the current quark mass and the pseudoscalar mass squared. One then ends up with slightly different lattice spacing effects and somewhat different statistical errors. We have performed also that analysis, using the current quark mass averaged over a range of timeslices around the central one in our lattice. The results differ by up to 2% from the ones presented above for finite lattice spacings but are indistinguishable after the continuum extrapolation.

Instead of the quark mass in units of r_0, we may also compute the combination $(M_s + \hat{M})/(F_K)_R$, where $(F_K)_R$ is the kaon decay constant. As its experimental value we take $(F_K)_R = 160(2)\,\mathrm{MeV}$. We note that electromagnetic effects cannot be subtracted in analogy to Eq. (1.10), chiefly because F_{K^0} is not known experimentally. We emphasize that this is truly an alternative procedure which amounts to computing the combination

$$\frac{M_s + \hat{M}}{(F_K)_R} = \frac{M}{\overline{m}} \left. \frac{1}{Z_P r_0^2 G_{PS}\left[1 + b_P a m_q\right]} \right|_{r_0^2 m_{PS}^2 = 1.5736} \times 1.5736\,, \tag{5.3}$$

where the ratio $M/\overline{m}$ and the renormalization constant Z_P have to be taken at a common scale for which we resort to the value $\mu = 1/(1.436 r_0)$ chosen in [32]. Discretization effects are clearly expected to be different in this case: they are known to be non-negligible in the product $r_0(F_{PS})_R$ [64]. A non-perturbative estimate being unavailable at present, we have to rely on the perturbative value $b_P = 1 + 0.153\, g_0^2$ [53]. Extrapolations in $r_0^2 m_{PS}^2$ and the continuum extrapolations are shown in Fig. 2b and Fig. 3b. Concerning the former, the mass-dependence of $1/\{G_{PS}[1 + b_P a m_q]\}$ is stronger than the mass dependence of R, but within our errors it is perfectly linear and the extrapolation is easily done. In comparison to the quark mass in units of r_0, we find discretization errors which are roughly only half as big.

In order to confirm that it is legitimate to perform an extrapolation linear in a^2, even though the improvement coefficient b_P is known only perturbatively, we have repeated the whole analysis after setting b_P to its tree-level value $b_P = 1$. Results after extrapolation changed by much less than a percent. Our final continuum result is

$$\frac{M_s + \hat{M}}{(F_K)_R} = 0.874(29)\,. \tag{5.4}$$

For illustration we may translate to physical units, setting $r_0 = 0.5$ fm [59] and $(F_K)_R = 160(2)\mathrm{MeV}$. We thus obtain

$$2\,M_{\mathrm{ref}} = M_s + \hat{M} = 143(5)\ \mathrm{MeV} \quad \text{from Eq. (5.2)}\,, \tag{5.5}$$

$$2\,M_{\mathrm{ref}} = M_s + \hat{M} = 140(5)\ \mathrm{MeV} \quad \text{from Eq. (5.4)}\,. \tag{5.6}$$

As will be discussed in more detail below, this assignment of physical units is ambiguous in the quenched approximation. One should be well aware that the solid results are given in Eq. (5.2) and Eq. (5.4).

Table 2
Extra-/interpolations in $r_0^2 m_{\mathrm{PS}}^2$ and resulting continuum limits (CL) including all errors

$r_0^2 m_{\mathrm{PS}}^2$	β	$Z_{\mathrm{M}} \frac{R}{r_0}$	$M_{\mathrm{s}} + \hat{M}/(F_{\mathrm{PS}})_{\mathrm{R}}$	$r_0(F_{\mathrm{PS}})_{\mathrm{R}}$	$m_{\mathrm{V}} r_0$	$(F_{\mathrm{PS}})_{\mathrm{R}}/m_{\mathrm{V}}$
1.5736	6.0	0.1939(30)	0.810(11)	0.3746(45)	2.428(32)	0.1543(26)
	6.1	0.2077(28)	0.824(10)	0.3952(47)	2.457(32)	0.1609(26)
	6.2	0.2160(30)	0.843(11)	0.4020(48)	2.361(40)	0.1701(32)
	6.45	0.2205(46)	0.851(19)	0.4070(60)	2.441(71)	0.1667(52)
	CL	0.2300(69)	0.874(27)	0.4146(94)	2.386(66)	0.1761(75)
3.0	6.0	0.1966(26)	1.450(17)	0.4063(47)	2.637(22)	0.1541(20)
	6.1	0.2104(26)	1.471(17)	0.4288(49)	2.666(20)	0.1609(20)
	6.2	0.2181(28)	1.501(18)	0.4363(51)	2.606(25)	0.1675(23)
	6.45	0.2236(37)	1.518(28)	0.4421(62)	2.677(42)	0.1652(32)
	CL	0.2324(57)	1.553(42)	0.4507(99)	2.645(41)	0.1709(49)

For future reference we list various dimensionless quantities both for $r_0^2 m_{\mathrm{PS}}^2 = 1.5736$ and for $r_0^2 m_{\mathrm{PS}}^2 = 3$ in Table 2. Our results before and after the continuum extrapolation can be found in that table.

6. Ambiguities in the quenched approximation

In Section 5 we have mainly used r_0 as our reference scale. However, in general one expects that by choosing different experimental inputs one will also get somewhat different results when working in the quenched approximation. Here we would like to quantify this ambiguity for our determination of $M_{\mathrm{s}} + \hat{M}$.

A first estimate is obtained by computing the combination $r_0(F_{\mathrm{K}})_{\mathrm{R}}$, using our results for the pseudoscalar decay constant including the non-perturbative renormalization factor Z_{A}, and comparing it to its experimental value. Of course, on the basis of the results for $M_{\mathrm{s}} + \hat{M}$ presented in Eqs. (5.5) and (5.6) one may not expect any significant deviation. However, the following detailed analysis may still be instructive, in particular since it yields $r_0(F_{\mathrm{K}})_{\mathrm{R}}$ in the quenched approximation.

The procedure to extract $r_0(F_{\mathrm{K}})_{\mathrm{R}}$ is entirely analogous to what was done in the previous section. The extrapolations in $r_0^2 m_{\mathrm{PS}}^2$ (for mass-degenerate quarks) and the continuum extrapolations are shown in Fig. 4a and Fig. 3c, respectively. In the continuum limit we find

$$\text{quenched:} \quad \left\{ r_0 Z_{\mathrm{A}} F_{\mathrm{PS}} \left[1 + b_{\mathrm{A}} a m_{\mathrm{q}} \right] \right\}_{r_0^2 m_{\mathrm{PS}}^2 = 1.5736} = 0.415(9) \tag{6.1}$$

compared to

$$\text{experiment:} \quad 0.5\,\mathrm{fm} \times (F_{\mathrm{K}})_{\mathrm{R}} = 0.405(5) \tag{6.2}$$

with the experimental value of $(F_{\mathrm{K}})_{\mathrm{R}}$. Clearly the result obtained in the quenched approximation agrees well with experiment when the approximate value $r_0 = 0.5\,\mathrm{fm}$ is employed. However, it would be premature to conclude that the ambiguity is small, since the agreement may be special to the case of $(F_{\mathrm{K}})_{\mathrm{R}}$.

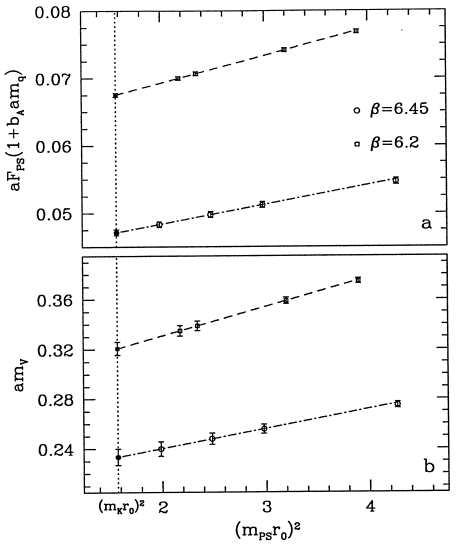

Fig. 4. Mass dependence of pseudoscalar decay constant and vector meson mass.

Another alternative to set the scale is provided by the nucleon mass, m_N. Compared with other widely used quantities like m_ρ, the nucleon has the advantage of being a stable hadron. Although we have not computed m_N ourselves, we can still use the precise published results obtained by the CP-PACS Collaboration [19] and combine them with the values of r_0/a reported in [59]. We obtain

$$\text{quenched:} \quad r_0 m_N \approx 2.6 \tag{6.3}$$

compared to

$$\text{experiment:} \quad 0.5\,\text{fm} \times m_N = 2.38\,, \tag{6.4}$$

which represents a 10% difference. Of course also the result for $M_s + \hat{M}$ in MeV would change by the same amount if one used m_N instead of r_0 or $(F_K)_R$ as experimental input. This may serve as a rough estimate of the inherent ambiguity in the quenched model.

In principle one could also use directly the results from recent comparisons of the quenched light hadron spectrum with experiment [19,65] to estimate this ambiguity. In Ref. [19] statistically significant deviations of up to 11% are observed when the scale is set by m_ρ, which, as a resonance, has a fairly large width. Since we consider it safer to set the scale by the nucleon mass, we have refrained from quoting this number as the typical uncertainty for the case at hand. However, using the published numbers of [19], it is not difficult to estimate the quenched results for the other hadron masses when one chooses m_N as input – at least within a precision of 2-3%. Interestingly it then turns out that the masses of the stable hadrons agree with experiment to within about 4%. On the other hand, for unstable hadrons one observes differences which can be as large as their widths. This may not be too surprising, since resonance effects are not controlled in the lattice calculation. In short, it is difficult to assess the relevance of the deviations

observed in the quenched hadron spectrum for our analysis, and thus we stick to our above estimate of around 10% for the ambiguity in question.

Finally, let us discuss the quark mass dependence of the flavour non-singlet vector meson masses in more detail. First we note that effects of the differences of quark masses can be shown to be unimportant in the same way as in Section 3 and we restrict our attention to the masses of mass-degenerate mesons ($m_i = m_j$). Our aim is to map out the quark mass dependence of $m_{\rm V}$ in the continuum limit: we pick certain values of $q \equiv m/m_{\rm s} = M/M_{\rm s}$, and for each of these values and for each lattice spacing we then perform an inter-/extrapolation of $m_{\rm V}$ as a function of the quark mass to determine $m_{\rm V}(m = q\,m_{\rm s})$. Here, $m_{\rm s} = 1.921\,m_{\rm ref}$ (see Eq. (1.1)) is used and $m_{\rm ref}$ is known from the previous section. At fixed value of q we then extrapolate $r_0 m_{\rm V}$ to the continuum limit including our data for all values of the lattice spacing, after observing that the lattice spacing dependence is very weak.

In Fig. 5, we plot the continuum results as a function of q. They are compared to $m_{\rm K^*}$, m_ρ and m_ϕ. Since all of these states are resonances, we also indicate their width in the figure. Additional reservations apply to the inclusion of the ϕ meson in this comparison. It is a mixture of flavour octet *and* singlet components, while the lattice calculation is for a pure octet state with mass-degenerate quarks: the disconnected quark diagrams occurring in the singlet channel are not accounted for, and mixing with glueballs is neglected. Although all these effects may be argued to be irrelevant in the quenched approximation, the experimental value in Fig. 5 does include them and it is somewhat surprising that our values for $m_{\rm V}$ at $q = 1$ come so close to m_ϕ.

If we were to ignore these problems and determined $M_{\rm s}$ from the requirement that $r_0 m_{\rm V}$ at that quark mass agrees with $r_0 m_\phi$, it is evident from Fig. 5 that we would obtain a result for $M_{\rm s}$ which is compatible with the numbers quoted in the previous section. However, the error would be considerably larger. Further continuum results such as $r_0 m_{\rm K^*}$, shown also in Fig. 4b and Fig. 3d, and $(F_{\rm K})_{\rm R}/m_{\rm K^*}$ are listed in Table 2 for future reference.

To summarize, we have directly seen ambiguities of about 10% owing to the use of the quenched approximation. This has to be kept in mind when quark masses in MeV are quoted. Still we have demonstrated that within the quenched approximation a total precision of 3% (see Eq. (5.2) and Eq. (5.4)) can be achieved.

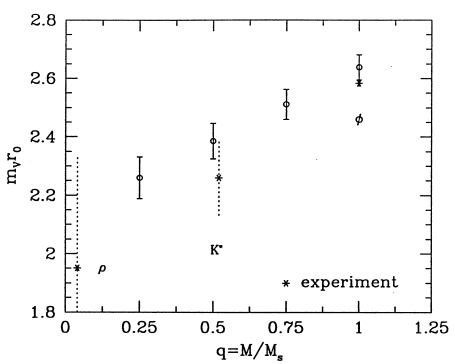

Fig. 5. Quark mass dependence of flavour non-singlet vector meson masses. Experimental masses are shown as asterisks and their width is indicated by a dotted line.

7. Discussion

Noting that ratios of light quark masses can at present best be calculated in chiral perturbation theory, we discussed a strategy to compute the overall scale of the light quark masses and applied it to the test-case of quenched QCD.

The problem has essentially two parts. First, the renormalization problem should be solved non-perturbatively. Here we have used the recent solution of the ALPHA collaboration [32,33] which connects the bare current quark masses to the renormalization group invariant ones. Second, one particular quark mass should be computed by matching with pseudoscalar meson masses. It is not necessary to perform this matching at physical values of the quark masses, because the parameters in the effective chiral Lagrangian are mass-independent. For both the quenched approximation and full QCD it appears convenient to use two different (flavours of) quarks with equal mass $M_{\rm ref}$ such that $m_{\rm PS}$ is equal to the kaon mass $m_{\rm K}$.

The ratio of $M_{\rm ref}$ to the physical quark masses can then be computed in chiral perturbation theory. In Section 3 we have shown that pseudoscalar masses, $m_{\rm PS}$, have *very little* dependence on the difference of the two quark masses in the quenched approximation. From this one has $2\,M_{\rm ref} \approx M_{\rm s} + \hat{M}$, which is also true in chiral perturbation theory (in full QCD!).

By making the identification $2\,M_{\rm ref} = M_{\rm s} + \hat{M}$ we have computed $(M_{\rm s} + \hat{M})r_0$ and $(M_{\rm s} + \hat{M})/(F_{\rm K})_{\rm R}$, incorporating all systematic errors (such as finite size effects), and have taken the continuum limit of these quantities. These solid results are given in Eq. (5.2) and Eq. (5.4).

A conversion of the results to physical units is necessarily ambiguous, since quenched QCD does not describe the real world. Depending on the choice of quantity somewhat different results in MeV are obtained. It is interesting to note that using either $r_0 = 0.5\,\text{fm}$ or $(F_{\rm K})_{\rm R} = 160\,\text{MeV}$ gives indistinguishable results at our level of precision of 3%. However, this does not mean that $M_{\rm s} + \hat{M}$ has to be very close to our quenched result also in full QCD. Indeed, we have estimated that replacing $(F_{\rm K})_{\rm R}$ by $m_{\rm N}$ (or other stable light hadron masses) would give quark masses in MeV, which are larger by about 10%.

Usually the running quark masses in the $\overline{\rm MS}$ scheme, $\overline{m}_{\overline{\rm MS}}(\mu)$, are quoted. Their relation to the renormalization group invariant quark masses, which we computed here, has been discussed in Section 2 of Ref. [32]. For convenience, we include a table with the perturbative conversion factors $\overline{m}_{\overline{\rm MS}}(\mu)/M$ computed by numerical integration of the renormalization group equations with the n-loop approximations of the renormalization group functions (β,τ in the notation of [32]) for $n = 2,3,4$. One should be aware that the result $\Lambda_{\overline{\rm MS}}^{(0)} = 238(19)$ MeV [32] enters the numbers of Table 3. The uncertainty in Λ translates into 1.5% in $\overline{m}_{\overline{\rm MS}}(\mu)/M$ at $\mu = 2$ GeV and 2.5% at $\mu = 1$ GeV. If desired, Table 3 may be used to estimate $\overline{m}_{\overline{\rm MS}}(\mu)$. A typical result combining Eqs. (5.6) and (1.1) and the table is

$$\overline{m}_{\rm s}(2\text{GeV}) = 97(4)\text{MeV} \quad \text{with 4-loop running in the } \overline{\rm MS} \text{ scheme}. \tag{7.1}$$

This illustrates that a high level of precision can be reached by state of the art lattice techniques.

Effects of dynamical fermions may first be examined in the theory with unphysically large quark masses. We have also given results for a reference mass which is roughly

Table 3
Factors to convert the renormalization group invariant mass into the $\overline{\rm MS}$ scheme at scale μ

μ [GeV]	$\overline{m}_{\overline{\rm MS}}(\mu)/M$		
	2-loop	3-loop	4-loop
1.0	0.80279	0.83585	0.84449
2.0	0.70388	0.71830	0.72076
4.0	0.64079	0.64880	0.64981
8.0	0.59549	0.60055	0.60105
90.0	0.49937	0.50105	0.50112

twice the strange quark mass. One should quantify what the effects of dynamical fermions are at such a point, where a good accuracy may be achieved, and then move on to the more chiral regime.

Also for some quantities not related directly to quark masses, precise results have been obtained. They refer to the continuum limit of the quenched approximation and are summarized in Table 2. Most notably, decay constants were computed with a precision not much worse than the experimental one. This was achieved using the method to compute hadronic correlation functions proposed in [55]. In this context we should also comment on the continuum extrapolations in the $\mathrm{O}(a)$ improved theory. They are certainly necessary! For the quark mass in units of r_0, the difference between its value at a lattice spacing $a = 0.1\,\mathrm{fm}$ and at $a = 0$ amounts to about 15%. Other quantities show smaller lattice spacing effects as was observed also in a finite volume study [60]. Although clearly one would have hoped for a weaker a-dependence, we note that their order of magnitude is not much different from what is known already for pure gauge theory observables [59].

Finally let us come back to the rôle of lattice QCD in determining parameters of the chiral Lagrangian. Figs. 2 and 4a show to what precision the quark mass dependence of observables in the pseudoscalar sector can be computed. Such information, once available in full QCD, will allow us to reduce the errors in the chiral Lagrangian. For instance, we have checked that just the mass independence of R puts strong restrictions on these parameters. As usual, estimates of the uncertainties is a delicate issue and a detailed investigation of the potential of this approach will be left for future work.

Acknowledgements

The project of computing light quark masses was started quite a while ago by the ALPHA collaboration. Here we presented the final results. The basis of our approach was developed together with M. Lüscher, S. Sint and P. Weisz. We would like to thank them for a most enjoyable collaboration. In particular, R.S. and H.W. thank M. Lüscher for numerous enlightening discussions. Furthermore, we appreciate useful correspondence with G. Ecker and D. Wyler on chiral perturbation theory and electromagnetic corrections. The numerical computations were performed on the APE100/Quadrics computers of DESY Zeuthen and on the Cray T3D at EPCC Edinburgh. We thank these institutions for their support. This work was in part supported by EPSRC grant GR/K41663 and PPARC grants GR/K55745 and GR/L29927.

Appendix A. Numerical details

A.1. Improvement coefficients, renormalization factors

Our calculations have been performed using the O(a) improved Wilson action defined in Ref. [45], which can be consulted for any unexplained notation. In particular, the improvement coefficients $c_{\rm sw}$ and $c_{\rm A}$ were taken from Eqs. (5.15) and (6.4) of that reference.

The renormalized axial current and pseudoscalar density for quark flavours i and j are defined as

$$(A_{\rm R})_\mu(x) = Z_{\rm A}\big(1 + b_{\rm A} a m_{\rm q}\big)(A_{\rm I})_\mu(x), \tag{A.1}$$

$$P_{\rm R}(x) = Z_{\rm P}\big(1 + b_{\rm P} a m_{\rm q}\big) P(x), \tag{A.2}$$

where $P(x) = \overline{\psi}_i(x)\gamma_5\psi_j(x)$, and the improved, unrenormalized axial current is given by

$$(A_{\rm I})_\mu(x) = \overline{\psi}_i(x)\gamma_\mu\gamma_5\psi_j(x) + a c_{\rm A}\frac{1}{2}\big(\partial^*_\mu + \partial_\mu\big)P(x). \tag{A.3}$$

The renormalization factor $Z_{\rm A}$ was calculated in [61], and here we have used its parameterization in Eq. (6.11) of that paper.

The renormalization factor $Z_{\rm M}$, which relates the current quark mass in the O(a) improved theory to the renormalization group invariant quark mass, has recently been determined [32]. In that paper also the scale- and scheme-dependent factor $Z_{\rm P}$ has been computed in the Schrödinger functional (SF) scheme at a fixed scale of $L = 1.436\, r_0$. Here we use their representation in terms of polynomial fit functions, viz.

$$Z_{\rm M}(g_0) = 1.752 + 0.321(\beta - 6) - 0.220(\beta - 6)^2, \tag{A.4}$$

$$Z_{\rm P}(g_0, L/a)_{L = 1.436\, r_0} = 0.5233 - 0.0362(\beta - 6) + 0.0430(\beta - 6)^2, \tag{A.5}$$

$$\beta = 6/g_0^2, \qquad 6.0 \leqslant \beta \leqslant 6.5.$$

As explained in Subsection A.2 of Ref. [32], the uncertainty in $Z_{\rm M}$ is split into a β-dependent part of 1.1%, which enters any continuum extrapolation, and a β-independent error of 1.3% which must be added (in quadrature) to the extrapolated result. The typical accuracy of $Z_{\rm P}$ as given by the above polynomial is 0.5%.

The factor $Z_{\rm M}$ renormalizes the lattice counterpart of the ratio $R(m_i, m_j)$ defined in Eq. (2.1). In the O(a) improved theory it is given by

$$R(m_i, m_j) = \frac{F_{\rm PS}}{G_{\rm PS}}\big[1 + (b_{\rm A} - b_{\rm P})\, a m_{\rm q}\big], \tag{A.6}$$

where

$$m_{\rm q} = \frac{1}{2}\big\{(m_{\rm q})_i + (m_{\rm q})_j\big\} = \frac{1}{4a}\left(\frac{1}{\kappa_i} + \frac{1}{\kappa_j} - \frac{2}{\kappa_{\rm c}}\right), \tag{A.7}$$

and κ_i, κ_j are the hopping parameters of flavours i and j.

The combination $b_A - b_P$ has been found to be small in perturbation theory [53] and also non-perturbatively [62,63]. A method how to determine the individual coefficients b_A and b_P non-perturbatively has been proposed in Ref. [66], but no results for our choice of action have been reported so far.

The values for the critical hopping parameter κ_c have been taken from Table 1 of Ref. [45]. When necessary they have been interpolated linearly to the desired β-value.

A.2. Hadronic correlation functions, reference scale

Our calculation of hadronic correlation functions using Schrödinger functional boundary conditions follows exactly the procedures outlined in a previous paper [55]. In particular, this reference contains the definitions of the correlation functions f_P, f_A^I, k_V^I and f_1, which we have computed to extract hadron masses and matrix elements for pseudoscalar and vector mesons.

Estimates for meson masses were obtained by averaging effective masses,

$$am_{\mathrm{eff},X}\big(x_0 + a/2\big) = \ln\big(f(x_0)/f(x_0 + a)\big), \quad X = \mathrm{PS,V}, \tag{A.8}$$

over a suitably chosen interval $t_{\min} \leqslant x_0 \leqslant t_{\max}$. Similarly, the ratio F_{PS}/G_{PS} was obtained by averaging the combination

$$\frac{F_{PS}}{G_{PS}} = \frac{1}{m_{PS}} \frac{f_A^I(x_0)}{f_P(x_0)}, \tag{A.9}$$

and the individual matrix elements F_{PS} and G_{PS} are extracted from

$$F_{PS} = 2\big(m_{PS} L^3\big)^{-1/2} \mathrm{e}^{(x_0 - T/2)m_{PS}} \frac{f_A^I(x_0)}{\sqrt{f_1}}, \tag{A.10}$$

$$G_{PS} = 2\big(m_{PS}/L^3\big)^{1/2} \mathrm{e}^{(x_0 - T/2)m_{PS}} \frac{f_P(x_0)}{\sqrt{f_1}}, \tag{A.11}$$

where again an average over the interval $[t_{\min}, t_{\max}]$ is taken. The averaging intervals used here were the same as those in Table 1 of Ref. [55].

We have also calculated an unrenormalized current quark mass defined by

$$m(x_0) = \frac{\frac{1}{2}\big(\partial_0^* + \partial_0\big) f_A(x_0) + c_A a \partial_0^* \partial_0 f_P(x_0)}{2 f_P(x_0)}. \tag{A.12}$$

The values for the current quark mass listed in Table 1 have been obtained by averaging $m(x_0)$ over the interval $T/4 \leqslant x_0 \leqslant 3T/4$.

For the hadronic radius r_0 which was used to set the scale, we have taken its parameterization quoted in [59], viz.

$$\ln(a/r_0) = -1.6805 - 1.7139\,(\beta - 6) + 0.8155\,(\beta - 6)^2 - 0.6667\,(\beta - 6)^3, \tag{A.13}$$

accounting for the uncertainty as quoted in [59]. In addition to the results obtained at $\beta = 6.0$ and 6.2, which have been published in [55], we have also computed correlation

Table 4
Simulation parameters

β	T/a	L/a	L/r_0	N_{meas}
6.0	32	16	2.981(12)	1000
6.1	40	24	3.795(17)	800
6.2	48	24	3.261(16)	800
6.45	64	32	3.060(17)	220

functions at $\beta = 6.1$ and 6.45. A brief summary of our simulation parameters including N_{meas}, the number of gauge field configurations for which the correlation functions were computed, is presented in Table 4.

References

[1] J. Gasser, H. Leutwyler, Phys. Rep. 87 (1982) 77.
[2] H. Leutwyler, hep-ph/9406283.
[3] H. Leutwyler, Phys. Lett. B 378 (1996) 313. hep-ph/9602366.
[4] C.R. Allton et al., Nucl. Phys. B 431 (1994) 667. hep-ph/9406263.
[5] C.R. Allton, V. Giménez, L. Giusti, F. Rapuano, Nucl. Phys. B 489 (1997) 427. hep-lat/9611021.
[6] V. Giménez, L. Giusti, F. Rapuano, M. Talevi, Nucl. Phys. B540 (1999) 472. hep-lat/9801028.
[7] L. Giusti, V. Giménez, F. Rapuano, M. Talevi, A. Vladikas, Nucl. Phys. B (Proc. Suppl.) 73 (1999) 210. hep-lat/9809037.
[8] UKQCD Collaboration, C.R. Allton et al., Phys. Rev. D 49 (1994) 474. hep-lat/9309002.
[9] R. Gupta, T. Bhattacharya, Phys. Rev. D 55 (1997) 7203. hep-lat/9605039.
[10] B.J. Gough, G.M. Hockney, A.X. El-Khadra, A.S. Kronfeld, P.B. Mackenzie, B.P. Mertens, T. Onogi, J.N. Simone, Phys. Rev. Lett. 79 (1997) 1622. hep-ph/9610223.
[11] M. Göckeler, R. Horsley, H. Perlt, P. Rakow, G. Schierholz, A. Schiller, P. Stephenson, Phys. Rev. D 57 (1997) 5562. hep-lat/9707021.
[12] A. Cucchieri, M. Masetti, T. Mendes, R. Petronzio, Phys. Lett. B 422 (1998) 212. hep-lat/9711040.
[13] A. Cucchieri, T. Mendes, R. Petronzio, J. High Energy Phys. 05 (1998) 006. hep-lat/9804007.
[14] D. Becirevic, Ph. Boucaud, J.P. Leroy, V. Lubicz, G. Martinelli, F. Mescia, Phys. Lett. B 444 (1998) 401. hep-lat/9807046.
[15] SESAM Collaboration, N. Eicker et al., Phys. Lett. B 407 (1997) 290. hep-lat/9704019.
[16] SESAM Collaboration, N. Eicker et al., Phys. Rev. D 59 (1999) 014509. hep-lat/9806027.
[17] T. Blum, A. Soni, M. Wingate, hep-lat/9902016.
[18] JLQCD Collaboration, S. Aoki et al., Phys. Rev. Lett. 82 (1999) 4392. hep-lat/9901019.
[19] CP-PACS Collaboration, S. Aoki et al., hep-lat/9904012.
[20] J. Bijnens, J. Prades, E. de Rafael, Phys. Lett. B 348 (1995) 226. hep-ph/9411285.
[21] M. Jamin, M. Münz, Z. Phys. C 66 (1995) 633. hep-ph/9409335.
[22] M. Jamin, Nucl. Phys. B (Proc. Suppl.) 64 (1998) 250. hep-ph/9709484.
[23] S. Narison, Phys. Lett. B 358 (1995) 113. hep-ph/9504333.
[24] S. Narison, hep-ph/9905264.
[25] K.G. Chetyrkin, D. Pirjol, K. Schilcher, Phys. Lett. B 404 (1997) 337. hep-ph/9612394.
[26] P. Colangelo, F.D. Fazio, G. Nardulli, N. Paver, Phys. Lett. B 408 (1997) 340. hep-ph/9704249.
[27] J. Prades, Nucl. Phys. B (Proc. Suppl.) 64 (1998) 253. hep-ph/9708395.
[28] F.J. Ynduráin, Nucl. Phys. B 517 (1998) 324. hep-ph/9708300.
[29] H.G. Dosch, S. Narison, Phys. Lett. B 417 (1998) 173. hep-ph/9709215.
[30] L. Lellouch, E. de Rafael, J. Taron, Phys. Lett. B 414 (1997) 195. hep-ph/9707523.
[31] K. Maltman, hep-ph/9904370.

[32] ALPHA Collaboration, S. Capitani, M. Lüscher, R. Sommer, H. Wittig, Nucl. Phys. B 544 (1999) 669. hep-lat/9810063.
[33] ALPHA Collaboration, S. Sint, P. Weisz, Nucl. Phys. B 545 (1999) 529. hep-lat/9808013.
[34] R. Dashen, Phys. Rev. 183 (1969) 1245.
[35] K. Maltman, D. Kotchan, Mod. Phys. Lett. A5 (1990) 2457.
[36] J.F. Donoghue, B.R. Holstein, D. Wyler, Phys. Rev. D 47 (1993) 2089.
[37] J. Bijnens, Phys. Lett. B 306 (1993) 343. hep-ph/9302217.
[38] R. Baur, R. Urech, Phys. Rev. D 53 (1996) 6552. hep-ph/9508393.
[39] J.F. Donoghue, private communication through D. Wyler.
[40] R. Sommer, Nucl. Phys. B 411 (1994) 839. hep-lat/9310022.
[41] J. Gasser, H. Leutwyler, Ann. Phys. 158 (1984) 142.
[42] J. Gasser, H. Leutwyler, Nucl. Phys. B 250 (1985) 465.
[43] J. Bijnens, G. Ecker, J. Gasser, hep-ph/9411232.
[44] M. Lüscher, S. Sint, R. Sommer, P. Weisz, Nucl. Phys. B 478 (1996) 365. hep-lat/9605038.
[45] M. Lüscher, S. Sint, R. Sommer, P. Weisz, U. Wolff, Nucl. Phys. B 491 (1997) 323. hep-lat/9609035.
[46] S.R. Sharpe, Phys. Rev. D 41 (1990) 3233.
[47] J.N. Labrenz, S.R. Sharpe, Phys. Rev. D 54 (1996) 4595. hep-lat/9605034.
[48] C.W. Bernard, M.F.L. Golterman, Phys. Rev. D 46 (1992) 853. hep-lat/9204007.
[49] C.W. Bernard, M.F.L. Golterman, Nucl. Phys. B (Proc. Suppl.) 30 (1993) 217.
[50] M. Booth, G. Chiladze, A.F. Falk, Phys. Rev. D 55 (1997) 3092. hep-ph/9610532.
[51] W. Bardeen, A. Duncan, E. Eichten, G. Hockney, H. Thacker, Phys. Rev. D 57 (1998) 1633. hep-lat/9705008.
[52] UKQCD Collaboration, K.C. Bowler et al., hep-lat/9910022.
[53] S. Sint, P. Weisz, Nucl. Phys. B 502 (1997) 251. hep-lat/9704001.
[54] T. Mendes, A. Cucchieri, R. Petronzio, Nucl. Phys. B (Proc. Suppl.) 73 (1999) 225. hep-lat/9810028.
[55] ALPHA Collaboration, M. Guagnelli, J. Heitger, R. Sommer, H. Wittig, Nucl. Phys. B 560 (1999) 465. hep-lat/9903040.
[56] J. Gasser, H. Leutwyler, Phys. Lett. B 184 (1987) 83.
[57] M. Lüscher, Lectures given at Summer School 'Fields, Strings and Critical Phenomena', Les Houches, France, Jun 28–Aug 5, 1988.
[58] M. Lüscher, Commun. Math. Phys. 104 (1986) 177.
[59] ALPHA Collaboration, M. Guagnelli, R. Sommer, H. Wittig, Nucl. Phys. B 535 (1998) 389. hep-lat/9806005.
[60] ALPHA Collaboration, J. Heitger, Nucl. Phys. B 557 (1999) 309. hep-lat/9903016.
[61] M. Lüscher, S. Sint, R. Sommer, H. Wittig, Nucl. Phys. B 491 (1997) 344. hep-lat/9611015.
[62] G.M. de Divitiis, R. Petronzio, Phys. Lett. B 419 (1998) 311. hep-lat/9710071.
[63] T. Vergata and ALPHA Collaborations, work in progress.
[64] H. Wittig, Nucl. Phys. B (Proc. Suppl.) 63 (1998) 47. hep-lat/9710013.
[65] F. Butler, H. Chen, J. Sexton, A. Vaccarino, D. Weingarten, Nucl. Phys. B 430 (1994) 179. hep-lat/9405003.
[66] T. Bhattacharya, S. Chandrasekharan, R. Gupta, W. Lee, S. Sharpe, hep-lat/9904011.

G

Effective chiral Lagrangians and lattice QCD

Nucl. Phys. B588 (2000) 377-399

ELSEVIER

Nuclear Physics B 588 (2000) 377–399

NUCLEAR PHYSICS B

www.elsevier.nl/locate/npe

Effective chiral Lagrangians and lattice QCD

ALPHA Collaboration

Jochen Heitger [a], Rainer Sommer [a], Hartmut Wittig [b,*]

[a] *DESY, Platanenallee 6, D-15738 Zeuthen, Germany*
[b] *CERN, Theory Division, CH-1211 Geneva 23, Switzerland*

Received 28 June 2000; accepted 26 July 2000

Abstract

We propose a general method to obtain accurate estimates for some of the "low-energy constants" in the one-loop effective chiral Lagrangian by means of simulating lattice QCD. In particular, the method is sensitive to those constants whose values are required to test the hypothesis of a massless up-quark. Initial tests performed in the quenched approximation confirm that good statistical precision can be achieved. As a byproduct we obtain an accurate estimate for the ratio of pseudoscalar decay constants, $F_{\rm K}/F_\pi$, in the quenched approximation, which lies 10% below the experimental result. The quantities that serve to extract the low-energy constants also allow a test of the scaling behaviour of different discretizations of QCD and a search for the effects of dynamical quarks.

PACS: 11.15.Ha; 12.38.Gc; 12.39.Fe; 14.65.Bt
Keywords: Quark masses; Lattice gauge theory; Chiral perturbation theory; Quantum chromodynamics; Monte Carlo

1. Introduction

Chiral Perturbation Theory (ChPT) [1,2] plays an important rôle in the study of low-energy phenomena in QCD. As is well known, ChPT is based on simultaneous expansions of scattering amplitudes or hadronic matrix elements in powers of momentum and the quark masses $m_{\rm u}$, $m_{\rm d}$ and $m_{\rm s}$, and the form of the effective chiral Lagrangian is entirely determined by chiral symmetry. Another feature is the emergence of a number of coupling constants at every given order, which incorporate the non-perturbative dynamics of QCD. These couplings — sometimes called "low-energy constants" — are *a priori* undetermined

* Corresponding author. On leave of absence from: Theoretical Physics, Oxford University, 1 Keble Road, Oxford OX1 3NP, UK.

E-mail address: hartmut.wittig@cern.ch (H. Wittig).

0550-3213/00/$ – see front matter
PII: S0550-3213(00)00490-9

and can be fixed through phenomenological constraints in conjunction with additional assumptions. Currently the typical accuracy which is achieved in the determination of the low-energy constants is not very high (for a review, see [3]).

It has been noted some time ago that the mass parameters m_{u}, m_{d} and m_{s} cannot be fixed unambiguously from symmetry considerations alone. The reason is that the effective chiral Lagrangian is invariant under a family of transformations of the quark masses, which can be absorbed into the low-energy constants [4]. In particular, this hidden symmetry of the chiral Lagrangian implies that one cannot distinguish between $m_{\mathrm{u}} = 0$ and $m_{\mathrm{u}} \approx 5$ MeV, whilst preserving all other phenomenological predictions. Thus, additional theoretical input beyond ChPT is required to decide whether $m_{\mathrm{u}} = 0$ is indeed realized in nature. An obvious strategy is then to sharpen the current estimates for the low-energy constants and check whether they are compatible with the condition that $m_{\mathrm{u}} = 0$.

Since $m_{\mathrm{u}} = 0$ represents a simple solution to the strong CP problem, this question has continued to attract a lot of attention, despite several plausible arguments, each of which independently rules out $m_{\mathrm{u}} = 0$ [5,6]. However, the problem has never been studied in a first principles approach starting from the QCD Lagrangian directly.

In this paper we propose and test a method to determine a large set of low-energy constants with good accuracy using lattice simulations. Given its technical feasibility, such an approach eliminates the use of theoretical assumptions in the specification of the chiral Lagrangian. In the context of testing $m_{\mathrm{u}} = 0$ the rôle of lattice calculations has recently been discussed by Cohen, Kaplan and Nelson [7]. We expand on their proposal by incorporating the information gained by studying the mass dependence of matrix elements in addition to that of the pseudoscalar masses. Furthermore, we present ready-to-use numerical procedures which increase the statistical precision and discuss the influence of lattice artefacts. The latter point is of great relevance because the effective chiral Lagrangian of Gasser and Leutwyler is not valid for non-zero lattice spacing.

Our method is generally applicable in simulations of QCD with or without dynamical quarks. This initial study mainly serves to test its accuracy and limitations, and for that purpose it is sufficient to apply it to lattice data obtained in the quenched approximation. As a consequence we also consider comparisons of our lattice data with the quenched version of ChPT, thereby extracting some of the low-energy constants relevant for the quenched theory.

On the basis of our lattice data we conclude that the mass dependence of matrix elements can be determined with high precision in lattice simulations. Furthermore, we show that low-energy constants in the chiral Lagrangian can be obtained with a typical, absolute statistical accuracy of ± 0.05 in the continuum limit. Systematic uncertainties due to neglected higher orders are estimated to be ± 0.2. However, a systematic study of the influence of higher orders in the chiral expansions has so far not been performed, owing to limitations in the range of light quark masses that one is currently able to explore. Future calculations at smaller quark masses will be required in order to settle this point.

The remainder of this paper is organized as follows. In Section 2 we recall the main concepts of ChPT. Our computational strategy is described in Section 3, and the numerical details are discussed in Section 4, focusing on the extrapolations to the continuum. Our

results are presented in Section 5, and Section 6 contains some concluding remarks. Two appendices list some details about expressions in partially quenched ChPT and explain our choice of additional low-energy constants in the quenched theory.

2. Chiral perturbation theory

In this section we repeat the main features of ChPT and specify our notation. In addition to standard ChPT we also discuss its quenched and partially quenched versions.

2.1. Standard ChPT and $m_{\rm u} = 0$

The effective chiral Lagrangian is written as a low-energy expansion [1,2]

$$\mathcal{L}_{\rm eff} = \mathcal{L}^{(2)}_{\rm eff} + \mathcal{L}^{(4)}_{\rm eff} + \cdots . \tag{2.1}$$

The leading contribution $\mathcal{L}^{(2)}_{\rm eff}$ contains two coupling constants F_0 and B_0. To lowest order F_0 coincides with the pion decay constant F_π. Throughout this paper we adopt a convention in which $F_\pi \approx 93$ MeV. At order p^4 additional couplings $\alpha_1, \alpha_2, \ldots, \alpha_{12}$ appear in the effective chiral Lagrangian.[1] The values of these couplings are not constrained by chiral symmetry. Furthermore they contain the divergences that arise if one goes beyond tree level and thus depend on the renormalization scale (and scheme). As mentioned in the introduction, experimental information at low energies is not sufficient to specify the values of the complete set of couplings $\alpha_1, \ldots, \alpha_{12}$. For this reason one has to add further theoretical constraints, which usually involve certain assumptions, such as large-$N_{\rm c}$ arguments. By applying such a procedure, the "standard" values of the low-energy constants in our convention for $N_{\rm f} = 3$ flavours read [1–3,8–11]

$$\begin{aligned}
&\alpha_1 = 0.2 \pm 0.4, && \alpha_6 = -0.5 \pm 0.4,\\
&\alpha_2 = 1.07 \pm 0.4, && \alpha_7 = -0.5 \pm 0.25,\\
&\alpha_3 = -4.4 \pm 1.4, && \alpha_8 = 0.76 \pm 0.4,\\
&\alpha_4 = -0.76 \pm 0.6, && \alpha_9 = 7.8 \pm 0.8,\\
&\alpha_5 = 0.5 \pm 0.6, && \alpha_{10} = -6.1 \pm 0.8.
\end{aligned} \tag{2.2}$$

Here the α_i's have been renormalized at scale $\mu = 4\pi F_\pi$, which will always be used in the remainder of this paper. The constants α_{11} and α_{12} are of little phenomenological interest and are not included here.

The question whether $m_{\rm u} = 0$ has been discussed at length in the literature [4–7]. The usual starting point is the observation that simultaneous transformations of the quark masses

$$m^\lambda_{\rm u} = m_{\rm u} + \lambda m_{\rm d} m_{\rm s}, \qquad m^\lambda_{\rm d} = m_{\rm d} + \lambda m_{\rm s} m_{\rm u}, \qquad m^\lambda_{\rm s} = m_{\rm s} + \lambda m_{\rm u} m_{\rm d}, \tag{2.3}$$

and coupling constants according to

[1] We adopt a convention in which the α_i's are related to the corresponding couplings L_i of Ref. [2] through $\alpha_i = 8(4\pi)^2 L_i$.

$$\alpha_6^\lambda = \alpha_6 + \lambda\frac{(4\pi F_0)^2}{4B_0}, \qquad \alpha_7^\lambda = \alpha_7 + \lambda\frac{(4\pi F_0)^2}{4B_0}, \qquad \alpha_8^\lambda = \alpha_8 - \lambda\frac{(4\pi F_0)^2}{2B_0}, \quad (2.4)$$

leaves the effective chiral Lagrangian invariant. Here, λ denotes an arbitrary parameter, and for $\lambda \neq 0$, $m_\mathrm{u} = 0$ one can generate an effective up-quark mass such that all predictions by ChPT, in particular for ratios of quark masses, remain unchanged. In order to test whether $m_\mathrm{u} = 0$ one has to determine the linear combination [5] $(2\alpha_8 - \alpha_5)$, which, however, is not directly accessible from phenomenology. The value of α_5 is obtained from the ratio of kaon to pion decay constants, F_K/F_π, but α_8 can only be inferred from the linear combination

$$\alpha_5 - 12\alpha_7 - 6\alpha_8, \quad (2.5)$$

which is related to the Gell-Mann–Okubo formula. Clearly this linear combination is invariant under the transformation of Eq. (2.4). As pointed out in [7] a choice for α_7 and α_8 which is compatible with $m_\mathrm{u} = 0$ is given by

$$m_\mathrm{u} = 0: \quad \alpha_8 = -0.9 \pm 0.4, \quad \alpha_7 = 0.25 \pm 0.25, \quad (2.6)$$

which is quite different from the corresponding numbers listed in Eq. (2.2). The task for lattice simulations is now to provide independent determinations of α_5, α_8 from linear combinations which are not invariant under Eq. (2.4), starting from the QCD Lagrangian. Provided that these estimates turn out to be sufficiently accurate, it should then be possible to test the hypothesis that $m_\mathrm{u} = 0$.

2.2. Partially quenched ChPT

The rôle of lattice simulations for the determination of the α_i's has already been stressed in [7,12], and most recently in [13]. In particular, it has been noted that simulations of "partially quenched" QCD, in which the sea and valence quarks can be chosen independently, may be useful as well as technically feasible. Thus, one is not forced to simulate at the physical values of the u, d and s quarks. Instead, the only requirement is that the pseudoscalar masses be small compared with the typical chiral scale of $\Lambda_\chi \approx 1$ GeV. Hence the use of moderately light sea and valence quark masses and their independent variation may be sufficient to extract the low-energy constants.

It has to be kept in mind, though, that the values of the α_i's have to be determined separately for $N_\mathrm{f} = 2$ and 3 flavours of dynamical quarks. This is a relevant point since there is currently not much experience with simulation algorithms for odd numbers of flavour.

Partially quenched ChPT has been studied to $\mathrm{O}(p^4)$ by a number of authors [12,14,15]. Here we focus on the one-loop expressions for pseudoscalar masses and decay constants obtained by Sharpe [14] for N_f *degenerate* flavours of sea quarks. For the remainder of this paper we also take over some of the notation used in that reference. In particular, we denote the mass of the sea quark by m_S, whereas the masses of the (in general non-degenerate) valence quarks are denoted by m_1, m_2. As in [14] we introduce the dimensionless parameters

$$y_{ij} = \frac{B_0(m_i + m_j)}{(4\pi F_0)^2}, \quad i, j \in \{1, 2, S\}. \tag{2.7}$$

By setting $\Lambda_\chi = 4\pi F_0$ in Eqs. (14) and (18) of Ref. [14], we obtain the generic formulae for the pseudoscalar mass and decay constant, i.e.,

$$m_{\rm PS}^2 = y_{12}(4\pi F_0)^2 \Bigg\{ 1 + \frac{1}{N_{\rm f}} \Bigg[\frac{y_{11}(y_{SS} - y_{11}) \ln y_{11} - y_{22}(y_{SS} - y_{22}) \ln y_{22}}{y_{22} - y_{11}} \Bigg] + y_{12}(2\alpha_8 - \alpha_5) + y_{SS} N_{\rm f} (2\alpha_6 - \alpha_4) \Bigg\}, \tag{2.8}$$

$$\frac{F_{\rm PS}}{F_0} = 1 - \frac{N_{\rm f}}{4}(y_{1S} \ln y_{1S} + y_{2S} \ln y_{2S}) + \frac{1}{2N_{\rm f}} \left(\frac{y_{11} y_{22} - y_{SS} y_{12}}{y_{22} - y_{11}} \ln \frac{y_{11}}{y_{22}} + y_{12} - y_{SS} \right) + y_{12} \frac{1}{2} \alpha_5 + y_{SS} \frac{N_{\rm f}}{2} \alpha_4. \tag{2.9}$$

Here the constants α_i are to be evaluated at scale $\mu = \Lambda_\chi = 4\pi F_0 \approx 1170$ MeV. These expressions will later be used to form quantities that allow for the extraction of the α_i's using lattice data.

2.3. Quenched ChPT

Quenched ChPT has originally been discussed in Refs. [16,17]. The complete chiral Lagrangian to order p^4 in quenched QCD has been studied by Colangelo and Pallante [18]. Their results form the basis of our analysis.

As is well known flavour singlets have to be treated differently in the quenched approximation: the decoupling of the η' from the pseudoscalar octet by means of the anomaly is not realized in the quenched theory. Therefore, the quenched chiral Lagrangian contains additional low-energy constants associated with flavour-singlet contributions. These include the singlet mass scale m_0 and the coupling constant α_Φ, which multiplies the kinetic term of the singlet field in the quenched chiral Lagrangian. The mass scale m_0 is usually expressed in terms of the parameter δ defined by

$$\delta = \frac{m_0^2}{3(4\pi F_0)^2}. \tag{2.10}$$

From various lattice studies (e.g., [19–22]) one expects $\delta \approx 0.1$. For α_Φ the available estimates have been summarized in [23] as $\alpha_\Phi \approx 0.6$.

Following Ref. [18] we restrict ourselves to the case of degenerate quarks. The complete results at one loop for the pseudoscalar mass and decay constant read [2]

$$m_{\rm PS}^2 = y(4\pi F_0)^2 \left\{ 1 - \left(\delta - \frac{2}{3} \alpha_\Phi y \right)[1 + \ln y] + \left(\left(2\alpha_8^{\rm q} - \alpha_5^{\rm q} \right) - \frac{\alpha_\Phi}{3} \right) y \right\}, \tag{2.11}$$

[2] In Ref. [18] a different combination of low-energy constants appears in the expression for $m_{\rm PS}^2$, since the authors use an alternative convention for the counterterms [24]. The convention employed in this paper is consistent with that used in standard and partially quenched ChPT.

$$\frac{F_{\rm PS}}{F_0} = 1 + y\,\frac{1}{2}\alpha_5^{\rm q}. \tag{2.12}$$

Here y is defined as

$$y = \frac{2B_0 m}{(4\pi F_0)^2}, \tag{2.13}$$

and $\alpha_8^{\rm q}$, $\alpha_5^{\rm q}$ denote the analogues of the low-energy constants α_8 and α_5 in the quenched theory.

3. Strategy

We now introduce the procedure to determine the low-energy constants from lattice data by studying the quark mass dependence of suitably defined *ratios* of pseudoscalar masses and matrix elements. In particular it is useful to investigate the mass dependence around some reference quark mass $m_{\rm ref}$. It is important to realize that this reference point does not have to coincide with a physical quark mass [25]. We only require that it should lie inside the range of simulated quark masses and within the domain of applicability of ChPT.

3.1. The ratios $R_{\rm M}$ and $R_{\rm F}$

Let us consider the case of degenerate valence quarks, $m_1 = m_2 = m$, either in the quenched approximation or in partially quenched QCD at a fixed value of the sea quark mass m_S. If we introduce

$$y = \frac{2B_0 m}{(4\pi F_0)^2}, \qquad y_{\rm ref} = \frac{2B_0 m_{\rm ref}}{(4\pi F_0)^2}, \qquad x = y/y_{\rm ref}, \tag{3.1}$$

then the ratios defined by

$$R_{\rm M}(x) = \left(\frac{F_{\rm PS}(y)}{G_{\rm PS}(y)}\right) \Bigg/ \left(\frac{F_{\rm PS}(y_{\rm ref})}{G_{\rm PS}(y_{\rm ref})}\right), \tag{3.2}$$

$$R_{\rm F}(x) = F_{\rm PS}(y)/F_{\rm PS}(y_{\rm ref}) \tag{3.3}$$

are universal functions of the parameter x, which measures the deviation from the reference point $y_{\rm ref}$. Here, $G_{\rm PS}$ denotes the matrix element of the pseudoscalar density between a pseudoscalar state and the vacuum, and the arguments of $F_{\rm PS}$, $G_{\rm PS}$ refer to the quark mass value at which the matrix elements have to be evaluated. Using the definition of the current quark mass in terms of $F_{\rm PS}$, $G_{\rm PS}$ and $m_{\rm PS}$ (see, for instance, Eqs. (2.1) and (2.2) in Ref. [25]), Eq. (3.2) can be rewritten as

$$R_{\rm M}(x) = \left(\frac{2y}{m_{\rm PS}^2(y)}\right) \Bigg/ \left(\frac{2y_{\rm ref}}{m_{\rm PS}^2(y_{\rm ref})}\right) = x\,\frac{m_{\rm PS}^2(y_{\rm ref})}{m_{\rm PS}^2(y)}. \tag{3.4}$$

Extracting the low-energy constants from the ratios R_X, $X = {\rm M}, {\rm F}$ instead of the masses and matrix elements themselves has several advantages:

- The ratios R_X can be computed with high statistical precision owing to the strong correlations between numerator and denominator;

- The renormalization factors of the axial current and the pseudoscalar density drop out in $R_{\rm M}$ and $R_{\rm F}$.[3] The ratios can therefore be readily extrapolated to the continuum limit, so that all dependence on the lattice spacing is eliminated. Strictly speaking it is only in the continuum limit that one is justified to compare the predictions of ChPT with lattice data;
- Since discretization errors are under good control in R_X the effects of dynamical quarks can be isolated unambiguously.

The high level of statistical accuracy of the ratios is crucial in order not to compromise the precision in the continuum limit. Extracting the low-energy constants from the x-dependence in the continuum limit in turn guarantees that these estimates will not be distorted by cutoff effects.

The simple renormalization and high precision of the ratios may also be exploited to perform scaling tests for different fermionic discretizations.

3.2. Expressions for $R_{\rm M}$ and $R_{\rm F}$ in ChPT

Below we give a list with the expressions for $R_{\rm M}$ and $R_{\rm F}$ in quenched and partially quenched ChPT. For simplicity we restrict ourselves to the case of degenerate valence quarks. The case of non-degenerate valence quarks in partially quenched ChPT is discussed in detail in Appendix A.

Note that we have not yet specified the reference point $y_{\rm ref}$. At this stage the precise definition of its numerical value is not needed, and we thus postpone its specification to Section 5, where we describe our numerical results.

We begin by considering $R_{\rm M}$ and $R_{\rm F}$ in quenched ChPT. By inserting Eq. (2.11) into Eq. (3.4) we obtain

$$R_{\rm M}^{\rm q}(x) = \frac{1-\left(\delta-\frac{2}{3}\alpha_\Phi\, y_{\rm ref}\right)(1+\ln y_{\rm ref})+y_{\rm ref}\left[\left(2\alpha_8^{\rm q}-\alpha_5^{\rm q}\right)-\frac{\alpha_\Phi}{3}\right]}{1-\left(\delta-\frac{2}{3}\alpha_\Phi\, x y_{\rm ref}\right)(1+\ln(x y_{\rm ref}))+x y_{\rm ref}\left[\left(2\alpha_8^{\rm q}-\alpha_5^{\rm q}\right)-\frac{\alpha_\Phi}{3}\right]}. \tag{3.5}$$

Provided that all masses and couplings are small, it is allowed to expand the denominator, which gives

$$\begin{aligned} R_{\rm M}^{\rm q}(x) = {} & 1+\delta\ln x-\frac{2}{3}\alpha_\Phi\, y_{\rm ref}\left[x\ln x+(x-1)\left(\frac{1}{2}+\ln y_{\rm ref}\right)\right] \\ & -y_{\rm ref}(x-1)\left(2\alpha_8^{\rm q}-\alpha_5^{\rm q}\right). \end{aligned} \tag{3.6}$$

Similarly we obtain

$$R_{\rm F}^{\rm q}(x) = \frac{1+x y_{\rm ref}\frac{1}{2}\alpha_5^{\rm q}}{1+y_{\rm ref}\frac{1}{2}\alpha_5^{\rm q}}, \tag{3.7}$$

which, after expanding the denominator, becomes

[3] For O(a) improved Wilson fermions, there remains a small mass-dependent renormalization proportional to $(b_{\rm A}-b_{\rm P})(x-1)am_{\rm ref}$ and $b_{\rm A}(x-1)am_{\rm ref}$ in the case of $R_{\rm M}$ and $R_{\rm F}$, respectively. Our experience has shown [25] that this can be safely neglected. In our calculations we set $b_{\rm A}$ and $b_{\rm P}$ equal to their one-loop perturbative values [26].

$$R_{\rm F}^{\rm q}(x) = 1 + y_{\rm ref}(x-1)\frac{1}{2}\alpha_5^{\rm q}. \tag{3.8}$$

In partially quenched ChPT it is useful to always define the reference point $y_{\rm ref}$ at

$$m_1 = m_2 = m_S = m_{\rm ref}, \qquad y_{\rm ref} = \frac{2B_0 m_{\rm ref}}{(4\pi F_0)^2}. \tag{3.9}$$

There are several possibilities to study the mass dependence of the ratios R_X. Let us first consider the case of equal sea and valence quark masses. The x-dependent part in R_X is then obtained by setting

$$\text{SS:} \quad m_1 = m_2 = m_S = x m_{\rm ref}, \tag{3.10}$$

which will be labelled "SS" in the following. By taking the appropriate limits in Eqs. (2.7) and (2.8) for the above choices of quark masses and inserting the resulting expressions into the definition of $R_{\rm M}$, we obtain, after expanding the denominator:

$$\begin{aligned} R_{\rm M}^{\rm SS}(x) = 1 &- \frac{1}{N_{\rm f}} y_{\rm ref}\big[x\ln x + (x-1)\ln y_{\rm ref}\big] \\ &- y_{\rm ref}(x-1)\big[(2\alpha_8 - \alpha_5) + N_{\rm f}(2\alpha_6 - \alpha_4)\big]. \end{aligned} \tag{3.11}$$

For $R_{\rm F}$ the corresponding result is

$$R_{\rm F}^{\rm SS}(x) = 1 - \frac{N_{\rm f}}{2} y_{\rm ref}\big[x\ln x + (x-1)\ln y_{\rm ref}\big] + y_{\rm ref}(x-1)\frac{1}{2}(\alpha_5 + N_{\rm f}\alpha_4). \tag{3.12}$$

For $m_1,\ m_2 \neq m_S$ the x-dependence can be mapped out using either the valence or the sea quarks. In the former case, which we label "VV" we define the x-dependent part through

$$\text{VV:} \quad m_1 = m_2 = x m_{\rm ref}, \quad m_S = m_{\rm ref} \tag{3.13}$$

instead of Eq. (3.10), which leads to the expressions

$$\begin{aligned} R_{\rm M}^{\rm VV}(x) = 1 &- \frac{1}{N_{\rm f}} y_{\rm ref}\big[(2x-1)\ln x + 2(x-1)\ln y_{\rm ref}\big] \\ &- y_{\rm ref}(x-1)\left[(2\alpha_8 - \alpha_5) + \frac{1}{N_{\rm f}}\right] \end{aligned} \tag{3.14}$$

$$\begin{aligned} R_{\rm F}^{\rm VV}(x) = 1 &- \frac{N_{\rm f}}{4} y_{\rm ref}\left[(x+1)\ln\left(\frac{1}{2}(x+1)\right) + (x-1)\ln y_{\rm ref}\right] \\ &+ y_{\rm ref}(x-1)\frac{1}{2}\alpha_5. \end{aligned} \tag{3.15}$$

A comparison of the expressions for $R_{\rm M}$ and $R_{\rm F}$ for the "SS" and "VV" cases shows that they are sensitive to different linear combinations of low-energy constants, depending on whether the x-dependence is defined using Eq. (3.10) or Eq. (3.13). In particular, we find that it is possible to extract directly from $R_{\rm M}^{\rm VV}(x)$ the linear combination $(2\alpha_8 - \alpha_5)$, which is relevant to the question of whether $m_{\rm u} = 0$.

There are several other possibilities to define the dependence of R_X on the quark masses, also allowing for non-degenerate valence quarks. Details are listed in Appendix A.

3.3. Extracting the low-energy constants

We now describe a method to determine the low-energy constants from the ratios R_X in the quenched and unquenched cases. To this end we choose two values of mass parameters, x_1, x_2, and introduce the quantity

$$\Delta R_X(x_1, x_2) = R_X(x_1) - R_X(x_2), \quad x_1 < x_2, \quad X = \mathrm{M},\ \mathrm{F}. \tag{3.16}$$

By inserting the expressions for the ratios R_X we can easily solve for the low-energy constants. For instance, from Eqs. (3.8) and (3.16) we find

$$\alpha_5^{\mathrm{q}} = 2\frac{\Delta R_{\mathrm{F}}^{\mathrm{q}}(x_1, x_2)}{(x_1 - x_2)\, y_{\mathrm{ref}}}. \tag{3.17}$$

Similar combinations of the α_i's can be obtained in partially quenched QCD. The explicit expressions are given in Appendix A, and one can easily convince oneself that they serve to determine α_4, α_5, α_6 and α_8.

The quantity $\Delta R_{\mathrm{M}}^{\mathrm{q}}$ is a special case, since it also depends on the low-energy constants δ and α_Φ, which only occur in the quenched theory. However, by inserting the estimates for δ and α_Φ quoted in the literature we can solve for $(2\alpha_8^{\mathrm{q}} - \alpha_5^{\mathrm{q}})$, i.e.,

$$\begin{aligned}\left(2\alpha_8^{\mathrm{q}} - \alpha_5^{\mathrm{q}}\right) = \left\{y_{\mathrm{ref}}(x_1 - x_2)\right\}^{-1}\Bigg\{&\delta \ln(x_1/x_2) - \Delta R_{\mathrm{M}}^{\mathrm{q}}(x_1, x_2) \\ &- \frac{2}{3}\alpha_\Phi\, y_{\mathrm{ref}}\left[x_1 \ln x_1 - x_2 \ln x_2 + (x_1 - x_2)\left(\frac{1}{2} + \ln y_{\mathrm{ref}}\right)\right]\Bigg\}.\end{aligned} \tag{3.18}$$

The expressions for R_X themselves can also be used in order to extract the low-energy constants from least-χ^2 fits over a suitably chosen interval in x. The differences ΔR_X, however, have the advantage that some of the lattice artefacts may cancel. Thus, instead of first extrapolating R_X to the continuum limit and then forming the differences ΔR_X, one may compute $\Delta R_X(x_1, x_2)$ at non-zero lattice spacing and then perform the continuum extrapolation. Obviously the results must be independent of the ordering of the two procedures, which offers an additional check against the influence of lattice artefacts. By contrast, if a fitting procedure is employed at non-zero lattice spacing then it is *a priori* not clear whether the continuum expressions for the ratios R_X are valid.

Our method to extract the low-energy constants is only viable if there is sufficient overlap between the region of validity of ChPT and the range of quark masses accessible in current lattice simulations. On present computers it is not possible to simulate very light quarks without suffering from large finite-volume effects. Furthermore, the fermion action and lattice spacings employed in this work do not allow the use of quark masses which are below approximately half of the strange quark mass. The reason is the occurrence of "exceptional configurations" [27,28], which correspond to unphysical zero modes of the lattice Dirac operator. Therefore, since one is restricted to a range of relatively large quark masses, one must check the results against the influence of higher orders in the chiral expansion: if large, these would modify the numerical estimates for the low-energy constants considerably. This will be discussed in more detail in Section 5.

4. Continuum limit of R_X and ΔR_X

The ratios R_X have been computed using the same quenched configurations as in our earlier papers [25,29]. Results for hadron and current quark masses, as well as for $F_{\rm PS}$ and $F_{\rm PS}/G_{\rm PS}$ are listed in Table 1 of Ref. [25]. Details of our numerical procedures are described in Appendix A of the same paper. Here we only mention that non-perturbative O(a) improvement [27,30,31] has been employed, and we will therefore assume that the remaining discretization errors are of order a^2.

In contrast to our earlier papers the statistical errors in this work have been estimated using a bootstrap procedure [32], with 200 bootstrap samples generated from the sets of gauge configurations. This allows us to keep a constant number of bootstrap samples at every value of the bare coupling, regardless of the number of configurations. By performing the continuum extrapolation of $R_X(x)$ for every bootstrap sample, our error procedure thus preserves the correlations in the mass parameter x. Throughout this paper we quote the symmetrized error from the central 68% of the bootstrap distribution.

The value of the reference quark mass $m_{\rm ref}$ is defined through the condition

$$(m_{\rm PS} r_0)^2\big|_{m=m_{\rm ref}} = 3, \tag{4.1}$$

a choice that has also been considered in Refs. [25,33]. For $F_0 = F_\pi = 93.3\,\text{MeV}$ the numerical value of $y_{\rm ref}$ is thus $y_{\rm ref} = 0.3398\ldots$. Lattice data for the hadronic radius r_0 [34] have been taken from Ref. [35]. For $r_0 = 0.5$ fm the definition of Eq. (4.1) corresponds to a pseudoscalar meson whose squared mass is roughly twice as large as the kaon mass squared, and therefore $m_{\rm ref} \approx m_{\rm s}$ (with "s" standing for "strange"). The results for $F_{\rm PS}$ and $F_{\rm PS}/G_{\rm PS}$ obtained for several values of the bare coupling have been interpolated in the current quark mass m to common values of $x = m/m_{\rm ref}$. To this end the two neighbouring points which straddle the value of x were used in a linear interpolation. If x was slightly outside the range of simulated quark masses, a linear extrapolation was performed using the three nearest points. The stability of this procedure was checked by varying the input masses and/or performing quadratic interpolations/extrapolations. Our sets of simulated quark masses cover the range $0.75 \leqslant x \leqslant 1.4$, and we have chosen increments of 0.05 to map out the mass dependence of $R_X(x)$.

In Fig. 1 we plot the ratios $R_{\rm M}(x)$ and $R_{\rm F}(x)$ against $(a/r_0)^2$ for three different values of x. The plots show that lattice artefacts are very small in general and are consistent with leading cutoff effects of order a^2. As a safeguard against higher-order lattice artefacts, we have excluded the points computed for our coarsest lattice ($a \approx 0.1$ fm) from the extrapolation. Results obtained by performing the extrapolations for all four values of the lattice spacing were entirely consistent, albeit with a smaller statistical error.

At non-zero lattice spacing the statistical precision is better than 0.3% and 0.2% for $R_{\rm M}$ and $R_{\rm F}$, respectively. In the continuum limit these figures are only slightly larger, namely 0.4% for $R_{\rm M}$ and 0.3% for $R_{\rm F}$. This demonstrates the high level of precision that can be achieved in the continuum limit. Furthermore, it is clear that the extrapolation is well controlled.

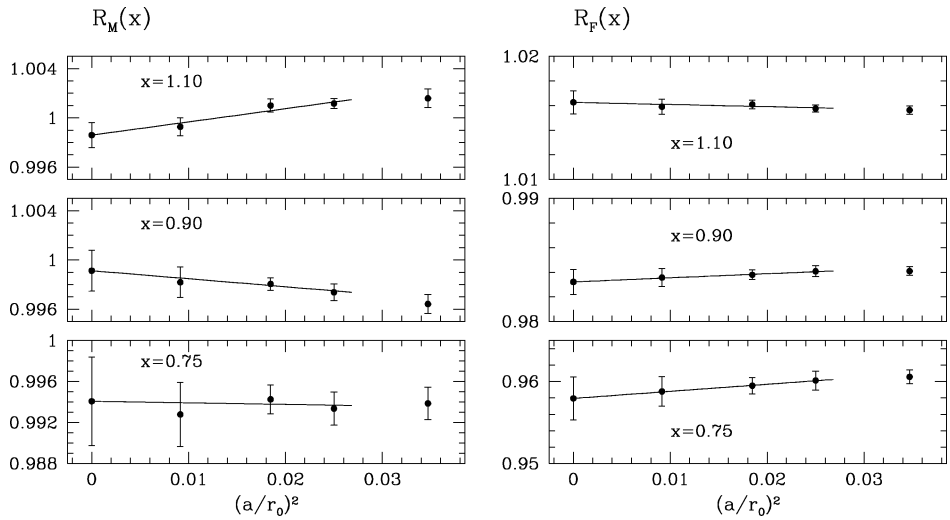

Fig. 1. Continuum extrapolations of $R_{\mathrm{M}}(x)$ and $R_{\mathrm{F}}(x)$ for selected values of the mass parameter x.

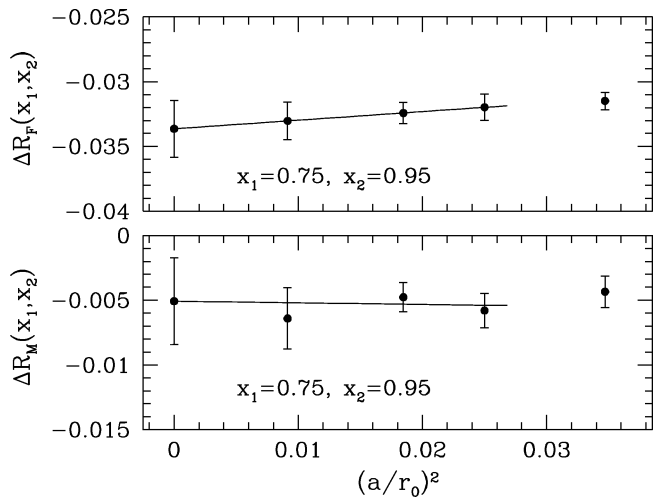

Fig. 2. Continuum extrapolations of ΔR_{M} and ΔR_{F}.

As mentioned in Section 3 the results for ΔR_X in the continuum limit can be obtained either directly from the continuum values of R_X or from a continuum extrapolation of ΔR_X computed at non-zero lattice spacing. The latter extrapolations are shown in Fig. 2 for a particular choice of x_1 and x_2. As in the case of the ratios R_X themselves the continuum limit is easy to control.

5. Results

We can now compare our results for the ratios R_X to the expressions predicted by ChPT. Since the numerical data have been obtained in the quenched approximation, we will focus on the determination of α_5^{q} and $(2\alpha_8^{\mathrm{q}} - \alpha_5^{\mathrm{q}})$.

5.1. Low-energy constants in quenched ChPT

The determination of α_5^{q} from Eq. (3.17) is straightforward, since it only depends on the mass parameters x_1 and x_2. However, in order to compute $(2\alpha_8^{\mathrm{q}} - \alpha_5^{\mathrm{q}})$ from Eq. (3.18) one must make a suitable choice of δ and α_Φ. Here we are going to consider two cases, namely

$$\text{Q1:} \quad \delta = 0.12 \pm 0.02, \quad \alpha_\Phi = 0, \tag{5.1}$$

$$\text{Q2:} \quad \delta = 0.05 \pm 0.02, \quad \alpha_\Phi = 0.5. \tag{5.2}$$

The reasoning which led us to consider these two distinct sets of parameters is described in Appendix B.

Our estimates for α_5^{q} and $(2\alpha_8^{\mathrm{q}} - \alpha_5^{\mathrm{q}})$ have been obtained from $\Delta R_{\mathrm{F}}(x_1, x_2)$ and $\Delta R_{\mathrm{M}}(x_1, x_2)$ for $x_1 = 0.75$ and $x_2 = 0.95$. This choice was motivated by the desire to go to the smallest possible quark masses, whilst maintaining a reasonably large x-interval in order to check the stability of the results against variations in the parameters x_1 and x_2. Following this procedure, we obtained the following estimates for the low-energy constants in quenched ChPT

$$\alpha_5^{\mathrm{q}} = 0.99 \pm 0.06, \tag{5.3}$$

$$\left(2\alpha_8^{\mathrm{q}} - \alpha_5^{\mathrm{q}}\right) = \begin{cases} 0.35 \pm 0.05 \pm 0.07, & \text{Q1}, \\ 0.02 \pm 0.05 \pm 0.07, & \text{Q2}. \end{cases} \tag{5.4}$$

Here, the first error is statistical, while the second (where quoted) is due to the variation of ± 0.02 in the value of δ for both parameter sets Q1 and Q2. These results can now be inserted into the expressions for the ratios R_{M} and R_{F}, Eqs. (3.6) and (3.8), respectively, and the resulting curves are compared with the data in Fig. 3(a)–(c).

The linearity of R_{F} predicted by one-loop quenched ChPT is well reproduced by the numerical data, resulting in very stable estimates for α_5^{q}. Although the result in Eq. (5.3) has been extracted from a fairly narrow x-interval, it provides a good representation of the data over the entire range of quark masses considered here. The determination of $(2\alpha_8^{\mathrm{q}} - \alpha_5^{\mathrm{q}})$ is also quite stable for both sets of values of δ, α_Φ, i.e., Q1 and Q2. In both cases a good description of the numerical data is achieved for $x \lesssim 1.2$, with $(2\alpha_8^{\mathrm{q}} - \alpha_5^{\mathrm{q}})$ extracted for Q1 tracing the data quite well even at the largest x-values.

Estimates for α_5^{q} and $(2\alpha_8^{\mathrm{q}} - \alpha_5^{\mathrm{q}})$ obtained from the continuum extrapolations of ΔR_{F} and ΔR_{M} shown in Fig. 2 are entirely consistent with Eqs. (5.3) and (5.4). The same is true if the low-energy constants are extracted directly from fits to $R_X(x)$ for x in the interval $0.75 \leqslant x \leqslant 0.95$; the results are numerically almost identical to those obtained using the differences ΔR_X.

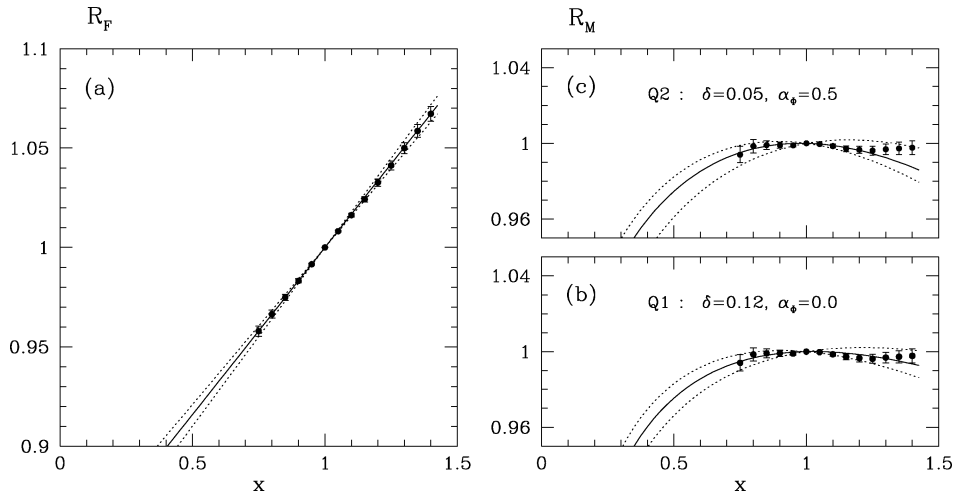

Fig. 3. (a): Data for the ratio R_{F} compared with the curve obtained by inserting the low-energy constant of Eq. (5.3); (b) and (c): the same for the ratio R_{M} using the low-energy constants of Eq. (5.4) for parameter sets Q1 and Q2, respectively. Dotted lines indicate the variation due to the statistical uncertainty in the extraction of the low-energy constants.

5.2. Effects of higher orders in the quark mass

Although the results presented in the last subsection suggest that the one-loop formulae for quenched ChPT offer a good description of the x-dependence of the ratios R_X, further work is needed to corroborate these findings by extending the range of quark masses under study to smaller values. For instance, the downward curvature observed in the prediction for R_{M} when $x < 0.75$ remains to be verified.

Furthermore, data at smaller quark masses will be required to systematically assess the influence of higher-order terms in the chiral expansion on the determination of the low-energy constants. Such terms manifest themselves in additional contributions proportional to x^2 in the formulae for R_X. Since the range $0.75 \leqslant x \leqslant 0.95$ corresponds to pseudoscalar meson masses between 590 and 670 MeV, it cannot be excluded that higher-order terms have a sizeable impact on the extraction of the α_i's.

Even without results at smaller masses there are several possibilities to study the effects of neglecting higher orders in ChPT on our estimates for α_5^{q} and $(2\alpha_8^{\mathrm{q}} - \alpha_5^{\mathrm{q}})$. We stress, however, that none of the methods described below can replace the systematic investigation of smaller quark masses.

An obvious way to proceed is to add a quadratic term to the expressions for $R_{\mathrm{F}}^{\mathrm{q}}$ and $R_{\mathrm{M}}^{\mathrm{q}}$. For instance, the modified expression for $R_{\mathrm{F}}^{\mathrm{q}}$ reads

$$R_{\mathrm{F}}^{\mathrm{q}}(x) \longrightarrow 1 + y_{\mathrm{ref}}(x-1)\frac{1}{2}\alpha_5^{\mathrm{q}} + y_{\mathrm{ref}}^2(x^2-1)\,d_{\mathrm{F}}, \tag{5.5}$$

with a similar quadratic term proportional to d_{M} in the case of $R_{\mathrm{M}}^{\mathrm{q}}$. One can now perform least-χ^2 fits over the *entire* range $0.75 \leqslant x \leqslant 1.4$, thereby extracting the low-energy constants as well as d_{F}, d_{M}. Because of the linearity of the data for R_{F} the only effect of

including x^2-terms in the determination of α_5^{q} is to increase its statistical error to ± 0.19. The estimates for $(2\alpha_8^{\mathrm{q}} - \alpha_5^{\mathrm{q}})$ are more sensitive: compared with Eqs. (5.4) their central values increase by 0.11 and 0.22 for the parameter sets Q1 and Q2, respectively, while the statistical error is increased to ± 0.12. The variation in the central values, or the larger statistical error in the case of α_5^{q}, may serve as an estimate of the uncertainty induced by neglecting higher orders.

An alternative, albeit naive, estimate of the effect in question is obtained by assuming that the chiral expansion converges like a geometric series. This implies that one expects the quadratic contributions to R_X to be roughly as large as the square of the linear ones. Here we consider $R_{\mathrm{F}}^{\mathrm{q}}$ as the generic case, since it does not involve logarithmic terms. Its linear contribution amounts to $\approx 16\%$ at $x = 1$, so that the quadratic term is estimated as $0.025\,x^2$. If we generalize this estimate, then the systematic uncertainty in $\Delta R_X(x_1, x_2)$ due to neglecting quadratic terms is given by

$$\text{syst. error in } \Delta R_X(x_1, x_2) \approx \pm 0.025\left(x_1^2 - x_2^2\right). \tag{5.6}$$

Through Eqs. (3.17) and (3.18) this is easily translated into systematic errors [4] on α_5^{q} and $(2\alpha_8^{\mathrm{q}} - \alpha_5^{\mathrm{q}})$, as

$$\text{syst. error in } \alpha_5^{\mathrm{q}} \approx \pm 0.25, \tag{5.7}$$

$$\text{syst. error in } \left(2\alpha_8^{\mathrm{q}} - \alpha_5^{\mathrm{q}}\right) \approx \pm 0.13, \tag{5.8}$$

which is of the same order of magnitude as the previous estimate.

Finally one can compare the expanded and unexpanded expressions for R_{M} and R_{F}, which differ at order x^2 (cf. Eqs. (3.5)–(3.8)). By extracting the low-energy constants from least-χ^2 fits to the ratios in Eqs. (3.5) and (3.7) we obtain yet another set of results. For α_5^{q} the central value is larger by 20%, whereas the result for $(2\alpha_8^{\mathrm{q}} - \alpha_5^{\mathrm{q}})$ remains essentially unchanged.

In order to present a synthesis of the various efforts to estimate the uncertainty due to neglecting higher orders, we note that the typical size of this systematic error amounts to ± 0.2 for both α_5^{q} and $(2\alpha_8^{\mathrm{q}} - \alpha_5^{\mathrm{q}})$.

5.3. *Application: the ratio F_{K}/F_π*

The result for α_5^{q} extracted from $R_{\mathrm{F}}^{\mathrm{q}}$ can be used to compute the ratio of the decay constants of the kaon and pion, F_{K}/F_π. In fact, one usually employs the reverse procedure by using the experimental result for F_{K}/F_π to extract the phenomenological value of α_5.

If we assume that contributions proportional to differences in the valence quark masses can be neglected, we can simply use the definition of $R_{\mathrm{F}}^{\mathrm{q}}(x)$ to compute F_{K}/F_π:

$$\frac{F_{\mathrm{K}}}{F_\pi} = \frac{R_{\mathrm{F}}^{\mathrm{q}}(x_{\mathrm{K}})}{R_{\mathrm{F}}^{\mathrm{q}}(x_\pi)} = 1 + y_{\mathrm{ref}}(x_{\mathrm{K}} - x_\pi)\frac{1}{2}\alpha_5^{\mathrm{q}}. \tag{5.9}$$

[4] Instead of the constant 0.025 in Eq. (5.6) the reader may supply an alternative value, depending on whether our estimate is deemed too optimistic or pessimistic.

Here the dimensionless mass parameters $x_{\rm K}$ and x_π are related to the kaon and pion masses by

$$x_{\rm K}\, y_{\rm ref} = \frac{m_{\rm K}^2}{(4\pi F_0)^2} = 0.1782, \tag{5.10}$$

$$x_\pi\, y_{\rm ref} = \frac{m_\pi^2}{(4\pi F_0)^2} = 0.0142, \tag{5.11}$$

where, as in Ref. [25], we have used $m_{\rm K} = 495$ MeV and $m_\pi = 139.6$ MeV. If the estimate for $\alpha_5^{\rm q}$ from Eq. (5.3) is inserted we find

$$\frac{F_{\rm K}}{F_\pi} = 1.081 \pm 0.005 \pm 0.017. \tag{5.12}$$

Here the first error is statistical and the second is the estimated uncertainty in $\alpha_5^{\rm q}$, due to neglecting quadratic terms. The above result is significantly smaller than the experimental value of $F_{\rm K}/F_\pi = 1.22$ [36].

A formula for $F_{\rm K}/F_\pi$ in one-loop quenched ChPT, which also accounts for differences in the valence quark masses, can be derived from Eqs. (18) and (20) of Ref. [37]. The low-energy constant that appears in the one-loop counterterm is the same as in the quenched degenerate case [18,24]. In our notation the full one-loop expression for $F_{\rm K}/F_\pi$ reads

$$\begin{aligned}\frac{F_{\rm K}}{F_\pi} = 1 + {} & y_{\rm ref}(x_{\rm K} - x_\pi)\,\frac{1}{2}\,\alpha_5^{\rm q} \\ & - \frac{1}{2}\left\{\left(\delta - \frac{\alpha_\Phi}{3}\, x_{\rm K}\, y_{\rm ref}\right) - \frac{3\delta\, x_{\rm K} - \alpha_\Phi\, y_{\rm ref} x_\pi (2x_{\rm K} - x_\pi)}{6(x_{\rm K} - x_\pi)}\,\ln\left(\frac{2x_{\rm K} - x_\pi}{x_\pi}\right)\right\}.\end{aligned} \tag{5.13}$$

Note that one recovers Eq. (5.9) when $\delta = \alpha_\Phi = 0$. For the two sets of parameters, Q1 and Q2, the results for $F_{\rm K}/F_\pi$ are evaluated as

$$\frac{F_{\rm K}}{F_\pi} = \begin{cases} 1.125 \pm 0.005 \pm 0.016 \pm 0.007, & \text{Q1}, \\ 1.110 \pm 0.005 \pm 0.017 \pm 0.007, & \text{Q2}, \end{cases} \tag{5.14}$$

where the additional third error is due to the variation of ± 0.02 in the input value for δ. While contributions proportional to differences in the quark masses enhance the result for $F_{\rm K}/F_\pi$ compared with Eq. (5.12), the value is still smaller than experiment by about 10%. Deviations of this order of magnitude are typical of quantities computed in the quenched approximation. This has previously been inferred from calculations of the hadron spectrum [21,33], and the results presented here firmly establish these findings for matrix elements of local currents as well. The fact that $F_{\rm K}/F_\pi$ is typically underestimated in quenched calculations has been observed before [38,39]. Note, however, that our estimates have much smaller uncertainties than those quoted in the other references.

Finally we remark that the enhancement in the estimate of $F_{\rm K}/F_\pi$ due to differences in the quark masses, demonstrates that these effects can be quite significant if the quark mass difference is as large as that between the physical light and strange quarks. By contrast, estimates of these effects based on masses in the region of that of the strange quark tend to be much smaller [25,40].

5.4. Partially quenched ChPT

In addition to our analysis of the quenched version of ChPT we can also tentatively use the expressions for R_{M} and R_{F} which are derived in the partially quenched theory. This essentially serves two purposes. On the one hand we can investigate to what extent the ratios R_X in quenched QCD are described by the formulae of partially quenched ChPT. If a severe mismatch is encountered it will signal that sea-quark effects are not accounted for. On the other hand, by extracting the α_i's using the expressions of partially quenched ChPT but quenched numerical data, we can test how much of the relevant physical information for the low-energy constants in full QCD is encoded in the mass dependence obtained in the quenched approximation. The subsequent calculation of quantities such as the ratio F_{K}/F_π and its comparison with experiment provides a quantitative criterion for this task. In this spirit we have investigated the cases labelled "SS" and "VV" discussed in Section 3.

If we employ the expression for $R_{\mathrm{F}}^{\mathrm{SS}}$, Eq. (3.12), we find that the linearity of the numerical data is incompatible with the additional logarithmic terms contained in the formula. As a consequence an acceptable representation of the data for R_{F} cannot be achieved on the basis of Eq. (3.12). We conclude that the mass dependence of the quenched decay constant is *incompatible* with the chiral behaviour predicted in full QCD!

By contrast, the expression for $R_{\mathrm{M}}^{\mathrm{SS}}$ fits the numerical data very well over almost the entire range in x. However, the disagreement between the data and $R_{\mathrm{F}}^{\mathrm{SS}}$ indicates that the "SS" formulae cannot be applied to the quenched data in any reasonable manner. Therefore, we refrain from quoting an estimate for $(2\alpha_8 - \alpha_5) + 3(2\alpha_6 - \alpha_4)$, even though a good modelling of the data for R_{M} can be achieved.

On the other hand, the expressions for both ratios obtained for the "VV" case do indeed lead to an acceptable representation of the data, at least for $x \lesssim 1$. Quoting only statistical errors, the results for the low-energy constants read

$$\alpha_5 = 0.75 \pm 0.06, \tag{5.15}$$

$$(2\alpha_8 - \alpha_5) = 0.15 \pm 0.05. \tag{5.16}$$

The curves corresponding to these values are shown in Fig. 4(a) and (b). While for $x \lesssim 1$ the curves fit the data quite well, they deviate much more at larger x than the corresponding quenched ones. Compared with the quenched case, the results for the α_i are roughly in the same ball park.

Using the value for α_5 extracted from $R_{\mathrm{F}}^{\mathrm{VV}}$ we can now compute the ratio F_{K}/F_π. Since the low-energy constants in the partially quenched and full theories are the same, we have used the expression derived in full QCD [2]. In our notation it reads

$$\begin{aligned}\frac{F_{\mathrm{K}}}{F_\pi} &= 1 + y_{\mathrm{ref}}(x_{\mathrm{K}} - x_\pi)\frac{1}{2}\alpha_5 \\ &\quad + \frac{y_{\mathrm{ref}}}{4}\Big\{(3x_\pi - 2x_{\mathrm{K}})\ln(x_\pi y_{\mathrm{ref}}) - x_{\mathrm{K}}\ln(x_{\mathrm{K}} y_{\mathrm{ref}}) \\ &\qquad - \frac{1}{2}(4x_{\mathrm{K}} - x_\pi)\ln\left(\frac{4x_{\mathrm{K}} - x_\pi}{3x_\pi}\right)\Big\}.\end{aligned} \tag{5.17}$$

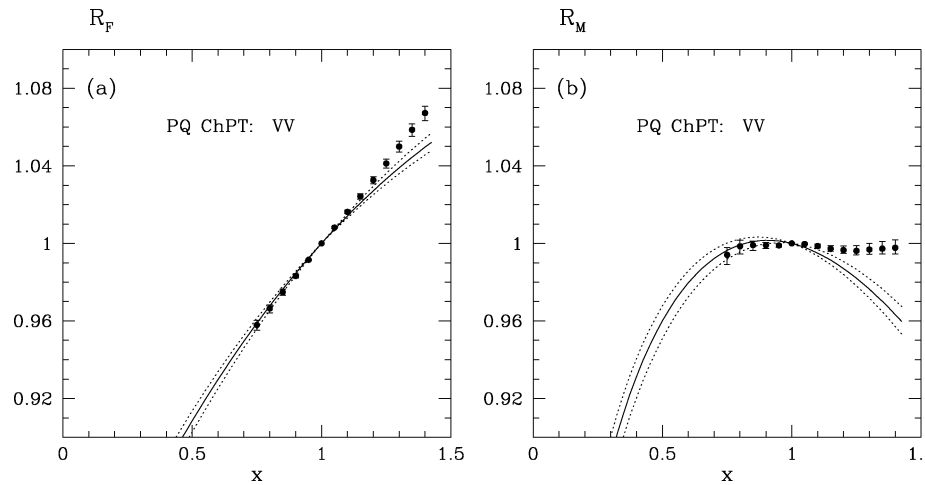

Fig. 4. The "VV" case in partially quenched ChPT. (a): Data for the ratio R_{F} compared with the curve obtained by inserting the low-energy constant of Eq. (5.15); (b): the same for the ratio R_{M} using the low-energy constants of Eq. (5.16). Dotted lines indicate the variation due to the statistical uncertainty in the extraction of the low-energy constants.

After inserting the numerical values for x_{K}, x_π, y_{ref} and α_5 one finds

$$\frac{F_{\mathrm{K}}}{F_\pi} = 1.228 \pm 0.005\,(\mathrm{stat}) \pm 0.016. \tag{5.18}$$

Here the uncertainty of ± 0.016 is due to neglecting higher orders. This result is actually compatible with the experimental value, which is not entirely surprising, since our estimate of $\alpha_5 = 0.75(6)$ agrees quite well with its phenomenological value of 0.5 ± 0.6 quoted in Eq. (2.2). These findings suggest that the valence quark mass dependence of the numerically determined ratios R_X in the region of the strange quark mass is only weakly distorted by neglecting dynamical quarks. The relevant quark mass effects which account for the difference between the quenched result Eq. (5.14) and the experimental value $F_{\mathrm{K}}/F_\pi = 1.22$, appear to be due to the very light up and down quarks in full QCD. Their non-linear effects can be efficiently accounted for by the formulae of partially quenched ChPT.

6. Summary and conclusions

In this paper we have proposed a general method to extract the low-energy constants in effective chiral Lagrangians by studying the mass dependence of suitably defined ratios of matrix elements and matching it to ChPT. The ratios are typically obtained with high statistical precision and can be extrapolated to the continuum limit in a straightforward manner. Thus, the method offers a conceptually clean way to determine the low-energy constants, since it is strictly speaking only in the continuum limit that a comparison of lattice data to ChPT can be performed.

The dimensionless ratios R_X are also interesting in their own right: they can be used to study the scaling behaviour of different fermionic discretizations without having to compute renormalization factors. Furthermore, the effects of dynamical quarks can be isolated unambiguously, since lattice artefacts are under good control.

In this initial study we have presented results for the quenched approximation. The typical value of the absolute statistical error of ± 0.05 in the low-energy constants confirms that the achievable precision is indeed quite high compared with "conventional" phenomenological determinations. The main limitation at present is that results at smaller quark masses are not available. It is therefore not possible to systematically investigate whether there is sufficient overlap between the range of simulated quark masses and the domain of validity of ChPT. As a consequence the present estimated uncertainty of ± 0.2 in the low-energy constants due to higher-order terms are fairly coarse. It is expected, though, that the simulation of smaller quark masses will be feasible within the formulation of QCD with a "twisted" mass term (tmQCD) [41]. In this construction the mass parameter protects against unphysical zero modes of the Dirac operator, which alleviates the problem of exceptional configurations encountered in simulations with Wilson fermions. Initial studies have shown promising results, and it is planned to exploit this method further in the present context.

Returning to the problem of examining the question of whether $m_{\mathrm{u}} = 0$, it is useful to recall that the problem can be solved through a reliable determination of α_8. In the quenched approximation we obtain

$$\alpha_8^{\mathrm{q}} = \begin{cases} 0.67 \pm 0.04\,(\mathrm{stat}) \pm 0.04, & \mathrm{Q1}, \\ 0.50 \pm 0.04\,(\mathrm{stat}) \pm 0.04, & \mathrm{Q2}, \end{cases} \tag{6.1}$$

where the second error is due to the variation in δ, and the additional uncertainty arising from neglecting higher orders is estimated to be ± 0.2. There is *a priori* no reason why the low-energy constant α_8^{q} should be numerically close to its counterpart in the full theory, and hence it would surely be premature to give a full assessment of the problem on the basis of our quenched results. Nevertheless, it is interesting to note that our results for α_8^{q} are quite close to the "standard" value for α_8, Eq. (2.2), which supports a non-vanishing up-quark mass. By contrast, given our data for the ratios R_X it would be very difficult to accommodate a large negative value, which is required for the up-quark to be massless (see Eq. (2.6)).

Finally we wish to add a few general comments on the philosophy of our approach. Provided that the quark masses used in simulations are small enough for the one-loop expressions of ChPT to apply, our procedures altogether avoid chiral extrapolations of lattice results, which are known to be quite difficult to control. The example of the computation of F_{K}/F_π shows that the problem can be separated in two parts. The information which involves quark masses near the chiral limit can be extracted safely in ChPT, whereas the mass dependence for masses in the region somewhat below the strange quark mass can be adequately studied in lattice QCD. The latter part is the additional theoretical input needed to determine some of the low-energy constants, which are not accessible from chiral symmetry considerations alone. In short, our method amounts to

exploiting the complementary character of ChPT and lattice QCD. The applicability of ChPT itself can be tested once quark masses somewhat smaller than those in our present work become accessible.

The next step is the application of our method to the case of dynamical quarks. Here the relevant formulae that will be required are listed in Appendix A. Simulations using either the O(a) improved Wilson action for $N_{\rm f} = 2$ flavours of dynamical quarks [42] or other improvement schemes [43] have already been performed [44–47]. Whereas an analysis of those results will be able to treat the two-flavour case, the extension to the physically most interesting case of $N_{\rm f} = 3$ flavours will require a significant amount of additional simulations. It is also worth investigating applications to the case of non-degenerate sea quarks and to try to determine the low-energy constant α_7 [13]. However, the main message of this paper is the following. In order to settle the question of whether $m_{\rm u} = 0$ one does not even require the same level of accuracy as that of the quenched results presented here. A satisfactory analysis of the problem in the case of three degenerate flavours is therefore quite a realistic prospect.

Acknowledgements

We are indebted to Gilberto Colangelo and Elisabetta Pallante for essential clarifications concerning the application of quenched ChPT. We are also grateful to Ruedi Burkhalter for useful correspondence. This work is part of the ALPHA Collaboration research programme. We thank DESY for allocating computer time on the APE/Quadrics computers at DESY-Zeuthen and the staff of the computer centre at Zeuthen for their support.

Appendix A. Partially quenched ChPT — the general case

In this appendix we list the expressions for $R_{\rm M}$ and $R_{\rm F}$, as well as for $\Delta R_{\rm M}$ and $\Delta R_{\rm F}$, in partially quenched QCD. In particular we discuss all possibilities to define the x-dependence of R_X, allowing also for non-degenerate valence quarks.

We start by considering the expressions in Eqs. (2.7)–(2.9). At the reference point we require all quark masses to coincide with $m_{\rm ref}$ (cf. Eq. (3.9)). Two cases, labelled "SS" and "VV" have already been discussed in Section 3.2. In addition to "VV", one can also study the x-dependence by varying the sea quark mass m_S for fixed, degenerate valence quarks:

$$\text{SS2:}\quad m_1 = m_2 = m_{\rm ref}, \quad m_S = x m_{\rm ref}. \tag{A.1}$$

For non-degenerate valence quarks one may define

$$\text{VS1:}\quad m_1 = x m_{\rm ref}, \quad m_2 = m_S = m_{\rm ref}, \tag{A.2}$$

$$\text{VS2:}\quad m_1 = m_{\rm ref}, \quad m_2 = m_S = x m_{\rm ref}. \tag{A.3}$$

In order to list the expressions for $R_{\rm M}$ and $R_{\rm F}$ for all cases SS, VV, ..., VS2 it is convenient to introduce the general parameterization

Table 1
The functions ρ and λ for the ratio $R_{\mathrm{M}}(x)$

	$\rho_{\mathrm{M}}(x; y_{\mathrm{ref}})$	$\lambda_{\mathrm{M}}(\alpha)$
SS	$x\ln x + (x-1)\ln y_{\mathrm{ref}}$	$(2\alpha_8 - \alpha_5) + N_{\mathrm{f}}(2\alpha_6 - \alpha_4)$
VV	$(2x-1)\ln x + 2(x-1)\ln y_{\mathrm{ref}}$	$(2\alpha_8 - \alpha_5) + \frac{1}{N_{\mathrm{f}}}$
SS2	$-(x-1)\ln y_{\mathrm{ref}}$	$N_{\mathrm{f}}(2\alpha_6 - \alpha_4) - \frac{1}{N_{\mathrm{f}}}$
VS1	$x\ln x + (x-1)\ln y_{\mathrm{ref}}$	$\frac{1}{2}(2\alpha_8 - \alpha_5)$
VS2	0	$\frac{1}{2}(2\alpha_8 - \alpha_5) + N_{\mathrm{f}}(2\alpha_6 - \alpha_4)$

Table 2
The functions ρ and λ for the ratio $R_{\mathrm{F}}(x)$

	$\rho_{\mathrm{F}}(x; y_{\mathrm{ref}})$	$\lambda_{\mathrm{F}}(\alpha)$
SS	$\frac{1}{2}\Big(x\ln x + (x-1)\ln y_{\mathrm{ref}}\Big)$	$-\frac{1}{2}(\alpha_5 + N_{\mathrm{f}}\alpha_4)$
VV	$\frac{1}{2}\Big(\frac{x+1}{2}\ln\frac{x+1}{2} + \frac{x-1}{2}\ln y_{\mathrm{ref}}\Big)$	$-\frac{1}{2}\alpha_5$
SS2	$\frac{1}{2}\Big(\frac{x+1}{2}\ln\frac{x+1}{2} + \frac{x-1}{2}\ln y_{\mathrm{ref}}\Big)$	$-\frac{N_{\mathrm{f}}}{2}\alpha_4$
VS1	$\frac{1}{4}\Big(\frac{x+1}{2}\ln\frac{x+1}{2} + \frac{x-1}{2}\ln y_{\mathrm{ref}} + \frac{1}{N_{\mathrm{f}}^2}\ln x\Big)$	$-\frac{1}{4}\Big(\alpha_5 + \frac{1}{N_{\mathrm{f}}}\Big)$
VS2	$\frac{1}{4}\Big(\frac{x+1}{2}\ln\frac{x+1}{2} + \frac{3(x-1)}{2}\ln y_{\mathrm{ref}} + \frac{N_{\mathrm{f}}^2-1}{N_{\mathrm{f}}^2}x\ln x\Big)$	$-\frac{1}{4}\alpha_5 - \frac{N_{\mathrm{f}}}{2}\alpha_4 + \frac{1}{4N_{\mathrm{f}}}$

$$R_{\mathrm{M}}(x) = 1 - \frac{y_{\mathrm{ref}}}{N_{\mathrm{f}}}\rho_{\mathrm{M}}(x; y_{\mathrm{ref}}) - y_{\mathrm{ref}}(x-1)\lambda_{\mathrm{M}}(\alpha), \tag{A.4}$$

$$R_{\mathrm{F}}(x) = 1 - N_{\mathrm{f}}\, y_{\mathrm{ref}}\, \rho_{\mathrm{F}}(x; y_{\mathrm{ref}}) - y_{\mathrm{ref}}(x-1)\lambda_{\mathrm{F}}(\alpha). \tag{A.5}$$

Here, ρ_{M} and ρ_{F} are functions of x and y_{ref}, λ_{M} and λ_{F} denote linear combinations of the low-energy constants, and $r(x)$ is a rational function of x. The expressions for ρ and λ are shown in Tables 1 and 2, respectively.

Using the functions ρ_X and λ_X, $X = \mathrm{M}, \mathrm{F}$, it is now quite easy to solve for particular linear combinations of low-energy constants by considering the differences $\Delta R_X(x_1, x_2)$ introduced in Eq. (3.16). With these definitions the linear combinations of low-energy constants denoted by $\lambda_X(\alpha)$, $X = \mathrm{M}, \mathrm{F}$ are simply given by

$$\lambda_{\mathrm{M}}(\alpha) = -\frac{\Delta R_{\mathrm{M}}(x_1, x_2) + \frac{y_{\mathrm{ref}}}{N_{\mathrm{f}}}(\rho_{\mathrm{M}}(x_1, y_{\mathrm{ref}}) - \rho_{\mathrm{M}}(x_2, y_{\mathrm{ref}}))}{y_{\mathrm{ref}}(x_1 - x_2)}, \tag{A.6}$$

$$\lambda_{\mathrm{F}}(\alpha) = -\frac{\Delta R_{\mathrm{F}}(x_1, x_2) + y_{\mathrm{ref}}\, N_{\mathrm{f}}(\rho_{\mathrm{F}}(x_1, y_{\mathrm{ref}}) - \rho_{\mathrm{F}}(x_2, y_{\mathrm{ref}}))}{y_{\mathrm{ref}}(x_1 - x_2)}. \tag{A.7}$$

By evaluating the right-hand side, using numerical data for ΔR_X, one can easily solve for the desired combination of α_i's.

Appendix B. Choices for δ and α_Φ

In this appendix we motivate our choices for the parameters δ and α_Φ specified in Eqs. (5.1) and (5.2). Here we will closely follow the analysis presented by the CP-PACS Collaboration [21], i.e., we consider the ratio

$$s = \frac{m_{\rm PS}^2(m_1,m_2)}{m_1+m_2}\cdot\frac{2m_1}{m_{\rm PS}^2(m_1,m_1)} \times \frac{m_{\rm PS}^2(m_1,m_2)}{m_1+m_2}\cdot\frac{2m_2}{m_{\rm PS}^2(m_2,m_2)}, \tag{B.1}$$

where the arguments in $m_{\rm PS}^2$ have been included in order to distinguish between degenerate and non-degenerate mesons. By inserting the expressions for $m_{\rm PS}^2$ in quenched ChPT for degenerate and non-degenerate quarks (cf. Eq. (9) in [16]) one obtains after expanding the denominator[5]

$$\begin{aligned} s = 1 &+ \delta\left(2 - \frac{y_{11}+y_{22}}{y_{11}-y_{22}}\ln\frac{y_{11}}{y_{22}}\right) \\ &+ \frac{\alpha_\Phi}{3}\left(-(y_{11}+y_{22}) + 2y_{11}\frac{y_{22}}{y_{11}-y_{22}}\ln\frac{y_{11}}{y_{22}}\right). \end{aligned} \tag{B.2}$$

In Ref. [21] the quantity t was defined as

$$t = 2 - \frac{y_{11}+y_{22}}{y_{11}-y_{22}}\ln\frac{y_{11}}{y_{22}}. \tag{B.3}$$

For $\alpha_\Phi = 0$ Eq. (B.2) reduces to a simple, linear relation between s and t:

$$s = 1 + \delta\cdot t, \tag{B.4}$$

with the slope given by δ. By plotting the numerically determined values for the ratio s against t for $\alpha_\Phi = 0$, CP-PACS concluded that all their data were enclosed within the "wedge" defined by $\delta = 0.08$–0.12. This wedge is represented in Fig. 5 by the solid lines.

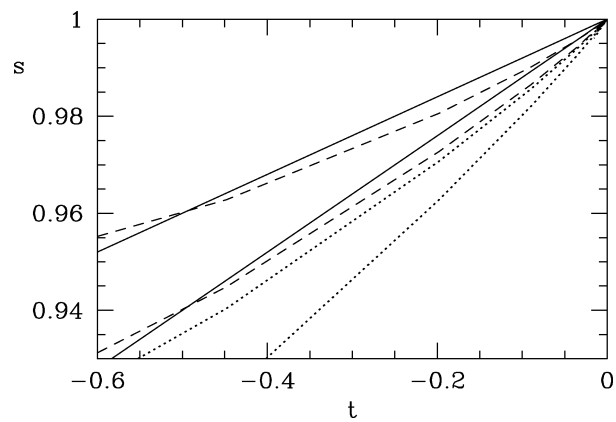

Fig. 5. The "wedges" defined through Eq. (B.2) for different values of δ and α_Φ as explained in the text.

[5] Note that the one-loop counterterms drop out in the expanded version of s.

So far the parameter α_Φ has not been considered in this kind of analysis. [6] We are now going to argue that a value of $\alpha_\Phi \approx 0.5$, as suggested by Sharpe in [23], is only compatible with the CP-PACS data enclosed by the solid wedge, if δ is chosen in the range 0.03–0.07. To this end we identify $m_1 = m_s$, so that $y_{11} = 0.343$. The mass ratio y_{11}/y_{22} is then varied between 1 and 24.4, where the latter number is the value of $2m_s/(m_u + m_d)$ computed in standard ChPT [48]. For $\delta = 0.08-0.12$, $\alpha_\Phi = 0$ one thus recovers the wedge denoted by the solid line in Fig. 5, which encloses the CP-PACS data.

If one combines $\delta = 0.08$–0.12 with the independent estimate of $\alpha_\Phi = 0.5$ from [23] one obtains instead the wedge defined by the dotted lines, which is clearly incompatible with CP-PACS's numerical data. Agreement can only be restored if δ is lowered. The dashed curves, which correspond to $\delta = 0.03$–0.07, $\alpha_\Phi = 0.5$, are again consistent with the wedge defined by the solid lines. These observations lead us to consider the two sets of parameters as specified in Eqs. (5.1) and (5.2).

References

[1] J. Gasser, H. Leutwyler, Ann. Phys. 158 (1984) 142.
[2] J. Gasser, H. Leutwyler, Nucl. Phys. B 250 (1985) 465.
[3] J. Bijnens, G. Ecker, J. Gasser, hep-ph/9411232.
[4] D.B. Kaplan, A.V. Manohar, Phys. Rev. Lett. 56 (1986) 2004.
[5] H. Leutwyler, Nucl. Phys. B 337 (1990) 108.
[6] H. Leutwyler, hep-ph/9609465.
[7] A.G. Cohen, D.B. Kaplan, A.E. Nelson, JHEP 11 (1999) 027, hep-lat/9909091.
[8] J. Bijnens, F. Cornet, Nucl. Phys. B 296 (1988) 557.
[9] J. Bijnens, Nucl. Phys. B 337 (1990) 635.
[10] C. Riggenbach, J. Gasser, J.F. Donoghue, B.R. Holstein, Phys. Rev. D 43 (1991) 127.
[11] D. Babusci et al., Phys. Lett. B 277 (1992) 158.
[12] S. Sharpe, N. Shoresh, Nucl. Phys. B (Proc. Suppl.) 83–84 (2000) 968, hep-lat/9909090.
[13] S. Sharpe, N. Shoresh, hep-lat/0006017.
[14] S.R. Sharpe, Phys. Rev. D 56 (1997) 7052, hep-lat/9707018.
[15] M.F.L. Golterman, K.C. Leung, Phys. Rev. D 57 (1998) 5703, hep-lat/9711033.
[16] C.W. Bernard, M.F.L. Golterman, Phys. Rev. D 46 (1992) 853, hep-lat/9204007.
[17] S.R. Sharpe, Phys. Rev. D 46 (1992) 3146, hep-lat/9205020.
[18] G. Colangelo, E. Pallante, Nucl. Phys. B 520 (1998) 433, hep-lat/9708005.
[19] Y. Kuramashi, M. Fukugita, H. Mino, M. Okawa, A. Ukawa, Phys. Rev. Lett. 72 (1994) 3448.
[20] T. Bhattacharya, R. Gupta, Phys. Rev. D 54 (1996) 1155, hep-lat/9510044.
[21] CP-PACS Collaboration, S. Aoki et al., Phys. Rev. Lett. 84 (2000) 238, hep-lat/9904012.
[22] W. Bardeen, A. Duncan, E. Eichten, H. Thacker, Nucl. Phys. B (Proc. Suppl.) 83–84 (2000) 215, hep-lat/9909128.
[23] S.R. Sharpe, Nucl. Phys. B (Proc. Suppl.) 53 (1997) 181, hep-lat/9609029.
[24] G. Colangelo, E. Pallante, private communication.
[25] ALPHA & UKQCD Collaborations, J. Garden, J. Heitger, R. Sommer, H. Wittig, Nucl. Phys. B 571 (2000) 237, hep-lat/9906013.
[26] S. Sint, P. Weisz, Nucl. Phys. B 502 (1997) 251, hep-lat/9704001.

[6] Terms proportional to α_Φ were also neglected in Ref. [22], where $\delta \approx 0.08$ was quoted.

[27] M. Lüscher, S. Sint, R. Sommer, P. Weisz, U. Wolff, Nucl. Phys. B 491 (1997) 323, hep-lat/9609035.
[28] W. Bardeen, A. Duncan, E. Eichten, G. Hockney, H. Thacker, Phys. Rev. D 57 (1998) 1633, hep-lat/9705008.
[29] ALPHA Collaboration, M. Guagnelli, J. Heitger, R. Sommer, H. Wittig, Nucl. Phys. B 560 (1999) 465, hep-lat/9903040.
[30] B. Sheikholeslami, R. Wohlert, Nucl. Phys. B 259 (1985) 572.
[31] M. Lüscher, S. Sint, R. Sommer, P. Weisz, Nucl. Phys. B 478 (1996) 365, hep-lat/9605038.
[32] B. Efron, SIAM Review 21 (1979) 460.
[33] UKQCD Collaboration, K.C. Bowler et al., Phys. Rev. D 62 (2000) 054506, hep-lat/9910022.
[34] R. Sommer, Nucl. Phys. B 411 (1994) 839, hep-lat/9310022.
[35] ALPHA Collaboration, M. Guagnelli, R. Sommer, H. Wittig, Nucl. Phys. B 535 (1998) 389, hep-lat/9806005.
[36] C. Caso et al., Eur. Phys. J. C 3 (1998) 1.
[37] M.F.L. Golterman, K.C. Leung, Phys. Rev. D 56 (1997) 2950, hep-lat/9702015.
[38] F. Butler, H. Chen, J. Sexton, A. Vaccarino, D. Weingarten, Nucl. Phys. B 421 (1994) 217, hep-lat/9310009.
[39] CP-PACS Collaboration, R. Burkhalter et al., Nucl. Phys. B (Proc. Suppl.) 73 (1999) 3, hep-lat/9810043.
[40] UKQCD Collaboration, C.R. Allton et al., Phys. Rev. D 49 (1994) 474, hep-lat/9309002.
[41] R. Frezzotti, P.A. Grassi, S. Sint, P. Weisz, Nucl. Phys. B (Proc. Suppl.) 83–84 (2000) 941, hep-lat/9909003.
[42] ALPHA Collaboration, K. Jansen, R. Sommer, Nucl. Phys. B 530 (1998) 185, hep-lat/9803017.
[43] Y. Iwasaki, Nucl. Phys. B 258 (1985) 141; Tsukuba Preprint UTHEP-118, 1983.
[44] UKQCD Collaboration, C.R. Allton et al., Phys. Rev. D 60 (1999) 034507, hep-lat/9808016.
[45] UKQCD Collaboration, J. Garden, Nucl. Phys. B (Proc. Suppl.) 83–84 (2000) 165, hep-lat/9909066.
[46] CP-PACS Collaboration, S. Aoki et al., Phys. Rev. D 60 (1999) 114508, hep-lat/9902018.
[47] CP-PACS Collaboration, A. Ali Khan et al., Nucl. Phys. B (Proc. Suppl.) 83–84 (2000) 176, hep-lat/9909050.
[48] H. Leutwyler, Phys. Lett. B 378 (1996) 313, hep-ph/9602366.

H

Non-perturbative renormalization of the static axial current in quenched QCD

Nucl. Phys. B669 (2003) 173-206

Available online at www.sciencedirect.com
SCIENCE DIRECT®
Nuclear Physics B 669 (2003) 173–206
NUCLEAR PHYSICS B
www.elsevier.com/locate/npe

Non-perturbative renormalization of the static axial current in quenched QCD

ALPHA Collaboration

Jochen Heitger [a], Martin Kurth [b], Rainer Sommer [c]

[a] *Westfälische Wilhelms-Universität Münster, Institut für Theoretische Physik, Wilhelm-Klemm-Strasse 9, D-48149 Münster, Germany*
[b] *University of Southampton, Department of Physics and Astronomy, Highfield, Southampton SO17 1BJ, United Kingdom*
[c] *Deutsches Elektronen-Synchrotron DESY, Zeuthen, Platanenallee 6, D-15738 Zeuthen, Germany*

Received 27 February 2003; accepted 23 June 2003

Abstract

We non-perturbatively calculate the scale dependence of the static axial current in the Schrödinger functional scheme by means of a recursive finite-size scaling technique, taking the continuum limit in each step. The bare current in the O(a) improved theory as well as in the original Wilson regularization is thus connected to the renormalization group invariant one. The latter may then be related to the current at the B-scale defined such that its matrix elements differ from the physical (QCD) ones by O($1/M$). At present, a (probably small) perturbative uncertainty enters in this step. As an application, we renormalize existing unimproved data on $F_{\mathrm{B}}^{\mathrm{bare}}$ and extrapolate to the continuum limit. We also study an interesting function $h(d/L, u)$ derived from the Schrödinger functional amplitude describing the propagation of a static quark–antiquark pair.

PACS: 11.15.Ha; 12.15.Hh; 12.38.Bx; 12.38.Gc; 12.39.Hg; 13.20.He; 14.65.Fy

Keywords: Lattice QCD; Heavy quark effective theory; Static approximation; Non-perturbative renormalization; Schrödinger functional; Renormalization group invariant

E-mail address: heitger@uni-muenster.de (J. Heitger).

0550-3213/$ – see front matter
doi:10.1016/S0550-3213(03)00552-2

1. Introduction

Since the decay constant $F_{\rm B}$, governing the leptonic decay of a B-meson, is an essential element in the quantitative analysis of the unitarity triangle, many lattice QCD investigations have worked towards its determination. However, with its large mass, the b-quark still escapes a direct numerical treatment [1] and effective theories have to be used to separate the large mass scale from the low-energy bound-state dynamics. (As an exception to this rule, it has recently been demonstrated that also finite-volume methods on lattices with a large number of points represent a possible alternative [2,3].)

The most natural and theoretically appealing effective theory is the *static approximation* [4]. It describes the large-mass limit of the theory and is the starting point for a $1/m$-expansion, the heavy quark effective theory. Yet the problems of this framework have been twofold in the past. (i) The renormalization properties of the static theory are different, i.e., the renormalization constant $Z_{\rm A}^{\rm stat}$ of the axial current in $(A_{\rm R}^{\rm stat})_0 = Z_{\rm A}^{\rm stat}(\mu)\bar{\psi}_{\rm d}\gamma_0\gamma_5\psi_{\rm b}^{\rm stat}$ becomes scale (μ) dependent, thereby entailing an additional uncertainty, and (ii) Monte Carlo computations of the matrix element itself are difficult. For these reasons, after a significant initial effort [5–12], the computation of $F_{\rm B}$ in the static approximation has received little attention in the recent past.

In the present work, we solve (i) by computing the renormalization factor that relates the bare operator in lattice regularization to the *renormalization group invariant* (*RGI*) *operator*. Denoting its matrix element by $\Phi_{\rm RGI}^{\rm stat}$, one then has a relation

$$F_{\rm B}\sqrt{m_{\rm B}} = C_{\rm PS}(M_{\rm b}/\Lambda_{\overline{\rm MS}})\Phi_{\rm RGI}^{\rm stat} + {\rm O}(1/M_{\rm b}) \tag{1.1}$$

with a function $C_{\rm PS}$ of the renormalization group invariant b-quark mass $M_{\rm b}$ in units of the Λ-parameter. It is scale independent, but in practice it is obtained perturbatively and an uncertainty due to perturbation theory remains, see Section 5. The important task of a lattice computation of the B-meson decay constant in the static approximation is to compute $\Phi_{\rm RGI}^{\rm stat}$.

Our strategy to arrive at $\Phi_{\rm RGI}^{\rm stat}$ from the bare matrix element follows the one used by the ALPHA Collaboration for the renormalization group invariant quark mass [13]. In this approach, an intermediate finite-volume renormalization scheme is used to follow the scale evolution non-perturbatively to high energies (O(100 GeV)), where then perturbation theory can safely be used to connect to the renormalization group invariants. For a more detailed explanation of the overall strategy we refer to Ref. [14] and for a preliminary report on our work to Refs. [15,16].

The present paper is organized as follows. In Section 2 we discuss our intermediate renormalization scheme, formulated in the Schrödinger functional (SF). It is based on the renormalization condition introduced in [17], but a modification has been necessary to achieve good statistical precision. Section 3 contains the numerical determination of the scale dependence of the current in the SF scheme which is independent of the lattice formulation. We also relate the current renormalized at some proper low scale to the RGI current. Section 4 gives our results for the lattice formulation dependent values of the Z-factor at this low scale. In Section 5 we then discuss Eq. (1.1) and explain in detail how our results are to be used. As an example we obtain $F_{\rm B_s}^{\rm stat}$ from published numbers of the

bare matrix element. We finish with a brief discussion of the results in Section 6. Details of the numerical and perturbative calculations are described in Appendices A–C.

2. Intermediate renormalization scheme

In this section we introduce our intermediate renormalization scheme. For reasons to be explained below, it differs from the one originally introduced in Ref. [17]. The perturbative calculations of Ref. [17] are extended to the new scheme in Appendix B.

We choose a mass-independent renormalization scheme, leading to simple renormalization group equations. The scheme is defined using the Schrödinger functional (SF) [18,19], i.e., the QCD partition function $\mathcal{Z} = \int_{T\times L^3} \mathrm{D}[A, \bar{\psi}, \psi]\, \mathrm{e}^{-S[A,\bar{\psi},\psi]}$ on a $T \times L^3$ cylinder in Euclidean space, where periodic boundary conditions in the spatial directions of length L and Dirichlet boundary conditions at times $x_0 = 0, T$ are imposed on the gluon and quark fields.[1] Their exact form can be found in Ref. [21]. Moreover, we set $T = L$ throughout, and the renormalization scale μ is identified with the inverse box extension, $1/L$. Such a finite-volume renormalization scheme is chosen, since it allows to study the scale dependence in the *continuum limit* for a large range of μ [13,22–24]. We can then relate the quantities renormalized at some low scale μ to the RGI quantities. Reviews of the strategy are found in [14,25,26], and for a more detailed description the reader should consult Ref. [13] which we will follow quite closely.

As detailed in [17], we consider the SF with vanishing boundary gauge fields and $\theta = 0.5$. These settings are identical to those used for the quark mass renormalization in [13] and were motivated by meeting the criteria of good statistical precision of the Monte Carlo results, well-behaved perturbative expansions of the renormalization group functions and minimization of lattice artifacts [27]. Static quarks are included as discussed in Ref. [17], and we use the notation of that reference. Throughout most of this paper, we formally stay in the framework of continuum QCD; some notation and basic formulae of the lattice regularized theory, in which the following expressions receive a precise meaning, are collected in Appendix A.

In contrast to the relativistic current, there is no axial Ward identity which protects the renormalized static-light axial vector current,

$$\big(A_{\mathrm{R}}^{\mathrm{stat}}\big)_0(x) = Z_{\mathrm{A}}^{\mathrm{stat}} \bar{\psi}_{\mathrm{l}}(x)\gamma_0\gamma_5\psi_{\mathrm{h}}(x), \tag{2.1}$$

from a scale dependence. Its scale evolution is governed by the renormalization group equation

$$\mu\,\frac{\partial \Phi}{\partial \mu} = \gamma(\bar{g})\Phi, \tag{2.2}$$

where

$$\Phi \equiv \Phi^{\mathrm{stat}} = \langle \mathrm{f}|\big(A_{\mathrm{R}}^{\mathrm{stat}}\big)_0|\mathrm{i}\rangle \tag{2.3}$$

[1] The spatial boundary conditions of the quark fields are only periodic up to a global phase θ [20], an additional 'kinematical' parameter.

is an arbitrary matrix element of the renormalized static current. The renormalization group function γ, the anomalous dimension, has a perturbative expansion

$$\gamma(\bar{g}) \overset{\bar{g}\to 0}{\sim} -\bar{g}^2\{\gamma_0 + \gamma_1\bar{g}^2 + \gamma_2\bar{g}^4 + \mathrm{O}(\bar{g}^6)\} \tag{2.4}$$

with a universal leading coefficient [28,29],

$$\gamma_0 = -\frac{1}{4\pi^2}, \tag{2.5}$$

and $\gamma_1, \gamma_2, \ldots$ depending on the chosen renormalization scheme.

Non-perturbatively, one computes the change of Φ under finite changes of the renormalization scale. For a scale factor of two, the induced change defines the *step scaling function*,

$$\sigma_{\mathrm{A}}^{\mathrm{stat}}(u) = \Phi(\mu/2)/\Phi(\mu) = Z_{\mathrm{A}}^{\mathrm{stat}}(2L)/Z_{\mathrm{A}}^{\mathrm{stat}}(L), \tag{2.6}$$

whose argument $u \equiv \bar{g}^2(L)$ is taken to be exactly the coupling defined in [24], and as always in the SF we have $\mu = 1/L$.

2.1. The old scheme

In Ref. [17], a normalization condition was formulated in terms of suitable correlation functions defined in the SF. It reads

$$Z_{\mathrm{A}}^{\mathrm{stat}}(L)X(L) = X^{(0)}(L) \quad \text{at vanishing quark mass,} \tag{2.7}$$

with

$$X(L) = \frac{f_{\mathrm{A}}^{\mathrm{stat}}(L/2)}{\sqrt{f_1^{\mathrm{stat}}}} \tag{2.8}$$

and $X^{(0)}(L)$ the tree-level value of $X(L)$. Here, $f_{\mathrm{A}}^{\mathrm{stat}}$ is a correlation function between a static-light pseudoscalar boundary source and A_0^{stat} in the bulk, and f_1^{stat} denotes the correlator between two such boundary sources at $x_0 = 0$ and $x_0 = T$:

$$f_{\mathrm{A}}^{\mathrm{stat}}(x_0) = -\frac{1}{2}\int \mathrm{d}^3\boldsymbol{y}\,\mathrm{d}^3\boldsymbol{z}\,\big\langle A_0^{\mathrm{stat}}(x)\bar{\zeta}_{\mathrm{h}}(\boldsymbol{y})\gamma_5\zeta_{\mathrm{l}}(\boldsymbol{z})\big\rangle, \tag{2.9}$$

$$f_1^{\mathrm{stat}} = -\frac{1}{2L^6}\int \mathrm{d}^3\boldsymbol{u}\,\mathrm{d}^3\boldsymbol{v}\,\mathrm{d}^3\boldsymbol{y}\,\mathrm{d}^3\boldsymbol{z}\,\big\langle\bar{\zeta}_{\mathrm{l}}'(\boldsymbol{u})\gamma_5\zeta_{\mathrm{h}}'(\boldsymbol{v})\bar{\zeta}_{\mathrm{h}}(\boldsymbol{y})\gamma_5\zeta_{\mathrm{l}}(\boldsymbol{z})\big\rangle. \tag{2.10}$$

(For the proper definition of the 'boundary quark and antiquark fields' $\zeta, \bar{\zeta}$ we refer to Refs. [17,21].) The two correlators are schematically depicted in Fig. 1, and their explicit form on the lattice is given in Eqs. (A.10) and (A.13) of Appendix A.1. In the ratio (2.8) both the multiplicative renormalization of the boundary quark fields and the mass counterterm of the static field cancel.

We now have to point out a drawback of this scheme that only becomes evident, when it is implemented numerically. Namely, the lattice step scaling function $\Sigma_{\mathrm{A}}^{\mathrm{stat}}(u, a/L)$ (cf. Eq. (A.20) for its definition), computed by means of Monte Carlo simulations, has

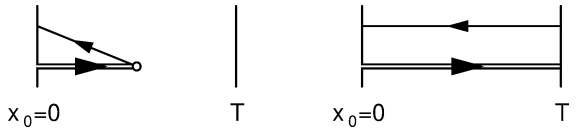

Fig. 1. Sketch of the correlation functions $f_{\mathrm{A}}^{\mathrm{stat}}(x_0)$ (left) and f_1^{stat} (right). The single and double lines represent light (i.e., relativistic) and static quark propagators, respectively.

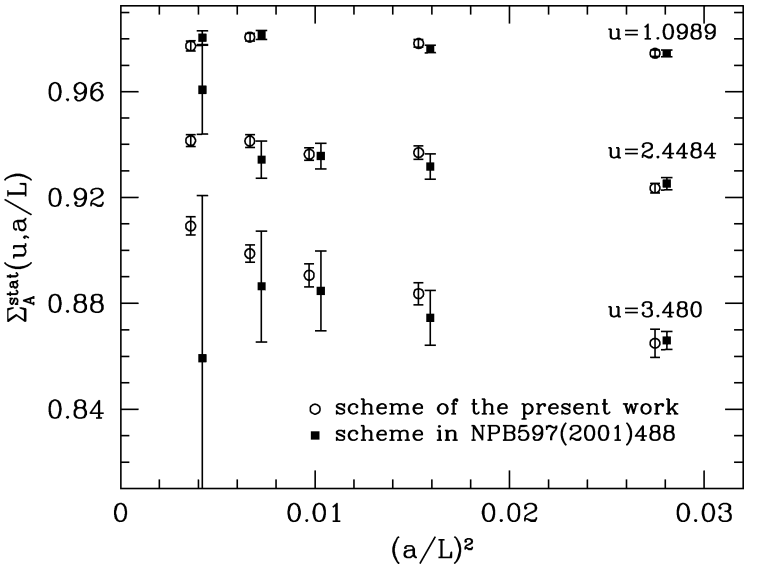

Fig. 2. Comparison of the numerical precision of the lattice step scaling function computed in the scheme of Ref. [17] with the new one introduced in Section 2.3, which will be used in the rest of this paper. (The symbols are slightly displaced for better readability.) The statistics of both computations is the same.

large statistical errors at $u \approx 1.5$ and larger. In particular, these errors grow with L/a. This can be inferred from the results tabulated in Appendix A.2 and is illustrated for three representative coupling values in Fig. 2. For $L/a = 12, 16$ (which amounts to also calculate $Z_{\mathrm{A}}^{\mathrm{stat}}$ for $2L/a = 24, 32$), already around $u \approx 1.5$ a precise determination of $\Sigma_{\mathrm{A}}^{\mathrm{stat}}(u, a/L)$ with a reasonable computational effort becomes impossible. The reason for this lies in the boundary correlator f_1^{stat} being part of the renormalization condition Eq. (2.7): it contains the static quark propagating over a distance $T = L$. Thus f_1^{stat} falls roughly like $\mathrm{e}^{-e_1 g_0^2 T/a}$ with $e_1 = \frac{1}{12\pi^2} \times 19.95$ [30] the leading coefficient of the self-energy of a static quark. On the other hand, the statistical errors fall much more slowly, leaving us with an exponential degradation of the signal-to-noise ratio.

To circumvent this problem, we now introduce a slightly modified renormalization scheme. (Therefore, for the rest of the paper, the scheme of Ref. [17]—if mentioned at all—will only be referred to by labeling the corresponding quantities with an additional 'old', e.g., $Z_{\mathrm{A}}^{\mathrm{stat}} \to Z_{\mathrm{A,old}}^{\mathrm{stat}}$.) The general idea is to replace f_1^{stat} containing a static and a light quark by two boundary-to-boundary correlation functions. One of them contains a

light quark–antiquark pair, the other a static quark–antiquark pair. Both can be computed with small statistical errors, the latter because the variance reduction method of Ref. [31] can be applied. Since the static-static boundary correlator has not been studied before, we discuss it in some detail.

2.2. The static-static boundary correlator f_1^{hh}

We define

$$f_1^{\mathrm{hh}}(x_3) \equiv -\frac{1}{2L^2}\int \mathrm{d}x_1\,\mathrm{d}x_2\,\mathrm{d}^3\boldsymbol{y}\,\mathrm{d}^3\boldsymbol{z}\,\big\langle \bar{\zeta}'_{\mathrm{h}}(\boldsymbol{x})\gamma_5\zeta'_{\mathrm{h}}(\boldsymbol{0})\bar{\zeta}_{\mathrm{h}}(\boldsymbol{y})\gamma_5\zeta_{\mathrm{h}}(\boldsymbol{z})\big\rangle, \tag{2.11}$$

represented graphically in the left part of Fig. 3. After integrating out the static quark fields, f_1^{hh} becomes the (trace of the) product of a timelike Wilson line and the complex conjugate one from boundary to boundary (see Eq. (B.1)). They are separated by $\boldsymbol{x}$ in space. This quantity is integrated over x_1, x_2 but retains a dependence on x_3. In the following we take $d \equiv |x_3|$ as its argument, where the periodicity of the system in the space directions restricts it to $0 \leqslant d \leqslant L/2$.

Upon renormalization the correlation function f_1^{hh} becomes

$$\big(f_1^{\mathrm{hh}}\big)_{\mathrm{R}}(d) = \mathrm{e}^{-2\delta m\times L}(Z_{\mathrm{h}})^4 f_1^{\mathrm{hh}}(d),$$

where Z_{h} is the wave function renormalization constant of a static boundary quark field and δm the linearly divergent static mass counterterm. Therefore, to study the properties of f_1^{hh} further, we form the finite ratio

$$h(d/L,u) \equiv \frac{(f_1^{\mathrm{hh}})_{\mathrm{R}}(d)}{(f_1^{\mathrm{hh}})_{\mathrm{R}}(L/2)} = \frac{f_1^{\mathrm{hh}}(d)}{f_1^{\mathrm{hh}}(L/2)} \quad \text{at } \bar{g}^2(L) = u. \tag{2.12}$$

Considered on the lattice, it has a continuum limit. As outlined in Appendix B.1, the one-loop coefficient $h^{(1)}(d/L)$ of the perturbative expansion

$$h(d/L,u) = 1 + u\,h^{(1)}(d/L) + u^2 h^{(2)}(d/L) + \cdots \tag{2.13}$$

is given by

$$h^{(1)}(d/L) = \frac{2}{3}\left(\frac{1}{2} - \frac{d}{L}\right)^2. \tag{2.14}$$

Remarkably, this form holds exactly on the lattice without any a/L-dependence. Some insight why this is so is presented in the appendix as well. At two-loop accuracy, we do not expect exact a-independence any more, but still one may hope that the favorable kinematics keep lattice artifacts small.

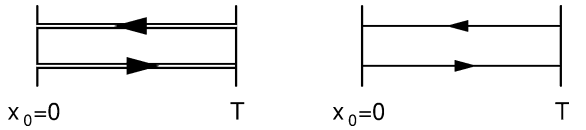

Fig. 3. The correlation functions $f_1^{\mathrm{hh}}(x_3)$ (left) and f_1 (right). The notation is the same as in Fig. 1.

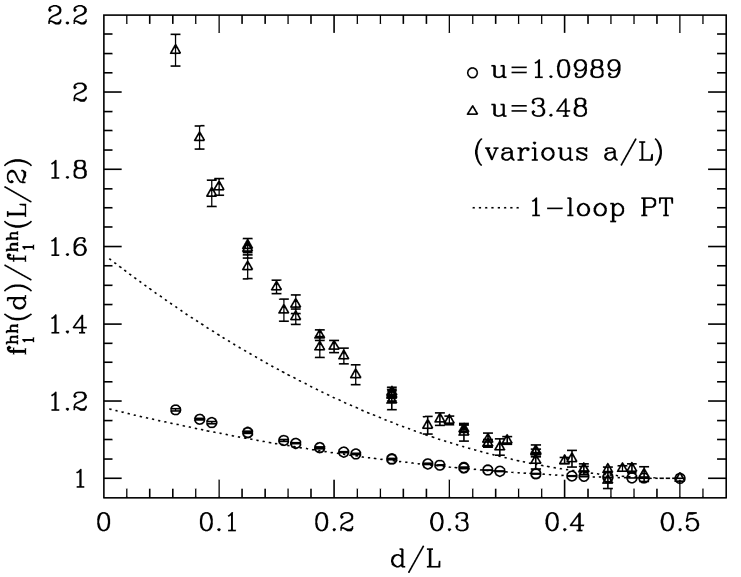

Fig. 4. Non-perturbative d-dependence of $h(d/L,u) = f_1^{\mathrm{hh}}(d)/f_1^{\mathrm{hh}}(L/2)$ at two (low and high) values of the coupling, compared to one-loop perturbation theory. As data points corresponding to various lattice resolutions are included, the figure also reflects the weak cutoff dependence of this ratio.

The one-loop expression is compared to results from our non-perturbative computation of f_1^{hh} for two representative values of the coupling in Fig. 4. The figure contains non-perturbative results for $L/a \in \{12, 16, 20, 24, 32\}$ but at the level of our statistical errors, which are about 1% and smaller, no lattice artifacts of the ratio h can be seen.

For low d, the non-perturbative data for h are well described by $c \times (L/d) + c'$, where the constant c grows with $u = \bar{g}^2$. Hence the correlation function contains a non-integrable short-distance singularity, which is the reason why we will not integrate over d in the following. It is easy to see that this singularity is absent up to and including the order u^2, but in higher-order terms in perturbation theory such a singularity may appear.

2.3. The new renormalization scheme

Choosing d at its maximum value to further keep discretization errors at a minimum, we specify our (non-perturbative) renormalization scheme by

$$Z_{\mathrm{A}}^{\mathrm{stat}}(L)\Xi(L) = \Xi^{(0)}(L) \quad \text{at vanishing quark mass,} \tag{2.15}$$

with

$$\Xi(L) = \frac{f_{\mathrm{A}}^{\mathrm{stat}}(L/2)}{[f_1 f_1^{\mathrm{hh}}(L/2)]^{1/4}}. \tag{2.16}$$

Here, f_1 is the correlator between two light-quark pseudoscalar boundary sources,

$$f_1 = -\frac{1}{2L^6}\int \mathrm{d}^3\boldsymbol{u}\,\mathrm{d}^3\boldsymbol{v}\,\mathrm{d}^3\boldsymbol{y}\,\mathrm{d}^3\boldsymbol{z}\,\big\langle \bar{\zeta}_1'(\boldsymbol{u})\gamma_5\zeta_2'(\boldsymbol{v})\bar{\zeta}_2(\boldsymbol{y})\gamma_5\zeta_1(\boldsymbol{z})\big\rangle, \tag{2.17}$$

depicted in the right part of Fig. 3. The form of f_1 and $f_1^{\rm hh}$ on the lattice is given in Eqs. (A.12) and (A.14) of Appendix A.1. As before, the combination of these correlators in the denominator of (2.16) is such that the boundary field renormalizations and the mass counterterm drop out and no other scale but L appears.

For $\theta = 0.5$ the perturbative calculation summarized in Appendix B now yields

$$\gamma_1^{\rm SF} = \frac{1}{(4\pi)^2}\big\{0.10(2) - 0.0477(13)\, N_{\rm f}\big\}, \tag{2.18}$$

which differs only little from the one in the old scheme [17].

Note that O(a) improvement [21,32] can be applied and is an important ingredient in practice to reduce the cutoff effects in the numerical simulations (see Appendix A). Returning to Fig. 2, one observes that the statistical errors of the lattice results are indeed much smaller in the new scheme.

3. Non-perturbative running and renormalization group invariant

In this section we present our quenched results on the evolution of $\Phi(\mu)$ over more than two orders of magnitude in μ. To this end we consider the evolution of $Z_{\rm A}^{\rm stat}$ under repeated changes of the scale (i.e., the box size L) by a factor of two at fixed bare parameters. Starting at some initial low-energy value (i.e., some large $L = L_{\rm max}$), one thereby climbs up the energy scale by repeated application of the inverse of the step scaling function until the perturbative domain at high energies (i.e., small $2^{-k}L_{\rm max}$) is reached, where finally the associated (scale and scheme independent) renormalization group invariant may be extracted. As in the previous section we keep the discussion in the continuum theory here; the underlying lattice calculations are described in Appendix A.

3.1. Step scaling function

The evolution of $Z_{\rm A}^{\rm stat}$ from size L to $2L$ is given by its step scaling function, $\sigma_{\rm A}^{\rm stat}(u)$, which has already been introduced in Eq. (2.6), but where it is understood that $Z_{\rm A}^{\rm stat}$ is defined in the new renormalization scheme according to Eq. (2.15).

As detailed in Appendix A.2, the sets of lattice parameters $(L/a, \beta, \kappa)$, which in practice are required to non-perturbatively compute $\sigma_{\rm A}^{\rm stat}(u)$, can be taken over from the quark mass renormalization [13]. The available coupling values u allow to trace the scale dependence of $Z_{\rm A}^{\rm stat}$ up to $L = 2L_{\rm max}$, where the scale $L_{\rm max}$ is implicitly defined through

$$\bar{g}^2(L_{\rm max}) = 3.48. \tag{3.1}$$

The sequence

$$u_k = \bar{g}^2\big(2^{-k}L_{\rm max}\big), \quad k = 0, \ldots, 8, \tag{3.2}$$

is known from Ref. [13], and thus the corresponding sequence

$$v_k \equiv \frac{Z_{\rm A}^{\rm stat}(2^{-k+1}L_{\rm max})}{Z_{\rm A}^{\rm stat}(2L_{\rm max})} = \frac{\Phi(2^{k-1}/L_{\rm max})}{\Phi((2L_{\rm max})^{-1})}, \qquad v_0 = 1, \tag{3.3}$$

Table 1
Results for the continuum step scaling function $\sigma_{\rm A}^{\rm stat}(u)$

u	$\sigma_{\rm A}^{\rm stat}(u)$
1.0989	0.9796(20)
1.3293	0.9746(25)
1.4300	0.9719(26)
1.5553	0.9668(27)
1.6950	0.9727(28)
1.8811	0.9632(28)
2.1000	0.9589(35)
2.4484	0.9432(27)
2.7700	0.9423(41)
3.4800	0.9154(41)

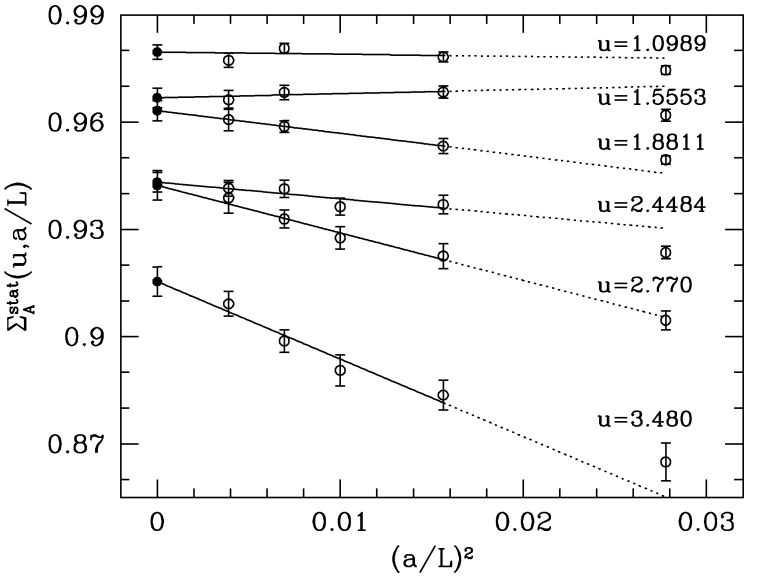

Fig. 5. Lattice step scaling function $\Sigma_{\rm A}^{\rm stat}$ and its continuum limit extrapolations for some selected values of u.

is simply given by

$$v_0 = 1, \qquad v_{k+1} = \frac{v_k}{\sigma_{\rm A}^{\rm stat}(u_k)}, \tag{3.4}$$

once the function $\sigma_{\rm A}^{\rm stat}(u)$ is available in the corresponding range of u.

The calculation of the lattice step scaling function and its subsequent continuum extrapolation yields the pairs u and $\sigma_{\rm A}^{\rm stat}(u)$ listed in Table 1. An impression of the quality of the continuum extrapolation is gained from Fig. 5, but for a more detailed account of the lattice simulations and data analysis we refer to Appendix A.2. An interpolating fit of $\sigma_{\rm A}^{\rm stat}(u)$ is shown in Fig. 6. The leading coefficients (s_0 and s_1, see Appendix C.1) of the interpolating polynomial are fixed to the perturbative predictions, Eqs. (B.14). This fit

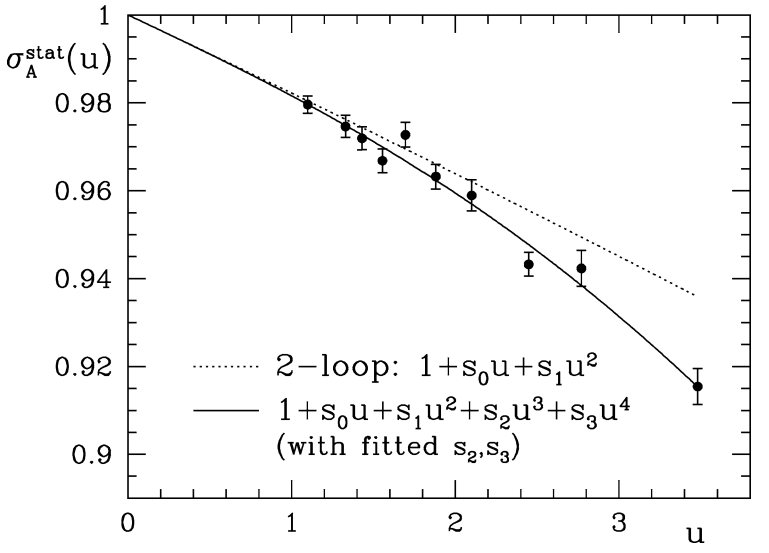

Fig. 6. Continuum step scaling function $\sigma_{\mathrm{A}}^{\mathrm{stat}}(u)$ and its polynomial fit.

is then inserted into the aforementioned recursion, and propagating all errors through the recursion we obtain

$$Z_{\mathrm{A}}^{\mathrm{stat}}(2L_{\max})/Z_{\mathrm{A}}^{\mathrm{stat}}(L) = 0.7551(47) \quad \text{at } L = 2^{-6}L_{\max}, \tag{3.5}$$

with the value of the coupling at this box size being $\bar{g}^2(2^{-6}L_{\max}) = 1.053(12)$ [13]. Let us emphasize once more that $L = 2L_{\max}$ and $L = 2^{-6}L_{\max}$ represent low- and high-energy scales, respectively, which in this way have been connected non-perturbatively. (Our data actually allow to go up to $L = 2^{-8}L_{\max}$.)

3.2. RGI matrix elements of the static axial current

We now proceed to relate the renormalized matrix element

$$\Phi(\mu) = Z_{\mathrm{A}}^{\mathrm{stat}}(L)\Phi_{\mathrm{bare}}(g_0), \quad \mu = 1/L, \tag{3.6}$$

at $L = 2L_{\max}$ to the renormalization group invariant one defined by[2]

$$\Phi_{\mathrm{RGI}} = \Phi(\mu)\big[2b_0\bar{g}^2(\mu)\big]^{-\gamma_0/2b_0}\exp\left\{-\int_0^{\bar{g}(\mu)}\mathrm{d}g\left[\frac{\gamma(g)}{\beta(g)} - \frac{\gamma_0}{b_0 g}\right]\right\}, \tag{3.7}$$

[2] In a loose notation, we take sometimes L and sometimes $\mu = 1/L$ as the argument of $\bar{g}$.

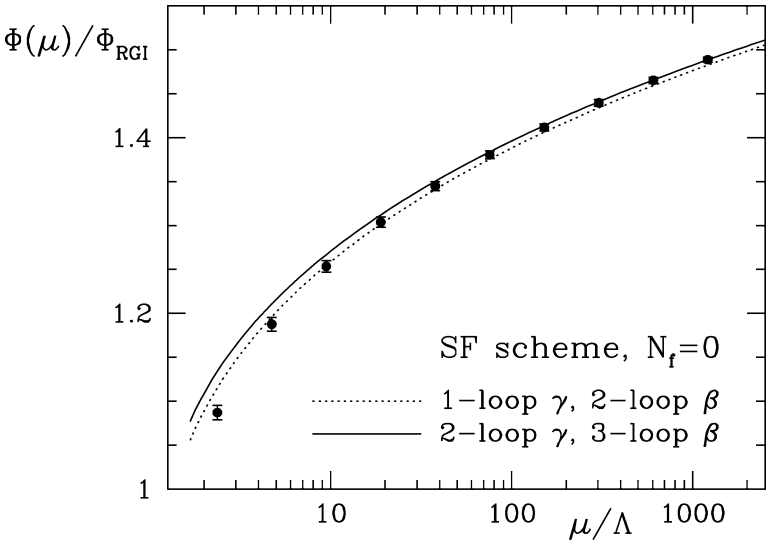

Fig. 7. Numerically computed values of the running matrix element of the static axial current in the SF scheme compared to perturbation theory. The dotted and solid lines are obtained from Eq. (3.7) using the 1/2- and 2/3-loop expressions for the γ- and β-functions, respectively, as well as $\Lambda L_{\max} = 0.211$ from Ref. [13].

with the universal leading-order coefficients $b_0 = 11/(4\pi)^2$ and $\gamma_0 = -1/(4\pi^2)$ of the β- and γ-functions, respectively. Casting this equation in the form

$$\frac{\Phi_{\rm RGI}}{\Phi((2L_{\max})^{-1})} = \frac{Z_{\rm A}^{\rm stat}(1/\mu)}{Z_{\rm A}^{\rm stat}(2L_{\max})}\big[2b_0\bar{g}^2(\mu)\big]^{-\gamma_0/2b_0}\exp\left\{-\int_0^{\bar{g}(\mu)}{\rm d}g\left[\frac{\gamma(g)}{\beta(g)}-\frac{\gamma_0}{b_0 g}\right]\right\},$$

with $\mu = 2^6/L_{\max}$, we see that the first factor is known from Eq. (3.5), while in the second one only couplings $\bar{g}^2 \leqslant 1.05$ contribute and it can safely be evaluated by perturbation theory. Still, for the perturbative error to be negligible, γ has to be known to two-loop accuracy and β to three-loop. Upon inserting $\bar{g}^2(2^6/L_{\max}) = 1.053$ and numerical integration of the second factor we find

$$\Phi(\mu)/\Phi_{\rm RGI} = 1.088(8) \quad \text{at } \mu = (2L_{\max})^{-1} \tag{3.8}$$

in the SF scheme. Entirely consistent numbers, with slightly larger errors, are obtained for $\Phi(\mu)/\Phi_{\rm RGI}$ if one switches to perturbation theory at $\mu = 2^7/L_{\max}$ or $\mu = 2^8/L_{\max}$ instead.

In Fig. 7 we compare the numerically computed running with the corresponding curves in perturbation theory. While good agreement with the perturbative approximation is seen at high scales, a growing difference of up to 5% becomes visible when μ is lowered to $\mu \approx 2.5\,\Lambda$.

Below it will be more convenient to specify the scale μ in Eq. (3.8) in terms of r_0 [33] instead of $L_{\max}$. Taking also the small error contribution from the uncertainty of $L_{\max}$ in units of r_0, $L_{\max}/r_0 = 0.718(16)$ [34], into account, the final result for the regularization

independent part $\Phi(\mu)/\Phi_{\rm RGI}$ of the total renormalization factor is

$$\Phi(\mu)/\Phi_{\rm RGI} = 1.088(10) \quad \text{at } \mu = (1.436\, r_0)^{-1}. \tag{3.9}$$

Note that this result refers to the *continuum limit* so that the error on $\Phi(\mu)/\Phi_{\rm RGI}$ of about 0.9% should only be added in quadrature to the proper matrix element under study *after* its continuum extrapolation.

4. $Z_{\rm A}^{\rm stat}$ at low scale and total renormalization factor

We still need to relate $(A_{\rm R}^{\rm stat})_0(\mu)$, renormalized at some appropriate scale μ, to the bare lattice operator. This amounts to computing $Z_{\rm A}^{\rm stat}$ at the low-energy matching scale $L = 2L_{\rm max} = 1.436\, r_0$, which is briefly explained in Appendix C.2. Since in this step the bare operator is involved, $Z_{\rm A}^{\rm stat}$ does depend—in contrast to the result of the previous section—on the choice of action. We have considered three different cases. The first two are the non-perturbatively O(a) improved action of Ref. [35], with $c_{\rm A}^{\rm stat} = -\frac{1}{4\pi} g_0^2$ (= one-loop) and separately with $c_{\rm A}^{\rm stat} = 0$. Their combination will in the future allow to study the influence of $c_{\rm A}^{\rm stat}$ on the continuum extrapolations of renormalized matrix elements. The third choice is the unimproved Wilson action which is of interest, because so far the best computations of the bare matrix element did not use improvement [10,11].

The numerical results for $Z_{\rm A}^{\rm stat}$ are shown in Fig. 8. For later use they are represented by interpolating polynomials,

$$Z_{\rm A}^{\rm stat}(g_0, L/a)\big|_{L=1.436\, r_0} = \sum_{i \geqslant 0} z_i (\beta - 6)^i, \tag{4.1}$$

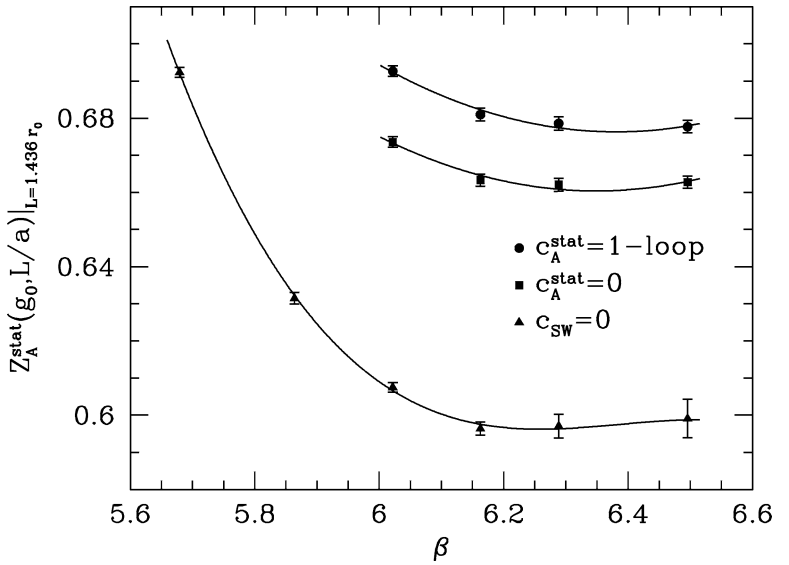

Fig. 8. Numerical results for $Z_{\rm A}^{\rm stat}(g_0, L/a)|_{L=1.436\, r_0}$ together with their interpolating polynomials.

Table 2
Coefficients of the interpolating polynomials, Eqs. (4.1) and (4.3). Uncertainties are discussed in the text

$c_{\rm sw}, c_{\rm A}$	$c_{\rm A}^{\rm stat}$	Applicability	i	z_i	f_i
non-perturbative	$-g_0^2/(4\pi)$	$6.0 \leqslant \beta \leqslant 6.5$	0	0.6944	0.6382
[35]			1	−0.0946	−0.0869
			2	0.1239	0.1139
non-perturbative	0	$6.0 \leqslant \beta \leqslant 6.5$	0	0.6750	0.6204
			1	−0.0838	−0.0771
			2	0.1200	0.1103
0, 0	0	$5.7 \leqslant \beta \leqslant 6.5$	0	0.6090	0.5598
			1	−0.1186	−0.1090
			2	0.3438	0.3160
			3	−0.2950	−0.2711

with coefficients z_i as listed in Table 2. The statistical uncertainty to be taken into account when using this formula is about 0.4%.

The total renormalization factor

The total renormalization factor to directly translate any bare matrix element $\Phi_{\rm bare}(g_0)$ of $A_0^{\rm stat}$ into the RGI matrix element, $\Phi_{\rm RGI}$, can be written as

$$Z_{\rm RGI}(g_0) = \left.\frac{\Phi_{\rm RGI}}{\Phi(\mu)}\right|_{\mu=(1.436\,r_0)^{-1}} \times Z_{\rm A}^{\rm stat}(g_0, L/a)\big|_{L=1.436\,r_0}. \tag{4.2}$$

We combine Eq. (4.1) with Eq. (3.9) and represent the total Z-factor by further interpolating polynomials,

$$Z_{\rm RGI}(g_0) = \sum_{i\geqslant 0} f_i(\beta-6)^i, \tag{4.3}$$

whose coefficients are also found in Table 2. These parametrizations of $Z_{\rm RGI}$ are to be used with an uncertainty of about 0.4%[3] at each β-value and an additional error of 0.9% (from $\Phi_{\rm RGI}/\Phi(\mu)$), which remains to be added in quadrature *after* performing a continuum extrapolation.

5. Matrix elements at finite values of the quark mass

In order to use results from the static theory, one still has to relate its renormalization group invariant matrix elements to those in QCD at finite values of the quark mass, m. This step may also be seen as a translation to another scheme, defined by the condition that matrix elements in the static effective theory renormalized in this scheme and at scale

[3] Only in the case $c_{\rm sw} = 0$ the error to be associated with the formulae for $Z_{\rm A}^{\rm stat}$ and $Z_{\rm RGI}$ grows to 0.5% at $\beta \approx 6.3$ and 0.8% at $\beta \approx 6.5$.

$\mu = m$ are the same as those in QCD up to $1/m$-corrections. This scheme is therefore denoted as the '*matching scheme*' [14]. Below, we will specify precisely which quark mass m is to be taken.

5.1. Conversion to the matching scheme

Let us write the relations for the special case of the matrix element of the axial current between the vacuum and the heavy-light pseudoscalar,

$$\Phi_{\rm RGI} = Z_{\rm RGI}\langle {\rm PS}|A_0^{\rm stat}|0\rangle. \tag{5.1}$$

We then have

$$F_{\rm PS}\sqrt{m_{\rm PS}} = \widehat{C}_{\rm PS}(\bar{m})\Phi_{\rm RGI} + {\rm O}(1/\bar{m}), \tag{5.2}$$

where $\bar{m}$ is the $\overline{\rm MS}$ quark mass at renormalization scale $\bar{m}$.[4] The function $\widehat{C}_{\rm PS}(\mu)$ is given by

$$\widehat{C}_{\rm PS}(\mu) = \left[2b_0\bar{g}^2(\mu)\right]^{\gamma_0/2b_0}\exp\left\{\int_0^{\bar{g}(\mu)} {\rm d}g\left[\frac{\gamma(g)}{\beta(g)} - \frac{\gamma_0}{b_0 g}\right]\right\}, \tag{5.3}$$

with $\bar{g}(\mu)$ the $\overline{\rm MS}$ running coupling and γ the anomalous dimension in the matching scheme. The latter is known to two loops [30,38–40] with γ_0 being the same as before and

$$\gamma_1 \equiv \gamma_1^{\rm match} = \gamma_1^{\overline{\rm MS}} - \frac{b_0}{3\pi^2}, \tag{5.4}$$

$$\gamma_1^{\overline{\rm MS}} = -\frac{1}{576\pi^4}\left(\frac{127}{2} + 28\zeta(2) - 5N_{\rm f}\right). \tag{5.5}$$

For illustration, $\widehat{C}_{\rm PS}(\mu)$ is plotted in the upper part of Fig. 9, where for the numerical evaluation the β-function is always taken at four-loop precision [41], while to estimate the perturbative uncertainty we show the result for the one-loop and the two-loop approximation of γ.

Eq. (5.3) can be rewritten in a form displaying explicitly that also this step is not restricted to perturbation theory. In terms of the renormalization group invariant quark mass, M, we have

$$F_{\rm PS}\sqrt{m_{\rm PS}} = C_{\rm PS}(M/\Lambda_{\overline{\rm MS}})\Phi_{\rm RGI} + {\rm O}(1/M), \tag{5.6}$$

where now only renormalization group invariants enter. To evaluate $C_{\rm PS}(M/\Lambda_{\overline{\rm MS}})$ in perturbative approximation, one changes the argument of the function $\widehat{C}_{\rm PS}$, Eq. (5.3), by

[4] Note that in [36] a similar equation with the pole mass instead of the $\overline{\rm MS}$ mass is written. At the two-loop order, which will be used below, this does formally not make any difference. However, the pole mass does not have a well-behaved perturbative expansion [37], and we therefore prefer a short-distance mass such as the $\overline{\rm MS}$ mass.

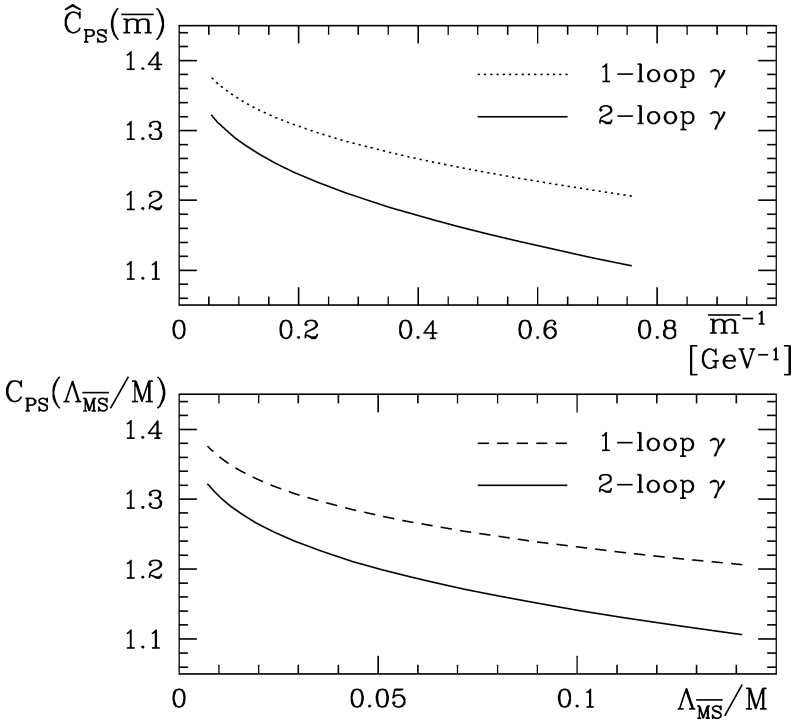

Fig. 9. Conversion factor to the matching scheme, which translates the RGI matrix element to the one at finite mass.

inserting

$$M/\bar{m}(\mu) = \left[2b_0\bar{g}^2(\mu)\right]^{-d_0/2b_0} \exp\left\{-\int_0^{\bar{g}(\mu)} \mathrm{d}g \left[\frac{\tau(g)}{\beta(g)} - \frac{d_0}{b_0 g}\right]\right\} \tag{5.7}$$

together with the condition $\bar{m}(m_{\overline{\mathrm{MS}}}) = m_{\overline{\mathrm{MS}}}$, where $\tau(\bar{g})$ denotes as usual the renormalization group function of the renormalized (running) quark mass with universal leading-order coefficient $d_0 = 8/(4\pi)^2$. A numerical evaluation (with the four-loop τ-function [42,43] in Eq. (5.7)) is shown in the lower part of Fig. 9. Eq. (5.6) is not only the cleanest form from a theoretical point of view but it is also practical, because the relation between bare quark masses in the O(a) improved lattice theory and the renormalization group invariant mass M is known non-perturbatively in the quenched approximation [44,45].

For later convenience we represent C_{PS} in terms of the variable $x \equiv 1/\ln(M/\Lambda_{\overline{\mathrm{MS}}})$ in a functional form motivated by Eq. (5.3),

$$C_{\mathrm{PS}} = x^{\gamma_0/2b_0}\left\{1 - 0.065\,x + 0.048\,x^2\right\}, \quad x = 1/\ln(M/\Lambda_{\overline{\mathrm{MS}}}) \leqslant 0.52, \tag{5.8}$$

with $b_0 = 11/(4\pi)^2$ and $\gamma_0 = -1/(4\pi^2)$. It describes the result for the two-loop approximation of the γ-function within less than 0.01%. Of course in this step a perturbative error is involved, which is difficult to estimate. Assuming a geometric growth

Table 3
Matrix elements of $A_0^{\rm stat}$ in units of r_0 for the light quark mass equal to the strange quark mass. Bare matrix elements come from Ref. [10], with the exception of $\beta = 6.0$ which is taken from Ref. [11]. The scale r_0/a [33] is used as determined in Ref. [34], and its uncertainty is already included here

$\beta = 6/g_0^2$	5.7	5.9	6.0	6.1	6.3
r_0/a	2.93(1)	4.48(2)	5.37(2)	6.32(3)	8.49(4)
$r_0^{3/2}\Phi_{\rm bare}$	4.75(25)	4.09(21)	3.94(13)	3.79(36)	4.00(29)
$r_0^{3/2}\Phi_{\rm RGI}$	2.99(16)	2.35(12)	2.21(7)	2.09(20)	2.20(16)

of the coefficients of the γ-function, we find that the γ_2-term would cause a change by around 1% at $\bar{m} = m_{\rm b,\overline{MS}}$ and by 2.5% at $\bar{m} = 1.2$ GeV. Thus one may attribute a 2–4% error due to the perturbative approximation, which could be much reduced by a computation of the three-loop anomalous dimension.

In principle, $C_{\rm PS}$ may be computed also non-perturbatively following the strategy outlined in Ref. [14]. It is then defined only up to $1/M$-terms, consistent with Eq. (5.6).

5.2. Application: first non-perturbative renormalization of $F_{\rm B_s}^{\rm stat}$

We now take bare matrix elements of $A_0^{\rm stat}$ for unimproved Wilson fermions from the literature to obtain an estimate for $F_{\rm B_s}$ in the static approximation. This exercise serves mainly to illustrate how to use our results.

5.2.1. The matrix elements are needed at a fixed value of the light quark mass. To avoid issues in the extrapolation to very light quarks, we here consider only $F_{\rm B_s}$. To fix the strange quark mass, we use that the sum of the light quark masses is to a good approximation proportional to the squared (light-light) pseudoscalar masses, $m_{\rm PS}^2({\rm l,l})$ [44], and interpolate the data for the decay constant of [10,11] as a function of $m_{\rm PS}^2({\rm l,l})r_0^2$ to $m_{\rm PS}^2({\rm s,s})r_0^2 = (2m_{\rm K}^2 - m_\pi^2)r_0^2 = 2m_{\rm K}^2 r_0^2/(1 + m_{\rm l}/m_{\rm s}) = 3.0233$. (To arrive at the latter, we employed $m_{\rm K}^2 r_0^2 = 1.5736$ [44] and $m_{\rm s}/m_{\rm l} = 24.4$ from chiral perturbation theory [46].) The resulting dimensionless numbers $r_0^{3/2}\Phi_{\rm bare}$ are listed in Table 3.

5.2.2. We renormalize by multiplying with Eq. (4.3), using the f_i from Table 2 ($c_{\rm sw} = c_{\rm A} = c_{\rm A}^{\rm stat} = 0$), take into account a 0.4–0.5% error from the non-universal part of the Z-factor at each value of g_0 and find the last line in Table 3. Assuming the leading linear behavior in the lattice spacing to dominate for $a/r_0 < 1/4$, we extrapolate to the continuum limit as shown in Fig. 10. Adding to the extrapolation error in quadrature also the 0.9% error contribution of $Z_{\rm RGI}$, which is independent of g_0, yields

$$r_0^{3/2}\Phi_{\rm RGI} = 1.93(34) \quad \text{at } a = 0. \tag{5.9}$$

5.2.3. Finally, inserting $M_{\rm b} r_0 = 17.6(5)$ [14,47] and $\Lambda_{\overline{\rm MS}} r_0 = 0.602(48)$ [13], one gets via the formula in Eq. (5.8)

$$C_{\rm PS}(M_{\rm b}/\Lambda_{\overline{\rm MS}}) = 1.23(3), \tag{5.10}$$

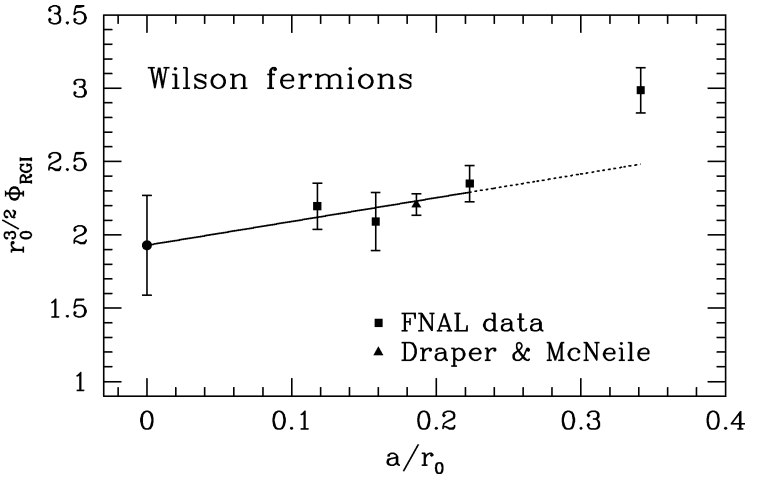

Fig. 10. Continuum extrapolation of the non-perturbatively renormalized matrix element of $A_0^{\rm stat}$ based on the unimproved Wilson data for $F_{\rm B}^{\rm bare}$ from Refs. [10,11].

where a 2% error for the perturbative approximation is assumed. With the experimental spin-averaged B-meson mass $m_{\rm B} = m_{\rm B_s} = 5.4\,\text{GeV}$, we then obtain from Eq. (5.6):

$$F_{\rm B_s}^{\rm stat} r_0 = 0.64(11), \tag{5.11}$$

$$F_{\rm B_s}^{\rm stat} = 253(45)\ \text{MeV} \quad \text{for } r_0 = 0.5\ \text{fm}. \tag{5.12}$$

The result contains all errors apart from the uncertainty owing to the quenched approximation. Evidently, the continuum extrapolation may be done much better, once O(a) improved results with sufficient precision and small lattice spacings are available.

6. Discussion

We have performed the scale dependent renormalization of $A_0^{\rm stat}$ by constructing a non-perturbative renormalization group in the Schrödinger functional scheme, and agreement with perturbation theory at large scales was demonstrated. The renormalization factors needed to extract the associated RG invariant are computed with good numerical accuracy, which is a crucial prerequisite for a controlled determination of $F_{\rm B}$ in the static limit. In Ref. [14] it was shown that the renormalization factors obtained in this way differ appreciably from earlier estimates [10] based on tadpole-improved perturbation theory [48]. Hence their non-perturbative computation is important.

We have not emphasized this so far, but our computation provides the scale dependence of *all* static-light bilinears

$$\mathcal{O}_\Gamma(x) = \bar{\psi}_{\rm l}(x)\Gamma\psi_{\rm h}(x). \tag{6.1}$$

They are renormalized by

$$(\mathcal{O}_{\gamma_k})_R(x) = Z_A^{\rm stat}\mathcal{O}_{\gamma_k},$$
$$(\mathcal{O}_{\gamma_0})_R(x) = \widetilde{Z}Z_A^{\rm stat}\mathcal{O}_{\gamma_0}, \qquad (\mathcal{O}_{\gamma_k\gamma_5})_R(x) = \widetilde{Z}Z_A^{\rm stat}\mathcal{O}_{\gamma_k\gamma_5}, \tag{6.2}$$

with a scale independent renormalization $\widetilde{Z}$. This pattern is due to the heavy quark spin symmetry which is exact on the lattice, and due to the chiral symmetry of the continuum theory. The latter means that the relative renormalization $\widetilde{Z}$ may be fixed by imposing a suitable chiral Ward identity [49] and is thus scale independent.

Returning to the case of most interest, $F_B^{\rm stat}$, our continuum extrapolation in Section 5.2 that uses unimproved data for the bare matrix elements from the literature and also quite large lattice spacings leaves much room for improvement of the present result, $F_{B_s}^{\rm stat} = 253(45)$ MeV. Apart from the obvious step of obtaining $O(a)$ improved bare matrix elements at small lattice spacings and extrapolating to the continuum, it will be necessary to estimate the $O(1/M)$ correction. There are two possible roads towards this goal.

An elegant and clean way is to compute the $1/M$-corrections directly as perturbations to the static effective theory. Again, the main problem here is renormalization. Indeed, this is a severe one, since mixing between operators of different dimensions has to be taken into account. This will require much more theoretical and numerical effort; but a possible strategy exists [14,47].

In the mean time, one may also compare the prediction from the static approximation to what one obtains at $M \approx M_c$ and also to the results obtained directly at $M = M_b$, most notably the ones of Refs. [2,3]. As emphasized in Refs. [50–52] this should be done in the continuum limit, since $O(a)$ errors get enhanced when the quark masses increase. At the charm quark mass these are sizable but can be extrapolated away, at least in the quenched approximation [53]. The comparison between finite-mass decay constants and $F_B^{\rm stat}$ is most conveniently done by comparing $F_{PS}\sqrt{m_{PS}}/C_{PS}(M/\Lambda_{\overline{MS}})$. Unfortunately, at present the error of the static result is still too large to draw any strong conclusions about $1/M$-corrections in F_B:

$$r_0^{3/2}\Phi_{RGI} = 1.93(34), \quad \text{static: Eq. (5.9)}, \tag{6.3}$$

$$r_0^{3/2}\frac{F_{B_s}\sqrt{m_{B_s}}}{C_{PS}(M_b/\Lambda_{\overline{MS}})} = 1.46(23), \quad \text{using } F_{B_s} = 192(30) \text{ MeV [2,3]}, \tag{6.4}$$

$$r_0^{3/2}\frac{F_{D_s}\sqrt{m_{D_s}}}{C_{PS}(M_c/\Lambda_{\overline{MS}})} = 1.29(5), \quad \text{using } F_{D_s} = 252(9) \text{ MeV [54]}. \tag{6.5}$$

Still, the difference of Eqs. (6.3) and (6.5) shows that there are significant $1/M$-corrections in the charm mass region.

As a more technical remark we point out that the function $h(d/L, u)$, Eq. (2.12), shows very small a-effects in the quenched approximation and may be worth studying to verify improvement with dynamical fermions.

Acknowledgements

We thank DESY for allocating computer time on the APE-Quadrics computers at DESY Zeuthen to this project. This work is also supported in part by the EU IHP Network on *Hadron Phenomenology from Lattice QCD* under grant HPRN-CT-2000-00145 and by the DFG Sonderforschungsbereich SFB/TR 9.

Appendix A. Computation of the lattice step scaling function

This appendix describes some details of the numerical simulations on the lattice and the subsequent calculations that we have performed in order to determine the step scaling function for $Z_{\rm A}^{\rm stat}$. At the beginning we also recall a few basic definitions and formulae, which are specific to the inclusion of static quarks and the correlation functions that are considered in the framework of the Schrödinger functional (SF). As the impact of the static quarks on O(a) improvement of the static-light sector has extensively been discussed in Ref. [17], the reader might consult this reference for further details and any unexplained notation.

A.1. Definitions

A.1.1. Lattice action

The total lattice action is given by the sum

$$S[U,\bar\psi_{\rm l},\psi_{\rm l},\bar\psi_{\rm h},\psi_{\rm h}] = S_{\rm G}[U] + S_{\rm F}[U,\bar\psi_{\rm l},\psi_{\rm l}] + S_{\rm h}[U,\bar\psi_{\rm h},\psi_{\rm h}], \tag{A.1}$$

where $S_{\rm G}$ and $S_{\rm F}$ are the standard pure gauge and O(a) improved Wilson actions for relativistic (light) quarks, see Eqs. (A.22)–(A.26) of Ref. [17], respectively, and $S_{\rm h}$ denotes the lattice action for the heavy quark:

$$S_{\rm h}[U,\bar\psi_{\rm h},\psi_{\rm h}] = a^4\sum_x \bar\psi_{\rm h}(x)\nabla_0^*\psi_{\rm h}(x). \tag{A.2}$$

The fields $\psi_{\rm h}$ and $\bar\psi_{\rm h}$ of the static effective theory are constrained in such a way (namely $P_+\psi_{\rm h}=\psi_{\rm h}$ and $\bar\psi_{\rm h}P_+=\bar\psi_{\rm h}$) that one is left with just two degrees of freedom per space-time point [4] and only the (time component of the) backward lattice derivative, ∇_μ^*, enters in the action (A.2). Hence, static quarks propagate only forward in time, which also reflects in the form of the associated quark propagator,

$$\begin{aligned} S_{\rm h}(x,y) &= U(x-a\hat{0},0)^{-1}U(x-2a\hat{0},0)^{-1}\cdots U(y,0)^{-1} \\ &\quad\times\theta(x_0-y_0)\delta(\boldsymbol{x}-\boldsymbol{y})P_+, \\ P_\pm &= \frac{1}{2}(1\pm\gamma_0), \end{aligned} \tag{A.3}$$

being just a straight timelike Wilson line.

To impose SF boundary conditions, Eqs. (A.1) and (A.2) are supplemented by

$$\begin{aligned} &\psi_{\rm l}(x)=0 \quad \text{if } x_0<0 \text{ or } x_0>L, \\ &\psi_{\rm h}(x)=0 \quad \text{if } x_0<0 \text{ or } x_0\geqslant L \end{aligned} \tag{A.4}$$

and

$$P_- \psi_{\rm l}(x)|_{x_0=0} = P_+ \psi_{\rm l}(x)|_{x_0=L} = 0, \tag{A.5}$$

while in the pure gauge part the spatial plaquettes at $x_0 = 0$ and $x_0 = L$ receive a non-trivial (and coupling dependent) weight, see Eq. (A.29) of Ref. [17]. In the discretization of the SF as described in [18,21] we choose zero boundary gauge fields throughout, $C = C' = 0$, which translates into the boundary conditions $U(x,k)|_{x_0=0} = U(x,k)|_{x_0=L} = 1$ for the lattice gauge field. Similarly, the light and static quark fields at $x_0 = 0, L$ are fixed to appropriate (space dependent) boundary functions; the corresponding boundary conditions are collected in Eqs. (3.2), (3.3) and (3.5) of Ref. [17] and not repeated here.

A.1.2. SF correlation functions

Observables are then defined as usual through a path integral involving the total action S. In this work we focus on SF correlation functions that are constructed from the O(a) improved static-light axial current

$$\big(A_{\rm I}^{\rm stat}\big)_0(x) = A_0^{\rm stat}(x) + a c_{\rm A}^{\rm stat} \delta A_0^{\rm stat}(x), \tag{A.6}$$

$$A_0^{\rm stat}(x) = \bar{\psi}_{\rm l}(x)\gamma_0\gamma_5\psi_{\rm h}(x), \tag{A.7}$$

$$\delta A_0^{\rm stat}(x) = \bar{\psi}_{\rm l}(x)\gamma_j\gamma_5\frac{1}{2}\big(\overleftarrow{\nabla}_j + \overleftarrow{\nabla}^*_j\big)\psi_{\rm h}(x). \tag{A.8}$$

Unless it is indicated differently, the improvement coefficient $c_{\rm A}^{\rm stat}$ is set to its one-loop perturbative value,

$$c_{\rm A}^{\rm stat} = -\frac{1}{4\pi}\, g_0^2, \tag{A.9}$$

computed in Refs. [55,56]. On the lattice, in terms of the boundary quark fields $\zeta, \ldots, \bar{\zeta}'$, the correlation functions of these fields, as well as the various types of pseudoscalar correlators from one boundary to the other that are needed in addition, read explicitly:

$$f_{\rm A}^{\rm stat}(x_0) = -a^6 \sum_{\boldsymbol{y},z} \frac{1}{2}\big\langle A_0^{\rm stat}(x)\, \bar{\zeta}_{\rm h}(\boldsymbol{y})\gamma_5\zeta_{\rm l}(z)\big\rangle, \tag{A.10}$$

$$f_{\delta{\rm A}}^{\rm stat}(x_0) = -a^6 \sum_{\boldsymbol{y},z} \frac{1}{2}\big\langle \delta A_0^{\rm stat}(x)\, \bar{\zeta}_{\rm h}(\boldsymbol{y})\gamma_5\zeta_{\rm l}(z)\big\rangle, \tag{A.11}$$

$$f_1 = -\frac{a^{12}}{L^6} \sum_{\boldsymbol{u},\boldsymbol{v},\boldsymbol{y},z} \frac{1}{2}\big\langle \bar{\zeta}'_i(\boldsymbol{u})\gamma_5\zeta'_j(\boldsymbol{v})\bar{\zeta}_j(\boldsymbol{y})\gamma_5\zeta_i(z)\big\rangle, \tag{A.12}$$

$$f_1^{\rm stat} = -\frac{a^{12}}{L^6} \sum_{\boldsymbol{u},\boldsymbol{v},\boldsymbol{y},z} \frac{1}{2}\big\langle \bar{\zeta}'_{\rm l}(\boldsymbol{u})\gamma_5\zeta'_{\rm h}(\boldsymbol{v})\bar{\zeta}_{\rm h}(\boldsymbol{y})\gamma_5\zeta_{\rm l}(z)\big\rangle, \tag{A.13}$$

$$f_1^{\rm hh}(x_3) = -\frac{a^8}{L^2} \sum_{x_1,x_2,\boldsymbol{y},z} \frac{1}{2}\big\langle \bar{\zeta}'_{\rm h}(\boldsymbol{x})\gamma_5\zeta'_{\rm h}(\boldsymbol{0})\bar{\zeta}_{\rm h}(\boldsymbol{y})\gamma_5\zeta_{\rm h}(z)\big\rangle. \tag{A.14}$$

Table 4
The ratio $\Xi_{\rm I}$ for $\theta = 0.5$ at tree-level

L/a	$\Xi_{\rm I}(0, L/a)$
6	−1.5964837518021
8	−1.5996643156321
10	−1.6011462370857
12	−1.6019540566018
16	−1.6027594410020
20	−1.6031330222299
24	−1.6033361949926
32	−1.6035384024722

Moreover we introduce the two ratios

$$X_{\rm I}(g_0, L/a) = \frac{f_{\rm A}^{\rm stat}(L/2) + ac_{\rm A}^{\rm stat} f_{\delta {\rm A}}^{\rm stat}(L/2)}{\sqrt{f_1^{\rm stat}}}, \tag{A.15}$$

$$\Xi_{\rm I}(g_0, L/a) = \frac{f_{\rm A}^{\rm stat}(L/2) + ac_{\rm A}^{\rm stat} f_{\delta {\rm A}}^{\rm stat}(L/2)}{[f_1\, f_1^{\rm hh}(L/2)]^{1/4}}, \tag{A.16}$$

which are constructed such that the (unknown) wave function renormalization factors of the boundary quark fields as well as the (linearly divergent) mass counterterm δm cancel out and only the static current remains subject to renormalization.

A.1.3. Renormalization

In Ref. [17] the renormalization constant $Z_{\rm A}^{\rm stat} \equiv Z_{\rm A,SF}^{\rm stat}$ entering the O(a) improved static axial current renormalized in the SF scheme,

$$\big(A_{\rm R}^{\rm stat}\big)_0 = Z_{\rm A}^{\rm stat}\big(1 + b_{\rm A}^{\rm stat} a m_{\rm q}\big)\big(A_{\rm I}^{\rm stat}\big)_0, \tag{A.17}$$

was defined in terms of the ratio Eq. (A.15) by imposing the renormalization condition (with m_0, $m_{\rm q}$ and $m_{\rm c}$ as defined in [17])

$$Z_{\rm A,old}^{\rm stat}(g_0, L/a)\, X_{\rm I}(g_0, L/a) = X_{\rm I}(0, L/a) \quad \text{at } m_0 = m_{\rm c}. \tag{A.18}$$

Thus, $Z_{\rm A,old}^{\rm stat}$ naturally runs with the scale $\mu = 1/L$. In the present context it will be referred to as the 'old' scheme, whereas the so-called 'new' scheme based on Eq. (A.16) is specified by

$$Z_{\rm A}^{\rm stat}(g_0, L/a)\, \Xi_{\rm I}(g_0, L/a) = \Xi_{\rm I}(0, L/a), \qquad m_0 = m_{\rm c}, \quad L = 1/\mu. \tag{A.19}$$

For $\theta = 0.5$, which is chosen in our simulations, the relevant values of the tree-level normalization constant $\Xi_{\rm I}(0, L/a)$ (or $\Xi_{\rm I}^{(0)}(a/L)$ in the notation of Appendix B summarizing the perturbative calculations) are collected in Table 4. As an aside we remark that $\Xi_{\rm I}(0, L/a) = X_{\rm I}(0, L/a)$ holds.

The critical quark mass is always understood to be defined from the non-perturbatively O(a) improved PCAC mass in the light quark sector as in Ref. [13] (i.e., for $\theta = 0$ and $T = L$, evaluating the associated combination of correlation functions at $x_0 = T/2$).

A.1.4. Lattice step scaling function

The lattice step scaling function of the static axial current is defined through

$$\Sigma_{\rm A}^{\rm stat}(u, a/L) = \frac{Z_{\rm A}^{\rm stat}(g_0, 2L/a)}{Z_{\rm A}^{\rm stat}(g_0, L/a)} \quad \text{at } \bar{g}^2(L) = u,\ m_0 = m_{\rm c}. \tag{A.20}$$

The additional condition $m_0 = m_{\rm c}$ from above, referring to lattice size L/a, defines the critical hopping parameter value, $\kappa = \kappa_{\rm c}$. Moreover, enforcing $\bar{g}^2(L)$ to take some prescribed value u fixes the bare coupling value $g_0^2 = 6/\beta$ to be used for given L/a. In this way $\Sigma_{\rm A}^{\rm stat}$ becomes a function of the renormalized coupling u, up to cutoff effects, and approaches its continuum limit as $a/L \to 0$ for fixed u.

A.2. Simulation details and results

As emphasized before, our quenched lattice simulation and the data analysis are analogous to Ref. [13], except that the boundary coefficient $c_{\rm t}$ is set to its two-loop perturbative value [57]:

$$c_{\rm t}^{\text{2-loop}} = 1 - 0.089\, g_0^2 - 0.030\, g_0^4. \tag{A.21}$$

The boundary $\mathrm{O}(a)$ improvement terms involving quark fields have to be multiplied with a coefficient $\tilde{c}_{\rm t}$, which is known to one-loop from [58], viz.

$$\tilde{c}_{\rm t}^{\text{1-loop}} = 1 - 0.018\, g_0^2. \tag{A.22}$$

Of course, owing to a priori unknown precision to which perturbation theory approximates these coefficients, linear lattice spacing errors are not suppressed completely, and we will come back to this issue later. As for the other contributing $\mathrm{O}(a)$ improvement coefficients, we used the non-perturbative values for $c_{\rm sw}$ and $c_{\rm A}$ of [35] for the relativistic fermions and the one-loop estimate (A.9) for $c_{\rm A}^{\rm stat}$ in the static-light axial current.

The renormalization constants $Z_{\rm A}^{\rm stat}(g_0, L/a)$ and $Z_{\rm A}^{\rm stat}(g_0, 2L/a)$ in Eq. (A.20) have been evaluated from the correlation functions in Eqs. (A.10)–(A.14), which were computed in a numerical simulation with $\theta = 0.5$. (The latter parameter specifies the boundary conditions of the quark fields, see, e.g., [20].) These simulations were performed on the APE-100 parallel computers with 128 to 512 nodes, employing for the updating of the gauge fields the same hybrid-overrelaxation algorithm as in [13,24] with two overrelaxation sweeps per heatbath sweep within a full iteration. This mix of updating was found to be close to optimal in [59]. Since the computation of SF correlators has already been detailed in Ref. [35] and Appendix A.2.2 of [13], we just mention that we differ from them only by using the implementation [60] of the SSOR-preconditioned BiCGStab inverter [61] to solve the lattice Dirac equation.

The computation of $f_1^{\rm hh}(d)$, where $d = |x_3|$ and $a \leqslant d \leqslant L/2$, amounts to evaluate Eq. (B.1). In order to improve the statistical precision of $f_1^{\rm hh}$, the links building up the observable are evaluated by a 10-hit multi-hit procedure [31], where each hit consists of a Cabibbo–Marinari heatbath update in three SU(2)-subgroups of SU(3). Translation invariance is fully exploited.

In order to keep autocorrelations small, the measurements of the correlation functions were always separated by $L/(2a)$ update iterations (and, respectively, five iterations in

the case of $f_1^{\rm hh}$). Statistical errors stem from a standard jackknife analysis, where we have checked explicitly for the statistical independence of the data by averaging them into bins of a few consecutive measurements beforehand. The total number of measurements itself was such that the statistical error of $\Sigma_{\rm A}^{\rm stat}$ was dominated by the uncertainty in $Z_{\rm A}^{\rm stat}(g_0, 2L/a)$. In general, the uncertainties in the coupling and in the value of $\kappa_{\rm c}$ would have to be propagated into the error of $\Sigma_{\rm A}^{\rm stat}$ as well. But as the former can be estimated to be much smaller than the statistical error of $\Sigma_{\rm A}^{\rm stat}$ and $\Sigma_{\rm A}^{\rm stat}$ is found to depend rather weakly on the bare (light) quark mass, we neglected both contributions in the final error estimate.

In Tables 5–7 we list our results on the step scaling functions of the static axial current[5] and—since they are available from our computations as well—of the pseudoscalar density defined as in [13]. The values of β and the critical hopping parameter $\kappa = \kappa_{\rm c}$ to be simulated were taken over from Ref. [13] without changes, which means to stay with $c_{\rm t}$ and $\tilde{c}_{\rm t}$ to one-loop accuracy in realizing the conditions $\bar{g}^2(L) = u$ and $m_0 = m_{\rm c}$. Note once more, however, that here, in contrast to [13], for the corresponding renormalization constants themselves—particularly when comparing the results for $Z_{\rm P}$ and $\Sigma_{\rm P}$ quoted in that previous work with those of the present one—the two-loop formula for $c_{\rm t}$, Eq. (A.21), has been used.

A.3. Continuum extrapolation of $\Sigma_{\rm A}^{\rm stat}$

For fixed coupling u the step scaling function defined in Eq. (A.20) has a continuum limit, $\sigma_{\rm A}^{\rm stat}(u)$. Neglecting for the moment the uncertainties on the correct values of $c_{\rm t}$, $\tilde{c}_{\rm t}$ and $c_{\rm A}^{\rm stat}$, we expect the leading-order cutoff effects to be quadratic in the lattice spacing,

$$\Sigma_{\rm A}^{\rm stat}(u, a/L) = \sigma_{\rm A}^{\rm stat}(u) + {\rm O}\big(a^2/L^2\big), \tag{A.23}$$

since $\mathrm{O}(a)$ improvement is employed. Based on this ansatz, Fig. 5 in Section 3 illustrates the continuum extrapolation of $\Sigma_{\rm A}^{\rm stat}$ for a representative subset of our available coupling values $u = \bar{g}^2(L)$. The coarsest lattices (with $L/a = 6$) have been omitted from the fits as a safeguard against higher order cutoff effects. For the remaining $a/L \leqslant 1/8$, the one-loop cutoff effects are quite small, see Fig. 12.

Although these extrapolations are entirely compatible with an approach to the continuum limit quadratic in a/L, we also have investigated extrapolations linear in a/L. These as well yield reasonable fits with consistent results and even comparable total χ^2/dof (when summing up the χ^2's belonging to the individual fits at the ten u-values) so that the form of the lattice spacing dependence cannot be decided on the basis of the data. Therefore, we have studied the influence of the imperfect (i.e., only perturbative) knowledge of some of the improvement coefficients in more detail.

Since the usage of the two-loop approximation (A.21) for $c_{\rm t}$ in the calculation of the correlation functions (and thereby also in the step scaling function $\Sigma_{\rm A}^{\rm stat}$) should cancel the main contributions from the related boundary terms, we only address its effect originating

[5] Here we do not tabulate the results on the static-static boundary correlator $f_1^{\rm hh}$ separately, but the numbers can be obtained from the authors upon request.

Table 5
Results for the step scaling function $\Sigma_{\rm P}$

$\bar{g}^2(L)$	β	κ	L/a	$Z_{\rm P}(g_0, L/a)$	$Z_{\rm P}(g_0, 2L/a)$	$\Sigma_{\rm P}(u, a/L)$
1.0989	9.5030	0.131514	6	0.8190(10)	0.7846(9)	0.9581(16)
	9.7500	0.131312	8	0.8107(9)	0.7786(12)	0.9604(18)
	10.0577	0.131079	12	0.8012(6)	0.7702(11)	0.9613(16)
	10.3419	0.130876	16	0.7956(8)	0.7625(15)	0.9584(21)
1.3293	8.6129	0.132380	6	0.7930(10)	0.7493(10)	0.9449(17)
	8.8500	0.132140	8	0.7827(11)	0.7402(11)	0.9456(19)
	9.1859	0.131814	12	0.7737(7)	0.7353(12)	0.9503(17)
	9.4381	0.131589	16	0.7666(11)	0.7274(18)	0.9488(27)
1.4300	8.5598	0.132453	8	0.7702(10)	0.7273(13)	0.9443(21)
	8.9003	0.132095	12	0.7610(6)	0.7223(14)	0.9491(21)
	9.1415	0.131855	16	0.7555(7)	0.7123(20)	0.9428(28)
1.5553	7.9993	0.133118	6	0.7666(7)	0.7165(16)	0.9346(23)
	8.2500	0.132821	8	0.7590(8)	0.7134(13)	0.9399(20)
	8.5985	0.132427	12	0.7473(10)	0.7035(13)	0.9414(21)
	8.8323	0.132169	16	0.7421(9)	0.6976(19)	0.9401(29)
1.6950	7.9741	0.133179	8	0.7442(11)	0.6939(15)	0.9325(24)
	8.3218	0.132756	12	0.7341(7)	0.6862(15)	0.9348(22)
	8.5479	0.132485	16	0.7277(13)	0.6805(18)	0.9352(30)
1.8811	7.4082	0.133961	6	0.7348(9)	0.6764(6)	0.9205(14)
	7.6547	0.133632	8	0.7258(7)	0.6691(15)	0.9219(23)
	7.9993	0.133159	12	0.7173(5)	0.6632(8)	0.9245(12)
	8.2415	0.132847	16	0.7117(13)	0.6604(20)	0.9279(33)
2.1000	7.3632	0.134088	8	0.7088(13)	0.6433(16)	0.9076(28)
	7.6985	0.133599	12	0.6971(8)	0.6385(24)	0.9160(36)
	7.9560	0.133229	16	0.6919(12)	0.6303(17)	0.9110(29)
2.4484	6.7807	0.134994	6	0.6845(10)	0.6110(12)	0.8925(21)
	7.0197	0.134639	8	0.6784(8)	0.6061(19)	0.8933(30)
	7.2025	0.134380	10	0.6733(8)	0.6021(12)	0.8943(21)
	7.3551	0.134141	12	0.6722(11)	0.6012(12)	0.8944(24)
	7.6101	0.133729	16	0.6661(5)	0.5962(10)	0.8950(17)
2.7700	6.5512	0.135327	6	0.6619(10)	0.5758(20)	0.8699(33)
	6.7860	0.135056	8	0.6541(13)	0.5751(17)	0.8792(31)
	6.9720	0.134770	10	0.6505(8)	0.5717(17)	0.8788(28)
	7.1190	0.134513	12	0.6482(9)	0.5705(10)	0.8802(19)
	7.3686	0.134114	16	0.6442(16)	0.5668(16)	0.8798(33)
3.4800	6.2204	0.135470	6	0.6173(8)	0.5067(11)	0.8208(21)
	6.4527	0.135543	8	0.6133(8)	0.5101(21)	0.8316(35)
	6.6350	0.135340	10	0.6112(11)	0.5078(19)	0.8307(35)
	6.7750	0.135121	12	0.6076(7)	0.5061(14)	0.8329(24)
	7.0203	0.134707	16	0.6063(7)	0.5097(11)	0.8406(21)

from the fixing of the renormalized coupling, the values of which were taken over from Ref. [13] with $c_{\rm t}$ still set to one-loop. Changing $c_{\rm t}$ from one- to two-loop also in this step then requires to adjust the bare coupling and the value of the critical quark mass accordingly before the simulations for $\Sigma_{\rm A}^{\rm stat}$ can be performed. We have done this analysis

Table 6
Results for the step scaling function $\Sigma_{\rm A}^{\rm stat}$ (in the 'new' scheme)

$\bar{g}^2(L)$	β	κ	L/a	$Z_{\rm A}^{\rm stat}(g_0, L/a)$	$Z_{\rm A}^{\rm stat}(g_0, 2L/a)$	$\Sigma_{\rm A}^{\rm stat}(u, a/L)$
1.0989	9.5030	0.131514	6	0.8926(7)	0.8698(8)	0.9745(12)
	9.7500	0.131312	8	0.8860(7)	0.8668(11)	0.9782(14)
	10.0577	0.131079	12	0.8800(6)	0.8630(11)	0.9806(14)
	10.3419	0.130876	16	0.8786(7)	0.8586(16)	0.9773(20)
1.3293	8.6129	0.132380	6	0.8733(8)	0.8458(9)	0.9686(13)
	8.8500	0.132140	8	0.8677(9)	0.8418(13)	0.9701(18)
	9.1859	0.131814	12	0.8635(7)	0.8401(13)	0.9729(17)
	9.4381	0.131589	16	0.8593(9)	0.8361(19)	0.9731(25)
1.4300	8.5598	0.132453	8	0.8593(7)	0.8328(13)	0.9692(17)
	8.9003	0.132095	12	0.8545(7)	0.8314(14)	0.9731(18)
	9.1415	0.131855	16	0.8516(6)	0.8238(23)	0.9674(28)
1.5553	7.9993	0.133118	6	0.8572(6)	0.8246(13)	0.9619(16)
	8.2500	0.132821	8	0.8517(6)	0.8248(13)	0.9684(17)
	8.5985	0.132427	12	0.8459(8)	0.8190(14)	0.9683(20)
	8.8323	0.132169	16	0.8425(9)	0.8141(20)	0.9662(26)
1.6950	7.9741	0.133179	8	0.8414(9)	0.8069(18)	0.9590(24)
	8.3218	0.132756	12	0.8359(8)	0.8074(13)	0.9659(19)
	8.5479	0.132485	16	0.8329(13)	0.8081(19)	0.9703(28)
1.8811	7.4082	0.133961	6	0.8362(7)	0.7939(7)	0.9495(11)
	7.6547	0.133632	8	0.8290(6)	0.7903(17)	0.9533(21)
	7.9993	0.133159	12	0.8247(7)	0.7907(12)	0.9588(16)
	8.2415	0.132847	16	0.8221(13)	0.7898(23)	0.9607(32)
2.1000	7.3632	0.134088	8	0.8193(10)	0.7732(20)	0.9436(26)
	7.6985	0.133599	12	0.8117(9)	0.7756(25)	0.9555(32)
	7.9560	0.133229	16	0.8081(12)	0.7704(21)	0.9533(29)
2.4484	6.7807	0.134994	6	0.8035(8)	0.7420(12)	0.9235(18)
	7.0197	0.134639	8	0.7945(7)	0.7444(19)	0.9370(26)
	7.2025	0.134380	10	0.7936(9)	0.7431(17)	0.9363(24)
	7.3551	0.134141	12	0.7930(10)	0.7465(17)	0.9414(24)
	7.6101	0.133729	16	0.7907(8)	0.7444(16)	0.9415(22)
2.7700	6.5512	0.135327	6	0.7886(9)	0.7133(19)	0.9045(26)
	6.7860	0.135056	8	0.7791(12)	0.7187(24)	0.9225(35)
	6.9720	0.134770	10	0.7786(9)	0.7223(23)	0.9276(31)
	7.1190	0.134513	12	0.7740(11)	0.7220(17)	0.9329(25)
	7.3686	0.134114	16	0.7755(16)	0.7281(30)	0.9388(43)
3.4800	6.2204	0.135470	6	0.7587(10)	0.6562(39)	0.8649(53)
	6.4527	0.135543	8	0.7496(11)	0.6624(29)	0.8837(41)
	6.6350	0.135340	10	0.7477(11)	0.6658(31)	0.8906(43)
	6.7750	0.135121	12	0.7451(11)	0.6696(22)	0.8988(32)
	7.0203	0.134707	16	0.7470(10)	0.6792(24)	0.9092(34)

for the largest fixed coupling, $u = 3.48$, where the uncertainty in $c_{\rm t}$ is largest and thus its effect most pronounced. At $L/a = 6$ the resulting change in $\Sigma_{\rm A}^{\rm stat}$ turns out to lie clearly inside the statistical errors, and this effect will even get smaller for decreasing a/L. On the other hand, if we just compute $\Sigma_{\rm A}^{\rm stat}$ with the one-loop value of $c_{\rm t}$ as in the

Table 7
Results for the step scaling function $\Sigma^{\rm stat}_{\rm A,old}$ (in the 'old' scheme)

$\bar{g}^2(L)$	β	κ	L/a	$Z^{\rm stat}_{\rm A,old}(g_0, L/a)$	$Z^{\rm stat}_{\rm A,old}(g_0, 2L/a)$	$\Sigma^{\rm stat}_{\rm A,old}(u, a/L)$
1.0989	9.5030	0.131514	6	0.8903(8)	0.8676(8)	0.9745(12)
	9.7500	0.131312	8	0.8846(7)	0.8635(11)	0.9762(14)
	10.0577	0.131079	12	0.8791(5)	0.8628(14)	0.9814(17)
	10.3419	0.130876	16	0.8773(9)	0.8601(21)	0.9804(26)
1.3293	8.6129	0.132380	6	0.8721(9)	0.8430(10)	0.9666(16)
	8.8500	0.132140	8	0.8664(10)	0.8428(14)	0.9728(19)
	9.1859	0.131814	12	0.8616(6)	0.8351(19)	0.9693(23)
	9.4381	0.131589	16	0.8580(10)	0.8370(48)	0.9755(57)
1.4300	8.5598	0.132453	8	0.8577(8)	0.8325(14)	0.9706(19)
	8.9003	0.132095	12	0.8535(6)	0.8332(21)	0.9761(26)
	9.1415	0.131855	16	0.8488(6)	0.8172(55)	0.9628(65)
1.5553	7.9993	0.133118	6	0.8552(7)	0.8243(19)	0.9639(23)
	8.2500	0.132821	8	0.8497(6)	0.8224(17)	0.9678(22)
	8.5985	0.132427	12	0.8441(8)	0.8198(26)	0.9712(32)
	8.8323	0.132169	16	0.8410(12)	0.8203(57)	0.9754(69)
1.6950	7.9741	0.133179	8	0.8411(11)	0.8079(20)	0.9606(26)
	8.3218	0.132756	12	0.8340(8)	0.8154(32)	0.9777(39)
	8.5479	0.132485	16	0.8328(16)	0.8076(87)	0.970(11)
1.8811	7.4082	0.133961	6	0.8336(7)	0.7904(7)	0.9482(12)
	7.6547	0.133632	8	0.8269(7)	0.7921(21)	0.9578(27)
	7.9993	0.133159	12	0.8232(5)	0.7863(20)	0.9551(25)
	8.2415	0.132847	16	0.8210(18)	0.798(12)	0.972(15)
2.1000	7.3632	0.134088	8	0.8172(13)	0.7778(24)	0.9518(33)
	7.6985	0.133599	12	0.8097(8)	0.7757(67)	0.9579(83)
	7.9560	0.133229	16	0.8091(21)	0.786(12)	0.971(14)
2.4484	6.7807	0.134994	6	0.8016(9)	0.7416(17)	0.9252(23)
	7.0197	0.134639	8	0.7941(9)	0.7399(37)	0.9317(48)
	7.2025	0.134380	10	0.7932(9)	0.7422(37)	0.9357(48)
	7.3551	0.134141	12	0.7901(13)	0.7382(54)	0.9344(70)
	7.6101	0.133729	16	0.7870(9)	0.756(13)	0.961(17)
2.7700	6.5512	0.135327	6	0.7863(10)	0.7132(34)	0.9070(45)
	6.7860	0.135056	8	0.7804(15)	0.7169(45)	0.9185(60)
	6.9720	0.134770	10	0.7759(10)	0.7121(55)	0.9177(72)
	7.1190	0.134513	12	0.7739(12)	0.7152(72)	0.9241(95)
	7.3686	0.134114	16	0.7732(30)	0.681(34)	0.880(43)
3.4800	6.2204	0.135470	6	0.7573(9)	0.6558(24)	0.8659(34)
	6.4527	0.135543	8	0.7501(9)	0.6560(77)	0.874(10)
	6.6350	0.135340	10	0.7476(15)	0.661(11)	0.885(15)
	6.7750	0.135121	12	0.7430(10)	0.659(16)	0.886(21)
	7.0203	0.134707	16	0.7474(13)	0.642(46)	0.859(61)

computation of the coupling, we found the results, now for $u = 2.77$ and $L/a = 6, 8$, to be indistinguishable within errors, too. We conclude that any small uncertainty present in $c_{\rm t}$ beyond the available two-loop estimate is numerically unimportant for the cutoff dependence of $\Sigma^{\rm stat}_{\rm A}$.

Regarding the O(a) improvement coefficient $\tilde{c}_{\rm t}$, we followed the same line as in [13] and assessed its influence on our results by artificially replacing the one-loop coefficient in the expression (A.22) by ten times its value. I.e., we set $\tilde{c}_{\rm t}$ to $\tilde{c}_{\rm t}' = 1 - 0.180\, g_0^2$ in some additional simulations at $u = 3.48$, and the outcome is that the corresponding estimates on $\Sigma_{\rm A}^{\rm stat}$ for $L/a = 6$ still differ by around 1.5%, while for $L/a = 8$ they already agree within their statistical errors. As this difference drops further for growing L/a and/or smaller couplings, a possible imperfection of $\tilde{c}_{\rm t}$ does not affect the results on $\Sigma_{\rm A}^{\rm stat}$ either.

Finally, we also checked for the influence of the O(a) improvement coefficient in the static-light axial current, $c_{\rm A}^{\rm stat}$, by analyzing our data with $c_{\rm A}^{\rm stat} = 0$ instead of the one-loop value (A.9). Whereas the related change in $Z_{\rm A}^{\rm stat}$ is of the order of a few percent and hence still substantial, it largely cancels in the ratio of Eq. (A.20) so that this effect is no more significant for $\Sigma_{\rm A}^{\rm stat}$ given its statistical errors.

All in all these findings demonstrate that at the level of our precision linear a-effects in the data on $\Sigma_{\rm A}^{\rm stat}$ are negligible, and extrapolations using $(a/L)^2$-terms as the dominant scaling violation are justified indeed.

Appendix B. Perturbation theory

This appendix provides a few details on the perturbative computations, which were required to obtain the one-loop expression for $h(d/L, u)$, Eq. (2.12), the two-loop anomalous dimension and the one-loop estimates of the discretization errors of the step scaling function $\Sigma_{\rm A}^{\rm stat}$. Note that here we restrict ourselves to the case of the modified (or 'new') scheme introduced via Eq. (2.15) in this paper, because the perturbation theory of the original scheme defined through Eq. (2.7) has been extensively discussed already in Ref. [17] where also more details on the different steps involved can be found.

The correlation functions $f_{\rm A}^{\rm stat}$, $f_{\delta{\rm A}}^{\rm stat}$ and f_1 are expanded in powers of the coupling g_0^2 as explained in [17] and [62], and the analogous expansion of $f_1^{\rm hh}$ is explained below.

B.1. The correlation function $f_1^{\rm hh}$

After integrating out the static quark fields, the correlation function $f_1^{\rm hh}$ can be written as

$$f_1^{\rm hh}(x_3) = \frac{a^2}{L^2} \sum_{x_1,x_2} \big\langle {\rm tr}\big\{ U(x,0)U(x+a\hat{0},0)\cdots U\big(x+(L-a)\hat{0},0\big) \times U\big((L-a)\hat{0},0\big)^{-1} U\big((L-2a)\hat{0},0\big)^{-1}\cdots U(0,0)^{-1}\big\}\big|_{x_0=0}\big\rangle, \tag{B.1}$$

where the trace is taken over color indices only.

Writing $U(x,\mu) = \exp\{g_0 a q_\mu(x)\}$, with the gluon field $q_\mu(x) = q_\mu^a(x)T^a$, where T^a are the anti-Hermitian generators of the gauge group, the function $f_1^{\rm hh}$ can be expanded in the bare coupling,

$$f_1^{\rm hh}(d) = 3 + g_0^2 f_1^{{\rm hh},(1)}(d) + {\rm O}\big(g_0^4\big), \quad d = |x_3|. \tag{B.2}$$

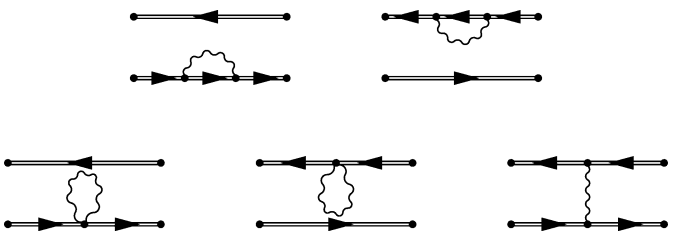

Fig. 11. One-loop diagrams contributing to f_1^{hh}. The two dots on the left are at $x_0 = 0$, the dots on the right are at $x_0 = L$.

Determining the one-loop coefficient $f_1^{\mathrm{hh},(1)}$ amounts to calculating and summing the diagrams shown in Fig. 11 using the gluon propagator $D_{\mu\nu}(x, y)$ (with SF boundary conditions) given in Ref. [58].

For comparison with the non-perturbative results shown in Fig. 4, Section 2.2, we consider the one-loop coefficient $h^{(1)}(d/L)$ of Eq. (2.13), which reads

$$h^{(1)}(d/L) = \frac{1}{3}\big\{f_1^{\mathrm{hh},(1)}(d) - f_1^{\mathrm{hh},(1)}(L/2)\big\}, \tag{B.3}$$

and which we can obtain analytically. (For the other quantities considered in this appendix, the diagrams are calculated numerically.) Only the last of the diagrams in Fig. 11 contributes, and we thus can write

$$\begin{aligned} &h^{(1)}(d/L) \\ &\quad= \frac{4a^6}{3L^4}\sum_{x_0,y_0}\sum_{x_1,y_1}\sum_{x_2,y_2}\big\{D_{00}(x,y)|_{x_3=d,\,y_3=0} - D_{00}(x,y)|_{x_3=L/2,\,y_3=0}\big\} \\ &\quad= \frac{4a^2}{3L^3}\sum_{p_3}\big\{\mathrm{e}^{ip_3 d} - \mathrm{e}^{ip_3 L/2}\big\}\sum_{x_0,y_0} d_{00}\big(x_0, y_0; (0,0,p_3)\big), \end{aligned} \tag{B.4}$$

with the momentum-space gluon propagator $d_{00}(x_0, y_0; \mathbf{p})$ defined in Ref. [58]. The $p_3 = 0$ term does not contribute to the sum, and using the explicit form of $d_{00}(x_0, y_0; \mathbf{p})$ for $\mathbf{p} \neq \mathbf{0}$, one can show that

$$a^2\sum_{x_0,y_0} d_{00}\big(x_0, y_0; (0,0,p_3)\big) = \frac{L}{\hat{p}_3^2} \tag{B.5}$$

with $\hat{p}_3 = \frac{2}{a}\sin\big(\frac{ap_3}{2}\big)$. Thus we see that $h^{(1)}(d/L)$ is just given in terms of the one-dimensional scalar propagator on a periodic lattice with length L, which has *no lattice artifacts*. This eventually leads to the result quoted in Eq. (2.14). The absence of any lattice spacing dependence is a consequence of the special kinematics, namely the summation over x_1, x_2, but will of course not be exact in higher orders of perturbation theory.

B.2. Anomalous dimensions

In order to precisely connect to the RGI current, it is important to obtain the anomalous dimension of the static-light axial current in the SF scheme at two-loop order. The

anomalous dimension is expanded as

$$\gamma(\bar{g}) = -\bar{g}^2\{\gamma_0 + \gamma_1^{\mathrm{SF}}\bar{g}^2 + \mathrm{O}(\bar{g}^4)\}, \tag{B.6}$$

with $\gamma_0 = -1/(4\pi^2)$ and the two-loop anomalous dimension in the SF scheme, γ_1^{SF}.

With the perturbative expansions for the various correlation functions, the ratio Ξ_{I} of Eq. (A.16) can be written as a series

$$\Xi_{\mathrm{I}}(g_0, a/L) = \Xi_{\mathrm{I}}^{(0)}(a/L) + g_0^2\,\Xi_{\mathrm{I}}^{(1)}(a/L) + \mathrm{O}(g_0^4). \tag{B.7}$$

Accordingly, this allows us to expand the SF renormalization constant $Z_{\mathrm{A}}^{\mathrm{stat}} = \Xi_{\mathrm{I}}^{(0)}/\Xi_{\mathrm{I}}$ (see Eq. (A.19)) as

$$Z_{\mathrm{A}}^{\mathrm{stat}} = Z_{\mathrm{A}}^{\mathrm{stat},(0)} + g_0^2 Z_{\mathrm{A}}^{\mathrm{stat},(1)} + \mathrm{O}(g_0^4). \tag{B.8}$$

With the one-loop relation between the bare lattice current and the renormalized static axial current in the $\overline{\mathrm{MS}}$ scheme, the anomalous dimension in the $\overline{\mathrm{MS}}$ scheme, Eq. (5.5) [38–40], can be converted into the SF scheme. The renormalization constant relating the SF scheme and the $\overline{\mathrm{MS}}$ scheme is obtained from the relation between the SF scheme and the bare lattice current, Eq. (B.8), the connection of the bare lattice current and a 'matching scheme' [63,64] and the relation between the latter and the $\overline{\mathrm{MS}}$ scheme [30]. Here the matching scheme is defined by the requirement that the renormalized static-light axial current at scale $\mu = m_{\mathrm{h}}$ equals the relativistic axial current with a heavy quark mass m_{h} up to terms of $\mathrm{O}(1/m_{\mathrm{h}})$, and the current in the relativistic theory is normalized by current algebra (imposing the chiral Ward identities).[6] Following the steps in Ref. [17], this analysis finally yields

$$\theta = 0.0: \quad \gamma_1^{\mathrm{SF}} = \frac{1}{(4\pi)^2}\{0.22(2) - 0.0552(13)N_{\mathrm{f}}\}, \tag{B.9}$$

$$\theta = 0.5: \quad \gamma_1^{\mathrm{SF}} = \frac{1}{(4\pi)^2}\{0.10(2) - 0.0477(13)N_{\mathrm{f}}\}, \tag{B.10}$$

$$\theta = 1.0: \quad \gamma_1^{\mathrm{SF}} = \frac{1}{(4\pi)^2}\{-0.08(2) - 0.0365(13)N_{\mathrm{f}}\}. \tag{B.11}$$

B.3. Discretization errors

The one-loop expansion at hand is also helpful to study discretization errors in the step scaling function. Using Eq. (B.8), the step scaling function at lattice spacing a is expanded as

$$\Sigma_{\mathrm{A}}^{\mathrm{stat}}(u, a/L) = 1 + u\,\Sigma_{\mathrm{A}}^{\mathrm{stat},(1)}(a/L) + \mathrm{O}(u^2), \tag{B.12}$$

and its continuum limit $\sigma_{\mathrm{A}}^{\mathrm{stat}}(u)$ as

$$\sigma_{\mathrm{A}}^{\mathrm{stat}}(u) = 1 + u\sigma_{\mathrm{A}}^{\mathrm{stat},(1)} + u^2\sigma_{\mathrm{A}}^{\mathrm{stat},(2)} + \mathrm{O}(u^3), \tag{B.13}$$

[6] Since the wording in Ref. [17] is not completely clear on this, we point out that $A_{\overline{\mathrm{MS}}}^{\mathrm{stat}}$ in that reference refers to what we call the $\overline{\mathrm{MS}}$ scheme here as well as in Ref. [17].

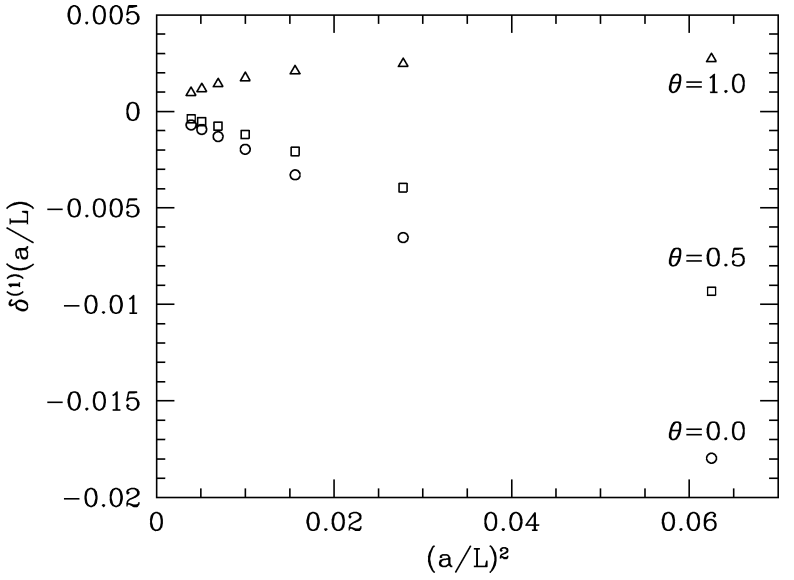

Fig. 12. Discretization errors of the step scaling function at one-loop level. The continuum extrapolation of the non-perturbative results uses $(a/L)^2 < 0.02$.

with

$$\sigma_{\mathrm{A}}^{\mathrm{stat},(1)} = \ln(2)\gamma_0,$$
$$\sigma_{\mathrm{A}}^{\mathrm{stat},(2)} = \frac{1}{2}\ln^2(2)\gamma_0^2 + \ln^2(2)b_0\gamma_0 + \ln(2)\gamma_1. \tag{B.14}$$

As a measure for the discretization errors, we define

$$\delta(u, a/L) = \frac{\Sigma_{\mathrm{A}}^{\mathrm{stat}}(u, a/L) - \sigma_{\mathrm{A}}^{\mathrm{stat}}(u)}{\sigma_{\mathrm{A}}^{\mathrm{stat}}(u)} \tag{B.15}$$

with a perturbative expansion

$$\delta(u, a/L) = \delta^{(1)}(a/L)u + \mathrm{O}\big(u^2\big). \tag{B.16}$$

The one-loop coefficient $\delta^{(1)}$ versus the lattice spacing squared is shown in Fig. 12 for different values of θ. In the range of lattice spacings where our non-perturbative calculation is performed, the discretization errors at one-loop level are smaller than $1\% \times u$, giving rise to the hope that also the non-perturbative discretization errors are reasonably small. A welcome feature of $\delta^{(1)}$ at $\theta = 0.5$ is that it is entirely dominated by the leading a^2/L^2-term in the a-expansion.

Appendix C. Continuum step scaling function and matching at $L = 1.436\,r_0$

In this last appendix we briefly discuss our parametrization (i.e., the interpolating fit) of the continuum step scaling function and some details on the calculation of $Z_{\rm A}^{\rm stat}$ at the matching scale $2L_{\rm max} = 1.436\,r_0$.

C.1. Fits and error determination in the scale evolution

As described in Appendix A.3, the continuum step scaling function $\sigma_{\rm A}^{\rm stat}(u)$ has been obtained by extrapolating the lattice data on $\Sigma_{\rm A}^{\rm stat}(u, a/L)$ at fixed u to the continuum limit. The next step is now to solve the recursion specified through Eqs. (3.1)–(3.4). In practice this is done by first representing the results for $\sigma_{\rm A}^{\rm stat}(u)$ in Table 1 by a fit and then solving the recursion, Eq. (3.4), with $\sigma_{\rm A}^{\rm stat}(u)$ given by the fit function.

Guided by the analysis for the step scaling function of the pseudoscalar density $\sigma_{\rm P}$ in Ref. [13] and the perturbative expansion discussed in Appendix B.3,

$$\sigma_{\rm A}^{\rm stat}(u) = 1 + s_0 u + s_1 u^2 + s_2 u^3 + \cdots + s_n u^{n+1} \tag{C.1}$$

is chosen as fit ansatz. The two non-trivial leading terms are restricted by perturbation theory,

$$s_0 = \sigma_{\rm A}^{\rm stat,(1)}, \qquad s_1 = \sigma_{\rm A}^{\rm stat,(2)}, \tag{C.2}$$

cf. Eqs. (B.14). Up to three additional free fit parameters were allowed for. All of these fits represent the data in Table 1 well, and we decided to quote the two-parameter fit (the curve of which is shown in Fig. 6) as the final result for the functional form of $\sigma_{\rm A}^{\rm stat}$. To check that the polynomial fits are stable, we also investigated fits where only s_0 or even no coefficient at all is constrained to its perturbative value. This leads to consistent results for $\sigma_{\rm A}^{\rm stat}(u)$; particularly the latter fit then reproduces the perturbative prediction for s_0.

Having chosen a definite expression for $\sigma_{\rm A}^{\rm stat}(u)$, the solution of the associated recursion is unique. Since the errors on the step scaling function stem from different simulation runs and are hence uncorrelated, the errors on the fit parameters in the polynomial (C.1) for $\sigma_{\rm A}^{\rm stat}(u)$ and those on the v_k's calculated from it can be estimated straightforwardly by the standard error propagation rules. Finally, by increasing the number of free fit parameters (while fixing s_0, s_1 to perturbation theory) as mentioned above, we convinced ourselves that the systematic error induced by the choice of fit functions is well under control: in fact, we then observed the expected pattern of finding slightly different errors but compatible results at comparably good overall fit quality.

C.2. Calculation of $Z_{\rm A}^{\rm stat}$ at the low-energy matching scale

The total renormalization factor $Z_{\rm RGI}$ introduced in Section 4 involves the value of the renormalization constant $Z_{\rm A}^{\rm stat}$ at our particular matching point: $Z_{\rm A}^{\rm stat}(g_0, L/a)|_{L=1.436\,r_0}$. As the latter connects a bare matrix element of the static-light axial current to the one renormalized in the SF scheme, this amounts to calculate $Z_{\rm A}^{\rm stat}$ for a range of bare couplings commonly used in simulations in physically large volumes.

Table 8
Results for $Z_{\rm A}^{\rm stat}(g_0, L/a)$ at fixed scale $L = 2L_{\rm max} = 1.436\,r_0$ with $c_{\rm t}$ being set to either one- or two-loop. The critical κ-values $\kappa = \kappa_{\rm c}$ [65] are the same as used for Table C.1 of Ref. [13]

L/a	$\beta = 6/g_0^2$	$c_{\rm t}^{\text{2-loop}}$		$c_{\rm t}^{\text{1-loop}}$	
		κ	$Z_{\rm A}^{\rm stat}$	κ	$Z_{\rm A}^{\rm stat}$
8	6.0219	0.13508	0.6926(15)	0.13504	0.6932(10)
10	6.1628	0.13565	0.6810(17)	0.13564	0.6824(16)
12	6.2885	0.13575	0.6786(18)	0.13574	0.6795(16)
16	6.4956	0.13559	0.6777(17)	0.13558	0.6763(18)

Table 9
Results for $Z_{\rm A}^{\rm stat}(g_0, L/a)$ at fixed scale $L = 2L_{\rm max} = 1.436\,r_0$ for $c_{\rm A}^{\rm stat} = 0$ and unimproved Wilson fermions (i.e., $c_{\rm sw} = 0$ and thus, $c_{\rm A} = c_{\rm A}^{\rm stat} = 0$ too), where $c_{\rm t}$ was kept at its two-loop value

L/a	$\beta = 6/g_0^2$	$c_{\rm A}^{\rm stat} = 0$		$c_{\rm sw} = 0$	
		κ	$Z_{\rm A}^{\rm stat}$	κ	$Z_{\rm A}^{\rm stat}$
4	5.6791	–	–	0.15268	0.6923(13)
6	5.8636	–	–	0.15451	0.6315(16)
8	6.0219	0.13508	0.6736(14)	0.15341	0.6075(13)
10	6.1628	0.13565	0.6633(17)	0.15202	0.5964(18)
12	6.2885	0.13575	0.6621(17)	0.15078	0.5971(32)
16	6.4956	0.13559	0.6627(17)	0.14887	0.5991(52)

To extract $Z_{\rm A}^{\rm stat}$ we exploit the fact that the required pairs $(L/a, \beta)$ that match the condition $L/a = 1.436\,r_0/a$ have already been determined for the relevant β-range in Appendix C of [13] by utilizing the known parametrization of $\ln(a/r_0)$ in terms of β from Ref. [34]. We thus could take over these pairs and computed $Z_{\rm A}^{\rm stat}$ for $\theta = 0.5$ from the renormalization condition (A.19) at the corresponding values $\kappa = \kappa_{\rm c}$ of the critical hopping parameter [65]. The results for $Z_{\rm A}^{\rm stat}(g_0, L/a)|_{L=1.436\,r_0}$ using the one- and two-loop expressions for $c_{\rm t}$, cf. Eq. (A.21), are given in Table 8. The difference originating from the two perturbative approximations for $c_{\rm t}$ is completely covered by the statistical errors so that we again consider $c_{\rm t}^{\text{2-loop}}$ to already account for the dominant part of the boundary cutoff effects in the gauge sector. Similarly to the discussion in Appendix A.3, the influence of the boundary improvement coefficient $\tilde{c}_{\rm t}$ in the fermionic sector can also be neglected at the level of our precision. The parametrization of the results for $Z_{\rm A}^{\rm stat}(g_0, L/a)|_{L=1.436\,r_0}$ by a polynomial fit in $(\beta - 6)$, with $c_{\rm t}^{\text{2-loop}}$ and $c_{\rm A}^{\rm stat}$ from one-loop perturbation theory, is quoted in Section 4, where the coefficients in the first block of Table 2 are to be combined with Eq. (4.1). The smooth dependence of $Z_{\rm A}^{\rm stat}$ on β in the studied region of bare couplings suggests that this representation can also be slightly extended down to $\beta = 6.0$ (even though we could not directly simulate that point for the same reason as in case of $Z_{\rm P}$ [13]), and we therefore regard it as a reliable representation of our data over the whole range $6.0 \leqslant \beta \leqslant 6.5$.

As in Appendix A.3, we also set $c_{\rm A}^{\rm stat} = 0$ instead of one-loop in the analysis of the data on $Z_{\rm A}^{\rm stat}(g_0, L/a)|_{L=1.436\,r_0}$, and the results are listed in the middle part of Table 9. In contrast to the step scaling function, which did not change appreciably under this

replacement of the value for $c_{\rm A}^{\rm stat}$, we observe an effect of about 3% in $Z_{\rm A}^{\rm stat}$ at the low-energy matching scale $L = 2L_{\rm max} = 1.436\,r_0$.

Furthermore, we addressed the case of unimproved Wilson fermions by also setting $c_{\rm sw} = 0$ in the relativistic fermion action and, after having computed the needed estimates of the critical hopping parameter for this situation, carried out the additional runs to determine the renormalization constant. In this case the pairs $(L/a, \beta)$ were extended to lower values of β in order to be able to make contact with the β-region that is typically employed in simulations to calculate the bare matrix element defining the B-meson decay constant, as, e.g., those in Refs. [10,11]. The resulting estimates on $Z_{\rm A}^{\rm stat}$ are shown in the right part of Table 9, and the corresponding polynomial representations for both aforementioned cases are as well found via Eq. (4.1) together with the two lower blocks of Table 2.

We conclude this discussion with the general remark that the uncertainties of the entering critical κ-values (of 1–2 and 2–4 on the last decimal place in the case of $c_{\rm sw} =$ non-perturbative and $c_{\rm sw} = 0$, respectively) do not affect the Z-factors significantly.

References

[1] N. Yamada, in: Lattice 2002, Proceedings of XXth International Symposium on Lattice Field Theory, Nucl. Phys. B (Proc. Suppl.) 119 (2003), hep-lat/0210035.
[2] M. Guagnelli, et al., Phys. Lett. B 546 (2002) 237, hep-lat/0206023.
[3] M. Guagnelli, et al., in: Lattice 2002, Proceedings of XXth International Symposium on Lattice Field Theory, Nucl. Phys. B (Proc. Suppl.) 119 (2003), hep-lat/0209113.
[4] E. Eichten, B. Hill, Phys. Lett. B 234 (1990) 511.
[5] C.R. Allton, et al., Nucl. Phys. B 349 (1991) 598.
[6] C. Alexandrou, et al., Phys. Lett. B 256 (1991) 60.
[7] APE Collaboration, C.R. Allton, et al., Phys. Lett. B 326 (1994) 295, hep-ph/9402343.
[8] C. Alexandrou, et al., Nucl. Phys. B 414 (1994) 815, hep-lat/9211042.
[9] C.W. Bernard, J.N. Labrenz, A. Soni, Phys. Rev. D 49 (1994) 2536, hep-lat/9306009.
[10] A. Duncan, et al., Phys. Rev. D 51 (1995) 5101, hep-lat/9407025.
[11] T. Draper, C. McNeile, Nucl. Phys. B (Proc. Suppl.) 34 (1994) 453, hep-lat/9401013.
[12] UKQCD Collaboration, A.K. Ewing, et al., Phys. Rev. D 54 (1996) 3526, hep-lat/9508030.
[13] ALPHA Collaboration, S. Capitani, et al., Nucl. Phys. B 544 (1999) 669, hep-lat/9810063.
[14] R. Sommer, in: Lattice 2002, Proceedings of XXth International Symposium on Lattice Field Theory, Nucl. Phys. B (Proc. Suppl.) 119 (2003), hep-lat/0209162.
[15] J. Heitger, Applications of non-perturbative renormalization, Contribution to 30th International Conference on High-Energy Physics (ICHEP 2000), Osaka, Japan, 27 July–2 August 2000, hep-ph/0010050.
[16] ALPHA Collaboration, J. Heitger, M. Kurth, R. Sommer, in: Lattice 2002, Proceedings of XXth International Symposium on Lattice Field Theory, Nucl. Phys. B (Proc. Suppl.) 119 (2003), hep-lat/0209078.
[17] ALPHA Collaboration, M. Kurth, R. Sommer, Nucl. Phys. B 597 (2001) 488, hep-lat/0007002.
[18] M. Lüscher, et al., Nucl. Phys. B 384 (1992) 168, hep-lat/9207009.
[19] S. Sint, Nucl. Phys. B 421 (1994) 135, hep-lat/9312079.
[20] S. Sint, R. Sommer, Nucl. Phys. B 465 (1996) 71, hep-lat/9508012.
[21] ALPHA Collaboration, M. Lüscher, et al., Nucl. Phys. B 478 (1996) 365, hep-lat/9605038.
[22] M. Lüscher, P. Weisz, U. Wolff, Nucl. Phys. B 359 (1991) 221.
[23] M. Lüscher, et al., Nucl. Phys. B 389 (1993) 247, hep-lat/9207010.
[24] M. Lüscher, et al., Nucl. Phys. B 413 (1994) 481, hep-lat/9309005.
[25] R. Sommer, Non-perturbative renormalization of QCD, Lectures given at 36th Internationale Universitätswochen für Kernphysik und Teilchenphysik, Schladming, Austria, 1–8 March 1997, hep-ph/9711243.

[26] M. Lüscher, Advanced lattice QCD, Lectures given at Les Houches Summer School in Theoretical Physics, Probing the Standard Model of Particle Interactions, Les Houches, France, 28 July–5 September 1997, hep-ph/9802029.
[27] ALPHA Collaboration, S. Sint, P. Weisz, Nucl. Phys. B 545 (1999) 529, hep-lat/9808013.
[28] M.A. Shifman, M.B. Voloshin, Sov. J. Nucl. Phys. 45 (1987) 292.
[29] H.D. Politzer, M.B. Wise, Phys. Lett. B 206 (1988) 681.
[30] E. Eichten, B. Hill, Phys. Lett. B 240 (1990) 193.
[31] G. Parisi, R. Petronzio, F. Rapuano, Phys. Lett. B 128 (1983) 418.
[32] K. Symanzik, Nucl. Phys. B 226 (1983) 187.
[33] R. Sommer, Nucl. Phys. B 411 (1994) 839, hep-lat/9310022.
[34] ALPHA Collaboration, M. Guagnelli, R. Sommer, H. Wittig, Nucl. Phys. B 535 (1998) 389, hep-lat/9806005.
[35] ALPHA Collaboration, M. Lüscher, et al., Nucl. Phys. B 491 (1997) 323, hep-lat/9609035.
[36] M. Neubert, Phys. Rep. 245 (1994) 259, hep-ph/9306320.
[37] M. Beneke, Phys. Rep. 317 (1999) 1, hep-ph/9807443.
[38] X. Ji, M.J. Musolf, Phys. Lett. B 257 (1991) 409.
[39] D.J. Broadhurst, A.G. Grozin, Phys. Lett. B 267 (1991) 105, hep-ph/9908362.
[40] V. Gimenez, Nucl. Phys. B 375 (1992) 582.
[41] T. van Ritbergen, J.A.M. Vermaseren, S.A. Larin, Phys. Lett. B 400 (1997) 379, hep-ph/9701390.
[42] K.G. Chetyrkin, Phys. Lett. B 404 (1997) 161, hep-ph/9703278.
[43] J.A.M. Vermaseren, S.A. Larin, T. van Ritbergen, Phys. Lett. B 405 (1997) 327, hep-ph/9703284.
[44] ALPHA, UKQCD Collaborations, J. Garden, et al., Nucl. Phys. B 571 (2000) 237, hep-lat/9906013.
[45] ALPHA Collaboration, M. Guagnelli, et al., Nucl. Phys. B 595 (2001) 44, hep-lat/0009021.
[46] H. Leutwyler, Principles of chiral perturbation theory, Lectures given at Hadrons 94 Workshop, Gramado, Brazil, 10–14 April 1994, hep-ph/9406283.
[47] ALPHA Collaboration, J. Heitger, R. Sommer, Nucl. Phys. B (Proc. Suppl.) 106 (2002) 358, hep-lat/0110016.
[48] G.P. Lepage, P.B. Mackenzie, Phys. Rev. D 48 (1993) 2250, hep-lat/9209022.
[49] S. Hashimoto, T. Ishikawa, T. Onogi, Nucl. Phys. B (Proc. Suppl.) 106 (2002) 352.
[50] C. Alexandrou, et al., Z. Phys. C 62 (1994) 659, hep-lat/9312051.
[51] R. Sommer, Phys. Rep. 275 (1996) 1, hep-lat/9401037.
[52] H. Wittig, Heavy Quarks on the lattice: status and perspectives, Lectures given at International School of Physics Enrico Fermi, Varenna, Italy, 8–18 July 1997, hep-lat/9710088.
[53] ALPHA Collaboration, J. Rolf, S. Sint, JHEP 12 (2002) 007, hep-ph/0209255.
[54] ALPHA Collaboration, A. Jüttner, J. Rolf, Phys. Lett. B 560 (2003) 59–63, hep-lat/0302016.
[55] C. Morningstar, J. Shigemitsu, Phys. Rev. D 57 (1998) 6741, hep-lat/9712016.
[56] K.I. Ishikawa, T. Onogi, N. Yamada, Nucl. Phys. B (Proc. Suppl.) 83–84 (2000) 301, hep-lat/9909159.
[57] ALPHA Collaboration, A. Bode, P. Weisz, U. Wolff, Nucl. Phys. B 576 (2000) 517, hep-lat/9911018.
[58] M. Lüscher, P. Weisz, Nucl. Phys. B 479 (1996) 429, hep-lat/9606016.
[59] B. Gehrmann, PhD thesis, 2002, hep-lat/0207016.
[60] ALPHA Collaboration, M. Guagnelli, J. Heitger, Comput. Phys. Commun. 130 (2000) 12, hep-lat/9910024.
[61] S. Fischer, et al., Comput. Phys. Commun. 98 (1996) 20, hep-lat/9602019.
[62] ALPHA Collaboration, S. Sint, P. Weisz, Nucl. Phys. B 502 (1997) 251, hep-lat/9704001.
[63] ALPHA Collaboration, M. Kurth, R. Sommer, Nucl. Phys. B 623 (2002) 271, hep-lat/0108018.
[64] A. Borrelli, C. Pittori, Nucl. Phys. B 385 (1992) 502.
[65] H. Wittig, private communication.

I

Lattice HQET with exponentially improved statistical precision

Phys. Lett. B581 (2004) 93-98

Available online at www.sciencedirect.com
SCIENCE DIRECT®
Physics Letters B 581 (2004) 93–98
PHYSICS LETTERS B
www.elsevier.com/locate/physletb

Lattice HQET with exponentially improved statistical precision

ALPHA Collaboration

Michele Della Morte [a], Stephan Dürr [a], Jochen Heitger [b], Heiko Molke [a], Juri Rolf [c], Andrea Shindler [d], Rainer Sommer [a]

[a] *DESY, Zeuthen, Germany*
[b] *Institut für Theoretische Physik, Universität Münster, Münster, Germany*
[c] *Institut für Physik, Humboldt Universität, Berlin, Germany*
[d] *NIC, Zeuthen, Germany*

Received 28 July 2003; received in revised form 3 November 2003; accepted 26 November 2003

Editor: G.F. Giudice

Abstract

We introduce an alternative discretization for static quarks on the lattice retaining the O(a)-improvement properties of the Eichten–Hill action. In this formulation, statistical fluctuations are reduced by a factor which grows exponentially with Euclidean time, x_0. For the first time, B-meson correlation functions are computed with good statistical precision in the static approximation for $x_0 > 1$ fm. At lattice spacings $a \approx 0.1$, 0.08, 0.07 fm, the B_s-meson decay constant is determined in the combined static and quenched approximation. A correction due to the finite mass of the b-quark is estimated by interpolating between the static result and a recent determination of F_{D_s}.

PACS: 11.15.Ha; 12.15.Hh; 12.38.Gc; 12.39.Hg; 13.20.He

Keywords: Lattice QCD; Heavy quark effective theory; Static approximation; Modified static actions; B-meson decay constant

1. B-physics matrix elements such as the B-meson decay constant F_B are obtained from lattice correlation functions at large Euclidean time. Considerable interest lies in the treatment of the b-quark in the leading order of HQET, the static approximation [1,2]: in this framework non-perturbative renormalization can be performed, the continuum limit exists and also $1/m_b$ corrections can in principle be taken into account [3–6].

Progress along this line has been hampered by large statistical errors in the static approximation. In particular it has been observed [7] that the errors of a B-meson correlation function roughly grow as

$$R_{\mathrm{NS}} \equiv \frac{\text{noise}}{\text{signal}} \propto \exp(x_0\Delta), \quad \Delta = E_{\mathrm{stat}} - m_\pi, \qquad (1)$$

where E_{stat} is the ground state energy of a B-meson in the static approximation with the Eichten–Hill action,[1]

[1] For a more precise definition of the theory and for any unexplained notation we refer to [3].

E-mail address: sommer@mail.cern.ch (R. Sommer).

0370-2693/$ – see front matter © 2003 Published by Elsevier B.V.
doi:10.1016/j.physletb.2003.11.064

$$S_{\rm h}^{\rm EH} = a^4 \sum_x \bar{\psi}_{\rm h}(x) D_0 \psi_{\rm h}(x), \tag{2}$$

$$D_0\psi_{\rm h}(x) = \frac{1}{a}\big[\psi_{\rm h}(x) - U^\dagger(x-a\hat{0},0)\psi_{\rm h}(x-a\hat{0})\big], \tag{3}$$

for the static quark [2]. Eq. (1) is problematic because the requirement $R_{\rm NS} \ll 1$ is satisfied only for x_0 of the order of Δ^{-1} and this time interval shrinks rapidly to zero in the continuum limit $a \to 0$ where $E_{\rm stat} \sim e_1 \times g_0^2/a$ with some number e_1. In the attempt to eliminate the discretization errors by reducing the lattice spacing, a, one is then limited more and more by unwanted contaminations by higher energy states and it has been very difficult to compute matrix elements in the static approximation [1,8–11]. Since the exponent in Eq. (1) is dominated by a divergent term, it is plausible that one may reduce it by changing the discretization. Here we will demonstrate that this is indeed possible while *remaining with roughly the same discretization errors.*

In [3] it has been shown that energy differences computed with the action Eq. (2) are O(a)-improved if the relativistic sector (light quarks and gluons) is O(a)-improved. Furthermore, apart from the usual mass dependent factor, $1 + b_{\rm A}^{\rm stat} a m_{\rm q}$, the static axial current,

$$A_0^{\rm stat}(x) = \bar{\psi}_{\rm l}(x)\gamma_0\gamma_5\psi_{\rm h}(x), \tag{4}$$

is on-shell O(a)-improved after adding only one correction term,

$$\big(A_{\rm I}^{\rm stat}\big)_0 = A_0^{\rm stat} + a c_{\rm A}^{\rm stat}\delta A_0^{\rm stat},$$
$$\delta A_0^{\rm stat}(x) = \bar{\psi}_{\rm l}(x)\gamma_j\gamma_5 \frac{\overleftarrow{\nabla}_j + \overleftarrow{\nabla}_j^*}{2}\psi_{\rm h}(x). \tag{5}$$

We want to retain these properties of the theory. They are guaranteed if the lattice Lagrangian is invariant under the following symmetry transformations (we do not list the usual ones such as parity and cubic invariance) [3].

(i) Heavy quark spin symmetry:

$$\psi_{\rm h} \to \mathcal{V}\psi_{\rm h}, \qquad \bar{\psi}_{\rm h} \to \bar{\psi}_{\rm h}\mathcal{V}^{-1},$$
$$\text{with } \mathcal{V} = \exp(-i\phi_i\epsilon_{ijk}\sigma_{jk}). \tag{6}$$

(ii) Local conservation of heavy quark flavor number:

$$\psi_{\rm h} \to {\rm e}^{i\eta(\mathbf{x})}\psi_{\rm h}, \qquad \bar{\psi}_{\rm h} \to \bar{\psi}_{\rm h}{\rm e}^{-i\eta(\mathbf{x})}. \tag{7}$$

Keeping these symmetries intact, there is little freedom to modify the action. We may, however, alter the way the gauge fields enter the discretized covariant derivative, D_0. To this end we choose

$$D_0\psi_{\rm h}(x) = \frac{1}{a}\big[\psi_{\rm h}(x) - W^\dagger(x-a\hat{0},0)\psi_{\rm h}(x-a\hat{0})\big], \tag{8}$$

with $W(x,0)$ a generalized gauge parallel transporter with the gauge transformation properties of $U(x,0)$. In particular, we take $W(x,0)$ to be a function of the link variables in the neighborhood of x, which is invariant under spatial cubic rotations and does have the correct classical continuum limit such that $D_0 = \partial_0 + A_0 + {\rm O}(a^2)$. This is enough to ensure that the universality class as well as O(a)-improvement are unchanged in comparison to Eq. (3). Since we expect the size of remaining higher-order lattice artifacts to be moderate if one keeps the action rather local, we here consider only choices where $W(x,0)$ is a function of gauge fields in the immediate neighborhood of x, $x + a\hat{0}$. We choose

$$W_{\rm S}(x,0) = V(x,0)\left[\frac{g_0^2}{5} + \left(\frac{1}{3}\,{\rm tr}\,V^\dagger(x,0)V(x,0)\right)^{1/2}\right]^{-1}, \tag{9}$$

$$W_{\rm A}(x,0) = V(x,0), \tag{10}$$

$$W_{\rm HYP}(x,0) = V_{\rm HYP}(x,0), \tag{11}$$

where

$$V(x,0) = \frac{1}{6}\sum_{j=1}^{3}\big[U(x,j)U(x+a\hat{j},0)U^\dagger(x+a\hat{0},j) + U^\dagger(x-a\hat{j},j)U(x-a\hat{j},0) \times U(x+a\hat{0}-a\hat{j},j)\big], \tag{12}$$

and where the so-called HYP-link, $V_{\rm HYP}(x,0)$, is a function of the gauge links located within a hypercube [12,13]. In the latter case we take the parameters $\alpha_1 = 0.75$, $\alpha_2 = 0.6$, $\alpha_3 = 0.3$ [12]. The choices (9)–(11) will be motivated further in [14]. It is worth pointing out that a covariant derivative of the general type used above has first been introduced in [15]. In this reference it was considered for the Kogut–Susskind action for relativistic quarks and with a different motivation.

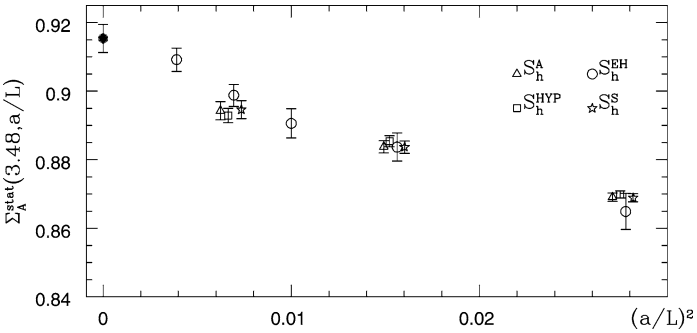

Fig. 1. The step scaling function $\Sigma_{\rm A}^{\rm stat}(3.48, a/L)$ for different choices of the action $S_{\rm h}$. Results for $S_{\rm h}^{\rm EH}$ were extrapolated to $\Sigma_{\rm A}^{\rm stat}(3.48, 0)$ [17] (•). In all cases $c_{\rm A}^{\rm stat}$ from 1-loop perturbation theory is used, which is sufficient since $\Sigma_{\rm A}^{\rm stat}(3.48, a/L)$ does not depend very sensitively on this improvement coefficient. For $S_{\rm h}^{\rm A}$, $S_{\rm h}^{\rm S}$ and $S_{\rm h}^{\rm HYP}$ points have been displaced on the horizontal axis for clarity.

2. Next we have to study the scaling behaviour of observables computed with the actions $S_{\rm h}^{\rm S}, S_{\rm h}^{\rm A}, S_{\rm h}^{\rm HYP}$ which are obtained by inserting $W_{\rm S}, W_{\rm A}, W_{\rm HYP}$ into Eqs. (8) and (2). In [14] this scaling behaviour is analyzed in depth for various observables and various choices for the static action in perturbation theory and non-perturbatively. Here we will present only one example. The necessity of such an investigation can be underlined by the following consideration.

The static potential can be seen as an energy for a static quark with action $S_{\rm h}$ and an antiquark with the corresponding $S_{\bar{\rm h}}$ [16]. Hence, the static force is one indicator for the scaling behaviour of these actions. In [13], rather large a^2-effects have been seen in the short-distance force for $S_{\rm h}^{\rm HYP}$ and $S_{\bar{\rm h}}^{\rm HYP}$.

One may therefore worry about large a-effects, in particular in correlation functions of the static-light axial current, where static and light quarks propagate also close to each other. With the new actions, $A_0^{\rm stat}$ is O(a)-improved once [14]

$$c_{\rm A}^{\rm stat} = -0.08237 g_0^2 + {\rm O}\big(g_0^4\big), \qquad \text{for } S_{\rm h} = S_{\rm h}^{\rm EH}, \tag{13}$$

$$c_{\rm A}^{\rm stat} = -0.1164(10) g_0^2 + {\rm O}\big(g_0^4\big), \quad \text{for } S_{\rm h} = S_{\rm h}^{\rm S}, S_{\rm h}^{\rm A}, \tag{14}$$

$$c_{\rm A}^{\rm stat} = -0.090(3) g_0^2 + {\rm O}\big(g_0^4\big), \qquad \text{for } S_{\rm h} = S_{\rm h}^{\rm HYP}, \tag{15}$$

is set in Eq. (5). The improvement coefficient $b_{\rm A}^{\rm stat}$ is set to its tree-level value $b_{\rm A}^{\rm stat} = 1/2$ in this Letter.

We consider now a step scaling function, $\Sigma_{\rm A}^{\rm stat}$, which gives the change of the renormalized static axial current in a Schrödinger functional (SF) scheme [17], when the renormalization scale is changed from $\mu = 1/L$ to $\mu = 1/(2L)$. Its continuum limit is known for a few values of L [17]. This quantity is thus a good observable to search for a-effects. In Fig. 1 we show $\Sigma_{\rm A}^{\rm stat}(3.48, a/L)$, where the first argument parameterizes L in terms of the SF-coupling $\bar{g}^2(L) = 3.48$. O(a)-improvement is employed as in [17] but we consider the different actions for the static quark introduced above. All of them lead to $\Sigma_{\rm A}^{\rm stat}(3.48, a/L)$ at finite a/L differing from the continuum limit by about the same amount. Supported also by further such studies [14], we conclude that within the set of actions studied none is particularly distinguished by its scaling behavior.

3. Let us now demonstrate that the statistical errors at large Euclidean time are reduced by the choices Eqs. (9)–(11). As a B-meson correlation function we choose

$$f_{\rm A}^{\rm stat}(x_0, \omega) = -\frac{1}{2}\big\langle \big(A_{\rm I}^{\rm stat}\big)_0(x)\mathcal{O}(\omega)\big\rangle,$$

$$\mathcal{O}(\omega) = \frac{a^6}{L^3}\sum_{\mathbf{y},\mathbf{z}} \bar{\zeta}_{\rm h}(\mathbf{y})\gamma_5\omega(\mathbf{y}-\mathbf{z})\zeta_{\rm l}(\mathbf{z}), \tag{16}$$

defined in the Schrödinger functional with $T = 3L/2$, $L/a = 24$, $\beta = 6/g_0^2 = 6.2$ and a vanishing background field [3]. Here, as a novelty compared to previous applications, a wave function $\omega(\mathbf{x})$ is introduced to construct an interpolating B-meson field in terms of the boundary quark fields $\zeta_{\rm l}$ and $\bar{\zeta}_{\rm h}$. It may be exploited to reduce the contribution of excited B-meson states to the correlation function, but this does not concern us yet. At the moment we simply consider

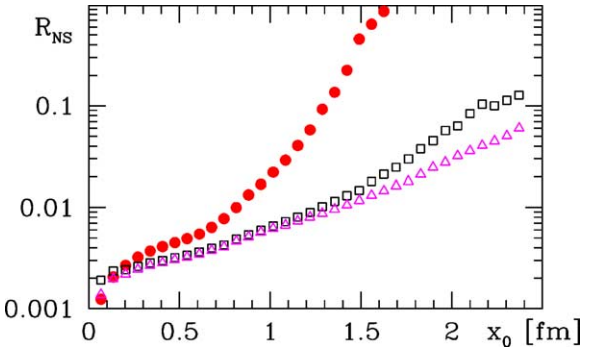

Fig. 2. The ratio $R_{\rm NS}$, Eq. (1), for the correlation function $f_{\rm A}^{\rm stat}$ for a statistics of 2500 measurements. Circles refer to $S_{\rm h}^{\rm EH}$ while squares and triangles to $S_{\rm h}^{\rm S}$ and $S_{\rm h}^{\rm HYP}$, respectively. $S_{\rm h}^{\rm A}$ behaves like $S_{\rm h}^{\rm S}$. Physical units are set by using $r_0 = 0.5$ fm [20,21].

$\omega(\mathbf{x}) = 1$ and form the ratio $R_{\rm NS}$, Eq. (1), for the different actions. From now on we set the light quark mass to the *strange quark mass*, taken from [18] following exactly [19] concerning the technical details.[2] Fig. 2 shows that in all cases $R_{\rm NS}$ grows exponentially with x_0. For the Eichten–Hill action, also the effective coefficient Δ, describing the growth for $x_0 = 1$–2 fm, is *roughly* given by $E_{\rm stat} - m_\pi$ in agreement with Eq. (1), while for the other actions this is not the case. Most importantly for the other actions, Δ is reduced by a factor around 4, and with the statistics in our example a distance of $x_0 \approx 2$ fm is reached with $S_{\rm h}^{\rm HYP}$ if one requires $R_{\rm NS} \leqslant 2\%$. The actions $S_{\rm h}^{\rm A}$, $S_{\rm h}^{\rm S}$ behave only slightly worse.

4. This reduction of statistical errors enables us to choose $\omega(\mathbf{x})$ such that a long and precise plateau is visible in the effective energy,

$$E_{\rm eff}(x_0,\omega) = \ln\bigl[f_{\rm A}^{\rm stat}(x_0-a,\omega)/f_{\rm A}^{\rm stat}(x_0+a,\omega)\bigr]\big/(2a), \quad (17)$$

as shown in Fig. 3. Neither position nor length of the plateau depend sensitively on the details of ω, as long as it is chosen such that the first excited state in the B-meson channel is canceled to a good approximation. For the figure as well as for the following, we have chosen $\omega \in \{\Omega_1, \Omega_2\}$ with

$$\Omega_1 = \omega_1 + \alpha\omega_3, \qquad \Omega_2 = \omega_2 + \alpha'\omega_4, \quad (18)$$

$$\omega_i(\mathbf{x}) = N_i^{-1} \sum_{\mathbf{n}\in\mathbf{Z}^3} \bar\omega_i\bigl(|\mathbf{x}-\mathbf{n}L|\bigr), \quad i = 1,2,3,$$
$$\bar\omega_1(r) = r_0^{-3/2}\mathrm{e}^{-r/a_0}, \qquad \bar\omega_2(r) = r_0^{-3/2}\mathrm{e}^{-r/(2a_0)},$$
$$\bar\omega_3(r) = r_0^{-5/2} r\mathrm{e}^{-r/(2a_0)}, \qquad \omega_4(\mathbf{x}) = L^{-3/2}, \quad (19)$$

where $a_0 = 0.1863 r_0$ and the (dimensionless) coefficients N_i are chosen such that $a^3\sum_{\mathbf{x}}\omega_i^2(\mathbf{x}) = 1$. The B-meson decay constant is then obtained from the renormalization group invariant matrix element [22]

$$\Phi_{\rm RGI}(x_0) = -Z_{\rm RGI}\bigl(1 + b_{\rm A}^{\rm stat} a m_{\rm q}\bigr) 2L^{3/2} \times \frac{f_{\rm A}^{\rm stat}(x_0)}{\sqrt{f_1(T',\omega)}} \mathrm{e}^{(x_0 - T'/2)E_{\rm eff}(x_0)} \quad (20)$$

of the static axial current, where

$$f_1(T,\omega) = -\frac{1}{2}\bigl\langle \mathcal{O}'(\omega)\mathcal{O}(\omega)\bigr\rangle,$$
$$\mathcal{O}'(\omega) = \frac{a^6}{L^3}\sum_{\mathbf{y},\mathbf{z}} \bar\zeta_{\rm l}'(\mathbf{y})\gamma_5\omega(\mathbf{y}-\mathbf{z})\zeta_{\rm h}'(\mathbf{z}). \quad (21)$$

The renormalization factor, $Z_{\rm RGI}$, relates the bare matrix element to the renormalization group invariant one [17]. Its regularization dependent part is computed exactly as in that reference, but for the new actions. In Table 1 we give results for $\Phi_{\rm RGI}(x_0)$ for three values of the lattice spacing and selected choices of T, T', x_0, highlighting what we selected for further analysis. These numbers do not change significantly if we vary the improvement coefficients $c_{\rm A}^{\rm stat}$ and $b_{\rm A}^{\rm stat}$, which are known only in perturbation theory, by factors of two. We thus extrapolate our results quadratically in the lattice spacing and arrive at our estimate for the continuum limit

$$r_0^{3/2}\Phi_{\rm RGI} = 1.74(13). \quad (22)$$

5. The result Eq. (22) may be used to compute $F_{\rm B_s}$ by taking account of the mass dependent function [17] $C_{\rm PS}(M_{\rm b}/\Lambda_{\overline{\rm MS}}) = F_{\rm B}\sqrt{m_{\rm B}}/\Phi_{\rm RGI} = 1.22(3)$, evaluated using the 3-loop anomalous dimension [23] and the associated matching coefficient between HQET and QCD [24]. $M_{\rm b}$ denotes the renormalization group invariant b-quark mass [4,5]. With

[2] Of course, these details matter only before taking the continuum limit.

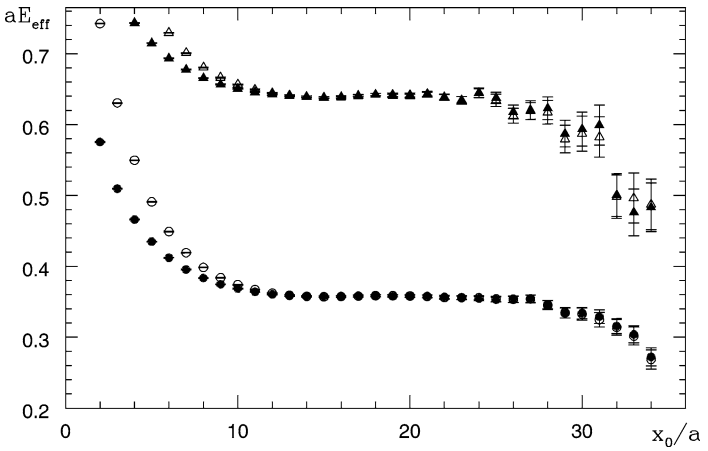

Fig. 3. Effective energies for wave functions Ω_1 (open symbols) and Ω_2 (filled symbols) using $S_{\rm h}^{\rm HYP}$ (circles) and $S_{\rm h}^{\rm S}$ (triangles). Results refer to a $24^3 \times 36$ lattice, $\beta = 6.2$.

Table 1
Decay constant in static approximation for action $S_{\rm h} = S_{\rm h}^{\rm HYP}$.

						$r_0^{3/2}\Phi_{\rm RGI}$			
β	a [fm]	L/a	T/a	T'/a	x_0/a	Ω_1	Ω_2	α	α'
6.0	0.093	16	24	24	12	1.794(30)	**1.797(28)**	0.278	−0.200
6.0	0.093	16	24	20	12	1.812(17)	1.796(17)	0.278	−0.200
6.0	0.093	16	24	24	10	1.784(30)	1.794(29)	0.278	−0.200
6.0	0.093	16	24	20	10	1.815(17)	1.793(17)	0.278	−0.200
6.1	0.079	24	30	30	15	1.834(59)	**1.830(55)**	0.756	0.022
6.1	0.079	24	30	30	12	1.822(59)	1.821(55)	0.756	0.022
6.2	0.068	24	36	36	18	1.685(76)	**1.724(74)**	0.351	−0.176
6.2	0.068	24	36	36	15	1.688(77)	1.728(75)	0.351	−0.176

this we arrive at $r_0 F_{\rm B_s}^{\rm stat} = 0.57(4)$ tantamount to $F_{\rm B_s}^{\rm stat} = 225(16)$ MeV with $r_0 = 0.5$ fm. A correction due to the finite mass of the b-quark can be computed by connecting the static result Eq. (22) and

$$r_0^{3/2} \frac{F_{\rm D_s}\sqrt{m_{\rm D_s}}}{C_{\rm PS}(M_{\rm c}/\Lambda_{\overline{\rm MS}})} = 1.33(7) \tag{23}$$

by a linear interpolation in the inverse meson mass. Here we have used recent computations of the $\rm D_s$-meson decay constant [25] and of the charm quark mass [19]. In this way we obtain

$$r_0 F_{\rm B_s} = 0.52(3) \to F_{\rm B_s} = 205(12)\ \text{MeV} \quad \text{with } r_0 = 0.5\ \text{fm}. \tag{24}$$

One may consider half of the difference to the static value, i.e., ≈5% as an additional uncertainty due to the interpolation used, but our personal estimate is that this error is smaller and it will soon be quantified [26].

One should remember that Eq. (24) refers to the quenched approximation and as in [25] a 12% scale ambiguity may be estimated from the slope of the linear interpolation.

6. An interesting point is that the potential in full QCD may be computed replacing the time-like links in the Wilson loop (or Polyakov loops) by the different W_i introduced above. In particular the "HYP-link potential" [13] may be used. Depending on which W_i is chosen, the static potentials differ from each other, but all of them approach the continuum limit with $\rm O(a^2)$ corrections if the action used for the dynamical fermions is $\rm O(a)$-improved. This property

follows from the considerations of [16] applied to the static actions introduced above, which satisfy all the necessary requirements. This virtue of, e.g., the HYP-link potential was not obvious before. Using it, better precision can be reached and some signs of string breaking [27] may become visible.

7. To summarize, we have shown that a modification of the Eichten–Hill static action can be found which keeps lattice artifacts in heavy–light correlation functions moderate but reduces statistical errors to a level making the region $x_0 > 1.5$ fm accessible. Furthermore, the new action can be used without change for dynamical fermions and also to compute the static potential with dynamical fermions. As a demonstration of the usefulness of this reduction of statistical errors, we have computed $F_{\mathrm{B_s}}$ in the quenched approximation, by joining the continuum limit of the static approximation estimated with the new action with the previously determined continuum limit of $F_{\mathrm{D_s}}$ by means of a linear interpolation. This procedure can systematically be improved by computing (1) the mass dependence around m_{c}, (2) the $1/m$ corrections to the static limit and (3) repeating the whole analysis with dynamical fermions. Work along these lines is in progress and a more detailed investigation of the properties of various static quark actions is in preparation.

Acknowledgements

We are grateful to M. Lüscher and F. Knechtli for comments on the manuscript. We thank DESY for allocating computer time on the APEmille computers at DESY Zeuthen to this project and the APE-group for its valuable help. This work is also supported by the EU IHP Network on Hadron Phenomenology from Lattice QCD under grant HPRN-CT-2000-00145 and by the Deutsche Forschungsgemeinschaft in the SFB/TR 09.

References

[1] E. Eichten, Talk delivered at the International Symposium of Field Theory on the Lattice, Seillac, France, 28 September–2 October, 1987.
[2] E. Eichten, B. Hill, Phys. Lett. B 234 (1990) 511.
[3] ALPHA Collaboration, M. Kurth, R. Sommer, Nucl. Phys. B 597 (2001) 488, hep-lat/0007002.
[4] ALPHA Collaboration, J. Heitger, R. Sommer, Nucl. Phys. B (Proc. Suppl.) 106 (2002) 358, hep-lat/0110016.
[5] R. Sommer, hep-lat/0209162.
[6] J. Heitger, M. Kurth, R. Sommer, hep-lat/0209078.
[7] S. Hashimoto, Phys. Rev. D 50 (1994) 4639, hep-lat/9403028.
[8] C.R. Allton, et al., Nucl. Phys. B 349 (1991) 598.
[9] C. Alexandrou, et al., Phys. Lett. B 256 (1991) 60.
[10] A. Duncan, et al., Phys. Rev. D 51 (1995) 5101, hep-lat/9407025.
[11] R. Sommer, Phys. Rep. 275 (1996) 1, hep-lat/9401037.
[12] A. Hasenfratz, F. Knechtli, Phys. Rev. D 64 (2001) 034504, hep-lat/0103029.
[13] A. Hasenfratz, R. Hoffmann, F. Knechtli, Nucl. Phys. B (Proc. Suppl.) 106 (2002) 418, hep-lat/0110168.
[14] M. Della Morte, A. Shindler, R. Sommer, in preparation.
[15] T. Blum, et al., Phys. Rev. D 55 (1997) 1133, hep-lat/9609036.
[16] S. Necco, R. Sommer, Nucl. Phys. B 622 (2002) 328, hep-lat/0108008.
[17] J. Heitger, M. Kurth, R. Sommer, hep-lat/0302019.
[18] ALPHA Collaboration, J. Garden, et al., Nucl. Phys. B 571 (2000) 237, hep-lat/9906013.
[19] ALPHA Collaboration, J. Rolf, S. Sint, JHEP 12 (2002) 007, hep-ph/0209255.
[20] R. Sommer, Nucl. Phys. B 411 (1994) 839, hep-lat/9310022.
[21] ALPHA Collaboration, M. Guagnelli, R. Sommer, H. Wittig, Nucl. Phys. B 535 (1998) 389, hep-lat/9806005.
[22] ALPHA Collaboration, M. Guagnelli, et al., Nucl. Phys. B 560 (1999) 465, hep-lat/9903040.
[23] K.G. Chetyrkin, A.G. Grozin, hep-ph/0303113.
[24] D.J. Broadhurst, A.G. Grozin, Phys. Rev. D 52 (1995) 4082, hep-ph/9410240.
[25] ALPHA Collaboration, A. Jüttner, J. Rolf, Phys. Lett. B 560 (2003) 59, hep-lat/0302016.
[26] ALPHA Collaboration, in preparation.
[27] K. Schilling, Nucl. Phys. B (Proc. Suppl.) 83 (2000) 140, hep-lat/9909152.

J

Non-perturbative heavy quark effective theory

J. High Energy Phys. 0402 (2004) 022

Published by Institute of Physics Publishing for SISSA/ISAS
Received: *December 15, 2003*
Accepted: *February 9, 2004*

Non-perturbative heavy quark effective theory

ALPHA Collaboration

Jochen Heitger

Westfälische Wilhelms-Universität Münster, Institut für Theoretische Physik
Wilhelm-Klemm-Strasse 9, D-48149 Münster, Germany
E-mail: heitger@uni-muenster.de

Rainer Sommer

Deutsches Elektronen-Synchrotron DESY, Zeuthen
Platanenallee 6, D-15738 Zeuthen, Germany, and
CERN, Theory Division
CH-1211 Geneva 23, Switzerland
E-mail: rainer.sommer@desy.de

Abstract: We explain how to perform non-perturbative computations in HQET on the lattice. In particular the problem of the subtraction of power-law divergences is solved by a non-perturbative matching of HQET and QCD. As examples, we present a full calculation of the mass of the b-quark in the combined static and quenched approximation and outline an alternative way to obtain the B-meson decay constant at lowest order. Since no excessively large lattices are required, our strategy can also be applied including dynamical fermions.

Keywords: Quark Masses and SM Parameters, B-Physics, Heavy Quarks Physics, Lattice QCD.

JHEP02(2004)022

Contents

JHEP02(2004)022

1. Introduction

The physics of the mixing and decays of B-mesons is essential for a determination of unknown CKM-matrix elements and thus for our understanding of the violation of CP-symmetry in Nature. It is also still promising for the discovery of physics beyond the standard model of particle physics. Unfortunately, many of the experimental observations can only be related to the standard model parameters if transition matrix elements of the effective weak hamiltonian are known. These matrix elements between hadron states are

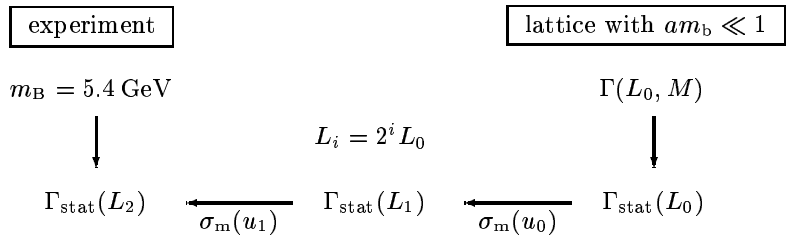

Figure 1: Relating experimental observables to properly renormalized HQET. Γ_stat is a renormalized quantity in HQET and $\sigma_\mathrm{m}(\bar{g}^2(L))$ connects $\Gamma_\mathrm{stat}(L)$ and $\Gamma_\mathrm{stat}(2L)$; their exact definitions will be given in the course of this paper. In the chosen example, the experimental observable is the mass of the B-meson.

only computable in a fully non-perturbative framework. They provide a strong motivation to study B-physics in lattice QCD. However, as the mass of the b-quark is larger than the affordable inverse lattice spacing in Monte Carlo simulations of lattice QCD, this quark escapes a direct treatment as a relativistic particle. Therefore, effective theories for the b-quark are being developed and used to compute the matrix elements in question [1, 2].

The first — and very promising — effective theory that was suggested is the Heavy Quark Effective Theory (HQET) [3, 4]. Like others, it is afflicted by a problem which remained unsolved so far: in general its parameters (the coefficients of the terms in the lagrangian) themselves have to be determined non-perturbatively, as briefly explained in section 2.2. In other words, the theory has to be renormalized non-perturbatively [5]. This fact is simply due to the mixing of operators of different dimensions in the lagrangian, requiring fine-tuning of their coefficients. If they were determined only perturbatively (in the QCD coupling), the continuum limit of the theory would not exist.

The issue is already present in the determination of the b-quark mass in the static approximation, i.e. in the lowest order of the effective theory. In [6] a strategy was introduced and successfully applied to this problem for the first time, and a general framework for a non-perturbative renormalization of HQET was sketched in [7]. The basic idea, illustrated in figure 1, is easily explained.

In a finite volume of linear extent $L_0 = \mathrm{O}(0.2\,\mathrm{fm})$, one may realize lattices with $am_\mathrm{b} \ll 1$ such that the b-quark can be treated as a standard relativistic fermion. At the same time the energy scale $1/L_0 = \mathrm{O}(1\,\mathrm{GeV})$ is still significantly below m_b and HQET applies quantitatively. Computing the same suitable observables in both theories relates the parameters of HQET to those of QCD. Then one moves, by an iterative procedure that we can still leave unspecified here, to larger and larger volumes and computes HQET observables. This yields the connection to a physically large volume (of linear extent $\mathrm{O}(2\,\mathrm{fm})$), where eventually the desired matrix elements are accessible.

Since in this way the parameters of HQET are determined from those of QCD, the predictive power of QCD is transfered to HQET. In addition to solving the renormalization problem of the effective theory, one also eliminates the usual need to determine more and more parameters of the theory from experiment as the effective theory is considered to higher and higher order.

JHEP02(2004)022

Although related, the strategy we propose here is not to be confused with the one for the computation of the running of the coupling and renormalization group invariant matrix elements as first suggested by Lüscher, Weisz and Wolff [8] and then developed by the ALPHA Collaboration. We will discuss the difference in section 5.2.4.

In this paper we define the effective theory in detail, discussing in particular its renormalization properties (section 2). We then explain the matching between QCD and HQET (section 3) as well as the finite-size strategy (section 4) in the general case. Section 5 provides two examples of applications using the effective theory at the lowest order in the inverse b-quark mass. The first one is the computation of the quark mass, where numerical results illustrate that indeed the power-law divergence can be subtracted non-perturbatively, retaining a very good precision for the final physical number. The second one, devoted to the B-meson decay constant, has not yet been applied numerically but is a useful and *simple* example to help in understanding our method. In section 6 we discuss the potential of our approach as well as the expected uncertainty due to the use of a finite order in the HQET expansion.

2. HQET on the lattice

In this section we define the effective field theory for QCD containing a heavy quark flavour in lattice regularization, starting from the formal $1/m$-expansion of the classical theory. We drop all terms involving the heavy anti-quark fields as they can be incorporated in complete analogy to those containing the heavy quark field $\psi_{\rm h}$ which we discuss in detail.[1] Renormalization properties are addressed but the proper choice of renormalization conditions and the physics content of the theory is deferred to the next section.

2.1 Definition of the effective theory

We consider QCD on the lattice. The explicit form of the gauge field and light fermion action, $S_{\rm rel}$, is not needed for our general discussion, but for some of the following statements to hold, an $\mathrm{O}(a)$ improved formulation is required, e.g. the one described in [9].[2] We denote the set of (bare) parameters of the theory with $N_{\rm f}$ relativistic quarks by $\mathcal{C}_{N_{\rm f}}$. Apart from the gauge coupling, g_0, and the quark masses, it will in general also cover some improvement coefficients [9].

As has been explained by Eichten and Hill [3, 4, 10], an effective field theory for hadrons (at rest) containing $N_{\rm f}-1$ light quarks and one heavy quark (b-quark) with mass m may be obtained by a formal $1/m$-expansion of the continuum QCD action and the fields, which appear in the correlation function under study. The action of the heavy quark is written in terms of the four-component field $\psi_{\rm h}$ satisfying

$$P_+\psi_{\rm h} = \psi_{\rm h}\,, \qquad \overline{\psi}_{\rm h}P_+ = \overline{\psi}_{\rm h}\,, \qquad P_+ = \frac{1}{2}(1+\gamma_0)\,. \tag{2.1}$$

[1] For simplicity we drop higher-dimensional operators in the effective field theory which involve only light quark fields and the gluon field. These terms contribute at higher order in $1/m$.

[2] $\mathrm{O}(a)$ improvement means that the continuum limit is reached with corrections of $\mathrm{O}(a^2)$.

Including terms up to the order $1/m^n$ in the expansion, the action, discretized on a Euclidean lattice, reads

$$S_{\rm HQET} = a^4 \sum_x \left\{ \mathcal{L}_{\rm stat}(x) + \sum_{\nu=1}^{n} \mathcal{L}^{(\nu)}(x) \right\}, \tag{2.2}$$

$$\mathcal{L}_{\rm stat}(x) = \overline{\psi}_{\rm h}(x) \left[\nabla_0^* + \delta m \right] \psi_{\rm h}(x), \tag{2.3}$$

$$\mathcal{L}^{(\nu)}(x) = \sum_i \omega_i^{(\nu)} \mathcal{L}_i^{(\nu)}(x), \tag{2.4}$$

where ∇_μ^* denotes the backward lattice derivative, δm has mass-dimension one, and the local composite fields $\mathcal{L}_i^{(\nu)}$ have mass-dimension $4+\nu$. Indeed, this form is suggested by a formal $1/m$-expansion at the classical level which yields[3]

$$\begin{aligned} & & \delta m &= 0, \\ \mathcal{L}_1^{(1)} &= \overline{\psi}_{\rm h} \left(-\frac{1}{2}\, \sigma \cdot \mathbf{B} \right) \psi_{\rm h}, & \omega_1^{(1)} &= \frac{1}{m}, \\ \mathcal{L}_2^{(1)} &= \overline{\psi}_{\rm h} \left(-\frac{1}{2}\, \mathbf{D}^2 \right) \psi_{\rm h}, & \omega_2^{(1)} &= \frac{1}{m} \end{aligned} \tag{2.5}$$

up to and including the order $1/m$. Here, $\mathbf{B}$ is a discretized version of the chromomagnetic field strength and $\mathbf{D}^2$ a lattice version of the covariant laplacian in three dimensions. Note that a term $m\,\overline{\psi}_{\rm h}(x)\psi_{\rm h}(x)$ has been removed from the action, since it only corresponds to a universal energy shift of all states containing a heavy quark. Removing it makes explicit that the dynamics of heavy-light systems is independent of the scale m at lowest order of $1/m$.

While the action is sufficient to obtain energy levels, for many applications one is interested in (e.g. electroweak transition matrix elements) it becomes necessary to also discuss correlation functions of composite fields. As an example we take the time component of the axial current. In the effective theory it is defined by an expansion similar to eq. (2.4),

$$A_0^{\rm HQET}(x) = \sum_{\nu=0}^{n} \mathcal{A}^{(\nu)}(x), \tag{2.6}$$

$$\mathcal{A}^{(0)}(x) = \alpha_0^{(0)} A_0^{\rm stat}(x), \quad A_0^{\rm stat}(x) = \overline{\psi}_{\rm l}(x)\gamma_0\gamma_5\psi_{\rm h}(x), \tag{2.7}$$

$$\mathcal{A}^{(\nu)}(x) = \sum_i \alpha_i^{(\nu)} \mathcal{A}_i^{(\nu)}(x), \qquad \nu > 0, \tag{2.8}$$

where a light quark field, $\psi_{\rm l}$, enters and $\mathcal{A}_i^{(\nu)}$ is of dimension $3+\nu$. One may then study for instance the correlator (with $(\overline{\psi}_i \Gamma \psi_j)^\dagger \equiv \overline{\psi}_j \gamma_0 \Gamma^\dagger \gamma_0 \psi_i$)

$$C_{\rm AA}^{\rm HQET}(x_0) = a^3 \sum_{\mathbf{x}} \left\langle A_0^{\rm HQET}(x) (A_0^{\rm HQET})^\dagger(0) \right\rangle. \tag{2.9}$$

At the classical level the fields are given by

$$\alpha_0^{(0)} = 1, \qquad \mathcal{A}_1^{(1)} = \overline{\psi}_{\rm l}\gamma_j\gamma_5 \overleftarrow{D}_j \psi_{\rm h}, \qquad \alpha_1^{(1)} = \frac{1}{m}. \tag{2.10}$$

[3] A short derivation may e.g. be found in [11].

In general, i.e. at the quantum level, expectation values are defined by a path integral

$$\langle \mathcal{O} \rangle = \frac{1}{Z} \int D[\varphi]\, \mathcal{O}[\varphi]\, \mathrm{e}^{-(S_{\mathrm{rel}}+S_{\mathrm{HQET}})}\,, \tag{2.11}$$

$$Z = \int D[\varphi]\, \mathrm{e}^{-(S_{\mathrm{rel}}+S_{\mathrm{HQET}})}\,, \tag{2.12}$$

over all fields with the standard measure, denoted here by $D[\varphi]$. An important ingredient in the definition of the effective field theory is that it is understood throughout that the *integrand* of the path integral is expanded *in a power series* in $1/m$, with power counting according to

$$\omega_i^{(\nu)} = \mathrm{O}\left(\frac{1}{m^\nu}\right), \qquad \alpha_i^{(\nu)} = \mathrm{O}\left(\frac{1}{m^\nu}\right). \tag{2.13}$$

In other words one replaces

$$\begin{aligned}\exp\{-(S_{\mathrm{rel}}+S_{\mathrm{HQET}})\} = \exp\left\{-\left(S_{\mathrm{rel}} + a^4\sum_x \mathcal{L}_{\mathrm{stat}}(x)\right)\right\} \times \\ \times\left\{1 - a^4\sum_x \mathcal{L}^{(1)}(x) + \frac{1}{2}\left[a^4\sum_x \mathcal{L}^{(1)}(x)\right]^2 - a^4\sum_x \mathcal{L}^{(2)}(x) + \cdots\right\}\end{aligned} \tag{2.14}$$

in eq. (2.11). The $1/m$-terms then appear only as insertions of local operators $\mathcal{O}_i^{(\nu)}(x)$ and $\mathcal{A}_i^{(\nu)}(x)$ into correlation functions, and the true path integral average is taken with respect to the action in the static approximation for the heavy quark, $S = S_{\mathrm{rel}} + a^4\sum_x \mathcal{L}_{\mathrm{stat}}(x)$.

Power counting leads us to expect that the static theory is *renormalizable*, requiring a finite number of parameters to be fixed to obtain a continuum limit. Indeed explicit perturbative [5] and [12]–[15] as well as non-perturbative [16] computations support that this is a genuine property of the static effective theory. Would one keep one of the $1/m$-terms in the exponent, as it is done in NRQCD, renormalizability would be lost and most of what we are concluding in this paper would not be true.

We are still left to discuss the renormalization of expectation values of the type (2.11) after inserting the expansion (2.14). This is just the problem of renormalizing correlation functions of local composite operators in the static effective theory. Power counting immediately leads to the conclusion: once *all local operators*, whose dimensions do not exceed the one of the highest-dimensional operator (i.e. $\nu \leq n$) and which have the proper symmetries, are included, their coefficients may be chosen such that all expectation values have a continuum limit (see e.g. ref. [17]). Of course, both the operators $\mathcal{L}_i^{(\nu)}(x)$ in the action and the ones in the effective operators such as $\mathcal{A}_i^{(\nu)}(x)$ have to be included. One may worry that due to the sums over all space-time points in eq. (2.14) contact terms appear, which lead to additional singularities. However, just like in the case of $\mathrm{O}(a)$ improvement discussed thoroughly in [9], the terms needed to remove these singularities are already present once all local operators with the appropriate dimensions are included.

The effective theory is now defined in terms of the set of parameters,

$$\mathcal{C}_{\mathrm{HQET}} \equiv \{c_k\} = \mathcal{C}_{N_{\mathrm{f}}-1} \cup \{\delta m\} \cup \{\omega_i^{(\nu)}\} \cup \{\alpha_j^{(\nu)}\} \cup \cdots\,, \qquad c_1 \equiv g_0^2\,. \tag{2.15}$$

The ellipses allow for coefficients of further composite operators which will be needed when their correlation functions are considered. For the continuum limit of this effective theory to exist, the parameters $\{c_k, k > 1\}$ have to be chosen properly as a function of g_0^2. Note that in the notation used here, the renormalization of the effective composite fields is included in the set of generalized coupling constants, $\mathcal{C}_{\rm HQET}$. E.g. at lowest order in $1/m$, the coefficient $\alpha_0^{(0)} \equiv Z_{\rm A}^{\rm stat}$ is the renormalization constant of the static axial current [14].

A few more remarks are in order.

- Once the proper degrees of freedom, namely the field $\psi_{\rm h}$, have been identified, the terms in the effective field theory are organized just by their mass-dimension. The expectation that the effective field theory has a continuum limit (is non-perturbatively renormalizable) is thus nothing but the usual expectation that composite operators mix only with operators of the same and lower dimension.

- The same argumentation is also the basis of Symanzik's discussion of cutoff effects of lattice theories and their removal order by order in a: [18]–[20] and [9]. An important consequence is that in general the $1/m$-expansion and the a-expansion are not independent but have to be considered as one expansion in terms of the dimension of the local operators. If we imagine to start with a theory with a set of operators identified by the formal continuum $1/m$-expansion, these operators will for instance mix under renormalization with operators of the same and lower dimension, which are allowed by the lattice symmetries but not by the continuum symmetries and which would therefore not be in the set of the operators one started with. To avoid this, one has to start immediately with the full set of operators of a given dimension, restricted only by the lattice symmetries. In other words we have to count $a = {\rm O}(1/m)$. This means also that $S_{\rm rel}$ has to be ${\rm O}(a)$ improved to go to order $1/m$.[4]

- Of course, symmetries restrict the terms that have to be taken into account. In general, out of the space-time symmetries we only have the 3-dimensional cubic group instead of the 4-dimensional hypercubic group. At the lowest order in $1/m$ there are additional symmetries: heavy quark spin-symmetry [21] and the local conservation of heavy quark number, which simplify ${\rm O}(a)$ improvement (see [14, section 2.2]).

- Furthermore it is convenient to formulate the effective theory only on-shell, i.e. for low energies as well as for correlation functions at physical separations. Then the argumentation of [9] can be taken over literally to show that the equations of motion (derived from the lowest-order action) can be used to reduce the set of operators $\mathcal{L}_i^{(\nu)}(x), \mathcal{A}_i^{(\nu)}(x), \ldots$. Following the same reference, operators obtained by multiplying those of dimension d by a light quark mass are to be counted as separate operators of dimension $d+1$.

[4] It may be possible to go to higher order in a than in $1/m$, when symmetries restrict the allowed mixings. An example is provided by ${\rm O}(a)$ improvement of the static effective theory [14]. Ways to extend this to higher orders in $1/m$ probably exist but we have not investigated this question systematically.

- Finally note that after using eq. (2.14), the determinant arising from the static quark action is just an irrelevant constant. In principle, loop effects of the heavy quark are still present in the coefficients c_k.

2.2 Power divergences and non-perturbative renormalization

The mixing of operators differing in dimensions by p translates into coefficients diverging (when $p > 0$) as a^{-p}. In the present context it actually has been checked in perturbation theory that these mixings are not forbidden by some accidental symmetry [5]. Due to such power divergences, perturbation theory is not sufficient to determine the coefficients c_k. An estimate of order g_0^{2l} would leave a perturbative remainder

$$\Delta c_k \sim g_0^{2(l+1)}\, a^{-p} \;\sim\; a^{-p}\,[\ln(a\Lambda)]^{-(l+1)} \;\stackrel{a\to 0}{\longrightarrow}\; \infty \tag{2.16}$$

with Λ the QCD Λ-parameter. This means that the continuum limit does not exist if the coefficients are determined only perturbatively.

Hence we conclude that a non-perturbative method is needed to determine (at least some of) the parameters $\{c_k\}$. Such a method will be introduced in the following two sections.

3. Matching of HQET and QCD

By QCD we denote the theory including a relativistic heavy quark, the b-quark, while with HQET we mean the theory where this quark is incorporated with the action defined in the previous section. The latter is an approximation to QCD when the coefficients $\mathcal{C}_{\rm HQET} = \{c_k\}$ are chosen correctly. Then we expect

$$\Phi^{\rm HQET}(M) = \Phi^{\rm QCD}(M) + {\rm O}\left(\frac{1}{M^{n+1}}\right) \tag{3.1}$$

for properly chosen observables, $\Phi^{\rm QCD}$, in QCD and their counterparts, $\Phi^{\rm HQET}$, in the effective theory. Amongst the many dependencies of $\Phi^{\rm QCD}$ we have indicated only the one on the heavy quark mass. To be free of any renormalization scheme dependence, we choose the renormalization group invariant (RGI) quark mass denoted by M [22]. In order for eq. (3.1) to hold, all other scales appearing in $\Phi^{\rm QCD}$ are assumed to be small compared to M. Choosing as a typical low-energy reference scale of QCD the energy scale $r_0^{-1}(\approx 400\,{\rm MeV})$ [23], defined in terms of the QCD force between static quarks, the combination $r_0 M$ has to be large. Thus the symbol ${\rm O}(1/M^n)$ is a short hand for ${\rm O}(1/[r_0 M]^n)$.

To give a *simple example* for a quantity $\Phi^{\rm QCD}$, one could take $\Phi^{\rm QCD} = C_{\rm AA}$, where

$$C_{\rm AA}(x_0) = Z_{\rm A}^2 a^3 \sum_{\mathbf{x}} \Big\langle A_0(x)(A_0)^\dagger(0)\Big\rangle \tag{3.2}$$

with the heavy-light axial current in QCD, $A_\mu = \overline{\psi}_{\rm l}\gamma_\mu\gamma_5\psi_{\rm b}$, and $Z_{\rm A}$ ensuring the natural normalization of the current consistent with current algebra [24, 25]. Then eq. (3.1) is valid for $\Phi^{\rm HQET} = {\rm e}^{-mx_0} C_{\rm AA}^{\rm HQET}(x_0)$ with $C_{\rm AA}^{\rm HQET}(x_0)$ from eq. (2.9) and in the region $1/x_0 \ll M$.

With the latter, kinematical, condition one takes care that the correlation functions are dominated by states with energies (the heavy quark mass being subtracted) small compared to M. Furthermore, the factor e^{-mx_0} accounts for the mass term that had been removed from the effective theory lagrangian as already mentioned after eq. (2.4). Which mass m is to be taken here, depends on the convention used to define δm. As will be explained further in section 5.1.1, at each order in $1/m$, the combination $m + \frac{1}{a}\ln(1 + a\delta m)$ is uniquely fixed by the matching of HQET and QCD. We emphasize again that the same mass m enters all correlation functions involving one heavy quark.

Let us now come to the main problem: determining the parameters in the effective theory such that this equivalence between HQET and QCD is true. First of all assume that the parameters of QCD have been fixed by requiring a set of observables, e.g. a set of hadron masses, to agree with experiment. It is then sufficient to impose

$$\Phi_k^{\mathrm{HQET}}(M) = \Phi_k^{\mathrm{QCD}}(M)\,, \qquad k = 1, \ldots, N_n\,, \tag{3.3}$$

to determine all parameters $\{c_k\,, k = 1, \ldots, N_n\}$ in the effective theory. Observables used originally to fix the parameters of QCD may be amongst these Φ_k^{QCD}. The matching conditions, eq. (3.3), define the set $\{c_k\}$ for any value of the lattice spacing (precisely speaking, for any value of a/r_0).

In principle, each Φ_k^{HQET} could be determined from a physical, experimentally accessible observable. However, this would reduce the predictive power of the effective theory since it contains more parameters than QCD. Particularly for increasing the order n of the $1/m$-expansion we then would need to use more and more experimental observables.

To preserve the predictability of the theory, we may instead insert some quantities $\Phi_k^{\mathrm{QCD}}(M)$ computed in the continuum limit of lattice QCD. This of course demands to treat the heavy quark as a relativistic particle on the lattice, seemingly in contradiction to the very reason to consider the effective theory: small enough lattice spacings to do this are very difficult to reach. An additional ingredient is thus necessary to make the idea practicable. It will be explained in the following section. At this stage the important point is that there are no theoretical obstacles to a non-perturbative matching. We end this section with some comments on details of the general matching procedure.

- The observables Φ are assumed to be renormalized. Eq. (3.3) is, however, used to fix the bare parameters in the action — for each value of g_0^2.

- When one increases the order n in the expansion, new quantities Φ_k have to be added, and at the same time, the parameters of the lower-order lagrangian, c_i, $i \leq N_{n-1}$, will change in general. This change is due to mixing of the operators and may thus be sizeable.

- It is convenient to take the continuum limit[5] of Φ_k^{QCD} before imposing eq. (3.3). If one decides not to do this, the lattice spacings on both sides of eq. (3.3) should be scaled together in order to reach the continuum limit in the effective theory.

[5] Or alternatively, work in a sufficiently improved lattice theory and at a small value of the lattice spacing.

- As mentioned already in the previous section, the terms necessary for Symanzik improvement are taken into account automatically, namely some of the equations (3.3) may be interpreted as improvement conditions. Working up to the order n, the resulting lattice HQET is correct up to

$$\text{error terms} = \mathrm{O}\left(\left(\frac{1}{m}\right)^{n+1}\right) = \mathrm{O}\left(M^{-(n+1)}(aM)^k\right), \qquad k = 0, 1, \ldots, n+1\,. \tag{3.4}$$

  Higher-order terms in $1/M$ have parametrically larger lattice spacing errors. For example, a treatment of the theory including the next-to-leading operators will give us the $(1/M)^0$-terms with $\mathrm{O}(a^2)$ errors and the linear $1/M$-corrections with $\mathrm{O}(a)$ uncertainties. Additional work would be necessary to suppress the discretization effects in the $1/M$-terms to $\mathrm{O}(a^2)$.

- There is a close analogy of our proposed matching procedure to what is done when the low-energy constants of the chiral effective lagrangian [26] are determined using lattice QCD. An important difference is, however, that the chiral expansion can be worked out analytically while here we still have to evaluate the resulting theory by Monte Carlo. The reason is that strong interactions remain; the lowest-order theory, the static approximation, is non-trivial.

4. The rôle of finite volume

From the theoretical point of view, the matching described in the previous section is sufficient. However, we should take into consideration what can be done in a numerical computation. To give a concrete example, let us assume that

$$\left(\frac{L}{a}\right)^3 \times \frac{T}{a} \leq 32^3 \times 64 \tag{4.1}$$

lattices can be simulated, numbers which are realistic for present computations in the quenched approximation, but too large for full QCD. We further assume that we deal with quantities which have negligible finite size effects when

$$L \geq 2\,\mathrm{fm}\,. \tag{4.2}$$

Then the smallest lattice spacing reachable is $a \approx 0.06\,\mathrm{fm}$, and this number will not be very different if the above assumptions are modified within reasonable limits. While such a lattice spacing is small enough to perform computations for charm quarks [27, 28], the subtracted bare mass of the b-quark is about $am_\mathrm{q} \approx 1$. In this situation lattice artifacts are expected to be very large and it is impossible to obtain the r.h.s. of eq. (3.3).

The situation becomes quite different when one considers observables Φ_k defined in finite volume with L considerably smaller than 2 fm and uses the generally accepted — and also much tested — assumption that *both QCD and HQET are applicable in a finite volume and the parameters in the lagrangians are independent of the volume.*

4.1 Matching in finite volume

Instead of eq. (3.3) we now consider (remember that N_n is the number of parameters in the effective theory):

$$\Phi_k^{\mathrm{HQET}}(L,M) = \Phi_k^{\mathrm{QCD}}(L,M)\,, \qquad k = 1,\ldots,N_n\,. \tag{4.3}$$

This will allow us to have much smaller lattice spacings on the r.h.s. in order to eventually approach the continuum limit. A typical choice is $L = L_0 \approx 0.2\,\mathrm{fm}$. As has been shown in the preliminary report of our work [6], eq. (4.3) can be evaluated very precisely for suitably selected quantities Φ_k^{QCD} and the continuum limit can actually be taken.

Concerning the l.h.s., we have to take into account that a-effects will certainly be significant when the resolution a/L of the finite space-time is too coarse. Hence the lattice spacings where the bare parameters $\{c_k(g_0)\}$ can be determined are $a = \mathrm{O}(0.02\,\mathrm{fm}) = \mathrm{O}(L_0/10)$. For such values of a, the computation of the physical observables in the infinite-volume theory ($L \approx 2\,\mathrm{fm}$ in practice) would again be impracticable, because lattices with too many points $(L/a)^4$ would be required. Therefore, a further step is necessary to make larger lattice spacings and thereby larger physical volumes available in the effective theory.

4.2 Finite-size scaling

Also for this step a well-defined procedure is easily found. First assume that all observables $\Phi_k^{\mathrm{HQET}}(L,M)$ have been made dimensionless by multiplication with appropriate powers of L. Next we define step scaling functions [8], F_k, by

$$\Phi_k^{\mathrm{HQET}}(sL,M) = F_k\left(\left\{\Phi_j^{\mathrm{HQET}}(L,M)\,,\, j = 1,\ldots,N_n\right\}\right), \quad k = 1,\ldots,N_n\,, \tag{4.4}$$

where typically one uses scale changes of $s = 2$. These dimensionless functions describe the change of the complete set of observables $\{\Phi_k^{\mathrm{HQET}}\}$ under a scaling of $L \to sL$, and we briefly sketch how they can be computed. One selects a lattice with a certain resolution a/L. The specification of $\Phi_j^{\mathrm{HQET}}(L,M)$, $j = 1,\ldots,N_n$, then fixes all (bare) parameters of the theory. The l.h.s. of eq. (4.4) is now computed, keeping the bare parameters fixed while changing $L/a \to L'/a = sL/a$. Repeating this for a few values of a/L, the continuum limit of F_k can be obtained by an extrapolation $a/L \to 0$.

An important practical detail is to choose the various quantities Φ_k^{HQET} such that each F_k depends only on a few Φ_j^{HQET} and the bare parameters c_k can be determined rather independently from each other. For instance, it is natural to identify the running Schrödinger functional coupling $\bar{g}^2(L)$ [8, 29] with $\Phi_1^{\mathrm{HQET}}(L,M)$ and to keep all of the light quark masses zero in these steps. In this way g_0^2 and the (light) bare quark masses are fixed independently of the parameters $\delta m, \omega_i^{(\nu)}, \alpha_i^{(\nu)}, \ldots$ coming from the heavy sector. In the quenched approximation or with two dynamical quarks, the set of bare parameters specifying the relativistic sector, $\mathcal{C}_{N_{\mathrm{f}}-1}$, can then be taken over from [22] and [29]–[31] without change.

A few steps — may be two — are necessary to reach a value of $L = \mathrm{O}(1\,\mathrm{fm})$, where at the same time contact can be made with resolutions a/L that are affordable to accommodate the suitable observables on a physically large lattice to realize the original matching

condition, eq. (3.3). (In our first example, section 5.1, this rôle will be played by the B-meson with its mass as the physical input.) We note that in principle the size of L_0 is rather arbitrary, but the following consideration is important. We are matching at a finite value of $1/m$ and a finite order n. Thus the final results will depend on which quantities have been used to perform the matching. If one chooses quantities with kinematics where the $1/m$-expansion is not accurate (or even not applicable), this will translate into badly determined parameters in the effective lagrangian and large final truncation errors. For this reason, L_0 has to be chosen such that the $1/m$-expansion is applicable which means

$$\frac{1}{L_0} \ll m\,, \tag{4.5}$$

and L_0 cannot be too small. From these considerations it appears that $L_0 \approx 0.2\,\mathrm{fm} - 0.4\,\mathrm{fm}$ is a good choice.

4.3 Evaluation of the physical observables in the effective theory

Physical observables usually have to be computed in large volume which, for practical reasons, means at lattice spacings around $1/20\,\mathrm{fm}$ to $1/10\,\mathrm{fm}$. In this region the bare parameters of the effective theory are determined as follows.

One chooses a suitable K such that

$$L_K = s^K L_0 \approx 1\,\mathrm{fm}\,. \tag{4.6}$$

Iterated applications of eq. (4.4) give rise to recursion relations, the solutions of which determine quantities $V_k \equiv \Phi_k^{\mathrm{HQET}}(L_K, M)$ in the larger volume of extent L_K. Next, regarding $\Phi_k^{\mathrm{HQET}}(L_K, M) = V_k$ as a requirement while setting the number of lattice points to $L_K/a = \mathrm{O}(10)$ just fixes the bare parameters $\mathcal{C}_{\mathrm{HQET}}$. These bare parameters are then known at values of the lattice spacing, where the computation of correlation functions in large volume is possible in the effective theory and masses and matrix elements can be extracted from their large-time behaviour.

Note that in the notation used here also the renormalization constants of the composite operators appearing in the correlation functions are amongst the "bare parameters". All quantities are thus renormalized entirely non-perturbatively.[6] One may still wonder how M itself is fixed. The answer to this question is provided by the first of the two examples, which we will use now to illustrate the general strategy.

5. Examples

In this section we supply two applications of our non-perturbative matching strategy of HQET and QCD that up to now was formulated in rather general terms: a full calculation of the b-quark mass in combined static and quenched approximations (section 5.1) and a proposal for a non-perturbative determination of multiplicatively renormalized matrix elements of the static-light axial current, which is different in spirit from ref. [16] and still awaits a numerical investigation.

[6] This represents an advantage in comparison to [16] where a last step using perturbation theory was necessary to get to the "matching scheme" [7, 16], which here we achieve by virtue of eq. (3.3).

5.1 The b-quark mass at lowest order

Several determinations of the mass of the b-quark, which use the static approximation on the lattice (HQET to order $(1/m)^0$), have been published [32]. They all rely on a perturbative estimate of δm [33]–[35] and suffer from a power-law divergence due to the mixing of $\overline{\psi}_{\rm h} D_0 \psi_{\rm h}$ and $\overline{\psi}_{\rm h}\psi_{\rm h}$ as discussed in section 2.2. Their precision is thus limited by the fact that a continuum limit can not be taken, and it is difficult to estimate the associated uncertainty. We here explain how a entirely non-perturbative computation can be done and will also give a first result, which can easily be improved in precision in the near future. This step is also a prerequisite to perform the matching of other quantities such as the axial current, since generically the quark mass enters in the matching step (4.3) for all Φ_k.

5.1.1 Strategy and basic formula

As indicated already in section 4, given a resolution a/L, we fix g_0^2 such that the finite-volume running coupling of ref. [29] takes a certain value. Furthermore we set the light quark masses to zero (with one exception which will be discussed). In the language of section 4 we have

$$\Phi_1^{\rm HQET} = \bar{g}^2(L)\,, \tag{5.1}$$

$$\Phi_{k+1}^{\rm HQET} = m_k^{\rm PCAC} = 0\,, \qquad k = 1, \ldots, N_{\rm f} - 1\,, \tag{5.2}$$

in terms of the PCAC masses of the light flavour number k, $m_k^{\rm PCAC}$, and the running coupling $\bar{g}^2(L)$ in the Schrödinger functional (SF) scheme [29]. Other choices are possible, but the above is convenient in view of the present numerical knowledge [22, 30, 31]. The box length L is then parametrized through $\bar{g}^2(L)$. A very useful feature of eqs. (5.1) and (5.2) is that they do not involve the heavy field at all and determine the bare coupling and quark masses independently of the heavy sector; in particular these conditions are independent of the order n of the expansion.

In this section we are only concerned with energies and remain at lowest order in $1/m$. The only additional parameter in the lagrangian to be fixed is $a\delta m$, i.e. one more condition corresponding to $k = N_{\rm f} + 1$ in eq. (4.3) is needed. We start from a time-slice correlation function projected onto spatial momentum zero containing one heavy quark (such as $C_{\rm AA}$, eq. (3.2)). Denoting it generically as $C(x_0)$, in the logarithmic derivative

$$\Gamma = \frac{1}{2a} \ln \left[\frac{C(x_0 - a)}{C(x_0 + a)} \right] \qquad \left(\frac{x_0}{L} \quad \text{fixed} \right) \tag{5.3}$$

all multiplicative renormalization factors of $C(x_0)$ cancel. Below we shall use $x_0/L = 1/2$, but other choices are possible. Replacing the fields in the correlation function $C(x_0)$ by the corresponding effective fields defines $C^{\rm HQET}(x_0)$ in the effective theory. In the static approximation, its logarithmic derivative, $\Gamma_{\rm stat}$, built as in eq. (5.3), depends on δm in the simple form

$$\Gamma_{\rm stat} = \Gamma_{\rm stat}|_{\delta m = 0} + \frac{1}{a} \ln(1 + a\delta m)\,, \tag{5.4}$$

as is easily seen from the explicit form of the static quark propagator. In large volume, which due to $x_0/L =$ constant also means large Euclidean time, $\Gamma = \Gamma(L, M)$ will turn into the mass of a b-hadron, say $m_{\rm B}$. It is now obvious that

$$\Phi^{\rm QCD}_{N_{\rm f}+1}(L, M) \equiv L\,\Gamma\,, \tag{5.5}$$

$$\begin{aligned}\Phi^{\rm HQET}_{N_{\rm f}+1}(L, M) &\equiv L\,(\Gamma_{\rm stat} + m) \\ &= L\,(\Gamma_{\rm stat}|_{\delta m=0} + m_{\rm bare})\,, \qquad m_{\rm bare} = m + \frac{1}{a}\ln(1 + a\delta m)\,,\end{aligned} \tag{5.6}$$

are sensible assignments to fix the combination $m_{\rm bare}$ via requiring

$$\Phi^{\rm QCD}_{N_{\rm f}+1}(L, M) = \Phi^{\rm HQET}_{N_{\rm f}+1}(L, M)\,. \tag{5.7}$$

Since δm and m always appear in the combination $m_{\rm bare}$, they may not be fixed separately, unless one arbitrarily defines δm by an additional condition.

Due to eq. (5.4), the step scaling function

$$\sigma_{\rm m}\left(\bar{g}^2(L)\right) \equiv 2L\,[\,\Gamma_{\rm stat}(2L, M) - \Gamma_{\rm stat}(L, M)\,] \tag{5.8}$$

is independent of $m_{\rm bare}$ and therefore also independent of M; at lowest order in $1/m$, energy differences in the effective theory do not depend on the heavy quark mass. The step scaling function (5.8) is thus a particularly simple realization of eq. (4.4). Together with the one for the running coupling [8, 29],

$$\sigma(u) = \bar{g}^2(2L)\big|_{\bar{g}^2(L)=u}\,, \tag{5.9}$$

it defines the sequence

$$\begin{aligned} u_0 &= \bar{g}^2(L_0)\,, & w_0 &= L\,\Gamma_{\rm stat}|_{L=L_0}\,, \\ u_{k+1} &= \sigma(u_k)\,, & w_{k+1} &= 2w_k + \sigma_{\rm m}(u_k)\,, \end{aligned} \tag{5.10}$$

which is easily seen to relate $\Gamma_{\rm stat}(L_K, M)$, with $L_K = 2^K L_0$, to $\Gamma_{\rm stat}(L_0, M)$ when the sequence $u_0, \ldots, u_{K-1}$ is known:

$$L_0\Gamma_{\rm stat}(L_K, M) = L_0\Gamma_{\rm stat}(L_0, M) + \sum_{k=0}^{K-1} 2^{-(k+1)}\sigma_{\rm m}(u_k)\,. \tag{5.11}$$

Suitable choices for u_0 and K then allow to arrive at $L_K = {\rm O}(1\,{\rm fm})$.

Finally one considers the energy $E_{\rm stat}$ of a B-meson in static approximation, given for example by

$$C^{\rm HQET}_{\rm AA}(x_0) \overset{x_0\to\infty}{\sim} A\exp(-x_0 E_{\rm stat}) \qquad (L \text{ large})\,. \tag{5.12}$$

The energy difference

$$\Delta E = E_{\rm stat} - \Gamma_{\rm stat}(L_K, M) \tag{5.13}$$

can be computed with one and the same lattice spacing (i.e. at the same bare parameters) for the two different terms on the r.h.s., but of course with different L. Combining eq. (5.7) imposed in small volume ($L = L_0$) with eqs. (5.11) and (5.13) to eliminate $m_{\rm bare}$ in $m_{\rm B} =$

$E_{\rm stat} + m_{\rm bare}$ (holding in the large-volume limit), we arrive at the basic equation

$$L_0 m_{\rm B} = L_0 \Gamma(L_0, M_{\rm b}) + \sum_{k=0}^{K-1} 2^{-(k+1)} \sigma_{\rm m}(u_k) + L_0 \Delta E \,. \tag{5.14}$$

It relates the mass of the B-meson to a quantity $\Gamma(L_0, M_{\rm b})$, computable in lattice QCD with a relativistic b-quark, and the energy differences ΔE and $\sigma_{\rm m}$ which are both defined and computable in the effective theory. All quantities on the r.h.s. may be evaluated in the continuum limit. Note that all of the terms in eq. (5.14) are independent of $m_{\rm bare}$ (because the unknown $m_{\rm bare}$, and thereby δm too, drop out in the differences), although logically eq. (5.7) has been used to fix it non-perturbatively. Our strategy has also been presented in a somewhat different way, which is closer in spirit and notation to standard HQET applications (but less rigorous), in [36].

Eq. (5.14) may be looked at in two different ways. Given the RGI mass of the b-quark, $M_{\rm b}$, eq. (5.14) provides a way to compute the mass of the B-meson. It is more interesting to turn this around: taking $m_{\rm B}$ from experiment and evaluating (in lattice QCD) $\Gamma(L_0, M)$ as a function of M, this equation may be solved for $M_{\rm b}$. Implicitly the bare parameter $m_{\rm bare}$ is thus fixed non-perturbatively, and the problem of a power-law divergence is solved.

We now give an example for a precise definition of the correlation function $C(x_0)$ and use the quenched approximation to demonstrate that the continuum limit can be reached in all steps while still a very interesting precision is attainable. The reader who is not interested in the numerical details may directly continue with section 5.2.

5.1.2 Correlation functions, O(a) improvement and spin-symmetry

In our numerical implementation we choose SF boundary conditions with all details as in [16], including $\theta = 1/2$, $T = L$ and $C = C' = 0$ in the notation of that paper. This means that O(a) improvement [9, 14] is fully implemented, except for uncertainties in the coefficients $c_{\rm A}^{\rm stat}$, $c_{\rm t}$ and $\widetilde{c}_{\rm t}$ originating from their only perturbative estimation. As in [16] it has been checked that the influence of these uncertainties on the observables considered here can be neglected compared to our statistical errors. We will therefore not mention O(a) terms any more and perform continuum extrapolations modelling the a-effects as O(a^2).

For our definition of Γ we consider the two correlation functions

$$f_{\rm A}(x_0) = -\frac{a^6}{2} \sum_{\mathbf{y},\mathbf{z}} \left\langle (A_{\rm I})_0(x)\, \overline{\zeta}_{\rm b}(\mathbf{y}) \gamma_5 \zeta_{\rm l}(\mathbf{z}) \right\rangle \,, \tag{5.15}$$

$$k_{\rm V}(x_0) = -\frac{a^6}{6} \sum_{\mathbf{y},\mathbf{z},k} \left\langle (V_{\rm I})_k(x)\, \overline{\zeta}_{\rm b}(\mathbf{y}) \gamma_k \zeta_{\rm l}(\mathbf{z}) \right\rangle \,, \tag{5.16}$$

where the label "I" on the axial and vector currents reminds us that their O(a) improved forms are used:

$$(A_{\rm I})_\mu(x) = \overline{\psi}_{\rm l}(x) \gamma_\mu \gamma_5 \psi_{\rm b}(x) + a c_{\rm A} \frac{1}{2} (\partial_\mu + \partial_\mu^*) \left\{ \overline{\psi}_{\rm l}(x) \gamma_5 \psi_{\rm b}(x) \right\} , \tag{5.17}$$

$$(V_{\rm I})_\mu(x) = \overline{\psi}_{\rm l}(x) \gamma_\mu \psi_{\rm b}(x) + a c_{\rm V} \frac{1}{2} (\partial_\nu + \partial_\nu^*) \left\{ i\, \overline{\psi}_{\rm l}(x) \sigma_{\mu\nu} \psi_{\rm b}(x) \right\} . \tag{5.18}$$

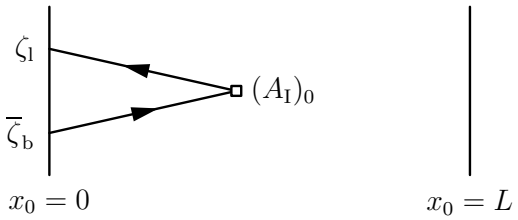

Figure 2: Illustration of the correlation function $f_{\rm A}$. For $k_{\rm V}$, the insertion of $(A_{\rm I})_0$ is replaced by $(V_{\rm I})_k$, whereas in case of $f_{\rm A}^{\rm stat}$ the operator in the bulk is $(A_{\rm I}^{\rm stat})_0$ connected to $\overline{\zeta}_{\rm h}$ (instead of $\overline{\zeta}_{\rm b}$) by a static quark propagator.

As a consequence of the heavy quark spin-symmetry, their partners in the effective theory coincide exactly at lowest order in $1/m$ and we thus define only one

$$C^{\rm HQET}(x_0) \equiv f_{\rm A}^{\rm stat}(x_0) = -\frac{a^6}{2}\sum_{\mathbf{y},\mathbf{z}} \left\langle (A_{\rm I}^{\rm stat})_0(x)\,\overline{\zeta}_{\rm h}(\mathbf{y})\gamma_5\zeta_{\rm l}(\mathbf{z})\right\rangle . \tag{5.19}$$

In these definitions, $\sum_{\mathbf{y},\mathbf{z}} \overline{\zeta}_{\rm b}(\mathbf{y})\gamma_5\zeta_{\rm l}(\mathbf{z})$ and $\sum_{\mathbf{y},\mathbf{z}} \overline{\zeta}_{\rm h}(\mathbf{y})\gamma_5\zeta_{\rm l}(\mathbf{z})$ are interpolating fields localized at the $x_0 = 0$ boundary of the SF, which create a state with the quantum numbers of a B-meson with momentum $\mathbf{p} = \mathbf{0}$, and for $\gamma_5 \to \gamma_k$ we have the quantum numbers of a B*. The correlation functions are schematically depicted in figure 2; more details can be found in [14].

Inserting $C(x_0) = f_{\rm A}(x_0)$ and $C(x_0) = k_{\rm V}(x_0)$ into eq. (5.3) defines $\Gamma_{\rm PS}$ and $\Gamma_{\rm V}$, respectively. Their partner in the effective theory is denoted as $\Gamma_{\rm stat}$. Due to the spin-symmetry, either $L\Gamma_{\rm PS} = L(\Gamma_{\rm stat} + m)$ or $L\Gamma_{\rm V} = L(\Gamma_{\rm stat} + m)$ are possible matching conditions at lowest order in $1/m$. At first order, one has to consider also separately the vector and the axial qvector correlators in the effective theory since these are split by the $\sigma\cdot\mathbf{B}$-term in the effective lagrangian. It is then convenient to define the matching condition as eq. (5.7) with the spin-average

$$\Gamma = \frac{1}{4}\left(\Gamma_{\rm PS} + 3\Gamma_{\rm V}\right) . \tag{5.20}$$

With this definition the matching condition (5.7) is independent of the coefficient of the $\sigma\cdot\mathbf{B}$-term also at first order in $1/m$, and hopefully $1/m$-effects are thereby minimized.

Having now completed our definition of Γ and $\Gamma_{\rm stat}$, we remind the reader that the mass of the light quark is set to zero and thus Γ is only a function of the heavy quark mass, M, and the linear extent of the SF-volume, L (if a-effects are neglected for the moment).

5.1.3 Matching

The essential steps of our strategy explained in section 5.1.1 are the matching at $L = L_0$ as the starting point, then connecting to $L = L_K$ and from there to the (infinite-volume) meson mass. In practice, proceeding from any choice of u_0 the sequence u_k is only known with a certain numerical precision and this has to be taken into account in the error analysis. Furthermore we want to take advantage of the numerical results of [22] for triples of $(L/a, \beta, \kappa)$ corresponding to fixed renormalized coupling and vanishing light quark mass

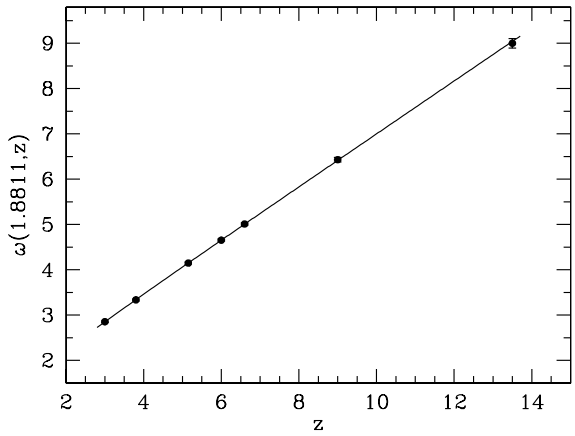

Figure 3: Continuum limit values of $L_0\Gamma(L_0, M)$ at fixed coupling $\bar{g}^2(L_0/2) = 1.8811$ as a function of $z = L_0 M$ and its fit function, determined in relativistic QCD but small volume [39]. The b-quark mass scale lies near $z \approx 6$.

in the quenched approximation, as well as of the known function $[r_0/a](\beta)$ and the value of $L_{\rm max}/r_0 = 0.718(16)$ [37], where $\bar{g}^2(L_{\rm max}) = 3.48$. So it is convenient to have $K = 2$ in previous formulae and to define (exactly) $L_2 = 2L_{\rm max} = 1.436\, r_0$. Then, applying the inverse of the step scaling function of the coupling [22] twice, we arrive at

$$u_0 = 2.455(28)\,, \qquad \sigma^{-1}(u_0) = 1.918(20)\,, \tag{5.21}$$

and end up with $L = L_0 = L_2/4 = 0.359\, r_0 \approx 0.18\,\mathrm{fm}$ for the linear extent of the matching volume. The matching of HQET and QCD is then supposed to be done at $u = u_0 \approx 2.4$. We could thus keep e.g. $u = 2.4484$ fixed, where the triples $(L/a, \beta, \kappa)$ are known [22], but only for $6 \leq L/a \leq 16$. The spacing of these lattices is still too large to comfortably accommodate a propagating b-quark. Instead it is better to work at a constant value of $u = 1.8811$, varying $6 \leq L/(2a) \leq 16$. Nevertheless, Γ is computed on the lattices with L/a points per direction, and the slight mismatch of $\sigma^{-1}(u_0)$ and 1.8811 will eventually be taken into account together with the overall error analysis.

We now have to determine $\Gamma(L, M)$, where in case of the relativistic theory L is always to be identified with the extent of the matching volume, L_0, from now on. In order to approach its continuum limit, we define

$$\Omega\left(u, z, \frac{a}{L}\right) = L\,\Gamma(L, M)|_{\bar{g}^2(L/2)=u\,,\,LM=z} \tag{5.22}$$

and extrapolate it as a function of a/L, viz.

$$\omega(u, z) = \lim_{a/L\to 0} \Omega\left(u, z, \frac{a}{L}\right), \tag{5.23}$$

for a few selected values of z and at fixed u. This requires to compute Ω with z and u fixed while changing L/a and therefore also β. A particular aspect in this step is that in imposing the condition of fixed z (at variable β), the relation between the bare quark mass, $m_{\rm q}$, and the RGI one, M, is needed, where several renormalization factors and improvement

coefficients enter. Although they had already been determined [22, 38], it turned out that it was desirable to improve their precision and to determine them directly in the range of β where they are needed in the present application. For this reason they were redetermined in ref. [39], and also ω as a function of z, eq. (5.23), was obtained by extrapolation in $a/L \to 0$ in that work. For the reader's convenience, we reproduce from [39] a graph of the continuum values $\omega(1.8811, z)$ together with the fit function

$$\omega(1.8811, z) = a_0 z + a_1 + a_2 \frac{1}{z}, \qquad a_0 = 0.581, \qquad a_1 = 1.226, \qquad a_2 = -0.358 \quad (5.24)$$

in figure 3. In the interval $5.2 \leq z \leq 6.6$, which is the relevant z-range to extract the RGI b-quark mass later, this parametrization describes $\omega(1.8811, z)$ with a precision of about 0.5%. A further global uncertainty of 0.9% has to be attributed to the argument z of the function ω (see ref. [39]). In order to also take the small statistical error and mismatch in u_0 into consideration at the end, we also need a numerical value for the derivative of $\omega'(1.8811, z)$ w.r.t. u. It was found to be constant in the interesting region [39]:

$$\left.\frac{\partial}{\partial u}\,\omega(u, z)\right|_{u=1.8811} = 0.70(1), \quad 6.0 \leq z \leq 6.6\,. \qquad (5.25)$$

For completeness we also quote the fit result for $\omega(1.8811, z)$, if instead of the spin-average (5.20) it is defined as the continuum limit of the effective energy $L\Gamma_{\rm PS}(L, M)$. With the same fit ansatz as in eq. (5.24), the coefficients then read

$$a_0 = 0.587, \qquad a_1 = 1.121, \qquad a_2 = -1.306 \qquad (\text{for } \Gamma \equiv \Gamma_{\rm PS})\,. \qquad (5.26)$$

The significantly larger a_2-term in this case compared to eq. (5.24) indicates that the spin-averaged combination Γ has smaller $1/m$-errors and should therefore be preferred in the implementation of the matching step.[7]

5.1.4 Finite-size scaling

The next step is the numerical determination of the step scaling function $\sigma_{\rm m}$, eq. (5.8), and then of the (M-independent difference) $L_0[\Gamma_{\rm stat}(L_K, M) - \Gamma_{\rm stat}(L_0, M)]$ as given by eq. (5.11).

At finite lattice spacing, the step scaling function is defined by

$$\Sigma_{\rm m}\left(u, \frac{a}{L}\right) = 2L\,[\,\Gamma_{\rm stat}(2L, M) - \Gamma_{\rm stat}(L, M)\,]|_{\bar{g}^2(L)=u}\,, \quad (5.27)$$

where, as mentioned earlier, the (light) quark mass is set to zero. The exact definition of the massless point does not play an important rôle; it is as in ref. [16]. In fact, we evaluated $\Sigma_{\rm m}$ directly from the correlation functions computed there, where details of the simulations can be found, too. Numerical results for $\Sigma_{\rm m}$ are listed in table 2 in the appendix. They are extrapolated to the continuum limit via

u	$\sigma_{\rm m}(u)$
2.4484	−0.205(18)
2.7700	−0.133(26)
3.4800	0.040(25)

Table 1: Results for the continuum step scaling function $\sigma_{\rm m}(u)$.

$$\Sigma_{\rm m}\left(u, \frac{a}{L}\right) = \sigma_{\rm m}(u) + c\,\frac{a^2}{L^2}\,. \qquad (5.28)$$

[7] In the preliminary computation of the b-quark's mass reported in refs. [6, 7], the matching was performed using only the energy in the pseudoscalar channel, $\Gamma_{\rm PS}$.

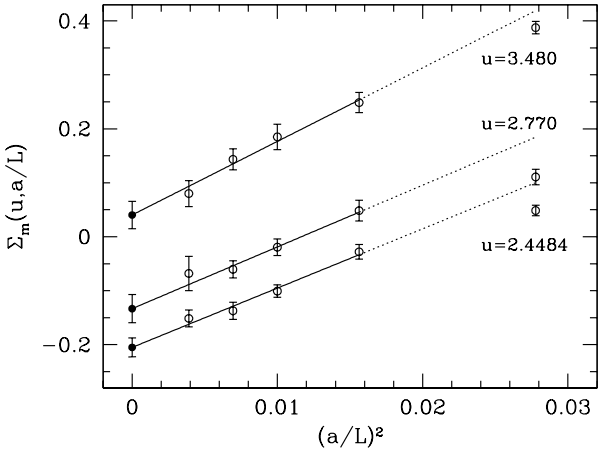

Figure 4: Lattice step scaling function $\Sigma_{\rm m}$ and its continuum limit extrapolation linear in $(a/L)^2$, which uses only the four smallest values of a/L.

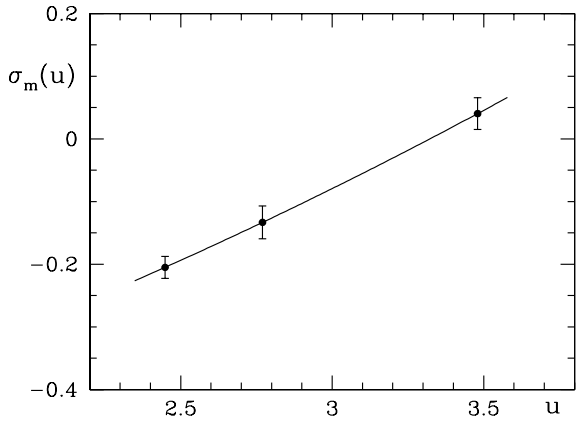

Figure 5: Continuum step scaling function $\sigma_{\rm m}(u)$ and its polynomial fit.

Given our data at various resolutions, this is a safe extrapolation (cf. figure 4) leading to continuum values reported in table 1. Setting now u_0 as in eq. (5.21), we want to compute (recall that $K = 2$ now)

$$L_0 \left[\Gamma_{\rm stat}(L_2, M) - \Gamma_{\rm stat}(L_0, M) \right] = \frac{1}{2}\sigma_{\rm m}(u_0) + \frac{1}{4}\sigma_{\rm m}(u_1)\,, \tag{5.29}$$

with $u_1 = \sigma(u_0) = 3.48(5)$ [22]. To this end it is convenient to represent the data of table 1 by a smooth fit function,

$$\sigma_{\rm m}(u) = s_0 + s_1 u + s_2 u^2\,, \tag{5.30}$$

shown in figure 5. This fit implies the numerical value

$$\frac{1}{2}\sigma_{\rm m}(u_0) + \frac{1}{4}\sigma_{\rm m}(u_1) = -0.092(11) \tag{5.31}$$

for the combination (5.29). Here the uncertainties in u_0, u_1 are neglected, since they would contribute only a negligible amount to the total error of eq. (5.31). Dropping the $s_2 u^2$-term in eq. (5.30) would give indistinguishable results.

5.1.5 The subtracted B-meson mass

As a last ingredient for the basic formula in eq. (5.14) we have to address $L_0\Delta E$, with ΔE the energy difference between the B-meson's static binding energy and the effective energy of the static-light correlator $f_{\rm A}^{\rm stat}$, eq. (5.13), at the same values of the lattice spacing. We evaluate this quantity starting from results for $aE_{\rm stat}(g_0)$ in the literature [40]. They are interpolated in the mass of the light quark to the strange quark mass (see also [16, section 5.2]) and then correspond to a $\rm B_s$-state. Since $\rm O(\mathit{a})$ improvement was not employed in the computation of ref. [40], we also need $\Gamma_{\rm stat}(L_2)$ for the unimproved theory. Given the simulation results reported in [16, appendix C.2], $a\Gamma_{\rm stat}(g_0, L/a)$ with $L = L_2 = 1.436\, r_0$ is straightforwardly obtained for $5.68 \le \beta = 6/g_0^2 \le 6.5$. These numbers are collected in table 3 of the appendix and well described by

$$a\Gamma_{\rm stat}\left(g_0, \frac{L}{a}\right)\Big|_{L=L_2} = 0.394 - 0.055\,(\beta-6) - 0.218\,(\beta-6)^2 + 0.229\,(\beta-6)^3 \qquad (5.32)$$

with an absolute uncertainty of less than ± 0.002 in the range of β mentioned.

The combination $L_0\Delta E$ is shown in figure 6. Its errors are dominated by those of $aE_{\rm stat}$. Since they are rather large and also the lattice spacings are not very small, we refrain from forming a continuum extrapolation. Instead we take

$$L_0\Delta E = 0.46(5) \qquad (5.33)$$

as our present estimate. As seen in the figure, its error encompasses the full range of results at finite a and the true continuum number is expected to be covered by it.

No doubt, a continuum limit with small error (at least a factor 3 smaller) can be achieved here in the near future, incorporating $\rm O(\mathit{a})$ improvement and using the alternative discretization of static quarks of ref. [41].

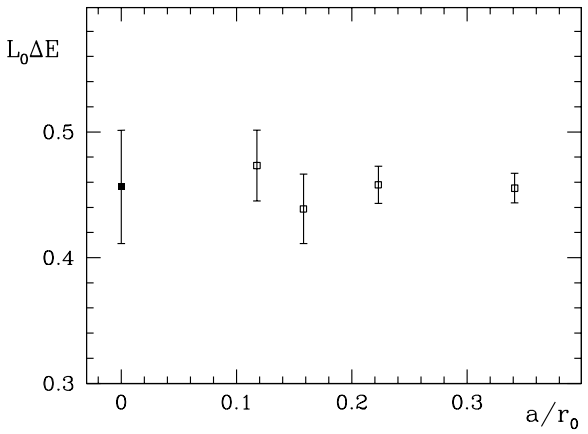

Figure 6: Subtracted, dimensionless $\rm B_s$-meson energy evaluated from the bare numbers of [40].

5.1.6 Determination of the quark mass

Now we are in the position to put all pieces together and solve the basic equation (5.14) for the b-quark mass. This amounts to determine the interception point of the function

$$\omega\left(\sigma^{-1}(u_0), z\right) = \omega(1.8811, z) + \Delta u \, \frac{\partial}{\partial u}\, \omega(u, z)\Big|_{u=1.8811}\,, \tag{5.34}$$

where $\Delta u = (\sigma^{-1}(u_0) - 1.8811) = 0.037(20)$ accounts for the slight mismatch in the couplings fixed, with the combination

$$\omega_{\rm stat} \equiv L_0 m_{\rm B} - \left\{ \frac{1}{2}\,\sigma_{\rm m}(u_0) + \frac{1}{4}\,\sigma_{\rm m}(u_1) \right\} - L_0 \Delta E\,. \tag{5.35}$$

All of the necessary quantities are known from the foregoing three subsections and the experimental spin-averaged B-meson mass $m_{\rm B} = m_{\rm B_s} = 5.40\,\mathrm{GeV}$ is taken as the physical input. As illustrated in figure 7, this procedure yields a value for $L_0 M_{\rm b}$ with an error. Together with $L_0/r_0 = L_{\rm max}/(2r_0) = 0.359$ it is converted to our central result

$$r_0 M_{\rm b} = 16.12(25)(15)\,. \tag{5.36}$$

Here the second error in parentheses stems from the additional 0.9% uncertainty of z in $\omega(u, z)$ that was mentioned in the context of eq. (5.24). With $r_0 = 0.5\,\mathrm{fm}$ this translates into

$$M_{\rm b} = 6.36(10)(6)\,\mathrm{GeV}\,, \qquad \overline{m}_{\rm b}\,(\overline{m}_{\rm b}) = 4.12(7)(4)\,\mathrm{GeV}\,, \tag{5.37}$$

where the running mass, $\overline{m}_{\rm b}(\mu)$, is evaluated with the four-loop renormalization group functions and in the $\overline{\rm MS}$ scheme.

One should remember that this result is valid up to $1/m$-corrections and it has been obtained in the quenched approximation. One may estimate the ambiguity due to setting the energy scale in the quenched approximation as usual. Varying the value of r_0 in fm by 10%, we obtain changes of about 260 MeV in $M_{\rm b}$ and 150 MeV in $\overline{m}_{\rm b}(\overline{m}_{\rm b})$. We

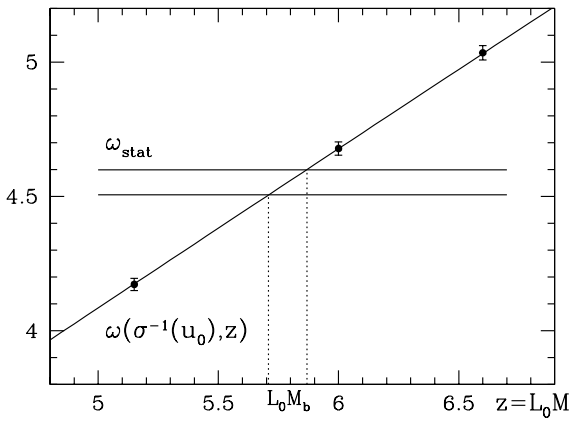

Figure 7: Graphical solution of the basic formula, eq. (5.14), for the dimensionless RGI b-quark mass, $z_{\rm b} \equiv L_0 M_{\rm b}$. The contributing pieces are repeated explicitly in eqs. (5.34) and (5.35).

emphasize, however, that the scale ambiguity can serve only as a rough guide to the impact of quenching. Finally, we also want to stress once more that in section 5.1.5 the contribution from the subtracted B-meson mass to our result on the b-quark mass is still based on ordinary Wilson fermion data and will be hopefully much improved soon.

5.2 The B-meson decay constant at lowest order

To lowest order in $1/m$, the bare matrix element

$$\mathcal{M}(g_0) = \langle \mathrm{B}(\mathbf{p}=\mathbf{0})|A_0^{\mathrm{stat}}(0)|0\rangle \tag{5.38}$$

evaluated with the static action together with a renormalization factor $Z_{\mathrm{A}}^{\mathrm{stat}}(g_0, aM_{\mathrm{b}})$ allows to determine the B-meson decay constant in static approximation [3]:

$$F_{\mathrm{B}}\sqrt{m_{\mathrm{B}}} = \lim_{a\to 0} Z_{\mathrm{A}}^{\mathrm{stat}}(g_0, aM_{\mathrm{b}})\mathcal{M}(g_0)\,. \tag{5.39}$$

The renormalization constant $Z_{\mathrm{A}}^{\mathrm{stat}}(g_0, aM_{\mathrm{b}})$ has already been computed in the quenched approximation [16], using a quite different method to the one described in this paper. However, the method of ref. [16] is not easily extended to include $1/m$-corrections. Therefore, as a second example of the use of our general strategy, we here describe an alternative method which may be extended to include $1/m$-corrections.

The key formula, valid up to corrections of $\mathrm{O}(1/m)$, has already appeared and was briefly discussed in Ref. [7]:

$$F_{\mathrm{B}}\sqrt{m_{\mathrm{B}}} = \frac{F_{\mathrm{B}}\sqrt{m_{\mathrm{B}}}\big|^{\mathrm{HQET}}}{\Phi^{\mathrm{HQET}}(L_2, M_{\mathrm{b}})} \times \frac{\Phi^{\mathrm{HQET}}(L_2, M_{\mathrm{b}})}{\Phi^{\mathrm{HQET}}(L_1, M_{\mathrm{b}})} \times \frac{\Phi^{\mathrm{HQET}}(L_1, M_{\mathrm{b}})}{\Phi^{\mathrm{HQET}}(L_0, M_{\mathrm{b}})} \times \Phi^{\mathrm{QCD}}(L_0, M_{\mathrm{b}})\,. \tag{5.40}$$

In the rest of this section we give precise definitions of the various factors and explain the formula in the general framework of sections 3 and 4. We assume that the b-quark mass is already known. Terms necessary for $\mathrm{O}(a)$ improvement are not written explicitly; they can easily be added.

5.2.1 Matching

As a preparation for the matching of the axial current and the associated determination of $Z_{\mathrm{A}}^{\mathrm{stat}} \equiv \alpha_0^{(0)}$, we start from $f_{\mathrm{A}}^{\mathrm{stat}}(x_0)$, defined in section 5.1.2. This correlation function renormalizes multiplicatively: $(f_{\mathrm{A}}^{\mathrm{stat}})_{\mathrm{R}} = Z_{\zeta_{\mathrm{h}}} Z_{\zeta_{\mathrm{l}}} Z_{\mathrm{A}}^{\mathrm{stat}} f_{\mathrm{A}}^{\mathrm{stat}}$. In order to eliminate the renormalization factors $Z_{\zeta_{\mathrm{h}}}, Z_{\zeta_{\mathrm{l}}}$ of the boundary quark fields, we consider in addition the boundary-to-boundary correlation,

$$f_1^{\mathrm{stat}} = -\frac{a^{12}}{2L^6} \sum_{\mathbf{u},\mathbf{v},\mathbf{y},\mathbf{z}} \left\langle \overline{\zeta}_{\mathrm{l}}{}'(\mathbf{u})\gamma_5\zeta_{\mathrm{h}}{}'(\mathbf{v})\,\overline{\zeta}_{\mathrm{h}}(\mathbf{y})\gamma_5\zeta_{\mathrm{l}}(\mathbf{z})\right\rangle\,, \tag{5.41}$$

which is renormalized as $(f_1^{\mathrm{stat}})_{\mathrm{R}} = (Z_{\zeta_{\mathrm{h}}} Z_{\zeta_{\mathrm{l}}})^2 f_1^{\mathrm{stat}}$. In the ratio

$$X\left(g_0, \frac{L}{a}\right) \equiv \frac{f_{\mathrm{A}}^{\mathrm{stat}}(L/2)}{\sqrt{f_1^{\mathrm{stat}}}} \tag{5.42}$$

the unwanted Z-factors cancel, and with the choice $x_0 = L/2$ it is also independent of the linearly divergent mass counterterm δm. The renormalized ratio is denoted by

$$\begin{aligned}\Phi^{\rm HQET}(L, M_{\rm b}) &\equiv X_{\rm R}\left(u, z_{\rm b}, \frac{a}{L}\right) \\ &= Z_{\rm A}^{\rm stat}(g_0, aM_{\rm b})\, X\left(g_0, \frac{L}{a}\right)\Big|_{\bar{g}^2(L)=u}, \qquad z_{\rm b} = LM_{\rm b}\,. \end{aligned} \tag{5.43}$$

Here, as wherever we do not mention the light quark masses explicitly, they are set to zero.

In QCD we define the corresponding quantities ($Z_{\rm A}$ denotes the standard renormalization constant for the QCD axial current [24, 25] and f_1 is the analogue of $f_1^{\rm stat}$ with $\zeta_{\rm h} \to \zeta_{\rm b}$)

$$Y\left(g_0, z_{\rm b}, \frac{L}{a}\right) = \frac{f_{\rm A}(L/2)}{\sqrt{f_1}}\,, \tag{5.44}$$

$$Y_{\rm R}\left(u, z_{\rm b}, \frac{a}{L}\right) = Z_{\rm A}(g_0)\, Y\left(g_0, z_{\rm b}, \frac{L}{a}\right)\Big|_{\bar{g}^2(L)=u}, \tag{5.45}$$

$$\Phi^{\rm QCD}(L, M_{\rm b}) = \lim_{a/L\to 0} Y_{\rm R}\left(u, z_{\rm b}, \frac{a}{L}\right), \tag{5.46}$$

and the matching equation to be imposed in the small volume (of extent L_0) is

$$\Phi^{\rm HQET}(L_0, M_{\rm b}) = \Phi^{\rm QCD}(L_0, M_{\rm b}) \qquad \text{with} \qquad \bar{g}^2(L_0) = u_0 = \text{fixed}\,. \tag{5.47}$$

While in agreement with the notation in previous sections $\Phi^{\rm HQET}$ on the l.h.s. has a lattice spacing dependence that is only implicit (cf. eq. (5.43)), for the r.h.s. the continuum limit is to be taken (cf. eq. (5.46)). In the quenched approximation, the particular value for u_0 may be chosen as in section 5.1.

5.2.2 Finite-size scaling

Computing the step scaling functions built as

$$\sigma_{\rm X}(u) \equiv \lim_{a/L\to 0} \frac{X(g_0, 2L/a)}{X(g_0, L/a)}\Big|_{\bar{g}^2(L)=u} \tag{5.48}$$

allows to reach larger values of L via the recursion

$$\Phi^{\rm HQET}(2L, M_{\rm b})\big|_{a=0} = \sigma_{\rm X}\left(\bar{g}^2(L)\right) \times \Phi^{\rm HQET}(L, M_{\rm b})\big|_{a=0}\,. \tag{5.49}$$

We note in passing that in eq. (5.48) we could have written $X \to X_{\rm R}$, since the same $Z_{\rm A}^{\rm stat}$ enters in numerator and denominator. For the following we assume eq. (5.49) to be iterated K times, connecting $\Phi^{\rm HQET}(L_0, M_{\rm b})$ to $\Phi^{\rm HQET}(L_K, M_{\rm b})$ with $L_K = 2^K L_0$, i.e. in a numerical implementation, details will be very similar to those described in section 5.1.4.

5.2.3 The decay constant

To finally arrive at $F_{\rm B}\sqrt{m_{\rm B}}$, one defines the renormalization constant in view of eq. (5.43),

$$Z_{\rm A}^{\rm stat}(g_0, aM_{\rm b}) = \frac{X_{\rm R}(u_K, z_{\rm b}, 0)}{X(g_0, L_K/a)} = \frac{\Phi^{\rm HQET}(L_K, M_{\rm b})|_{a=0}}{X(g_0, L_K/a)}\,, \qquad u_K = \bar{g}^2(L_K)\,, \tag{5.50}$$

and — bearing in mind that $\Phi^{\rm HQET}(L_K, M_{\rm b})|_{a=0}$ via eq. (5.49) and the matching condition (5.47) may be evolved back to the *renormalized* quantity $\Phi^{\rm QCD}(L_0, M_{\rm b})$ in QCD — replaces $Z_{\rm A}^{\rm stat}(g_0, aM_{\rm b})$ in eq. (5.39) by rewriting:

$$F_{\rm B}\sqrt{m_{\rm B}} = \rho(u_K) \times \Phi^{\rm HQET}(L_K, M_{\rm b})\big|_{a=0}\,, \tag{5.51}$$

$$\rho(u) = \lim_{a/L\to 0} R\left(u, \frac{a}{L}\right), \qquad R\left(u, \frac{a}{L}\right) \equiv \left.\frac{\mathcal{M}(g_0)}{X(g_0, L/a)}\right|_{\bar{g}^2(L)=u}. \tag{5.52}$$

Although we have chosen only u and a/L as arguments for R, it does depend on the masses of the light quarks used for the evaluation of the matrix element $\mathcal{M}$. These masses have to be set (or extrapolated) to the physical ones to obtain the correct matrix element in question; conveniently, the light quark masses are put to zero in all other quantities as mentioned above. In this way the effective theory is renormalized in a (light quark) mass-independent renormalization scheme.

Choosing as an example $K = 2$, we may combine all ingredients into the expression

$$F_{\rm B}\sqrt{m_{\rm B}} = \rho(u_2) \times \sigma_{\rm X}(u_1) \times \sigma_{\rm X}(u_0) \times \Phi^{\rm QCD}(L_0, M_{\rm b})\,, \tag{5.53}$$

where the various factors correspond one to one to those in eq. (5.40) but are now rigorously defined and can be computed in the continuum limit. Our notation is most appropriate for the lowest order in $1/m$. At higher order, additional matching equations and step scaling functions have to be defined and $\sigma_{\rm X}$ will depend on $M_{\rm b}$, which is not the case at lowest order in $1/m$. In fact, at this order all the (heavy quark) mass dependence of $F_{\rm B}\sqrt{m_{\rm B}}$ is contained in $\Phi^{\rm QCD}(L_0, M_{\rm b})$ that is calculable in small-volume lattice QCD with a relativistic b-quark [42].

5.2.4 Relation to other approaches

We finally want to compare the strategy of renormalizing $A_0^{\rm stat}$, presented in this paper, to the one of [14, 16], which followed the general ALPHA Collaboration strategy of obtaining the renormalization group invariant matrix elements of composite operators non-perturbatively and then using (continuum) perturbative results to find the operators normalized in the matching scheme at finite renormalization scale. (A recent review is ref. [7].) For the application to the HQET, the natural renormalization scale is then the mass of the b-quark.

Remaining strictly at lowest order in $1/m$, there is no mixing with lower-dimensional operators. Consequently, perturbation theory can be applied. In particular the large-mass behaviour of $F_{\rm B}\sqrt{m_{\rm B}}$, which is given by the mass dependence of $Z_{\rm A}^{\rm stat}$, is computable leading to the asymptotics [43, 44][8]

$$\lim_{M_{\rm b}\to\infty}\left[\ln\left(\frac{M_{\rm b}}{\Lambda_{\overline{\rm MS}}}\right)\right]^{\gamma_0/(2b_0)} F_{\rm B}\sqrt{m_{\rm B}} = \Phi_{\rm RGI}^{\rm stat} = \text{constant}\,,$$

$$\gamma_0 = -\frac{1}{4\pi^2}\,, \qquad b_0 = \frac{11 - \frac{2}{3}(N_{\rm f}-1)}{16\pi^2}\,. \tag{5.54}$$

[8]The leading-order coefficient b_0 of the β-function is taken for $N_{\rm f} - 1$ flavours, since the b-quark does not contribute. Note that here $N_{\rm f} - 1 = 0$ corresponds to the quenched approximation.

Furthermore, the function $C_{\rm PS}(M_{\rm b}/\Lambda_{\overline{\rm MS}}) = F_{\rm B}\sqrt{m_{\rm B}}/\Phi^{\rm stat}_{\rm RGI}$ is known perturbatively up to and including $\bar{g}^4(\overline{m}_{\rm b})$-corrections to the leading-order equation (5.54) [45]–[50]. These perturbative computations, like our non-perturbative method, are based on the renormalization of the static axial current where the finite part is determined by matching, eq. (3.3). We denote this renormalization scheme by the "matching scheme" [7, 16].[9]

A finite, renormalized static axial current can of course also be defined by other renormalization conditions involving a renormalization scale μ in a suitably chosen intermediate scheme. Matrix elements $\Phi_{\rm inter}(\mu)$ of the renormalized current in this scheme will then not necessarily satisfy eq. (3.1), but it is easy to see that

$$\lim_{\mu\to\infty}\,[\,8\pi b_0\alpha(\mu)\,]^{-\gamma_0/(2b_0)}\,\Phi_{\rm inter}(\mu) = \Phi^{\rm stat}_{\rm RGI}\,, \qquad \alpha = \frac{\bar{g}^2}{(4\pi)}\,, \tag{5.55}$$

is independent of the intermediate renormalization scheme. In ref. [16] a finite-volume scheme was adopted, which allows to evaluate the limit in eq. (5.55) through some finite-size scaling steps followed by perturbative evolution at very high μ. The results obtained in this way are then combined with the perturbative approximation of $C_{\rm PS}(M_{\rm b}/\Lambda_{\overline{\rm MS}})$. Owing to this last step, they are accurate up to relative errors of order $\bar{g}^6(\overline{m}_{\rm b})$. This discussion should have made evident that the essential difference of the method presented here is not the absence of these perturbative errors, which are expected to be quite small, but rather the tempting possibility to *include* $1/m$*-corrections*.

6. Uncertainties and perspectives

Following the general strategy introduced in this paper opens the possibility to perform clean non-perturbative computations using the lattice regularized HQET. The dangerous power-law divergences are subtracted non-perturbatively through the matching in small volume. This is not only a theoretical proposal: in section 5.1 we showed that in a concrete physics application the statistical errors of Monte Carlo results are quite moderate. In fact they can be expected to be even smaller, when an alternative discretization of the static approximation is employed [41].

We emphasize that the result for the b-quark mass in section 5.1 is valid up to $1/M_{\rm b}$-corrections. If we had used $\Gamma = \Gamma_{\rm PS}$ instead of the spin-averaged energy in the matching step, a 0.4 GeV higher number for $M_{\rm b}$ would have been obtained. We do not regard this shift as a realistic estimate of the magnitude of $1/M_{\rm b}$-corrections but believe that they are significantly smaller, as indicated by the smallness of the associated coefficient a_2 in the numerically determined quark mass dependence of the spin-averaged energy, eq. (5.24). Nevertheless it is clear that a precision determination of $M_{\rm b}$ requires to take the $1/M_{\rm b}$-corrections into account, even if only to show that they are small.

In general one may argue that the matching step (carried out at order $1/M_{\rm b}^n$) contains $1/(L_0 M_{\rm b})^{n+1}$-uncertainties in addition to the unavoidable $1/(r_0 M_{\rm b})^{n+1}$-terms (we remind the reader that we take $1/r_0 \approx 0.4\,\text{GeV}$ as a typical QCD scale). Whether or

[9] Non-perturbatively, the matching scheme is unique up to higher orders in $1/m$; in perturbation theory, a residual scheme dependence due to the choice of the other renormalized parameters, such as $\bar{g}$, remains.

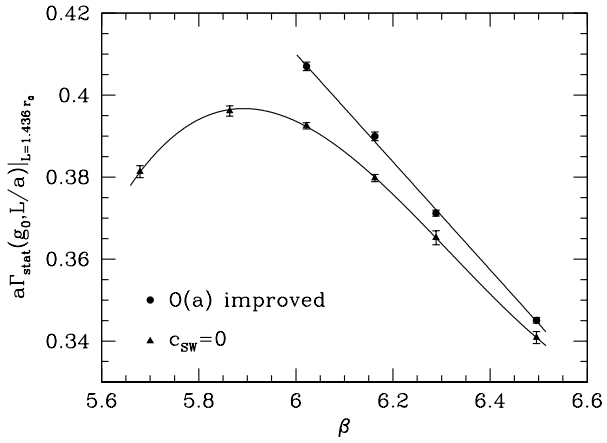

Figure 8: Numbers for $a\Gamma_{\rm stat}(g_0, L/a)|_{L=1.436\,r_0}$ from table 3 and its polynomial fit functions for O(a) improved and unimproved Wilson fermions.

not the former terms are larger than the latter can only be decided if the linear extent of the matching volume, L_0, is varied. Increasing it would demand even smaller lattice spacings.

Since $1/M_{\rm b}$-corrections are computable, they should be determined to arrive at precision computations for B-physics observables, e.g. for the phenomenologically interesting B-$\overline{\rm B}$ mixing amplitude. On the other hand we expect $(1/M_{\rm b})^2$-corrections to be very difficult in practice, because they require also O(a^2) improvement of the whole theory. Fortunately, $(1/M_{\rm b})^2$-corrections do not appear to be very important [42] but, as in every expansion, this issue has to be studied case by case.

An attractive property of our strategy is that it does not involve any particularly large lattices and therefore all the steps outlined in the present work can also be performed with dynamical fermions. These calculations are presumably no more difficult than for instance those of refs. [51]–[53] in the light meson sector.

Acknowledgments

We would like to thank M. Della Morte, A. Shindler and U. Wolff for useful discussions and comments on the manuscript. This work is part of the ALPHA Collaboration research plan. We thank DESY for allocating computer time on the APEmille computers at DESY Zeuthen to this project and the APE-group for its valuable help. We further acknowledge support by the EU IHP Network on *Hadron Phenomenology from Lattice QCD* under grant HPRN-CT-2000-00145 and by the Deutsche Forschungsgemeinschaft in the SFB/TR 09.

A. Detailed numerical results

In this appendix we collect some of the numerical results underlying the computation of the b-quark's mass in section 5.1.

JHEP02(2004)022

$\bar{g}^2(L)$	$\beta = 6/g_0^2$	κ	L/a	$a\Gamma_{\rm stat}(L)$	$a\Gamma_{\rm stat}(2L)$	$\Sigma_{\rm m}(u, a/L)$
2.4484	6.7807	0.134994	6	0.3082(6)	0.3123(6)	0.049(10)
	7.0197	0.134639	8	0.2899(4)	0.2881(7)	−0.028(13)
	7.2025	0.134380	10	0.2747(4)	0.2697(4)	−0.101(12)
	7.3551	0.134141	12	0.2621(5)	0.2564(5)	−0.137(16)
	7.6101	0.133729	16	0.2444(2)	0.2396(4)	−0.151(16)
2.7700	6.5512	0.135327	6	0.3282(6)	0.3374(10)	0.111(14)
	6.7860	0.135056	8	0.3068(8)	0.3098(9)	0.048(19)
	6.9720	0.134770	10	0.2916(4)	0.2907(6)	−0.019(15)
	7.1190	0.134513	12	0.2795(4)	0.2769(5)	−0.060(16)
	7.3686	0.134114	16	0.2592(6)	0.2570(8)	−0.068(32)
3.4800	6.2204	0.135470	6	0.3629(6)	0.3952(7)	0.388(12)
	6.4527	0.135543	8	0.3399(5)	0.3554(11)	0.249(19)
	6.6350	0.135340	10	0.3219(6)	0.3311(10)	0.185(23)
	6.7750	0.135121	12	0.3081(3)	0.3141(7)	0.143(20)
	7.0203	0.134707	16	0.2858(3)	0.2883(7)	0.080(24)

Table 2: Results for the lattice step scaling function $\Sigma_{\rm m}$. For the intermediate quantity $\Gamma_{\rm stat}(L)$ the argument M is suppressed, since it is evaluated at $m_{\rm bare} = 0$ and so does not depend on M.

		O(a) improved		$c_{\rm sw} = 0$	
L/a	$\beta = 6/g_0^2$	κ	$a\Gamma_{\rm stat}$	κ	$a\Gamma_{\rm stat}$
4	5.6791	—	—	0.15268	0.381(2)
6	5.8636	—	—	0.15451	0.396(1)
8	6.0219	0.13508	0.407(1)	0.15341	0.393(1)
10	6.1628	0.13565	0.390(1)	0.15202	0.380(1)
12	6.2885	0.13575	0.371(1)	0.15078	0.365(2)
16	6.4956	0.13559	0.345(1)	0.14887	0.341(2)

Table 3: Numerical results for $a\Gamma_{\rm stat}$ at $L = 1.436\, r_0$ for O(a) improved and unimproved Wilson fermions (i.e. $c_{\rm sw} = 0$ and also $c_{\rm A}^{\rm stat} = 0$ in the latter case). The corresponding simulation parameters are reproduced from [16, appendix C.2.] for completeness.

The numerical data on the static-light meson correlator in the Schrödinger functional (SF), which are necessary to evaluate its logarithmic derivative $\Gamma_{\rm stat}$, see eqs. (5.3) and (5.19), have already been obtained in the context of the non-perturbative renormalization of the static-light axial current, ref. [16]. Hence we refer the reader to this work for more details. In table 2 we list the numerical results on the lattice step scaling function $\Sigma_{\rm m}$, defined through eq. (5.27).

Another ingredient in the determination of $M_{\rm b}$ is the subtracted B-meson energy ΔE, eq. (5.13), which amounts to calculate the static effective energy $\Gamma_{\rm stat}$ at $L = 1.436\, r_0$. Our quenched results for this quantity, both for the O(a) improved case (with non-perturbative $c_{\rm sw}$ from [54] and the 1-loop value [55] for the coefficient $c_{\rm A}^{\rm stat}$ to improve the static-light axial current) as well as for the unimproved theory (where both improvement coefficients

are set to zero), are shown in table 3 and figure 8. These numbers are well represented by the polynomial expressions

$$a\Gamma_{\rm stat}\left(g_0,\frac{L}{a}\right)\Big|_{L=1.436\,r_0} = \begin{cases} 0.410 - 0.132\,(\beta-6) \\ \text{for } 6.0 \le \beta = 6/g_0^2 \le 6.5 \text{ and } c_{\rm sw} = \text{non-perturbative} \\ \\ 0.394 - 0.055\,(\beta-6) - 0.218\,(\beta-6)^2 + 0.229\,(\beta-6)^3 \\ \text{for } 5.68 \le \beta = 6/g_0^2 \le 6.5 \text{ and } c_{\rm sw} = 0 \end{cases},$$

where their absolute uncertainty is below ± 0.001 and ± 0.002 in the indicated ranges of β, respectively. In section 5.1.5 we restrict the analysis only to the case of unimproved Wilson fermions, $c_{\rm sw} = 0$, but the O(a) improved parametrization may be required when also O(a) improved data on the static binding energy $E_{\rm stat}$ at various lattice spacings will become available.

References

[1] N. Yamada, *Heavy quark physics and lattice QCD*, *Nucl. Phys.* **119** *(Proc. Suppl.)* (2003) 93 [hep-lat/0210035].

[2] A.S. Kronfeld, *Heavy quarks and lattice QCD*, hep-lat/0310063.

[3] E. Eichten, *Heavy quarks on the lattice*, *Nucl. Phys.* **4** *(Proc. Suppl.)* (1988) 170.

[4] E. Eichten and B. Hill, *An effective field theory for the calculation of matrix elements involving heavy quarks*, *Phys. Lett.* **B 234** (1990) 511.

[5] L. Maiani, G. Martinelli and C.T. Sachrajda, *Nonperturbative subtractions in the heavy quark effective field theory*, *Nucl. Phys.* **B 368** (1992) 281.

[6] ALPHA collaboration, J. Heitger and R. Sommer, *A strategy to compute the b-quark mass with non-perturbative accuracy*, *Nucl. Phys.* **106** *(Proc. Suppl.)* (2002) 358 [hep-lat/0110016].

[7] R. Sommer, *Non-perturbative renormalization of HQET and QCD*, *Nucl. Phys.* **119** *(Proc. Suppl.)* (2003) 185 [hep-lat/0209162].

[8] M. Lüscher, P. Weisz and U. Wolff, *A numerical method to compute the running coupling in asymptotically free theories*, *Nucl. Phys.* **B 359** (1991) 221.

[9] M. Lüscher, S. Sint, R. Sommer and P. Weisz, *Chiral symmetry and O(a) improvement in lattice QCD*, *Nucl. Phys.* **B 478** (1996) 365 [hep-lat/9605038].

[10] E. Eichten and B. Hill, *Static effective field theory:* $1/m$ *corrections*, *Phys. Lett.* **B 243** (1990) 427.

[11] B.A. Thacker and G.P. Lepage, *Heavy quark bound states in lattice QCD*, *Phys. Rev.* **D 43** (1991) 196.

[12] E. Eichten and B. Hill, *Renormalization of heavy-light bilinears and* $F_{\rm B}$ *for Wilson fermions*, *Phys. Lett.* **B 240** (1990) 193.

[13] P. Boucaud, L.C. Lung and O. Pene, *B meson decay constant on the lattice and renormalization*, *Phys. Rev.* **D 40** (1989) 1529.

[14] ALPHA collaboration, M. Kurth and R. Sommer, *Renormalization and O(a)-improvement of the static axial current*, *Nucl. Phys.* **B 597** (2001) 488 [hep-lat/0007002].

[15] ALPHA collaboration, M. Kurth and R. Sommer, *Heavy quark effective theory at one-loop order: an explicit example*, *Nucl. Phys.* **B 623** (2002) 271 [hep-lat/0108018].

[16] ALPHA collaboration, J. Heitger, M. Kurth and R. Sommer, *Non-perturbative renormalization of the static axial current in quenched QCD*, *Nucl. Phys.* **B 669** (2003) 173 [hep-lat/0302019].

[17] J.C. Collins, *Renormalization*, 1st ed. Cambridge University Press, Cambridge, 1984.

[18] K. Symanzik, *Continuum limit and improved action in lattice theories, 1. Principles and ϕ^4 theory*, *Nucl. Phys.* **B 226** (1983) 187.

[19] K. Symanzik, *Continuum limit and improved action in lattice theories, 2. O(n) nonlinear sigma model in perturbation theory*, *Nucl. Phys.* **B 226** (1983) 205.

[20] M. Lüscher and P. Weisz, *On-shell improved lattice gauge theories*, *Commun. Math. Phys.* **97** (1985) 59.

[21] N. Isgur and M.B. Wise, *Weak decays of heavy mesons in the static quark approximation*, *Phys. Lett.* **B 232** (1989) 113.

[22] ALPHA collaboration, S. Capitani, M. Lüscher, R. Sommer and H. Wittig, *Non-perturbative quark mass renormalization in quenched lattice QCD*, *Nucl. Phys.* **B 544** (1999) 669 [hep-lat/9810063].

[23] R. Sommer, *A new way to set the energy scale in lattice gauge theories and its applications to the static force and α_s in* SU(2) *Yang-Mills theory*, *Nucl. Phys.* **B 411** (1994) 839 [hep-lat/9310022].

[24] M. Bochicchio, L. Maiani, G. Martinelli, G.C. Rossi and M. Testa, *Chiral symmetry on the lattice with Wilson fermions*, *Nucl. Phys.* **B 262** (1985) 331.

[25] M. Lüscher, S. Sint, R. Sommer and H. Wittig, *Non-perturbative determination of the axial current normalization constant in O(a) improved lattice QCD*, *Nucl. Phys.* **B 491** (1997) 344 [hep-lat/9611015].

[26] J. Gasser and H. Leutwyler, *Chiral perturbation theory to one loop*, *Ann. Phys. (NY)* **158** (1984) 142.

[27] ALPHA collaboration, J. Rolf and S. Sint, *A precise determination of the charm quark's mass in quenched QCD*, *J. High Energy Phys.* **12** (2002) 007 [hep-ph/0209255].

[28] ALPHA collaboration, A. Jüttner and J. Rolf, *A precise determination of the decay constant of the D_s- meson in quenched QCD*, *Phys. Lett.* **B 560** (2003) 59 [hep-lat/0302016].

[29] M. Lüscher, R. Sommer, P. Weisz and U. Wolff, *A precise determination of the running coupling in the* SU(3) *Yang-Mills theory*, *Nucl. Phys.* **B 413** (1994) 481 [hep-lat/9309005].

[30] ALPHA collaboration, A. Bode et al., *First results on the running coupling in QCD with two massless flavors*, *Phys. Lett.* **B 515** (2001) 49 [hep-lat/0105003].

[31] ALPHA collaboration, M. Della Morte et al., *Recent results on the running coupling in QCD with two massless flavours*, *Nucl. Phys.* **119** *(Proc. Suppl.)* (2003) 439 [hep-lat/0209023].

[32] S.M. Ryan, *Heavy quark physics from lattice QCD*, *Nucl. Phys.* **106** *(Proc. Suppl.)* (2002) 86 [hep-lat/0111010].

JHEP02(2004)022

[33] G. Martinelli and C.T. Sachrajda, *Computation of the b-quark mass with perturbative matching at the next-to-next-to-leading order*, *Nucl. Phys.* **B 559** (1999) 429 [hep-lat/9812001].

[34] F. Di Renzo and L. Scorzato, *The residual mass in lattice heavy quark effective theory to α^3 order*, *J. High Energy Phys.* **02** (2001) 020 [hep-lat/0012011].

[35] H.D. Trottier, N.H. Shakespeare, G.P. Lepage and P.B. Mackenzie, *Perturbative expansions from Monte Carlo simulations at weak coupling: Wilson loops and the static-quark self-energy*, *Phys. Rev.* **D 65** (2002) 094502 [hep-lat/0111028].

[36] L. Lellouch, *Phenomenology from lattice QCD*, *Nucl. Phys.* **117** *(Proc. Suppl.)* (2003) 127 [hep-ph/0211359].

[37] ALPHA collaboration, M. Guagnelli, R. Sommer and H. Wittig, *Precision computation of a low-energy reference scale in quenched lattice QCD*, *Nucl. Phys.* **B 535** (1998) 389 [hep-lat/9806005].

[38] ALPHA collaboration, M. Guagnelli et al., *Non-perturbative results for the coefficients $b_{\rm m}$ and $b_{\rm A}$-$b_{\rm P}$ in O(a) improved lattice QCD*, *Nucl. Phys.* **B 595** (2001) 44 [hep-lat/0009021].

[39] ALPHA collaboration, J. Heitger and J. Wennekers, *Effective heavy-light meson energies in small-volume quenched QCD*, hep-lat/0312016.

[40] A. Duncan et al., *Properties of B mesons in lattice QCD*, *Phys. Rev.* **D 51** (1995) 5101 [hep-lat/9407025].

[41] ALPHA collaboration, M. Della Morte et al., *Lattice HQET with exponentially improved statistical precision*, *Phys. Lett.* **B 581** (2004) 93 [hep-lat/0307021].

[42] J. Heitger et al., in preparation.

[43] M.A. Shifman and M.B. Voloshin, *On annihilation of mesons built from heavy and light quark and anti-$B_0 \leftrightarrow B_0$ oscillations*, *Sov. J. Nucl. Phys.* **45** (1987) 292.

[44] H.D. Politzer and M.B. Wise, *Leading logarithms of heavy quark masses in processes with light and heavy quarks*, *Phys. Lett.* **B 206** (1988) 681.

[45] X.D. Ji and M.J. Musolf, *Subleading logarithmic mass dependence in heavy meson form-factors*, *Phys. Lett.* **B 257** (1991) 409.

[46] D.J. Broadhurst and A.G. Grozin, *Two loop renormalization of the effective field theory of a static quark*, *Phys. Lett.* **B 267** (1991) 105 [hep-ph/9908362].

[47] V. Gimenez, *Two loop calculation of the anomalous dimension of the axial current with static heavy quarks*, *Nucl. Phys.* **B 375** (1992) 582.

[48] D.J. Broadhurst and A.G. Grozin, *Matching QCD and HQET heavy - light currents at two loops and beyond*, *Phys. Rev.* **D 52** (1995) 4082 [hep-ph/9410240].

[49] A.G. Grozin, *Decoupling of heavy quark loops in light-light and heavy- light quark currents*, *Phys. Lett.* **B 445** (1998) 165 [hep-ph/9810358].

[50] K.G. Chetyrkin and A.G. Grozin, *Three-loop anomalous dimension of the heavy-light quark current in HQET*, *Nucl. Phys.* **B 666** (2003) 289 [hep-ph/0303113].

[51] CP-PACS collaboration, A. Ali Khan et al., *Light hadron spectroscopy with two flavors of dynamical quarks on the lattice*, *Phys. Rev.* **D 65** (2002) 054505 [hep-lat/0105015].

JHEP02(2004)022

[52] UKQCD collaboration, C.R. Allton et al., *Effects of non-perturbatively improved dynamical fermions in QCD at fixed lattice spacing*, *Phys. Rev.* **D 65** (2002) 054502 [hep-lat/0107021].

[53] JLQCD collaboration, S. Aoki et al., *Light hadron spectroscopy with two flavors of O(a)-improved dynamical quarks*, *Phys. Rev.* **D 68** (2003) 054502 [hep-lat/0212039].

[54] M. Lüscher, S. Sint, R. Sommer, P. Weisz and U. Wolff, *Non-perturbative O(a) improvement of lattice QCD*, *Nucl. Phys.* **B 491** (1997) 323 [hep-lat/9609035].

[55] C.J. Morningstar and J. Shigemitsu, *One-loop matching of lattice and continuum heavy-light axial vector currents using nrqcd*, *Phys. Rev.* **D 57** (1998) 6741 [hep-lat/9712016].

JHEP02(2004)022

K

Effective heavy-light meson energies in small-volume quenched QCD

J. High Energy Phys. 0402 (2004) 064

Published by Institute of Physics Publishing for SISSA/ISAS

Received: *December 15, 2003*
Revised: *February 20, 2004*
Accepted: *February 25, 2004*

Effective heavy-light meson energies in small-volume quenched QCD

ALPHA Collaboration

Jochen Heitger and Jan Wennekers*

Westfälische Wilhelms-Universität Münster, Institut für Theoretische Physik
Wilhelm-Klemm-Strasse 9, D-48149 Münster, Germany
E-mail: heitger@uni-muenster.de, jan.wennekers@desy.de

Abstract: We study effective energies of heavy-light meson correlation functions in lattice QCD and a small volume of $(0.2\ \mathrm{fm})^4$ to non-perturbatively calculate their dependence on the heavy quark mass in the continuum limit. Our quenched results obtained here constitute an essential intermediate step of a first fully non-perturbative computation of the b-quark's mass in the static approximation that has recently been presented as an application of a new proposal to non-perturbatively renormalize the Heavy Quark Effective Theory. The renormalization constant and the improvement coefficients relating the renormalized current and subtracted quark mass are determined in the relevant parameter region at weak couplings, which allows to perform the numerical simulations at several, precisely fixed values of the renormalization group invariant heavy quark mass in a range from 3 GeV to 15 GeV.

Keywords: B-Physics, Heavy Quarks Physics, Lattice QCD.

*Present address: DESY, Theory Group, Notkestrasse 85, D-22603 Hamburg, Germany.

JHEP02(2004)064

Contents

JHEP02(2004)064

1. Introduction

During the last years, the elementary particle physics community has seen a growing interest and activity in the study of B-meson physics and its phenomenology. While on the experimental side this interest reflects in the various facilities that are currently running to explore CP-violation in the B-system [1, 2, 3], it is nourished on the theoretical side by the demand to determine transition matrix elements of the effective weak hamiltonian in order to interpret the experimental observations within (or beyond) the standard model and to (over-)constrain the unitarity triangle. For the computations of such matrix elements between low-energy hadron states to become valuable contributions in this field, they have to be carried out non-perturbatively, which is the domain of QCD on the lattice. However, in contrast to light quarks which as widely spread objects are predominantly exposed to large-volume limitations, heavy quarks are extremely localized ($1/m_{\mathrm{b}} \simeq 1/(4\,\mathrm{GeV}) \simeq 0.04$ fm) and thus also require very fine lattice resolutions, because otherwise one would face huge discretization errors. Mainly for this reason, realistic simulations of heavy-light systems involving a b-quark (even in the quenched approximation) are impossible so far [4].

A theoretically very appealing way out of this restriction is to recourse to the *Heavy Quark Effective Theory (HQET)* [5, 6]. This comes at a prize, though. As a consequence of its different renormalization properties, physical quantities deriving from expectation values calculated in the effective theory are affected by power-law divergences in the lattice spacing that can not be subtracted perturbatively in a clean way: the continuum limit ceases to exist, unless the theory is renormalized non-perturbatively [7].

Only recently, an approach to overcome these deficiencies has been developed from a solution for the problem of a completely non-perturbative computation of the b-quark

mass in the static approximation *including* the power-divergent subtraction [8] to a new method addressing the general class of renormalization problems in HQET [9]. At its root stands the insight that these power-law divergences can be removed by a *non-perturbative matching procedure to relativistic QCD in a finite volume*. In fact, the *smallness* of the physical volume represents a characteristic feature in this strategy — since only then one is capable to incorporate and simulate the b-quark as a relativistic fermion — and motivates the investigation of QCD observables in a small-volume setup presented in this work. Here we will concentrate on the non-perturbative heavy quark mass dependence of effective heavy-light meson energies in the continuum limit, whose numerical knowledge is crucial to apply the proposal of ref. [9] to the determination of the b-quark's mass in leading order of HQET.[1] An extension to also examine the mass dependence of a few more quantities, which aims at quantitative non-perturbative tests of HQET by comparing static results with those obtained along the large quark mass limit in small-volume QCD, is in progress [12].

In section 2 we first recall the main ideas of the general matching strategy between HQET and QCD of ref. [9] (section 2.1), then introduce our observables considered (section 2.2) and finally describe how these can be calculated as functions of the (renormalized) mass of the heavy quark by numerical simulations (section 2.3). Section 3.1 is devoted to some intermediate results on a renormalization constant and improvement coefficients that are needed to renormalize the heavy quark mass in the relevant parameter range. Our central results on the mass dependence of the heavy-light meson energies are discussed in section 3.2, and we conclude in section 4.

In the calculations reported here we still stay in the quenched approximation. We want to emphasize, however, that this study of the heavy quark mass dependence of suitable observables (as an important part of the general non-perturbative approach to HQET of [9]) can be expected to be numerically implementable as well for QCD with dynamical fermions at a tolerable computing expense, because on basis of the experiences made in refs. [13, 14] the use of the QCD Schrödinger functional brings us in a favourable position where in physically small to intermediate volumes dynamical simulations are definitely easier than with the standard formulation.

2. Computational strategy

For the rest of this paper we will focus on meson observables derived from heavy-light correlation functions in finite volume and their dependence on the heavy quark mass in the continuum limit. Before we explain in detail how this dependence can be singled out in an actual numerical computation, we want to clarify the special rôle of QCD in a *finite* volume as a material component of the more general idea advocated in ref. [9] to non-perturbatively renormalize HQET; therefore, it suggests itself to briefly summarize this idea in the first subsection.

[1] For another method to determine $m_{\rm b}$ and $F_{\rm B}$, which also starts from lattice QCD in small volume but employs extrapolations of finite-volume effects in the heavy quark mass, see refs. [10, 11].

2.1 From QCD in small volume to non-perturbatively renormalized HQET

A long-standing problem with lattice computations in HQET is the occurrence of power-law divergences during the renormalization process (cf. refs. [15, 16, 17]), implied by the allowed mixings of operators of different dimensions coming with coefficients $\{c_k\}$ that contain inverse powers of the lattice spacing a. At each order of the HQET expansion parameter ($1/m$, where m is the heavy quark mass), new such free parameters c_k arise, which in principle are adjustable by a matching to QCD; but owing to incomplete cancellations when performing this matching only in perturbation theory, one is always left with a perturbative remainder that still stays divergent as $a \to 0$. Therefore, the continuum limit does not exist.

Already HQET in leading order, the static approximation, exhibits this unwanted phenomenon. In this case the kinetic and the mass terms in the static action mix under renormalization and give rise to a local mass counterterm $\delta m \propto 1/a$, the self-energy of the static quark, which causes a linearly divergent truncation error if one relies on an only perturbative subtraction of this divergence. A prominent example for a quantity suffering from it is the b-quark mass itself: past computations in the static approximation [18] were limited to finite lattice spacings, and the continuum limit was impossible to reach.

A viable strategy to solve this severe problem of power divergences is provided by a *non-perturbative matching of HQET and QCD in finite volume* [8, 9]. To integrate the present work into the broader context of ref. [9], we reproduce the central line of reasoning here. Let us consider QCD consisting of (generically $N_{\rm f}-1$) light quarks and a heavy quark, typically the b-quark. In the effective theory, the dynamics of the heavy quark is governed by the HQET action, which formally is an expansion in inverse powers of the heavy quark mass. (For further details see e.g. section 2 of ref. [9].) On the renormalized level, the effective theory discretized on a lattice can be defined in terms of parameters $\{c_k\}$ that comprise those specifying the light quark sector (e.g. the bare gauge coupling, $g_0^2 \equiv c_1$, and the masses of the light quarks) and coefficients of local composite fields in the $1/m$-expansion of the lattice action, supplemented by further coefficients belonging to local composite operators which will be needed when including their correlation functions into the renormalization program. In other words, if these parameters are chosen correctly, HQET and QCD are expected to be equivalent in the sense that $\Phi^{\rm HQET}(M) = \Phi^{\rm QCD}(M) + {\rm O}(1/M^{n+1})$ holds for suitable observables Φ in both theories, where for simplicity only the dependence on the heavy quark mass, here represented by the scheme and scale independent (and thus theoretically unambiguous) renormalization group invariant quark mass, M, is stressed. Now suppose that in some way the parameters of QCD have already been fixed to proper values. Then the parameters $\{c_k\}$ in the effective theory may just be determined through its relation to QCD by requiring a set of matching conditions:

$$\Phi_k^{\rm HQET}(L, M) = \Phi_k^{\rm QCD}(L, M)\,, \qquad k = 1, \ldots, N_n\,. \tag{2.1}$$

In this equation, the index k labels the elements of the parameter set $\{c_k\}$ defining the effective theory up to $1/M^{n+1}$-corrections (where, for instance, the additive mass renormalization δm mentioned above is amongst them), and the conditions (2.1) determine the

c_k for any value of the lattice spacing. Moreover, we have already indicated the dependence of the observables Φ_k in eq. (2.1) on another variable which will become important in the following: the linear extent L of a *finite* volume.

To substantiate this L-dependence, we note that in order to circumvent the difficulties with the power-law divergences from the start, the matching equations (2.1) are understood as *non-perturbative conditions* in which both sides are to be calculated with the aid of numerical simulations. From the practical point of view, this in turn also means that one must be able to simulate the b-quark as a relativistic fermion. Hence, the linear extent L of the matching volume (i.e. where eq. (2.1) should hold) has to be chosen with care. On the one hand, it should fulfill $LM \gg 1$ to apply HQET quantitatively on the l.h.s. of (2.1), i.e. to suppress $1/m$-corrections, and on the other hand one has to ensure $aM \ll 1$ on the r.h.s. to treat the heavy quark flavour in the relativistic theory and avoid large lattice artifacts so that the continuum limit is under control. Taking these constraints together, while at the same time keeping the number of lattice points manageable for present-day computers, one then ends up with a volume for imposing the matching conditions (2.1) that is physically small; in our application later it will turn out to be of the order of $(0.2\ \mathrm{fm})^4$.

Having highlighted QCD in finite volume as key ingredient for the practical realization of the non-perturbative matching, we close this subsection with a few remarks on the subsequent (but not less important) steps that are involved to adopt it as a general approach for non-perturbative computations using the lattice regularized HQET. These steps, together with two applications of the proposal as a whole, are also worked out in ref. [9], which the reader should consult for a thorough discussion.

- Rather than directly identifying the quantities Φ_k entering (2.1) with physical, experimentally accessible observables (by which one would sacrifice the predictability of the effective theory), they must be properly chosen as renormalized quantities computable in the continuum limit of lattice QCD, which in turn necessitates the use of a small volume as explained before. Of course, their explicit form still depends on the application in question. One may think e.g. of hadronic matrix elements or, as in the computations reported in the following sections, effective masses (respectively, energies) that are deduced from the decay of two-point heavy-light correlation functions.

- Apparently, although these matching conditions to fix the parameters of HQET are perfectly legitimate (since the underlying lagrangian does not 'know' anything about the finite volume), one still has to make contact to a physical situation, where the interesting quantities of the infinite-volume theory can be extracted at the end. Employing the same lattice resolution as in the small volume computation, however, would again demand too many lattice points. This gap between the small volume with its fine lattice resolution on the one side and larger lattice spacings, and thereby also larger physical volumes, on the other is bridged by a recursive finite-size scaling procedure inspired by ref. [19]. As a result, the Φ_k^{HQET} are obtained at some larger volume of extent $L = \mathrm{O}(1\ \mathrm{fm})$, where the resolutions a/L are such that at the same lattice spacings (i.e. at the same bare parameters) volumes with $L \simeq 2$ fm — to accommodate physical observables in the infinite-volume theory — are affordable.

JHEP02(2004)064

- Finally, the approach requires a physical, dimensionful input. This usually amounts to relate the observables $\Phi_k^{\rm HQET}$ of the effective theory calculated in large volume to some experimental quantity. Which quantity this actually might be has to be decided when a concrete application is addressed. (E.g., in the application to compute $\overline{m}_{\rm b}$, it is the B-meson mass [9].)

2.2 Lattice setup and observables

In our investigation of QCD in a small volume we distinguish between a light ('l') and a heavy ('h') quark flavour. The lattice regularized theory is formulated in a Schrödinger functional (SF) cylinder of extent $L^3 \times T$ [20, 21]: the gluon and quark fields are subject to periodic (Dirichlet) boundary conditions in spatial (temporal) directions, and — if not explicitly stated otherwise — we assume $T = L$ from now on. In principle, the aforementioned matching strategy between HQET and QCD is not restricted to the SF as the only possible finite-volume scheme to treat the involved heavy-light systems in the relativistic theory, but in this way its practical implementation will much profit from known non-perturbative results on the renormalized quantities that will be needed in the following.

Starting from the O(a) improved heavy-light axial and vector currents,

$$(A_{\rm I})_\mu(x) = \overline{\psi}_{\rm l}(x)\gamma_\mu\gamma_5\psi_{\rm h}(x) + ac_{\rm A}\frac{1}{2}(\partial_\mu + \partial^*_\mu)\left\{\overline{\psi}_{\rm l}(x)\gamma_5\psi_{\rm h}(x)\right\}, \tag{2.2}$$

$$(V_{\rm I})_\mu(x) = \overline{\psi}_{\rm l}(x)\gamma_\mu\psi_{\rm h}(x) + ac_{\rm V}\frac{1}{2}(\partial_\nu + \partial^*_\nu)\left\{i\,\overline{\psi}_{\rm l}(x)\sigma_{\mu\nu}\psi_{\rm h}(x)\right\}, \tag{2.3}$$

(where numerical values for the coefficients $c_{\rm A}$ and $c_{\rm V}$ in the quenched approximation are taken from refs. [22, 23]), we construct their correlation functions in the SF [24, 25] as

$$f_{\rm A}(x_0) = -\frac{a^6}{2}\sum_{\boldsymbol{y},\boldsymbol{z}}\left\langle (A_{\rm I})_0(x)\overline{\zeta}_{\rm h}(\boldsymbol{y})\gamma_5\zeta_{\rm l}(\boldsymbol{z})\right\rangle, \tag{2.4}$$

$$k_{\rm V}(x_0) = -\frac{a^6}{6}\sum_{\boldsymbol{y},\boldsymbol{z},k}\left\langle (V_{\rm I})_k(x)\overline{\zeta}_{\rm h}(\boldsymbol{y})\gamma_k\zeta_{\rm l}(\boldsymbol{z})\right\rangle, \tag{2.5}$$

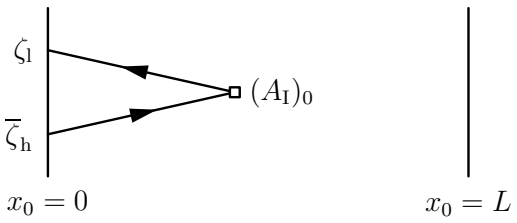

Figure 1: Illustration of the correlation function $f_{\rm A}$, while in $k_{\rm V}$ the insertion of $(A_{\rm I})_0$ is replaced by $(V_{\rm I})_k$.

schematically drawn in figure 1. Based on these, we define L-dependent energies in both channels by combining the usual forward and backward difference operators to take the logarithmic derivatives

$$\Gamma_{\rm PS}(L,M) \equiv -\frac{1}{2}\left(\partial_0 + \partial_0^*\right)\ln\left[\,f_{\rm A}(x_0,M)\right]\Big|_{x_0=L/2}, \tag{2.6}$$

$$\Gamma_{\rm V}(L,M) \equiv -\frac{1}{2}\left(\partial_0 + \partial_0^*\right)\ln\left[\,k_{\rm V}(x_0,M)\right]\Big|_{x_0=L/2}, \qquad T = L, \tag{2.7}$$

in which all multiplicative renormalization factors drop out. These observables also depend on the bare coupling, g_0, and — as the light quark mass is put to zero in the actual computations — on the heavy quark mass variable which, as already in section 2.1, one

may conveniently set to be the *renormalization group invariant (RGI)* mass of the heavy quark, M. Having in mind the corresponding correlators in the effective theory, where in the static (i.e. infinite-mass) limit the two currents fall together owing to the heavy quark spin-symmetry, we also form their spin-averaged combination

$$\Gamma_{\rm av} \equiv \frac{1}{4}\left(\Gamma_{\rm PS} + 3\Gamma_{\rm V}\right), \tag{2.8}$$

which is expected to deviate from the static limit by the smallest $1/m$-corrections [9].

2.3 Determination of the heavy quark mass dependence

As mentioned before and detailed in refs. [8, 9], the non-perturbative matching between HQET and QCD can be applied to determine the mass of the b-quark in the static approximation. To achieve this goal, the quantities Φ_k in eq. (2.1) have to be identified with suitable observables that can be calculated by numerical simulations. Since we want to evaluate them in the continuum limit, we have to ensure a situation with fixed renormalized parameters, along which the limit $a/L \to 0$ may be performed. In regard of the (suppressed as well as indicated) dependences in the matching conditions (2.1), this means that for each value of L/a we have to make particular choices for the gauge coupling and the quark masses in the light and heavy sectors, respectively. The first two of them are immediately offered by

$$\Phi_1^{\rm HQET} = \bar{g}^2(L) = \text{constant}\,, \tag{2.9}$$
$$\Phi_2^{\rm HQET} = m_{\rm l} = 0\,, \tag{2.10}$$

where $\bar{g}^2$ denotes the renormalized finite-volume coupling in the SF scheme that runs with the box size L [26] and $m_{\rm l} \equiv m_{\rm l}^{\rm PCAC}$ is the PCAC current quark mass of the light flavour. These conditions allow to readily benefit from earlier work, because when fixing $\bar{g}^2$ to one of the values used for the (quenched) computation of the non-perturbative quark mass renormalization in [27], they translate into triples $(L/a, \beta = 6/g_0^2, \kappa_{\rm l})$ that can directly be taken over from this reference.[2]

For the computation of the b-quark's mass in leading order of HQET one yet needs one more condition in order to fix the parameter $a\delta m$ in the static lagrangian. Following [8, 9], the most natural candidates for this purpose are now the pseudoscalar and spin-averaged energies of the form (2.6) and (2.8) introduced in section 2.2. For $k = 3$, eq. (2.1) then turns into

$$L(\Gamma_{\rm stat} + m) \equiv \Phi_3^{\rm HQET}(L, M) = \Phi_3^{\rm QCD}(L, M) \equiv L\Gamma_{\rm X}\,, \tag{2.11}$$

where $\Gamma_{\rm X} = \Gamma_{\rm X}(L, M)$, $\rm X = PS, av$, are defined in *QCD and small volume with a relativistic b-quark* and carry the entire quark mass dependence. On the l.h.s., $\Gamma_{\rm stat}$ denotes the analogue of $\Gamma_{\rm X}$ in the effective theory, where the heavy quark entering the correlator (2.4) is treated in the static approximation, and implicitly contains the problematic, linearly divergent mass counterterm $a\delta m$. The matching equation (2.11) may be connected to a

[2] In this case the lattice action's hopping parameter associated with the light quark flavour, $\kappa_{\rm l}$, just equals the critical hopping parameter, $\kappa_{\rm c}$, as a consequence its very definition: $m_{\rm l}(\kappa_{\rm c}) = 0$, see ref. [27].

physical quantity in large volume (the B-meson mass [9]) by finite-size scaling (cf. section 2.1). But without going into further, unnecessary details we only note that this yields a (dimensionless) equation, which apart from $\Gamma_{\rm X}(L,M)$ only contains energy differences computable in the static theory — such that the counterterm $a\delta m$ cancels out — and the experimental mass of the B-meson. Since all pieces in that equation can be evaluated non-perturbatively and in the continuum limit, the quantitative knowledge of $\Gamma_{\rm X}(L,M)$ as a function of M in the relevant quark mass region finally allows to solve it for the desired numerical value of the non-perturbatively renormalized RGI mass of the b-quark, $M_{\rm b}$, in the static approximation [9].

So the task is here to non-perturbatively determine the heavy quark mass dependence of the effective heavy-light meson energies $\Gamma_{\rm X}(L,M)$. It thus remains to discuss how we fix the linear size of the finite volume, $L = L_0$, and a set of dimensionless quark mass values,

$$z \equiv L_0 M = \text{constant}\,, \tag{2.12}$$

at which the numerical computation of $\Gamma_{\rm X}$ for various lattice spacings takes place in practice.

We answer this question again on basis of the present numerical knowledge in the framework of the SF. Among the available constant values of the renormalized SF coupling that belong to different sets of triples $(L/a, \beta, \kappa_{\rm l})$ known from ref. [27] we fix, as was initially required by the condition (2.9),

$$\bar{g}^2\left(\frac{L_0}{2}\right) = 1.8811\,, \tag{2.13}$$

where the (inverse) lattice spacing varies within $6 \leq L_0/(2a) \leq 16$. This choice is particularly convenient, because from the same reference one then finds that L_0 is given in units of a certain maximal size, $L_{\rm max}$, of the SF box, namely

$$L_0 = \frac{L_{\rm max}}{2} = 0.36\, r_0 \approx 0.18 \text{ fm}\,, \tag{2.14}$$

which is implicitly defined by $\bar{g}^2(L_{\rm max}) = 3.48$ and, through its relation to the hadronic radius $r_0 = 0.5$ fm [28], also known in physical units: $L_{\rm max}/r_0 = 0.718(16)$ [29]. Indeed, from a closer inspection of the parameters corresponding to the condition (2.13) (see table 1) one may convince oneself that an accompanying volume of some small extent as (2.14) is a sensible compromise between the associated resolutions being small enough to comfortably accommodate a propagating (albeit the system size confining) b-quark and being able to consider heavy quark masses large enough to suppress $\mathrm{O}(1/z)$-corrections (i.e. $z \gg 1$ but not too large to avoid a substantial enhancement of cutoff effects) as well as to cover the physical RGI b-quark mass scale itself.

In order to satisfy eq. (2.12) for the intended numerical values z while L/a and β are changed to approach the continuum limit, we still have to relate the RGI mass of the heavy quark, M, to the corresponding hopping parameter $\kappa_{\rm h}$ as the simulation parameter for the bare heavy quark mass in the lattice action. One possibility would be to employ the ($\mathrm{O}(a)$

improved) relation between the RGI and the bare PCAC quark mass, $m_{\rm h}$, viz.

$$M = \frac{M}{\overline{m}_{\rm h}(\mu_0)} \frac{Z_{\rm A}(g_0)(1+b_{\rm A}am_{\rm q,h})}{Z_{\rm P}(g_0,L_0)(1+b_{\rm P}am_{\rm q,h})} \times m_{\rm h} + {\rm O}\left(a^2\right), \qquad \mu_0 = \frac{1}{L_0}, \tag{2.15}$$

where $\overline{m}_{\rm h}(\mu_0)$ denotes the running heavy quark mass renormalized at the scale $\mu_0 = 1/L_0$ in the SF scheme and (the inverse of) its *ratio* to the RGI mass M, the first factor on the r.h.s., is inferable from the literature as will be elaborated on after eq. (2.19). The numerator and denominator in the second factor account for the renormalization of the axial current and the pseudoscalar density in the O(a) improved theory, respectively. Here, the subtracted bare heavy quark mass is defined as usual by $m_{\rm q,h} = m_{0,\rm h} - m_{\rm c}$ with $m_{\rm c}$ the critical value of the bare quark mass $m_{0,\rm h}$, which in terms of the hopping parameters is given by $am_{\rm q,h} = \frac{1}{2}(\kappa_{\rm h}^{-1} - \kappa_{\rm c}^{-1})$. Although the involved renormalization factors are in principle known from refs. [27, 30] in the quenched case, this would demand additional simulations to appropriately tune $\kappa_{\rm h}$ — and thereby the PCAC mass $m_{\rm h}$ as a secondary quantity composed of correlation functions (cf. eq. (3.3)) — until the condition (2.12) is met with sufficient precision.

However, a safer (and also more economic) way to estimate $\kappa_{\rm h}$ such that a constant $z = L_0 M$ can be enforced in advance *without* any additional tuning runs is as follows. Recall that alternatively the renormalized quark mass can be written in terms of the O(a) improved subtracted bare quark mass, $\widetilde{m}_{\rm q,h}$, as

$$\overline{m}_{\rm h} = Z_{\rm m}\, \widetilde{m}_{\rm q,h}\,, \qquad \widetilde{m}_{\rm q,h} = m_{\rm q,h}(1 + b_{\rm m} am_{\rm q,h})\,, \tag{2.16}$$

where non-perturbative estimates on the improvement coefficient $b_{\rm m}$ and the finite combination of renormalization constants

$$Z(g_0) \equiv \frac{Z_{\rm m}(g_0,L) Z_{\rm P}(g_0,L)}{Z_{\rm A}(g_0)} \tag{2.17}$$

have been published in ref. [30] for the quenched approximation. The latter identity may then be used to eliminate the (in the SF scheme unknown) renormalization factor $Z_{\rm m}$ in eq. (2.16) in favour of numerically known ones. The decomposition of the RGI heavy quark mass analogous to (2.15) now assumes the form:

$$M = \frac{M}{\overline{m}_{\rm h}(\mu_0)} \frac{Z(g_0) Z_{\rm A}(g_0)}{Z_{\rm P}(g_0,L_0)} \times m_{\rm q,h}(1 + b_{\rm m} am_{\rm q,h}) + {\rm O}\left(a^2\right), \qquad \mu_0 = \frac{1}{L_0}\,. \tag{2.18}$$

The last piece to be addressed in this equation is the universal, regularization independent ratio of the RGI quark mass to the renormalized mass at fixed renormalization scale, which for later reference we call

$$h(L_0) \equiv \frac{M}{\overline{m}_{\rm h}(\mu_0)}\,, \qquad \mu_0 = \frac{1}{L_0}\,. \tag{2.19}$$

In a mass independent renormalization scheme such as the SF it is flavour independent and, according to ref. [27], can be expressed as

$$h(L_0) = \frac{Z_{\rm P}(L_0)}{Z_{\rm P}(2^{-6}L_{\rm max})} \times \left[2b_0 \bar{g}^2(\mu)\right]^{-d_0/(2b_0)} \exp\left\{ - \int_0^{\bar{g}(\mu)} {\rm d}g \left[\frac{\tau(g)}{\beta(g)} - \frac{d_0}{b_0 g} \right] \right\} \tag{2.20}$$

set	L/a	$\beta = 6/g_0^2$	κ_l	$\bar{g}^2(L/2)$	$\bar{g}^2(L)$	Z_P
A	12	7.4082	0.133961(8)	1.8811(22)	2.397(17)	0.6764(6)
B	16	7.6547	0.133632(6)	1.8811(28)	2.393(18)	0.6713(8)
C	20	7.8439	0.133373(2)	1.8811(22)	2.379(22)	0.6679(8)
D	24	7.9993	0.133159(4)	1.8811(38)	2.411(20)	0.6632(8)
E	32	8.2415	0.132847(3)	1.8811(99)	2.397(52)	0.6575(13)

Table 1: Our parameter sets that refer to the light quark sector and have fixed SF coupling, $\bar{g}^2(L/2) = 1.8811$. The parameters L/a, β and $\kappa_\mathrm{l} \equiv \kappa_\mathrm{c}$ of A, B, D and E are taken over from [27] without changes, whereas we performed new simulations to add with C a further lattice resolution for this work. Moreover, the renormalization constants $Z_\mathrm{P} = Z_\mathrm{P}(g_0, L/a)$ differ from those of [27] in that they have been computed in the context of [31] using the two-loop value [32] for the boundary improvement coefficient c_t.

with $L_0 = L_\mathrm{max}/2$, $\mu = 2^6/L_\mathrm{max}$ and b_0, d_0 the leading-order coefficients in the perturbative expansions of the renormalization group functions of the running coupling and quark mass, $\beta(\bar{g})$ and $\tau(\bar{g})$. In the ratio of Z_P-factors we encounter a scale evolution through changes by finite step sizes in the SF renormalization scale $L = 1/\mu$ that has been non-perturbatively computed in [27], whereas the remainder lives in the high-energy regime where the coupling is reasonably small to evaluate it in perturbation theory. Since in eq. (2.14) we just chose the linear extent L_0 of the small volume, where the non-perturbative matching to the relativistic theory is to be performed, as a proper multiple of the scale L_max, a numerical estimate for $h(L_0)$ in the continuum limit, eq. (2.19), can be directly extracted from the results already published in [27] and will be quoted in section 3.2 later on.

Our simulation parameters, which fix via eqs. (2.9), (2.10) and (2.13) the physics in the relativistic sector and via eq. (2.14) the size of the matching volume where to determine the non-perturbative heavy quark mass dependence of our observables, are summarized in table 1. Values for the other quantities, which have to be inserted into eq. (2.18) in order to obey the condition (2.12) of constant $z = L_0 M$, will be specified when we come to describe the actual calculation of the z-dependence of $\Gamma_\mathrm{X} = \Gamma_\mathrm{X}(L_0, M)$, $\mathrm{X} = \mathrm{PS}, \mathrm{av}$, in section 3.2.

At this stage we still want to direct the reader's attention to an issue that can already be foreseen to become a potential limitation in any application of the numerically computed quark mass dependence: even with eq. (2.18), the dimensionless mass parameter z can only be fixed through quantities known to a certain precision. In particular, the improvement coefficient b_m and the renormalization factor Z are only available from ref. [30][3] for $6.0 \leq \beta \leq 6.756$, which are significantly lower than the β-s of table 1 we are interested in. It hence appears quite difficult to reliably guess from the numbers in [30] values for b_m and Z in the β-region relevant here and, even more, to quantitatively assess the additional error contribution those estimates would then be afflicted with. Since this constitutes a dominant source of uncertainty, which would also propagate into any quantity that explicitly derives

[3]The β-range considered in [30] was chosen to cover values commonly used to simulate O(a) improved quenched QCD in physically large volumes. Similarly, the results from determinations through chiral Ward identities with mass non-degenerate quarks [33, 34] refer to this region and are not applicable here, too.

from the z-dependence of the observables studied here — such as, for instance, the b-quark mass through the matching of HQET and QCD [9] —, we first determine $b_{\rm m}$ and Z exactly for the β-values of table 1 and also improve their numerical precision.

3. Results

We now present the numerical results of our (quenched) computation of the heavy-light meson energies $\Gamma_{\rm X}(L_0, M)$, X = PS, av, which — as outlined in the previous subsection — basically consists of two parts: first, we determine $b_{\rm m}$ and Z in the β-range relevant for a matching in physically small volume in order to be able to fix the RGI heavy quark mass to a set of desired values $z = L_0 M$ with sufficient precision, and second, the $L_0\Gamma_{\rm X}(L_0, M)$ are calculated at these values of z in the continuum limit. This will then allow for smooth representations of the energies as functions of z, which eventually may be used to interpolate them to the b-quark scale, $z_{\rm b} = L_0 M_{\rm b}$ [9].

3.1 Coefficients $b_{\rm A} - b_{\rm P}$, $b_{\rm m}$ and renormalization factor Z for $7.4 \lesssim \beta \lesssim 8.2$

Here we proceed in the spirit of ref. [30], where the idea of *imposing improvement conditions at constant physics* was advocated. In that work, which considered a range $6.0 \leq \beta \leq 6.756$ of bare couplings commonly used in large-volume simulations, this was realized by keeping constant the ratios L/r_0 and $T/L = 3/2$ (supplemented by the SF-specific choices $C = C' = 0$ and $\theta = 0.5$). However, despite $\ln(a/r_0)$ as a function of β needed to fix L/r_0 to some suitable value for given L/a is available for $5.7 \leq \beta \leq 6.92$ [35] and even beyond [36], the condition of constant L/r_0 can not be transfered to the present situation. The reason lies in the fact that for β-values in the range we are interested in, $7.4 \lesssim \beta \lesssim 8.2$, enforcing an improvement condition such as $L/r_0 = {\rm O}(1)$ would lead to prohibitively large values of L/a in the simulations. Therefore, to replace the latter, we exploit one of the already built in elements of the matching strategy between HQET and QCD as explained in the foregoing section: namely, as for the computation of the energies $\Gamma_{\rm X}$ on the QCD side we have to work along a line of constant physics in bare parameter space anyway, we can directly adopt the pairs $(L/a, \beta)$ of table 1, which correspond to $L/L_{\rm max} = 1/2 = 0.36 r_0/L_{\rm max}$ and simultaneously to a constant renormalized coupling of $\bar{g}^2(L/2) = 1.8811$ (see eqs. (2.14) and (2.13)). Within the present application, this constitutes a much more natural and equally admissible choice of improvement condition and thereby, in the same way as in ref. [30], the improvement coefficients $b_{\rm A} - b_{\rm P}$ and $b_{\rm m}$ as well as the renormalization constant Z become smooth functions of g_0^2 but exactly in the region where they are needed.

Following [30] — and also referring to this reference for any unexplained details —, the improvement coefficient $b_{\rm m}$ and the renormalization constant Z (as well as the difference of coefficients $b_{\rm A} - b_{\rm P}$, though it does not enter the subsequent computations in section 3.2) can be determined by studying QCD with non-degenerate quarks. This is particularly advantageous in case of the quenched approximation at hand, since then the structure of the O(a) improved theory stays quite simple. For instance, the improvement of the off-diagonal bilinear fields $X^{\pm} = X^1 \pm i\, X^2$, $X = A_\mu, P$, emerging as a consequence of

the broken isospin symmetry, is the same as in the degenerate case, except that the b-coefficients now multiply cutoff effects proportional to the average $\frac{1}{2}(am_{\mathrm{q},i} + am_{\mathrm{q},j})$ of the subtracted bare quark masses, $m_{\mathrm{q},i} = m_{0,i} - m_{\mathrm{c}}$, which themselves are separately improved for each quark flavour:

$$\widetilde{m}_{\mathrm{q},i} = m_{\mathrm{q},i}(1 + b_{\mathrm{m}} a m_{\mathrm{q},i})\,. \tag{3.1}$$

(Here and below the indices i, j label the different quark flavours.) Identifying, for instance, the flavours in the isospin doublet with a light and a heavy quark as before, the corresponding PCAC relation reads

$$\partial_\mu A_\mu^{\pm}(x) = (m_{\mathrm{l}} + m_{\mathrm{h}}) P^{\pm}(x)\,, \tag{3.2}$$

and the renormalization constants Z_{A} and Z_{P} that come into play upon renormalization are just those known in the theory with two mass degenerate quarks.

Accordingly, the fermionic correlation functions defined in the SF and involving the axial current and the pseudoscalar density [24] generalize to $f_{\mathrm{A}}^{ij}(x_0) = -\frac{1}{2}\left\langle A_0^+(x) O^-\right\rangle$ and $f_{\mathrm{P}}^{ij}(x_0) = -\frac{1}{2}\left\langle P^+(x) O^-\right\rangle$, with pseudoscalar boundary sources decomposed as $O^{\pm} = O^1 \pm i\, O^2$ where $O^a = a^6 \sum_{\boldsymbol{y},\boldsymbol{z}} \bar{\zeta}(\boldsymbol{y})\gamma_5 \frac{1}{2}\tau^a \zeta(\boldsymbol{z})$. Then the improved bare PCAC (current) quark masses[4] as functions of the timeslice location x_0 are given by

$$m_{ij}\left(x_0; \frac{L}{a}, \frac{T}{L}, \theta\right) = \frac{\tilde{\partial}_0 f_{\mathrm{A}}^{ij}(x_0) + a c_{\mathrm{A}} \partial_0^* \partial_0 f_{\mathrm{P}}^{ij}(x_0)}{2\, f_{\mathrm{P}}^{ij}(x_0)}\,, \tag{3.3}$$

where only here we explicitly indicate their additional dependence on L/a, T/L and the periodicity angle θ of the fermion fields. In the degenerate case, $i = j$, the correlators assume the standard form as introduced earlier [24, 25], and m_{ij} just reduces to the current quark mass of a single quark flavour that is prepared by a corresponding choice of equal values for the associated hopping parameters, $\kappa_i = \kappa_j$. Also the precise definition of the lattice derivatives in eq. (3.3) matters. As it is written there, $\tilde{\partial}_0 = \frac{1}{2}(\partial_0 + \partial_0^*)$ denotes the average of the usual forward and backward derivatives, but as in ref. [30] we have employed the improved derivatives

$$\tilde{\partial}_0 \to \tilde{\partial}_0\left(1 - \frac{1}{6}\, a^2 \partial_0^* \partial_0\right), \qquad \partial_0^* \partial_0 \to \partial_0^* \partial_0 \left(1 - \frac{1}{12}\, a^2 \partial_0^* \partial_0\right) \tag{3.4}$$

as well, which (when acting on smooth functions) have $\mathrm{O}(g_0^2 a^2, a^4)$ errors only.

To enable their numerical calculation, the desired coefficients $b_{\mathrm{A}} - b_{\mathrm{P}}$, b_{m} and the finite factor $Z = Z_{\mathrm{m}} Z_{\mathrm{P}}/Z_{\mathrm{A}}$ have to be isolated. This can be achieved by virtue of the identity

$$\begin{aligned} m_{ij} = Z\Bigg[&\frac{1}{2}\left(m_{\mathrm{q},i} + m_{\mathrm{q},j}\right) + \frac{1}{2}\, b_{\mathrm{m}} \left(a m_{\mathrm{q},i}^2 + a m_{\mathrm{q},j}^2\right) - \\ &- \frac{1}{4}\left(b_{\mathrm{A}} - b_{\mathrm{P}}\right) a \left(m_{\mathrm{q},i} + m_{\mathrm{q},j}\right)^2\Bigg] + \mathrm{O}\left(a^2\right), \end{aligned} \tag{3.5}$$

[4] This expression for the PCAC masses is only $\mathrm{O}(a)$ improved up to a factor $1 + \frac{1}{2}(b_{\mathrm{A}} - b_{\mathrm{P}})(am_{\mathrm{q},i} + am_{\mathrm{q},j})$ for quark mass dependent cutoff effects.

which is obtained if one equates the two available expressions for the O(a) improved renormalized quark masses, i.e. in terms of the current quark and the subtracted bare quark masses (as they appear for the degenerate case in eq. (2.15) and thereafter). Forming ratios of suitable combinations of degenerate and non-degenerate current quark masses in the representation (3.5) allows to derive the following direct estimators for $b_{\rm A} - b_{\rm P}$, $b_{\rm m}$ and Z [30]:

$$R_{\rm AP} = \frac{2\,(2m_{12} - m_{11} - m_{22})}{(m_{11} - m_{22})(am_{\rm q,1} - am_{\rm q,2})} = b_{\rm A} - b_{\rm P} + {\rm O}\left(am_{\rm q,1} + am_{\rm q,2}\right), \tag{3.6}$$

$$R_{\rm m} = \frac{4\,(m_{12} - m_{33})}{(m_{11} - m_{22})(am_{\rm q,1} - am_{\rm q,2})} = b_{\rm m} + {\rm O}\left(am_{\rm q,1} + am_{\rm q,2}\right), \tag{3.7}$$

with $m_{0,3} = \frac{1}{2}(m_{0,1} + m_{0,2})$, apart from other quark mass independent lattice artifacts of O(a). For the renormalization constant Z an analogous expression holds even up to O(a^2) corrections,

$$R_Z = \frac{m_{11} - m_{22}}{m_{\rm q,1} - m_{\rm q,2}} + (b_{\rm A} - b_{\rm P} - b_{\rm m})(am_{11} + am_{22}) = Z + {\rm O}\left(a^2\right), \tag{3.8}$$

provided that the correct value for $b_{\rm A} - b_{\rm P} - b_{\rm m} = R_{\rm AP} - R_{\rm m}$ (only involving correlation functions with mass degenerate quarks) is inserted.

Concerning the simulation parameters, we argued above that it is most natural to choose L/a and β exactly as listed in table 1 of the preceding section. Moreover, values for the bare quark masses have to be selected. Here we considered two pairs of values for them,

$$\begin{aligned} &\text{choice 1}: \quad m_{0,\rm l} = m_{\rm c} \;\Leftrightarrow\; Lm_{\rm l} \approx 0\,, \quad Lm_{\rm h} \approx 0.5\,, \\ &\text{choice 2}: \quad m_{0,\rm l} = m_{\rm c} \;\Leftrightarrow\; Lm_{\rm l} \approx 0\,, \quad Lm_{\rm h} \approx 2.6\,; \end{aligned} \tag{3.9}$$

to comply with the heavy-light notation before we identify the bare quark masses as $m_{0,1} = m_{0,\rm l}$ and $m_{0,2} = m_{0,\rm h}$ with associated PCAC masses $m_{11} \equiv m_{\rm l}$ and $m_{22} \equiv m_{\rm h}$. With the first choice (corresponding to $z \approx 1$) $Lm_{\rm h}$ is close to the value used in ref. [30], which has the advantage that there this condition was also investigated in perturbation theory and the encountered O(a) ambiguities were not enormous. On the contrary, the second one (corresponding to $z \approx 5$) is motivated by the typical quark mass region that we have to deal with when probing our non-degenerate, heavy-light quark system in the next subsection. Maintaining these conditions to sufficient accuracy requires some prior simulations to tune the hopping parameter $\kappa_{\rm h}$ belonging to the heavy flavour's bare mass appropriately, whereas by $\kappa_{\rm l} = \kappa_{\rm c}$ taken over from the known values of ref. [27] the light quark mass is set to zero. The final simulation parameters to determine the quantities $R_{\rm X}$, ${\rm X} = {\rm AP}, {\rm m}, Z$, in question can be drawn from the triples $(L/a, \beta, \kappa_{\rm l})$ of table 1 specifying the light quark sector (except that, only here, $T = 3L/2$), while the bare heavy quark mass is set through $\kappa_{\rm h}$ given in the second columns of tables 2 and 3. There one can also see that the bare current quark mass $Lm_{\rm h}$ has been fixed within a few percent to the values dictated by (3.9) to keep physics constant.[5]

set	$\kappa_{\rm h}$	$Lm_{\rm h}$	$b_{\rm A}-b_{\rm P}$	$b_{\rm m}$	Z
A	0.132728	0.4778(7)	−0.0008(14)	−0.6217(17)	1.0941(3)
B	0.132711	0.4621(7)	−0.0059(22)	−0.6218(27)	1.0916(3)
C	—	0.4572(6)	−0.0057(23)	−0.6228(28)	1.0900(3)
D	0.132553	0.4539(5)	−0.0072(21)	−0.6260(27)	1.0882(2)
E	0.132395	0.4508(5)	−0.0077(25)	−0.6312(32)	1.0859(2)

Table 2: Numerical results on the improvement coefficients $b_{\rm A}-b_{\rm P}$ and $b_{\rm m}$ and on the renormalization constant Z, based on statistics varying between O(900) measurements (A) and O(200) measurements (E). These numbers refer to 'choice 1' in eq. (3.9), where the heavy quark mass is kept at $Lm_{\rm h}\approx 0.5$, while $Lm_{\rm l}$ indeed turned out to be compatible with zero up to tiny deviations of O(0.03) (A) and O(0.01) (sets B–E). For C, we interpolated results obtained with $L/a = 16, 24$ to $L/a = 20$. Amongst others, $b_{\rm m}$ and Z are needed to fix the renormalized heavy quark mass in the simulations reported in section 3.2.

set	$\kappa_{\rm h}$	$Lm_{\rm h}$	$b_{\rm A}-b_{\rm P}$	$b_{\rm m}$	Z
A	0.126040	2.7100(6)	0.0489(3)	−0.5401(4)	1.0855(2)
B	0.128028	2.6112(6)	0.0239(5)	−0.5621(7)	1.0867(2)
C	—	2.6709(5)	0.0151(6)	−0.5744(9)	1.0867(2)
D	0.129595	2.5456(5)	0.0103(5)	−0.5811(8)	1.0859(1)
E	0.130246	2.5035(5)	0.0051(6)	−0.5927(9)	1.0845(1)

Table 3: The same as in table 2 but for 'choice 2' of the heavy quark mass: $Lm_{\rm h}\approx 2.6$.

The Monte Carlo simulation details and the technical aspects of the analysis to compute the observables (3.6)–(3.8) from the measured fermionic correlation functions are essentially the same as in ref. [30]. In particular, these secondary quantities have been averaged over the central timeslices $L/(2a),\ldots,(T-L/2)/a$ to increase statistics, and their statistical errors were estimated by the jackknife method. Another issue that deserves to be mentioned is the occurrence of the third mass parameter $m_{0,3}$ in the determination of $b_{\rm m}$, which has to be set properly to ensure the required (but subtle) cancellation leading to the expression (3.7) for the estimator $R_{\rm m}$. As in terms of the hopping parameters this amounts to form the combination $\kappa_3 = 2\kappa_1\kappa_2/(\kappa_1+\kappa_2)$, the condition $\frac{1}{2}(m_{0,1}+m_{0,2})-m_{0,3}=0$ can be satisfied in practice only up to roundoff errors, which might cause a systematic uncertainty in simulations with single precision arithmetics. But in contrast to ref. [30], where this effect had to be taken into account carefully, the exact numerical value of κ_3 was now calculated in double precision directly in the simulation program itself so that a rounding error contribution (reflecting some possible remnant imperfection in the cancellation via $m_{0,3}$) to the error on $R_{\rm m}$ can be neglected here.

Our non-perturbative results on $b_{\rm A}-b_{\rm P}$, $b_{\rm m}$ and Z, which we obtained from the numerical simulation data along these lines using improved derivatives throughout, are also

[5]Similar to the situation in ref. [30], this is to a good precision equivalent to keeping fixed the corresponding renormalized masses $Lm_{\rm R} = LZ_{\rm A}m/Z_{\rm P}$, because also over our range of considered couplings the entering renormalization constant barely varies.

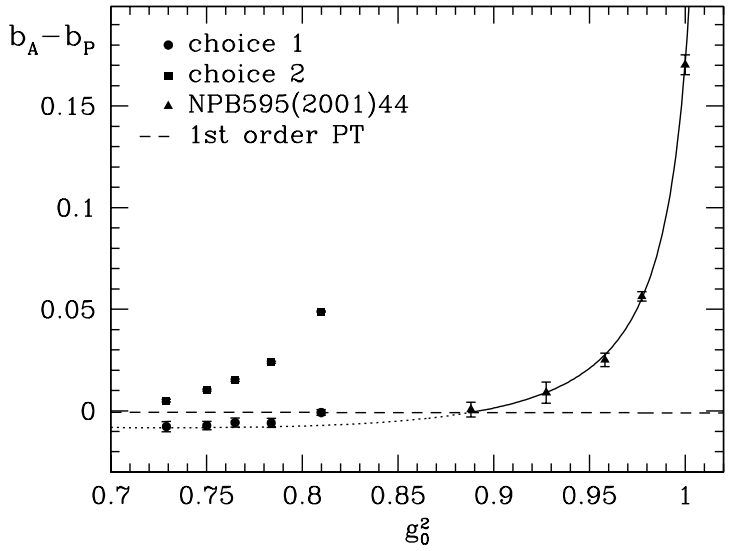

Figure 2: Non-perturbative results for $b_{\rm A} - b_{\rm P}$ in the considered region of bare couplings for our two choices of quark masses (cf. eq. (3.9)), together with the corresponding results at larger g_0^2 from [30] (triangles) and the prediction from one-loop perturbation theory. The solid line gives the rational fit function that was quoted in [30] to well describe the numerical simulation results obtained there.

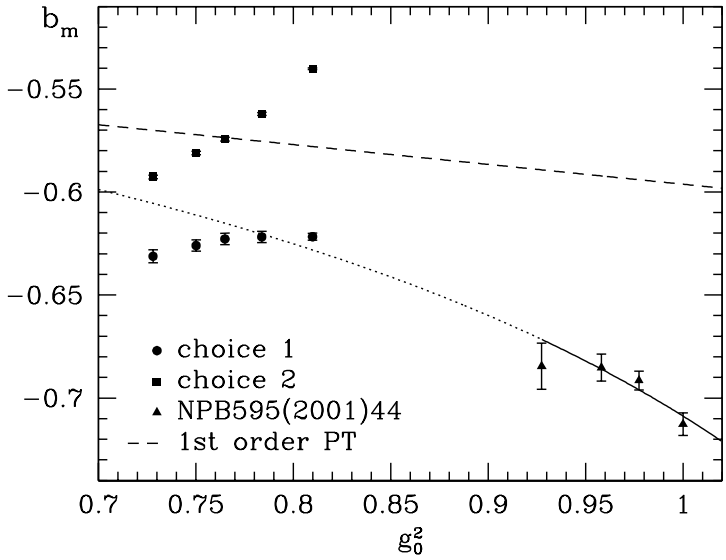

Figure 3: The same as in figure 2 but for the improvement coefficient $b_{\rm m}$. In view of the leading perturbative behaviour that one expects to be approached in the limit $g_0^2 \to 0$, the curvature seen in our results hints at a more complicated structure of (unknown) higher-order terms.

collected in tables 2 and 3.[6] As a consequence of the fact that all renormalized quantities have been fixed in units of L while the ratio $L/L_{\rm max}$ and thereby also the renormalized

[6]We note in passing that memory and processor-topology restrictions of the APEmille parallel computers in use prevented us from directly simulating $L/a = 20$ lattices at an earlier stage of our work. Therefore, we employed $16^3 \times 30$ and $24^3 \times 30$ lattices and a linear interpolation in $1/L$ to arrive at the results for set C in tables 2 and 3.

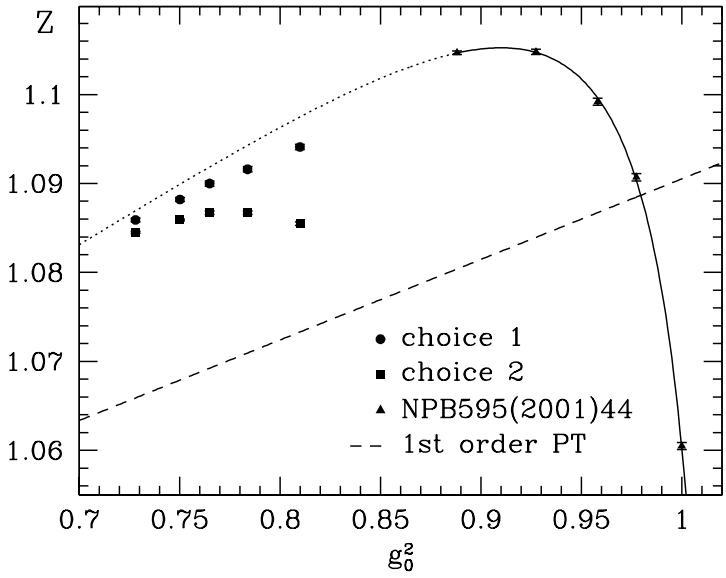

Figure 4: The same as in figure 2 but for the renormalization constant Z.

SF coupling are kept constant, the estimates $R_{\rm X}$ become smooth functions of the bare coupling, $g_0^2 = 6/\beta$. This is well fulfilled in figures 2–4, where our results are shown in conjunction with those at larger couplings of the earlier work [30] together with the one-loop perturbative predictions [37, 30]. One observes that the estimates for $b_{\rm A} - b_{\rm P}$ and Z corresponding to 'choice 1' of quark masses are roughly consistent with the fit functions quoted in ref. [30] for larger couplings, if one assumes them to be even valid far beyond the β-region where the underlying data were actually taken. Nonetheless, this was not obvious from the beginning, since despite the quark mass values being comparable in that case the conditions defining the associated lines of constant physics are different.

For $b_{\rm m}$ the situation is more intricate. Here a naive prolongation of the curve from [30] to weak couplings (dottet line in figure 3) does not give the right g_0^2-behaviour for this region. We infer this from the fact that the difference of the dotted line to our results does not seem to be compatible with being of $\mathrm{O}(a)$. In other words, if the improvement condition of [30] were used also in the region of weaker couplings, the points would look quite differently, and we have to conclude that a simple approach to one-loop perturbation theory is not an adequate representation for the continuation of the triangles in figure 3. This underlines the importance of using particularly adapted improvement conditions, which may be used in the coupling range actually relevant for the desired application. The example of $b_{\rm m}$ thus illustrates that our redetermination of the b-coefficients and the Z-factor indeed eliminates a source of uncontrollable error.

On the other hand, the results from 'choice 2' (i.e. with the quark mass $m_{\rm h}$ being larger) fall significantly apart throughout, because the a-effects are generically larger in that case. But this only reveals an expected, inevitable property of the procedure applied: any other estimate $R_{\rm X}$ (e.g. stemming from a different choice of renormalization condition) may yield a different functional dependence upon g_0^2, but its differences are again smooth functions that must vanish in the continuum limit with a rate proportional to a/L (for

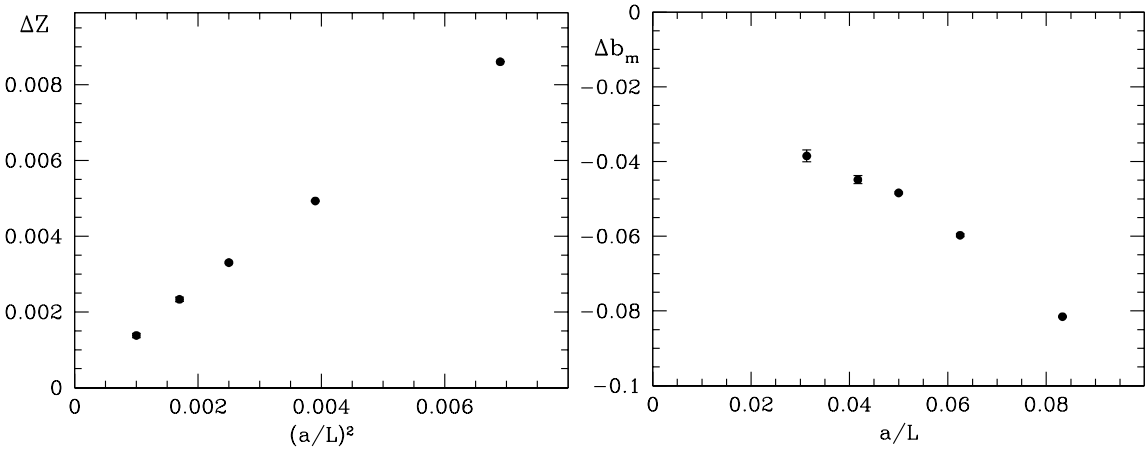

Figure 5: Left: Difference of the results on the renormalization constant Z, obtained from the two heavy quark mass choices, versus $(a/L)^2$. Right: The same for the improvement coefficient $b_{\rm m}$ where, however, the ambiguity inherent in any improvement condition imposed is of $\mathrm{O}(a)$.

improvement coefficients) or even $(a/L)^2$ (for renormalization constants). These intrinsic $\mathrm{O}(a^n)$ ambiguities, $n = 1, 2$, imply that rather than a numerical value at some given β, the essential information lies in the *correct* g_0^2*-dependence* of the results for the estimators $R_{\rm X}$, $\mathrm{X} = \mathrm{AP}, \mathrm{m}, Z$, resulting from working at fixed physics while varying β.

To demonstrate the last statement, we also investigated a few alternative improvement conditions, which are either realized by defining the estimators $R_{\rm X}$ with standard instead of improved derivatives (as in [30]) or directly by the two different quark mass settings that we already have at our disposal through the choices in eq. (3.9). As an example we plot in the left part of figure 5 the difference $\Delta Z(g_0^2) = Z(g_0^2)|_{\,\rm choice\,1} - Z(g_0^2)|_{\,\rm choice\,2}$ versus $(a/L)^2$, which clearly shows a linear approach towards zero. Other cases behave similarly, e.g. the $\mathrm{O}(a)$ ambiguities for $\Delta b_{\rm m}(g_0^2) = b_{\rm m}(g_0^2)|_{\,\rm choice\,1} - b_{\rm m}(g_0^2)|_{\,\rm choice\,2}$ in the right part of figure 5 are found to be very small and rapidly decreasing in magnitude as $a/L \to 0$.

As a further (and less direct) check for the universality of the continuum limit we consider a physical quantity that depends on $b_{\rm m}$ and Z in a more implict way, namely the energy $L_0\Gamma_{\rm PS}(L_0, M, g_0)$ introduced in eq. (2.6) of the previous section. In fixing z while computing $L_0\Gamma_{\rm PS}$ for various lattice resolutions, the just determined results on $b_{\rm m}$ and Z enter via eq. (2.18), and hence it is interesting to confront the lattice spacing dependences of $L_0\Gamma_{\rm PS}|_{\,b_{\rm m},Z:\,\rm choice\,1}$ and $L_0\Gamma_{\rm PS}|_{\,b_{\rm m},Z:\,\rm choice\,2}$ with eachother. We did this exercise for $z = 9$ (where, due to the large quark mass, a-effects are already very pronounced) and anticipate results from the following section in figure 6 to display the two data sets and its continuum extrapolations linear in $(a/L)^2$. From the nice agreement of the continuum limits[7] we infer once more that our results (on $b_{\rm m}$ and Z) correctly model — within each choice of improvement condition separately — the respective g_0^2-dependences, entailing convergence to the continuum limit with leading corrections of $\mathrm{O}(a^2)$.

[7]The fact that in this case the cutoff effects in $L_0\Gamma_{\rm PS}$ are larger with $b_{\rm m}, Z$ from 'choice 1' (where the quark mass fixed is smaller) is not so surprising, since via 'choice 2' as improvement condition (where $z \approx 5$) one is closer to the line in parameter space with $z = 9$ along which $L_0\Gamma_{\rm PS}$ is computed.

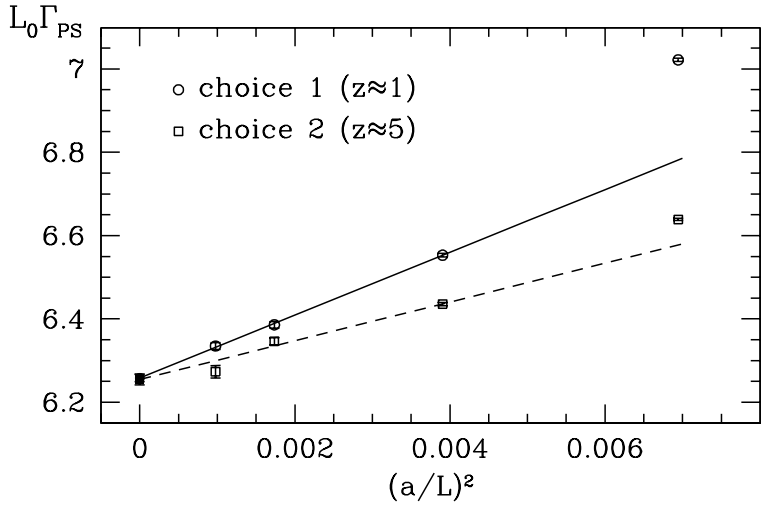

Figure 6: $L_0\Gamma_{\rm PS}(L_0, M, g_0)$, where the results on $b_{\rm m}, Z$ from both renormalization conditions corresponding to eq. (3.9) were used to keep the dimensionless RGI heavy quark mass fixed to $z = L_0 M = 9$ while varying $\beta = 6/g_0^2$ and thus a/L. Assuming quadratic scaling violations and discarding the coarsest lattice in the (unconstrained) extrapolations, the continuum limits coincide. A more thorough discussion of the continuum extrapolations of the observables $\Gamma_{\rm X}$, X = PS, av, will follow in section 3.2.

3.2 Heavy-light meson energies

Supposing the parameters β and $\kappa_{\rm l}$ at each L/a $(= L_0/a)$ to be appropriately fixed to comply with the conditions $\bar{g}^2(L_0/2) = 1.8811 =$ constant and $m_{\rm l} = 0$, eqs. (2.13) and (2.10), we still have to prescribe a sequence of dimensionless quark mass values z in order to be able to map out the heavy quark mass dependence of the observables $\Gamma_{\rm X}$, X = PS, av, over a reasonable range that encloses the RGI mass scale of the b-quark itself. To this end we split, according to the discussion around eq. (2.18) in section 2.3, $z = L_0 M$ into the product

$$z = L_0 \times h(L_0) \times Z_{\rm m} \times m_{\rm q,h}(1 + b_{\rm m} a m_{\rm q,h})\,, \qquad Z_{\rm m} = \frac{Z\, Z_{\rm A}}{Z_{\rm P}}\,. \tag{3.10}$$

For $b_{\rm m}(g_0^2)$ and $Z(g_0^2)$ we decided to use the results of table 2 from 'choice 1' of quark mass settings, mainly because especially for $b_{\rm m}$ the g_0^2-dependence is weaker and with the corresponding value of the (heavy) quark mass fixed in their determination we more resemble the condition that in ref. [30] was found favourable also from the perturbative point of view. $Z_{\rm A}(g_0^2)$ is known in O(a) improved quenched QCD via the formula [38]

$$Z_{\rm A} = \frac{1 - 0.8496\, g_0^2 + 0.0610\, g_0^4}{1 - 0.7332\, g_0^2}\,, \qquad g_0^2 \leq 1\,, \tag{3.11}$$

while the required values of $Z_{\rm P}(g_0, L_0/a)$ have already been quoted in the last column of table 1 and, as was said after eq. (2.20), the universal factor

$$h(L_0) = 1.531(14)\,, \qquad L_0 = \frac{L_{\rm max}}{2}\,, \tag{3.12}$$

could be extracted from the data published in ref. [27]. Given some value of z one is aiming at, the relation between the subtracted bare (heavy) quark mass and the hopping parameter,

$$am_{\rm q,h} = \frac{1}{2}\left(\frac{1}{\kappa_{\rm h}} - \frac{1}{\kappa_{\rm c}}\right), \tag{3.13}$$

then allows to straightforwardly solve eq. (3.10) for $\kappa_{\rm h}$ and, together with $\kappa_{\rm l}$ as quoted in table 1 of section 2.3, yields the pairs $(\kappa_{\rm l}, \kappa_{\rm h})$ of hopping parameters, for which the numerical simulations with the computation of the heavy-light correlation functions have been performed.[8]

Of course, the uncertainties to be associated with the various pieces entering eq. (3.10) translate into an error on z, which has to be taken into account also for any quantity regarded as a *function of* z. More precisely, the resulting error on z consists of a g_0-dependent part and a universal, g_0-independent one: while the former comes from the uncertainties of $b_{\rm m}$, Z and $Z_{\rm P}$ quoted in the tables plus an error (of 0.8% at $\beta \approx 7.4$ down to 0.4% for $\beta \geq 7.8$ [38]) on $Z_{\rm A}$, the latter stems from the overall uncertainty of 0.9% on $h(L_0)$ in the continuum limit and hence has only to be added in quadrature *after* a continuum extrapolation of the respective z-dependent quantity under study.[9]

The final parameter sets employed in the Monte Carlos simulations consist of the triples $(L/a, \beta, \kappa_{\rm l})$ in table 1 and the $\kappa_{\rm h}$-values we arrived at as described before; they are listed together with the corresponding values of the dimensionless RGI heavy quark mass, z, and the g_0-dependent error part of the latter in table 4 at the end of this section. For the technical details of the runs to produce the numerical data on the SF heavy-light meson correlators, from which the logarithmic derivatives (2.6) and (2.7) are evaluated, we refer to the simulations reported in ref. [31] (and its appendix A.2. in particular) to non-perturbatively renormalize the static-light axial current. The number of measurements in the statistical samples is comparable to what was accumulated to get the results in tables 2 and 3.

Table 4 also contains the numerical results for $L_0\Gamma_{\rm PS}$ and $L_0\Gamma_{\rm av}$ at all values of z that were considered. To ease notation, we set

$$\Omega_{\rm X}\left(u, z, \frac{a}{L}\right) \equiv L_0\Gamma_{\rm X}(L_0, M, g_0)\Big|_{\bar{g}^2(L_0/2)=u\,,\, L_0M=z}, \qquad {\rm X} = {\rm PS}, {\rm av}\,, \tag{3.14}$$

and denote its continuum limits as

$$\omega_{\rm X}(u, z) \equiv \lim_{a/L\to 0} \Omega_{\rm X}\left(u, z, \frac{a}{L}\right), \qquad {\rm X} = {\rm PS}, {\rm av}\,. \tag{3.15}$$

In table 4 both the statistical errors of $\Omega_{\rm X}$ (in square brackets) as well as the combined statistical and g_0-dependent, z-induced uncertainties (in parentheses) are given, the latter

[8] Due to the fact that the non-perturbative values for $b_{\rm m}$ in the relevant β-range lie around -0.6, the relation $z = L_0 h(L_0) Z_{\rm m} m_{\rm q,h}(1 + b_{\rm m} a m_{\rm q,h})$ can not be inverted in favour of $am_{\rm q,h}$ (and thereby $\kappa_{\rm h}$) for arbitrarily high z-values. In case of our largest z (= 13.5), for instance, this already restricts the possible inverse lattice spacings in table 4 to $L/a = 16 - 32$.

[9] Note that also this error can in principle be reduced further by increasing the precision of the continuum step scaling functions of ref. [27].

being obtained by including the propagation of the g_0-dependent part of the error on z. As an outcome of this error analysis we find that summing up the various errors on the factors in eq. (3.10) quadratically (since they are uncorrelated) and multiplying with the numerically estimated slopes $|[\partial\Omega_{\rm X}/\partial z]\,(g_0)|$ yields a contribution of about 0.3% or less to the final uncertainties on $\Omega_{\rm X}$.

As we work in the O(a) improved theory, the numbers for $\Omega_{\rm PS}$ and $\Omega_{\rm av}$ can now be extrapolated linearly in a^2 to the continuum limit.[10] However, based on the experience made in perturbation theory (see section 5 of ref. [39]) that the discretization errors primarily depend on the mass of the heavy quark, $aM = z \times a/L$, we expect some deviation from a leading linear behaviour in a^2 for the coarsest lattices as z grows. Since our non-perturbative data qualitatively confirm this picture, we again adopt perturbation theory as a guide to get a rough estimate for the quark mass value where this deviation sets in. In [39] the heavy quark mass dependence of the discretization errors in a typical matrix element of the heavy-light axial current, similarly constructed from SF correlators as our energy observables, indicates a breakdown of O(a) improvement beyond $(a\overline{m}_{\rm h}^{\overline{\rm MS}})^2 \approx 0.2$, which with $\overline{m}_{\rm h}^{\overline{\rm MS}} \approx 0.7M$ [40] approximately corresponds to $aM \approx 0.64$. From this we deduce the following *two-step criterium* to carefully perform the continuum extrapolations of $\Omega_{\rm X}$, X = PS, av, for the various values of z:

1. In view of the z-dependence of the size of the lattice artifacts, only allow for fits which start at and beyond the minimal L/a such that $aM < 0.6$ approximately holds.

2. Among these, the n-point fit must agree with the $(n+1)$-point one within errors but the former, which omits the coarsest of the lattices meeting 1. and thereby has the larger error, gives the final estimate of the continuum limit.

The resulting continuum extrapolations for the subset $z \in \{5.15, 6.0, 9.0, 13.5\}$ of available z-values are displayed in figure 7. As it turns out when applying this fitting procedure, the continuum limits then have to be extracted from fits discarding the $L/a = 12$ lattice in case of $z \in \{3.0, 3.8, 5.15, 6.0, 6.6\}$, the $L/a = 12, 16$ lattices in case of $z = 9.0$ and even the $L/a = 12, 16, 20$ lattices for the heaviest mass, $z = 13.5$. The numbers of table 4 in Italics are the continuum limit results for all z, based on these fits.

To further corroborate our results from this prescription, we in addition considered an alternative fit ansatz that also accounts for a term cubic in a. Again, it is to some extent guided by the aforementioned finding of ref. [39] that in perturbation theory the cutoff effects in the regime of large quark masses are approximately a function of aM and not of aM and a/L separately. In the O(a) improved case at hand (and here for the example of $\Omega_{\rm av}$, omitting the argument u for a moment), such an ansatz may therefore be written as:

$$\Omega_{\rm av}\left(z, \frac{a}{L}\right) = \omega_{\rm av}(z)\left[1 + \rho_2\, z^3 \left(\frac{a}{L}\right)^3\right] + \rho_1(z)\left(\frac{a}{L}\right)^2, \tag{3.16}$$

where by a z-dependent parameter ρ_1 we after all admit a still more general form for the a^2-term. Performing a simultaneous fit of all available $\Omega_{\rm av}$ data (no cut on aM), we then

[10] As in [27, 31], the influence of the only perturbatively known SF-specific boundary improvement coefficients $c_{\rm t}$ and $\widetilde{c}_{\rm t}$ is negligible at the level of our precision.

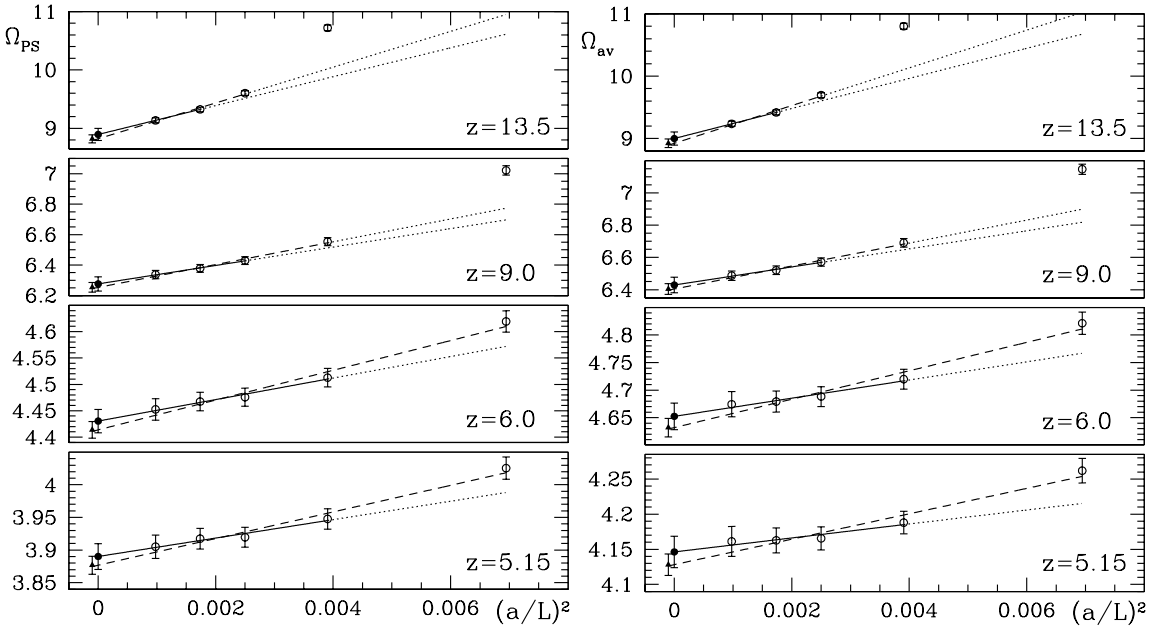

Figure 7: Continuum extrapolations of $\Omega_{\rm PS}(1.8811, z, a/L)$ (left) and $\Omega_{\rm av}(1.8811, z, a/L)$ (right) for representative values of z. As explained in the text, the number of coarsest lattices to be skipped in the fits depends on z. The final continuum limits are taken from the solid fit functions, which are compatible with the dashed extrapolations omitting one point less.

arrive at continuum limits in complete accordance with the former, having comparable or even smaller errors: $\omega_{\rm av}(z) \in \{2.86(1), 3.34(1), 4.15(3), 4.65(2), 5.00(2), 6.39(3), 8.99(6)\}$ for $z = 3.0, \ldots, 13.5$. But keeping in mind that for $aM \approx 0.6 - 0.8$ the perturbative a-expansion entirely breaks down [39], we take the continuum limits of table 4 from the linear extrapolations in $(a/L)^2$ imposing a cut on aM as a safeguard against any uncontrollable higher-order behaviour as our final results, which within their (larger) errors are moreover also consistent with the values at smallest lattice resolution. All told, we thus are confident that possible systematic uncertainties in the fitting procedure are already well covered by these estimates.

For future reference (i.e. in particular for the non-perturbative determination of the b-quark's mass in ref. [9]) we introduce for the dimensionless, spin-averaged heavy-light meson energy in small volume the further abbreviation

$$\Omega\left(u, z, \frac{a}{L}\right) \equiv \Omega_{\rm av}\left(u, z, \frac{a}{L}\right), \qquad \omega(u, z) \equiv \omega_{\rm av}(u, z)\,. \tag{3.17}$$

To parametrize the z-dependence of our continuum values $\omega(1.8811, z)$ by a smooth fit function, we make the ansatz $a_0 z + a_1 + a_2/z$, which is justified by the theoretical expectation that heavy-light meson correlation functions of the type studied here decay with a leading term proportional to the heavy quark mass, up to some low-energy scale of $\mathrm{O}(\Lambda_{\rm QCD})$ and $1/m$-corrections. Since the simulation data for the various z at given β were produced on the same gauge field backgrounds, possible correlations in z had to be taken into account in this fit. Hence weperformed it on basis of the jackknife samples that were built from the

z	set	$\kappa_{\rm h}$	$z(g_0)$	$\Omega_{\rm PS}$	$\Omega_{\rm av}$
3.0	A	0.129571	3.000(12)	2.534(11)[5]	2.916(11)[6]
	B	0.130445	3.000(13)	2.485(10)[4]	2.869(11)[6]
	C	0.130876	3.000(13)	2.465(10)[5]	2.856(12)[8]
	D	0.131115	3.000(13)	2.471(11)[7]	2.863(14)[12]
	E	0.131349	3.000(13)	2.458(13)[10]	2.858(18)[16]
	CL			*2.451(13)*	*2.852(18)*
3.8	A	0.128310	3.800(16)	3.094(13)[5]	3.408(14)[6]
	B	0.129552	3.800(16)	3.039(12)[4]	3.356(13)[6]
	C	0.130185	3.800(16)	3.019(12)[5]	3.341(13)[8]
	D	0.130553	3.800(16)	3.022(12)[7]	3.345(15)[11]
	E	0.130940	3.800(17)	3.011(15)[10]	3.342(19)[16]
	CL			*3.002(16)*	*3.334(19)*
5.15	A	0.126055	5.150(21)	4.025(17)[5]	4.262(17)[6]
	B	0.127991	5.150(22)	3.948(16)[5]	4.188(16)[6]
	C	0.128989	5.150(22)	3.920(15)[5]	4.166(16)[8]
	D	0.129586	5.150(22)	3.917(16)[7]	4.163(18)[11]
	E	0.130242	5.150(23)	3.905(18)[11]	4.161(21)[16]
	CL			*3.890(20)*	*4.146(22)*
6.0	A	0.124528	6.000(25)	4.619(20)[5]	4.821(20)[6]
	B	0.126967	6.000(25)	4.513(18)[5]	4.720(18)[6]
	C	0.128214	6.000(25)	4.476(17)[5]	4.688(18)[8]
	D	0.128964	6.000(25)	4.467(18)[8]	4.679(19)[11]
	E	0.129796	6.000(27)	4.453(20)[11]	4.674(23)[15]
	CL			*4.430(22)*	*4.652(24)*
6.6	A	0.123383	6.600(27)	5.049(22)[5]	5.232(22)[6]
	B	0.126222	6.600(28)	4.912(20)[5]	5.100(20)[6]
	C	0.127656	6.600(28)	4.866(19)[5]	5.059(20)[8]
	D	0.128518	6.600(28)	4.852(19)[8]	5.045(21)[10]
	E	0.129477	6.600(30)	4.835(22)[11]	5.037(24)[15]
	CL			*4.806(24)*	*5.009(26)*
9.0	A	0.117762	9.000(39)	7.022(31)[5]	7.146(31)[5]
	B	0.122987	9.000(39)	6.554(27)[5]	6.690(27)[6]
	C	0.125309	9.000(38)	6.429(25)[6]	6.572(26)[7]
	D	0.126670	9.000(38)	6.378(26)[8]	6.521(26)[10]
	E	0.128175	9.000(40)	6.337(28)[12]	6.487(29)[15]
	CL			*6.277(47)*	*6.429(48)*
13.5	B	0.113764	13.500(69)	10.721(47)[5]	10.801(47)[5]
	C	0.120094	13.500(60)	9.603(40)[6]	9.695(40)[7]
	D	0.122808	13.500(58)	9.324(38)[8]	9.418(38)[9]
	E	0.125575	13.500(61)	9.136(40)[12]	9.235(41)[14]
	CL			*8.89(10)*	*9.00(11)*

Table 4: Heavy quark masses $z = L_0 M$ with g_0-dependent error and associated results for $\Omega_{\rm X}(u, z, a/L)$, X = PS, av, $u = 1.8811$, with the total g_0-dependent part of the error in parentheses and the only statistical one of $\Omega_{\rm X}$ in square brackets. Continuum limits (see text) are displayed in Italics.

JHEP02(2004)064

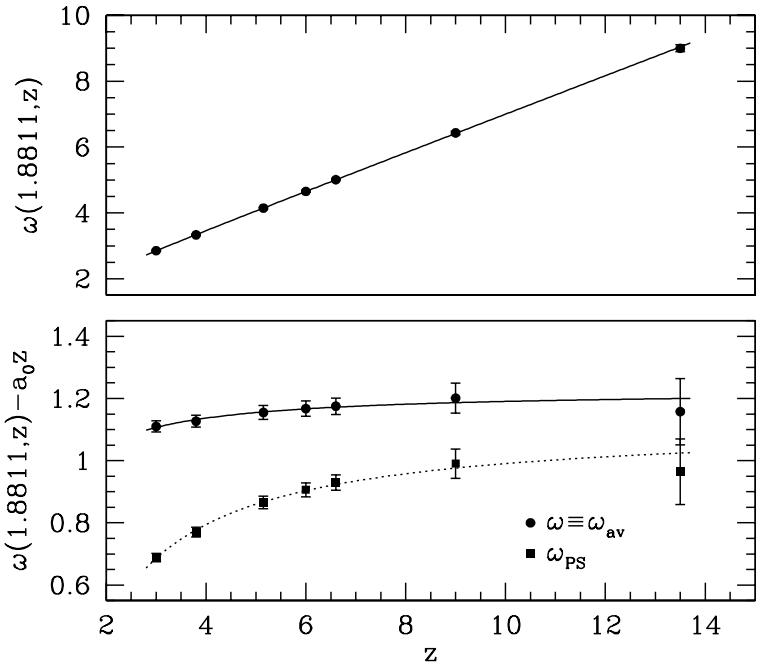

Figure 8: Continuum limit values $\omega(1.8811, z)$ of the spin-averaged energies $\Omega(1.8811, z, a/L)$, at fixed coupling $\bar{g}^2(L_0/2) = 1.8811$, as a function of $z = L_0 M$ and its fit function (top). The bottom graph has the linear term, $a_0 z$, subtracted and also includes the pseudoscalar case, $\omega_{\rm PS}(1.8811, z)$, for comparison.

raw data and passed through the whole analysis, and we end up with the parametrization

$$\omega(1.8811, z) = a_0 z + a_1 + a_2 \frac{1}{z}\,, \qquad a_0 = 0.581\,, \qquad a_1 = 1.226\,, \qquad a_2 = -0.358\,, \quad (3.18)$$

the graph of which is shown in the upper diagram of figure 8 to well represent our data. In the interval $5.2 \le z \le 6.6$, which for instance is the relevant z-range to calculate the RGI b-quark mass by means of the non-perturbative matching to HQET in ref. [9], this parametrization describes $\omega(1.8811, z)$ with a precision of about 0.5%. As already mentioned, a further uncertainty of 0.9% that enters only indirectly through the argument z of the function ω (and thus remains to be added in quadrature at the end) originates from the universal part $h(L_0)$ in eq. (3.10) of the renormalization factor relating the bare to the RGI quark mass.

For later use of the result (3.18) it is also necessary to have a numerical estimate for the derivative $\omega'(1.8811, z)$ w.r.t. u, in order to compensate for a possible slight mismatch in the imposed condition of fixed renormalized coupling. From an additional simulation with $L/a = 24$ and a nearby coupling of $\bar{g}^2(L_0/2) = 1.95$ (and assuming the a-effect of the derivative to be negligible) we found this derivative to be constant in the central region

$$6.0 \le z \le 6.6: \qquad \frac{\partial}{\partial u}\,\omega(u, z)\Big|_{u=1.8811} = 0.70(1)\,, \qquad (3.19)$$

which is the required one in the context of the immediate application discussed in [9].

Finally, we give as well the fit result for $\omega_{\rm PS}(1.8811, z)$ for comparison, i.e. if in the definition (3.14) the effective energy in the pseudoscalar channel alone, $\Gamma_{\rm PS}(L_0, M, g_0)$, would be used instead of the spin-averaged combination. By an analogous analysis with the same ansatz for the fit function as in eq. (3.18) we obtain the coefficients

$$a_0 = 0.587\,, \qquad a_1 = 1.121\,, \qquad a_2 = -1.306 \qquad (\text{for } \Gamma_{\rm X} = \Gamma_{\rm PS})\,. \tag{3.20}$$

The fact that the absolute value of a_2 is evidently larger than in the spin-averaged case is illustrated by the shape of the subtracted fits in the bottom diagram of figure 8 and confirms our earlier claim that with $\Gamma_{\rm X} = \Gamma_{\rm av}$ the matching condition (2.11) becomes *independent of the coefficient of the chromomagnetic field strength term in the HQET lagrangian also at first order in* $1/m$. Therefore, the use of $\Omega \equiv \Omega_{\rm av} \equiv L_0\Gamma_{\rm av}$ (and eq. (3.18) for its heavy quark mass dependence in the continuum limit) is preferable for later applications to HQET, since the $1/m$-errors arising at leading order will generically be smaller then.

4. Conclusions

In this work we have computed the non-perturbative heavy quark mass dependence of effective energies derived from heavy-light meson correlation functions by means of numerical simulations. A particular aspect of this computation is the *use of a physically small volume* (of a linear extent of O(0.2 fm)): it is a prerequisite to treat the heavy quark flavour in lattice regularization as a relativistic particle and thus may be looked at as a 'device' that serves to non-perturbatively renormalize HQET with the method of matching the effective theory to small-volume QCD, proposed and applied in ref. [9].

Among the several improvement coefficients and renormalization constants that are needed to accurately keep fixed the renormalized (heavy) quark mass while the observables of interest approach their continuum limits, we determined those relating the renormalized to the subtracted bare quark mass in a range of weaker couplings relevant here ($7.4 \lesssim \beta = 6/g_0^2 \lesssim 8.2$) with high precision. Even in the region of the b-quark mass and slightly beyond we still find our results on the meson energies under study to be rather mildly cutoff dependent so that the continuum extrapolations can be well controlled.

The quenched numerical results obtained in section 3.2 directly pass into the — for the first time entirely non-perturbative — calculation of the b-quark mass in the static approximation of [9, 41]. Moreover, our quantitative investigation of the quark mass dependence in relativistic heavy-light systems in finite volume can easily be extended to other heavy-light bilinears and matrix elements, which then opens the possibility to perform genuinely non-perturbative tests of HQET and to estimate the size of the $1/m$-corrections to the static theory. We will focus on these issues in a separate publication [12].

Finally, considering the small-volume investigation presented here in the light of the more general framework [9] of a non-perturbative matching between HQET and QCD, it is an obvious practical advantage that they can be transfered to also include dynamical quarks in the (hopefully near) future without requiring exceedingly large computing resources.

JHEP02(2004)064

Acknowledgments

This work is part of the ALPHA Collaboration research programme. The largest part of the numerical simulations has been performed on the APEmille computers at DESY Zeuthen, and we thank DESY for allocating computer time to this project as well as the staff of the computer centre at Zeuthen for their support. In addition we ran on the PC cluster of the University of Münster a C-code based on the MILC Collaboration's public lattice gauge theory code [42], which in its version incorporating Schrödinger functional correlation functions was kindly provided to us by A. Jüttner. We are also grateful to R. Sommer for useful discussions and a critical reading of the manuscript. This work was supported in part by the EU IHP Network on *Hadron Phenomenology from Lattice QCD* under grant HPRN-CT-2000-00145.

References

[1] BaBar collaboration, J.J. Back, *B decays at* BaBar, *Nucl. Phys.* **121** *(Proc. Suppl.)* (2003) 239 [hep-ex/0308069].

[2] Belle collaboration, M. Yamauchi, *New results from Belle*, *Nucl. Phys.* **117** *(Proc. Suppl.)* (2003) 83.

[3] HERA-B collaboration, A. Zoccoli, *First results from the HERA-B experiment*, *Nucl. Phys.* **A 715** (2003) 280.

[4] N. Yamada, *Heavy quark physics and lattice QCD*, *Nucl. Phys.* **119** *(Proc. Suppl.)* (2003) 93 [hep-lat/0210035].

[5] E. Eichten, *Heavy quarks on the lattice*, *Nucl. Phys.* **4** *(Proc. Suppl.)* (1988) 170.

[6] E. Eichten and B. Hill, *An effective field theory for the calculation of matrix elements involving heavy quarks*, *Phys. Lett.* **B 234** (1990) 511.

[7] L. Maiani, G. Martinelli and C.T. Sachrajda, *Nonperturbative subtractions in the heavy quark effective field theory*, *Nucl. Phys.* **B 368** (1992) 281.

[8] ALPHA collaboration, J. Heitger and R. Sommer, *A strategy to compute the B quark mass with non-perturbative accuracy*, *Nucl. Phys.* **106** *(Proc. Suppl.)* (2002) 358 [hep-lat/0110016].

[9] ALPHA collaboration, J. Heitger and R. Sommer, *Non-perturbative heavy quark effective theory*, *J. High Energy Phys.* **02** (2004) 022 [hep-lat/0310035].

[10] G.M. de Divitiis, M. Guagnelli, R. Petronzio, N. Tantalo and F. Palombi, *Heavy quark masses in the continuum limit of quenched lattice QCD*, *Nucl. Phys.* **B 675** (2003) 309 [hep-lat/0305018].

[11] G.M. de Divitiis, M. Guagnelli, F. Palombi, R. Petronzio and N. Tantalo, *Heavy-light decay constants in the continuum limit of quenched lattice QCD*, *Nucl. Phys.* **B 672** (2003) 372 [hep-lat/0307005].

[12] J. Heitger, A. Jüttner, R. Sommer and J. Wennekers, in preparation.

[13] ALPHA collaboration, A. Bode et al., *First results on the running coupling in QCD with two massless flavors*, *Phys. Lett.* **B 515** (2001) 49 [hep-lat/0105003].

[14] ALPHA collaboration, M. Della Morte et al., *Simulating the Schrödinger functional with two pseudo-fermions*, hep-lat/0307008.

[15] G. Martinelli and C.T. Sachrajda, *Computation of the b-quark mass with perturbative matching at the next-to-next-to-leading order*, *Nucl. Phys.* **B 559** (1999) 429 [hep-lat/9812001].

[16] F. Di Renzo and L. Scorzato, *The residual mass in lattice heavy quark effective theory to α^3 order*, *J. High Energy Phys.* **02** (2001) 020 [hep-lat/0012011].

[17] H.D. Trottier, N.H. Shakespeare, G.P. Lepage and P.B. Mackenzie, *Perturbative expansions from Monte Carlo simulations at weak coupling: Wilson loops and the static-quark self-energy*, *Phys. Rev.* **D 65** (2002) 094502 [hep-lat/0111028].

[18] S.M. Ryan, *Heavy quark physics from lattice QCD*, *Nucl. Phys.* **106** *(Proc. Suppl.)* (2002) 86 [hep-lat/0111010].

[19] M. Lüscher, P. Weisz and U. Wolff, *A numerical method to compute the running coupling in asymptotically free theories*, *Nucl. Phys.* **B 359** (1991) 221.

[20] M. Lüscher, R. Narayanan, P. Weisz and U. Wolff, *The Schrödinger functional: a renormalizable probe for nonabelian gauge theories*, *Nucl. Phys.* **B 384** (1992) 168 [hep-lat/9207009].

[21] S. Sint, *On the Schrödinger functional in QCD*, *Nucl. Phys.* **B 421** (1994) 135 [hep-lat/9312079].

[22] M. Lüscher, S. Sint, R. Sommer, P. Weisz and U. Wolff, *Non-perturbative $O(a)$ improvement of lattice QCD*, *Nucl. Phys.* **B 491** (1997) 323 [hep-lat/9609035].

[23] M. Guagnelli and R. Sommer, *Non-perturbative $O(a)$ improvement of the vector current*, *Nucl. Phys.* **63** *(Proc. Suppl.)* (1998) 886 [hep-lat/9709088].

[24] M. Lüscher, S. Sint, R. Sommer and P. Weisz, *Chiral symmetry and $O(a)$ improvement in lattice QCD*, *Nucl. Phys.* **B 478** (1996) 365 [hep-lat/9605038].

[25] ALPHA collaboration, J. Heitger, *Scaling investigation of renormalized correlation functions in $O(a)$ improved quenched lattice QCD*, *Nucl. Phys.* **B 557** (1999) 309 [hep-lat/9903016].

[26] M. Lüscher, R. Sommer, P. Weisz and U. Wolff, *A precise determination of the running coupling in the* SU(3) *Yang-Mills theory*, *Nucl. Phys.* **B 413** (1994) 481 [hep-lat/9309005].

[27] ALPHA collaboration, S. Capitani, M. Lüscher, R. Sommer and H. Wittig, *Non-perturbative quark mass renormalization in quenched lattice QCD*, *Nucl. Phys.* **B 544** (1999) 669 [hep-lat/9810063].

[28] R. Sommer, *A new way to set the energy scale in lattice gauge theories and its applications to the static force and α_s in* SU(2) *Yang-Mills theory*, *Nucl. Phys.* **B 411** (1994) 839 [hep-lat/9310022].

[29] ALPHA collaboration, M. Guagnelli, R. Sommer and H. Wittig, *Precision computation of a low-energy reference scale in quenched lattice QCD*, *Nucl. Phys.* **B 535** (1998) 389 [hep-lat/9806005].

[30] ALPHA collaboration, M. Guagnelli et al., *Non-perturbative results for the coefficients $b_{\rm m}$ and $b_{\rm A} - b_{\rm P}$ in $O(a)$ improved lattice QCD*, *Nucl. Phys.* **B 595** (2001) 44 [hep-lat/0009021].

JHEP02(2004)064

[31] ALPHA collaboration, J. Heitger, M. Kurth and R. Sommer, *Non-perturbative renormalization of the static axial current in quenched QCD*, *Nucl. Phys.* **B 669** (2003) 173 [hep-lat/0302019].

[32] ALPHA collaboration, A. Bode, P. Weisz and U. Wolff, *Two loop computation of the Schrödinger functional in lattice QCD*, *Nucl. Phys.* **B 576** (2000) 517 [hep-lat/9911018], errata *ibid.* **B600** (2001) 453, *ibid.* **B608** (2001) 481.

[33] G.M. de Divitiis and R. Petronzio, *Non-perturbative renormalization constants on the lattice from flavour non-singlet Ward identities*, *Phys. Lett.* **B 419** (1998) 311 [hep-lat/9710071].

[34] T. Bhattacharya, R. Gupta, W.-J. Lee and S.R. Sharpe, *$O(a)$ improved renormalization constants*, *Phys. Rev.* **D 63** (2001) 074505 [hep-lat/0009038].

[35] S. Necco and R. Sommer, *The $N_f = 0$ heavy quark potential from short to intermediate distances*, *Nucl. Phys.* **B 622** (2002) 328 [hep-lat/0108008].

[36] M. Guagnelli, R. Petronzio and N. Tantalo, *The lattice scale at large β in quenched QCD*, *Phys. Lett.* **B 548** (2002) 58 [hep-lat/0209112].

[37] S. Sint and P. Weisz, *Further results on $O(a)$ improved lattice QCD to one-loop order of perturbation theory*, *Nucl. Phys.* **B 502** (1997) 251 [hep-lat/9704001].

[38] M. Lüscher, S. Sint, R. Sommer and H. Wittig, *Non-perturbative determination of the axial current normalization constant in $O(a)$ improved lattice QCD*, *Nucl. Phys.* **B 491** (1997) 344 [hep-lat/9611015].

[39] ALPHA collaboration, M. Kurth and R. Sommer, *Heavy quark effective theory at one-loop order: an explicit example*, *Nucl. Phys.* **B 623** (2002) 271 [hep-lat/0108018].

[40] ALPHA collaboration, J. Garden, J. Heitger, R. Sommer and H. Wittig, *Precision computation of the strange quark's mass in quenched QCD*, *Nucl. Phys.* **B 571** (2000) 237 [hep-lat/9906013].

[41] ALPHA, in preparation.

[42] http://www.physics.indiana.edu/~sg/milc.html.

JHEP02(2004)064

L

Non-perturbative tests of heavy quark effective theory

J. High Energy Phys. 0411 (2004) 048

Published by Institute of Physics Publishing for SISSA/ISAS

Received: *July 23, 2004*
Revised: *October 15, 2004*
Accepted: *November 17, 2004*

Non-perturbative tests of heavy quark effective theory

ALPHA Collaboration

Jochen Heitger

Westfälische Wilhelms-Universität Münster, Institut für Theoretische Physik
Wilhelm-Klemm-Strasse 9, D-48149 Münster, Germany
E-mail: heitger@uni-muenster.de

Andreas Jüttner

Humboldt Universität Berlin, Institut für Physik
Newtonstrasse 15, D-12489 Berlin, Germany
E-mail: juettner@phys.soton.ac.uk

Rainer Sommer*

CERN, Theory Division, CH-1211 Geneva 23, Switzerland
E-mail: rainer.sommer@desy.de

Jan Wennekers

Deutsches Elektronen-Synchrotron DESY, Theory Group
Notkestrasse 85, D-22603 Hamburg, Germany
E-mail: jan.wennekers@desy.de

Abstract: We consider QCD with one massless quark and one heavy quark in a finite volume of linear extent $L_0 \approx 0.2$ fm. In this situation, HQET represents an expansion in terms of $1/z = 1/(mL_0)$, which we test by a non-perturbative computation of quenched current matrix elements and energies, taking the continuum limit of lattice results. These are seen to approach the corresponding renormalization group invariant matrix elements of the static effective theory as the quark mass becomes large. We are able to obtain estimates of the size of the $1/m$-corrections to the static theory, which are also of practical relevance in our recent strategy to implement HQET non-perturbatively by matching to QCD in a finite volume.

Keywords: B-Physics, Heavy Quarks Physics, Lattice QCD, Phenomenological Models.

*On leave from: DESY Zeuthen, Platanenallee 6, D-15738 Zeuthen, Germany

JHEP11(2004)048

Contents

1. Introduction

It is expected that the dynamics of QCD simplifies in the limit of large masses of the charm and beauty quarks. For external states with a single heavy quark, transition amplitudes are expected to be described by an effective quantum field theory, the Heavy Quark Effective Theory (HQET) [1, 2, 3]. For details of the proper kinematics where this theory applies, and also for a guide to the original literature we refer the reader to reviews [4, 5]. To prepare for the following presentation, we only note that HQET applies to matrix elements between hadronic states, where these hadrons are both at rest and do not represent high excitations. HQET then provides an expansion of the QCD amplitudes in terms of $1/m$, the inverse of the heavy quark mass(es). The HQET lagrangian of a heavy quark is given by[1]

$$\mathcal{L}_{\mathrm{HQET}}(x) = \overline{\psi}_{\mathrm{h}}(x)\left[D_0 + m - \frac{\omega_{\mathrm{kin}}}{2m}\,\mathbf{D}^2 - \frac{\omega_{\mathrm{spin}}}{2m}\,\sigma\cdot\mathbf{B}\right]\psi_{\mathrm{h}}(x) + \cdots\,, \tag{1.1}$$

where the ellipsis stands for higher-dimensional operators with coefficients of $\mathrm{O}(1/m^2)$. Following power counting arguments, this effective theory is renormalizable at any finite order in $1/m$ [6, 7]. A significant number of perturbative matching computations have been carried out (see [8, 9] and references therein), in order to express the parameters of HQET

[1] We write here the velocity-zero part, since non-vanishing velocities will not be relevant to our discussion.

JHEP11(2004)048

$(m, \omega_{\rm spin}, \ldots)$ in terms of the QCD parameters. The very possibility of performing this matching reflects good evidence that HQET does represent an effective theory for QCD.

Nowadays, HQET is a standard phenomenological tool to describe decays of heavy-light hadrons and their transitions in terms of a set of hadronic matrix elements, which are usually determined from experiments. Its phenomenological success is illustrated, for example, by the determination of the Cabibbo-Kobayashi-Maskawa matrix element $V_{\rm cb}$: its value determined from inclusive $b \to c$ transitions agrees with the one extracted from exclusive ones [10, 11] and HQET enters in both determinations. Similarly, HQET hadronic matrix elements, such as $\lambda_1 \propto \omega_{\rm kin} \langle {\rm B}| - \overline{\psi}_{\rm h} \mathbf{D}^2 \psi_{\rm h} |{\rm B}\rangle$, extracted from different experiments tend to agree [11, 12, 13]. As a small caveat concerning these phenomenological tests, we note that some of them involve both the beauty and the charm quark, and one may suspect that the effective theory is not very accurate for the latter.

Additional, independent tests of HQET are thus of both theoretical and phenomenological interest. In [14] some euclidean correlation functions, which are gauge invariant and infrared-finite, were studied in perturbation theory. There it was verified at one-loop order that their (large-distance) $m \to \infty$ asymptotics is described by the correlation functions of the properly renormalized effective theory. This comparison was performed after separately taking the continuum limit of the lattice regularized effective theory and of QCD.

In general, lattice gauge theory calculations allow a variation of the heavy quark mass and the performance of *non*-perturbative tests. However, if one is interested in the comparison of QCD and HQET in the *continuum limit*, one has to first respect the condition

$$m \ll \frac{1}{a}\,, \tag{1.2}$$

and then to do an extrapolation to zero lattice spacing, $a = 0$. Given the present restrictions in the numerical simulations of lattice field theories, a direct comparison at large mass can only be done in a finite volume of linear size significantly smaller than 1 fm.

Before discussing this further, we note that in the charm quark mass region the continuum limit can also be taken in a large volume [15, 16, 17]. In particular, a recent study concentrated on the decay constant $F_{\rm D_s}$, where many previous estimates found evidence for large $1/m$-corrections. After taking the continuum limit and non-perturbatively renormalizing the lowest-order HQET, ref. [18] finds only a rather small difference between lowest-order HQET and the QCD results. Although this investigation was restricted to the quenched approximation, it provides some further evidence of the usefulness of HQET — maybe even for charm quarks. For related work, see [19]–[31] and references therein.

In this paper we study the large-mass behaviour of correlation functions in a finite volume of size $L \times L^3$, with Dirichlet boundary conditions in time and periodic boundary conditions in space, i.e. we work in the framework of the QCD Schrödinger functional [32, 33]. Keeping all distances in the correlation functions of order L, the energy scale $1/L$ takes over the rôle usually played by small (residual) momenta, and at fixed L, HQET can be considered to be an expansion of QCD in terms of the dimensionless variable

$$\frac{1}{z} \equiv \frac{1}{ML}\,, \tag{1.3}$$

where we take M to be the renormalization group invariant (RGI) mass of the heavy quark (see eq. (3.6)).[2] With the choice $L \approx 0.2$ fm, today's lattice techniques allow us to increase z beyond $z = 10$, while the continuum limit can still be controlled well [34, 35]. One is thus able to verify that the large-z behaviour is described by the effective theory, which is the primary purpose of this paper. Of course, the coefficients a_i in expansions $\Phi = a_0 + a_1/z + a_2/z^2 + \cdots$ are functions of ΛL (with Λ the intrinsic QCD scale) such that $a_i(\Lambda L) \to c_i \times (\Lambda L)^i$ and $a_i(\Lambda L)/z^i \to c_i \times (\Lambda/M)^i$ as $\Lambda L \to \infty$. Since we only work at one value of L, the dependence on ΛL will be suppressed in the rest of this paper.

After a discussion of the QCD observables under investigation (section 2), we give their HQET expansion (section 3) and confront them with Monte Carlo results at finite values of $1/z$ (section 4). In our conclusions we also discuss the usefulness of our results for a non-perturbative matching of HQET to QCD [36].

2. Observables

We introduce our observables starting from correlation functions defined in the continuum Schrödinger functional (SF) [32, 33]. For the reader who is unfamiliar with this setting, we give a representation of these correlation functions in terms of operator matrix elements below.

We take a $T \times L^3$ geometry with $T/L = \mathrm{O}(1)$ fixed. The boundary conditions are periodic in space, where for the fermion fields, and only for those, a phase is introduced:

$$\psi(x + \hat{k}L) = \mathrm{e}^{i\theta}\psi(x)\,, \quad \overline{\psi}(x + \hat{k}L) = \overline{\psi}(x)\mathrm{e}^{-i\theta}\,, \qquad k = 1, 2, 3\,. \tag{2.1}$$

In the numerical investigation of section 4, we will set $T = L$ and $\theta = 0.5$. Dirichlet conditions are imposed at the $x_0 = 0$ and $x_0 = T$ boundaries. Their form as well as the action are by now standard [32, 33, 37] and we do not repeat them here. Multiplicatively renormalizable, gauge-invariant correlation functions can be formed from local composite fields in the interior of the manifold and from boundary quark fields. Boundary fields, located at the $x_0 = 0$ surface are denoted by $\overline{\zeta}, \zeta$ and create fermions and anti-fermions. Their partners at $x_0 = T$ are $\overline{\zeta}', \zeta'$. We shall need flavour labels, "l" denoting a massless flavour, "b" a heavy but finite-mass flavour and "h" the corresponding field in the effective theory. The heavy-light axial vector and vector currents then read

$$A_\mu(x) = \overline{\psi}_{\mathrm{l}}(x)\gamma_\mu\gamma_5\psi_{\mathrm{b}}(x)\,, \qquad V_\mu(x) = \overline{\psi}_{\mathrm{l}}(x)\gamma_\mu\psi_{\mathrm{b}}(x)\,. \tag{2.2}$$

2.1 Correlation functions

In our tests we shall consider the correlation functions

$$f_{\mathrm{A}}(x_0) = -\frac{1}{2}\int \mathrm{d}^3\mathbf{y}\,\mathrm{d}^3\mathbf{z}\,\left\langle A_0(x)\,\overline{\zeta}_{\mathrm{b}}(\mathbf{y})\gamma_5\zeta_{\mathrm{l}}(\mathbf{z})\right\rangle\,, \tag{2.3}$$

$$k_{\mathrm{V}}(x_0) = -\frac{1}{6}\sum_k\int \mathrm{d}^3\mathbf{y}\,\mathrm{d}^3\mathbf{z}\,\left\langle V_k(x)\,\overline{\zeta}_{\mathrm{b}}(\mathbf{y})\gamma_k\zeta_{\mathrm{l}}(\mathbf{z})\right\rangle\,, \tag{2.4}$$

[2] We continue to use m as a generic symbol for the quark mass when its precise definition is irrelevant, sometimes even not distinguishing the renormalized mass from the bare one. However, when precisely defined functions of the quark mass are considered, only the properly defined M is used.

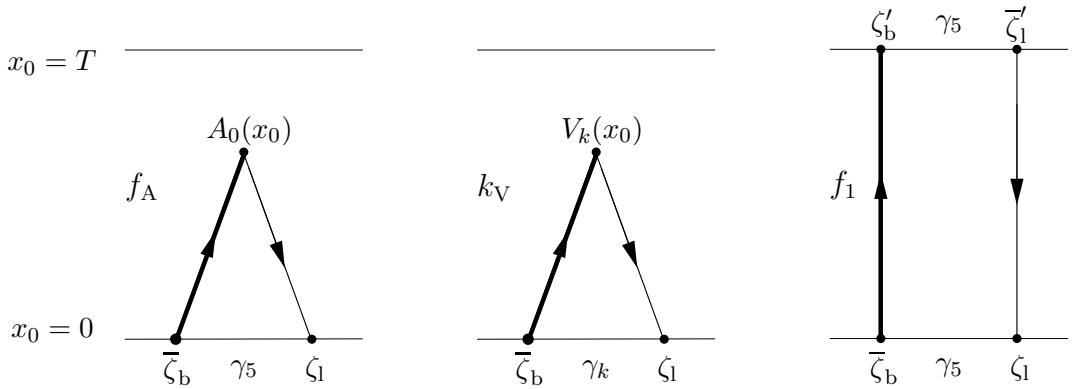

Figure 1: The Schrödinger functional correlation functions $f_{\rm A}$, $k_{\rm V}$ and f_1. For k_1, in the rightmost diagram γ_5 is replaced by γ_k.

as well as the boundary-to-boundary correlations

$$f_1 = -\frac{1}{2L^6}\int \mathrm{d}^3\mathbf{y}\,\mathrm{d}^3\mathbf{z}\,\mathrm{d}^3\mathbf{y}'\,\mathrm{d}^3\mathbf{z}'\,\left\langle\overline{\zeta}'_{\rm l}(\mathbf{y}')\gamma_5\zeta'_{\rm b}(\mathbf{z}')\,\overline{\zeta}_{\rm b}(\mathbf{y})\gamma_5\zeta_{\rm l}(\mathbf{z})\right\rangle, \tag{2.5}$$

$$k_1 = -\frac{1}{6L^6}\sum_k\int \mathrm{d}^3\mathbf{y}\,\mathrm{d}^3\mathbf{z}\,\mathrm{d}^3\mathbf{y}'\,\mathrm{d}^3\mathbf{z}'\,\left\langle\overline{\zeta}'_{\rm l}(\mathbf{y}')\gamma_k\zeta'_{\rm b}(\mathbf{z}')\,\overline{\zeta}_{\rm b}(\mathbf{y})\gamma_k\zeta_{\rm l}(\mathbf{z})\right\rangle. \tag{2.6}$$

They are illustrated in figure 1.

Let us discuss the function $f_{\rm A}(x_0)$ in some detail. It describes the creation of a (finite-volume) $\mathbf{p} = 0$ heavy-light pseudoscalar meson state, $|\varphi_{\rm B}(L)\rangle$, through quark and antiquark boundary fields which are separately projected onto momentum $\mathbf{p} = 0$. "After" propagating for a euclidean time interval x_0, the axial current operator $\mathbb{A}_0$ initiates a transition to a state, $|\Omega'(L)\rangle$, with the quantum numbers of the vacuum. The correlation function $f_{\rm A}(x_0)$, taken in the middle of the manifold, can thus be written in terms of Hilbert space matrix elements,

$$f_{\rm A}\left(\frac{T}{2}\right) = \mathcal{Z}^{-1}\langle\Omega(L)|\,\mathbb{A}_0|B(L)\rangle \equiv \mathcal{Z}^{-1}\langle\Omega(L)|\Omega'(L)\rangle\,, \qquad |B(L)\rangle = \mathrm{e}^{-T\mathbb{H}/2}|\varphi_{\rm B}(L)\rangle\,, \tag{2.7}$$

where $\mathbb{H}$ is the QCD hamiltonian and

$$\mathcal{Z} = \langle\Omega(L)|\Omega(L)\rangle\,, \qquad |\Omega(L)\rangle = \mathrm{e}^{-T\mathbb{H}/2}|\varphi_0(L)\rangle\,. \tag{2.8}$$

Here, $|\varphi_0(L)\rangle$ denotes the Schrödinger functional intrinsic boundary state. It has the quantum numbers of the vacuum. Because the definition of our correlation functions contains integrations over all spatial coordinates, all states appearing in our analysis are eigenstates of spatial momentum with eigenvalue zero. The operator $\mathrm{e}^{-T\mathbb{H}/2}$ suppresses high-energy states. When expanded in terms of eigenstates of the hamiltonian, $|\Omega(L)\rangle$ and $|B(L)\rangle$ are thus dominated by contributions with energies of at most $\Delta E = \mathrm{O}(1/L)$ above the ground state energy in the respective channel (recall that we take $T = \mathrm{O}(L)$). This explains why, at large time separation $x_0 \geq \mathrm{O}(1/m)$, HQET is expected to describe the large-mass behaviour of the correlation function, also in the somewhat unfamiliar framework of the Schrödinger functional.[3]

[3]More generally, HQET will apply to correlation functions at large euclidean separations.

JHEP11(2004)048

Equations similar to the above hold for $k_{\rm V}$; one only needs to replace pseudoscalar states by vector ones. Finally, the boundary-to-boundary correlator may be represented as

$$f_1 = \mathcal{Z}^{-1}\langle B(L)|B(L)\rangle\,. \tag{2.9}$$

Since the boundary quark fields $\zeta, \overline{\zeta}, \ldots$ are multiplicatively renormalizable [38], this holds also for the states $|\varphi_0(L)\rangle$ and $|\varphi_{\rm B}(L)\rangle$.

It now follows that the ratios

$$Y_{\rm PS}(L,M) \equiv \frac{f_{\rm A}(T/2)}{\sqrt{f_1}}\,, \qquad Y_{\rm V}(L,M) \equiv -\frac{k_{\rm V}(T/2)}{\sqrt{k_1}}\,, \qquad R(L,M) \equiv -\frac{f_{\rm A}(T/2)}{k_{\rm V}(T/2)} \tag{2.10}$$

are finite quantities when we adopt the convention that A_μ, V_μ denote the renormalized currents. As is immediately clear from the foregoing discussion,

$$Y_{\rm PS}(L,M) = \frac{\langle\Omega(L)|\,\mathbb{A}_0|B(L)\rangle}{\|\,|\Omega(L)\rangle\,\|\;\|\,|B(L)\rangle\,\|} \tag{2.11}$$

(or $Y_{\rm V}(L,M)$) becomes proportional to the pseudoscalar (or vector) heavy-light decay constant as $L \to \infty$. We shall study the large-M behaviour of these quantities at fixed L in the following sections.

For the same purpose we define effective energies

$$\Gamma_{\rm PS}(L,M) \equiv -\frac{\mathrm{d}}{\mathrm{d}x_0}\ln\left[f_{\rm A}(x_0)\right]\Big|_{x_0=T/2} = -\frac{f'_{\rm A}(T/2)}{f_{\rm A}(T/2)}\,, \tag{2.12}$$

$$\Gamma_{\rm V}(L,M) \equiv -\frac{\mathrm{d}}{\mathrm{d}x_0}\ln\left[k_{\rm V}(x_0)\right]\Big|_{x_0=T/2} = -\frac{k'_{\rm V}(T/2)}{k_{\rm V}(T/2)}\,. \tag{2.13}$$

These may be written in terms of matrix elements of the hamiltonian. E.g., we have

$$\Gamma_{\rm PS}(L,M) = \frac{\langle B'(L)|\,\mathbb{H}\,|B(L)\rangle}{\langle B'(L)|B(L)\rangle} - \frac{\langle\Omega(L)|\,\mathbb{H}\,|\Omega'(L)\rangle}{\langle\Omega(L)|\Omega'(L)\rangle}\,, \tag{2.14}$$

with $|B'(L)\rangle = \mathbb{A}_0{}^\dagger|\Omega(L)\rangle$ and $\langle B'(L)|B(L)\rangle = \langle\Omega(L)|\Omega'(L)\rangle$. Expanding in terms of energy eigenfunctions, one sees immediately that $\Gamma_{\rm PS}(L,M) = \sum_i \beta_i E_B^{(i)} - \sum_i \alpha_i E_\Omega^{(i)}$, where $E_B^{(i)}$ are the (finite-volume) energy levels in the heavy-light pseudoscalar meson sector and $E_\Omega^{(i)}$ those with vacuum quantum numbers. The coefficients β_i, α_i have a strong dependence on i, which labels the energy excitations; states with $E^{(i)} - E^{(0)} \gg 1/L$ are suppressed exponentially in the sum. For $z = ML \gg 1$, the effective energy $\Gamma_{\rm PS}(L,M)$ is hence expected to be given by HQET.

To summarize, $Y_{\rm PS}$, $Y_{\rm V}$ and R are (ratios of) matrix elements between low-energy heavy-light and vacuum-like states. HQET at order $(1/m)^n$ should describe them up to corrections of the order of $1/(ML)^{n+1}$. The energies Γ, eqs. (2.12) and (2.13), share the same property. It is then possible to test HQET by studying the large-z asymptotics of these observables!

3. Large-z asymptotics: effective theory predictions

We now turn our attention to the effective theory predictions for the observables introduced above.

JHEP11(2004)048

3.1 Current matrix elements

At the classical level it is expected that they can be described by a power series in $1/z$ with $z = ML$. This has been checked explicitly in [14]: the expansion in $1/z$ is asymptotic, non-analytic terms are of the type e^{-z} and are thus very small for, say, $z > 4$. The leading term in the expansion for each of the correlation functions in eqs. (2.3)–(2.6) is given by exactly the same expressions, evaluated with the simple replacement $\psi_{\mathrm{b}} \to \psi_{\mathrm{h}}$ etc. and by dropping all terms of $\mathrm{O}(1/m)$ in the action associated with eq. (1.1). This corresponds to the static limit, where the heavy quark does not propagate in space. We denote the corresponding observables (in the effective theory) with a superscript "stat", e.g.

$$f_{\mathrm{A}}(x_0) \to f_{\mathrm{A}}^{\mathrm{stat}}(x_0)\,,$$

and also introduce

$$X(L) \equiv \frac{f_{\mathrm{A}}^{\mathrm{stat}}(T/2)}{\sqrt{f_1^{\mathrm{stat}}}} \tag{3.1}$$

that is easily seen to be mass independent from the form of the static propagator (both in the formal continuum theory and in lattice regularization at finite lattice spacing [37]). An example for the correspondence of the effective theory and QCD at the classical level is

$$X(L) = \lim_{z\to\infty} Y_{\mathrm{PS}}(L,M) = \lim_{z\to\infty} Y_{\mathrm{V}}(L,M)\,. \tag{3.2}$$

In the quantum theory there are logarithmic modifications of such relations. Of course, they have their origin in the scale dependent renormalization of the effective theory. For example, due to the renormalization of the axial current in the effective theory, the renormalized ratio[4]

$$X_{\mathrm{R}}(L,\mu) = Z_{\mathrm{A}}^{\mathrm{stat}}(\mu) X_{\mathrm{bare}}(L) \tag{3.3}$$

depends logarithmically on the chosen renormalization scale μ. It further depends on the chosen renormalization scheme, but the renormalization group invariant

$$X_{\mathrm{RGI}}(L) = \lim_{\mu\to\infty} \Big\{ \big[2b_0\bar{g}^2(\mu)\big]^{-\gamma_0/(2b_0)}\; X_{\mathrm{R}}(L,\mu) \Big\} = Z_{\mathrm{RGI}} X_{\mathrm{bare}}(L)\,, \tag{3.4}$$

$$b_0 = \frac{11}{(4\pi)^2}\,, \quad \gamma_0 = -\frac{1}{(4\pi^2)} \qquad (N_{\mathrm{f}} = 0)\,, \tag{3.5}$$

does not. The renormalization constant Z_{RGI} is computable in lattice QCD [39]. Above, b_0 and γ_0 are given for the case of a vanishing number of flavours as is appropriate for the quenched approximation, which we will employ in the following section.

The large-z behaviour of the QCD observables is then given by the corresponding renormalization group invariants of the effective theory, together with logarithmically mass

[4] One should *not* identify $\mu = 1/L$ here, as it was done in the computation of the scale dependence of the static axial current in [39]. Note also that in the ratio X other renormalization factors cancel in the effective theory, just as they do in QCD.

dependent functions that will be called C below. As arguments of these functions we choose the renormalization group invariant mass M (in units of the Λ parameter), since this can be fixed in the lattice computations without perturbative uncertainties: the relation between the bare quark masses in the lattice regularization, which we use [40], and M has been non-perturbatively computed in [41, 42, 35]. The scheme independent M describes the limiting behaviour of any running mass $\overline{m}(\mu)$ for large μ via

$$\lim_{\mu\to\infty}\left\{\left[2b_0\bar{g}^2(\mu)\right]^{-d_0/(2b_0)}\,\overline{m}(\mu)\right\} = M\,, \qquad d_0 = \frac{8}{(4\pi)^2} \qquad (N_{\rm f}=0)\,. \tag{3.6}$$

The following predictions are then obtained (see also section 5.1 of ref. [39]):

$$Y_{\rm PS}(L,M) \;\stackrel{M\to\infty}{\sim}\; C_{\rm PS}\left(\frac{M}{\Lambda_{\overline{\rm MS}}}\right) X_{\rm RGI}(L)\left(1+{\rm O}\left(\frac{1}{z}\right)\right), \qquad z=ML\,, \tag{3.7}$$

$$Y_{\rm V}(L,M) \;\stackrel{M\to\infty}{\sim}\; C_{\rm V}\left(\frac{M}{\Lambda_{\overline{\rm MS}}}\right) X_{\rm RGI}(L)\left(1+{\rm O}\left(\frac{1}{z}\right)\right), \tag{3.8}$$

$$R(L,M) \;\stackrel{M\to\infty}{\sim}\; C_{\rm PS/V}\left(\frac{M}{\Lambda_{\overline{\rm MS}}}\right)\left(1+{\rm O}\left(\frac{1}{z}\right)\right). \tag{3.9}$$

Here, the function $C_{\rm PS}(M/\Lambda_{\overline{\rm MS}})$ has the asymptotics

$$C_{\rm PS}\left(\frac{M}{\Lambda_{\overline{\rm MS}}}\right) \;\stackrel{M\to\infty}{\sim}\; \left(\ln\frac{M}{\Lambda_{\overline{\rm MS}}}\right)^{-\gamma_0/(2b_0)}\left\{1+{\rm O}\left(\frac{\ln\left[\ln\left(M/\Lambda_{\overline{\rm MS}}\right)\right]}{\ln\left(M/\Lambda_{\overline{\rm MS}}\right)}\right)\right\}; \tag{3.10}$$

to within this accuracy, $C_{\rm V}$ shares this asymptotic behaviour. In practice, the functions $C_{\rm X}(M/\Lambda_{\overline{\rm MS}})$, ${\rm X}={\rm PS},{\rm V},{\rm PS/V}$, are obtained by solving the perturbative renormalization group equations along the lines of section 5.1 of ref. [39], where more details can be found. In particular we always use the four-loop perturbative approximation of the β-function [43] and the three-loop approximation to the anomalous dimension γ of the currents, which has recently been computed [9]. Taking the n-loop approximation to γ, the resulting relative error in the functions $C_{\rm X}$ is of order α^n with α evaluated at a scale of the order of the heavy quark mass. Explicit expressions for the functions $C_{\rm X}$ are given in appendix B.

In order to study whether their α^n-error is a limiting factor, we first note that changing the order from three-loop to four-loop in the β-function makes only a tiny difference. Next we plot $C_{\rm X}$, ${\rm X}={\rm PS},{\rm PS/V}$, using γ at n loops in figure 2. We observe a reasonable behaviour of the asymptotic perturbative series and take half of the difference between the two-loop and three-loop approximations for γ as our uncertainty. This uncertainty will be almost negligible with respect to our statistical errors. Note that without the three-loop computations of [9] such a statement would not have been possible.

For completeness we remind the reader that eqs. (3.7)–(3.9) are afflicted by the usual problem of identifying power corrections. Asymptotically, at large M, the higher-order logarithmic (perturbative) corrections in $C_{\rm X}$ dominate over the $1/z^n$ power corrections. However, as just discussed, in the interesting range of z, the perturbative corrections are under reasonable control and it makes sense to investigate the power corrections if they are significantly larger. Note that this problem is not present if the effective theory is renormalized non-perturbatively [36].

JHEP11(2004)048

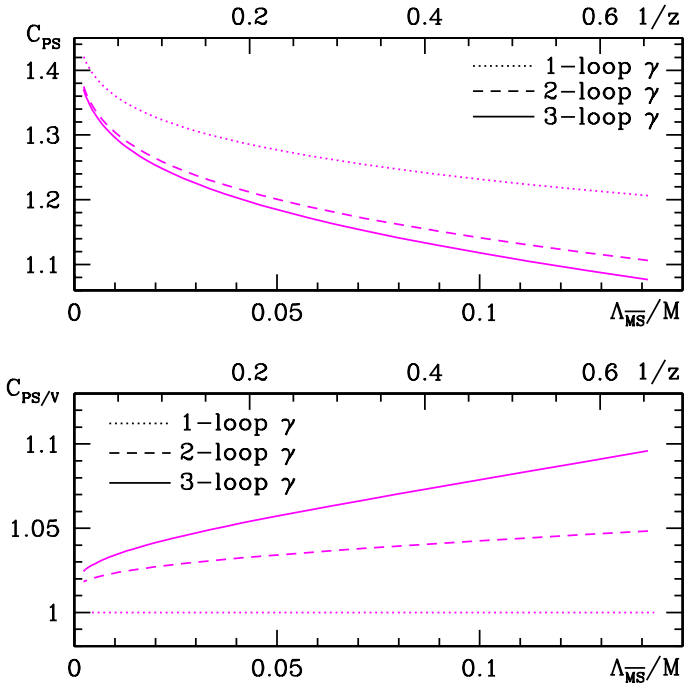

Figure 2: The functions $C_{\rm PS}$ and $C_{\rm PS/V}$ evaluated in different approximations of perturbation theory. In relating $\Lambda_{\overline{\rm MS}}/M$ to $z = ML$, we used [41] $\Lambda_{\overline{\rm MS}} r_0 = 0.602$ and $L/r_0 = L_{\rm max}/(2r_0) = 0.359$. (Setting $r_0 = 0.5$ fm, this actually corresponds to $L \approx 0.2$ fm.)

3.2 Energies

Next we concentrate on the energies Γ. Clearly, because of the term $m\overline{\psi}_{\rm h}(x)\psi_{\rm h}(x)$ in the lagrangian (1.1), they grow (roughly linearly) with the mass. For the case of hadron masses, mass formulae have been written down [44]; for instance, the one for the B-meson mass reads:

$$m_{\rm B} = m + \bar{\Lambda} + \frac{1}{2m}\,(\lambda_1 + d_{\rm B}\lambda_2) + {\rm O}\left(\frac{1}{m^2}\right), \qquad d_{\rm B} = 3 \tag{3.11}$$

(and the same formula holds for the B*-meson except that $d_{\rm B} \to d_{\rm B^*} = -1$). The matrix element $\lambda_1 = \frac{1}{2}\omega_{\rm kin}\langle{\rm B}|-\overline{\psi}_{\rm h}\mathbf{D}^2\psi_{\rm h}|{\rm B}\rangle$ was mentioned already in the introduction, and $\lambda_2 = \frac{1}{2d_{\rm B}}\,\omega_{\rm spin}\langle{\rm B}|-\overline{\psi}_{\rm h}\sigma\cdot\mathbf{B}\,\psi_{\rm h}|{\rm B}\rangle$. Some cautioning remark concerning the above formula is in order. It suggests that the binding energy $\bar{\Lambda} = m_{\rm B} - m + {\rm O}(1/m)$ may be obtained as a prediction of HQET. However, there is no unique non-perturbative definition of the mass m, which should be subtracted. As a consequence, $\bar{\Lambda}$ has an ambiguity of order $\Lambda_{\rm QCD}$, which may then also propagate into a significant ambiguity in λ_1 extracted from eq. (3.11).

We nevertheless start our discussion of the effective energies Γ from a trivial generalization of eq. (3.11):

$$\begin{aligned}\Gamma_{\rm av}(L,M) &\equiv \frac{1}{4}\big[\Gamma_{\rm PS}(L,M) + 3\,\Gamma_{\rm V}(L,M)\big] \\ &= m + \bar{\Lambda}(L) + \frac{1}{2m}\,\lambda_1(L) + {\rm O}\left(\frac{1}{m^2}\right),\end{aligned} \tag{3.12}$$

where $\lambda_1(L)$ again summarizes the effect of the $\overline{\psi}_{\rm h}\mathbf{D}^2\psi_{\rm h}$-perturbation to the static action. We have cancelled a λ_2-term by considering the spin-averaged combination of the energy. While one ought to be careful with the interpretation of sub-leading terms in $1/M$, the large-mass behaviour of $\Gamma_{\rm av}(L,M)$ is given by

$$L\Gamma_{\rm av}(L,M) \stackrel{M\to\infty}{\sim} C_{\rm mass}\left(\frac{M}{\Lambda_{\overline{\rm MS}}}\right)\times z + {\rm O}\left(\left(\frac{1}{z}\right)^0\right), \tag{3.13}$$

with ($\overline{m}_{\overline{\rm MS}}(\overline{m}_*)=\overline{m}_*$)

$$C_{\rm mass}\left(\frac{M}{\Lambda_{\overline{\rm MS}}}\right) = \frac{m_Q}{M} = \frac{\overline{m}_*}{M}\,\frac{m_Q}{\overline{m}_*} \tag{3.14}$$

and m_Q being the pole mass. Here the first factor on the right-hand side is known very precisely in perturbation theory (up to four loops [45, 46]), but it is well known that the perturbative series for the second factor is not very well behaved and even the three-loop term [47] is still rather significant. We will discuss this uncertainty in $C_{\rm mass}$ together with the numerical results in the following section.[5]

Let us now consider the sub-leading terms in eq. (3.12). Taking energy differences, m drops out and e.g. $\bar{\Lambda}(L)-\bar{\Lambda}(L')$ can be computed unambiguously from the static effective theory. It does not depend on any convention adopted for m in eq. (3.12). In our numerical computations, however, we investigated only one value of L. As an example of another observable unaffected by the ambiguity in m, we therefore look at the combination

$$\Xi(L,M) = \frac{L}{4}\left[\frac{f'_{\rm A}(T/4)}{f_{\rm A}(T/4)} - \frac{f'_{\rm A}(T/2)}{f_{\rm A}(T/2)} + 3\,\frac{k'_{\rm V}(T/4)}{k_{\rm V}(T/4)} - 3\,\frac{k'_{\rm V}(T/2)}{k_{\rm V}(T/2)}\right]. \tag{3.15}$$

The HQET prediction for this quantity is

$$\Xi(L,M) = \Xi_{\rm stat}(L) + \frac{1}{2z}\,\Xi_{\rm kin}(L) + {\rm O}\left(\frac{1}{z^2}\right), \tag{3.16}$$

with

$$\Xi_{\rm stat}(L) = L\left[\frac{(f_{\rm A}^{\rm stat})'(T/4)}{f_{\rm A}^{\rm stat}(T/4)} - \frac{(f_{\rm A}^{\rm stat})'(T/2)}{f_{\rm A}^{\rm stat}(T/2)}\right], \tag{3.17}$$

defined in the static effective theory. Since it is an energy, Ξ does not require any renormalization. The first-order correction in $1/z$ is given entirely by matrix elements of $\overline{\psi}_{\rm h}(x)\mathbf{D}^2\psi_{\rm h}(x)$. Its coefficient is fixed using the reparametrization invariance of the effective theory, first discussed in ref. [48]. To see this, one considers the matrix elements of $\overline{\psi}_{\rm h}(x)\mathbf{D}^2\psi_{\rm h}(x)$ to be computed in dimensional regularization. Then reparametrization invariance is valid, and the coefficient of the operator renormalized by minimal subtraction is the inverse $\overline{\rm MS}$ quark mass [49, 50], whose renormalization scale dependence cancels against the one of the matrix element. From eq. (3.6) it hence follows that the prefactor of

[5] We note that eqs. (3.13) and (3.14) are the only ones where m_Q enters the coefficient functions relating the RGI matrix elements of HQET to the QCD observables. In all other cases, m_Q has been eliminated and only M appears. Thus, there is no particular reason to expect that any of the perturbative expressions (for the various anomalous dimension functions) is badly behaved.

JHEP11(2004)048

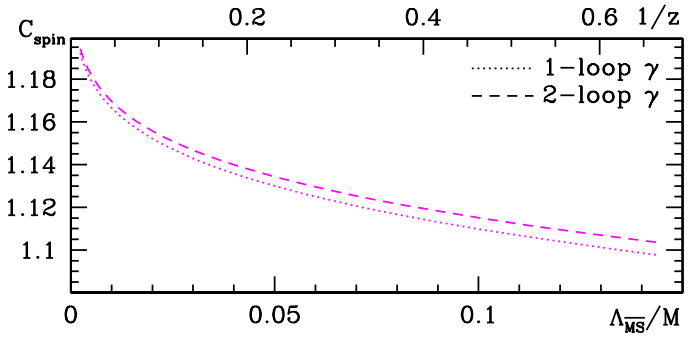

Figure 3: The function $C_{\rm spin}$ evaluated in perturbation theory.

the renormalization group invariant matrix element of $\overline{\psi}_{\rm h}(x)\mathbf{D}^2\psi_{\rm h}(x)$ is $1/(2M)$, as used in eq. (3.16). In that equation, $\Xi_{\rm kin}(L)$ is the matrix element made dimensionless by a factor L. In the following, the exact expression for $\Xi_{\rm kin}(L)$ will be irrelevant. It rather suffices to know that it does not depend on the mass.

We point out that, in writing down the quantum mechanical representation of Ξ, states play a rôle for which only the operator $\mathrm{e}^{-T\mathbb{H}/4}$ is effective to suppress higher energy contributions, while in our other observables $\mathrm{e}^{-T\mathbb{H}/2}$ suppresses high energies. For the quantity Ξ, HQET is thus expected to be accurate only at larger values of z. This variable should roughly be a factor of 2 larger than for the other observables.

Finally, in the difference

$$\Delta_\Gamma(L,M) \equiv \Gamma_{\rm PS}(L,M) - \Gamma_{\rm V}(L,M) \tag{3.18}$$

the lowest-order term that contributes in the effective theory is $\overline{\psi}_{\rm h}(x)\sigma\cdot\mathbf{B}\,\psi_{\rm h}(x)$. With $C_{\rm spin}$ constructed from the anomalous dimension of this operator in the effective theory, $\gamma^{\rm spin}$ [51, 52], we thus have

$$L\Delta_\Gamma(L,M) \stackrel{M\to\infty}{\sim} C_{\rm spin}\left(\frac{M}{\Lambda_{\overline{\rm MS}}}\right)\frac{X^{\rm spin}_{\rm RGI}(L)}{z}\left(1+\mathrm{O}\Big(\frac{1}{z}\Big)\right), \tag{3.19}$$

where the leading asymptotics of the function $C_{\rm spin}(M/\Lambda_{\overline{\rm MS}})$ is of the form

$$C_{\rm spin}\left(\frac{M}{\Lambda_{\overline{\rm MS}}}\right) \stackrel{M\to\infty}{\sim} \left(\ln\frac{M}{\Lambda_{\overline{\rm MS}}}\right)^{-\gamma_0^{\rm spin}/(2b_0)}\left\{1+\mathrm{O}\left(\frac{\ln\left[\ln\left(M/\Lambda_{\overline{\rm MS}}\right)\right]}{\ln\left(M/\Lambda_{\overline{\rm MS}}\right)}\right)\right\} \tag{3.20}$$

with the universal coefficient (cf. appendix B)

$$\gamma_0^{\rm spin} = \frac{6}{(4\pi)^2} - d_0\,, \tag{3.21}$$

and $X^{\rm spin}_{\rm RGI}$ being again a renormalization group invariant matrix element, defined in the static effective theory.[6] The relative perturbative uncertainty of $C_{\rm spin}$ is $\mathrm{O}(\alpha^2)$, since here the three-loop anomalous dimension is not known. As illustrated in figure 3, the difference

[6] Alternatively, one can also construct a difference of squared energies as the product $L^2\Gamma_{\rm av}\Delta_\Gamma$, which then behaves as $C_{\rm mag}X^{\rm spin}_{\rm RGI}\,(1+\mathrm{O}(1/z))$ for $M\to\infty$, where $C_{\rm mag}$ is introduced in appendix B as well.

between the one-loop anomalous dimension and the two-loop one is tiny. Since this may, however, be accidental rather than representing the behaviour of the series, we shall take the size of the three-loop term met in $C_{\rm PS}$, figure 2, as our uncertainty. A better estimate of this uncertainty would require the knowledge of $\gamma_2^{\rm spin}$.

4. Quantitative tests of the effective theory

We have tested the predictions of the effective theory applied to the *quenched approximation* of QCD by evaluating the observables for one geometry, namely $T = L \equiv L_0$, and for $\theta = 0.5$. The use of the quenched approximation should not be worrying in this context, since it is of course used both in the effective theory and in QCD. Furthermore, although we set the light quark mass to zero, $1/L_0$ provides an infrared cutoff and there are no singularities in the chiral limit.

The numerical simulations are done on lattices with various resolutions a/L_0 followed by a continuum extrapolation. In all cases, L_0 is fixed by imposing

$$\bar{g}^2\left(\frac{L_0}{2}\right) = 1.8811\,, \tag{4.1}$$

where $\bar{g}(L)$ is the renormalized coupling at length scale L in the SF scheme [53]. It is known that $L_0 \approx 0.2$ fm [41, 36]. The (purely technical) reasons for the precise definition (4.1) are detailed in ref. [36]. Table 1 of ref. [35] lists the bare coupling g_0 for each resolution L_0/a, and this reference also explains how the bare quark masses are fixed to ensure a massless light quark and a prescribed value M for the heavy quark.

4.1 Results in the static approximation

Some of the leading-order terms in the HQET expansions described in the previous section are known exactly due to the spin symmetry [54, 55], but for two of the expansions we have computed the non-trivial leading order from a lattice simulation in static approximation.

The first one is the matrix element of the time component of the axial current, $X_{\rm RGI}(L)$ in eq. (3.4). Indicating explicitly also the dependence on the bare coupling g_0 and the lattice spacing a, it is given by

$$X_{\rm RGI}(L_0) = \lim_{a/L_0\to 0} Z_{\rm RGI}(g_0)\, X\left(g_0, \frac{L_0}{a}\right). \tag{4.2}$$

From the relation of X to the very definition of the renormalization factor $Z_{\rm RGI}$, as detailed in ref. [39], one obtains the explicit form

$$Z_{\rm RGI}\, X = \frac{\Phi_{\rm RGI}}{\Phi(\mu = 1/L_0)} \times \left.\frac{\left(f_1^{\rm hh}\, f_1\right)^{1/4}}{\sqrt{f_1^{\rm stat}}}\right|_{L=L_0} \times [X]_{\rm tree-level} \tag{4.3}$$

for the right-hand side of eq. (4.2). All quantities that enter the above expression have been defined in the latter reference. For its numerical evaluation we take the non-perturbatively O(a) improved action of [40] for the light quarks and the improved discretizations of [56]

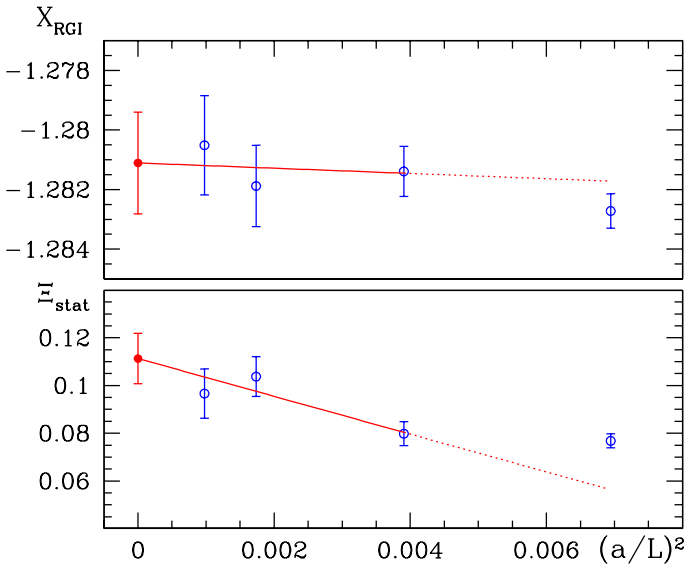

Figure 4: Continuum limit extrapolations of $X_{\rm RGI}(L_0)$ (top) and $\Xi_{\rm stat}(L_0)$ (bottom). The fits adopt simulation data generated with the HYP-link static quark action, see text. The a/L independent part of the error of $X_{\rm RGI}$ is *not* included in the graph.

for the heavy quark. We note in passing that, using the data of [39], we first evaluated this quantity with the Eichten-Hill action for the heavy quark [1]. However, this resulted in an order of magnitude larger error for $X_{\rm RGI}$ at $L_0/a = 32$.

The limit $a/L_0 \to 0$ is taken by a linear fit in $(a/L_0)^2$ as illustrated in the upper diagram of figure 4, referring to the data set from a simulation with the static quark action built from HYP-links [57, 56]. We quote the result from a fit with $L_0/a \geq 16$ as our continuum result,

$$X_{\rm RGI}(L_0) = -1.281(9)\,, \tag{4.4}$$

which also receives an error contribution from the (regularization independent) factor $\Phi_{\rm RGI}/\Phi(1/L_0)$ in eq. (4.3) [39]. Including all points with $L_0/a \geq 12$ in the fit yields a compatible continuum value with smaller error. In the same way we obtain (cf. eq. (3.17) and the lower diagram of figure 4):

$$\Xi_{\rm stat}(L_0) = 0.11(1)\,. \tag{4.5}$$

4.2 Results at finite M and comparison

The finite-mass (quenched) QCD observables are obtained from similar extrapolations of lattice results at finite a/L. However, as the variable z is increased, the quark mass in lattice units grows at a given resolution a/L. A perturbative computation [14] as well as our non-perturbative study suggest that O(a) improvement may be trusted only below a certain value of the quark mass in lattice units. It is therefore necessary to impose a cut on the quark mass. For a given z, this cut translates into estimates of the coarsest lattice resolutions beyond which the lattice data are to be omitted from the continuum

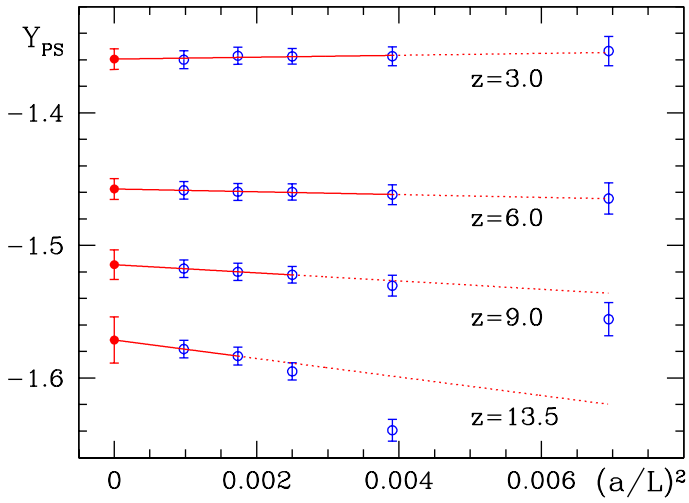

Figure 5: Continuum extrapolations for some z-values spanning the entire range of z. The linear fit in $(a/L)^2$ is shown by the full line and extended also to those values of a/L that did not participate in the fit by a dotted line.

extrapolations. As in ref. [35] we impose $aM < 0.6$ and follow this reference on all other details of the lattice computations as well as the extraction of the continuum limits. For illustration we just show the continuum extrapolations of $Y_{\rm PS}(L, M)$, $L = L_0$, at selected values of z in figure 5. In addition we mention a few features equally true for the continuum limit extrapolations of the other observables, which enter our investigation but are not shown in figures.

- The slopes in a/L are rather small.
- The error in the continuum limit grows with z, because less lattices can be used in the extrapolation at large z.
- The continuum limit is compatible with the values at the smallest two lattice spacings. Its error is conservative.

In appendix A we collect our numerical results both at finite lattice spacing and in the continuum limit.

We are now ready to compare the continuum results with the predictions of HQET. Before that, we remind the reader that energies of order $2/L$ still contribute significantly to our observables. It is thus possible that the $1/M$-expansion breaks down earlier in our finite-volume situation than it does in large volume. However, our numerical results do not give any indication of such a behaviour.

Let us start with the current matrix elements. The prediction for the matrix element of the axial current is $Y_{\rm PS}(L, M)/C_{\rm PS} = X_{\rm RGI}(L) + {\rm O}(1/z)$. In this combination, plotted in figure 6, the perturbatively computed coefficient $C_{\rm PS}(M/\Lambda_{\overline{\rm MS}})$ compensates a significant part of the mass dependence of $Y_{\rm PS}$. The finite-mass $Y_{\rm PS}/C_{\rm PS}$ is obviously well compatible with approaching the static result, eq. (4.4), as $1/z \to 0$. To quantify the deviations

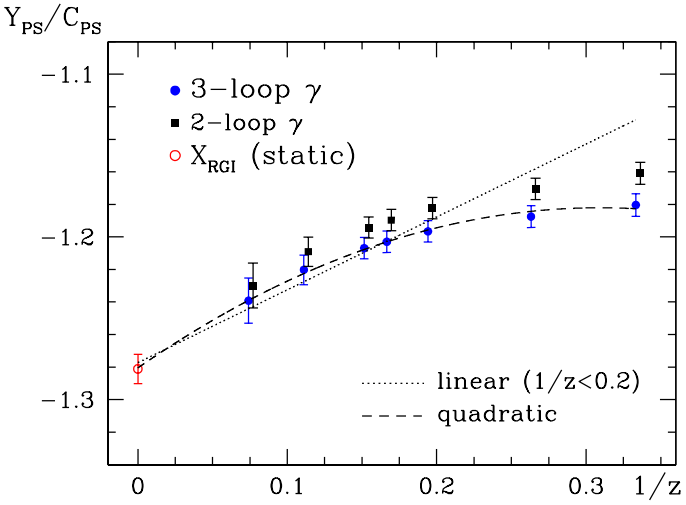

Figure 6: The ratio $Y_{\rm PS}(L,M)/C_{\rm PS}(M/\Lambda_{\overline{\rm MS}})$ with $C_{\rm PS}$ using the two- and the three-loop anomalous dimension of the static axial current. Error bars do not contain the perturbative uncertainty in $C_{\rm PS}$. The fits shown refer to the three-loop evaluation of $C_{\rm PS}$ and include the result for $X_{\rm RGI}$ in the static limit. (Points using only the two-loop anomalous dimension are slightly displaced here.)

from the static limit at finite z, we fit all data points, including $1/z = 0$, to first- and second-order polynomials in $1/z$:

$$\frac{Y_{\rm PS}}{C_{\rm PS}} = a_0 + \frac{a_1}{z} + \cdots . \tag{4.6}$$

In these fits also the uncertainty in $C_{\rm PS}$ is taken into account (i.e. half of the difference between $C_{\rm PS}$ evaluated with the two-loop and three-loop anomalous dimension). We perform them separately to the data in the range $1/z < 0.2$, which means masses around the b-quark mass and higher [36], and over the whole range, see table 1. Comparing a_1 obtained from the quadratic fit over the whole range ($z = 3.0$–13.5) and the linear fit for $1/z < 0.2$ ($z \geq 5.15$), the change is not so small. This indicates that a precise identification of the first-order correction is not possible with our precision and range of z. However, the rough magnitude of $a_1 \approx 0.6$ can be inferred and, more importantly, it is clear that the overall magnitude of $1/z$-corrections is reasonably small. It is also relevant to remember that eq. (4.6) is only an approximate parametrization of the z-dependence, since the renormalization of the higher-dimensional operators in the effective theory will introduce logarithmic modifications of the simple power series. It is thus conceivable that these logarithms account for some of the curvature seen in figure 6.

For the ratio of matrix elements $R(L,M)$, eq. (3.9), the lowest-order term in the $1/z$-expansion is fixed to be 1 by the spin symmetry of the static theory. As is reflected by figure 7, the results at finite $1/z$ are well compatible with this, if the function $C_{\rm PS/V}$ is evaluated including at least the two-loop anomalous dimensions. Fits to $R/C_{\rm PS/V}$ are performed in complete analogy to eq. (4.6). The corresponding parameters of table 1 are again of order unity. In that table we also include the parameters of the analogous fits to the quantity $Y_{\rm V}/C_{\rm V}$.

JHEP11(2004)048

	Linear		Quadratic		
Quantity	a_0	a_1	a_0	a_1	a_2
z-range: 3.0–13.5					
$Y_{\rm PS}/C_{\rm PS}$			$-1.281(7)$	0.64(8)	$-1.0(2)$
$Y_{\rm V}/C_{\rm V}$			$-1.281(7)$	$-0.63(9)$	0.3(2)
$R/C_{\rm PS/V}$			1.0	$-0.89(1)$	1.06(3)
$L\Gamma_{\rm av}/(z\,C_{\rm mass})$			1.0	0.42(3)	0.14(10)
$L\Delta_\Gamma/C_{\rm spin}$			0.0	$-1.69(6)$	0.8(2)
Ξ			0.109(8)	0.7(1)	$-0.8(3)$
z-range: 5.15–13.5					
$Y_{\rm PS}/C_{\rm PS}$	$-1.277(7)$	0.45(4)	$-1.281(8)$	0.7(1)	$-1.3(5)$
$Y_{\rm V}/C_{\rm V}$	$-1.281(9)$	$-0.59(6)$	$-1.281(7)$	$-0.6(1)$	0.2(6)
$R/C_{\rm PS/V}$	1.0	$-0.722(7)$	1.0	$-0.91(1)$	1.18(5)
$L\Gamma_{\rm av}/(z\,C_{\rm mass})$	1.0	0.44(2)	1.0	0.41(6)	0.2(3)
$L\Delta_\Gamma/C_{\rm spin}$	0.0	$-1.56(4)$	0.0	$-1.62(6)$	0.4(2)
Ξ	0.112(8)	0.54(7)	0.110(9)	0.6(2)	$-0.5(7)$

Table 1: Fit parameters describing the z-dependences of the form $a_0 + a_1/z + a_2/z^2$. Where the constant term, a_0, is listed without an error, it is constrained to the prediction of the static effective theory. (In case of the entire z-range, only the quadratic fit results are given.) All these fits have an acceptable goodness-of-fit.

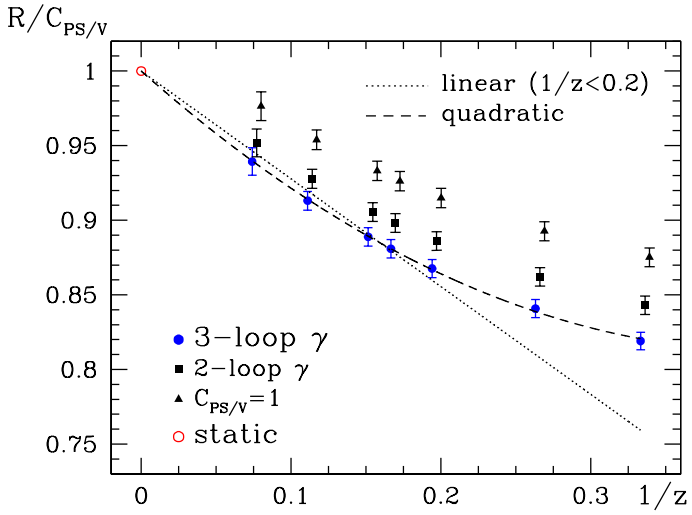

Figure 7: As in figure 6. The fits use the evaluation of $C_{\rm PS/V}$ with the two-loop matching coefficient between HQET and QCD; they are constrained to the prediction of the static effective theory. (On the level of perturbative orders, two-loop matching belongs to the three-loop anomalous dimension of the currents, cf. appendix B).

Turning our attention to the effective energies, introduced in section 2.1, a first rough test of HQET is the behaviour of the spin-averaged energy $\Gamma_{\rm av}$. Figure 8 confirms the expectation that the combination $L\Gamma_{\rm av}/(z\,C_{\rm mass})$ approaches 1 up to $1/z$-corrections as $1/z \to 0$ (see eq. (3.13)). Note that the $(1/z)^2$-corrections in $\Gamma_{\rm av}$ are very small, which is of

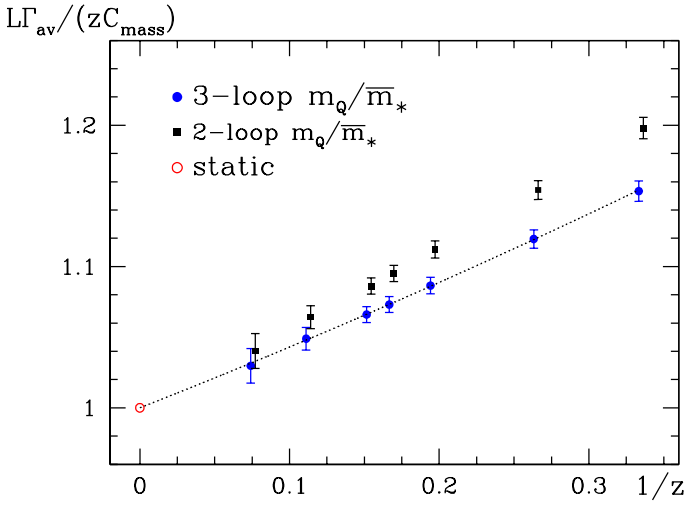

Figure 8: Quadratic fit over the entire z-range of the combination $L\Gamma_{\rm av}/(z\,C_{\rm mass})$, which is constrained to approach 1 in the static limit. It employs the three-loop relation between the pole and the $\overline{\rm MS}$ mass; the results using this relation to only two loops are also depicted for comparison.

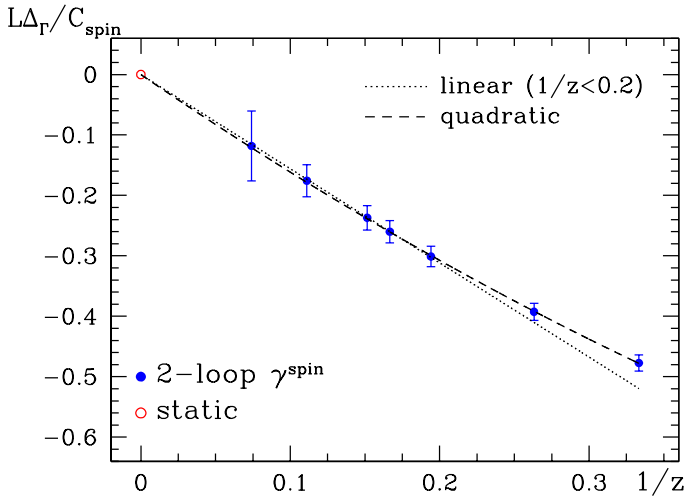

Figure 9: Fits in $1/z$ constrained to the static result and referring to the two-loop evaluation of $C_{\rm spin}$. The linear fit is only based on the heavier quark mass points with $z = 5.15$–13.5, while the quadratic one (i.e. also allowing for a $1/z^2$-term) includes all points.

particular interest for the computation of the b-quark mass in static approximation [36, 35]. There the quantity $\Gamma_{\rm av}$ was used in order to non-perturbatively match the quark mass of the effective theory to the one in QCD. The dominant error in the final estimate for the quark mass, $M_{\rm b}$, is expected to originate from this matching and is of order $M_{\rm b} \times (1/z)^2$. From the values of a_2 and $z_{\rm b} \equiv m_{\rm b} L \approx 5$, we may estimate the relative error to be roughly of the order of $0.2 \times (1/5)^2 \approx 1\%$. As seen from the figure, this conclusion is not very much affected either by the perturbative uncertainty visible in the graph as a difference between the two-loop and three-loop approximations for the pole mass m_Q in eq. (3.14); the $1/z^2$-curvature is not very different.

JHEP11(2004)048

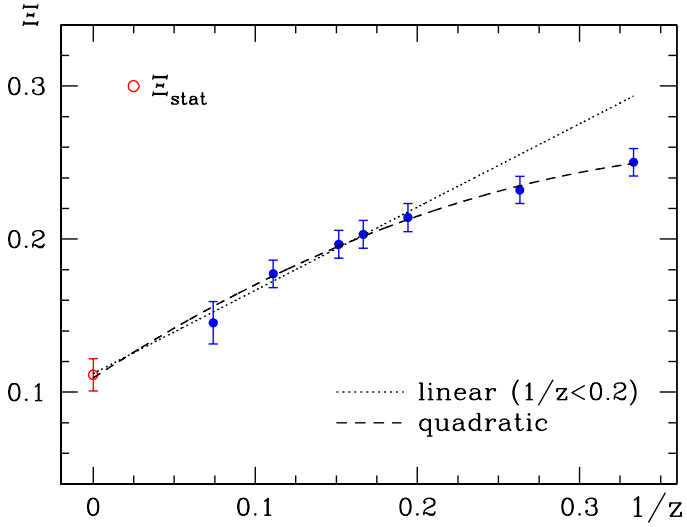

Figure 10: Linear and quadratic fits of the observable Ξ as in figures 6–9, where the static data point, $\Xi_{\rm stat}$, is included in the fits.

The spin splitting $\Delta_\Gamma(L, M)$, which vanishes in the static limit, is displayed in figure 9. It is in good agreement with the HQET prediction but exhibits a rather large $1/z$-coefficient.[7]

Finally, we successfully test eq. (3.16) in figure 10. Recall that a simple kinematical consideration leads one to expect the $1/z$-expansion to only be applicable at smaller values of $1/z$ for this observable (cf. section 3.2). On the other hand, reparametrization invariance allows to exclude logarithmic modifications of the $1/z$-term; in contrast to our other tests, figure 10 does not involve any perturbative conversion factor.

5. Conclusions

All of the comparisons of QCD observables with the predictions of HQET discussed in this work represent tests of the effective theory, which it passed successfully. As a significant improvement of earlier non-perturbative (lattice) tests, these comparisons are performed after first taking the *continuum limit* of the *non-perturbatively renormalized* quantities. Thus, worries that $\mathrm{O}(a)$ effects, in particular those that grow with the quark mass, may afflict the large-mass behaviour in QCD are removed.

For a precise judgement of figures 6–10 it is important to be aware of the level of precision of renormalization and matching. The renormalization problem of the static axial current has been solved non-perturbatively in [39] and with this information all points at $1/z = 0$ are known without any residual perturbative uncertainty. For the quantity Ξ shown

[7] We note that the slope $X^{\rm spin}_{\rm RGI}(L)$ is computable in the effective theory in a very similar way to $X_{\rm RGI}$, because the associated operator $\overline{\psi}_{\rm h}\sigma\cdot\mathbf{B}\,\psi_{\rm h}$ does not mix with any other; its renormalization may be computed non-perturbatively using the methods of ref. [39]. The comparison of the result to the data at finite mass would presumably be limited in precision by the present perturbative uncertainty in $C_{\rm spin}$. This limitation is likely to apply to the (large-volume) mass splitting between the B*- and the B-meson as well.

in figure 10, this is also true at finite $1/z$. However, in general we need to know the functions $C_{\rm X}$, which relate the QCD observables at finite mass M (and thus finite $z = ML$) to the renormalization group invariants of the effective theory, such as $X_{\rm RGI}$ in figure 6. While the latter are unambiguously defined and have been computed non-perturbatively, the former are known only in perturbation theory and have errors of order α^n, with α evaluated at the scale of the heavy quark mass. We have discussed these errors. On a phenomenological level they are under control due to the computations [58, 9], except for $C_{\rm spin}$, where a next-to-next-to-leading-order computation is not yet available. Still, one should remember that — strictly speaking — the isolation of $1/m$-corrections by looking at the difference to the leading-order HQET result is only possible when $C_{\rm X}$ is known non-perturbatively: parametrically, $\mathrm{O}([\alpha(m)]^n)$ corrections are always larger than $\mathrm{O}(1/m)$. Nevertheless, our results in figures 6–10 are compatible with the z^{-n} power corrections dominating over the perturbative ones in the accessible range of z. Fitting them by a simple polynomial in $1/z$, the coefficients turn out to be of order 1 as naively expected. Therefore, at the b-quark mass, which corresponds to $z_{\rm b} \equiv m_{\rm b}L \approx 5$ for our value of $L = L_0 \approx 0.2$ fm, the effective theory is very useful.

Beyond the general interest of providing a non-perturbative test for HQET, these results are important for the programme of ref. [36]. There it was suggested to determine the $1/m_{\rm b}$-corrections to B-physics matrix elements from a simulation of HQET on the lattice. The coefficients c_k of the various terms in the HQET lagrangian and of the effective composite fields are to be determined by matching HQET and QCD in a finite volume, and it was proposed to employ a value of L similar to L_0 in this step. This value has to be large enough such that (i) $z_{\rm b}$ is in the range where HQET is applicable with small corrections, yet (ii) L_0 has to be small enough to allow for the computation of the QCD observables at $m = m_{\rm b}$ with small a-effects. From table 1 we conclude that $L = L_0$ is indeed promising. In fact, in the previous section we roughly estimated that the correction to the static limit computation of the RGI b-quark mass [34, 36] is only of the order of 1%.

However, this application appears to be a particularly favourable case and it would be of advantage to have a larger value of $z_{\rm b}$ (i.e. larger L) in the matching step to suppress higher-order terms. Our analysis suggests that this is indeed possible, since we may determine QCD observables rather precisely in, say, the entire range $z \geq 5$ by combining QCD results at finite z with the static limit. Choosing, for instance, $L \approx 2L_0$ in the matching step, one needs the QCD observables for $z \approx 10$. The errors of the quadratic fit functions evaluated at $z = z_{\rm b} = 10$ are typically 30%–50% smaller than the errors of the neighbouring points seen in figures 6–10. Proceeding in this way, namely taking the fit functions as representations of the QCD observables in finite volume (of course within their errors), one may obtain the HQET parameters as functions of the quark mass and infer predictions for all quark masses larger than the minimal one considered. With the entire matching done non-perturbatively, the final HQET results will differ from QCD by $\mathrm{O}(1/m^2)$ if $1/m$-terms are properly included. No perturbative errors as in $C_{\rm X}$ enter in this programme.

We finally remind the reader that in the quantities discussed in this paper, as well as in the matching step just described, we are dealing with matrix elements of a mixture of energy eigenstates where states with energy of $\mathrm{O}(1/L)$ contribute. Hence the $1/m$-

expansion for the large-volume B-physics matrix elements may be expected to behave even better and should be well under control, once this is the case for the matching step.

Acknowledgments

We would like to thank M. Della Morte, T. Mannel, T. Feldmann and N. Tantalo for useful discussions. This work is part of the ALPHA Collaboration research programme. The largest part of the numerical simulations has been performed on the APEmille computers at DESY Zeuthen, and we thank DESY for allocating computer time to this project as well as the staff of the computer center at Zeuthen for their support. In addition we ran a C-code based on the MILC Collaboration's public lattice gauge theory code [59] on the PC cluster of the University of Münster. This work is supported in part by the EU IHP Network on *Hadron Phenomenology from Lattice QCD* under grant HPRN-CT-2000-00145 and by the Deutsche Forschungsgemeinschaft in the SFB/TR 09.

A. Results at finite lattice spacing

For any details on the lattice simulations and the subsequent analysis of the numerical data, the reader is referred to [35] and references therein. In table 2 we therefore directly list the results on the observables studied in this work at finite values of the lattice spacing as well as in the continuum limit. As already mentioned in section 4, the latter have been extracted by linear extrapolations $(a/L)^2 \to 0$ of the $\mathrm{O}(a)$ improved lattice data following the same procedure as adopted in ref. [35].

L/a	$Y_{\mathrm{PS}}(L,M)$	$Y_{\mathrm{V}}(L,M)$	$R(L,M)$	$L\Delta_\Gamma(L,M)$	$\Xi(L,M)$
			$z = 3.0$		
12	−1.35(1)	−1.581(7)	0.869(8)	−0.509(10)	0.245(4)
16	−1.357(7)	−1.576(7)	0.874(6)	−0.512(10)	0.256(5)
20	−1.357(6)	−1.575(7)	0.875(5)	−0.521(11)	0.259(6)
24	−1.357(6)	−1.576(7)	0.874(5)	−0.522(13)	0.259(8)
32	−1.360(7)	−1.577(7)	0.875(5)	−0.533(14)	0.246(9)
CL	*−1.359(8)*	*−1.576(8)*	*0.875(6)*	*−0.537(15)*	*0.250(9)*
			$z = 3.8$		
12	−1.39(1)	−1.591(7)	0.884(8)	−0.419(13)	0.226(4)
16	−1.392(7)	−1.584(7)	0.890(6)	−0.423(12)	0.240(5)
20	−1.391(6)	−1.582(7)	0.892(5)	−0.430(12)	0.240(6)
24	−1.391(6)	−1.582(7)	0.891(5)	−0.431(13)	0.241(8)
32	−1.394(7)	−1.583(7)	0.892(5)	−0.441(15)	0.228(9)
CL	*−1.394(8)*	*−1.581(8)*	*0.893(6)*	*−0.444(16)*	*0.232(9)*

Table 2: *(Continued).*

L/a	$Y_{\rm PS}(L,M)$	$Y_{\rm V}(L,M)$	$R(L,M)$	$L\Delta_\Gamma(L,M)$	$\Xi(L,M)$
			$z = 5.15$		
12	−1.44(1)	−1.609(7)	0.904(8)	−0.315(17)	0.200(4)
16	−1.438(7)	−1.596(7)	0.910(6)	−0.320(15)	0.215(5)
20	−1.437(6)	−1.592(7)	0.913(5)	−0.328(15)	0.216(6)
24	−1.437(6)	−1.591(7)	0.913(5)	−0.327(16)	0.218(8)
32	−1.436(7)	−1.589(7)	0.914(5)	−0.341(17)	0.210(9)
CL	*−1.435(8)*	*−1.586(8)*	*0.915(6)*	*−0.343(19)*	*0.214(9)*
			$z = 6.0$		
12	−1.46(1)	−1.620(7)	0.913(8)	−0.270(20)	0.186(4)
16	−1.462(7)	−1.604(7)	0.920(6)	−0.276(17)	0.203(5)
20	−1.460(6)	−1.597(7)	0.923(5)	−0.283(17)	0.205(6)
24	−1.460(6)	−1.595(7)	0.924(5)	−0.282(17)	0.207(8)
32	−1.458(7)	−1.593(7)	0.924(5)	−0.296(19)	0.198(9)
CL	*−1.457(8)*	*−1.589(8)*	*0.926(6)*	*−0.297(21)*	*0.203(9)*
			$z = 6.6$		
12	−1.48(1)	−1.629(7)	0.918(8)	−0.243(21)	0.178(4)
16	−1.477(8)	−1.609(7)	0.926(6)	−0.251(19)	0.196(5)
20	−1.474(6)	−1.601(7)	0.930(5)	−0.258(19)	0.198(6)
24	−1.474(6)	−1.599(7)	0.930(5)	−0.257(19)	0.201(8)
32	−1.473(7)	−1.596(7)	0.931(5)	−0.270(20)	0.191(9)
CL	*−1.471(8)*	*−1.591(8)*	*0.933(6)*	*−0.271(23)*	*0.197(9)*
			$z = 9.0$		
12	−1.56(1)	−1.678(7)	0.933(8)	−0.166(31)	0.149(4)
16	−1.530(8)	−1.633(7)	0.943(6)	−0.182(27)	0.172(5)
20	−1.522(6)	−1.618(7)	0.948(5)	−0.190(25)	0.176(6)
24	−1.520(6)	−1.612(7)	0.950(5)	−0.189(25)	0.180(8)
32	−1.517(7)	−1.608(7)	0.951(5)	−0.200(26)	0.170(9)
CL	*−1.515(11)*	*−1.600(12)*	*0.954(7)*	*−0.202(30)*	*0.177(9)*
			$z = 13.5$		
16	−1.639(8)	−1.713(7)	0.961(6)	−0.106(47)	0.139(5)
20	−1.595(7)	−1.659(7)	0.967(5)	−0.123(39)	0.149(5)
24	−1.583(7)	−1.640(7)	0.970(6)	−0.126(37)	0.157(8)
32	−1.578(7)	−1.631(7)	0.973(6)	−0.132(39)	0.142(9)
CL	*−1.571(17)*	*−1.619(18)*	*0.976(9)*	*−0.137(66)*	*0.145(14)*

Table 2: Lattice results on the quantities of this work for different values of the dimensionless renormalization group invariant heavy quark mass, $z = ML$, with $L \equiv L_0 \approx 0.2$ fm. The full sets of simulation parameters can be inferred from tables 1 and 4 of ref. [35], where also the results for $L\Gamma_{\rm av}$ were published. The quoted errors cover the statistical as well as the systematic uncertainties, including those originating from the fact that in the numerical simulations z can only be fixed within some finite precision. Continuum limits are displayed in italics.

B. Perturbative conversion factors between QCD and HQET

In this appendix we provide details on the numerical evaluation of the perturbative approximations of the conversion functions $C_{\rm X}(M/\Lambda_{\overline{\rm MS}})$ (X = PS, V, PS/V, spin) that translate the matrix elements and energies obtained in the effective theory to those in *quenched* QCD at finite values of the heavy quark mass. Also the case of the conversion factor $C_{\rm mass}(M/\Lambda_{\overline{\rm MS}})$, which relates the heavy quark's pole mass m_Q to the renormalization group invariant quark mass M, will be addressed.

Let us begin with the definition of the conversion functions for matrix elements of the heavy-light currents. Parametrized with the $\overline{\rm MS}$ mass $\overline{m}_*$, implicitly defined through

$$\overline{m}_{\overline{\rm MS}}(\overline{m}_*) = \overline{m}_* \,, \tag{B.1}$$

we write them for X = PS and V as

$$\widehat{C}_{\rm X}(\overline{m}_*) \equiv \left[2b_0\bar{g}^2(\overline{m}_*)\right]^{\gamma_0^{\rm X}/(2b_0)} \exp\left\{\int_0^{\bar{g}(\overline{m}_*)} {\rm d}g \left[\frac{\gamma^{\rm X}(g)}{\beta(g)} - \frac{\gamma_0^{\rm X}}{b_0 g}\right]\right\}. \tag{B.2}$$

Here, $\beta(g) = -g^3 b_0 - g^5 b_1 + \ldots$ is the four-loop anomalous dimension [43] of the renormalized coupling $\bar{g}(\mu)$ in the $\overline{\rm MS}$ scheme with the leading- and next-to-leading-order coefficients $b_0 = 11/(4\pi)^2$ and $b_1 = 102/(4\pi)^4$. In eq. (B.2) we have introduced the anomalous dimensions in the matching scheme

$$\gamma^{\rm X}(g) = -g^2\left\{\gamma_0^{\rm X} + \gamma_1^{\rm X} g^2 + \gamma_2^{\rm X} g^4 + \cdots\right\}. \tag{B.3}$$

At one-loop order they are the universal ones [60, 61],

$$\gamma_0^{\rm PS} = \gamma_0^{\rm V} = -\frac{1}{4\pi^2}\,, \tag{B.4}$$

and at higher order they are related to the anomalous dimensions $\gamma^{{\rm X},\overline{\rm MS}}(g)$ of the corresponding effective theory operator in the $\overline{\rm MS}$ scheme via

$$\gamma_1^{\rm X} = \gamma_1^{{\rm X},\overline{\rm MS}} + 2b_0 c_1^{\rm X}\,, \tag{B.5}$$

$$\gamma_2^{\rm X} = \gamma_2^{{\rm X},\overline{\rm MS}} + 4b_0(c_2^{\rm X} + \gamma_0^{\rm X} k) + 2b_1 c_1^{\rm X} - 2b_0[c_1^{\rm X}]^2\,. \tag{B.6}$$

For X = PS and V, the $\overline{\rm MS}$ two-loop anomalous dimensions are known from [62, 63, 64] and the three-loop ones from ref. [9].[8]

The coefficients

$$c_1^{\rm PS} = -\frac{2}{3}\frac{1}{4\pi^2}\,, \qquad c_2^{\rm PS} = -4.2\,\frac{1}{(4\pi^2)^2}\,, \tag{B.7}$$

$$c_1^{\rm V} = -\frac{4}{3}\frac{1}{4\pi^2}\,, \qquad c_2^{\rm V} = -11.5\,\frac{1}{(4\pi^2)^2} \tag{B.8}$$

[8] Note that, since in HQET the anomalous dimension of the quark bilinears does not depend on their Dirac structure, $\gamma_n^{{\rm PS},\overline{\rm MS}} = \gamma_n^{{\rm V},\overline{\rm MS}}$ holds for all n.

originate from the matching of the effective theory operators renormalized in the $\overline{\rm MS}$ scheme to the physical ones in QCD [1, 65, 58], while the term proportional to

$$k = -\frac{1}{3\pi^2} \tag{B.9}$$

is due to a reparametrization: the matching was originally done at the matching scale expressed in terms of the heavy quark's pole mass, m_Q. Using the perturbative expansion for the ratio $\overline{m}_*/m_Q$ [66],

$$\frac{\overline{m}_*}{m_Q} = 1 + k\,\bar{g}^2(\overline{m}_*) + \cdots\,, \tag{B.10}$$

the pole mass can be replaced by $\overline{m}_*$.

Next, we turn to the chromomagnetic operator $\overline{\psi}_{\rm h}\sigma\cdot\mathbf{B}\,\psi_{\rm h}$. If, for the moment, we follow the common practice that in the HQET expansion its matrix element is understood to multiply the inverse pole mass, $1/m_Q$, the associated conversion function $\widehat{C}_{\rm mag}$ would be given by eq. (B.2) with an expansion (B.3) for X = mag and the universal one-loop coefficient [67, 68]

$$\gamma_0^{\rm mag} = \frac{6}{(4\pi)^2}\,. \tag{B.11}$$

With the two-loop anomalous dimension $\gamma_1^{\rm mag,\,\overline{\rm MS}}$ in the effective theory given in [51, 52] one finds

$$\gamma_1^{\rm mag} = \gamma_1^{\rm mag,\,\overline{\rm MS}} + 2b_0 c_1^{\rm mag}\,, \qquad c_1^{\rm mag} = \frac{13}{6}\,\frac{1}{4\pi^2}\,, \tag{B.12}$$

where $c_1^{\rm mag}$ was determined in [67]. In view of eq. (3.19), however, we are rather interested in a function $C_{\rm spin}$, which multiplies $1/M$. In other words, the conversion function $\widehat{C}_{\rm spin}$ must also include the factors $\overline{m}_*/m_Q$ and $M/\overline{m}_*$ in order to cancel the conventional factor $1/m_Q$ in the HQET expansion in favour of $1/M$. Using the relation

$$\frac{M}{\overline{m}_*} = \left[2b_0\bar{g}^2(\overline{m}_*)\right]^{-d_0/(2b_0)} \exp\left\{-\int_0^{\bar{g}(\overline{m}_*)} {\rm d}g\left[\frac{\tau(g)}{\beta(g)} - \frac{d_0}{b_0 g}\right]\right\}, \tag{B.13}$$

where $\tau(g) = -g^2 d_0 - g^4 d_1 + \cdots$ denotes the quark mass anomalous dimension in the $\overline{\rm MS}$ scheme in QCD (known up to four loops [45, 46] with leading coefficient $d_0 = 8/(4\pi)^2$), and the ratio (B.10), we then obtain eqs. (B.2) and (B.3) for X = spin and

$$\gamma_0^{\rm spin} = \gamma_0^{\rm mag} - d_0 = \frac{6}{(4\pi)^2} - d_0\,, \tag{B.14}$$

$$\gamma_1^{\rm spin} = \gamma_1^{\rm mag} - d_1 + 2b_0 k = \gamma_1^{\rm mag,\,\overline{\rm MS}} - d_1 + 2b_0(c_1^{\rm mag} + k)\,, \tag{B.15}$$

with $\gamma_1^{\rm mag}$ from eq. (B.12).

For the special case of the ratio of pseudoscalar and vector current matrix elements, X = PS/V, all but the contributions from the matching cancel and one gets

$$\widehat{C}_{\rm PS/V}(\overline{m}_*) \equiv \exp\left\{\int_0^{\bar{g}(\overline{m}_*)} {\rm d}g \frac{\gamma^{\rm PS}(g) - \gamma^{\rm V}(g)}{\beta(g)}\right\}. \tag{B.16}$$

To parametrize the mass dependence of energy observables (such as $\Gamma_{\rm av}$ in eq. (3.12) of section 3.2), we also define

$$\widehat{C}_{\rm mass}(\overline{m}_*) \equiv \frac{m_Q}{\overline{m}_*}\,\frac{\overline{m}_*}{M}\,, \tag{B.17}$$

where in this case the highest available perturbative precision is achieved by taking the four-loop τ-function [45, 46] in $\overline{m}_*/M$ together with the three-loop expression for $m_Q/\overline{m}_*$ [47].

Finally, changing the argument of the various $\widehat{C}_X$ to the renormalization group invariant ratio $M/\Lambda_{\overline{\rm MS}}$ via (B.13), we straightforwardly arrive at the conversion functions

$$C_{\rm X}\left(\frac{M}{\Lambda_{\overline{\rm MS}}}\right) = \widehat{C}_{\rm X}\left(\overline{m}_*\right) \qquad \text{with X} = \text{PS, V, PS/V, mass, spin}\,. \tag{B.18}$$

We evaluate all occurring integrals in the above expressions exactly (sometimes numerically), truncating anomalous dimensions and the β-function as specified. Also eq. (B.1) is solved numerically. For practical purposes, such as repeated use in the fits of the heavy quark mass dependence of our QCD observables, a parametrization of all conversion functions in terms of the variable

$$x \equiv \frac{1}{\ln\left(M/\Lambda_{\overline{\rm MS}}\right)} \tag{B.19}$$

was determined from a numerical evaluation. The functions decompose into a prefactor encoding the leading asymptotics as $x \to 0$, multiplied by a polynomial in x, which guarantees at least 0.2% precision for $x \le 0.6$:

$$C_{\rm PS}(x) = \begin{cases} x^{\gamma_0^{\rm PS}/(2b_0)}\left\{1 - 0.065\,x + 0.048\,x^2\right\} & \text{2-loop } \gamma^{\rm PS} \\ x^{\gamma_0^{\rm PS}/(2b_0)}\left\{1 - 0.068\,x - 0.087\,x^2 + 0.079\,x^3\right\} & \text{3-loop } \gamma^{\rm PS} \end{cases}, \tag{B.20}$$

$$C_{\rm V}(x) = \begin{cases} x^{\gamma_0^{\rm V}/(2b_0)}\left\{1 - 0.180\,x + 0.099\,x^2\right\} & \text{2-loop } \gamma^{\rm V} \\ x^{\gamma_0^{\rm V}/(2b_0)}\left\{1 - 0.196\,x - 0.222\,x^2 + 0.193\,x^3\right\} & \text{3-loop } \gamma^{\rm V} \end{cases}, \tag{B.21}$$

$$C_{\rm PS/V}(x) = \begin{cases} 1 + 0.117\,x - 0.043\,x^2 & \text{2-loop } \gamma^{\rm PS,V} \\ 1 + 0.124\,x + 0.187\,x^2 - 0.102\,x^3 & \text{3-loop } \gamma^{\rm PS,V} \end{cases}, \tag{B.22}$$

$$C_{\rm mass}(x) = \begin{cases} x^{d_0/(2b_0)}\left\{1 + 0.247\,x + 0.236\,x^2\right\} & \text{2-loop } \frac{m_Q}{\overline{m}_*} \\ x^{d_0/(2b_0)}\left\{1 + 0.179\,x + 0.694\,x^2 + 0.065\,x^3\right\} & \text{3-loop } \frac{m_Q}{\overline{m}_*} \end{cases}, \tag{B.23}$$

$$C_{\rm spin}(x) = \begin{cases} x^{\gamma_0^{\rm spin}/(2b_0)}\left\{1 + 0.066\,x\right\} & \text{1-loop } \gamma^{\rm spin} \\ x^{\gamma_0^{\rm spin}/(2b_0)}\left\{1 + 0.087\,x - 0.021\,x^2\right\} & \text{2-loop } \gamma^{\rm spin} \end{cases}. \tag{B.24}$$

Apart from the function $C_{\rm mass}$, the pole mass does not appear in any of the above perturbative expressions; they relate observables in the effective theory to those in QCD and are parametrized by the RGI mass M, which is unambiguously defined in terms of the (short-distance) running quark mass (see eq. (3.6)). Thus, their perturbative expansion is expected to be a regular short-distance expansion. In particular, it is not expected to suffer from the bad behaviour of the series (B.10).

References

[1] E. Eichten and B. Hill, *An effective field theory for the calculation of matrix elements involving heavy quarks*, *Phys. Lett.* **B 234** (1990) 511.

[2] H.D. Politzer and M.B. Wise, *Effective field theory approach to processes involving both light and heavy fields*, *Phys. Lett.* **B 208** (1988) 504.

[3] H. Georgi, *An effective field theory for heavy quarks at low-energies*, *Phys. Lett.* **B 240** (1990) 447.

[4] M. Neubert, *Heavy quark symmetry*, *Phys. Rept.* **245** (1994) 259 [hep-ph/9306320].

[5] T. Mannel, *Effective theory for heavy quarks*, lectures at *35th Internationale Universitätswochen für Kern- und Teilchenphysik*, Schladming, Austria, 2 – 9 March 1996 [hep-ph/9606299].

[6] B. Grinstein, *The static quark effective theory*, *Nucl. Phys.* **B 339** (1990) 253.

[7] W. Kilian and T. Mannel, *On the renormalization of heavy quark effective field theory*, *Phys. Rev.* **D 49** (1994) 1534 [hep-ph/9307307].

[8] A.G. Grozin, *Lectures on perturbative HQET, I*, hep-ph/0008300.

[9] K.G. Chetyrkin and A.G. Grozin, *Three-loop anomalous dimension of the heavy-light quark current in HQET*, *Nucl. Phys.* **B 666** (2003) 289 [hep-ph/0303113].

[10] Particle Data Group collaboration, K. Hagiwara et al., *Review of particle physics*, *Phys. Rev.* **D 66** (2002) 010001.

[11] S. Stone, *Experimental results in heavy flavor physics*, plenary talk at *International Europhysics Conference on High-Energy Physics (HEP 2003)*, Aachen, Germany, 17 – 23 July 2003, *Eur. Phys. J.* **C 33** (2004) S129 [hep-ph/0310153].

[12] M. Battaglia et al., *The CKM matrix and the unitarity triangle*, *Proceedings of the CKM Unitarity Triangle Workshop*, Geneva, Switzerland, 13 – 16 February 2002 [hep-ph/0304132].

[13] BaBaR collaboration, B. Aubert et al., *Determination of the branching fraction for $B \to X_c \ell \nu$ decays and of $|V_{cb}|$ from hadronic mass and lepton energy moments*, *Phys. Rev. Lett.* **93** (2004) 011803 [hep-ex/0404017].

[14] ALPHA collaboration, M. Kurth and R. Sommer, *Heavy quark effective theory at one-loop order: an explicit example*, *Nucl. Phys.* **B 623** (2002) 271 [hep-lat/0108018].

[15] C. Bernard et al., *Lattice results for the decay constant of heavy-light vector mesons*, *Phys. Rev.* **D 65** (2002) 014510 [hep-lat/0109015].

[16] ALPHA collaboration, J. Rolf and S. Sint, *A precise determination of the charm quark's mass in quenched QCD*, *J. High Energy Phys.* **12** (2002) 007 [hep-ph/0209255].

[17] ALPHA collaboration, A. Jüttner and J. Rolf, *A precise determination of the decay constant of the D_s-meson in quenched QCD*, *Phys. Lett.* **B 560** (2003) 59 [hep-lat/0302016].

[18] ALPHA collaboration, J. Rolf et al., *Towards a precision computation of F_{B_s} in quenched QCD*, *Nucl. Phys.* **129** *(Proc. Suppl.)* (2004) 322 [hep-lat/0309072].

[19] C. Alexandrou et al., *The leptonic decay constants of $\bar{Q}q$ mesons and the lattice resolution*, *Z. Physik* **C 62** (1994) 659 [hep-lat/9312051].

JHEP11(2004)048

[20] R. Sommer, *Beauty physics in lattice gauge theory*, *Phys. Rept.* **275** (1996) 1 [hep-lat/9401037].

[21] H. Wittig, *Leptonic decays of heavy quarks on the lattice*, *Int. J. Mod. Phys.* **A 12** (1997) 4477 [hep-lat/9705034].

[22] A.X. El-Khadra, A.S. Kronfeld, P.B. Mackenzie, S.M. Ryan and J.N. Simone, *B and D meson decay constants in lattice QCD*, *Phys. Rev.* **D 58** (1998) 014506 [hep-ph/9711426].

[23] JLQCD collaboration, S. Aoki et al., *Heavy meson decay constants from quenched lattice QCD*, *Phys. Rev. Lett.* **80** (1998) 5711.

[24] C.W. Bernard et al., *Lattice determination of heavy-light decay constants*, *Phys. Rev. Lett.* **81** (1998) 4812 [hep-ph/9806412].

[25] D. Becirevic et al., *Non-perturbatively improved heavy-light mesons: masses and decay constants*, *Phys. Rev.* **D 60** (1999) 074501 [hep-lat/9811003].

[26] UKQCD collaboration, K.C. Bowler et al., *Decay constants of B and D mesons from non-perturbatively improved lattice QCD*, *Nucl. Phys.* **B 619** (2001) 507 [hep-lat/0007020].

[27] CP-PACS collaboration, A. Ali Khan et al., *Decay constants of B and D mesons from improved relativistic lattice QCD with two flavours of sea quarks*, *Phys. Rev.* **D 64** (2001) 034505 [hep-lat/0010009].

[28] UKQCD collaboration, L. Lellouch and C.J.D. Lin, *Standard Model matrix elements for neutral B meson mixing and associated decay constants*, *Phys. Rev.* **D 64** (2001) 094501 [hep-ph/0011086].

[29] S.M. Ryan, *Heavy quark physics from lattice QCD*, *Nucl. Phys.* **106** *(Proc. Suppl.)* (2002) 86 [hep-lat/0111010].

[30] G.M. de Divitiis, M. Guagnelli, R. Petronzio, N. Tantalo and F. Palombi, *Heavy quark masses in the continuum limit of lattice QCD*, *Nucl. Phys.* **B 675** (2003) 309 [hep-lat/0305018].

[31] G.M. de Divitiis, M. Guagnelli, F. Palombi, R. Petronzio and N. Tantalo, *Heavy-light decay constants in the continuum limit of lattice QCD*, *Nucl. Phys.* **B 672** (2003) 372 [hep-lat/0307005].

[32] M. Lüscher, R. Narayanan, P. Weisz and U. Wolff, *The Schrödinger functional: a renormalizable probe for non-abelian gauge theories*, *Nucl. Phys.* **B 384** (1992) 168 [hep-lat/9207009].

[33] S. Sint, *On the Schrödinger functional in QCD*, *Nucl. Phys.* **B 421** (1994) 135 [hep-lat/9312079].

[34] ALPHA collaboration, J. Heitger and R. Sommer, *A strategy to compute the B quark mass with non-perturbative accuracy*, *Nucl. Phys.* **106** *(Proc. Suppl.)* (2002) 358 [hep-lat/0110016].

[35] ALPHA collaboration, J. Heitger and J. Wennekers, *Effective heavy-light meson energies in small-volume quenched QCD*, *J. High Energy Phys.* **02** (2004) 064 [hep-lat/0312016].

[36] ALPHA collaboration, J. Heitger and R. Sommer, *Non-perturbative heavy quark effective theory*, *J. High Energy Phys.* **02** (2004) 022 [hep-lat/0310035].

[37] ALPHA collaboration, M. Kurth and R. Sommer, *Renormalization and $O(a)$ improvement of the static axial current*, *Nucl. Phys.* **B 597** (2001) 488 [hep-lat/0007002].

JHEP11(2004)048

[38] S. Sint, *One-loop renormalization of the QCD Schrödinger functional*, *Nucl. Phys.* **B 451** (1995) 416 [hep-lat/9504005].

[39] ALPHA collaboration, J. Heitger, M. Kurth and R. Sommer, *Non-perturbative renormalization of the static axial current in quenched QCD*, *Nucl. Phys.* **B 669** (2003) 173 [hep-lat/0302019].

[40] ALPHA collaboration, M. Lüscher, S. Sint, R. Sommer, P. Weisz and U. Wolff, *Non-perturbative $O(a)$ improvement of lattice QCD*, *Nucl. Phys.* **B 491** (1997) 323 [hep-lat/9609035].

[41] ALPHA collaboration, S. Capitani, M. Lüscher, R. Sommer and H. Wittig, *Non-perturbative quark mass renormalization in quenched lattice QCD*, *Nucl. Phys.* **B 544** (1999) 669 [hep-lat/9810063].

[42] ALPHA collaboration, M. Guagnelli et al., *Non-perturbative results for the coefficients b_m and $b_A - b_P$ in $O(a)$ improved lattice QCD*, *Nucl. Phys.* **B 595** (2001) 44 [hep-lat/0009021].

[43] T. van Ritbergen, J.A.M. Vermaseren and S.A. Larin, *The four-loop beta function in Quantum Chromodynamics*, *Phys. Lett.* **B 400** (1997) 379 [hep-ph/9701390].

[44] A.F. Falk and M. Neubert, *Second-order power corrections in the heavy quark effective theory, 1. Formalism and meson form-factors*, *Phys. Rev.* **D 47** (1993) 2965 [hep-ph/9209268].

[45] K.G. Chetyrkin, *Quark mass anomalous dimension to $O(\alpha_s^4)$*, *Phys. Lett.* **B 404** (1997) 161 [hep-ph/9703278].

[46] J.A.M. Vermaseren, S.A. Larin and T. van Ritbergen, *The four-loop quark mass anomalous dimension and the invariant quark mass*, *Phys. Lett.* **B 405** (1997) 327 [hep-ph/9703284].

[47] N. Gray, D.J. Broadhurst, W. Grafe and K. Schilcher, *Three-loop relation of quark (modified) $\overline{MS}$ and pole masses*, *Z. Physik* **C 48** (1990) 673.

[48] M.E. Luke and A.V. Manohar, *Reparametrization invariance constraints on heavy particle effective field theories*, *Phys. Lett.* **B 286** (1992) 348 [hep-ph/9205228].

[49] W. Kilian and T. Ohl, *Renormalization of heavy quark effective field theory: quantum action principles and equations of motion*, *Phys. Rev.* **D 50** (1994) 4649 [hep-ph/9404305].

[50] R. Sundrum, *Reparameterization invariance to all orders in heavy quark effective theory*, *Phys. Rev.* **D 57** (1998) 331 [hep-ph/9704256].

[51] G. Amoros, M. Beneke and M. Neubert, *Two-loop anomalous dimension of the chromomagnetic moment of a heavy quark*, *Phys. Lett.* **B 401** (1997) 81 [hep-ph/9701375].

[52] A. Czarnecki and A.G. Grozin, *HQET chromomagnetic interaction at two loops*, *Phys. Lett.* **B 405** (1997) 142 [hep-ph/9701415].

[53] M. Lüscher, R. Sommer, P. Weisz and U. Wolff, *A precise determination of the running coupling in the* SU(3) *Yang-Mills theory*, *Nucl. Phys.* **B 413** (1994) 481 [hep-lat/9309005].

[54] N. Isgur and M.B. Wise, *Weak decays of heavy mesons in the static quark approximation*, *Phys. Lett.* **B 232** (1989) 113.

[55] N. Isgur and M.B. Wise, *Weak transition form-factors between heavy mesons*, *Phys. Lett.* **B 237** (1990) 527.

[56] ALPHA collaboration, M. Della Morte et al., *Lattice HQET with exponentially improved statistical precision*, *Phys. Lett.* **B 581** (2004) 93 [hep-lat/0307021].

JHEP11(2004)048

[57] A. Hasenfratz and F. Knechtli, *Flavor symmetry and the static potential with hypercubic blocking*, *Phys. Rev.* **D 64** (2001) 034504 [hep-lat/0103029].

[58] D.J. Broadhurst and A.G. Grozin, *Matching QCD and HQET heavy-light currents at two loops and beyond*, *Phys. Rev.* **D 52** (1995) 4082 [hep-ph/9410240].

[59] http://www.physics.indiana.edu/~sg/milc.html.

[60] M.A. Shifman and M.B. Voloshin, *On annihilation of mesons built from heavy and light quark and $\bar{B}^0 \leftrightarrow B^0$ oscillations*, *Sov. J. Nucl. Phys.* **45** (1987) 292.

[61] H.D. Politzer and M.B. Wise, *Leading logarithms of heavy quark masses in processes with light and heavy quarks*, *Phys. Lett.* **B 206** (1988) 681.

[62] X.-D. Ji and M.J. Musolf, *Subleading logarithmic mass dependence in heavy meson form-factors*, *Phys. Lett.* **B 257** (1991) 409.

[63] D.J. Broadhurst and A.G. Grozin, *Two-loop renormalization of the effective field theory of a static quark*, *Phys. Lett.* **B 267** (1991) 105 [hep-ph/9908362].

[64] V. Gimenez, *Two-loop calculation of the anomalous dimension of the axial current with static heavy quarks*, *Nucl. Phys.* **B 375** (1992) 582.

[65] E. Eichten and B. Hill, *Renormalization of heavy-light bilinears and f_B for Wilson fermions*, *Phys. Lett.* **B 240** (1990) 193.

[66] R. Tarrach, *The pole mass in perturbative QCD*, *Nucl. Phys.* **B 183** (1981) 384.

[67] E. Eichten and B. Hill, *Static effective field theory: 1/m corrections*, *Phys. Lett.* **B 243** (1990) 427.

[68] A.F. Falk, B. Grinstein and M.E. Luke, *Leading mass corrections to the heavy quark effective theory*, *Nucl. Phys.* **B 357** (1991) 185.

JHEP11(2004)048

Dank

gilt

- meiner Familie und insbesondere meiner Frau Margret und unseren Kindern Tizian, Thalia und Tristan, die meine Arbeit stets mit Geduld, Verständnis und oft auch Verzicht begleitet und unterstützt haben;
- den Mitgliedern der ALPHA-Kollaboration und dabei vor allem meinen Kollegen M. Della Morte, R. Frezzotti, M. Guagnelli, K. Jansen, A. Jüttner, J. Rolf, R. Sommer, J. Wennekers, H. Wittig und U. Wolff für die fruchtbare und meinen wissenschaftlichen Werdegang der letzten Jahre prägende Zusammenarbeit;
- sowie G. Münster und unserer Arbeitsgruppe für die harmonische Atmosphäre am Institut für Theoretische Physik der WWU Münster.